NASA/CP—2000–209959

The 1999 NASA Aerospace Battery Workshop

J.C. Brewer, Compiler
Marshall Space Flight Center, Marshall Space Flight Center, Alabama

Proceeding of a workshop sponsored by the
NASA Aerospace Flight Battery Systems Program
and held in Huntsville, Alabama, November 16–18, 1999

May 2000

The NASA STI Program Office...in Profile

Since its founding, NASA has been dedicated to the advancement of aeronautics and space science. The NASA Scientific and Technical Information (STI) Program Office plays a key part in helping NASA maintain this important role.

The NASA STI Program Office is operated by Langley Research Center, the lead center for NASA's scientific and technical information. The NASA STI Program Office provides access to the NASA STI Database, the largest collection of aeronautical and space science STI in the world. The Program Office is also NASA's institutional mechanism for disseminating the results of its research and development activities. These results are published by NASA in the NASA STI Report Series, which includes the following report types:

- TECHNICAL PUBLICATION. Reports of completed research or a major significant phase of research that present the results of NASA programs and include extensive data or theoretical analysis. Includes compilations of significant scientific and technical data and information deemed to be of continuing reference value. NASA's counterpart of peer-reviewed formal professional papers but has less stringent limitations on manuscript length and extent of graphic presentations.

- TECHNICAL MEMORANDUM. Scientific and technical findings that are preliminary or of specialized interest, e.g., quick release reports, working papers, and bibliographies that contain minimal annotation. Does not contain extensive analysis.

- CONTRACTOR REPORT. Scientific and technical findings by NASA-sponsored contractors and grantees.

- CONFERENCE PUBLICATION. Collected papers from scientific and technical conferences, symposia, seminars, or other meetings sponsored or cosponsored by NASA.

- SPECIAL PUBLICATION. Scientific, technical, or historical information from NASA programs, projects, and mission, often concerned with subjects having substantial public interest.

- TECHNICAL TRANSLATION. English-language translations of foreign scientific and technical material pertinent to NASA's mission.

Specialized services that complement the STI Program Office's diverse offerings include creating custom thesauri, building customized databases, organizing and publishing research results...even providing videos.

For more information about the NASA STI Program Office, see the following:

- Access the NASA STI Program Home Page at ***http://www.sti.nasa.gov***

- E-mail your question via the Internet to help@sti.nasa.gov

- Fax your question to the NASA Access Help Desk at (301) 621–0134

- Telephone the NASA Access Help Desk at (301) 621–0390

- Write to:
  NASA Access Help Desk
  NASA Center for AeroSpace Information
  7121 Standard Drive
  Hanover, MD 21076–1320
  (301)621–0390

NASA/CP—2000–209959

The 1999 NASA Aerospace Battery Workshop

J.C. Brewer, Compiler
Marshall Space Flight Center, Marshall Space Flight Center, Alabama

Proceeding of a workshop sponsored by the
NASA Aerospace Flight Battery Systems Program
and held in Huntsville, Alabama, November 16–18, 1999

National Aeronautics and
Space Administration

Marshall Space Flight Center • MSFC, Alabama 35812

May 2000

Available from:

NASA Center for AeroSpace Information
7121 Standard Drive
Hanover, MD 21076–1320
(301) 621–0390

National Technical Information Service
5285 Port Royal Road
Springfield, VA 22161
(703) 487–4650

Preface

This document contains the proceedings of the 32nd annual NASA Aerospace Battery Workshop, hosted by the Marshall Space Flight Center on November 16-18, 1999. The workshop was attended by scientists and engineers from various agencies of the U.S. Government, aerospace contractors, and battery manufacturers, as well as international participation in like kind from a number of countries around the world.

The subjects covered included nickel-hydrogen, nickel-cadmium, silver-zinc, and lithium-ion technologies.

Introduction

The NASA Aerospace Battery Workshop is an annual event hosted by the Marshall Space Flight Center. The workshop is sponsored by the NASA Aerospace Flight Battery Systems Program which is managed out of NASA Glenn Research Center and receives support in the form of overall objectives, guidelines, and funding from Code S, NASA Headquarters.

The 1999 Workshop was held on three consecutive days and was divided into five sessions. The first day consisted of a General Session and a Nickel-Hydrogen Session. The second day consisted of two Lithium-Ion Sessions with the first two papers (nickel-hydrogen and silver-zinc) placed in the first session due to scheduling constraints. The third and final day was a second Nickel-Hydrogen Session.

On a personal note, I would like to take this opportunity to thank all of the many people that contributed to the organization and production of this workshop:

The NASA Aerospace Flight Battery Systems Program, for their financial support as well as their input during the initial planning stages of the workshop;

Huntsville Hilton, for doing an outstanding job in providing an ideal setting for this workshop and for the hospitality that was shown to all who attended;

Marshall Space Flight Center employees, for their help in mailing the various correspondence, registering attendees, handling the audience microphones, and flipping transparencies during the workshop.

Finally, I want to thank all of you that attended and/or prepared and delivered presentations for this workshop. You were the key to the success of this workshop.

Jeff Brewer
NASA Marshall Space Flight Center

Table of Contents

Preface iii

Introduction v

General Session 1

Status of the Space Battery R&D at Tsukuba Space Center, NASDA
Y. Sone, T. Suzuki, X. Liu, H. Kusawake, K. Kanno, and S. Kuwajima, National Space Development Agency of Japan (NASDA) 3

Summary of JPL Activities
Paul Timmerman and Subbarao Surampudi, Jet Propulsion Laboratory 31

In-orbit Earth Radiation Budget Satellite (ERBS) Battery Switch
Anisa Ahmad, Marlon Enciso, and Gopalakrishna Rao, NASA Goddard Space Flight Center 65

Super Capacitor Development at NASA MSFC
David K. Hall, NASA Marshall Space Flight Center 87

Calorimetric Measurements on a 32 Ah Li/MnO_2 Cell for the X-38 Crew Return Vehicle
Eric Darcy, NASA Johnson Space Center; and Chris Johnson, Boeing-Seattle 111

Low Temperature Performance of Two Nickel-Hydrogen Designs
Dr. Dean W. Maurer, Loral Skynet; and Dr. Dawn See, Imperial College of Science, Technology, and Medicine 131

Nickel-Hydrogen Session I 137

High DOD LEO Life Cycle Testing
Jeff Dermott, Eagle-Picher Technologies, LLC 139

Launch and Early Orbit Phase Simulation Tests on Nickel Hydrogen Batteries
P.J. Johnson, S.W. Donley, and B. Starritt, TRW Space & Electronics Group 153

EOS-PM Nickel-Hydrogen Cell Initial Life Test Report
R.F. Tobias, TRW Space & Electronics Group 171

High Conductivity Composite Sleeves for Nickel Hydrogen Cells
K.C. Snyder, Eagle-Picher Technologies, LLC 193

Progress in the Development of 5.5 Inch Nickel Hydrogen Battery Cells
Jack N. Brill, Robert Brown, and Fred Sill, Eagle-Picher Technologies, LLC 213

Lithium-Ion Session I 229

Dependence of Positive Plate Design and Temperature on the Performance of Nickel-Hydrogen Cells
Hari Vaidyanathan, COMSAT Laboratories 231

Comparison of Separation Performance for Four Variables in Rechargeable Silver/Zinc Cells
Harlan Lewis, NSWC Crane Division; and Albert Himy, J.J. McMullen Associates 249

Thermal Aspects of Lithium Ion Cells
H. Frank, P. Shakkottai, R. Bugga, M. Smart, C.K. Huang, P. Timmerman, and S. Surampudi, Jet Propulsion Laboratory 275

Pulse Testing of the Eagle-Picher Lithium-Ion System
Chad Kelly and Beth Parmley, Eagle-Picher Technologies, LLC 287

Lithium-Ion Cell Storage Study
Leonine Lee and Gopalakrishna M. Rao, NASA Goddard Space Flight Center 303

Engineering and Abuse Testing of Panasonic Lithium-Ion Battery and Cells
Judith A. Jeevarajan, Lockheed Martin / NASA Johnson Space Center; and Bobby J. Bragg, NASA Johnson Space Center 317

Lithium-Ion Session II 349

Characterization and Simulated LEO Cycling of STRV Lithium-Ion Battery Modules
Chuck Lurie and Philip Johnson, TRW Space and Electronics Group 351

SAFT Space Li-Ion Development Status
Dr. Yannick Borthomieu, SAFT Defense and Space Division 369

Performance Characteristics of Lithium-Ion Prototype Batteries for Mars Surveyor Program 2001 Lander
M.C. Smart, B.V. Ratnakumar, L. Whitcanack, and S. Surampudi, Jet Propulsion Laboratory; J. Byers, Lockheed Martin Astronautics Corporation; and R.A. Marsh, Wright-Patterson Air Force Base 411

Performance Characteristics of Lithium Ion Prototype Cells for 2003 Mars Sample Return Athena Rover
B.V. Ratnakumar, M.C. Smart, R. Ewell, and S. Surampudi, Jet Propulsion Laboratory; and R. Marsh, Wright-Patterson Air Force Base 455

Development of a 70 Ah Li-ion Cell for Aerospace Applications
Jim DeGruson, Eagle-Picher Technologies, LLC 495

Nickel-Hydrogen Session II 515

Computational Fluid Dynamics Modeling of Nickel Hydrogen Batteries
R. Cullion, W.B. Gu, and C.Y. Wang, Pennsylvania State University; and P. Timmerman, Jet Propulsion Laboratory 517

Validation of the Static Model for Nickel-Hydrogen Cells
Lawrence H. Thaller, The Aerospace Corporation 537

Nickel-Hydrogen Life Modeling
Robert A. Brown, Eagle-Picher Technologies, LLC 553

Nickel-Hydrogen Cell Positive Precharge Signatures
Chuck Lurie, TRW Space and Electronics Group 567

Strain Gage Temperature Effects and the van der Waals' Equation
Dean W. Maurer, Loral Skynet 585

1999 NASA Aerospace Battery Workshop Attendance List 591

General Session

Status of the Space Battery R&D at Tsukuba Space Center, NASDA

Y. Sone, T. Suzuki, X. Liu, H. Kusawake, K. Kanno, and S. Kuwajima

Electronic and Information Technology Department
Office of Research and Development
National Space Development Agency of Japan
(NASDA)

NASDA Launch Schedule of NASDA Projects

Past and Future Space Development Programs

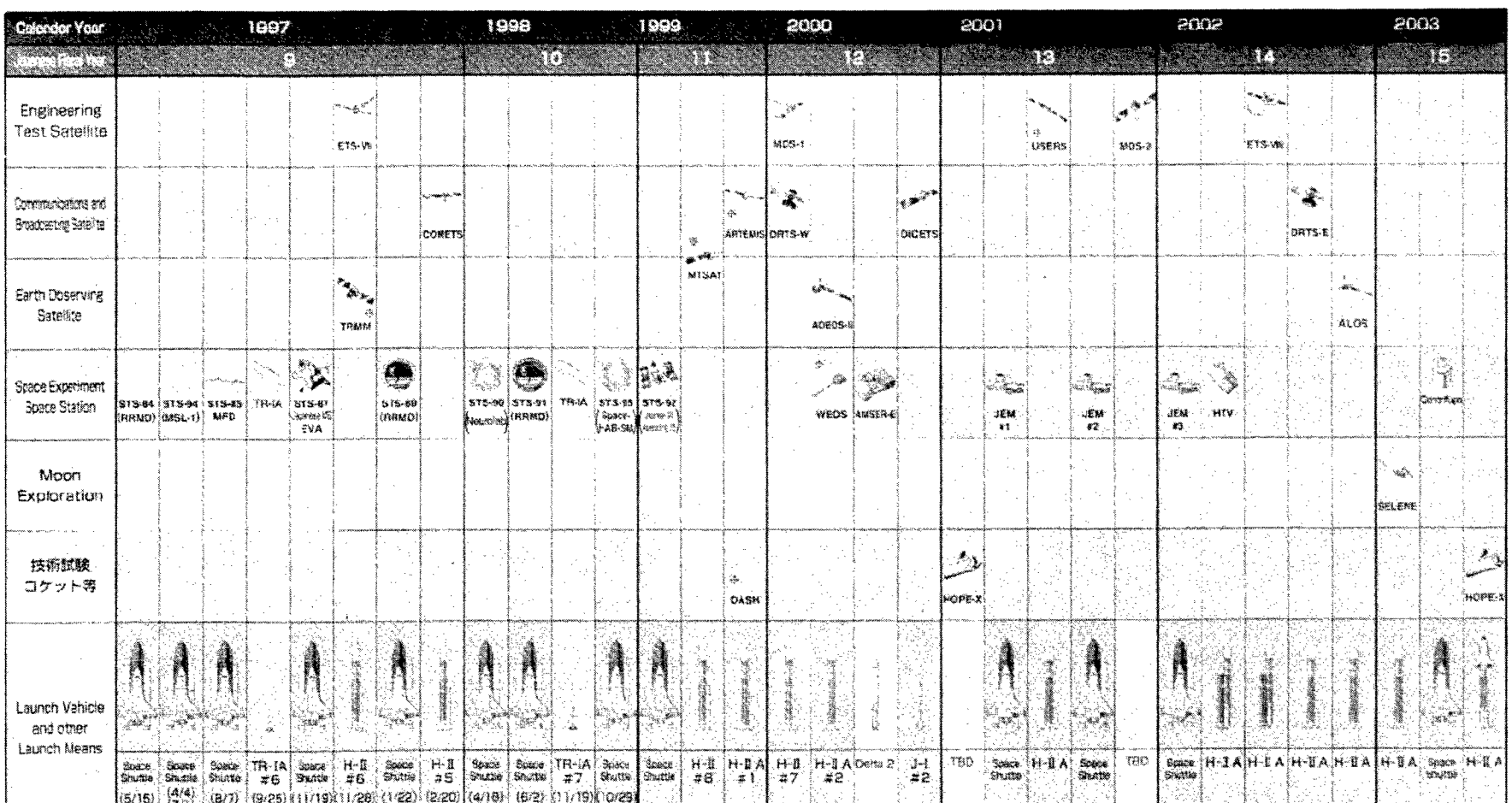

(Launch dates are indicated in the Eastern Standard Time)

※Other Agency's Payload

Launch Vehicle and Other Launch Means

- H-II Rocket
- J-I Rocket
- TR-IA Rocket
- H-II A Rocket
- Space Shuttle

ADEOS-II	Advanced Earth Observing Satellite II
ALOS	Advanced Land Observing Satellite
ARTEMIS	Advanced Relay and Technology Mission Satellite
COMETS	Communications and Broadcasting Engineering Test Satellite
DASH	Demonstrator of Atmospheric Flight with Hypersonic Speed
DRTS	Data Relay Test Satellite
ETS	Engineering Test Satellite
HOPE-X	H-II Orbiting Plane-X
HTV	H-IIA Transfer Vehicle
JEM	Japanese Experiment Module
MFD	Manipulator Flight Demonstration Program
MDS	Mission Demonstration Satellite
MDS-1	Evaluating Components and Devices Mission (tentative)
MDS-2	Lidar Experiment Mission (tentative)
MSL-1	First Microgravity Science Laboratory
MTSAT	Multi-purposes Transportation Satellite
DICETS	Optical Inter-orbit Communications Engineering Test Satellite
RRMD	Realtime Radiation Monitoring Device
SELENE	Selenological Engineering Explore
TR-IA	Test Rocket for Space Experiment
TRMM	Tropical Rainfall Measuring Mission
USERS	Unmanned Space Experiment Recovery (tentative)
VDP	Vehicle Evaluation Payload
WEDS	Whale Ecology Observation Satellite
Centrifuge	Biological Research Facility
Neurolab	Neuroscience Experiment

http://yyy.tksc.nasda.go.jp/Home/Projects/index_j.html

NASDA | Development of Space Batteries at NASDA

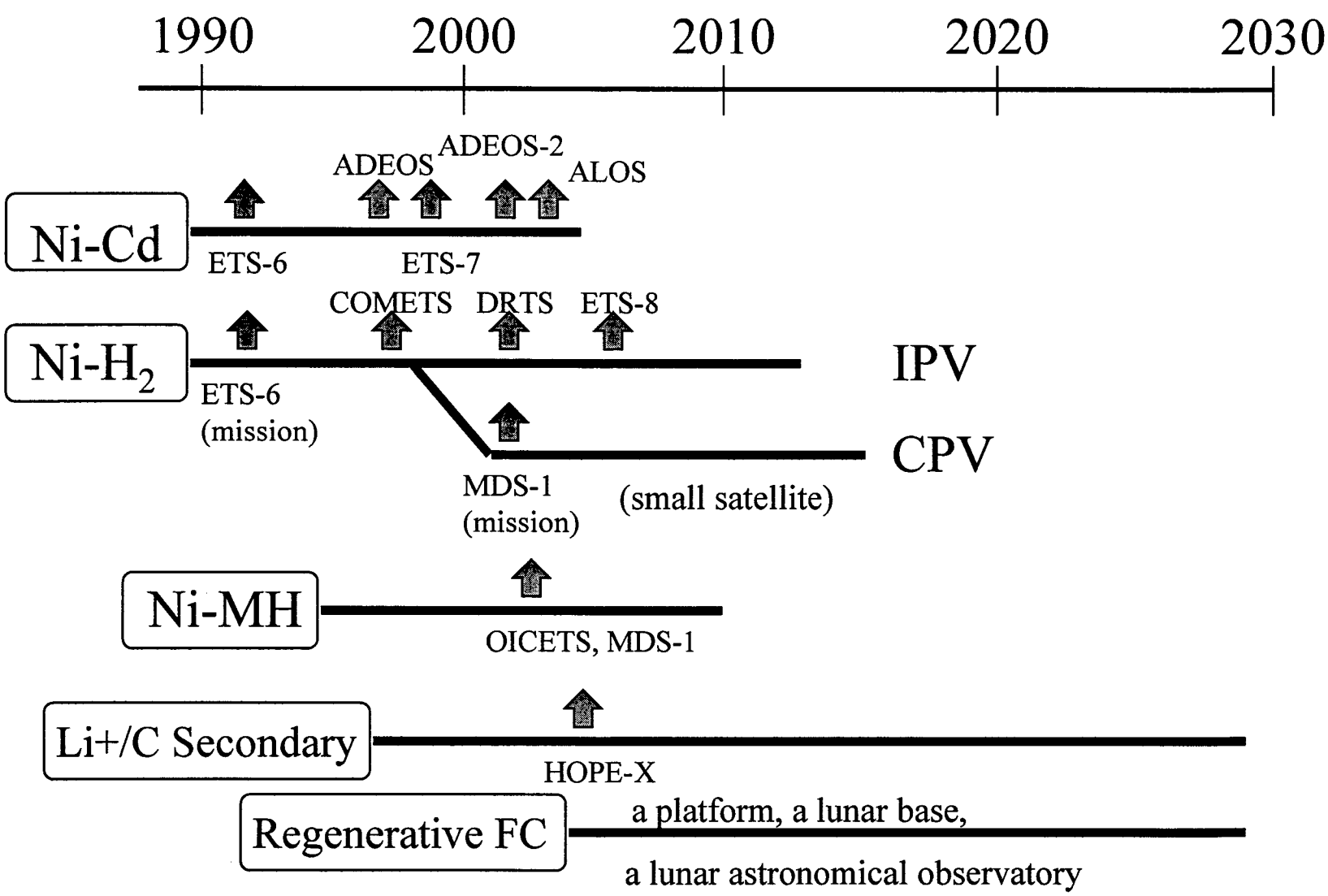

NASDA

Battery Main Schedule

Cell	Capacity	Satellite	Requirement	Launch Schedules
Standard Ni-Cd [1)]	50 Ah	ADEOS-II	LEO 3 Years	2,000 summer
Advanced Ni-Cd [1)]	50 Ah	ALOS	LEO 5 Years	2,003 winter
Ni-MH	13 Ah	OICETS	LEO 1 Year	2,001 winter
	20 Ah	MDS-1	GTO 1 Year	2,000 spring
IPV Ni-H_2	50 Ah	DRTS series	GEO 10 Years	2,000 spring
	100 Ah	ETS-VIII	GEO 10 Years	2,002 autumn
CPV Ni-H_2 [2)]	5 Ah	MDS-1	GTO 1 Year	2,000 spring

[1)] 'Standard Ni-Cd' is a conventional Ni-Cd cell, while 'Advanced Ni-Cd' has negative electrodes with organic plate treatment.

[2)] CPV Ni-H2 is going to be launched to demonstrate its performance in the orbit.

NASDA

CPV Ni-H_2 Battery

- CPV type Ni-H_2 Battery

CPV type Ni-H2 battery will be launched as one of the missions of MDS-1.

We are going to demonstrate its performance in order to apply it to the future missions.

NASDA

CPV Ni-H_2 Battery

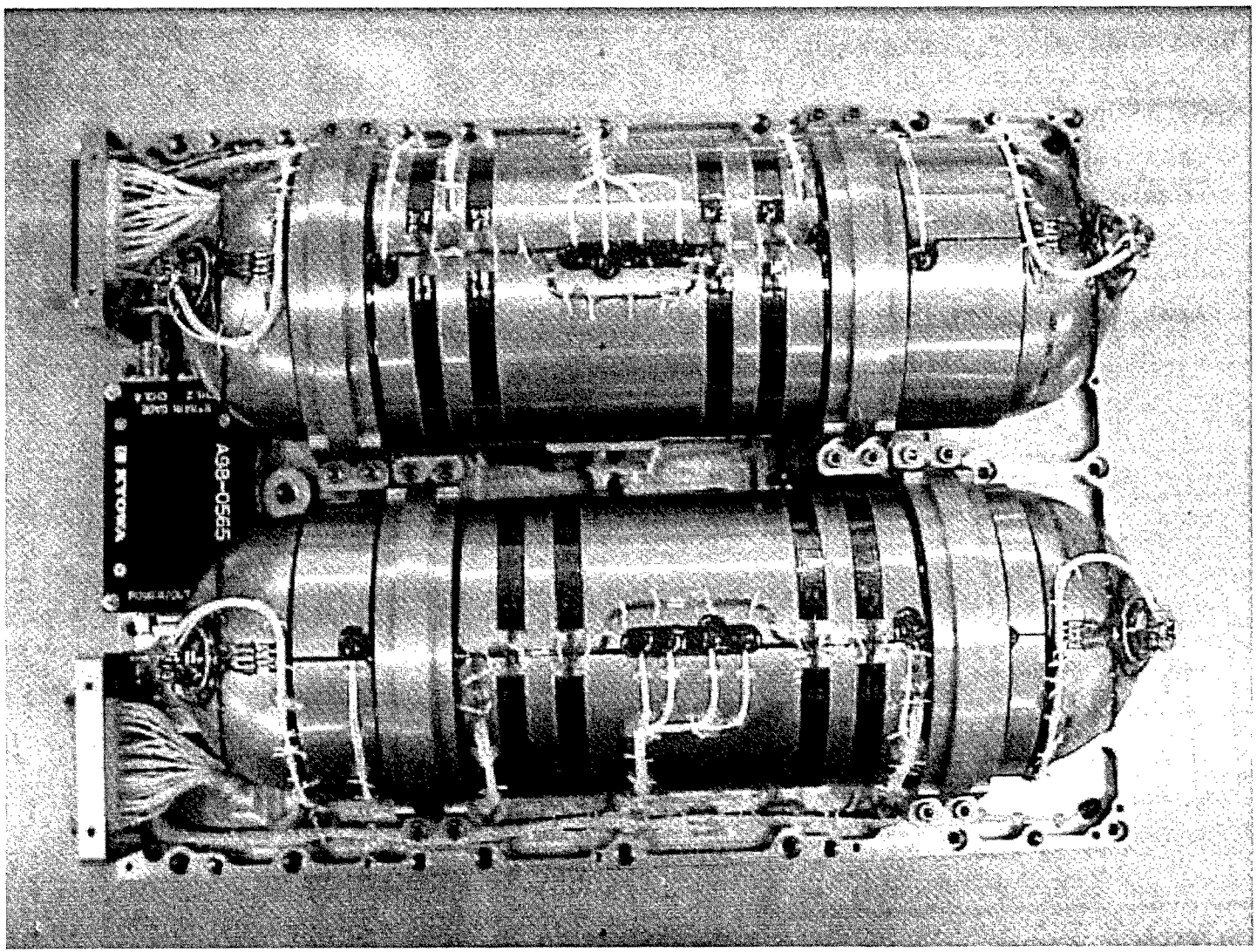

Demonstration Model

NASDA

CPV Ni-H_2 Battery

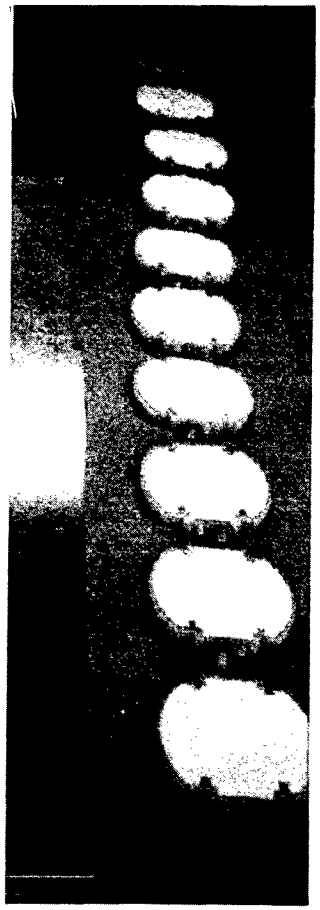

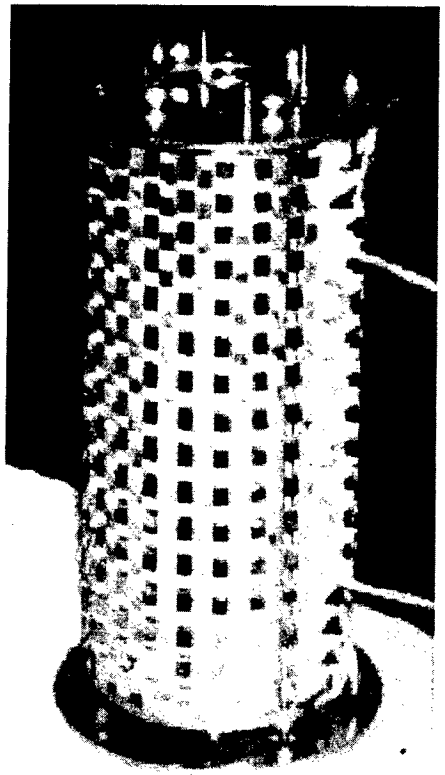

Inside Structure of CPV

Capacity	5 Ah battery (16 cells in series)
Energy Density	ca. 35 Wh/kg (1 CPV)
Total Weight	11.7 kg
Total Size	300mm x 400mm x132mm
Permitted Temperature	0~30°C

Specification

NASDA

Advanced Ni-Cd

- Advanced Ni-Cd

The advanced Ni-Cd battery/cell has negative electrodes with organic treatment. We tested the battery performance by LEO mode with high DOD.

NASDA

Advanced Ni-Cd

We tested the performance with high DOD by V/T control.
The V/T curve we used though our measurements is as follows,

$$V = \{1.557 - 0.015 \times (8-L) - 0.00294 \times T\} \times 6$$

V ; Volt.,
L ; V/T level,
T ; Temp.(°C)

Test Sample	50Ah Ni-Cd with organic treated negative electrodes	
Simulated Orbit	LEO	
Charge Time	60 min.	
Discharge Time	30 min.	
Ambient Temperature	20 degrees C	
DOD	40%	50%
Current Charge	40 A	40 A
Current Discharge	40 A	50 A
Number of Cells with Series Connection	6 cells	6 cells

NASDA

Advanced Ni-Cd

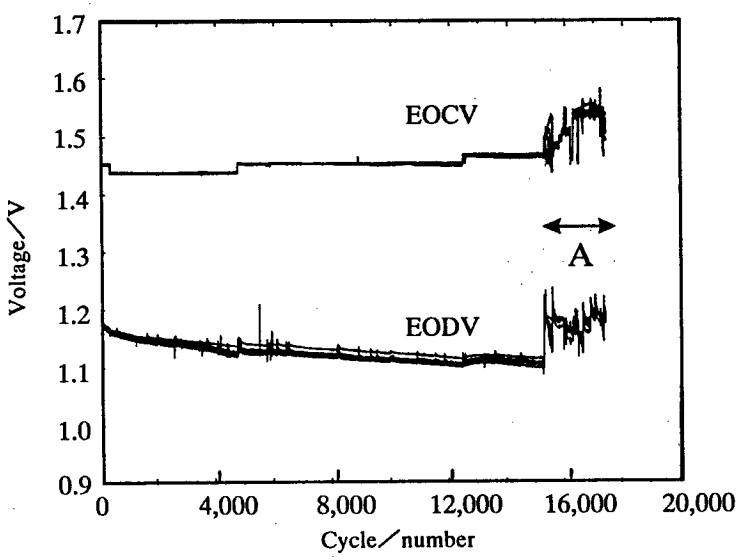

Fig. Trend data of life cycle test with DOD=40%

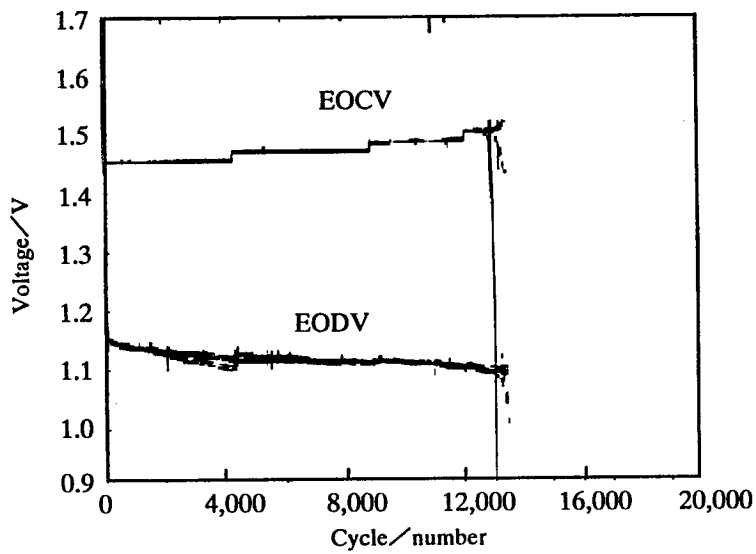

Fig. Trend data of life cycle test with DOD=50%

We observed rather stable performance in the test with DOD=40%, while we found two 'dead short' cells in the test with DOD=50% at ca. 13,500th cycle.
When the test with DOD=40% passed ca. 15,000 cycles, we checked the V/T conditions as respect to DOD and temperature. (area A). We have now switched back to the test with DOD=40%.

NASDA

Advanced Ni-Cd

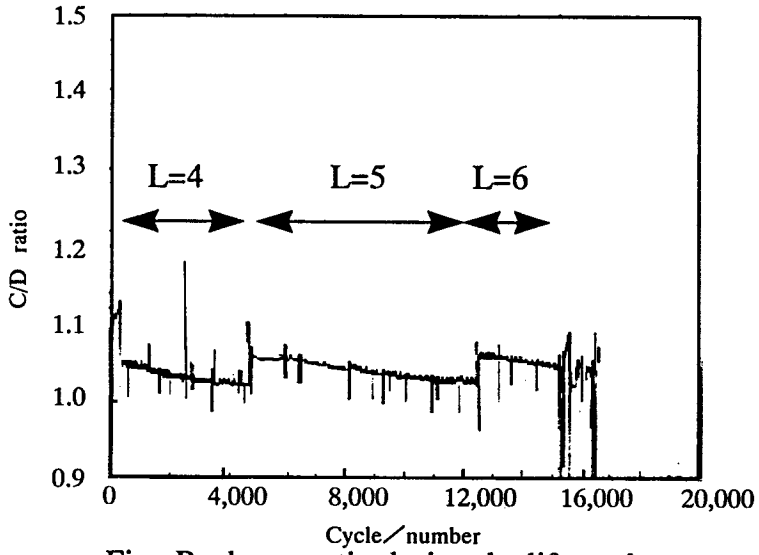

Fig. Recharge ratio during the life cycle test with DOD=40%

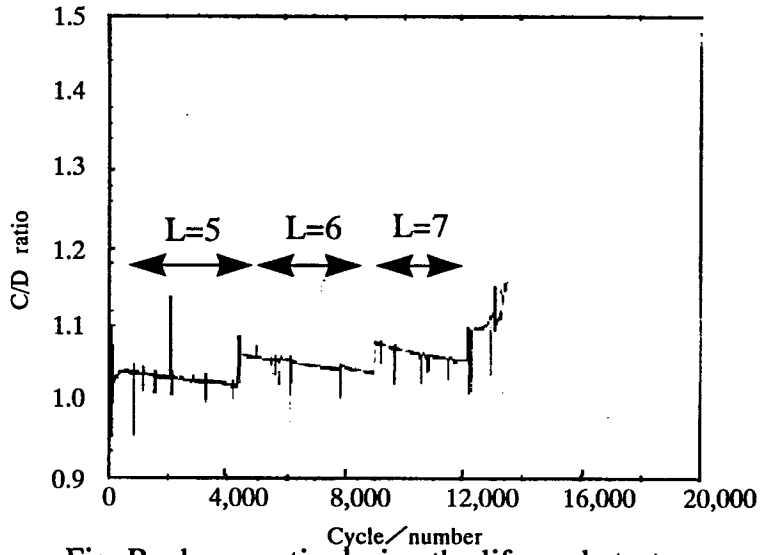

Fig. Recharge ratio during the life cycle test with DOD=50%

These figures show the recharge ratio (C/D ratio). The V/T level was always changed to keep the C/D ratio between 1.0 and 1.1.

Advanced Ni-Cd

NASDA decided to apply this battery/cell to ALOS project.
In order to predict the battery performance in the orbit, we decided to start new tests. The test conditions are as follows.
V/T curve;

$$V = \{1.529 - 0.012 \times (8-L) - 0.00315 \times T\} \times 5$$

V ; Volt.,
L ; V/T level,
T ; Temp.(°C)

Test Sample	50Ah Ni-Cd with organic treated negative electrodes	
Simulated Orbit	LEO(ALOS Simulations)	
Charge Time	64 min.	
Discharge Time	34.5 min.	
Ambient Temperature	10 degrees C	
DOD	20%	25%
Charge Current	12.5 A	14.3 A
Discharge Current	20.87 A	24.35 A
Number of Cells with Series Connection	5 cells	5 cells

NASDA

Lithium Ion Secondary Cell

- Lithium Ion Secondary Cell

As reported '1998 NASA Aerospace Battery Workshop,' we started the study of 10 and 30Ah lithium ion secondary cells in 1997.

We also started the study of 100 Ah lithium ion secondary cell, in 1998. In order to accelerate the R&D of lithium ion cells, the partnership between NASDA and companies has started.

NASDA

Lithium Ion Secondary Cell

Cell Style		Elliptic Cylinder
Electrode	Positive Electrode	LiCoO2
	Negative Electrode	Graphite Carbon
Capacity	Nominal / Typical	100Ah / 106 Ah
Weight		2.8 kg
Dimensions		130 mm (W) x 50 mm (D) x 207 mm (H)
Energy Density	per Weight	136 Wh/kg
	per Volume	309 Wh/L
Charge Voltage / Higher Limited Voltage		3.98 V
Discharge Voltage	Nominal Voltage	3.6 V
	Lower Limited Voltage	2.75 V

Mitsubishi Electric Co. (MELCO) and Japan Storage Battery Co (JSB) have been cooperating for the development of lithium ion secondary battery for space applications. In 1998 we decided to collaborate with these companies to accelerate our R&D of lithium ion secondary battery for the NASDA future satellites.

- MELCO is going to establish the battery system including the charge method. For example, MELCO studies the electric circuits, safety unit, etc. It will also evaluate the safety of the battery system.
- JSB checks the single cell performance. Life cycle test, safety test of cells, storage effect are included in its study.
- NASDA focuses the evaluation on the long term performance as a battery.

Lithium Ion Secondary Cell

The following is the test conditions for Lithium Ion Secondary Cells

Test Sample	100 Ah Lithium Ion Secondary Cell		
Simulated Orbit	LEO		GEO
Charge Time	60 min.		22 hours 48 min.
Discharge Time	30 min.		72 min.
Ambient Temperature	15 degrees C (12 degrees C)		
DOD	25%	40%	80%
Charge Current / Constant Voltage 1)	30 A / 19.75 V	50 A / 19.75 V	10 A / 19.75
Discharge Current	50 A	80 A	67 A
Number of Cells with Series Connection	5 cells	5 cells	5 cells

1) The charge method is so-called CC-CV (constant current - constant voltage) control.

NASDA

Lithium Ion Secondary Cell

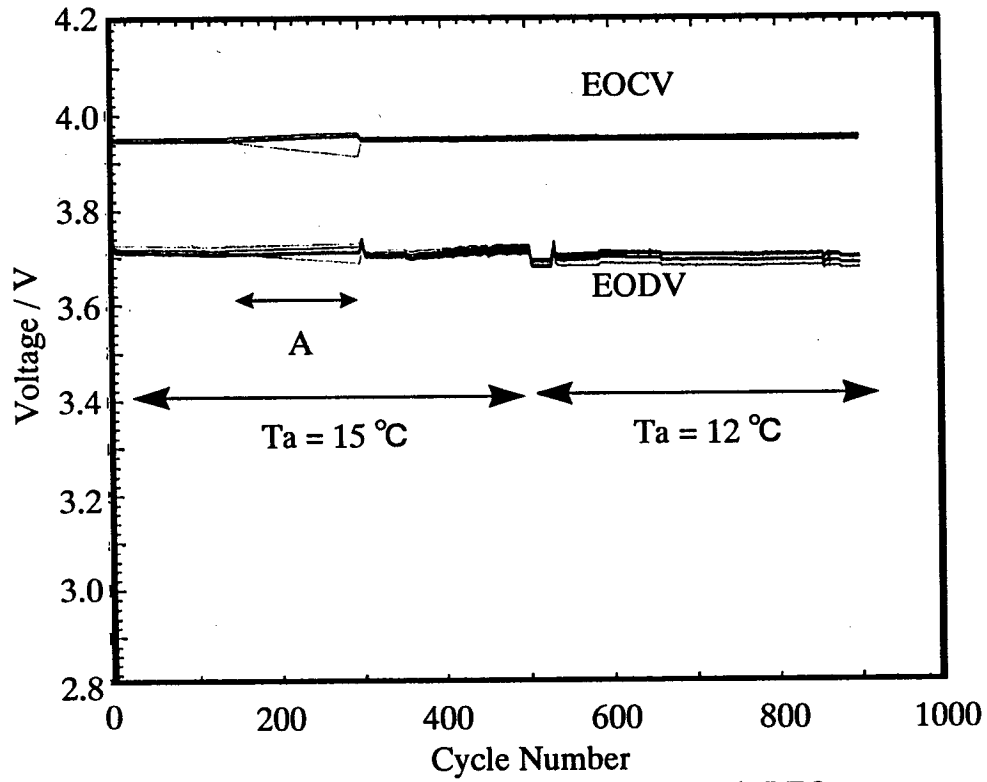

Fig. The trend data with DOD=25%, LEO

After ca.170th cycle, one of the cells started to show the lower EODV and EOCV(area A). The reason for these lower voltage seemed to reflect the difference of state of charge (SOC). In order to equalize SOC condition, we discharged each cell down to 2.75V at 300th cycle. After this treatment, the battery showed a better performance, again.

At 500th cycle, we decreased the ambient temperature (Ta) by 3℃, which decreased the EODV slightly.

NASDA

Lithium Ion Secondary Cell

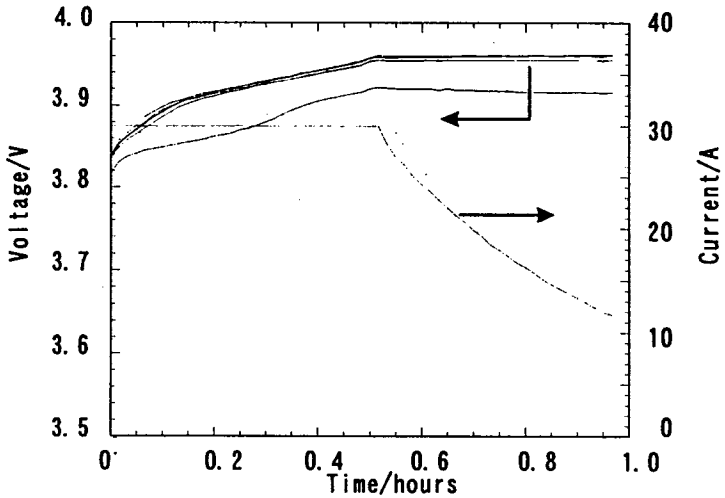

Fig. Charge curve among LEO cycles.
Cycle number = 280

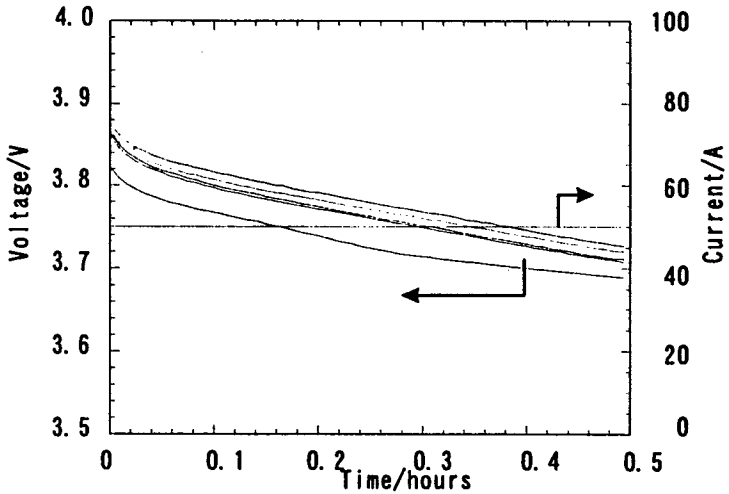

Fig. Discharge curve among LEO cycles.
Cycle number = 280

Fig. The Charge and Discharge curve of the test with DOD=25%

This is one of the cycle data before the SOC control. A single cell showed both lower EOCV and EODV.

NASDA

Lithium Ion Secondary Cell

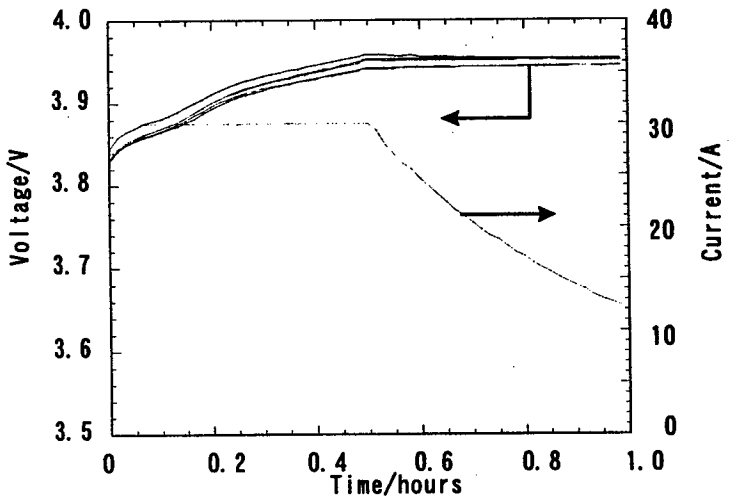

Fig. Charge curve among LEO cycles.
Cycle number = 954

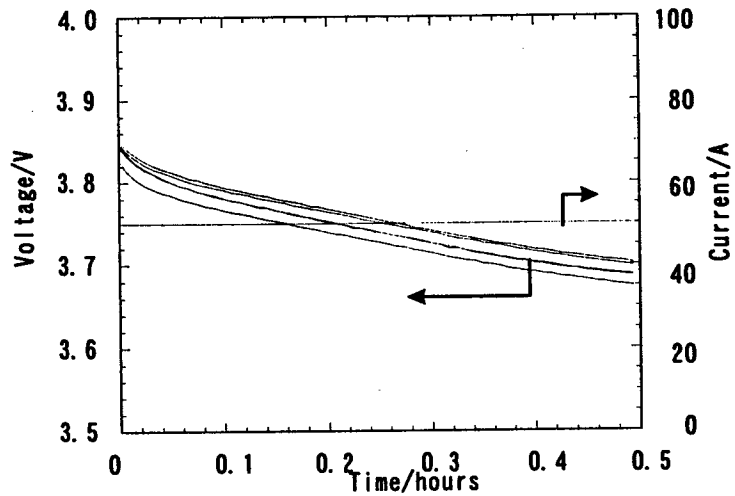

Fig. Discharge curve among LEO cycles.
Cycle number = 954

Fig. The Charge and Discharge curve of the test with DOD=25%

This is one of the latest cycle performances of the battery with DOD=25%. After the treatment at 300th cycle, the difference of voltage was reduced.

NASDA | Lithium Ion Secondary Cell

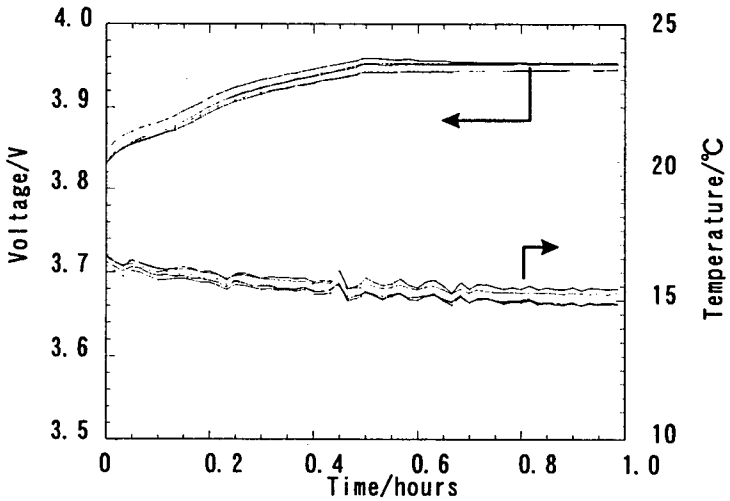

Fig. Charge curve among LEO cycles.
Cycle number = 954

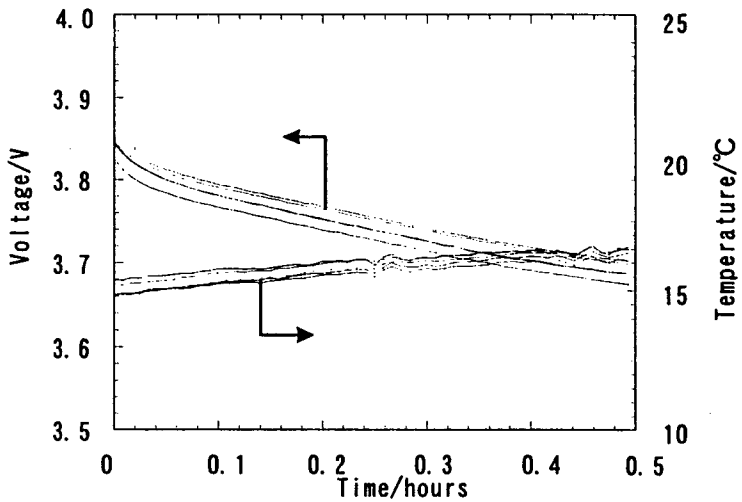

Fig. Discharge curve among LEO cycles.
Cycle number = 954

Fig. The Charge and Discharge curve of the test with DOD=25%

These figures show the temperature change through one cycle.

NASDA

Lithium Ion Secondary Cell

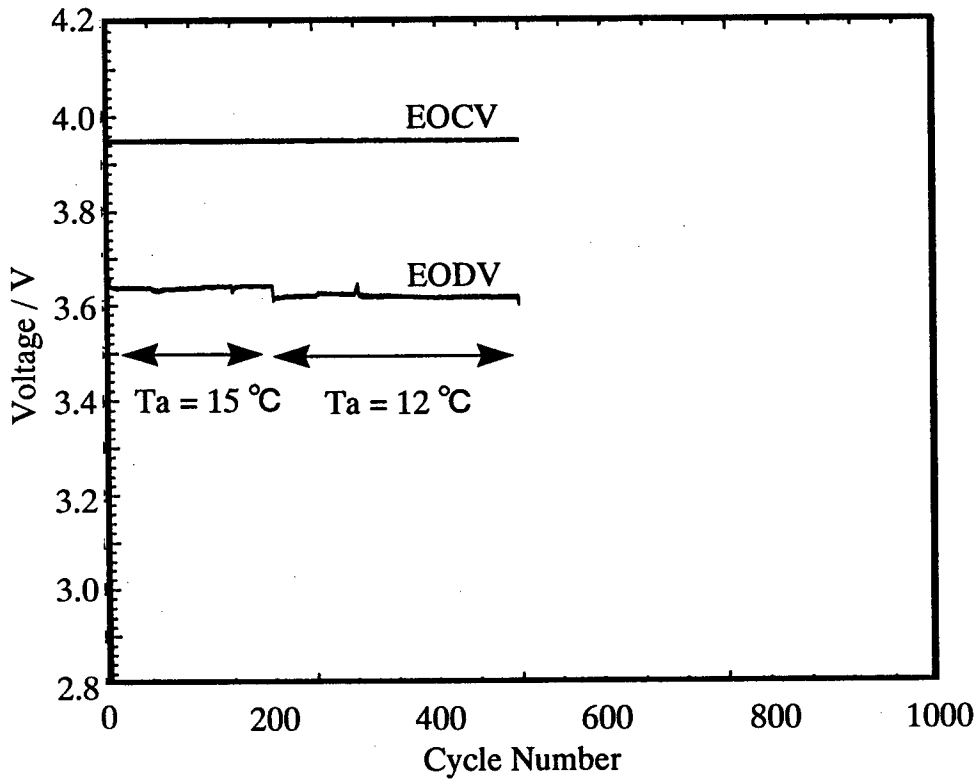

Fig. The trend data of with DOD=40%, LEO.

The performance of the cells in this battery still seem to coincide with each other. At 500th cycle, we decreased the ambient temperature (Ta) by 3℃.

NASDA

Lithium Ion Secondary Cell

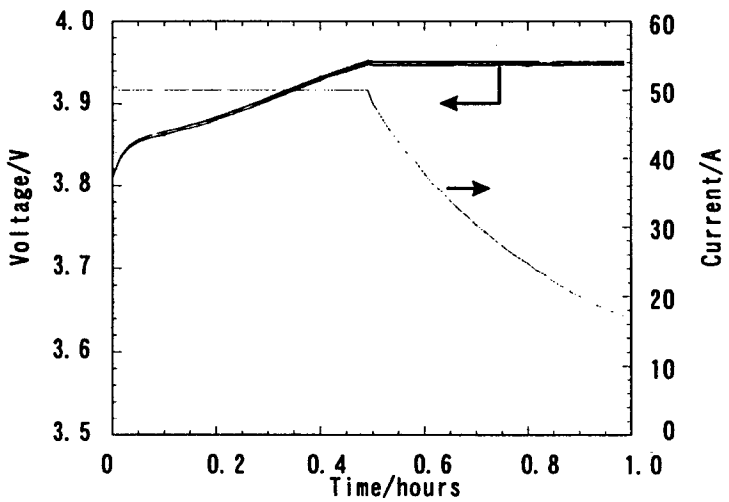

Fig. Charge curve among LEO cycles.
Cycle number = 280

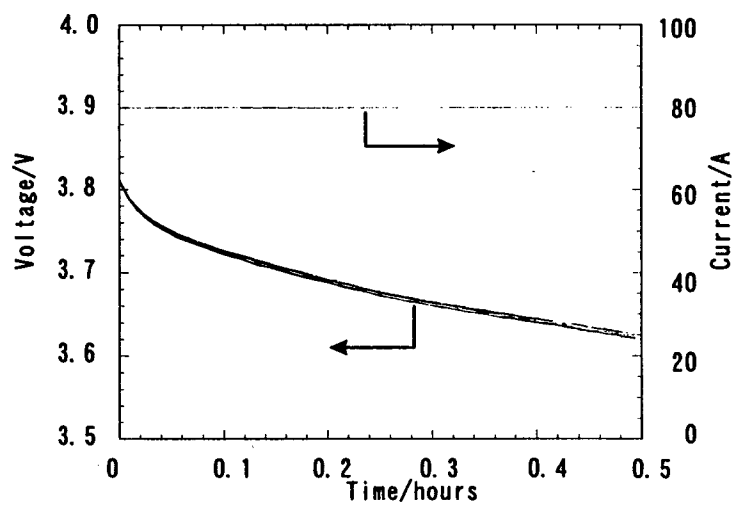

Fig. Discharge curve among LEO cycles.
Cycle number = 280

Fig. The Charge and Discharge curve of the test with DOD=40%

These results were obtained at 280th cycle. In this measurement, cells connected in series showed the same performance. The cells kept the same SOC conditions.

NASDA

Lithium Ion Secondary Cell

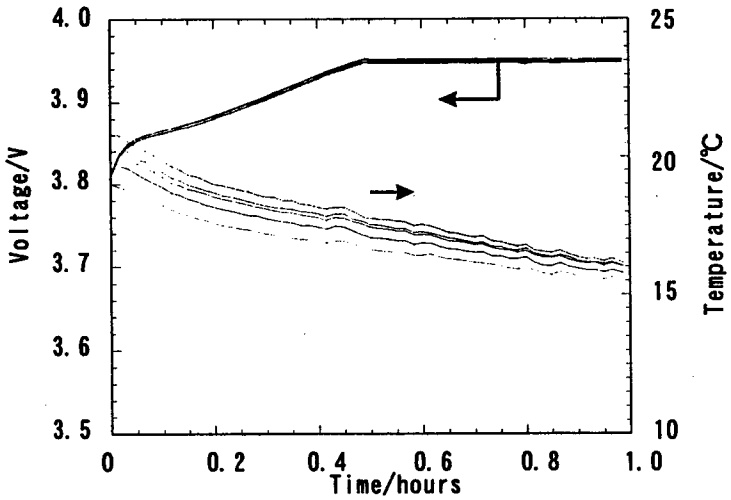

Fig. Charge curve among LEO cycles.
Cycle number = 280

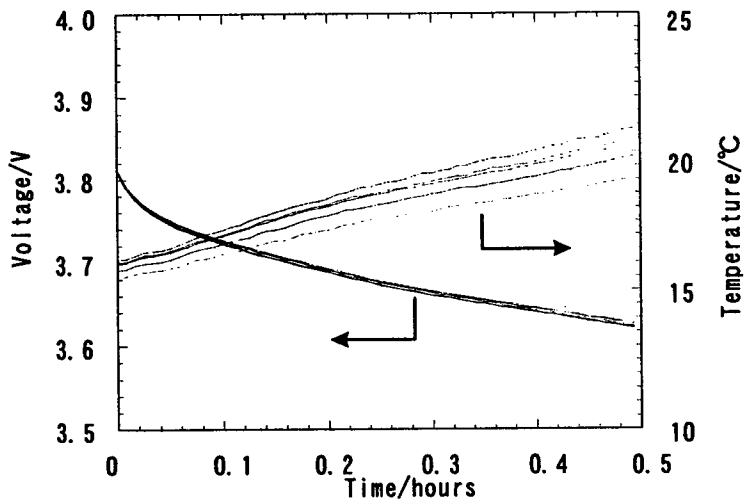

Fig. Discharge curve among LEO cycles.
Cycle number = 280

Fig. The Charge and Discharge curve of the test with DOD=40%

These figures show the temperature change through one cycle with DOD=40%.

NASDA

Lithium Ion Secondary Cell

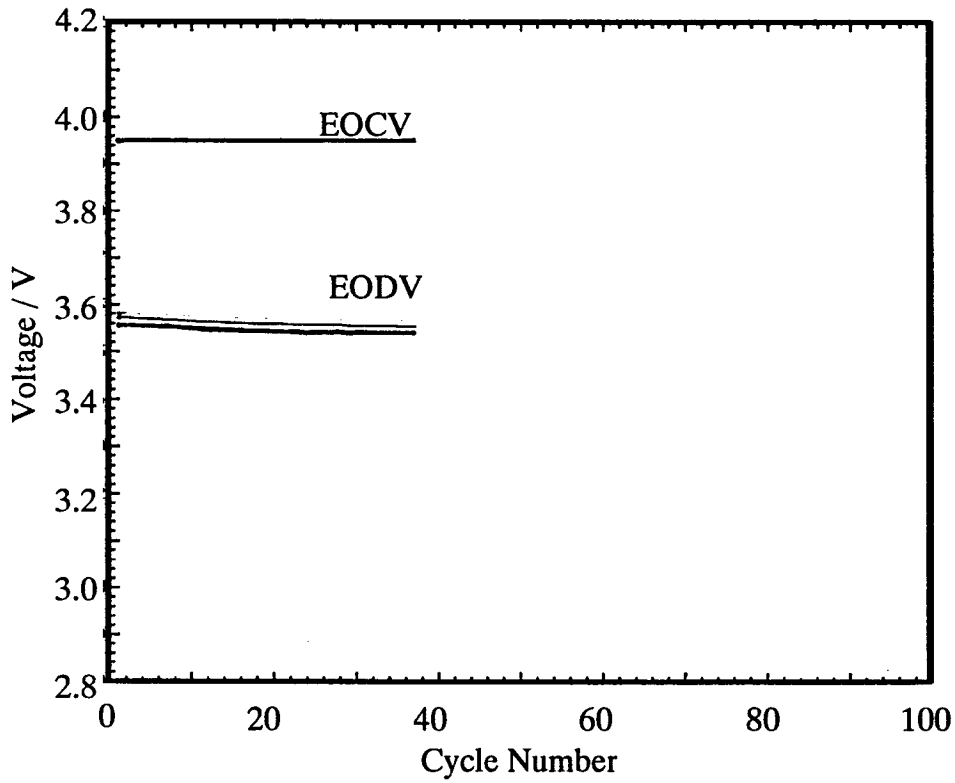

Fig. The trend data of with DOD=80%, GEO.

GEO life cycle test was also started.

NASDA

Lithium Ion Secondary Cell

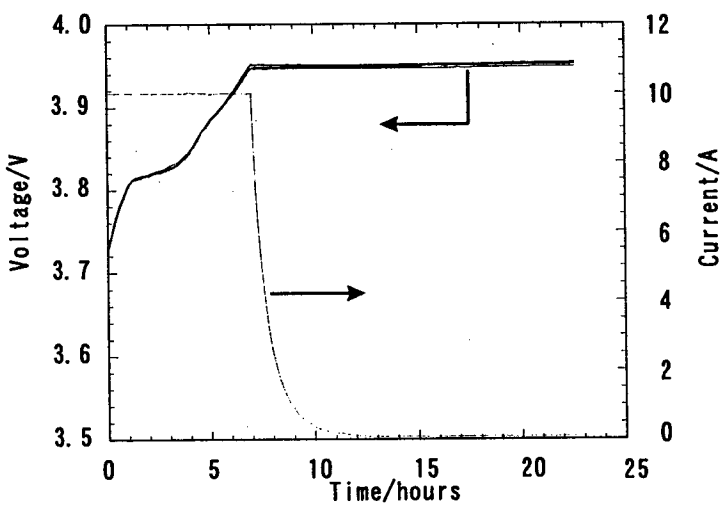

Fig. Charge curve among GEO cycles.
Cycle number = 42

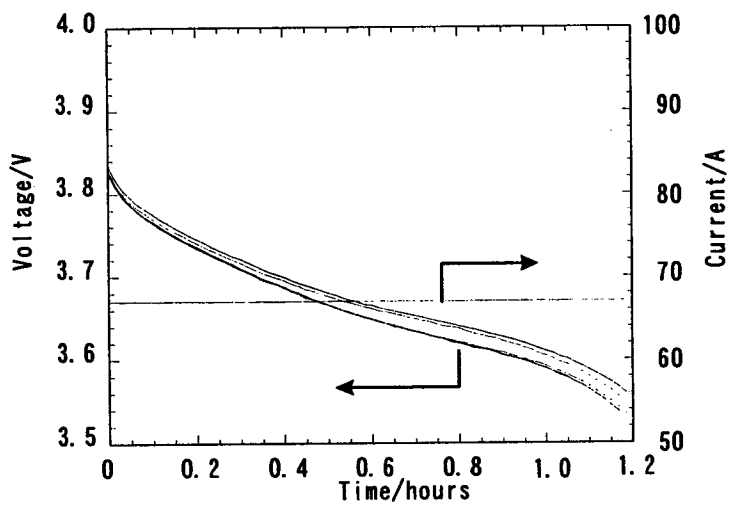

Fig. Discharge curve among GEO cycles.
Cycle number = 42

Fig. The Charge and Discharge curve of the test with DOD=80%

Charge and discharge curves of GEO cycle test are shown above. Stable performance could be observed.

NASDA

Lithium Ion Secondary Cell

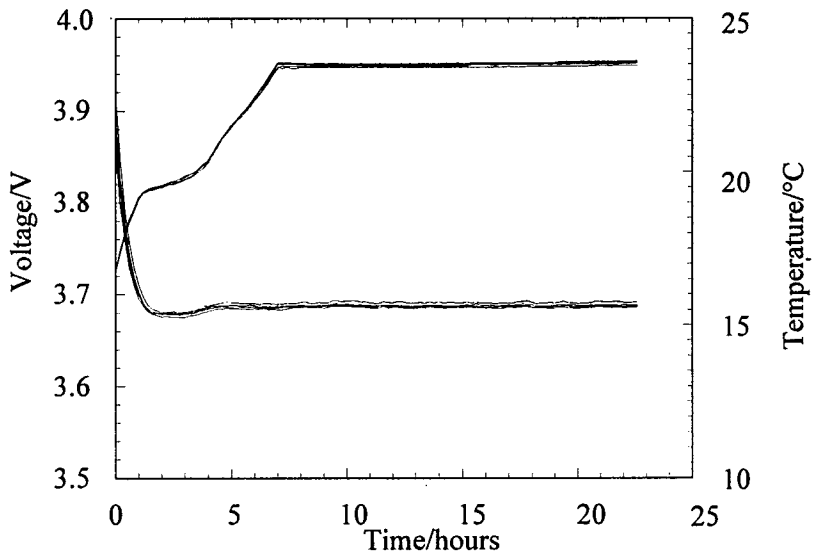

Fig. Charge curve among GEO cycles.
Cycle number = 42

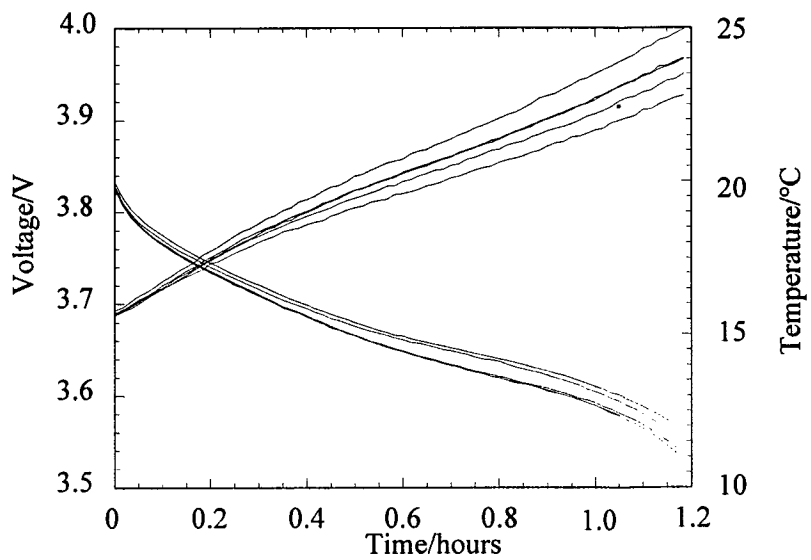

Fig. Discharge curve among GEO cycles.
Cycle number = 42

Fig. The Charge and Discharge curve of the test with DOD=80%

These figures shows the temperature change through one GEO cycle with DOD=80%.

NASDA

Lithium Ion Secondary Cell

-Next Plan-

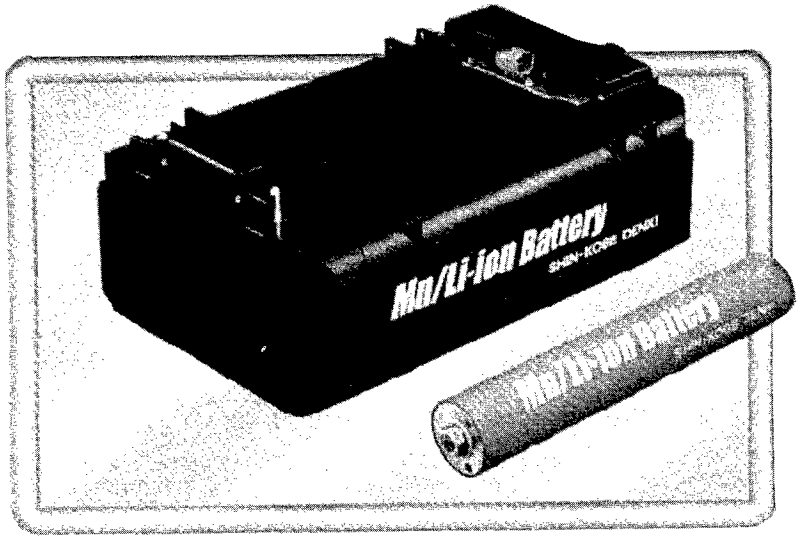

Cell Style		Cylinder
Electrode	positive electrode	LiMnO2
	negative electrode	Non-graphite Carbon
Capacity		90 Ah
Weight		3.3 kg
Dimensions		Φ 67mm x 410 mm
Energy Density	per weight	104 Wh/kg
	per volume	237 Wh/L
Charge Voltage / Higher Limited Voltage		4.2 V
Discharge Voltage	Nominal Voltage	3.8 V
	Lower Limited Voltage	2.5 V

Above battery/cell is under development by the cooperation of Nissan Motor Co. and Shinkobe Electric Machinery Co. We will start our tests from spring. The point of this cell is the electrode material. $LiMnO_2$ and non-graphite carbon is used for the positive and negative electrode, respectively.

NASDA

Summary

- CPV type Ni-H_2 Battery

  CPV type Ni-H2 battery 'demonstration model' was introduced. It will be launched in 2,000.

- Advanced Ni-Cd

  The performances of 50Ah advanced Ni-Cd battery/cell with high DOD were shown. We observed rather stable performance with over 15,000 life cycles in the test with DOD=40%.

  The orbital simulation for ALOS will be started.

- Lithium Ion Secondary Cell

  The cycle data of 100Ah lithium ion secondary cell were shown. Two modes of LEO and one mode of GEO cycle test are to be continued.

SUMMARY OF JPL ACTIVITES

Paul Timmerman
Subbarao Surampudi

Paul.J.Timmerman@jpl.nasa.gov
ELECTROCHEMICAL SYSTEMS GROUP

Outline

JPL Program Summary
Ni-H2 Cell Testing
Li-Ion Technology
NASA Telecons
Battery Laboratory

Paul.J.Timmerman@jpl.nasa.gov
ELECTROCHEMICAL SYSTEMS GROUP

JPL Flight Program Summary

Solar System Exploration

Deep Space 1 - Asteroid Rendezvous
Deep Space 2 - Mars Penetrator
Mars Global Surveyor
Mars Surveyor '98
Stardust - Comet Sample Return
Europa Orbiter - Jupiter Lunar System Explorer
Mars Surveyor 2001
Mars "03 Lander and Rover

Paul.J.Timmerman@jpl.nasa.gov
ELECTROCHEMICAL SYSTEMS GROUP

JPL Flight Program Summary (cont'd)

Earth Sciences

ACRIMSAT - Active Cavity Radiometer Irradiance Monitor
TOPEX/Poseidon - Ocean Topography Experiment
Jason-1 - Ocean Topography Experiment Follow-On
QuikScat /Seawinds - Ocean Winds Tracking

Astrophysics

Genesis - Solar Dust Return

Paul.J.Timmerman@jpl.nasa.gov
ELECTROCHEMICAL SYSTEMS GROUP

Deep Space 1

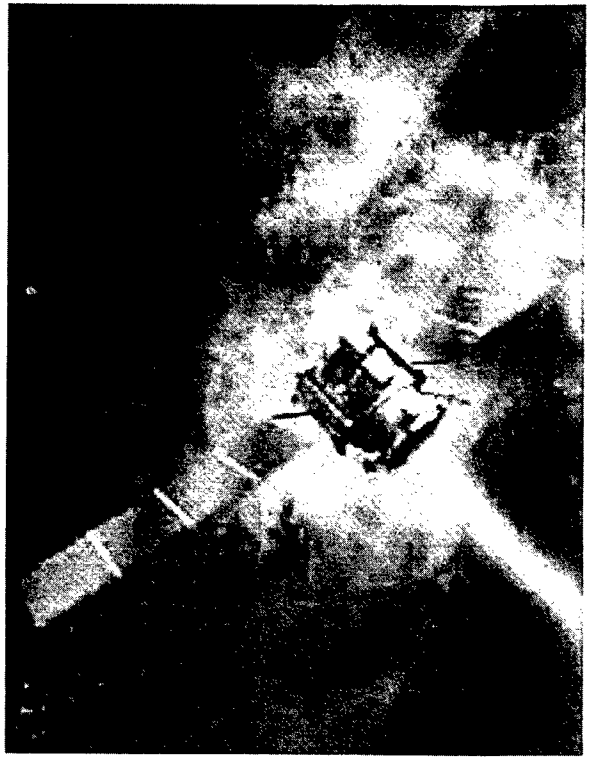

Mission:
Its first destination was the near-Earth steroid Braille. Deep Space 1 flew by this asteroid on July 28, 1999. The New Millennium Program is conducting to demonstrate new technologies in the environment of space.

Launch:
October 24, 1998 from Cape Canaveral, Florida.

Completion:
Deep Space 1 began thrusting toward Comet Wilson-Harrington less than 36 hours after encountering Braille.

Batteries: CPV NiH2, 12AH, 11-Cell, Dual String

Paul.J.Timmerman@jpl.nasa.gov
ELECTROCHEMICAL SYSTEMS GROUP

NASA BATTERY WORKSHOP - 1999

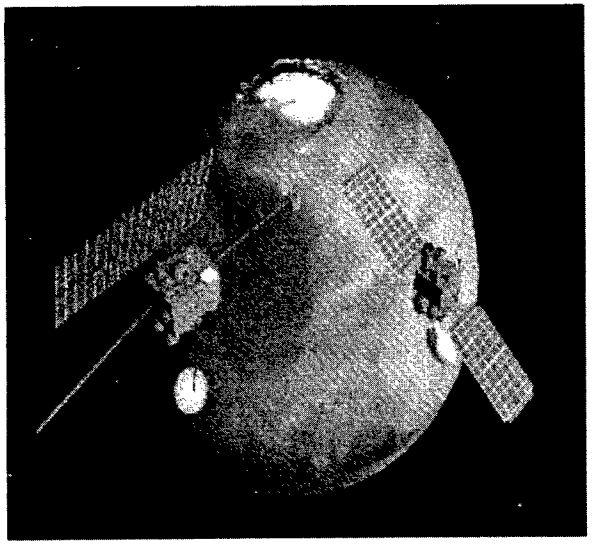

MARS GLOBAL SURVEYOR

Launched 6 Nov. 1996

Regulated Direct Energy Transfer System

- 4 Solar Array Panels (2 GaAs, 2 Si) Capable of Generating 667 W @ Aphelion
- 2 - 20 Amp-hr Nickel Hydrogen (NiH2) Batteries
- 28 Vdc +/-2% Regulated Bus

BATTERY

- 2 BATTERIES / 8 NiH_2 CP V'S PER BATTERY
- VOLTAGE MONITORED AT BATTERY AND HALF BATTERY LEVEL
- 2 STRAIN GAUGES AND 2 TEMPERATURE SENSORS PER BATTERY
- CHARGE CONTROL: V/T WITH PRESSURE AND AHR INTEGRATION

REGIME

- 11 MONTH CRUISE (THREE 40% DOD CYCLES)
- MODIFIED AEROBRAKING (TO MAINTAIN S/A INTEGRITY)
- ~8500 MAPPING CYCLES (29% DOD) AND ~14,000 RELAY CYCLES (24% DOD)

JPL

Paul.J.Timmerman@jpl.nasa.gov

ELECTROCHEMICAL SYSTEMS GROUP

NASA BATTERY WORKSHOP - 1999

MGS EONV TREND

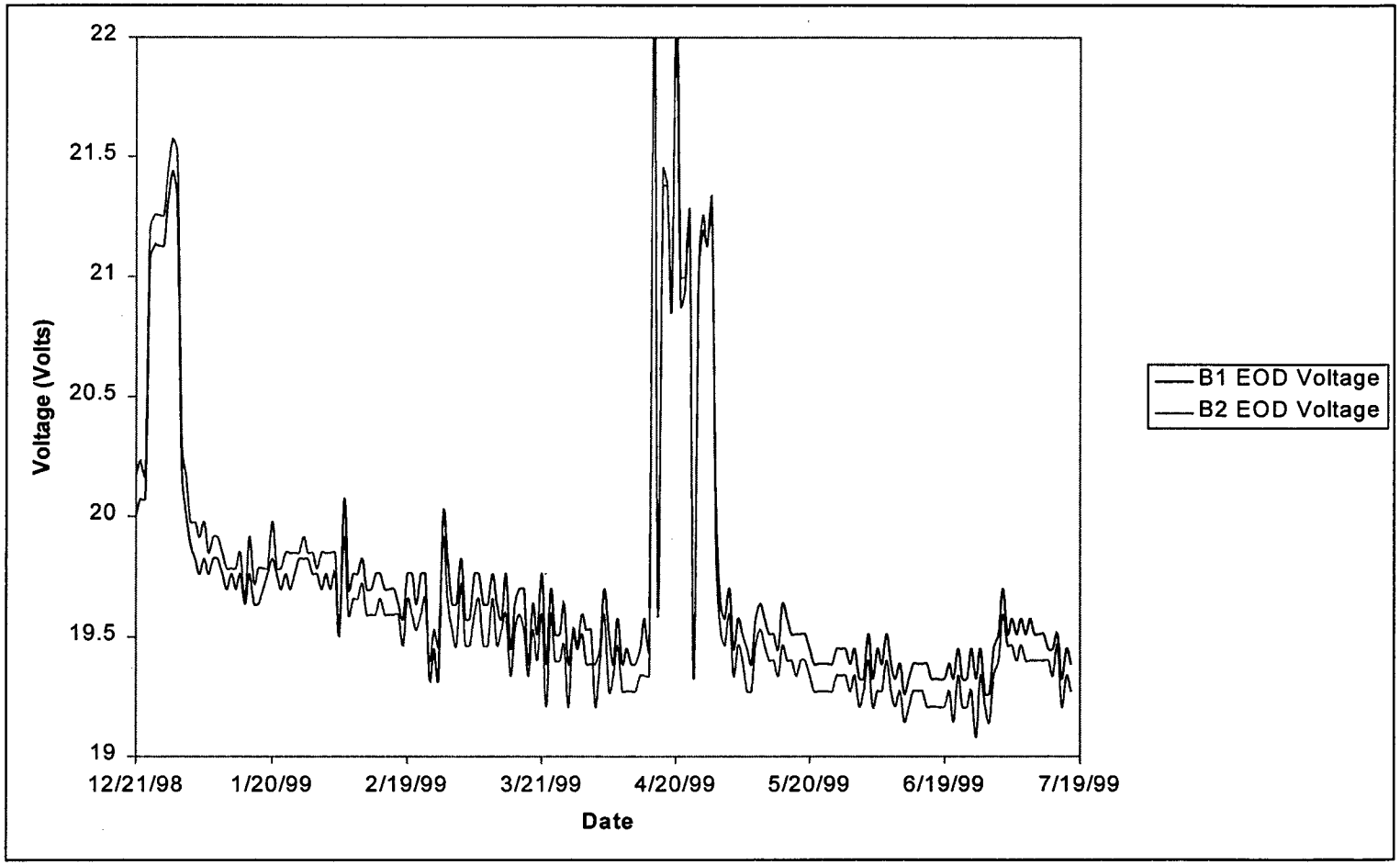

JPL
Paul.J.Timmerman@jpl.nasa.gov
ELECTROCHEMICAL SYSTEMS GROUP

NASA BATTERY WORKSHOP - 1999

MARS SURVEYOR '98

Mars Climate Orbiter
Launch: Dec 10, 199
Mars Orbit: Sep 23, 1999

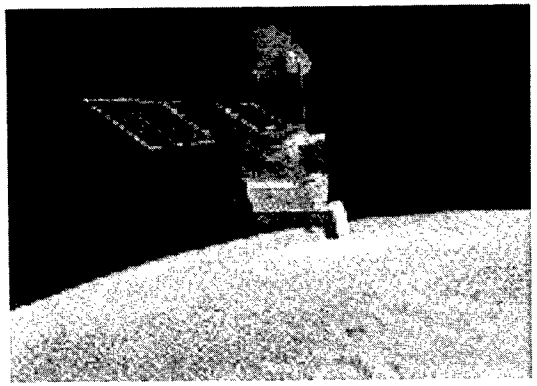

Mars Polar Lander
Launch: Jan 3, 1999
Mars Landing: Dec 3, 1999

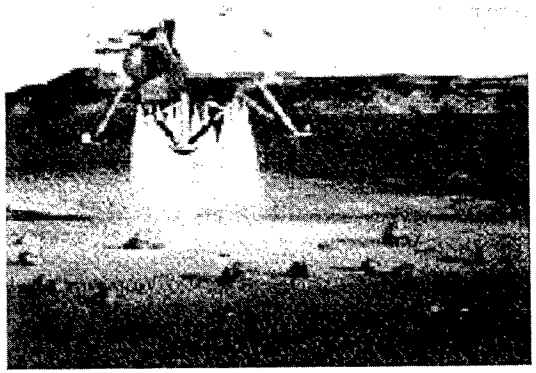

ORBITER BATTERY REQUIREMENTS 13,500 CYCLES @ 50% DOD

BOTH ORBITER AND LANDER WILL USE 2.5" 2-CELL CPV NiH_2 BATTERIES

- **16 Amp-Hour capacity (RNHC-16-1, Lot 5)**
- **11 CPVs for the orbiter and 11 CPVs and one IPV for the lander**
- **Rabbit Ear, Teflon coated wall, 31% KOH**

LANDER WILL CARRY TWO PROBES FOR THE DS-2 MISSION

JPL

Paul.J.Timmerman@jpl.nasa.gov
ELECTROCHEMICAL SYSTEMS GROUP

NASA BATTERY WORKSHOP - 1999

MARS MICROPROBE DS-2

Mission:
Characterize Martian Sub-surface soil
Aft body plus forebody ~2Kg
Demonstrate Key Technologies for future missions
(low temp performance, flex cabling, Telecom-on-a-chip)

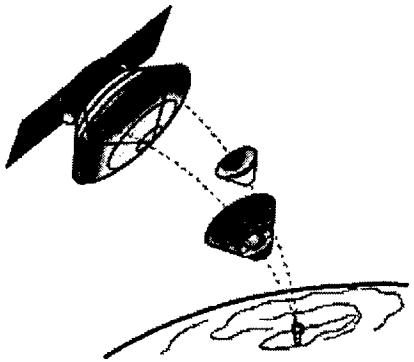

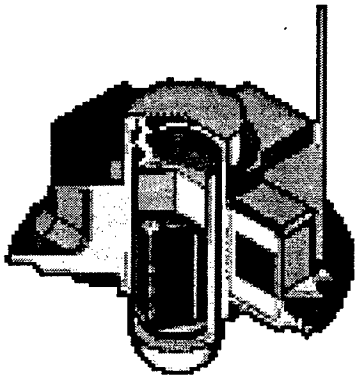

Batteries:
Lithium-Thionyl Chloride
- 80°C Environment
80,000 g shock,
Voltage 6-14 V,
550 mAhr capacity @ -80°
Yardney Technical Products

JPL

Paul.J.Timmerman@jpl.nasa.gov
ELECTROCHEMICAL SYSTEMS GROUP

NASA BATTERY WORKSHOP - 1999

STARDUST

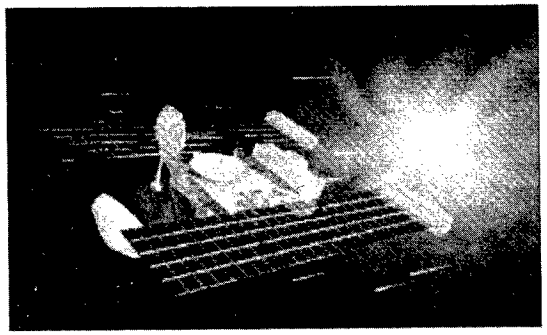

Sample Return Mission -- The STARDUST mission will fly within approximately 100 kilometers (62 miles) of the comet Wild-2 in early 2004 and collect cometary dust and volatiles. The comet samples are made up of ancient pre-solar interstellar grains and nebular condensates that were incorporated into comets at the birth of the solar system. During cruise, STARDUST will collect contemporary particles that recently came to our solar system from the interstellar medium. This interstellar dust was first discovered by Ulysses in 1993 and later confirmed by the Galileo mission. STARDUST will return to the Earth in January of 2006 and drop off the samples using a streamlined, low-cost reentry capsule.

BATTERY REGIME

- LOW CYCLE LIFE (~200 CYCLES @<71% DOD)
- 7 YEAR CRUISE + 1 YEAR PRELAUNCH

BATTERY DESIGN

- 2.5" 2-CELL CPV NiH_2 BATTERIES
- 16 AMP-HOUR CAPACITY(RNHC16-1 Lot 6)
- CELL DESIGN SIMILAR TO MSP '98

SAMPLE RETURN CAPSULE BATTERY

- LITHIUM/SULFUR DIOXIDE
- SAFT AMERICA

Paul.J.Timmerman@jpl.nasa.gov
ELECTROCHEMICAL SYSTEMS GROUP

JPL

NASA BATTERY WORKSHOP - 1999

Europa Orbiter

Europa Orbiter

Missions:
Explore the Frozen Oceans on Moon of Jupiter and look for signs of Life

Batteries: Cold and Wet

Solar Probe

Mission:This first exploration mission to the Sun's Corona seeks a new understanding of a star by flying through its corona.

Batteries: Hot and Dry

JPL
Paul.J.Timmerman@jpl.nasa.gov
ELECTROCHEMICAL SYSTEMS GROUP

Mars Surveyor 2001

This mission will allow scientists to study the ancient climate and geologic history of Mars,investigate the role water may have played on Mars in the past and search for evidence of ancient life.

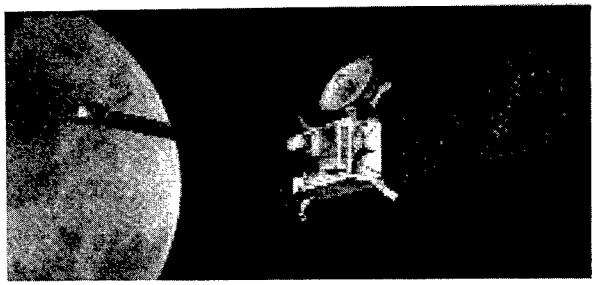

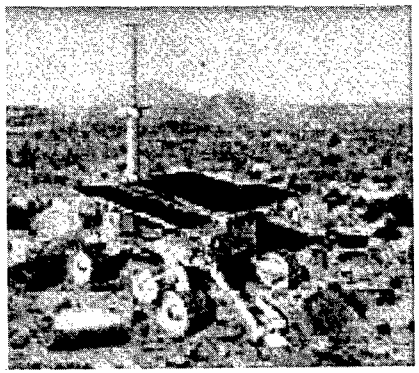

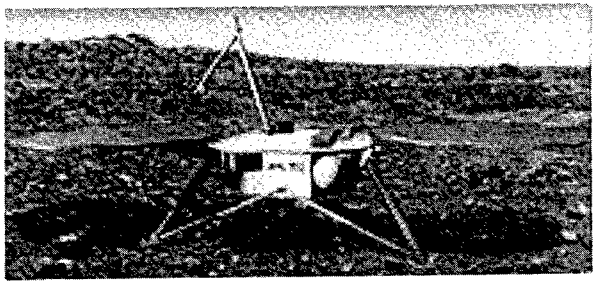

The Mars Surveyor 2001Orbiter

Mission:

Orbiter launches on March 7, 2001.

It will arrive at Mars on Dec. 10, 2001.

Battery:

NiH2 2.5" CPV RNHC16-1 or 16-9

Mars Surveyor 2001 Rover / Lander

Mission:

Launch on April 3, 2001.

Land on Mars on Jan. 27, 2002.

Batteries:

Lander: Li-Ion batteries, 7AH size

Rover: Same Li-SO_4 D-Cells as used in "98

JPL

Paul.J.Timmerman@jpl.nasa.gov

ELECTROCHEMICAL SYSTEMS GROUP

ACRIMSAT - Active Cavity Radiometer Irradiance Monitor:

Mission: Study of the Solar Activity

System Contractor: Hughes (in STV)

Launch: 2000

Completion: TBD

Batteries: Ni-H_2 ?

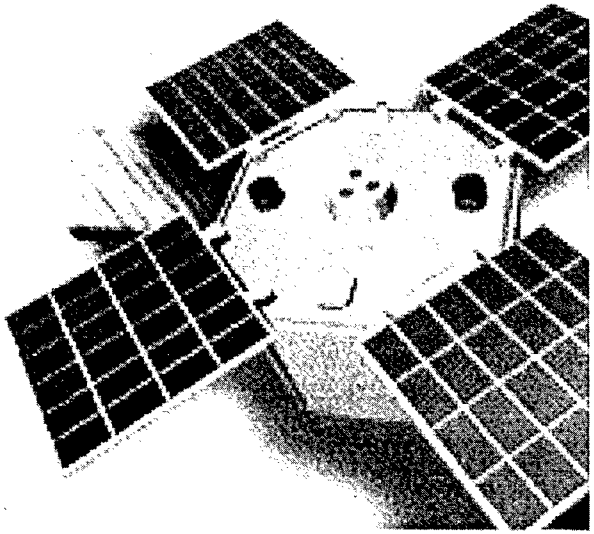

Paul.J.Timmerman@jpl.nasa.gov
ELECTROCHEMICAL SYSTEMS GROUP

NASA BATTERY WORKSHOP - 1999

TOPEX

TOPEX/POSEIDON

PRIME CONTRACTOR - FAIRCHILD
MODULAR POWER SUBSYSTEM / McDac
NASA STANDARD BATTERY (3 x 22 CELL)
50 Amp-Hr CELLS / GATES AEROSPACE
PELLON 2505 SEPARATOR / Eagle-Picher
NONPASSIVATED POS / TEFLONATED NEG

LAUNCH AUGUST 10, 1992

BATTERY OPERATIONAL STRATEGY

- **LIMIT PEAK CHARGE TO LESS THAN 24 AMPS**
- **LIMIT RECHARGE RATIO (C/D) TO 105 (+/-3%)**
- **OPERATE AT LOWEST PRACTICAL (V/T 3 FULL SUN, V/T 4 ECLIPSES)**
- **AVOID HIGH CHARGE CURRENTS DURING FULL SUN PERIODS**
- **CURRENT STATUS - OVER 85 MONTHS SUCCESSFUL OPERATION**

JPL

Paul.J.Timmerman@jpl.nasa.gov
ELECTROCHEMICAL SYSTEMS GROUP

NASA BATTERY WORKSHOP - 1999

TOPEX END OF NIGHT BATTERY VOLTAGE PREDICTION

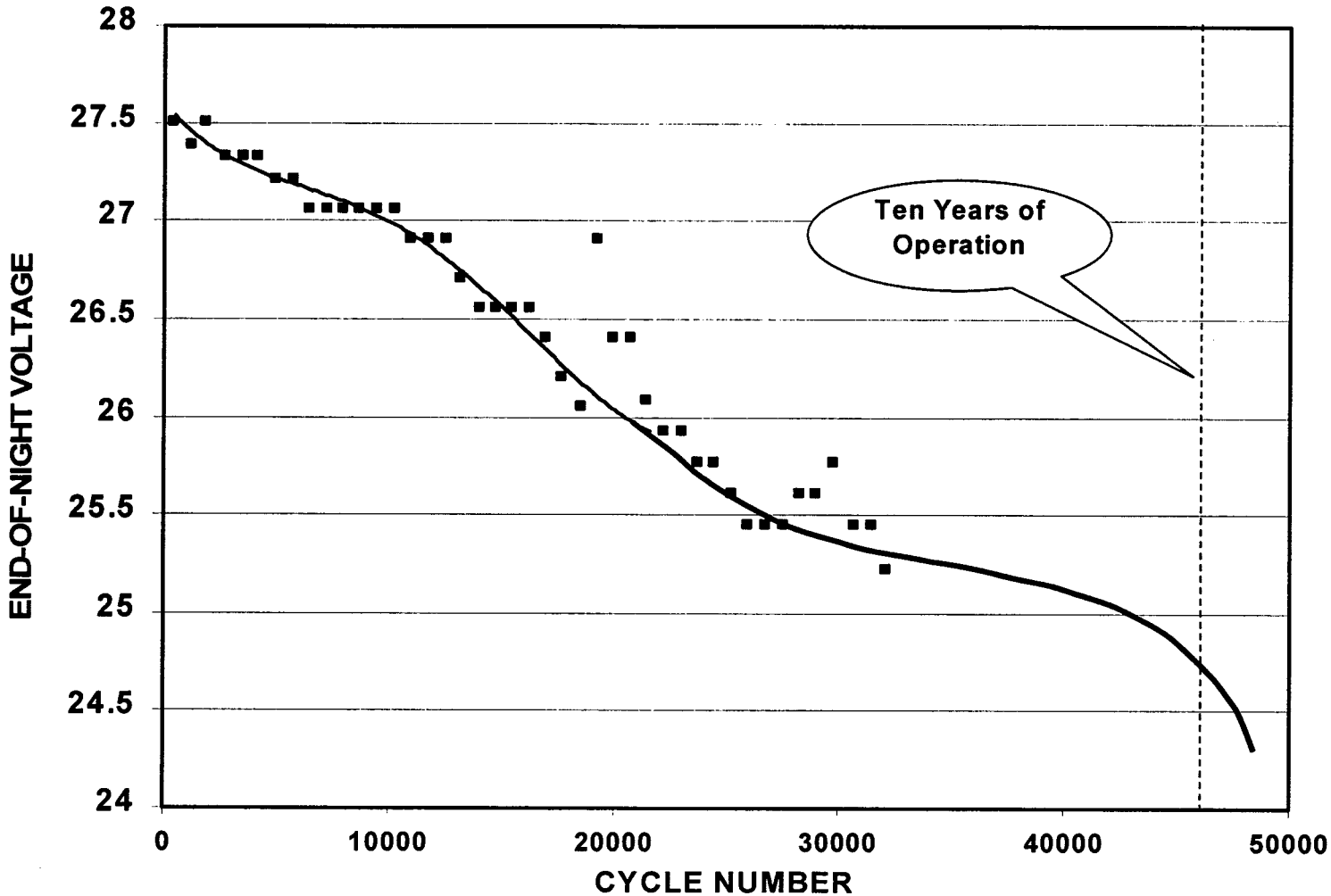

Paul.J.Timmerman@jpl.nasa.gov
ELECTROCHEMICAL SYSTEMS GROUP

Jason-1

Mission: Follow-up Mission to TOPEX

Spacecraft Contract: ESA/France/AS

Launch: 2000

Completion: TBD

Batteries: Single String Ni-H_2 IPV / SAFT

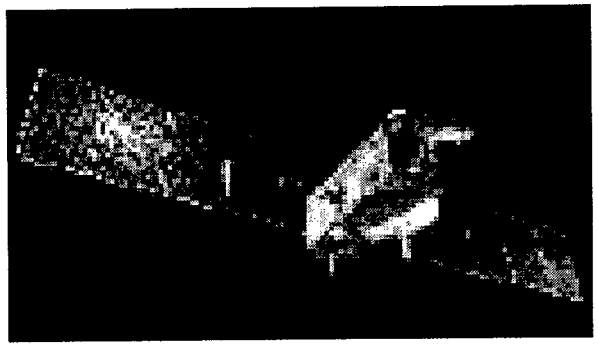

Beyond 2000:
Jason-1

Paul.J.Timmerman@jpl.nasa.gov
ELECTROCHEMICAL SYSTEMS GROUP

QuikScat /Seawinds

Mission: Microwave radiometery - measuring wind speed and direction over Earth's oceans.

System Contractor: Ball Aerospace

Launch: June 19, 1999

Completion: TBD

Batteries: E.P. CPV Ni-H_2

Paul.J.Timmerman@jpl.nasa.gov
ELECTROCHEMICAL SYSTEMS GROUP

Genesis

Mission:

Return solar matter for compositional analysis in terrestrial laboratories. Ultra pure materials will be exposed to the solar wind for two years.

System:

This system is to use the New X2000 power subsystem under development at JPL.

Batteries:

RNH16-9, 11 Cell, CPV Ni-H_2

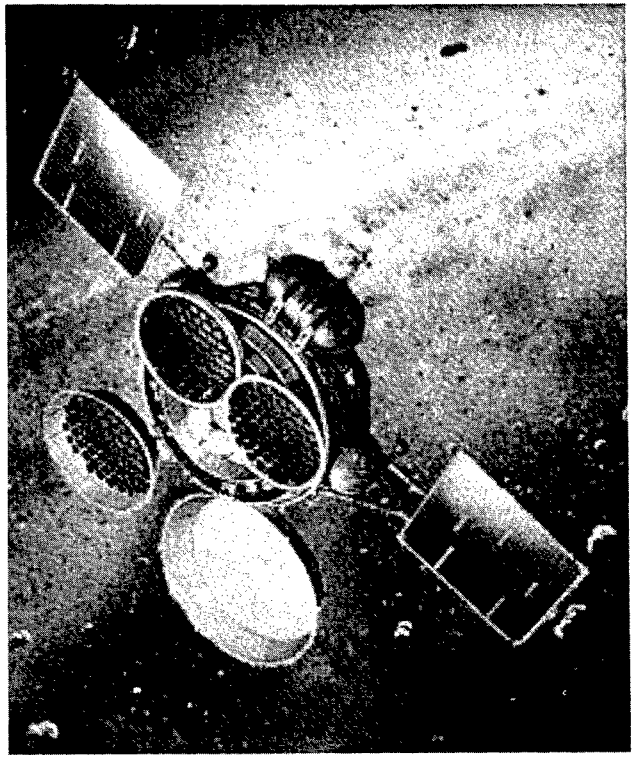

Paul.J.Timmerman@jpl.nasa.gov
ELECTROCHEMICAL SYSTEMS GROUP

NASA BATTERY WORKSHOP - 1999

GRACE (Gravity Recovery and Climate Experiment) Produce a new model of the Earth's gravity field with unprecedented accuracy every 12 to 15 days for five years. Launch 2001,

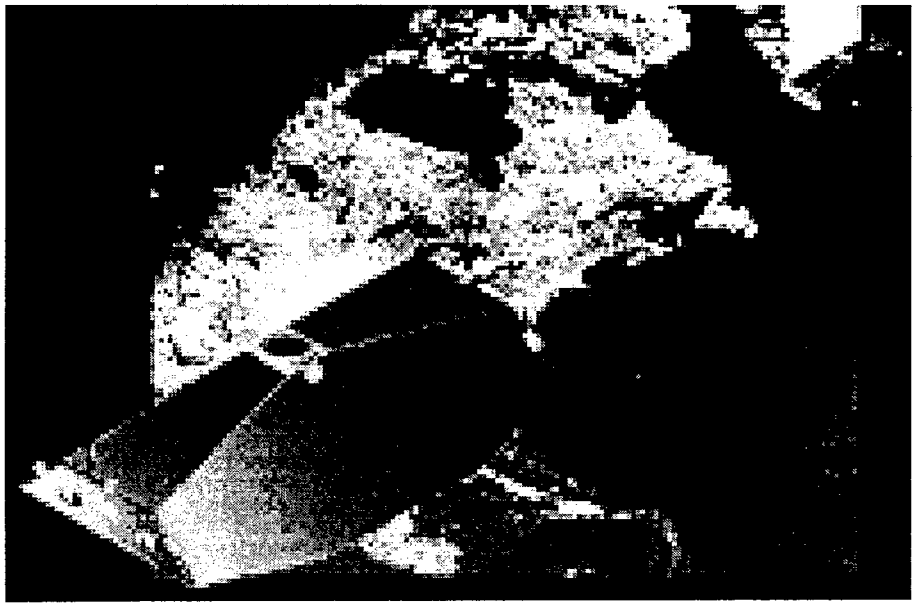

System Contract: German

Battery: CPV NiH2

JPL

Paul.J.Timmerman@jpl.nasa.gov
ELECTROCHEMICAL SYSTEMS GROUP

CELL TESTING

Ni-H_2

2.5" CPV Characterization - On Going

3.5" CPV Characterization - On Going

MGS Simulation - Over 2300 Cycles

Ni-Cd

Topex Simulation - 21Occultations on Zero Degree Pack

Paul.J.Timmerman@jpl.nasa.gov
ELECTROCHEMICAL SYSTEMS GROUP

CPV EVALUATION

TECHNOLOGY STATUS

NUMEROUS BATTERIES FLYING OR BEING BUILT

PREVIOUS MECHANICAL PROBLEMS HAVE BEEN ELIMINATED

MISSIONS USING CPV

NEW MILLENIUM DS-1, MARS '98 (ORBITER AND LANDER), MARS 2001 ORBITER

STARDUST, GENESIS, GRACE,SIRTF, GOES

PROGRAM

PROCURE REPRESENTATIVE SAMPLES FROM FLIGHT LOTS

DEVELOP A PERFORMANCE DATABASE - CHARACTERIZATION TESTS

PERFORM MISSION SIMULATION TESTING

PROVIDE SUPPORT TO PROGRAMS THROUGH TELCONS AND WORKSHOP

FOLLOW DEVELOPMENT OF NEW DESIGNS

JPL

Paul.J.Timmerman@jpl.nasa.gov

ELECTROCHEMICAL SYSTEMS GROUP

2.5'' CPV DESIGNS

SIZES CURRENTLY MANUFACTURED BY E.P.

RNHC 4-1	(12 UNITS)
RNHC 6-1	(77 UNITS)
RNHC 10-1	(335 UNITS)
RNHC 12-3	(81 UNITS)
RNHC 16-1	(147 UNITS)

Paul.J.Timmerman@jpl.nasa.gov
ELECTROCHEMICAL SYSTEMS GROUP

2.5" CPV EVALUATION

BACKGROUND

HISTORY OF FAILURES DURING VIBRATION AND REDESIGNS

STATUS

OBTAINED THREE (RNHC 10-1) CPV UNITS FROM EAGLE-PICHER

CHARACTERIZATION TESTS IN PROGRESS

INITIAL CAPACITY 11.3 AHR

PLANS

CONTINUE ELECTRICAL CHARACTERIZATION

COMPILE RESULTS AND ISSUE REPORT

JPL

Paul.J.Timmerman@jpl.nasa.gov

ELECTROCHEMICAL SYSTEMS GROUP

NASA BATTERY WORKSHOP - 1999

20 AH CPV Prorated Battery Discharge for Four Rates
Following 10 degree C/10 16 hour charge

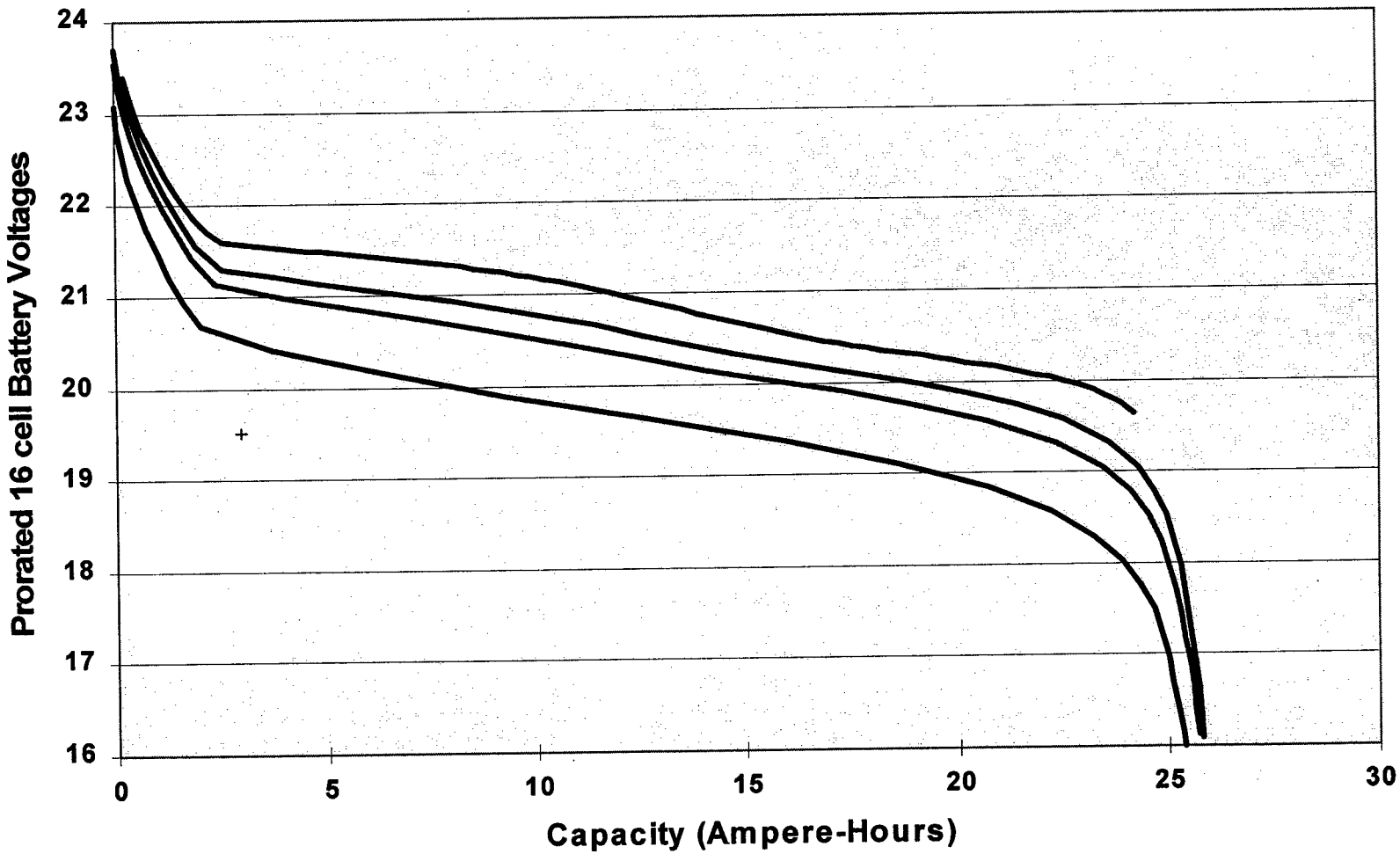

Paul.J.Timmerman@jpl.nasa.gov
ELECTROCHEMICAL SYSTEMS GROUP

3.5" CPV EVALUATION

3 Cells in MGS Characterization Tests

Insert Information Here

3 Cells in MGS Simulation Test

Provides Mission Leading Information

Shows Characteristic Pressure Decline

Unusual Charge Control Regime Uses VT and Switch to Trickle

Paul.J.Timmerman@jpl.nasa.gov
ELECTROCHEMICAL SYSTEMS GROUP

NASA BATTERY WORKSHOP - 1999

MGS Simulation Prorated Battery Voltages

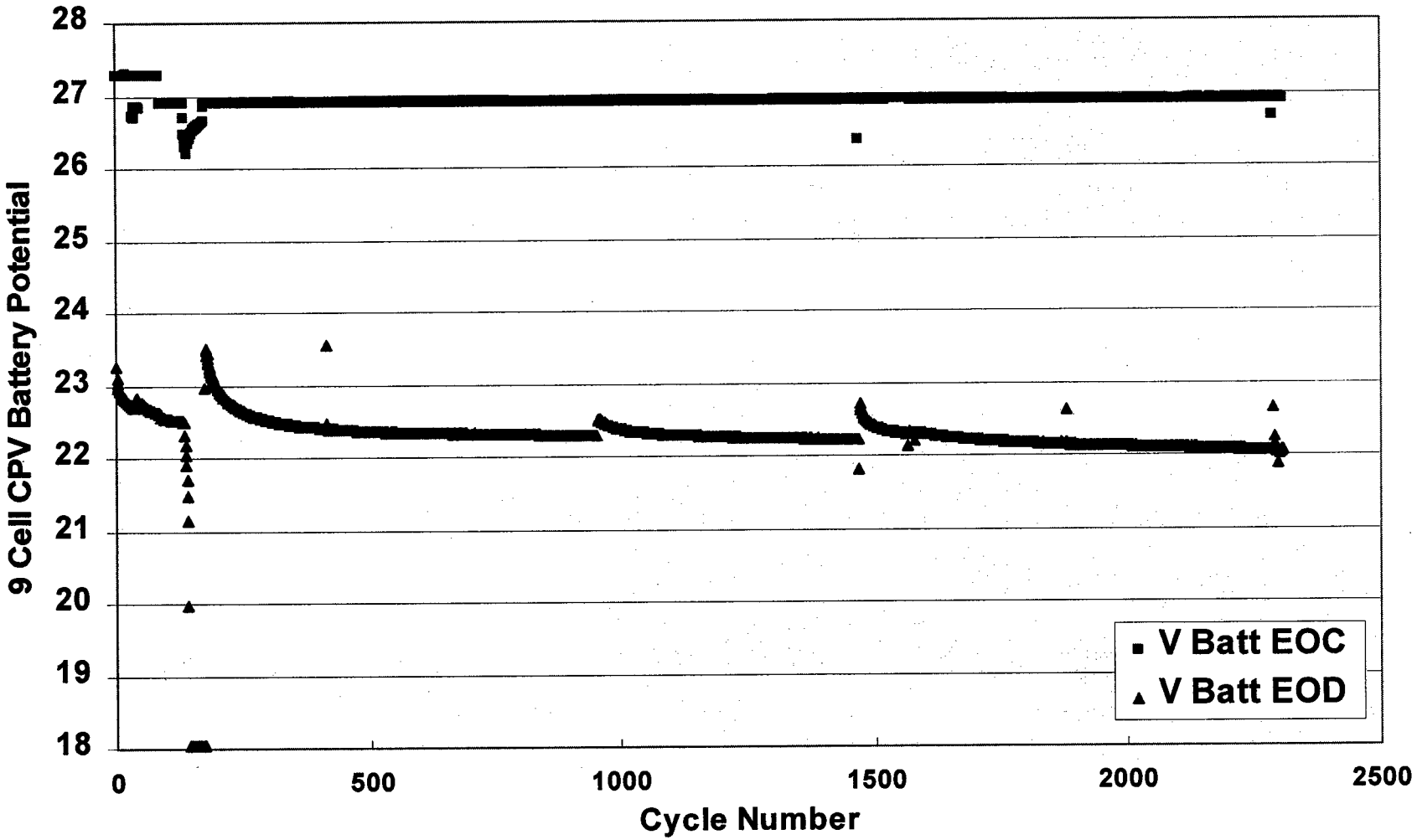

Paul.J.Timmerman@jpl.nasa.gov
ELECTROCHEMICAL SYSTEMS GROUP

Ni-H2 Modeling

GOALS

DEVELOP A NIH_2 BATTERY PERFORMANCE MODEL

MODEL FLIGHT TYPE CELLS WITH INTERNAL DETAILS

COMBINED ELECTROCHEMCIAL / ELECTRICAL / THERMAL MODEL

APPROACH

COMPUTATION FLUID DYNAMICS (CFD)

EXCELLENT INDUSTRY SUPPORT (S/W TOOLS)

EASIER TO IMPLIMENT EQUATION THAN PREVIOUS MODELS

QUICK SOLUTIONS PROVIDED

PROVIDES FIRST CONVECTION SOLUTION

EASY TO CHANGED GRANULARITYOF MODEL - DETAILS

JPL

Paul.J.Timmerman@jpl.nasa.gov
ELECTROCHEMICAL SYSTEMS GROUP

Li-Ion ASSESSMENT

OBJECTIVES

GENERATE PERFORMANCE CHARACTERIZATION DATA

IDENTIFY POTENTIAL ISSUES AND WORK TOWARD RESOLUTION

DETERMINE FLIGHT READYNESS OF TECHNOLOGY

APPROACH

PARTICIPATE IN THE JOINT AIR FORCE / NASA PROGRAM

CHARACTERIZE CELL PERFORMANCE FROM MULTIPLE VENDORS

DOCUMENT MANUFACTURING PROCEDURES

DEVELOP METHODS/FACILITIES FOR EVAULATION

DEVELOP MODELS FOR BATTERY PERFORMANCE PREDICTIONS

COMMUNICATE FLIGHT INFORMATION TO BATTERY COMMUNITY

JPL

Paul.J.Timmerman@jpl.nasa.gov

ELECTROCHEMICAL SYSTEMS GROUP

Li-Ion ASSESSMENT

STATUS

BASELINE CHEMISTRY SELECTED WITH LOW TEMP ELECTROLYTE
EVALUATION OF FOUR VENDORS FOR MARS "01 LANDER COMPLETED
YARDNEY SELECTED FOR "01 LANDER BATTERY DEVELOPMENT
EVALUATION OF TWO VENDORS FOR MARS "03 ROVER IN PROGRESS
EXTENDED LIFE CYCLE TESTING AND STORAGE TESTING IN PROGRESS
IMPROVED COMPONENTS RESEARCH ONGOING

PLANS

CONTINUE THE EVALUATION OF CELLS FROM 5AH to 25 AH INCLUDING:
CONTINUE COLD TEMPERATURE CYCLING
STORAGE / CRUISE TESTING
RATE AND TEMPERATURE EFFECTS / VARIABLE TEMP CYCLING
PULSE TESTING
CHARGE CONTROL DEVELOPMENT
AC IMPEADANCE
FAILURE ANALSYS

JPL
Paul.J.Timmerman@jpl.nasa.gov
ELECTROCHEMICAL SYSTEMS GROUP

TELECONS

NASA Ni-Cd BATTERY OPERATIONS TELECON

FUNCTIONING FOR ~5 YEARS

CONCENTRATION IS ON MPS S/C

TOPEX,GRO,UARS,EUVE

ALSO LOOKS AT NEWER EXPLORERS

GSFC, BERKELY, JPL PARTICIPATION

BENEFITS ALL PARTIES INVOLVED

JPL

Paul.J.Timmerman@jpl.nasa.gov
ELECTROCHEMICAL SYSTEMS GROUP

TELECONS

Ni-H2 BATTERY OPERATIONS TELECON

NEW ACTIVITY IN 1999
DAVE PICKETT CONSULTS ON CALLS
LARGE PARTICIPATION BY NASA AND CONTRACTORS
DETAILED ANALYSIS OF S/C PERFORMANCE
DISCUSSIONS OF GENERAL INTEREST
ONGOING "WORKSHOP ATMOSPHERE"
PARTICIPANTS BRING IN THEIR ISSUES/QUESTIONS

JPL
Paul.J.Timmerman@jpl.nasa.gov
ELECTROCHEMICAL SYSTEMS GROUP

FLIGHT BATTERY STORAGE PROGRAM

GOALS

DEVELOP FLIGHT BATTERY REUSE PROGRAM

BUILD BATTERY STORAGE FACILITY

COLLECT FLIGHT SPARE BATTERIES FROM FPO'S

MAINTAIN SPARES UNDER QC PROGRAM (FHLP)

PROVIDE BATTERIES TO NEW PROGRAMS - FAST!

BRIDGE THE PROGRAM GAP

JPL

Paul.J.Timmerman@jpl.nasa.gov
ELECTROCHEMICAL SYSTEMS GROUP

FLIGHT BATTERY STORAGE PROGRAM

PLAN

SECURE MONEY TO BUY/LEASE FACILITY

CO-OPERATE WITH FLIGHT HA/W LOGISTICS PROG

SOLICIT FPO'S FOR SPARES

MAINTAIN SPARES INVENTORY AND LOGS

ADVERTIZE AVAILABILITY TO NEW PROGRAMS

EXTRACT COMPENSATION FROM FPO TO FUND

JPL

Paul.J.Timmerman@jpl.nasa.gov
ELECTROCHEMICAL SYSTEMS GROUP

BATTERY LABORATORY

STATUS

THREE MACCOR CYCLERS OPERATING

OVER ONE HUNDRED CHANNELS AVAILABLE

LAB OPERATING AT NEAR CAPACITY

BATTLAB SERVER OPERATING

REMOTE CONNECTIONS TO SERVER IN PLACE

ROOM TEMP FACILITY UPGRADE COMPLETED

JPL

Paul.J.Timmerman@jpl.nasa.gov
ELECTROCHEMICAL SYSTEMS GROUP

In-orbit Earth Radiation Budget Satellite (ERBS) Battery Switch

Anisa Ahmad
Marlon Enciso
Gopalakrishna Rao
Code 563, Power Systems Branch
Electrical Systems Center
Applied Engineering and Technology Directorate
NASA/Goddard Space Flight Center
Greenbelt, Maryland 20771

ERBS Spacecraft

- Launched October 5, 1984
  - 610 km circular orbit, 57 degrees inclination
  - 3 instruments:
    - Earth Radiation Budget Experiment (ERBE) Scanner, ERBE Non-Scanner, Stratospheric Aerosol Gas Experiment (SAGE) II
  - ERBE Scanner failed in 1990
  - ERBE Non-Scanner & SAGE II collecting 99 % data
- SAGE II - provides long term global trending of ozone, aerosol, water vapor and nitrogen dioxide
- Spacecraft is needed to be in operation until launch of SAGE III + ~ 6 months

ERBS Power System & Battery History

- Peak Power Tracker Standard Power Regulator Unit (SPRU)
- Launched with Two 22-cell 50 Ah NiCd Batteries (GE/GAB)
- Battery Charging using VT Mode & Constant Current Mode
  - VT 6, avg. C/D = ~1.16, avg. T = 10 C, avg. DOD= 9% (max=14%)
- Half Battery differential voltage (Cell Balance) began to diverge in 9/89 (Bat 1 increased to 200 mV & Bat 2 to over 450 mV by 7/90)
- Battery load sharing divergence
  - VT Level for both batteries reduced from VT 6 to VT 5 in 1/92
  - VT Level for both batteries reduced from VT 5 to VT 4 in 7/92

ERBS Battery Cell Failures

- Aug. 1992, cell short on Battery # 1
  - Cell Balance increased from 90 mV to 1.2 V
  - Temperature Rise greater than 5 degrees C
  - VT reduced from VT 4 to VT 3
- Sept. 1992, 2nd Cell shorted on Battery # 1
  - Cell Balance increased from 1.2 to 2.5 V (Max. possible Cell Balance in telemetry)
  - Temperature Rise greater than 5 degrees C
- October 1992 Battery # 1 taken off-line
- Battery # 2 supporting all loads

ERBS Battery Cell Failures (Continued)

- June 1993, cell short on Battery # 2
  - Cell Balance increased from 50 mV to 1.28 V
  - Temperature Rise greater than 5 degrees C
- July 1993, 2nd Cell shorted on Battery # 2
  - Cell Balance increased from 1.25 to 2.5 V
  - Temperature Rise greater than 5 degrees C
- Battery # 1 & Battery # 2 both have 20 cells
  - Attempts made to bring Battery # 1 back on-line 8/93
  - Unsuccessful due to poor load sharing - Battery # 2 was healthier of two batteries
- Battery # 2 (20 cells) continued to support all loads

ERBS Battery # 1 & # 2 Cell Failures

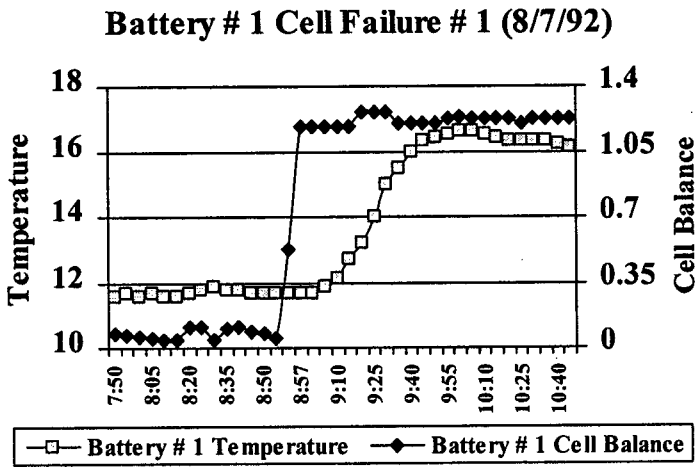

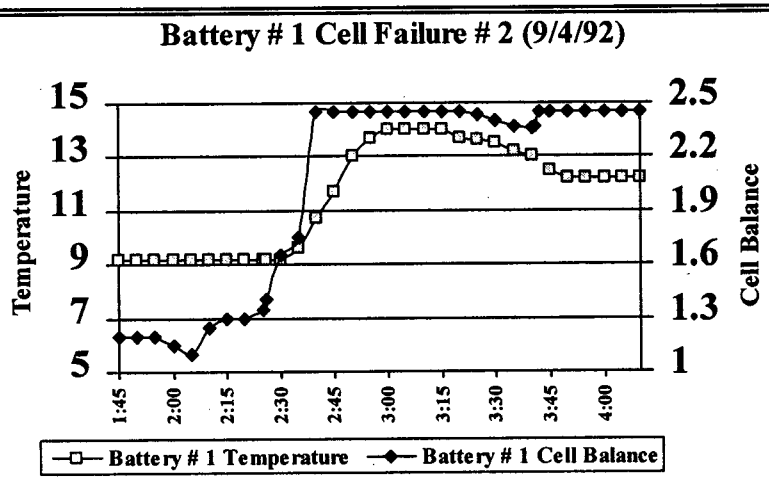

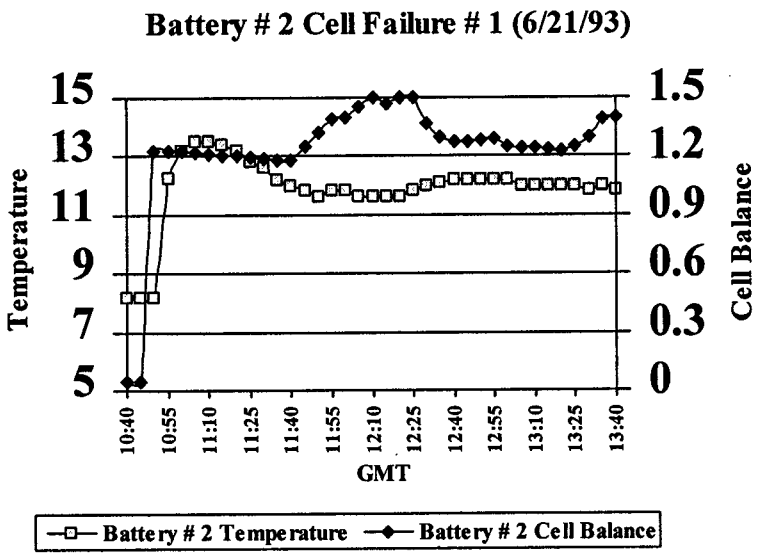

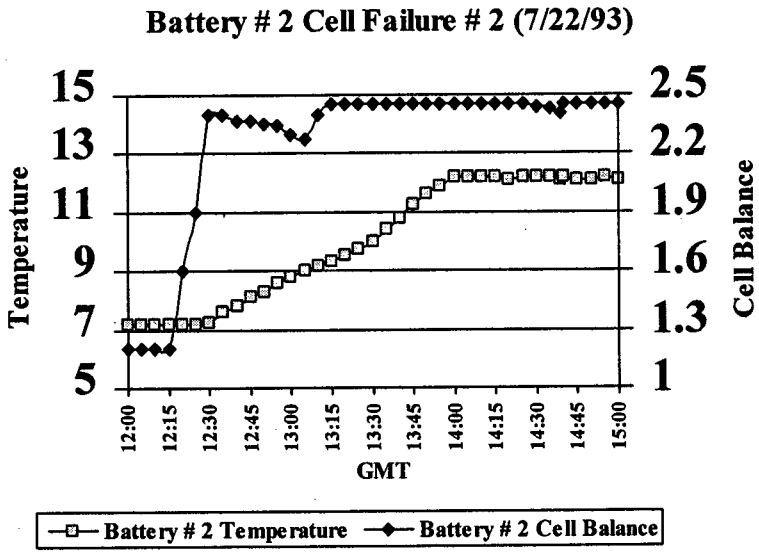

20-Cell ERBS Battery # 2 Operation

- Manual battery charging by uplinked commands switching between three Constant Current Modes (CCM)
  - VT charge mode cannot be used
  - Charged at beginning & end of orbit day at 2.74 Amps
  - Middle of orbit day charged at 11.4 Amps
  - 5 Amp discharge rate used during full sun periods & during less than 7% DOD orbital nights to minimize battery overcharge
  - CCM changed every orbit to maintain C/D of ~1.1& End of Night (EON) cell V > 24 V
  - C/D Ratio lowered to 1.02 by 3/94 to further minimize overcharge
  - Battery Temp: 3 - 5 degrees C, DOD: 7 - 14 %
  - 11.4 A rate varied from 0 to ~ 40 min.
  - Battery discharge period varies from 0 - 55 min due to orbit inclination and fixed solar array

ERBS Spacecraft Failures

- 5 of 6 Gyros failed
- ERBE scanner instrument failed on 2/90
- Command Memory # 1 & # 2 subject to random Bit Flips since launch
- Command Memory # 2 failed on 10/93
- Digital telemetry Unit # 1 failed on 4/98

Battery # 2 Additional Cell Failures

- 6/98 Cell balance began to dip from the maximum telemetry value of 2.5 to 2.0 V at EON
- 7/27/98 ERBS completed 5 years of operation on a single 20-cell battery.
- 10/98 EON V decreased below 24 V.
- 11/98 EON V decreased further by 1 Volt (23.1 V).
  - Only a 0.9 degrees C temperature rise seen over the entire orbit.
  - No Cell Balance change observed
- 12/7/98 EON V reached 21.68 V and a 5 degree temperature rise. Additional Cell failure.

10/98 - 11/98 Battery # 2 Voltage Drop

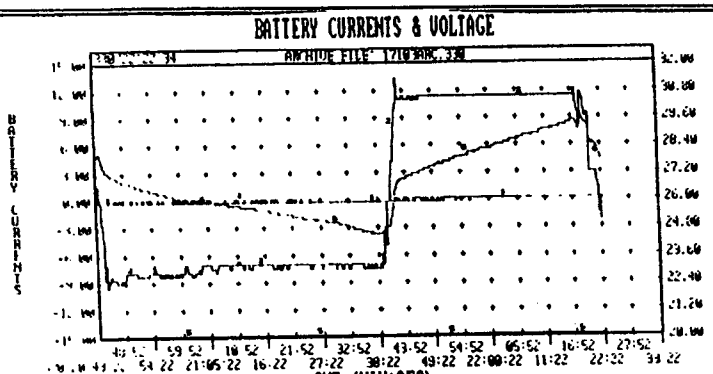

ITEM	MNEMONIC	MAX	MIN	SCALE SIDE
1	FB1HII	0.20	-0.20	LEFT
2	FB2HII	13.40	-5.40	LEFT
5	FB1V	13.40	13.40	RIGHT
7	FB2V	29.75	24.53	RIGHT

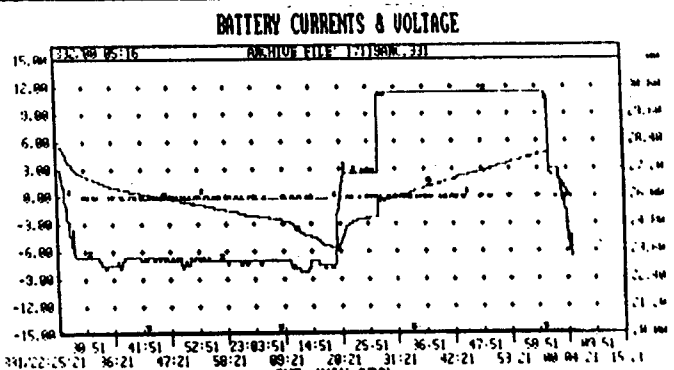

ITEM	MNEMONIC	MAX	MIN	SCALE SIDE
1	FB1HII	0.20	-0.20	LEFT
2	FB2HII	11.40	-0.20	LEFT
5	FB1V	13.40	13.40	RIGHT
7	FB2V	28.24	23.77	RIGHT

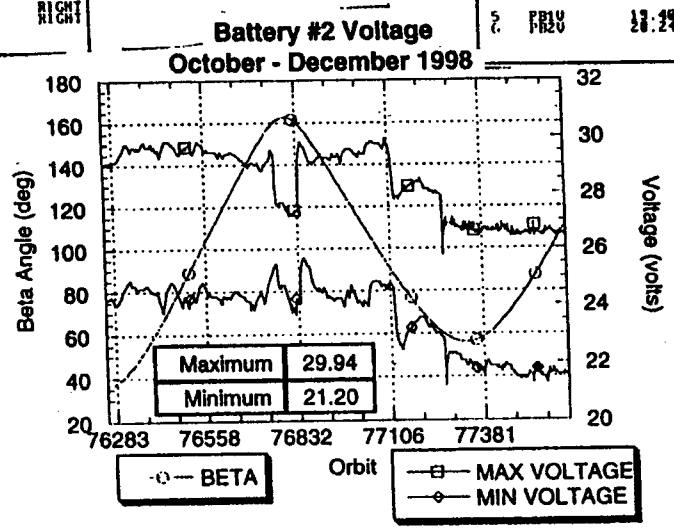

12/98 Battery # 2 Cell Failure

BATTERY TEMP and PRESSURE

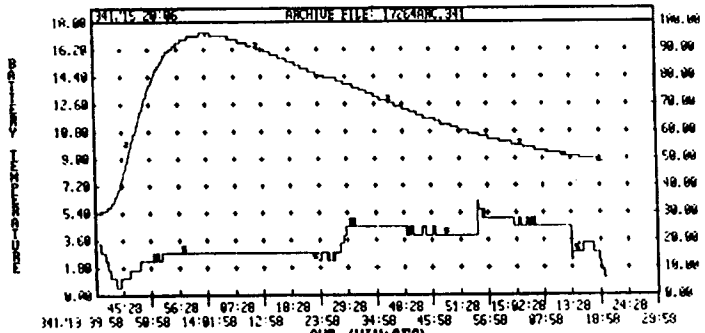

ITEM	MNEMONIC	MAX	MIN	SCALE SIDE
2	PB2TP	17.39	5.42	LEFT
5	PB2P	34.54	3.14	RIGHT

BATTERY CURRENTS & VOLTAGE

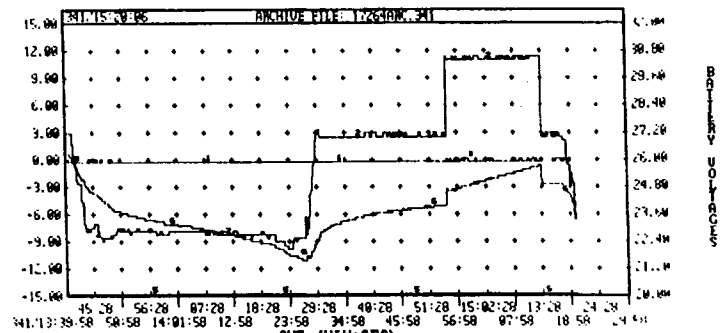

ITEM	MNEMONIC	MAX	MIN	SCALE SIDE
1	PB1NII	9.20	-9.20	LEFT
2	PB2NII	11.40	-9.80	LEFT
5	PB1V	19.40	19.40	RIGHT
6	PB2V	26.33	21.58	RIGHT

BATTERY CELL BALANCE

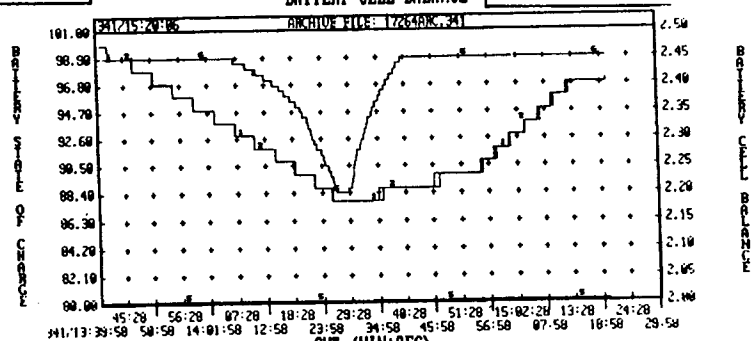

ITEM	MNEMONIC	MAX	MIN	SCALE SIDE
1	PA1SOC	100.00	87.81	LEFT
2	PA2SOC	100.00	87.81	LEFT
5	PB1CB	1.88	1.87	RIGHT
6	PB2CB	2.45	2.20	RIGHT

Battery # 2 Additional Cell Failures (Continued)

- Battery # 2 @ 18 - 19 cells (?)
  - YAW Maneuver accomplished on 12/25/98
- January 15, 1999 Battery # 2 lost another cell and EON V dropped to 20.4 V with a simultaneous temperature rise of ~ 20 degrees C
  - Battery # 2 @ 17 - 18 cells (?)
- Attitude Control System and Transponder are unreliable at V < 20 V
- Battery charging unstable. Battery going to VT charge control mode instead of 5 A discharge mode (default charge mode)
- Battery Voltage reached 19.67 V
- Spacecraft went into a B-dot mode where the spacecraft tumbled twice per orbit.
- Spacecraft attitude system stabilized, battery charging stabilized and battery EON V reached 20.4 V

1/99 Battery # 2 Cell Failure

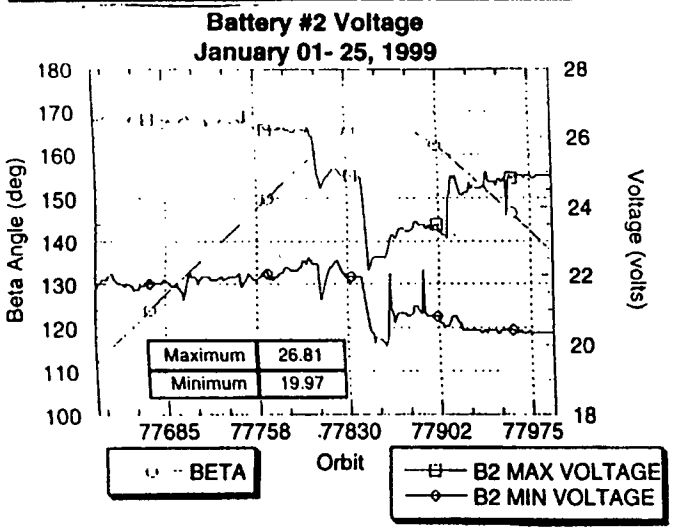

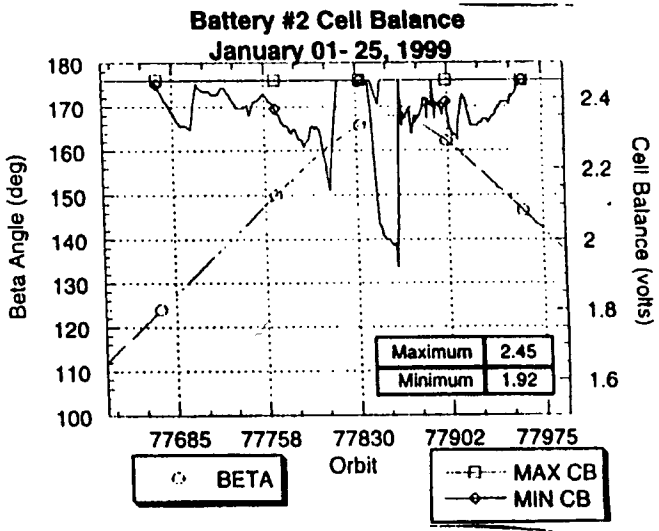

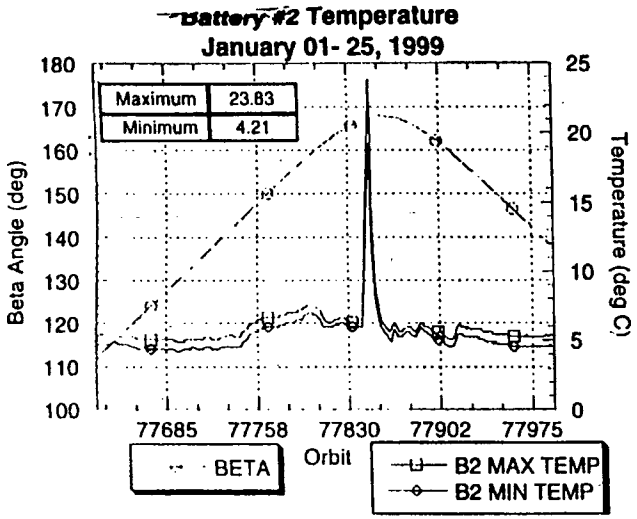

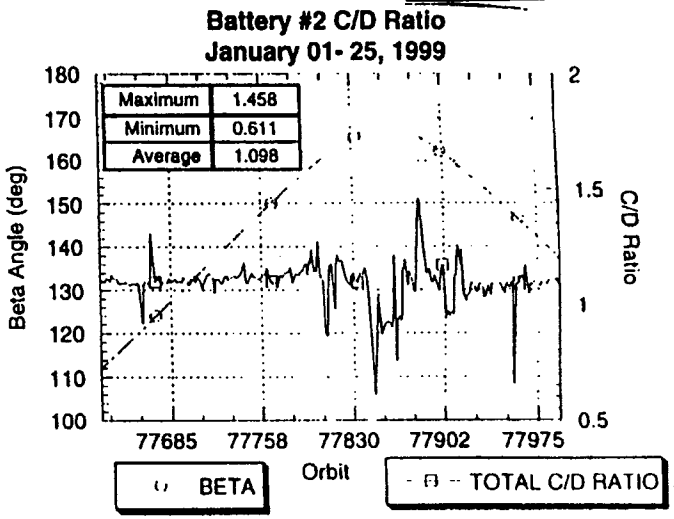

Battery Operations Dilemma

- Predicted Battery # 2 Voltage < 20 V at upcoming (2/3/99) Yaw maneuver
- Battery # 1 has been open circuit for > 5 years. The Voltage via telemetry is at the low rail of 19.4 Volts. Battery # 1 has 20 out of 22 cells (last time it was on-line)
- Risk of bringing Battery # 1 on-line:
  - Battery # 2 being drained to charge Battery # 1 (Voltage going below min. safety V)
  - Relay concern: Being vaporized, or arcing
  - Poor sharing of batteries under parallel configuration (Battery # 1 stuck on-line)

Battery Management Decision

- Bring Battery # 1 on-line on January 26, 1999
- Attempt two-Battery Operation
- Take Battery # 2 off-line if Battery #1 alone could support the spacecraft load

Bringing Battery # 1 On-Line

- Brought Battery # 1 online during the orbital day so voltage doesn't drop below 20 V.
- Goal - Keep Battery # 2 adequately charged while charging up Battery # 1.
  - Orbit # 1 - Battery # 1 relay connected - Voltage immediately rose from 19.4 to 22.44 V and Bat # 1 began charging.
  - Orbit # 2 - Charge Bat # 1 @ 3 A for 5 Min (Bat # 2 off-line)
  - Orbit # 3 - Charge Bat # 1 @ 3 A for 16 min (Bat # 2 off-line) Discharge Bat # 1 for 4 min (Bat # 2 off-line)
  - Orbit # 4- Charge Bat # 1 @ 11 A for 15 min (Bat # 2 off-line) Discharge Bat # 1 for 15 min (Bat # 2 off-line) at beg. of night
  - Continue charging scenario by increasing Battery # 1 charge time and discharge time with Battery # 2 off-line

Stabilization of Battery # 1

- As Battery # 1 got fully charged - Battery # 2 did not discharge during eclipse & Battery # 1 discharged during orbital day to charge Battery # 2
  - Battery # 2 was over charging
- Battery # 2 was disabled 32 hours after bringing Battery # 1 on-line
- Spacecraft Voltage reached: 25.95 - 29.57 V
  - Prior to 1/26/99: 20.35 - 24.72 V
- Battery # 1 Charged at NASA VT 1 (1.5 V/cell @ 5 C) for 3 orbits to ascertain fully charged battery
  - Battery Current & Temperature closely monitored to minimize overcharge

Present Battery Operations and Performance

- Battery charged by a power command load uplinked at least twice per day (default VT mode overridden)
- 3 CCM rates being used to charge battery (Same as for Battery # 2, before being taken off-line)
- Battery # 1 C/D Ratio being maintained at ~ 1.05
- Battery # 1 Voltage: 23.58 - 30.8 V
- Cell Balance:
  - 2.45 for first month after Battery # 1 brought online
  - 0.89 - 2.45 V from 2/99 - 5/99
  - Since 5/99, 2.13 - 2.45 V
- Temperature: 1.97 - 6.84 degrees C
  - Higher temperature at Beta 0 (Full Sun)

Present Battery Operations

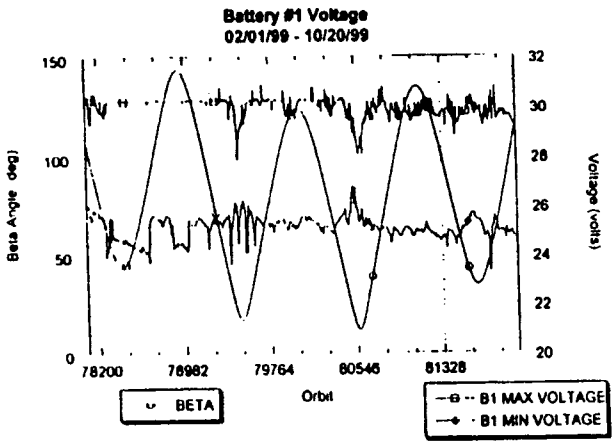

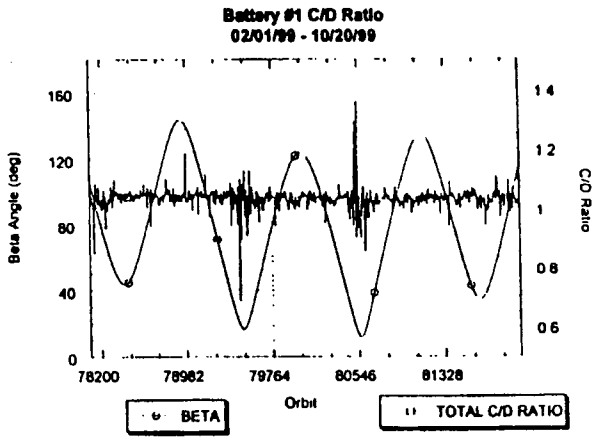

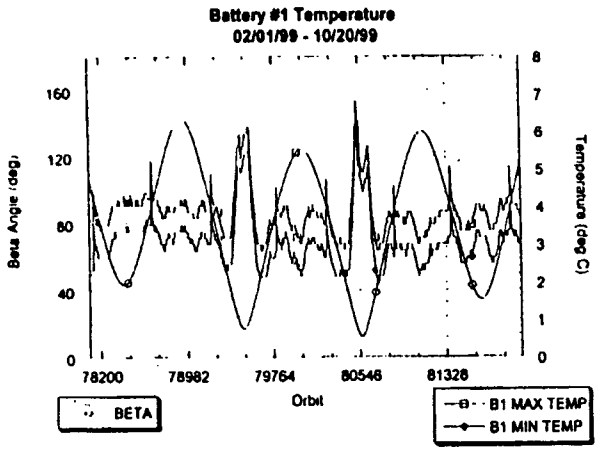

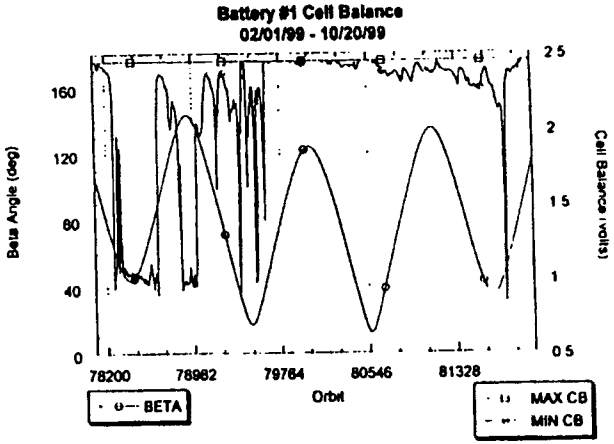

Summary

- Battery # 1 adequately supporting load
- Cell Balance divergence needs to be monitored
- Power System closely monitored
- New Power Command Loads must be uplinked every 22 hrs
  - Concern in case of ground power failure or loose commanding with spacecraft (Leonids Meteor storm, Y2K)
- SAGE III scheduled for launch in April 2000
- > 15 YEARS SUCCESSFUL LEO OPERATION SUPPORTING SPACECRAFT LOAD
- FIRST EVER KNOWN ON-BOARD "STORED" BATTERY (even with two failed cells) BROUGHT INTO OPERATION

Acknowledgments

- NASA HQ
- NASA/GSFC Management
  - J. Dezio, E. Macie, R. Sodanao et. al.
- Facility Operations Team
  - L. Nihal and Company
- Ball Aerospace
  - Z. Emsley and P. Lyman

Super Capacitor Development At NASA MSFC

David K. Hall / ED11

Electrical Power Subsystems Team

NASA Marshall Space Flight Center

Super Capacitor Development

- **Concept**
- **Proof of Concept Testing**
- **Areas of Focus**
  - Classifications of Super Capacitors
  - Chemical Double Layer Capacitors
  - Psuedocapacitors (Electrochemical)
- **An Added Advantage**

Concept

- Problem: Need for a lighter weight energy source that can deliver high power pulses while maintaining minimum voltage sag. Applications include electromechanical actuators (EMA's), and electric vehicles.
- Hybrid Power Source Rationale: Combine the energy density of a conventional power source with the power density of a capacitor bank to yield a high-power, high energy power source capable of pulse power applications that weighs less than a conventional source sized for the same application.

Proof of Concept Testing

- Tests performed using a 25 hp EMA in a hydraulic rate vs. load bench loaded to 15 klb. with a 270 V Lead acid battery bank and a 270 V, 5 farad capacitor bank (Panasonic) made by AU-SPI.
- Results showed voltage in Batt. Only tests sagged 40%, while Batt/Cap. configuration's voltaged sagged only 13%.

Test Set-up

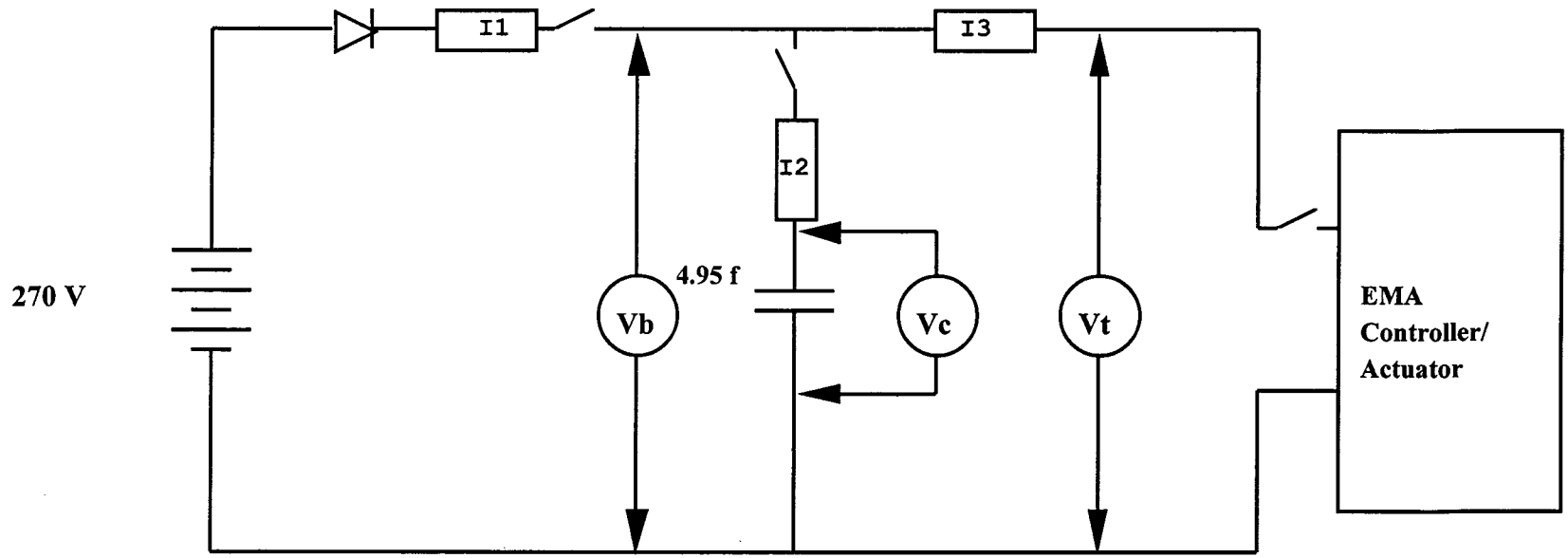

Proof of Concept Testing

- Repeated the tests with "flight type" batteries sized to do the task in the Battery Only configuration, and for a hybrid Batt/Cap configuration.
- Selected primary Ag-Zn batteries for pulse discharge capabilities. Wanted to limit bus voltage sag to 15% or less.
- Selected an 80 A-hr Ag-Zn for Battery Only tests, and a 20 A-hr Ag-Zn to be used in the hybrid configuration with the 5 Farad capacitor bank.

Battery Only - 15 kLb Test

Voltage Sag 7% initially to approx. 5%.

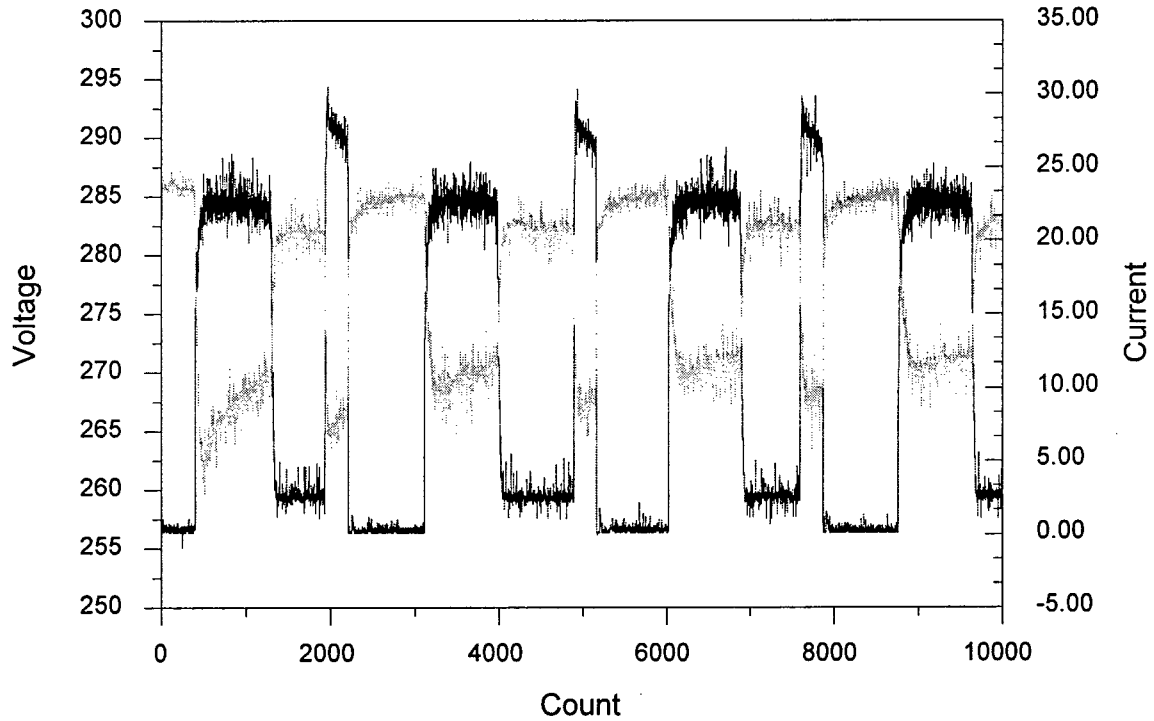

Current -------
Voltage -------

80 A-hr Ag-Zn: 450 Lbs.

Batt./Cap 15kLb Test

Voltage Sag 6% constant.

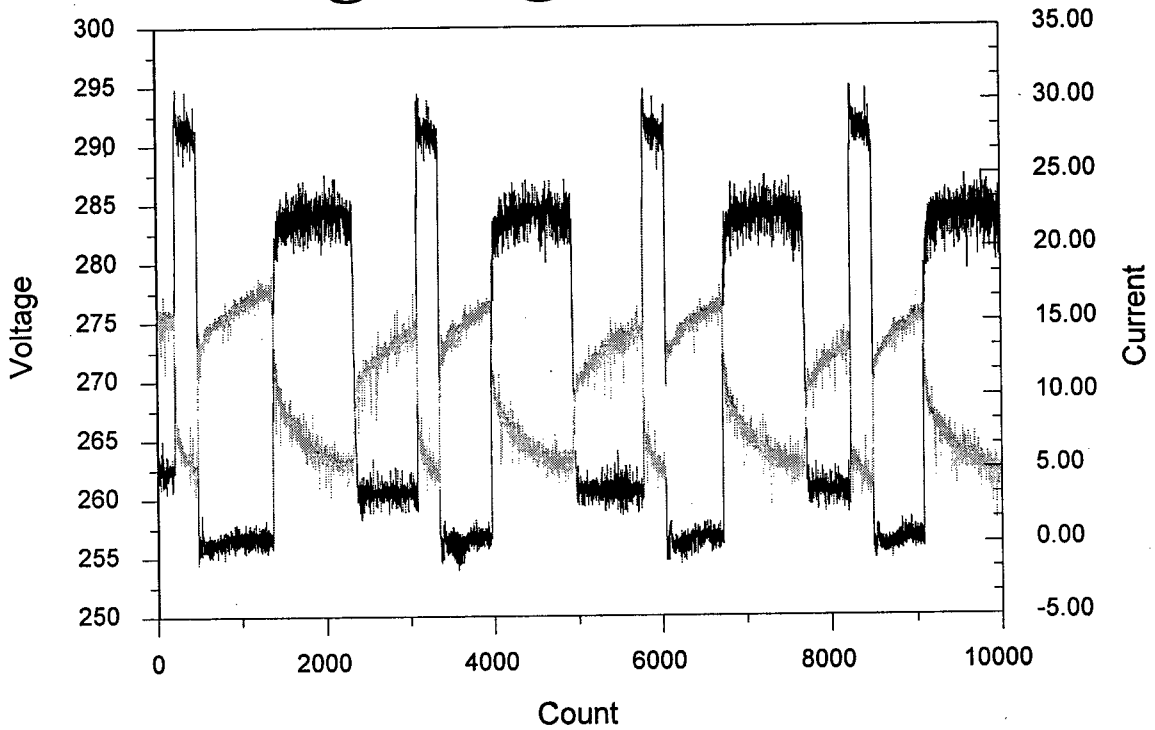

Current -------
Voltage -------

20 A-hr Ag-Zn: 100 Lbs, Cap. 85 Lbs.
Total: 185 Lbs. ***59% WEIGHT SAVINGS***

Classification of Super Capacitors

- By Electrode Type
  - Activated Carbon Powder
  - Carbon/Metal Fiber
  - Activated Synthetic Carbon
  - Doped Conducting Polymer Films on Carbon Cloth
  - Mixed Metal Oxides Deposited on Conductive Foils
- By Electrolyte Type
  - Aqueous
  - Organic
  - Solid
- By Energy Storage Mechanism
  - Double Layer Capacitance
  - Pseudocapacitance

MSFC Focus

- Electrode Types; carbon/metal fiber (Ni-C), mixed metal oxides and carbides deposited on conductive foils (Ru-O, V-Nitride).
- Electrolyte Type; Aqueous, Potasium Hydroxide and Sulfuric Acid.
- Energy Storage Mechanism; double layer capacitance (Ni-C, V-N), and pseudocapacitance (RuO).

Ni-C CDL

- Electrodes are sinter bonded to metalic current collectors in a bi-polar configuration.
- Carbon powder has very high surface area properties. *Approx. 2500 m^2/g.*

Ni-C CDL Sinter Bonding

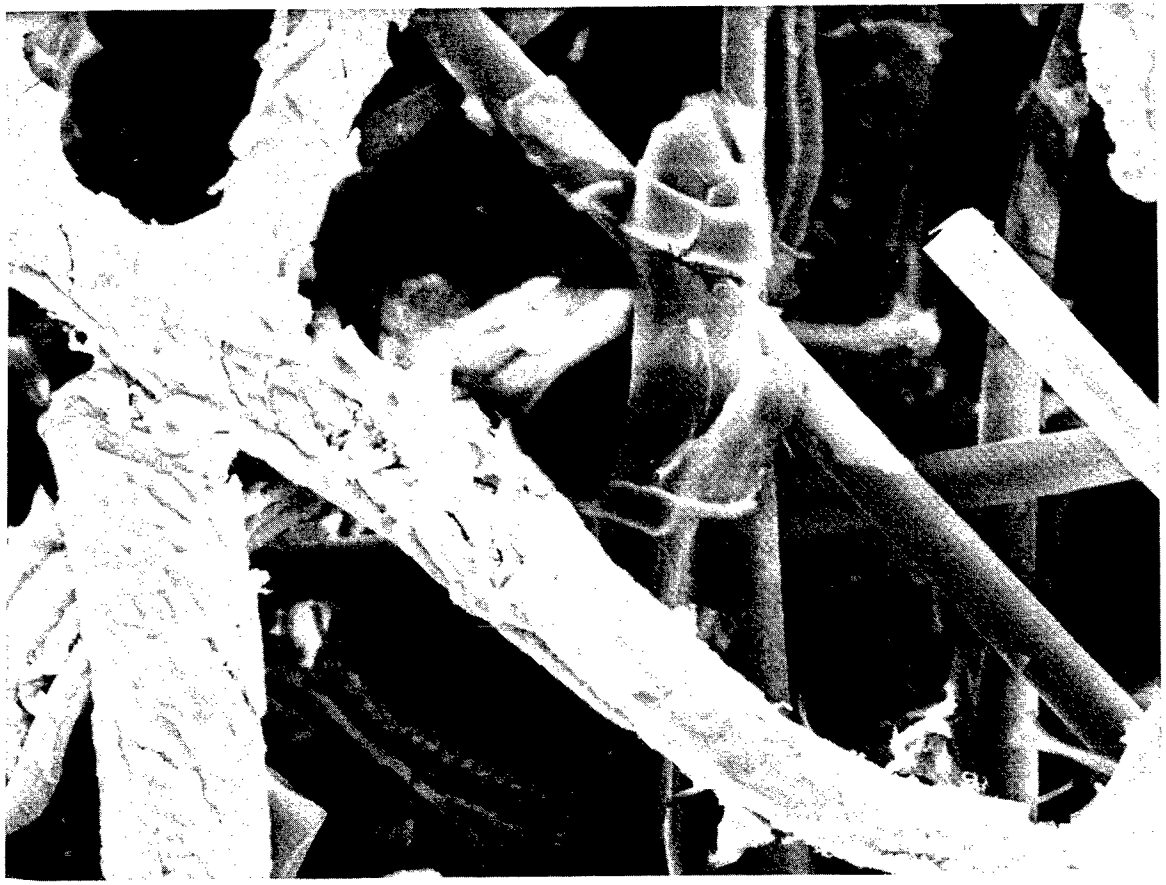

Ni-C CDL Electrode Material

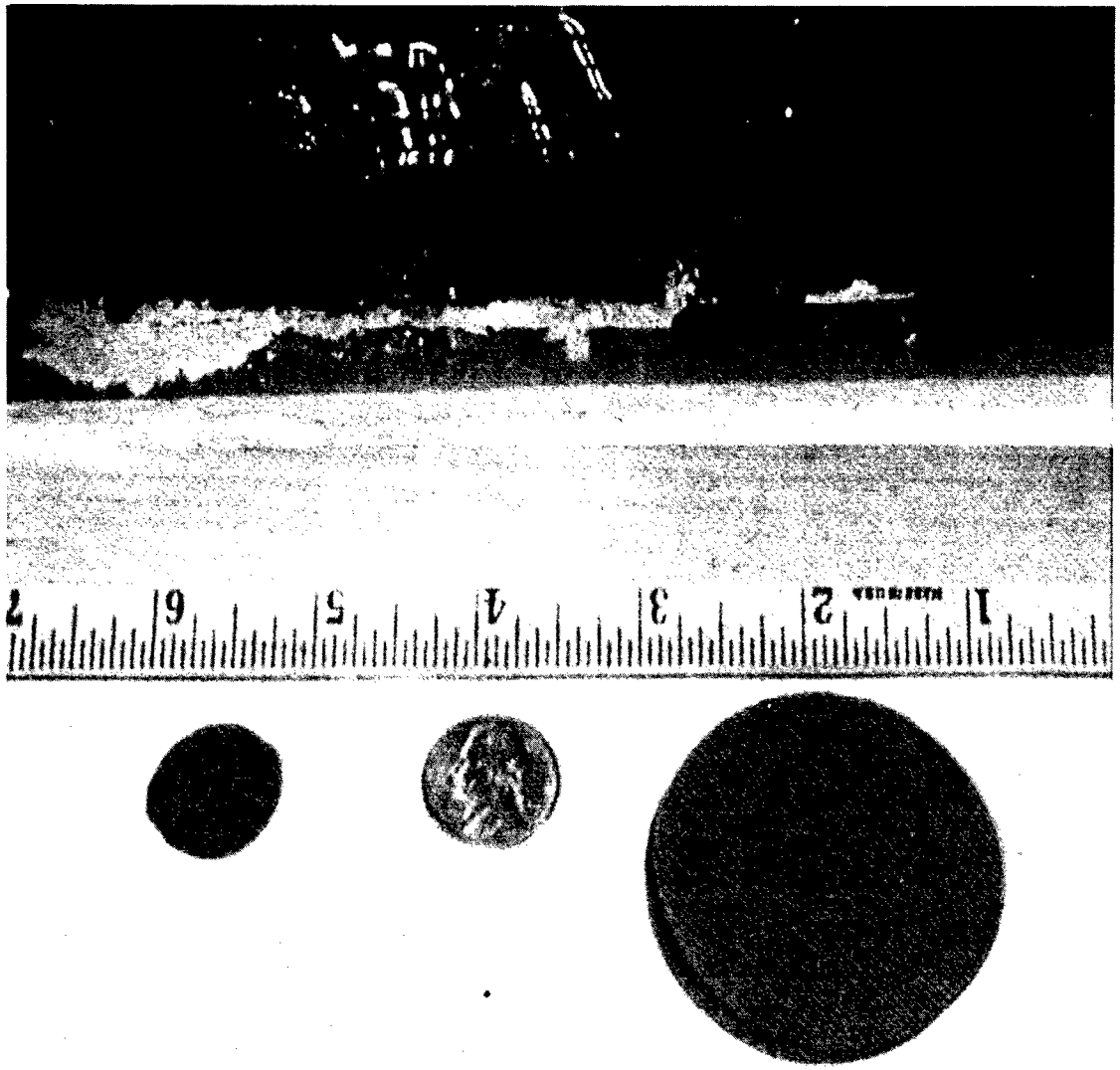

Ni-C CDL 1 F, 300 V Cap Bank

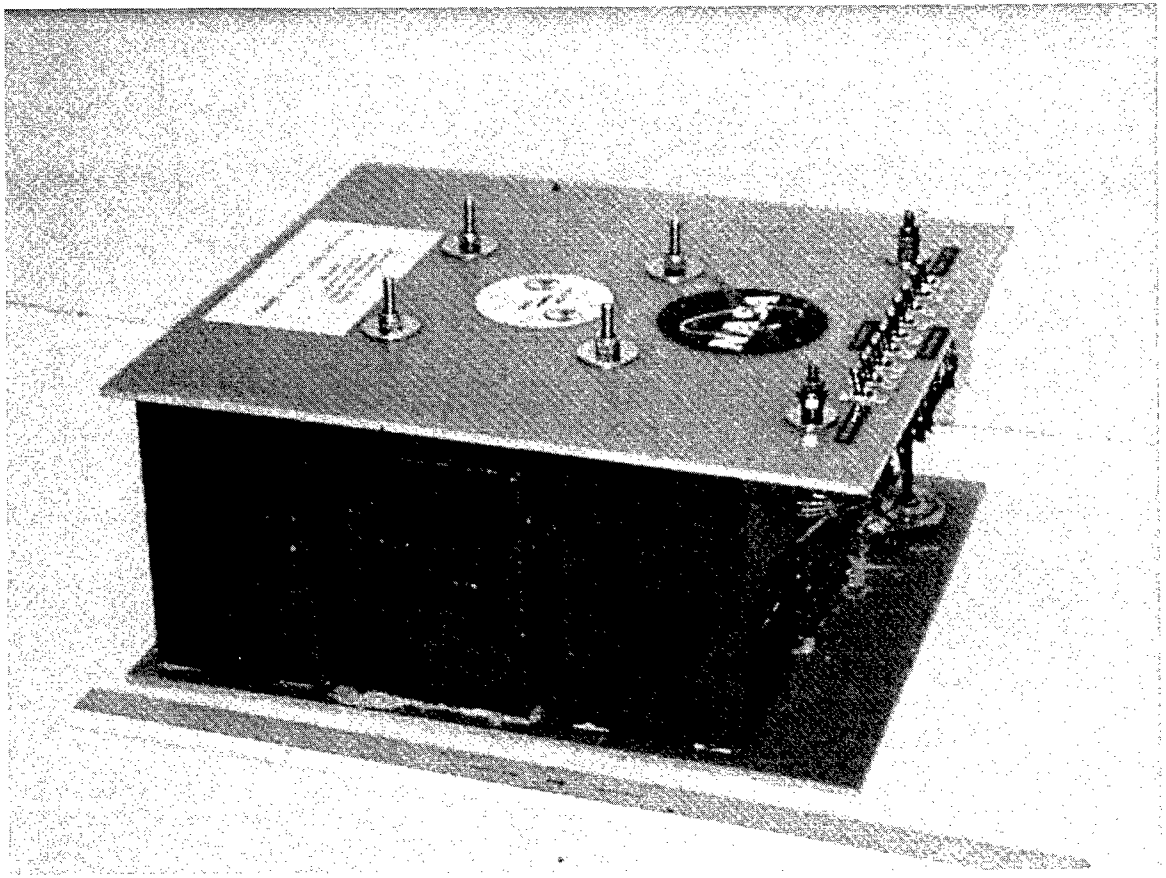

Ru-Oxide Psuedo-Cap

- Utilizes a Redox reaction, "fast battery" characteristics along with high capacitance.
- Target of > 10 W/g power density.

Ruthenium Oxide "psuedo-cap"

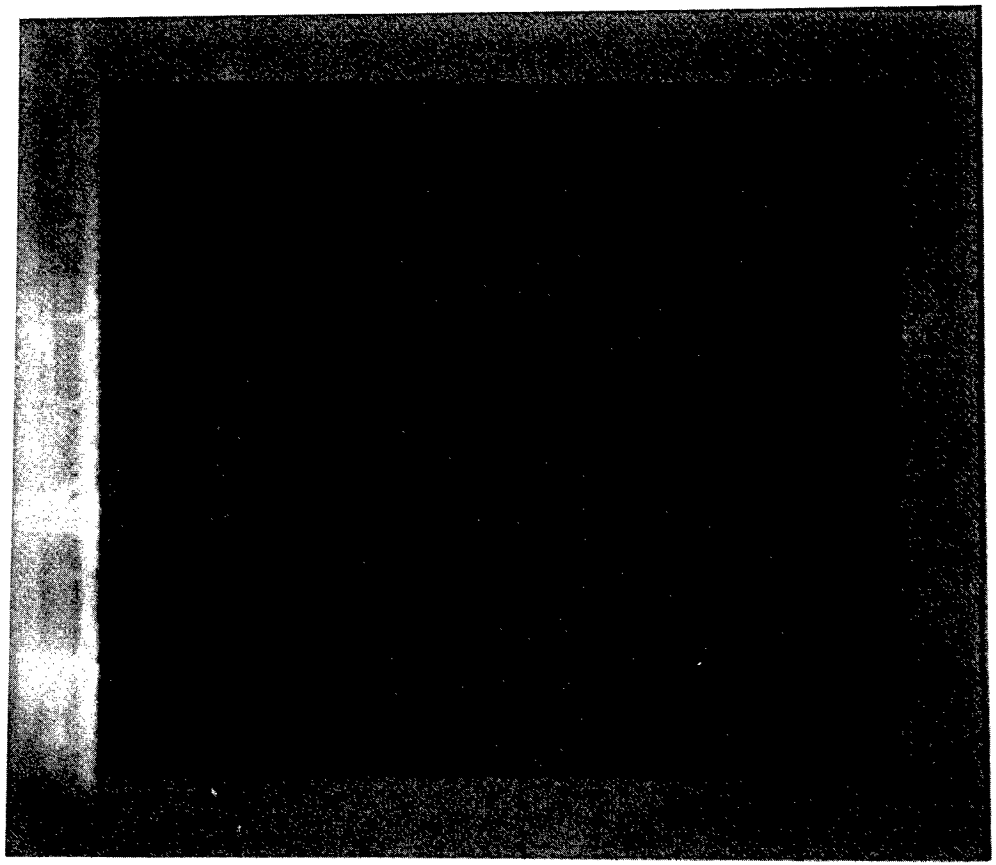

Ru-Oxide 2 F, 30 V Capacitor

Added Advantage

- Other testing has shown that use of Super Capacitors in hybrid power sources not only improves pulse loading power performance, but also extends battery life.
- *Data shown taken from a 0.5 F, 5 V, 6 cell Vanadium Nitride super capacitor. (GSM Protocall profile 217 Hz, 13% duty cycle, 0.16 - 1.3 A load.)*

Ultracapacitor extends the run time of alkaline battery

T/J Technologies Inc.

Minimum Potential vs. Run Time

3 AAA Alkaline Cells with and without T/J Capacitor at RT

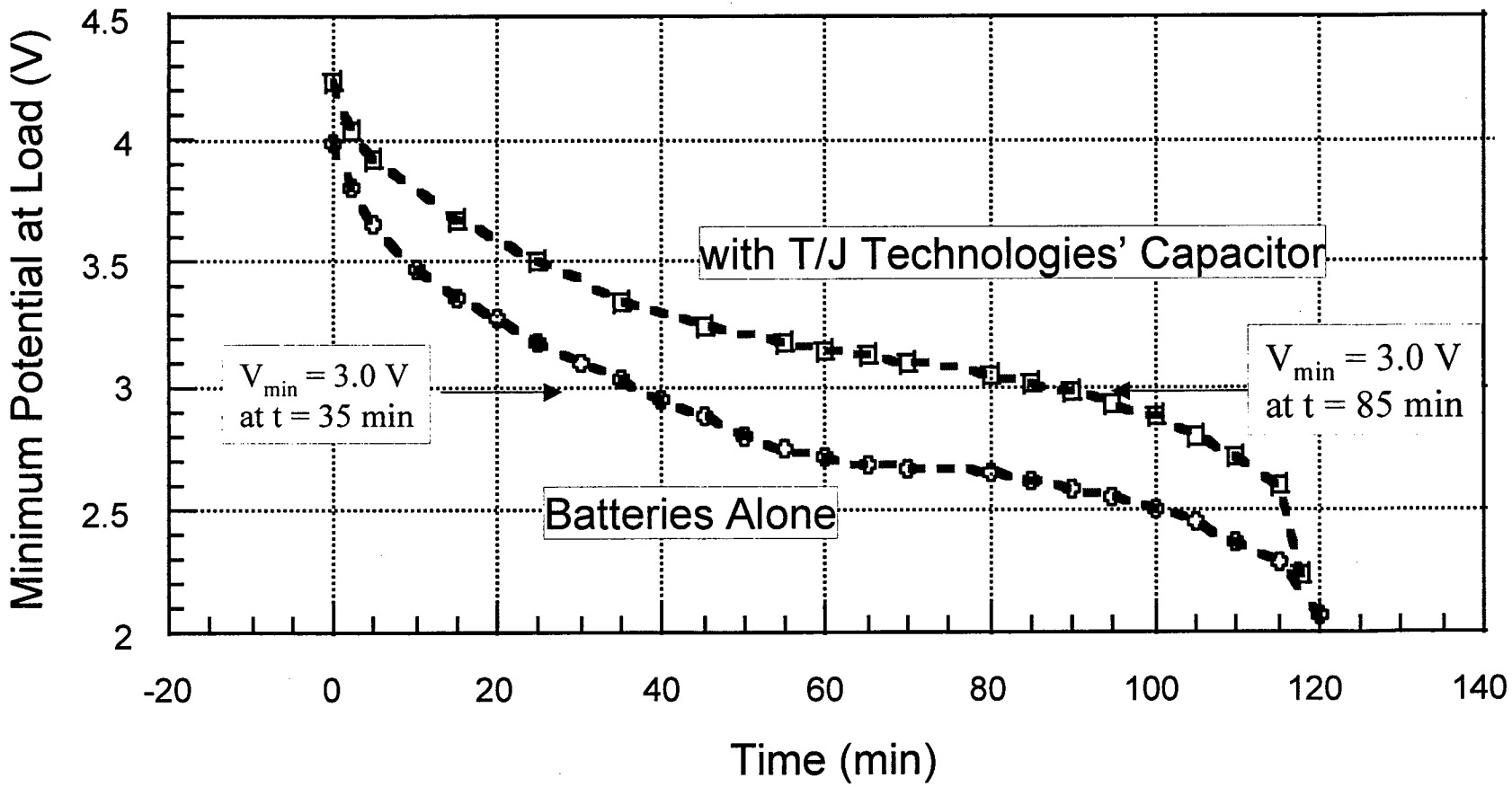

Run time extension vs. minimum voltage

T/J Technologies Inc.

3 AAA Alkaline Cells with T/J Capacitor at Room Temperature

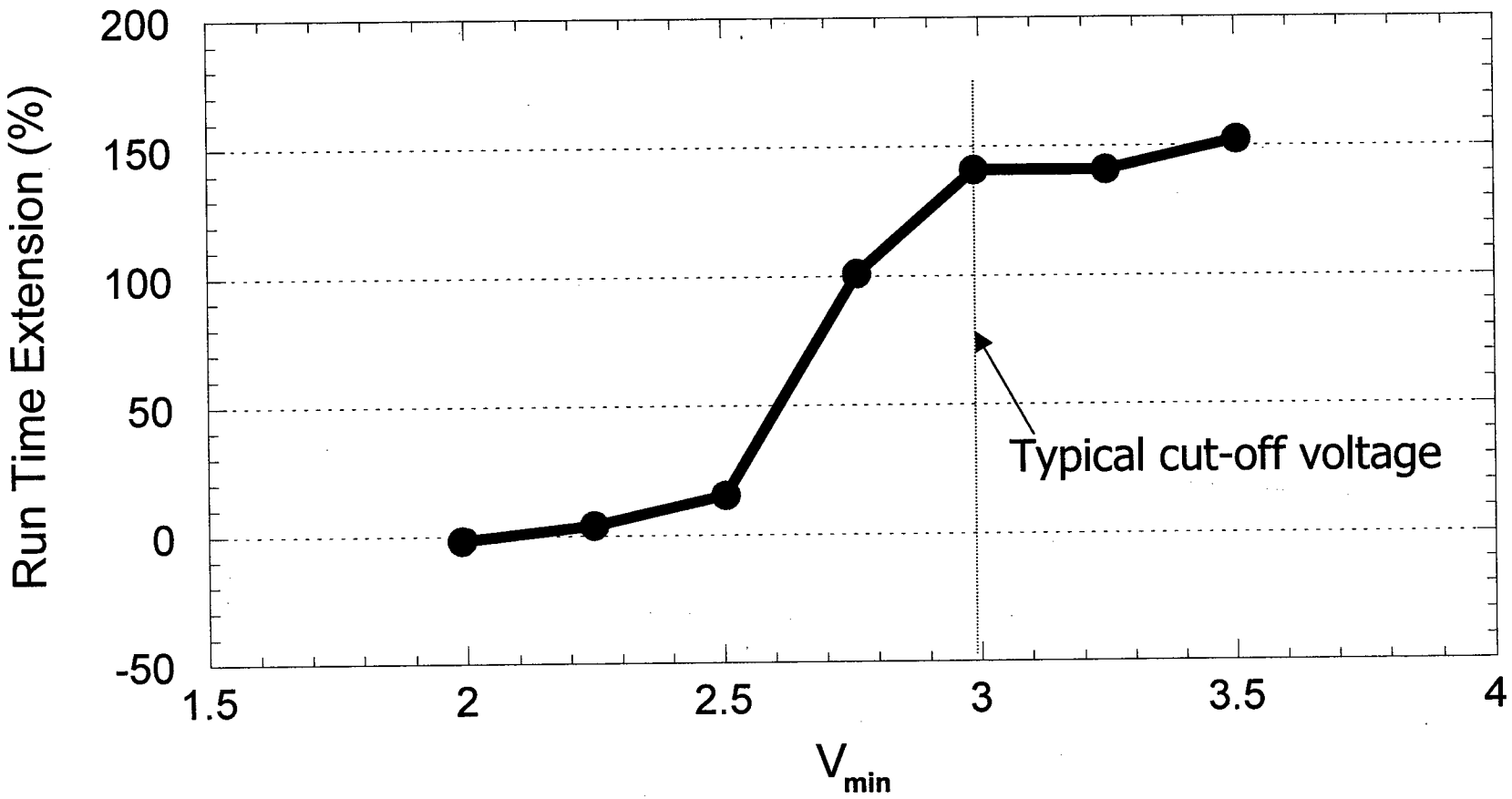

Ultracapacitor enhances battery performance at low temperature

T/J Technologies Inc.

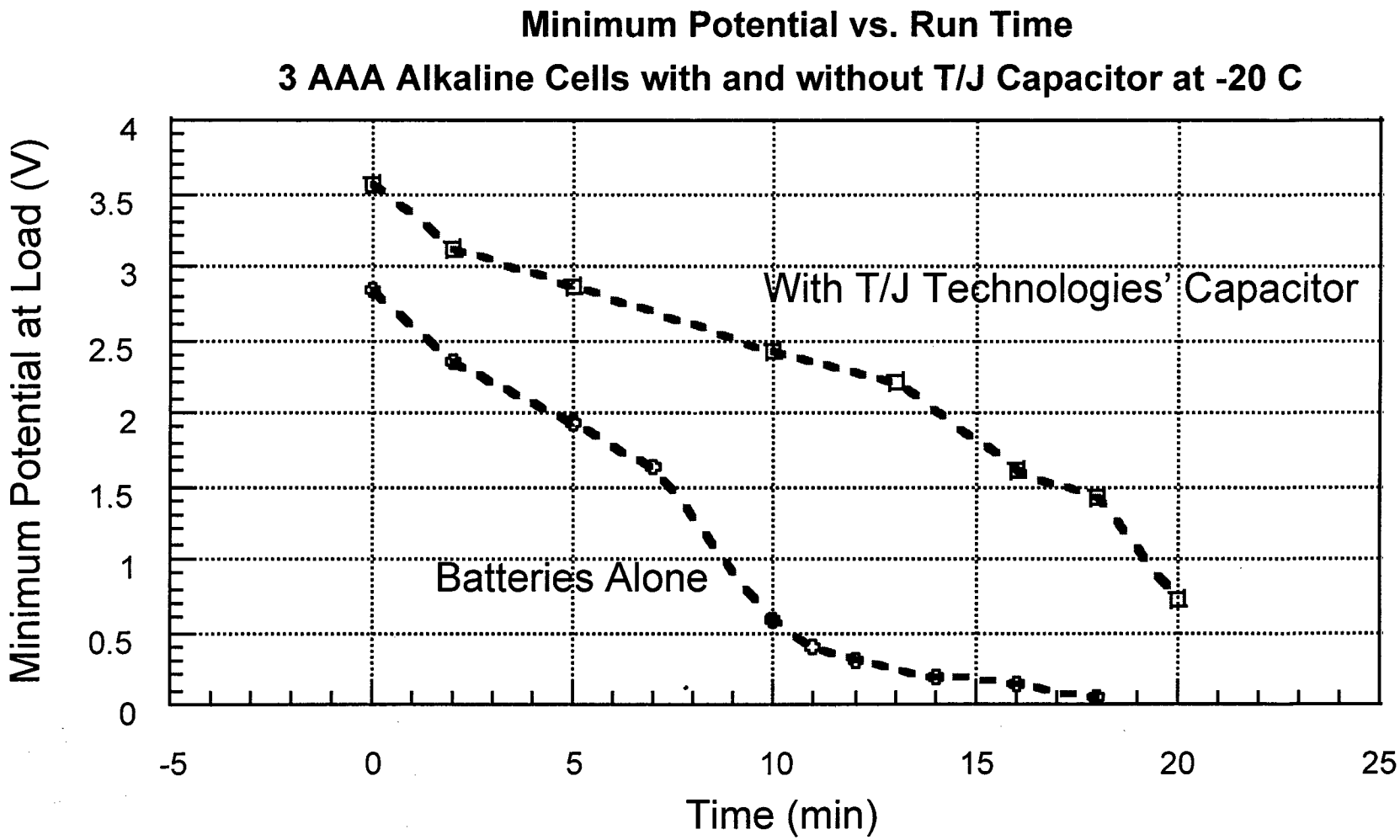

Reference Material

- Merryman, Stephen A. and Hall, David K., "Chemical Double-Layer Capacitor Power Source for an Electromechanical Thrust Vector Control Actuator," published in *AIAA Journal of Propulsion and Power*, Vol. 11, No. 1, January-February 1996.
- "Hybrid Electrical Power Source for Thrust Vector Control Electromechanical Actuation," D. K. Hall and S. A. Merryman, published in the Proceedings of the 30th Intersociety Energy Conversion Engineering Conference, Orlando, FL, July 31-August 4, 1995.
- Yoshida, A., Nishino, A., and Ohara, K., "Electric Double-Layer Capacitors for High Rate Charge-Discharge Uses," *Proceedings of The Second International Seminar on Double Layer Capacitors and Similar Energy Storage Devices*, Florida Educational Seminars, Inc., Deerfield Beach, FL, December 1992.
- Kurzweil, P. and Dietrich, G., "Double Layer Capacitors for Energy Storage Devices in Space Applications," *Proceedings of The Second International Seminar on Double Layer Capacitors and Similar Energy Storage Devices*, Florida Educational Seminars, Inc., Deerfield Beach, FL, December 1992.

Reference Material

- Rose, M. F., Lai, J. and Levy, S., "High Energy Density Double-Layer Capacitors for Energy Storage Applications," *Proceedings of the Power Conversion Intelligent Motion Conference*, Los Angeles, CA, June 1991.
- Burke, A. F., "Technology Update - Capacitors for Electric Vehicle Drivelines," *Proceedings of The Second International Seminar on Double Layer Capacitors and Similar Energy Storage Devices*, Florida Educational Seminars, Inc., Deerfield Beach, FL, December 1992.

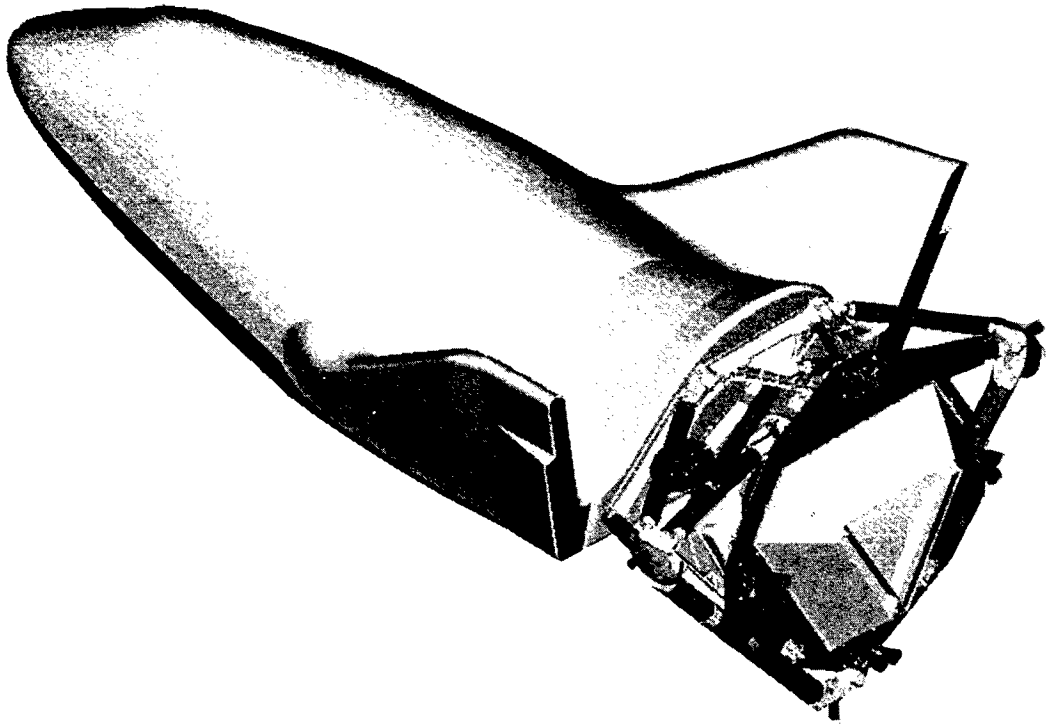

Calorimetric Measurements on a 32 Ah Li/MnO_2 Cell for the X-38 Crew Return Vehicle

by
Eric Darcy/NASA-JSC and Chris Johnson/Boeing-Seattle

Presented at the
1999 NASA Aerospace Battery Workshop

Agenda

- Introduction
- Battery and Cell Description
- Thermal Vacuum Performance
- Comparison of Dewar vs Heat Conduction Calorimetry
  - Theory
  - Experiments
  - Results
- Preliminary Findings
- Future Work

Introduction

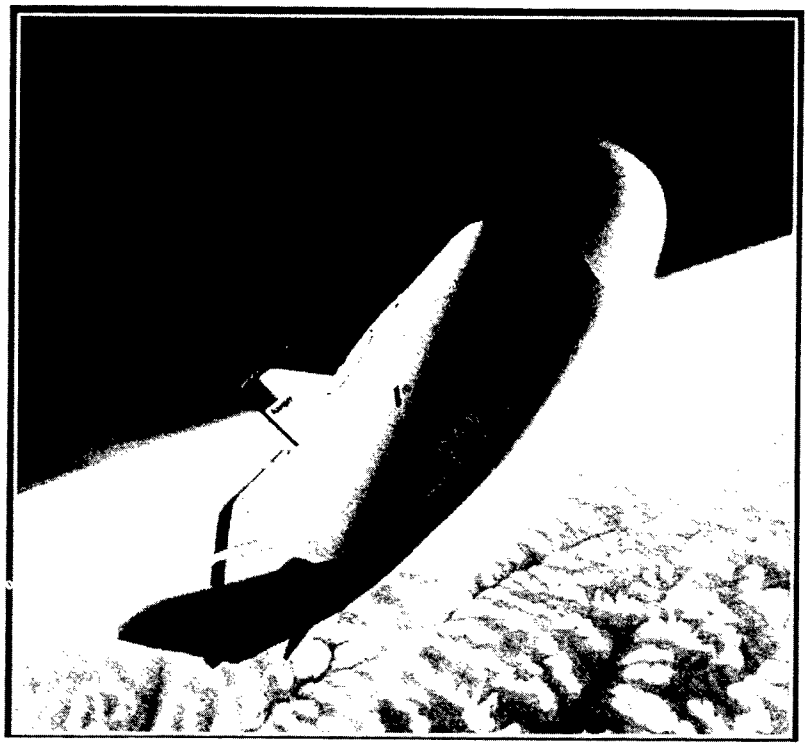

- Crew Return Vehicle Objectives
  - return ill or injured crew
  - evacuate crew from ISS
  - return crew if Shuttle is grounded
- X-38 Objective
  - Demonstrate the design in a unmanned spaceflight test (Feb 2002)
- X-38 Vehicle has 3 battery systems
  - Spacecraft
    - 28V In-Cabin NiMH (400 Ah total)
    - 270V high power (27 Ah total)
  - Deorbit Propulsion Stage (DPS)
    - 32V Li/MnO_2 (1400 Ah)

32V DPS Lithium Primary Battery

- Design Features
  - Li/MnO_2 32Ah cell (P/N M62) from Friemann & Wolf, Germany
  - Battery Module consists of 144 cells in a 12P-12S configuration
  - 4 Battery Modules per DPS
  - 350 Ah per Battery Module at 50A to 25V starting at 0 degC
  - 7 hour discharge rate
  - Refurbished by replacing cell strings
  - Battery Module Size
    - 620 mm wide, 620 mm deep, 206 mm tall
    - 79 kg

350Ah Li/MnO_2 Battery Module for X-38

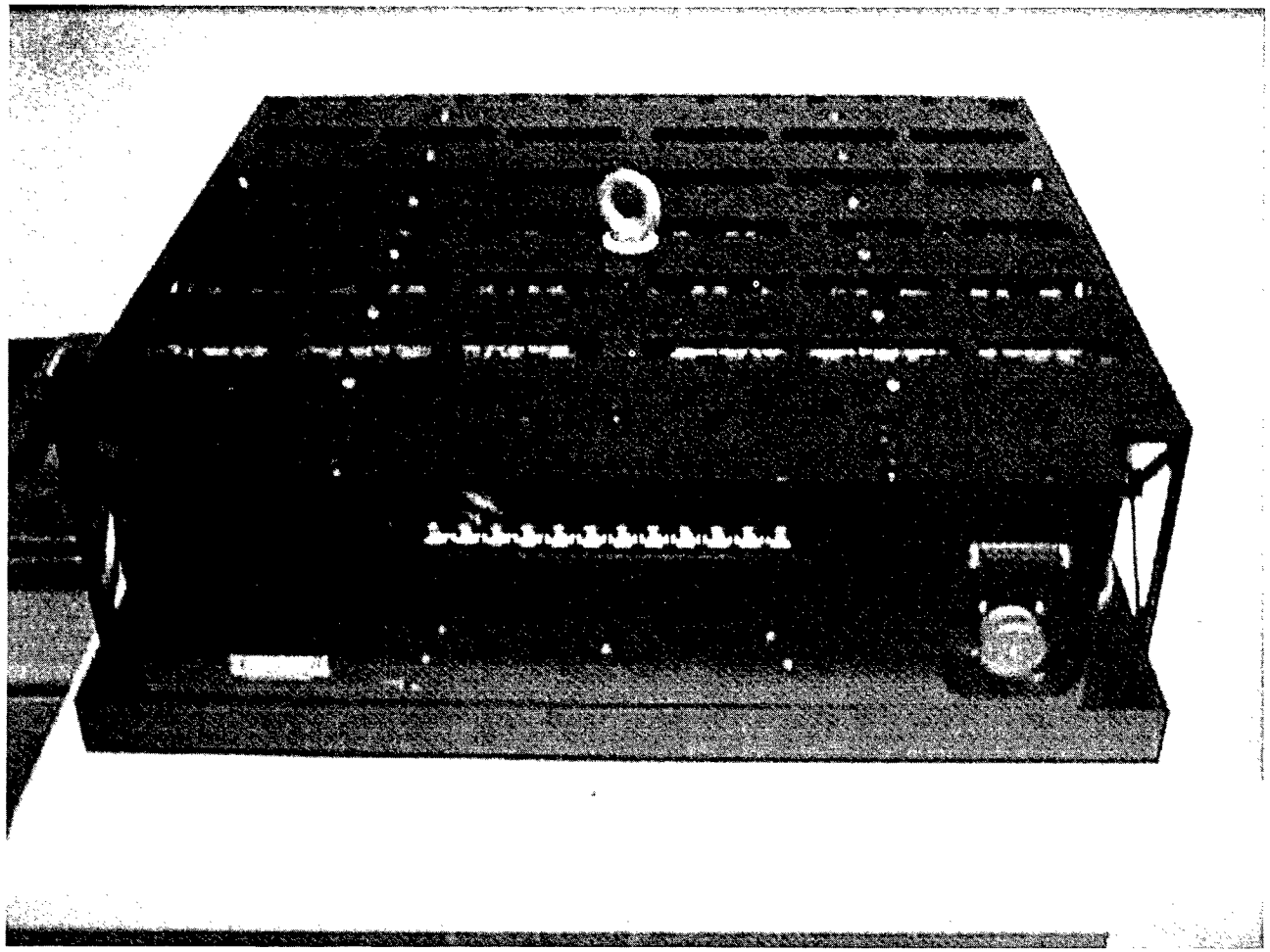

Friemann & Wolf Part No. 49815-000.000

Li/MnO_2 Cell Description (P/N M62)

- Similar to commercial M25 cell
- Capacity = 32 Ah
- Mass = 354 g
- Diameter = 42 mm
- Height = 133 mm
- Spirally wound
- Hermetically sealed
- Vent = opens at 10-17 atms

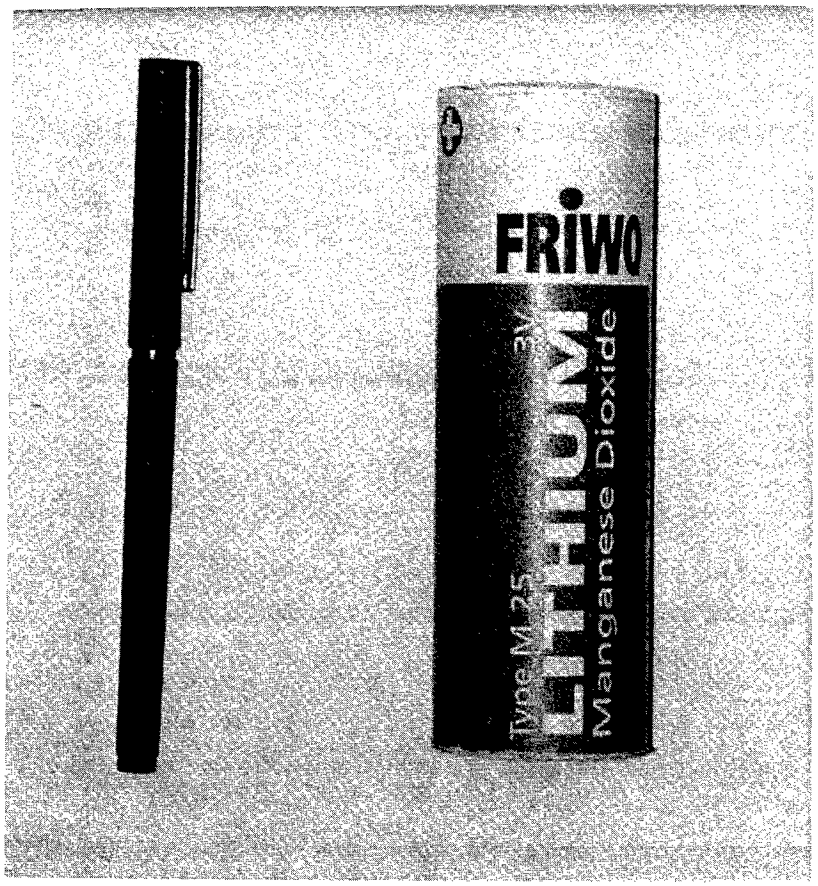

Battery String of 12 cells

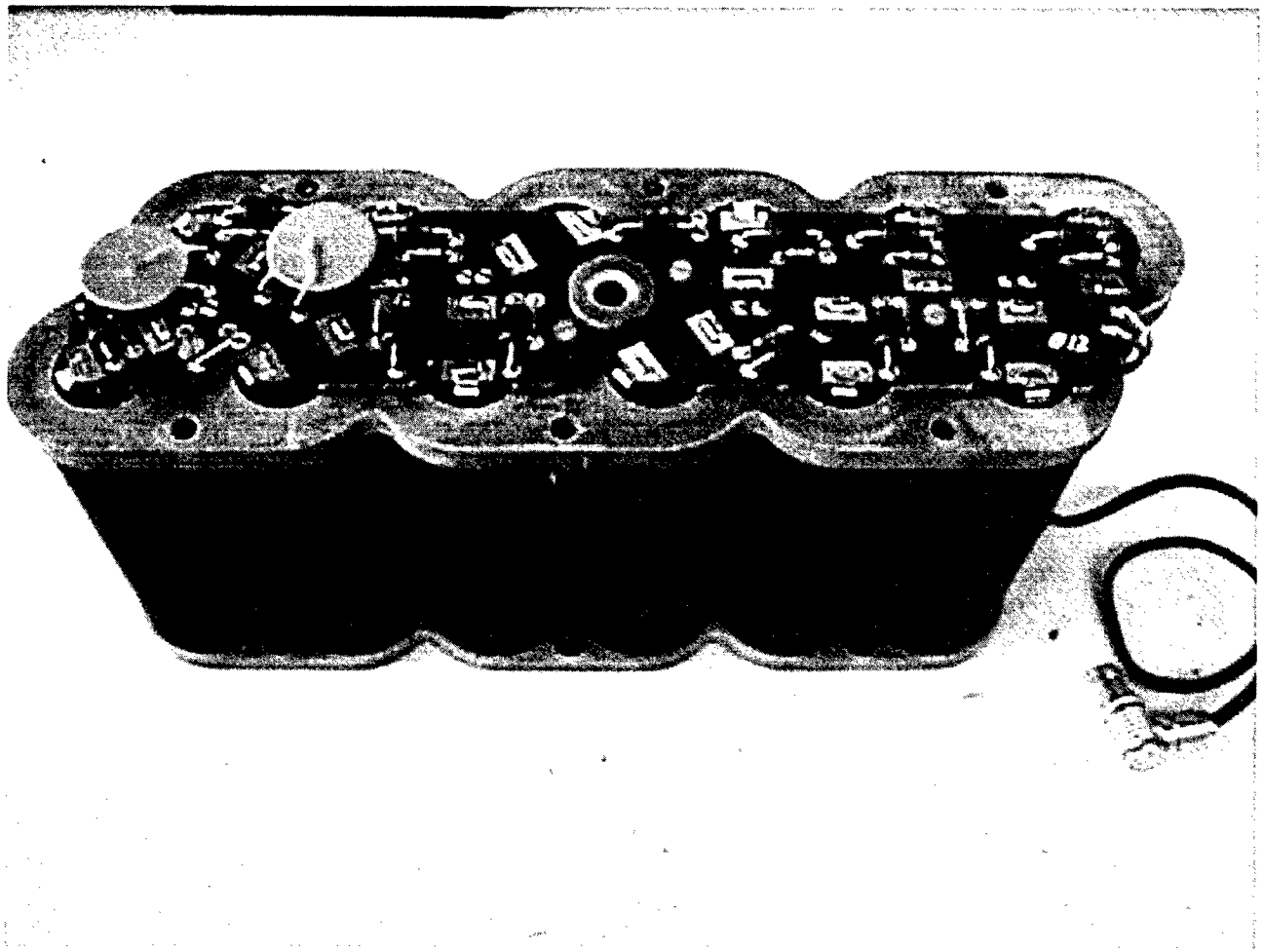

Battery Module Without Top Cover

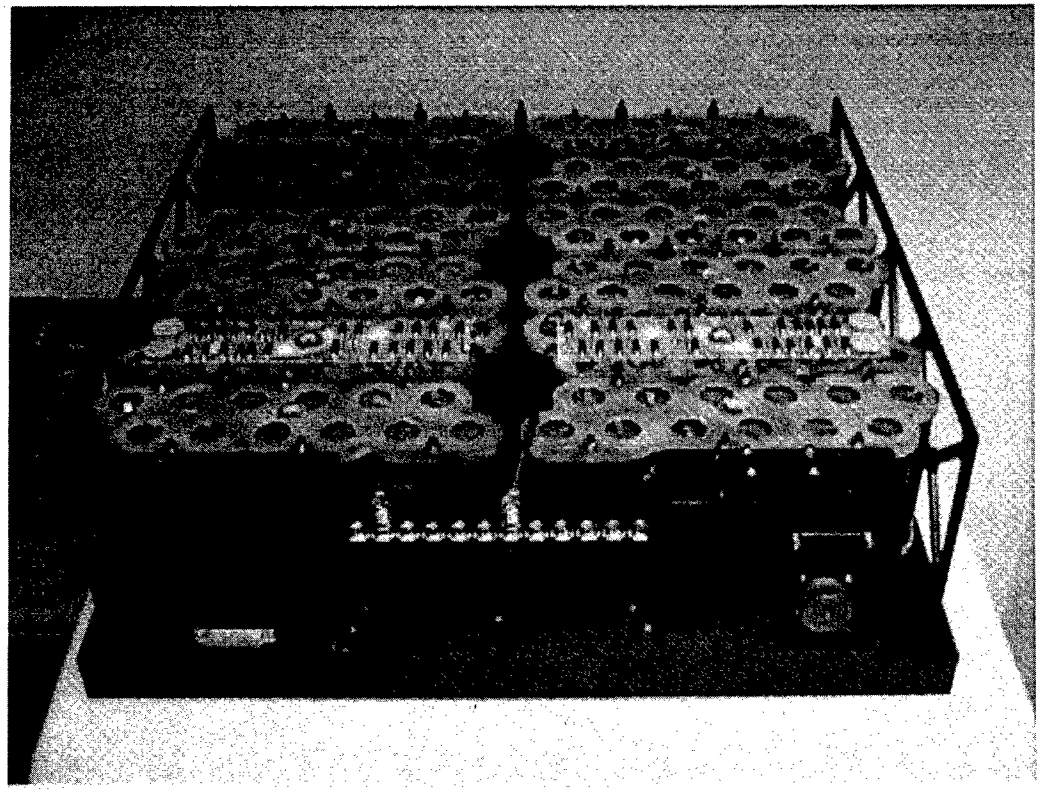

2 Views of the DPS

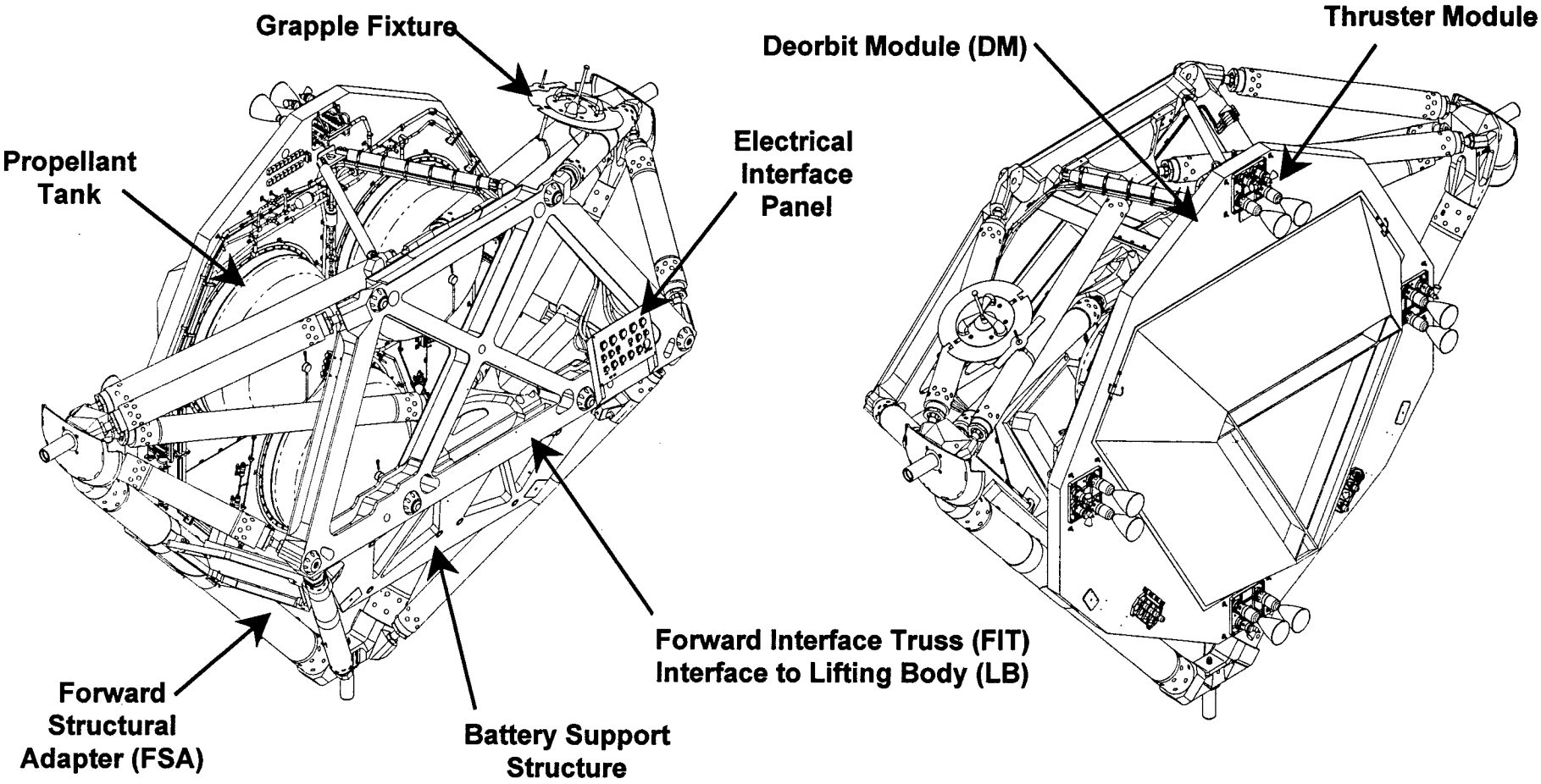

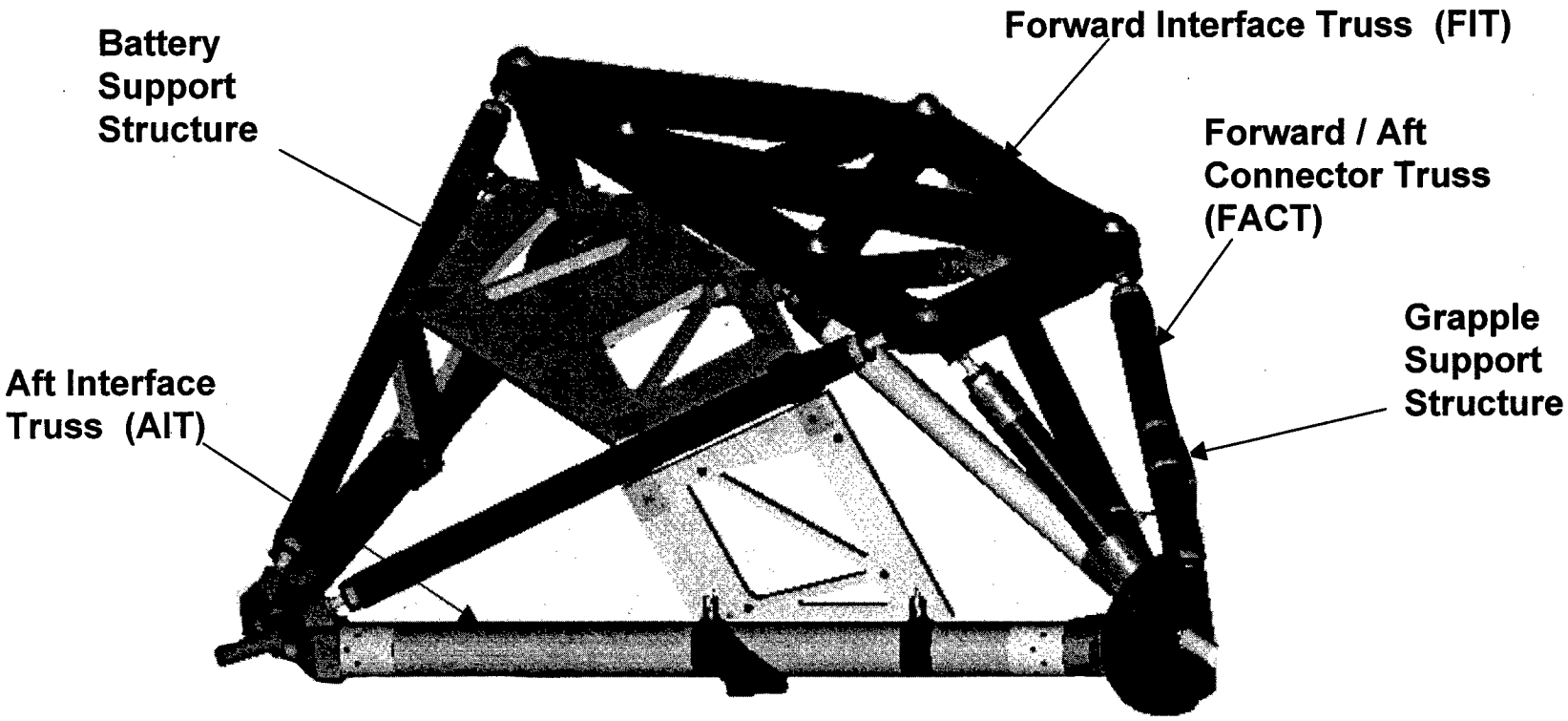

Forward Structural Adapter

1st Thermal Vacuum Test Results

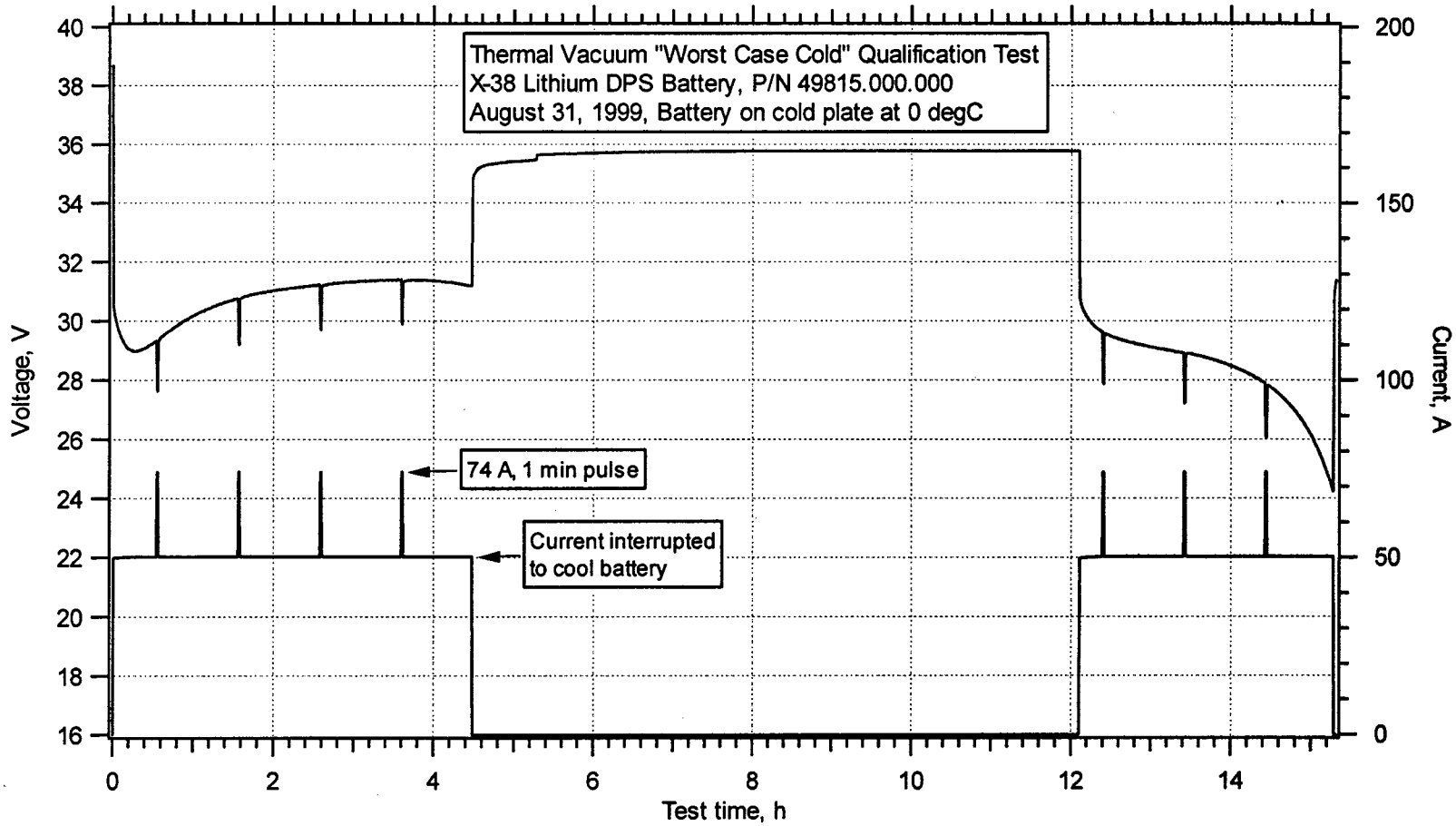

Thermal Vacuum Test Results

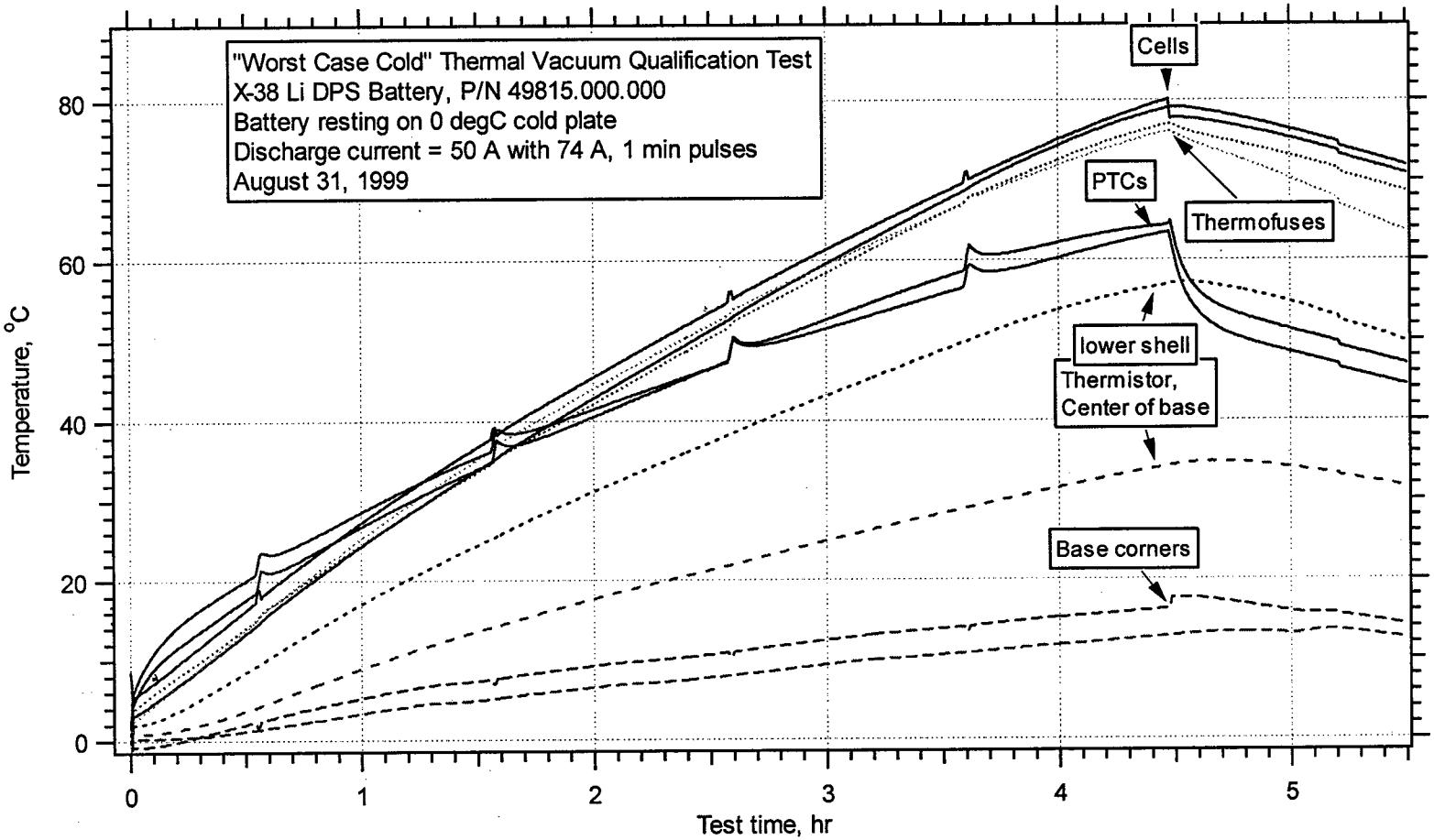

What is needed to improve battery thermal design?

- Cell thermal properties must be known accurately
  - Cell heat capacity, C_p, (cal/g/C)
    - No values found in the literature for Li/MnO_2 cells
    - Drop calorimetry
  - Cell heat generation, Q, (W)
    - No values found in the literature for Li/MnO_2 cells
    - Heat conduction calorimetry
- Battery heat conduction bottlenecks must be improved
  - From cell to the structure of the battery
- Battery must take full advantage of heat dissipation modes
  - Conduction to the DPS/battery structure
  - Radiation to the DPS propellant tanks

Two Drop Calorimetric Methods to get Cell C_p

- Adiabatic dewar method
  - Water in a dewar at 26 C
    - known mass of water
    - dewar assumed adiabatic
  - Cell at 55 C dropped into water
    - cell mass at 354 g
  - Cell C_p calculated from rise in temp of water/cell mixture
    - water C_p is known
  - Simple, inexpensive
- Theory
  - Heat inside dewar at start
    - $Q_{init} = (mC_p\Delta T)_{cell} + (mC_p\Delta T)_{water}$
  - Heat inside dewar at end
    - $Q_{final} = ((mC_p)_{cell} + (mC_p)_{water})T_{final}$
  - $Q_{init} = Q_{final}$, solve for cell C_p

- Heat conduction method
  - Oil bath maintained at 20 C inside water bath maintained at lower temp (16 C)
  - Cell at 33.8 C dropped into oil
  - Oil heating drops as cell heat is dissipated in the oil
  - (-1) * heater counts ~ to cell W
  - Custom instrument, expensive
- Theory
  - $E = \int Q\, dt = \int mC_p\, dT$
  - $C_p = E / m(T_2 - T_1)$
  - where $E = k^* E_{exp}$
  - where
    - E_{exp} = area under thermogram
    - k = cal/integrated counts

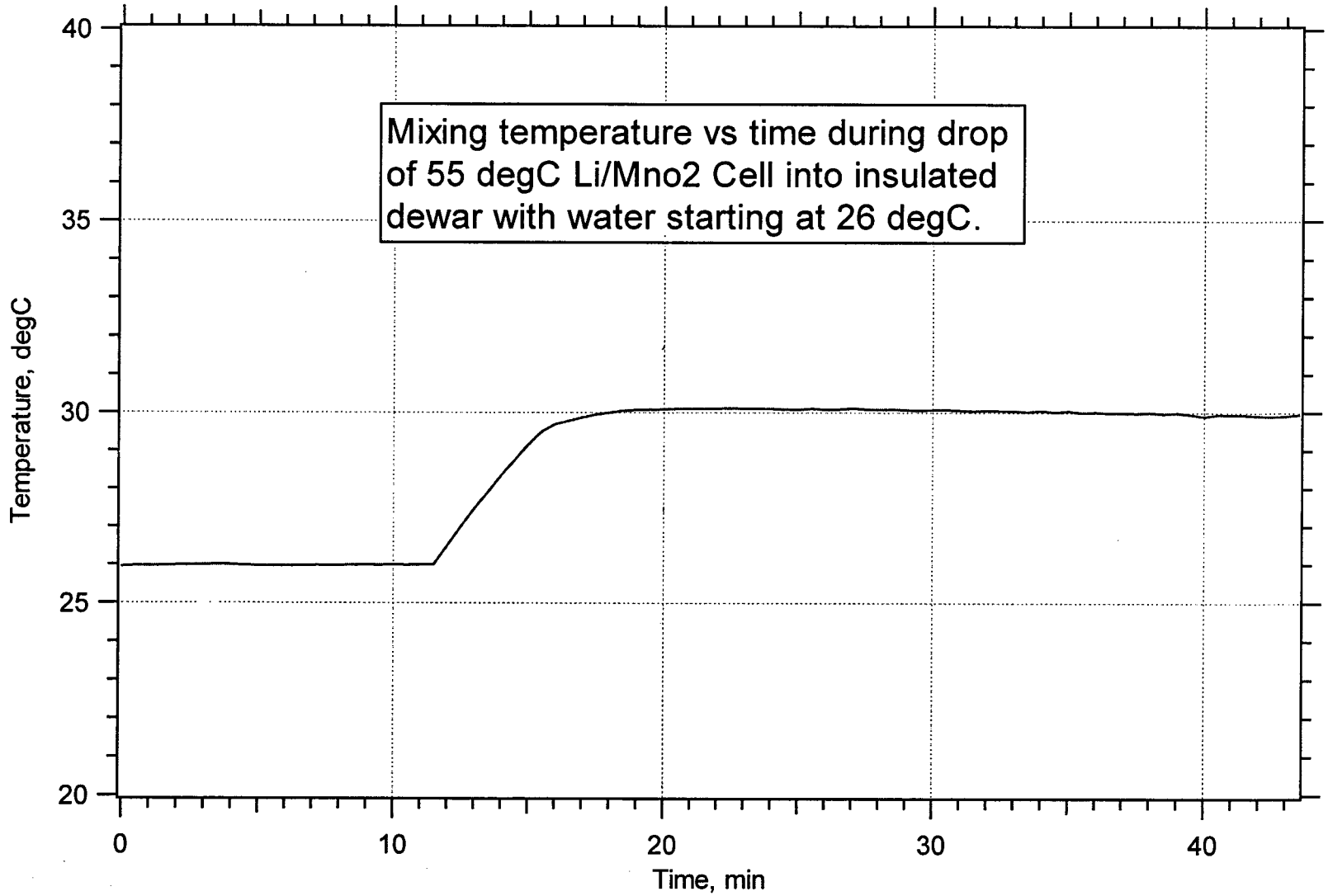
Mixing temperature vs time during drop of 55 degC Li/Mno2 Cell into insulated dewar with water starting at 26 degC.
Temperature, degC
40
35
30
25
20
0
10
20
30
40
Time, min

Heat Conduction Calorimeter

~~Boeing Calorimeter~~

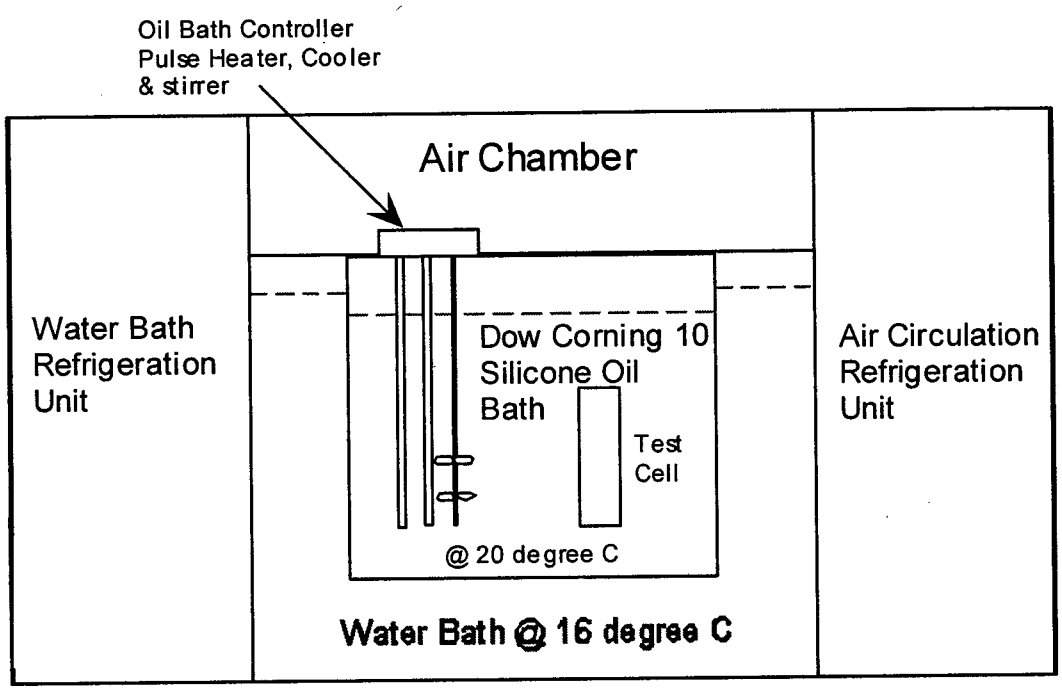

Eric Darcy/281-483-9055

NASA-Johnson Space Center, Houston, TX

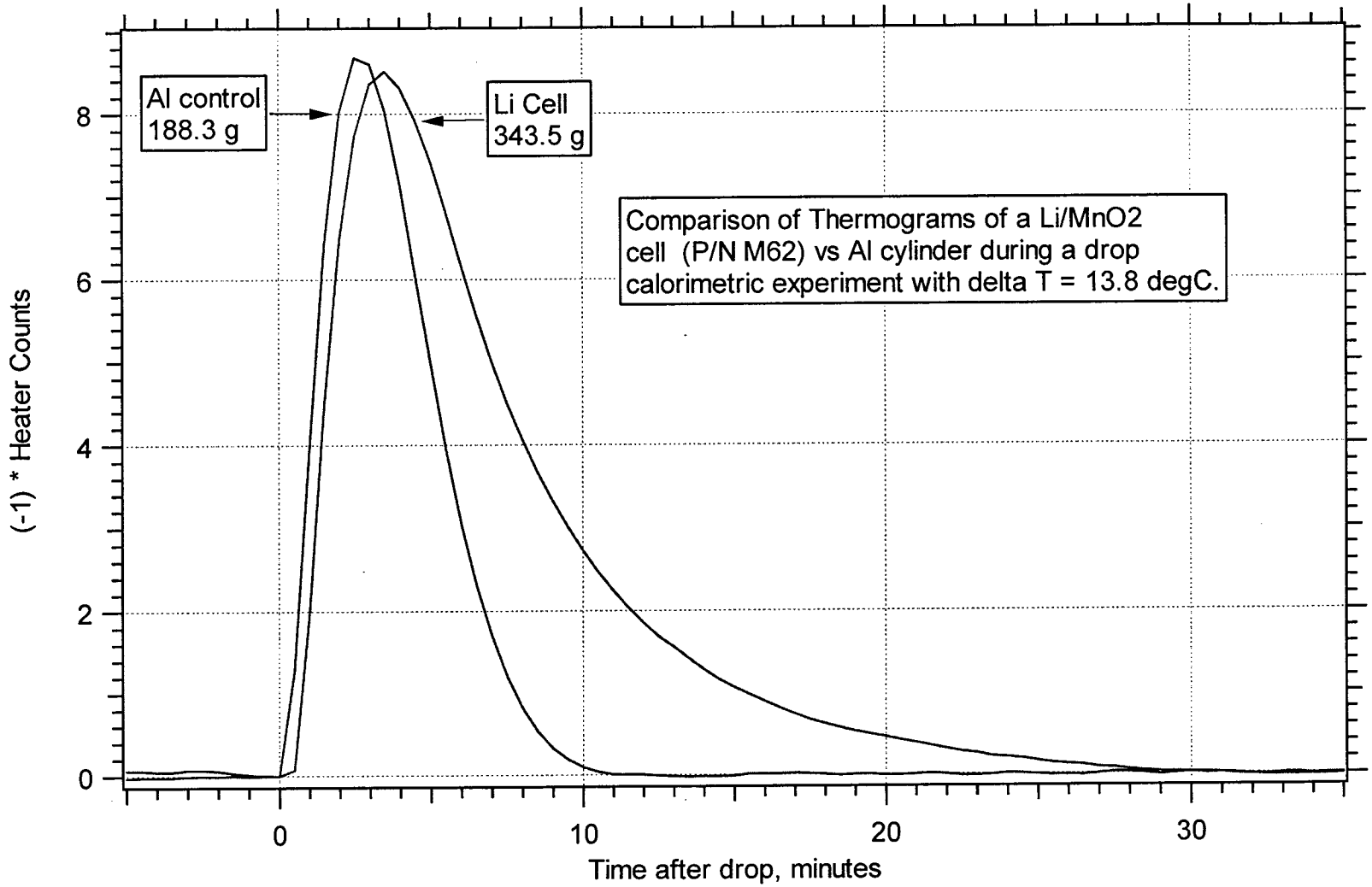

Results

- Adiabatic Dewar Method
  - Control = Al cylinder, 226g
    - Cp obtained = 0.249 cal/g/C
    - True Cp = 0.215 cal/g/C
    - 16% overestimation of true value
  - Cell data from 3 drops
    - complete cell, 354 g
    - Cp = 0.254 cal/g/C
    - s.d. = 0.0154 cal/g/C or 6%
    - 90% conf. Int.= +/- 17%
- Heat Conduction Method
  - Control = Al cylinder, 188.3 g
    - Cp obtained = 0.214 cal/g/C
      - based on 1W = 1000 heater counts
      - calibrated by energy balance with known power input into a resistor
      - <0.5% difference with true value
    - establish k factor = [integrated heater counts/cal]
  - Cell data from X drops
    - cell stripped of shrink wrap, 343 g
    - Cp = 0.203 cal/g/C
    - s.d. = TBD
    - 90% conf. Int. = +/- TBD

Preliminary Findings

- Difference between methods is significant
  - Cp difference is 20%
    - can not be explained by 11 g shrink wrap
- Possible source of errors with each method
  - Dewar method
    - small mixing temp rise (~ 4 degC) requires very accurate and precise temperature measurements
    - small errors in delta T measurement can propagate errors significantly
    - heat losses through top of dewar could be significant
  - Heat conduction method
    - small errors in delta T measurement
    - heat losses through top of oil bath are minimized by surrounding water and air bath
- Heat conduction appears to be more accurate and precise

Future Work

- Determine cell heat generation during 4.2 A discharge
  - Compare both methods
  - Calibrate both with a known power input through a resistor
  - Obtain effective thermoneutral potential, E_{tn} vs SOC
    - $Q = (E_{tn} - L.V.)\ I$
    - calculate heat generation at different discharge rates
- Improve battery heat conduction bottlenecks
  - From cell to the structure of the battery
- Take full advantage of heat dissipation modes
  - Conduction to the DPS/battery structure
  - Radiation to the DPS propellant tanks

Low Temperature Performance of Two Nickel Hydrogen Designs

By
Dr. Dean W. Maurer[1]
Loral Skynet
PO Box 7018
Bedminster, NJ 07921
And
Dr. Dawn M. See[2]
Imperial College of Science, Technology and Medicine
Dept. of Materials
Prince Consort Road
London SW7 2BP, UK

Introduction

The Telstar 5, 6 & 7 spacecraft owned and operated by Loral Skynet and built by Space Systems/ Loral utilize the patented[3] Loral "Cold Charge" protocol in their battery operation. This protocol provides an approximately 25% capacity enhancement by charging at a very low temperature and subsequently discharging while ramping the temperature up from the end of charge temperature to as high as 30 °C. It was of interest to measure the relative effects of the low temperature charge and the temperature-ramped discharge on flight-quality cells of the two different cell designs used in the Telstar 4 program where this protocol is not used. The Telstar 401 cell is a conventional 3.5" COMSAT design (50 AH) with asbestos separators and the Telstar 402R cell is a 3.5" modified Mantech design (45 AH) with a single layer of Zircar separator.

The cell cycling facility used for the experimental work was designed and built some years ago by the AT&T Bell Labs (when Skynet was part of AT&T) for life testing of Telstar battery cells. When Skynet became part of Loral, this facility was donated to the University of South Carolina (USC). The work was carried out by one of us[2] as part of a graduate study program. The data were also intended for use in model verification of the USC first-principles nickel-hydrogen cell model.

Experimental

After selection of the flight battery cells, a number of the remaining cells from the production lots were selected for this work. The cells were placed in a temperature chamber in a horizontal position with a thermocouple attached to the cell midsection. Some of the selected cells included strain gages. The 401 cells were cycled three times at each test temperature. The cycle consisted of a charge for 16 hours at C/10 and a discharge at C/2 to 0.8 volts followed by a 3 hour open circuit stand to equilibrate the temperature. The 402R cells had two cycles at each temperature. First they were charged at C/10 for 20 hours and discharged at C/2 to 0.8 volts at constant temperature and then

[1] presenter
[2] formerly with University of South Carolina
[3] J. Hall, US Patent #5,395,706 (1995) and J. Lenhart, J. Hall and A. Applewhite, US Patent # 5,617,006 (1997)

cycled again with the temperature increased during the discharge from the end-of-charge temperature to about 30 °C by the end of the discharge. Figure 1 is a plot of the temperature and pressure for the test run at –20 °C. The pressure fluctuation which was observed on the ramped-temperature test is an artifact caused by voltage noise on the strain gage wiring; this was eliminated on subsequent tests. Note that the temperature

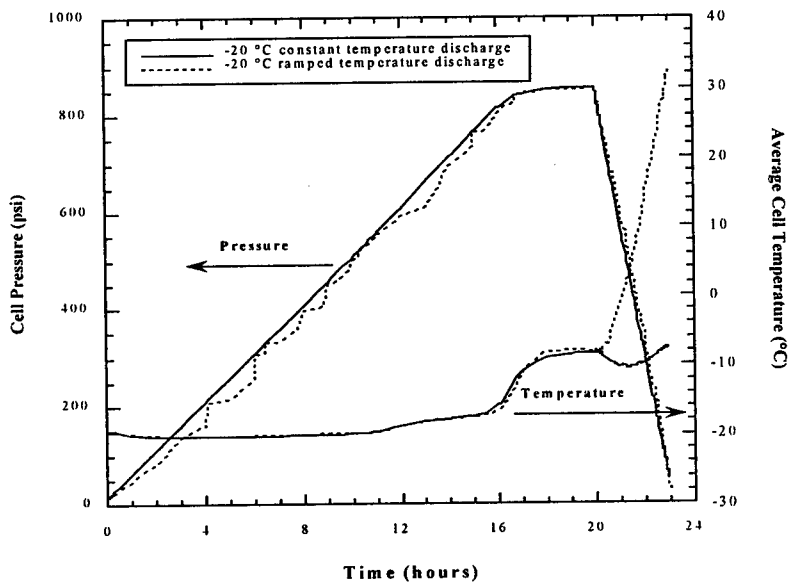

Fig 1 Pressure and Temperature Responses for the 402R Cells at –20 °C

chamber was not able to maintain the temperature during the overcharge portion of the charge. In addition, the pressure is essentially flat after 16 hours of charge, which indicates minimal capacity difference between the two cycling procedures.

Results

The discharge curves for the test shown in Figure 1 are shown in Figure 2. The temperature ramping results in a "normal" discharge curve such as one would expect at higher temperatures, whereas the "constant" temperature discharge has the voltage depressed during the second half of the discharge as well as slightly less capacity. Figure 3 shows the ramped temperature discharge curves for all of the 402R tests.

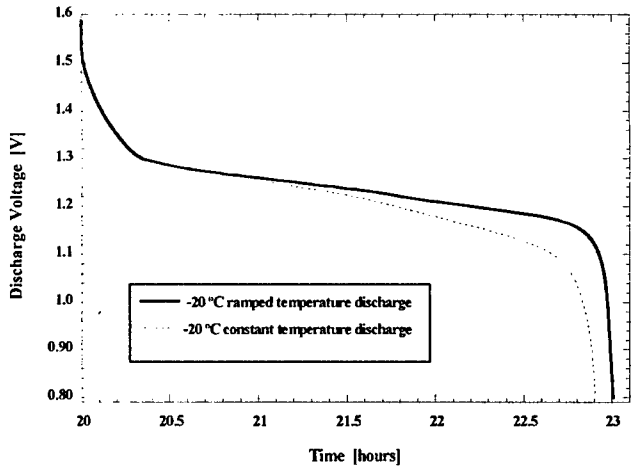

Figure 2 Discharge Curves for the 402R Cells at –20 °C

Note the uniformity of the discharge plateau voltages. The capacity achieved for each test is representative of the charging temperature. The results of these tests is further summarized in Figure 4 where the capacity is plotted vs. temperature for each of the temperatures in the 402R tests. The ramped discharge provides only

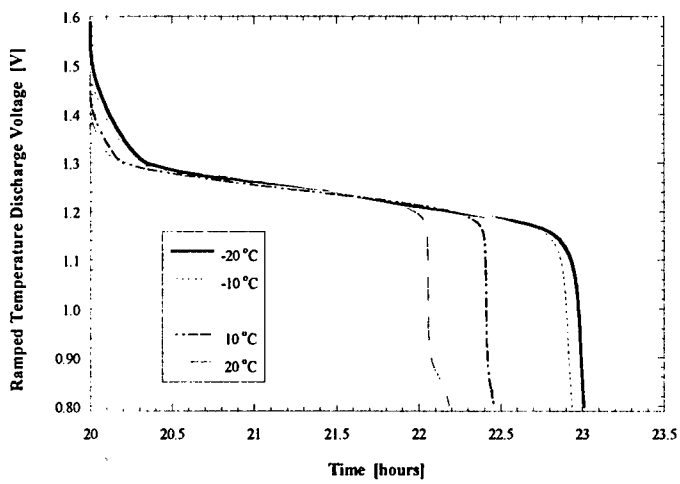

Figure 3 Ramped Temperature Discharge Curves for All 402R Tests

~3% greater capacity than the "constant" temperature, but that the difference in capacity between +20 and –20 °C is of the order of 50%! The difference between a more usual operating temperature of +10°C and the –20 °C data is still 25%. Similarly the effect shown in Figure 2 is also presented in Figure 5 in terms of the specific energy vs. temperature. In this case, there is a 5% difference at –20 °C, and a 40% energy density advantage between +20 and –20 °C.

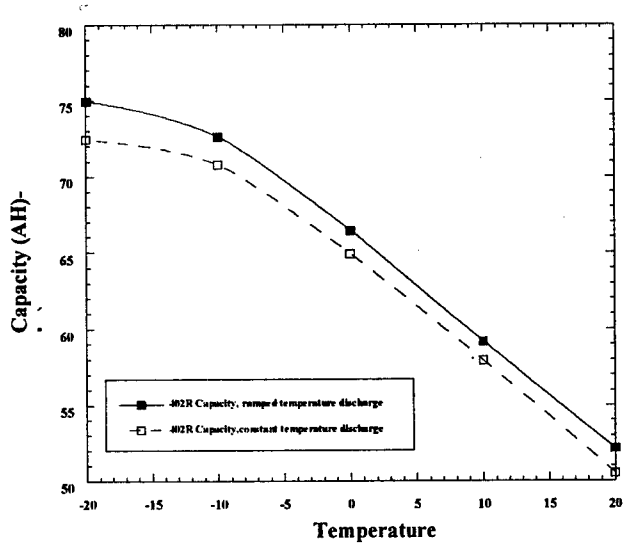

Figure 4 Ramped vs. Constant Temperature Capacity for 402R Tests

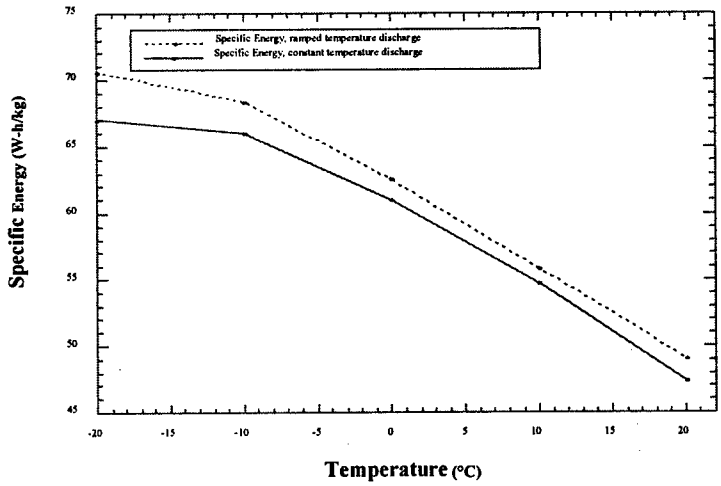

Figure 5 Specific Energy vs. Temperature for 402R Cells

Finally the 402R cell data and the 401 cell data are compared in Figure 6. In this case the direct result is shown as well as a curve in which the 401 cell data are "normalized" by the ratio of the nameplate capacities of the cells. The only justification offered is that the nickel electrodes are approximately the same area in each design and the cell capacities differ only by the number of electrodes.

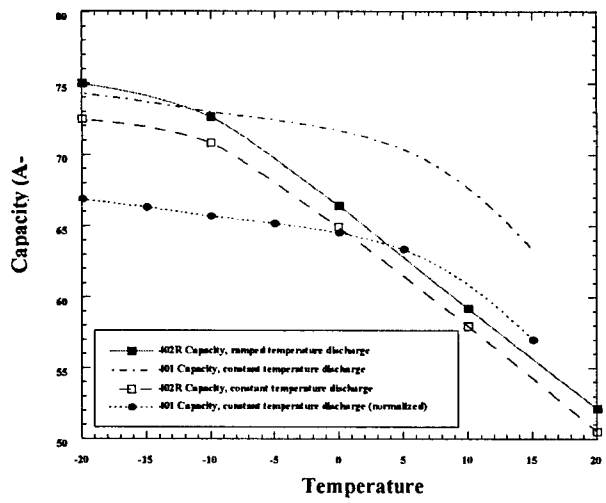

Figure 6 Capacity Data for 401 and 402R Cells vs. Temperature

In Figure 6 it can be seen that:

1) The capacity of the 401 cells below about 5 °C is relatively flat but above that temperature it has about the same slope as the 402R cells. Presumably this is due to the decreased conductivity of the asbestos separator at lower temperatures.
2) The unadjusted capacity of the asbestos cells at –20 °C is about the same as the capacity of the Zircar cells with fewer electrodes.
3) The "normalized" capacity of the 401 cells at higher temperature is about equal to the 402R cells but the 402R cells are ~12% higher at the low temperature.

Conclusions

These studies support the generally held expectation that the Mantech cell design offers some performance advantages over the original COMSAT design (the COMSAT design is after all nearly 25 years old). More importantly the studies show a pronounced advantage in operating at very low temperatures: a 25% advantage at –20°C compared to the more usual +10°C. How this temperature control is achieved in orbit is left as an exercise for the thermal engineer.

Acknowledgements

The authors would like to thank Dr. Ralph White of the Center of Electrochemical Engineering at the University of South Carolina for his continued support, encouragement and useful discussions. We also thank Dr. B. Vyas and his group at Lucent Technologies/ Bell Labs for their technical assistance and training during the transfer of the facilities. Finally we acknowledge the additional financial support of the Office of Research and Development of the United States Government.

Nickel-Hydrogen Session I

EAGLE PICHER
Eagle-Picher Technologies, LLC

POWER Subsystems

HIGH DOD [illegible] LE TESTING

Jeff Dermott
Eagle-Picher Technologies, LLC
Joplin, Missouri

- Life Test at 70% DOD was started 4 years ago.
- Original intent was to qualify cells produced at the Range Line Facility (RLF).
- Test data is useful for high DOD cell design.

- Standard Acceptance Test cooling cart.
- Cells mounted in aluminum cooling blocks (minimize dome to dome thermal gradients).
- Test temperature controlled at 0C based on average upper dome temperature.
- Nameplate capacity of cells is 56 AH.

EAGLE PICHER
Eagle-Picher Technologies, LLC

POWER Subsystems

LIFETIME

- Test Uses High Rate 70% DOD Cycles to Accumulate Wear on the Cells
- Every 1000 Cycles the Cells are Run for 100 Cycles at 40% DOD as a Health Check

LIFETIME

- Test Temperature = 0C
- 70% DOD Cycles:
  - Charge at a C Rate With a Taper at the End of Charge
  - Discharge at a 1.2C Rate for 35 Minutes
  - RR = 105% to 110%, Total Cycle Time = 90 Minutes
- 40% DOD Cycles:
  - Charge at a C/2 Rate With a Taper at the End of Charge
  - Discharge at a C/1.45 Rate for 35 Minutes
  - RR = 105%, Total Cycle Time = 90 Minutes

EAGLE PICHER
Eagle-Picher Technologies, LLC

POWER Subsystems

DESCR[illegible] IN TEST

Cell Lot	Identifier	Positive Porosity	Positive Thick.	Electrolyte (%KOH)	# of Cells
Boiler Plate	Control	80% (slurry)	0.030"	31%	3
Boiler Plate	BP-V3	80% (slurry)	0.035"	26%	4
Boiler Plate	BP-V4	84% (slurry)	0.035"	26%	4
Engineer. Models	EM-V2	80% (slurry)	0.035"	31%	3
Pre-Flight	PFC	84% (dry sinter)	0.034	26%	2

✦ All cells are in pressure vessels.

EAGLE PICHER
Eagle-Picher Technologies, LLC

POWER Subsystems

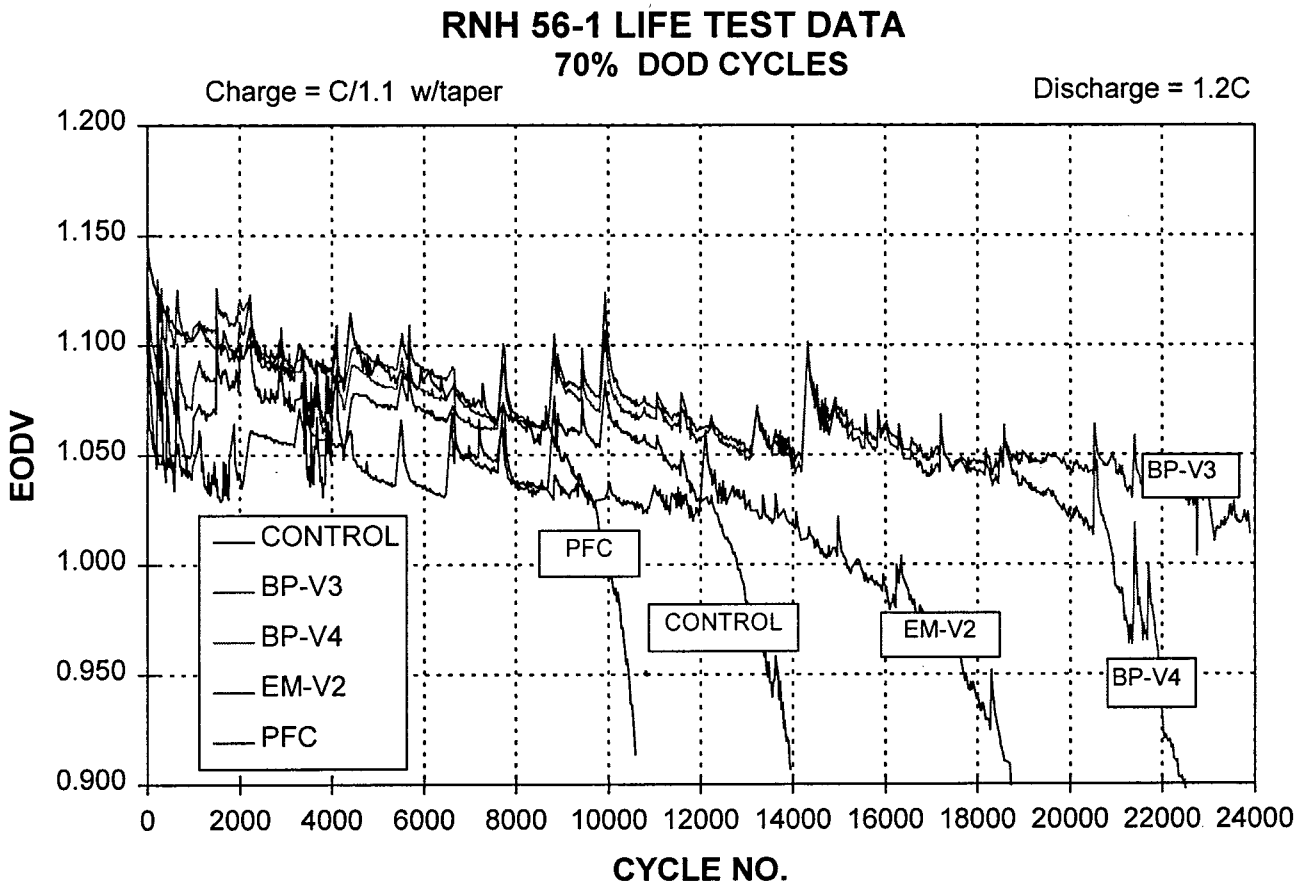

EAGLE PICHER
Eagle-Picher Technologies, LLC

POWER Subsystems

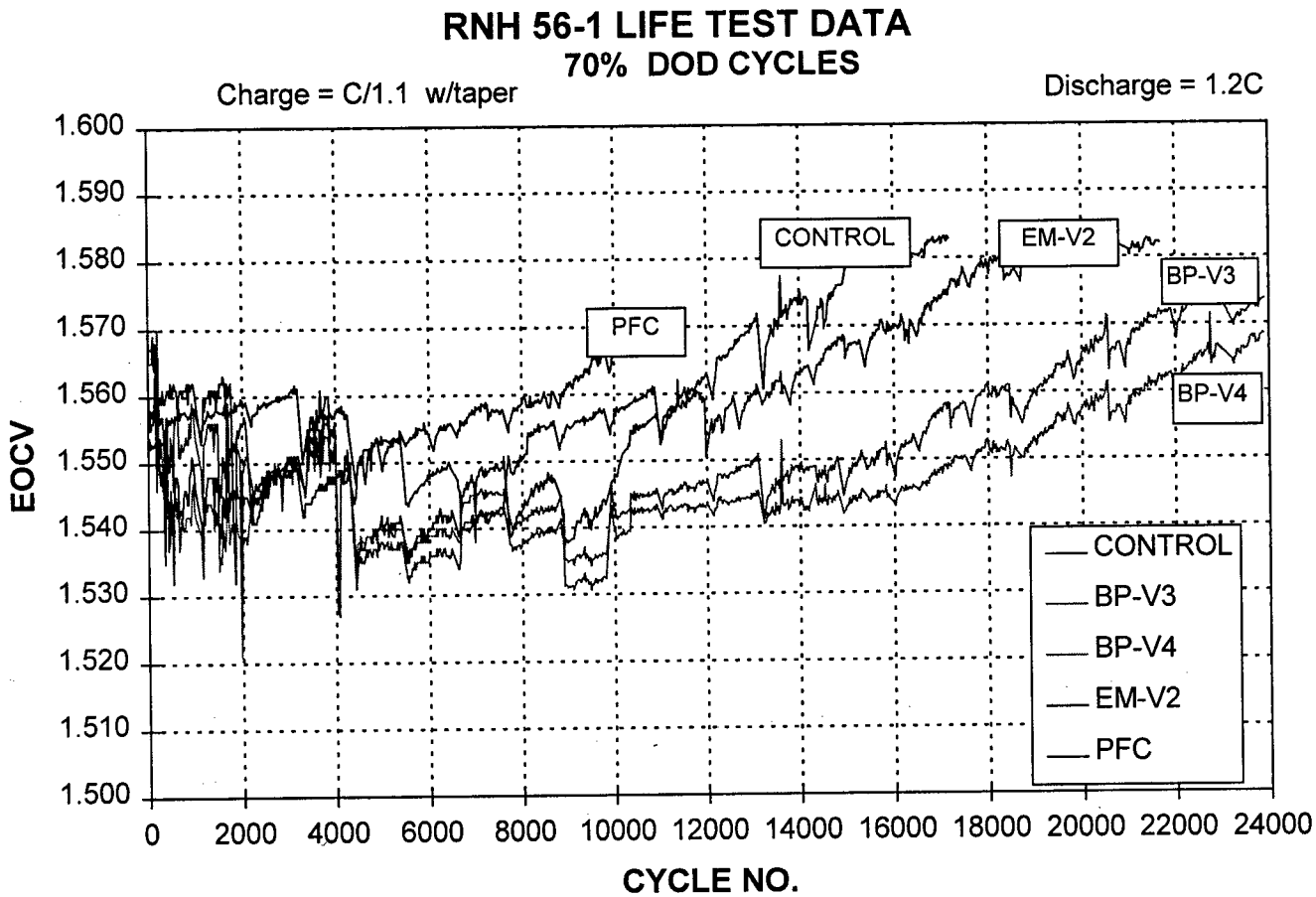

EAGLE PICHER
Eagle-Picher Technologies, LLC

POWER Subsystems

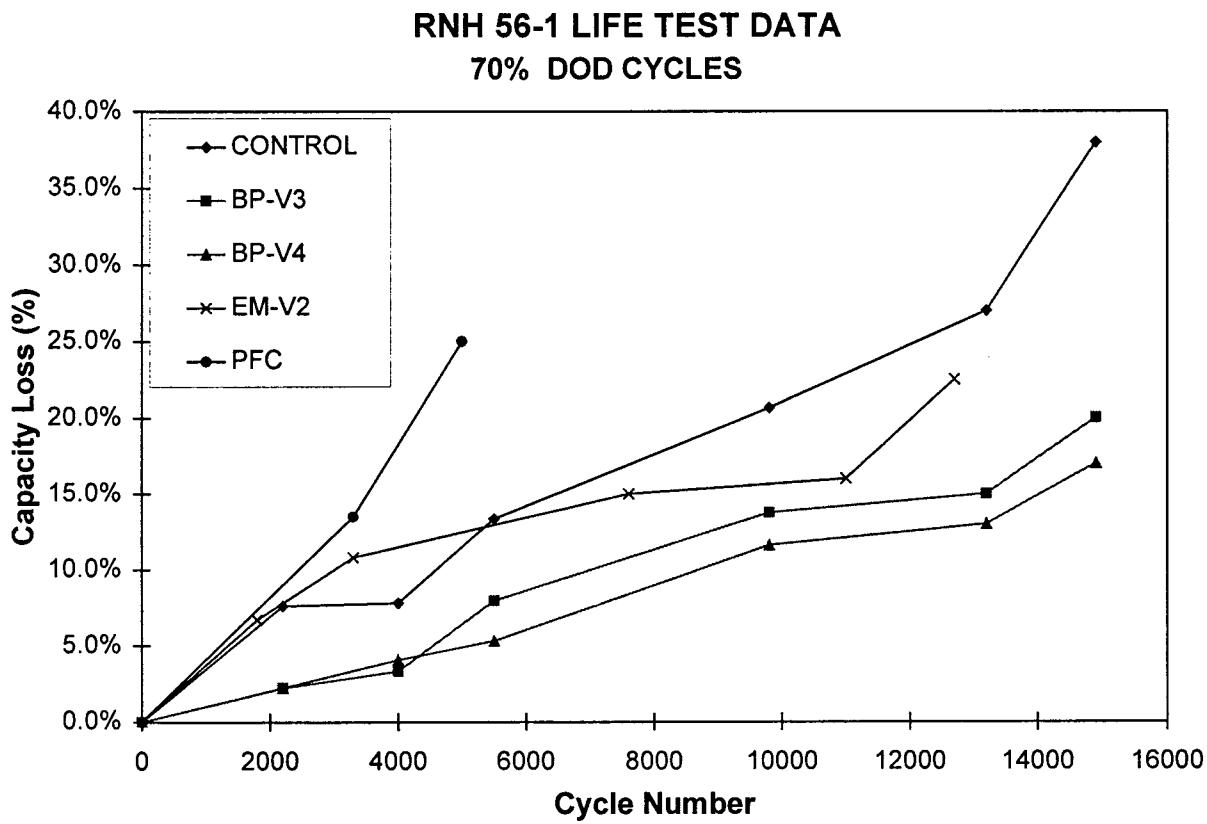

CELL [illegible] TESTS

- Two cells were removed from the test @cycle 15,800 for EOL performance characterization.
- These cells were a Control and BP-V4.
- The BOL Acceptance test was repeated on the cells.

CAPACITY TO 1.0V

CELL	0 deg C (AH)		10 deg C (AH)		20 deg C (AH)	
	BOL	EOL	BOL	EOL	BOL	EOL
Control	67.4	40.3	63.1	41.9	53.4	38.5
BP-V4	64.2	50.6	60.1	49.2	52.3	43.9

- Cells showed EOC pressure increase of 100 psig.
- BOL Specific Energy = 50 whr/kg (Control)
- BOL Specific Energy = 53 whr/kg (BP-V4)

- 35mil electrode cells have provided equivalent cycle life to the 30mil electrodes.
- 26% KOH cells have shown superior cycle life 31%KOH cells.
- Slurry electrodes have shown superior cycle life to dry sinter electrodes
- Cycle count is significant and can be used to update existing cycle life models.

AC[illegible]TS

- *Chris Guilfoyle:* Eagle-Picher Technologies, LLC
- *David Judd:* Eagle-Picher Technologies, LLC
- *Dan DeBiccari:* Space Systems/Loral

THE 1999 NASA AEROSPACE BATTERY WORKSHOP

LAUNCH AND EARLY ORBIT PHASE SIMULATION TESTS ON NICKEL HYDROGEN BATTERIES

P. J. JOHNSON *, S. W. DONLEY and B. STARRITT

TRW Space & Electronics Group
One Space Park, Redondo Beach, CA 90278

*E-mail: philip.johnson@physics.org

Abstract.

A series of experiments has been carried out with the objective of evaluating the performance of nickel-hydrogen batteries for a variety of scenarios that may be encountered pre-launch and during the early phases of launch and transfer orbit. Temperature of the battery was found to be a critical parameter. Excessive overcharge was found to be of no benefit for subsequent battery performance.

INTRODUCTION

This presentation describes a series of experiments designed to elucidate the behavior of nickel-hydrogen batteries subject to various launch site and early orbit phase scenarios. The on-station performance has been the subject of a series of life tests, which have been reported elsewhere [1].

There were several purposes behind these test: to gather information that could be used to accurately determine the battery capacity available at liftoff (Charge Stand and Capacity Maintenance Tests), to determine the battery behavior and effectiveness of charging at a specific voltage (Transfer Orbit Operation Simulation), and to optimize the pre-launch battery charge operations (Launch Preparedness Simulation and Trickle Charge During Cool-Down). The liftoff capacity determination and the transfer orbit operation data are used to estimate the energy available at spacecraft separation to support deployment contingencies.

PHASES

- Launch Pad

  This covers the period from the final pre-launch recondition to ignition

- Ascent

  This covers the period from ignition to spacecraft separation from the launch vehicle

- Transfer Orbit

  This covers spacecraft separation, solar array deployment, and station acquisition

These three phases cover the time from the final on the ground charge to the first post eclipse charge when the spacecraft is on-station.

TEST OUTLINE

- Charge Stand Matrix
- Launch Preparedness Simulation
  - Temperature
  - Charge return
- Transfer Orbit Operation Simulation
- Trickle charge during cool-down
- Capacity Maintenance Tests
  - Normal Trickle Charge
  - Low-rate Trickle Charge
  - Very Low-rate Trickle Charge

Normal rate for trickle charge is C/100; Low-rate trickle charge is C/330 and very low-rate trickle charge is C/1000. The "Trickle charge during cool-down test was combined with the capacity maintenance tests.

TEST ARTICLE

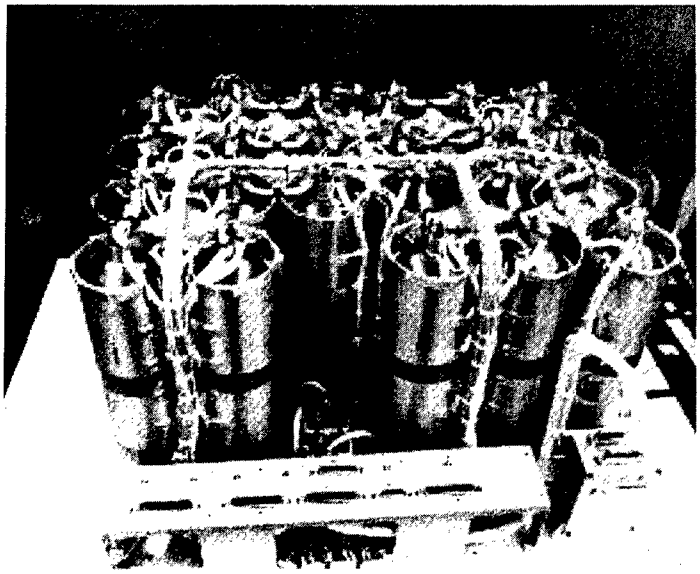

The battery under test comprised of 23 series connected 98 Ah cells. The cells were provided by Eagle-Picher LLC of Joplin, MO. They were a dual stack back-to-back design with a single layer Zircar™ separator. The battery was designed, manufactured and tested by TRW Space and Electronics Group.

The cells were assembled into an Engineering Model (EM) battery with full flight configuration. Each cell is constrained within an aluminum sleeve. Electrical insulation is provided by a layer of Cho-therm™ coated on both sides with RTV-11. The cell sleeves were then mounted on an aluminum baseplate. The 23 cells were arranged in an 6 x 4 array, with the spare 'slot' used to accommodate battery electronics.

DIFFERENCES BETWEEN CELL AND BATTERY TESTS

There are differences between the way cells and batteries are tested:

CELLS:	BATTERIES:
Tested isothermally to within 3°C	Cold plate held at constant temperature. Battery allowed to float thermally as it would operationally.
Discharged at constant current, C/2	Discharged at constant power as defined by system power budget.
One hour open circuit stand between charge and discharge phases	Four hour stand on trickle charge (C/100) between charge and discharge phases

Cells undergo an industry standard acceptance test on receipt from the manufacturer. This allows comparison of a given lot of cells with previous lots of cells, which may have been procured for different missions with considerably different operational characteristics, for example GEO and LEO missions. The testing of cells closely followed the guidelines given in reference 2.

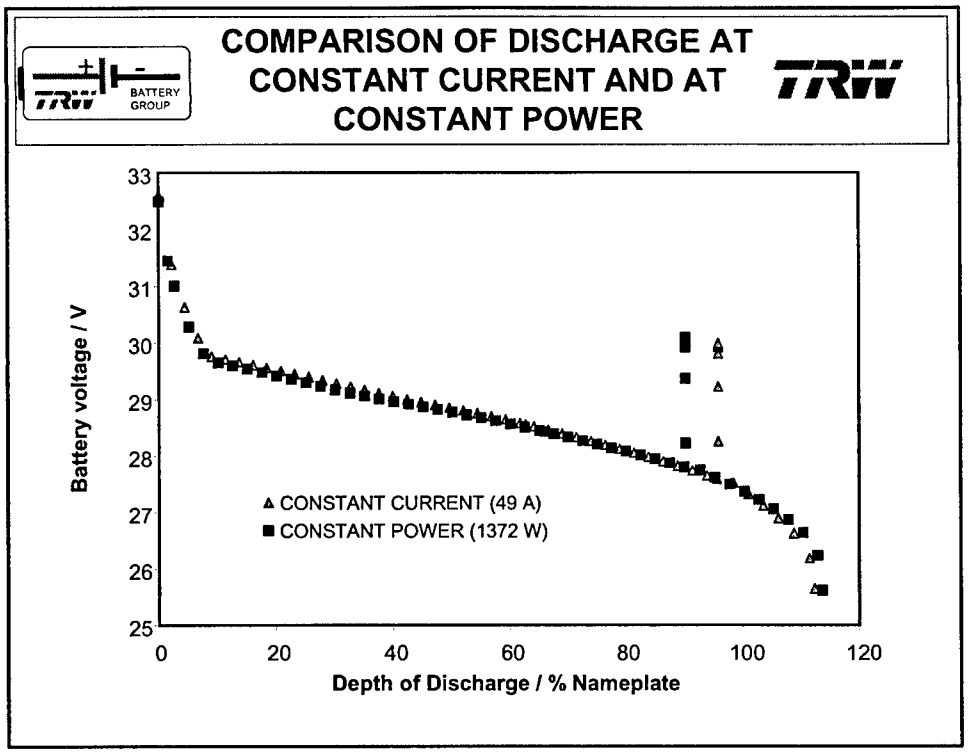

The discharge was interrupted when the battery temperature reached 27°C and the battery was allowed to cool on open circuit until its temperature had reached 18°C, when the discharge was resumed. Discharge was terminated when the battery voltage reached a lower limit of 24.15 V, which corresponded to an average of 1.05 V per cell. Note that this occurred much later than the maximum expected operational depth of discharge of 65%.

CHARGE STAND MATRIX

TEST	CAPACITY / Ah	NOTES
Reference 20°C	94·65	
72 hour stand at 20°C	76·64	81% of Reference

The matrix consisted of one reference capacity cycle followed by one charge-discharge cycle with a 72 hour stand time. The stand time began once the battery had reached thermal equilibrium. The temperature was measured as the average of the cell sleeve top temperatures. In each cycle the charge and stand was held at 20°C while the discharge commenced with the battery stabilized at 4°C. The capacity returned after the 72-hour open-circuit stand at 81% of the reference test compares favorably with the result obtained during cell acceptance testing.

TEMPERATURE LIMITED CHARGING

TEST TEMPERATURE		CAPACITY / Ah	VOLTAGE @ 1·32 h / V	NOTES
START	FINISH			
13°C	27°C	104·85	28·713	Tripped after 13·20 h on charge
13°C	18°C	100·36	28·892	Tripped after 12·03 h on charge
21°C	22°C	69·39	*	Tripped after 8·33 h on charge
21°C	27°C	92·58	28.860	Tripped after 12·00 h on charge
25°C	27°C	74·70	28·710	Tripped after 9·50 h on charge

* DISCHARGE TERMINATED EARLY

The battery was charged to a preset end-of-charge temperature at the sleeve-top, followed by equilibration at 4°C (39°F) and discharge to 24.15 V (the battery was fully discharged to measure capacity but voltage data are recorded after 79·2 minutes, corresponding to 65% DOD).

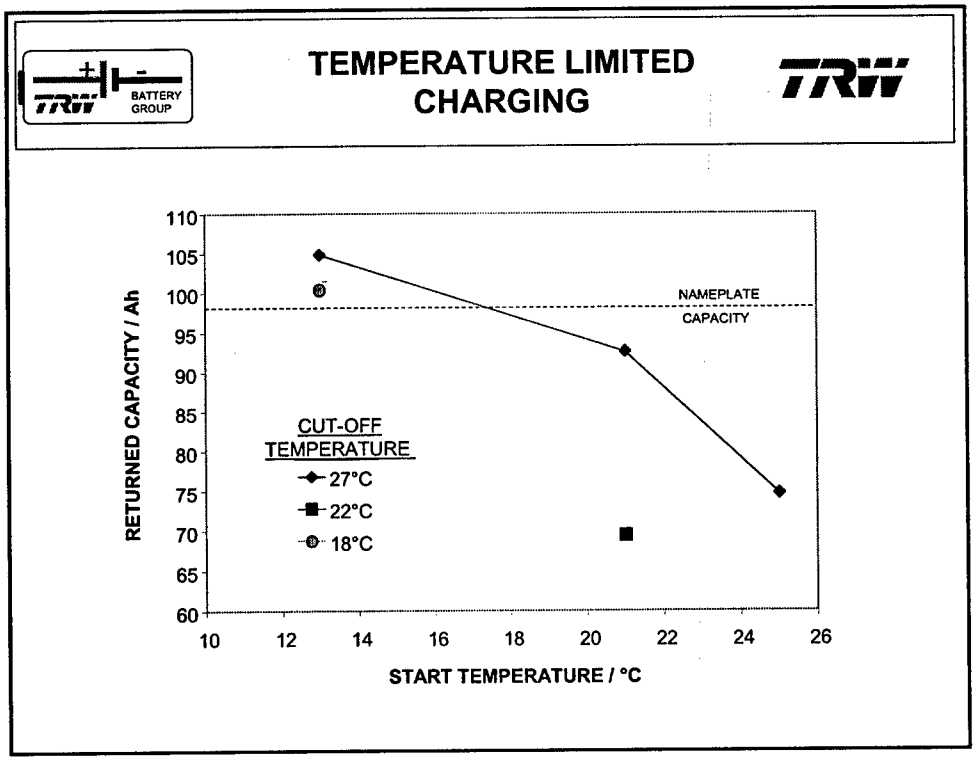

The above chart shows the delivered capacity at 4°C following a temperature limited charge. The temperature limit and the charge start temperature were variables. Capacity in excess of nameplate was only achieved at the lowest start temperature. Raising the cut off temperature from 18°C to 27°C led to only a marginal increase in delivered capacity.

CHARGE RETURN AFTER RECONDITIONING

TEST	CAPACITY / Ah	VOLTAGE @ 1·32 h / V	NOTES
ID#1 140%	101·18	28·68	Over Temperature after 13·2 h on charge
ID#2 160%	100·68	28·60	First (of three) Over Temperature after 13·1 h on charge
ID#3 185%	105·61	28·62	First (of three) Over Temperature after 13·2 h on charge. Cooling fault.
ID#4 110%	90·73	28·99	
ID#3 185% R	102·38	28·65	First (of four) Over Temperature after 13·2 h on charge. R = Retest.
ID#6 120%	100.36	28.89	Performed during temperature tests
ID#7 132%	104.85	28.71	Performed during temperature tests

In this series of tests, the battery was discharged to 24.15 V and the delivered capacity multiplied by the recharge ratio was then recharged at constant current. Note that only when the recharge ratio was less than 140% could the battery be recharged without interruption.

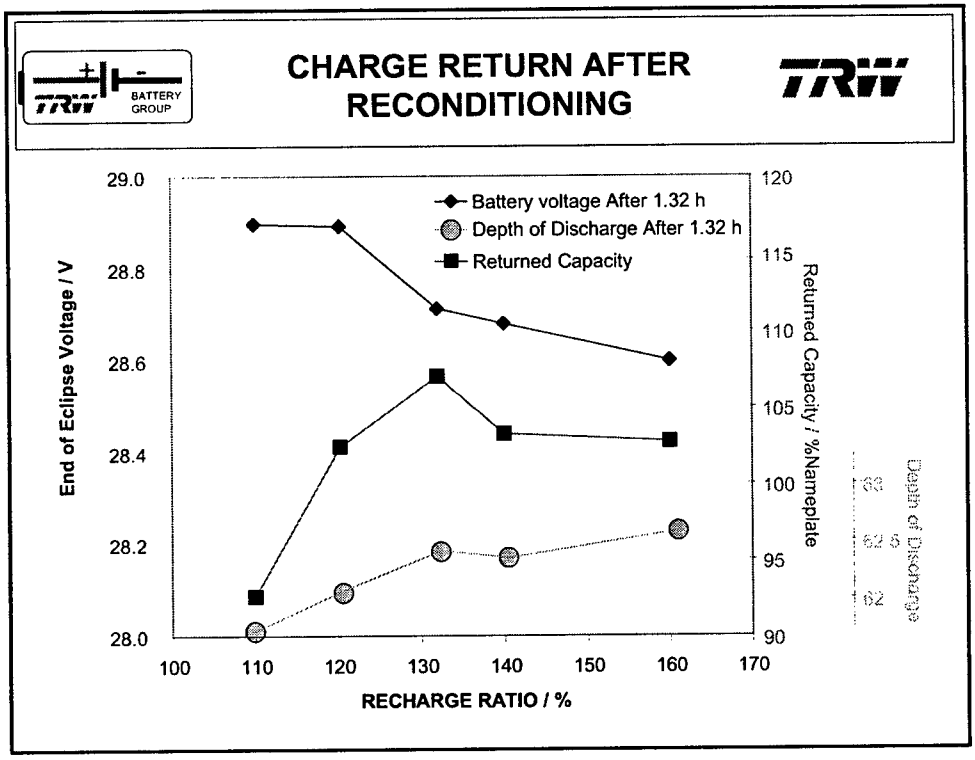

This chart shows the results of the launch pad simulation tests to determine optimum recharge ratio following a reconditioning. Optimum capacity is obtained with a recharge ratio of 130%. Higher recharge ratios necessitate interruption of the charge phase to prevent the battery overheating. This may explain the poorer capacity response at high recharge ratios. Excessive overcharge depresses the discharge voltage during the useful part of the discharge curve, I.e., during the maximum of 1.32 h of eclipse discharge. Depth of discharge also increases slightly to compensate for this voltage depression.

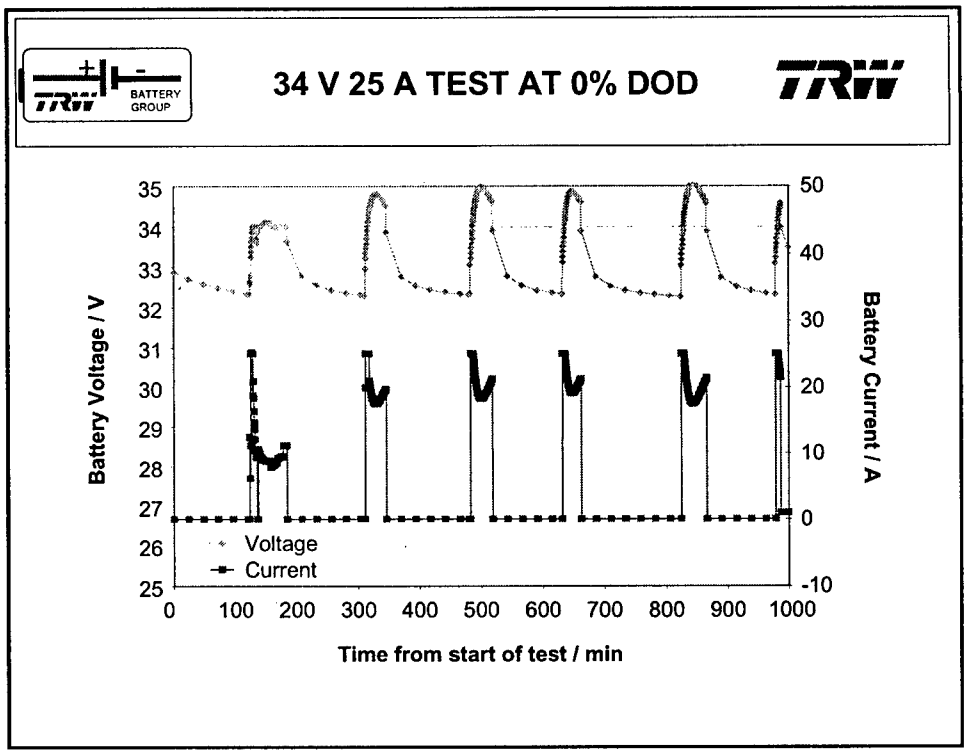

As the battery is fully charged all the charge current is converted to heat and the battery temperature rose quickly to its safety limit.

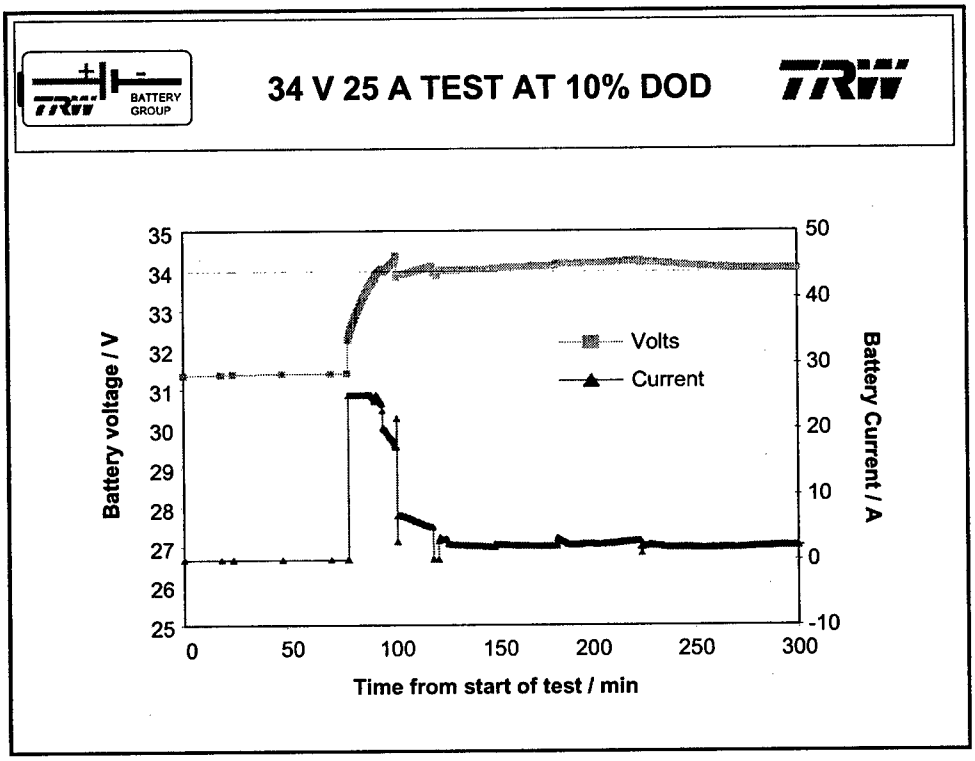

The response curve starting at 10% DOD is shown above. At the start of charge the charge is current limited. Little heat is generated when the charging efficiency is high and 6·5 Ah is returned to the battery before its voltage begins to throttle the charge current. As the battery is still cool, the current falls rapidly, and a steady state is reached after approximately one hour on charge, and now the battery resistance is 17 Ω. The average battery temperature was below 8°C throughout the entirety of the charge phase of this test.

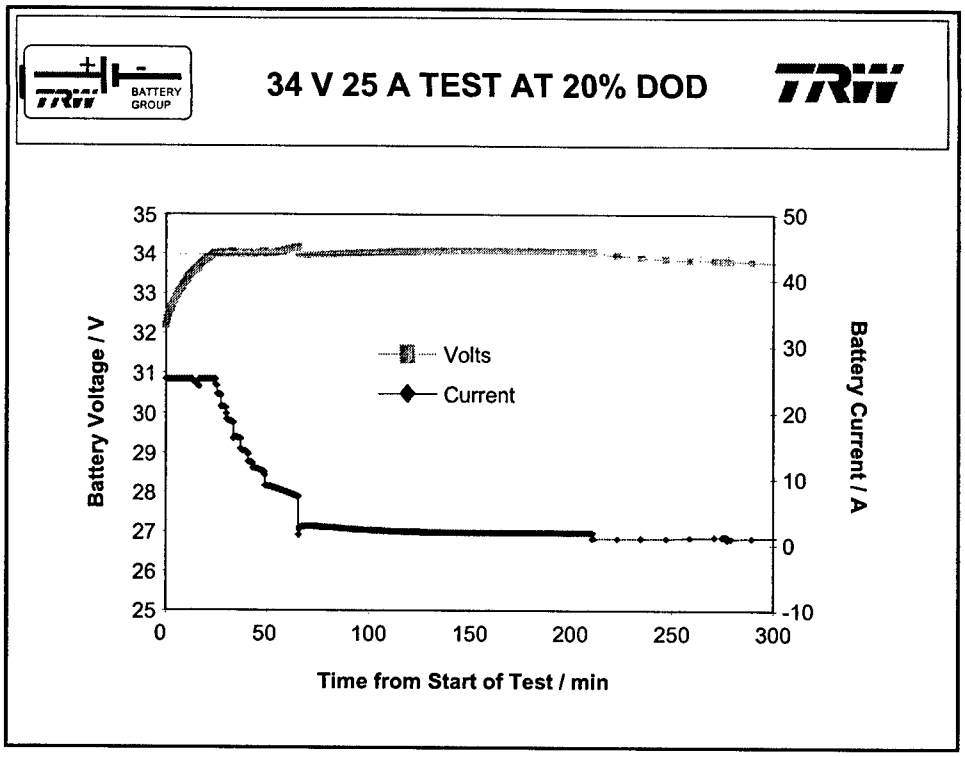

A similar response is achieved starting at 20% DOD, as shown in this figure. 24 minutes into charge the battery voltage restricts the current and by two hours into the test steady state is once again reached with the battery resistance at 17 Ω. Following charge, the discharge cycle delivered 101·64 Ah. The average battery temperature was below 6°C throughout the entirety of the charge phase of this test.

CAPACITY MAINTENANCE

TEST	CAPACITY / Ah	NOTES
Standard Capacity	111·05	Charge 14 h @ C / 10, trickle 1 A for 4 h, open 2 h.
Capacity Maintenance 1	99·02	Trickle 300 mA for 42 min., 98 mA for 8h 48 min.
Capacity Maintenance 2	84·53	Trickle 300 mA for 42 min., open 24 h, 106 mA for 9h 27 min.
Capacity Maintenance 3	87·48	Trickle 300 mA for 42 min., 98 mA for 33 h 09 min.

The capacity maintenance tests were preceded by a standard reference capacity test to demonstrate the battery was fully reconditioned after it had been on open circuit following the transfer orbit simulation tests. The capacity returned (111·05 Ah) compared favorably with the standard capacity value obtained in the preceding test (113·70 Ah).

The first capacity maintenance cycle had no experimental stand period. Following charge, the trickle charge rate was 300 mA until thermal stability at 22°C was obtained. The period spent on trickle charge was recorded for use in the subsequent tests. Temperature was reduced to 4°C prior to discharge, and trickle charge at 98±5 mA was applied during this cool down period. A capacity of 99·02 Ah was delivered.

Cycle 2 was the same as cycle 1 with the addition of a 24-hour stand at 22°C. This test delivered 84·53 Ah, suggesting that 14·49 Ah (14·8% of nameplate) were lost during the stand period.

Cycle 3 repeated cycle 2 but with 98 mA trickle charge applied during the stand period. This test delivered 87·48 Ah, some 2·95 Ah more than cycle 2. As the trickle charge only added 0·098 x 24 h = 2·35 Ah, this difference cannot be attributed to the trickle charge alone. As the application of trickle charge necessitates the application of an over-potential to the battery, it seems reasonable to assume that the applied potential acted as a 'float' voltage and reduced the self discharge rate of the battery.

SUMMARY

- A low start of charge temperature gives best charge acceptance
- Excessive overcharge yields little benefit. Optimum recharge ratio for capacity is 130%, but for voltage is 110%
- Battery polarization can prevent thermal runaway; fully charged batteries do not polarize sufficiently.
- Trickle charge during battery cool-down from an over-temperature condition is unnecessary

REFERENCES

1. "Orbital simulation life tests of nickel-hydrogen batteries with additional non-eclipse cycles", P. J. Johnson, S. W. Donley, and D. C. Verrier, J. Power Sources 76 (1998) 210-214.
2. "NASA Handbook for Nickel-Hydrogen Batteries", J. D. Dunlop, G. M. Rao, and T. Y. Yi, NASA Reference Publ. 1314, Sept. 1993.

ACKNOWLEDGEMENTS

The authors are indebted to:

- Many colleagues at Space Park for their constructive comments and fruitful discussions
- The staff of TRW's battery test facility who performed these experiments and collected the data
- The US Government for funding this work and the program sponsor for permission to publish this paper

TRW

EOS-PM Nickel-Hydrogen Cell Initial Life Test Report

R. F. Tobias
TRW Space And Electronics Group
Redondo Beach, California

The 1999 NASA Aerospace Battery Workshop
The Huntsville Hilton
Huntsville, Alabama
November 16-18, 1999

EOS-PM

TRW

- Objective- To provide cloud, precipitation, sea surface temperature, terrestrial and oceanic productivity and atmospheric temperature data for Global Modeling
- Launch on a Delta II MELV in December 2000
- Polar, sun synchronous, 705 km orbit with the 1:30 PM nodal crossing
- Spacecraft weight is approximately , 2,933 Kg
- Six year mission

Spacecraft Configuration

TRW

Overall Dimensions
(Stowed)
X= 255.9 in.
Y= 98.1 in.
Z= 105.9 in.

Overall Dimensions
(Deployed)
X= 316.7 in.
Y= 657.8 in.
Z= 164.4 in. (Bus)
Z= 190.1 in. (S/A)

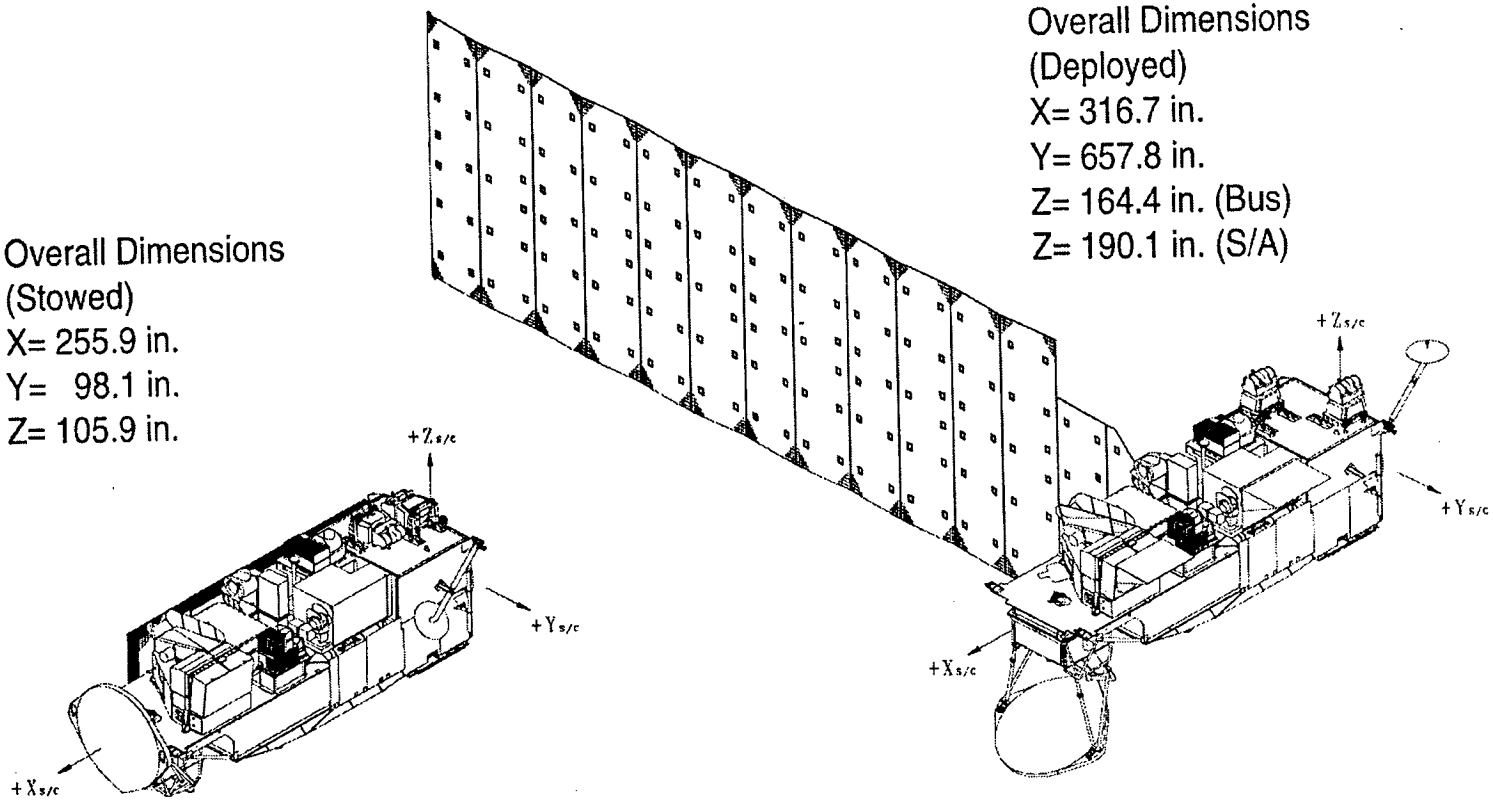

Electrical Power

TRW

- EPS via software provides power management, load shedding control, and battery management
- Electrical power is provided by the solar array and flight battery modules on orbit and a flight battery or ground power during prelaunch preparations
- Spacecraft power is nominally 22.0 - 38.6 Vdc
- Circuit protection is provided by fusing, battery clamping overvoltage protection, bonding and grounding , and EMC controls
- Battery consists of 24 series-wired 160 Ah NiH2 cells contained in two-12 cell modules
  - Rate of charge is automatically controlled by charge determination and depth-of-discharge control software

Battery Assembly

TRW

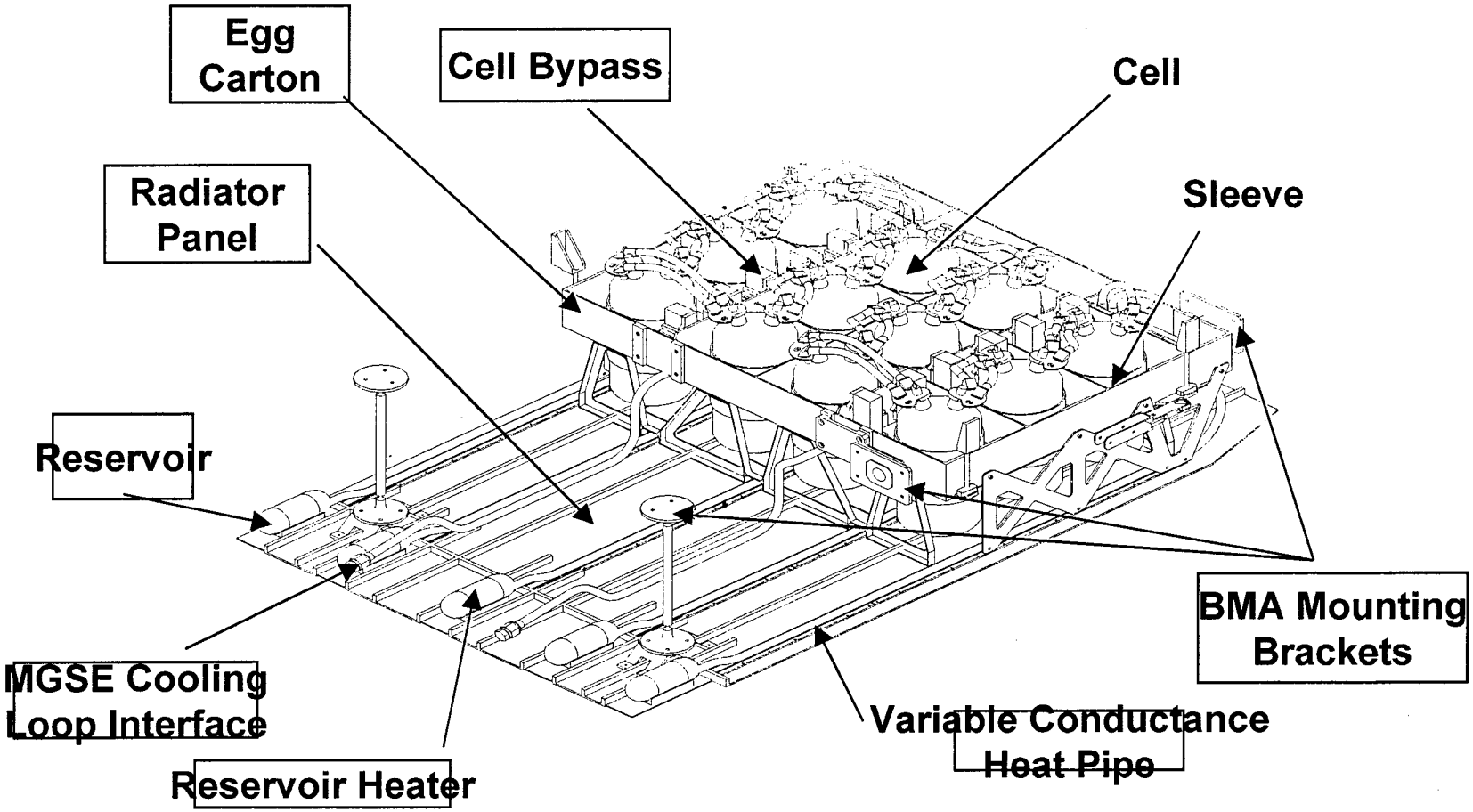

NiH_2 160 AH Cell

TRW

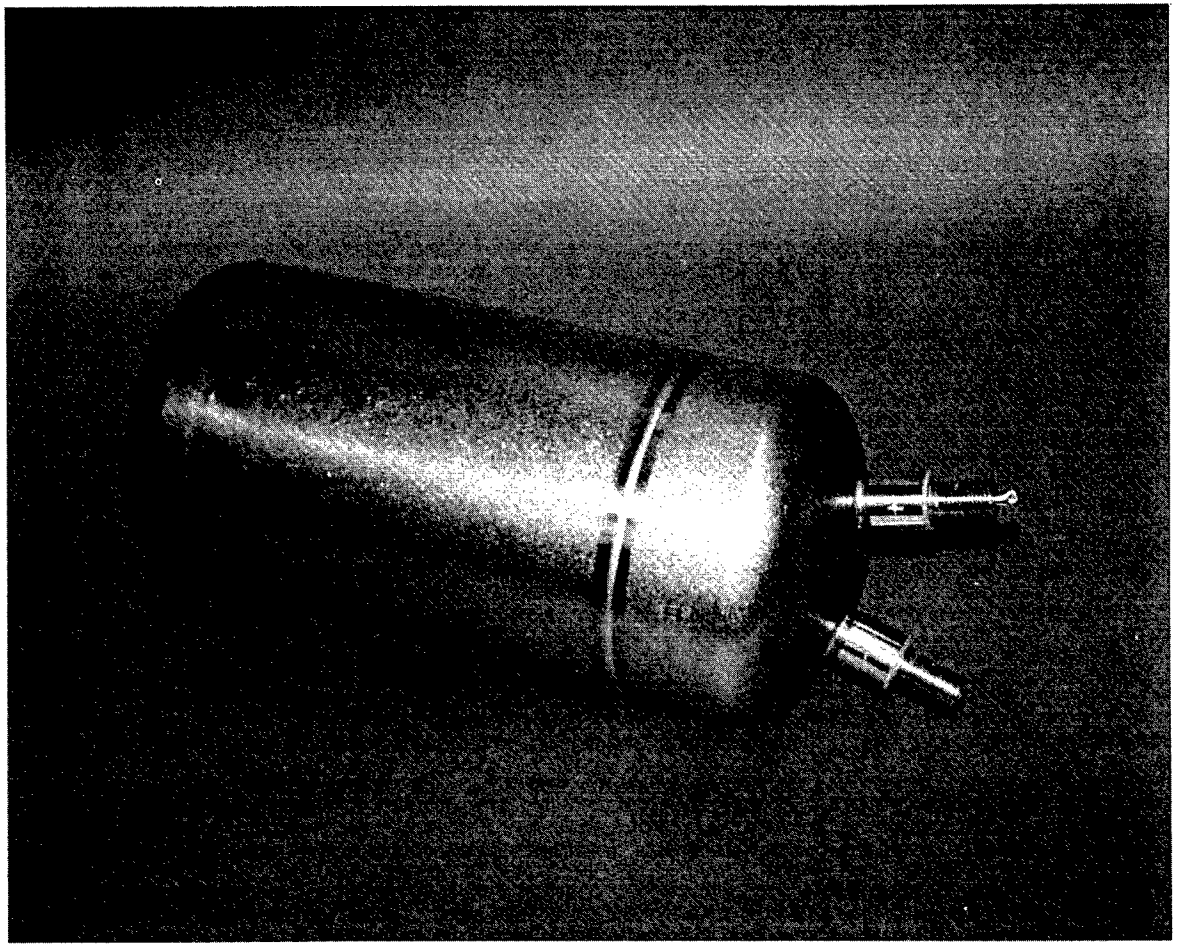

Cell Design

TRW

• Configuration	
– Stack	Single
– Electrode arrangement	Back-to-Back
– Bussing	"Pineapple shape"
• Internal coating	Zirconium oxide wall wick with catalyzed wall stripes
• Terminals	
– Seals	Ziegler nylon compression
– Placement	Rabbit ears
• Negative Electrodes	
– Number	64
– Substrate	Electro etched nickel foil
– Pt Loading	8 mg/cm^2

Cell Design (con't)

TRW

- Positive Electrodes
  - Number — 64
  - Plaque — Slurry
  - Thickness — 0.030 inch
  - Porosity — 80 %
  - Impregnation — Aqueous electrochemical
  - Active Material Loading — 1.65 g/cc void
- Separator
  - Type — Zircar
  - Layers — Two
- Electrolyte
  - Type — KOH
  - Concentration — 31 %
  - Precharge — Nickel

Experimental Design

TRW

- Test consists of two 6-cell packs
- Configuration designed to simulate conductive thermal design of the spacecraft battery
- Cells mounted in aluminum sleeves and placed on a mounting platform which contains cooling coils to control temperature
- Entire assembly is located in an insulated chamber

Cell / Sleeve Arrangement

TRW

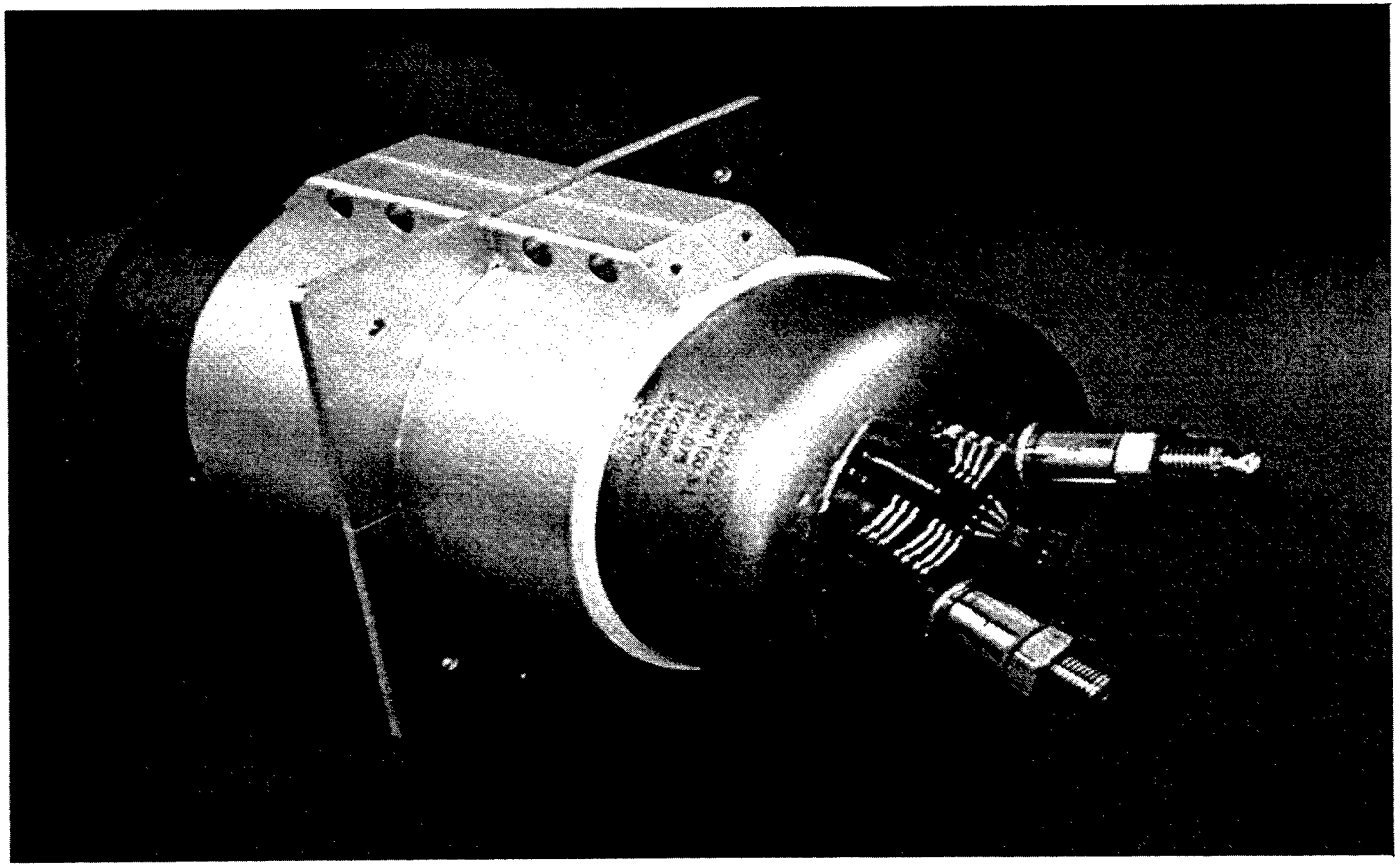

Bottom View of Cell Pack

TRW

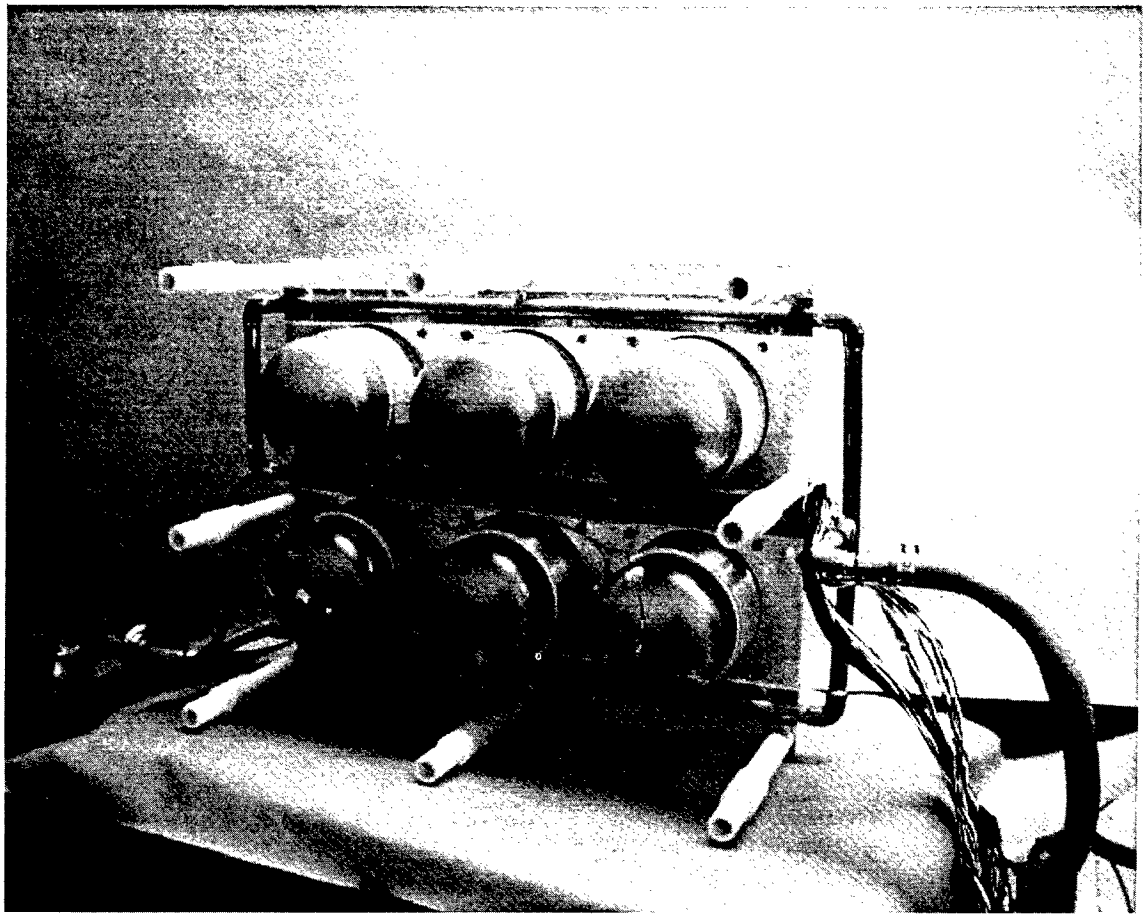

Cell Packs

TRW

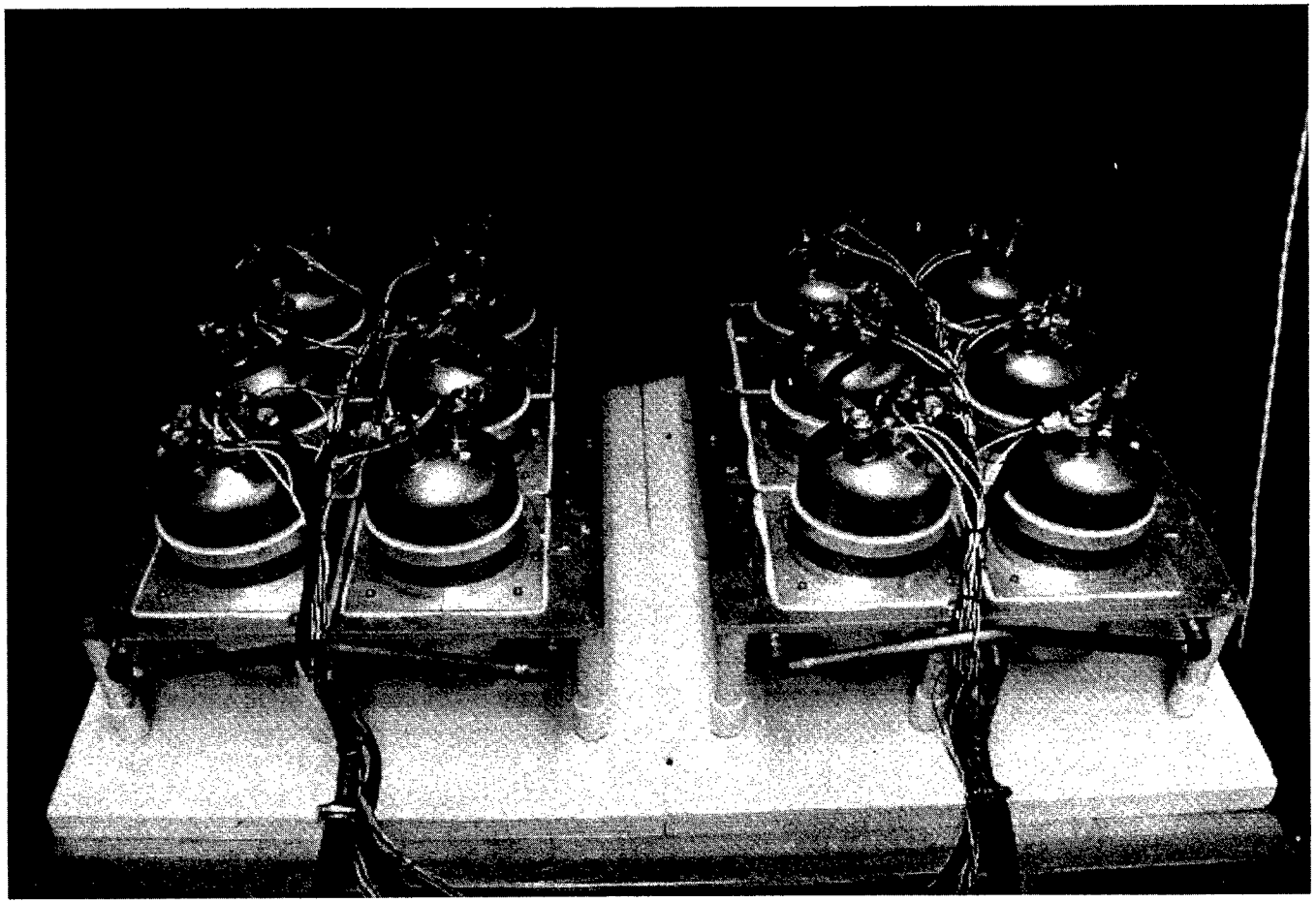

Experimental Setup

TRW

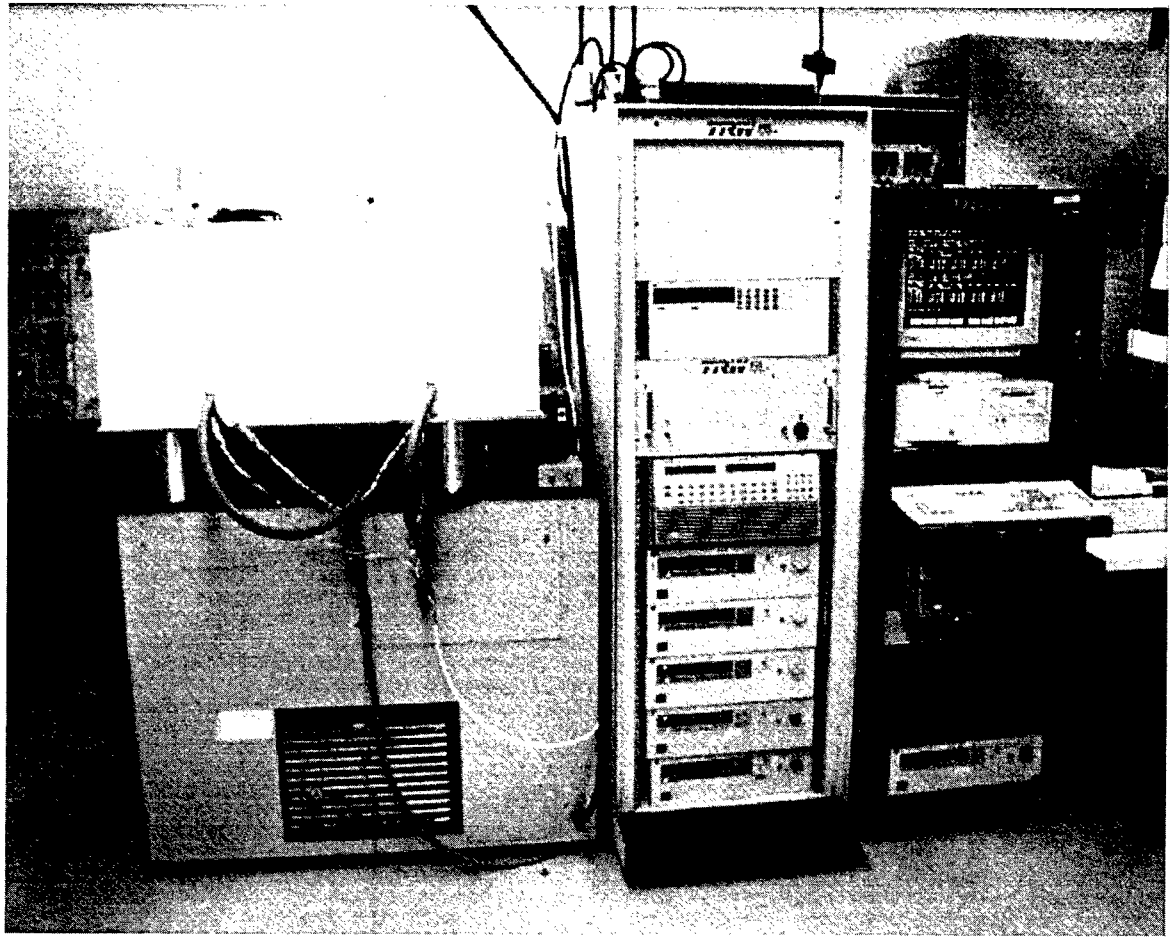

Experimental Conditions

TRW

- Real Time LEO Condition
- Total orbit time: 94.6 minutes
- Depth-of-discharge: 25 % nominal
- Constant power discharge: 550 watts for 34.8 minutes
- Charge to a given RR:
  - Initial current Approximately 45 amps
  - Taper current To 32 amps
  - Trickle current 1.6 amps for 2 minutes minimum

Baseline Capacities
Cell Potential vs Time

TRW

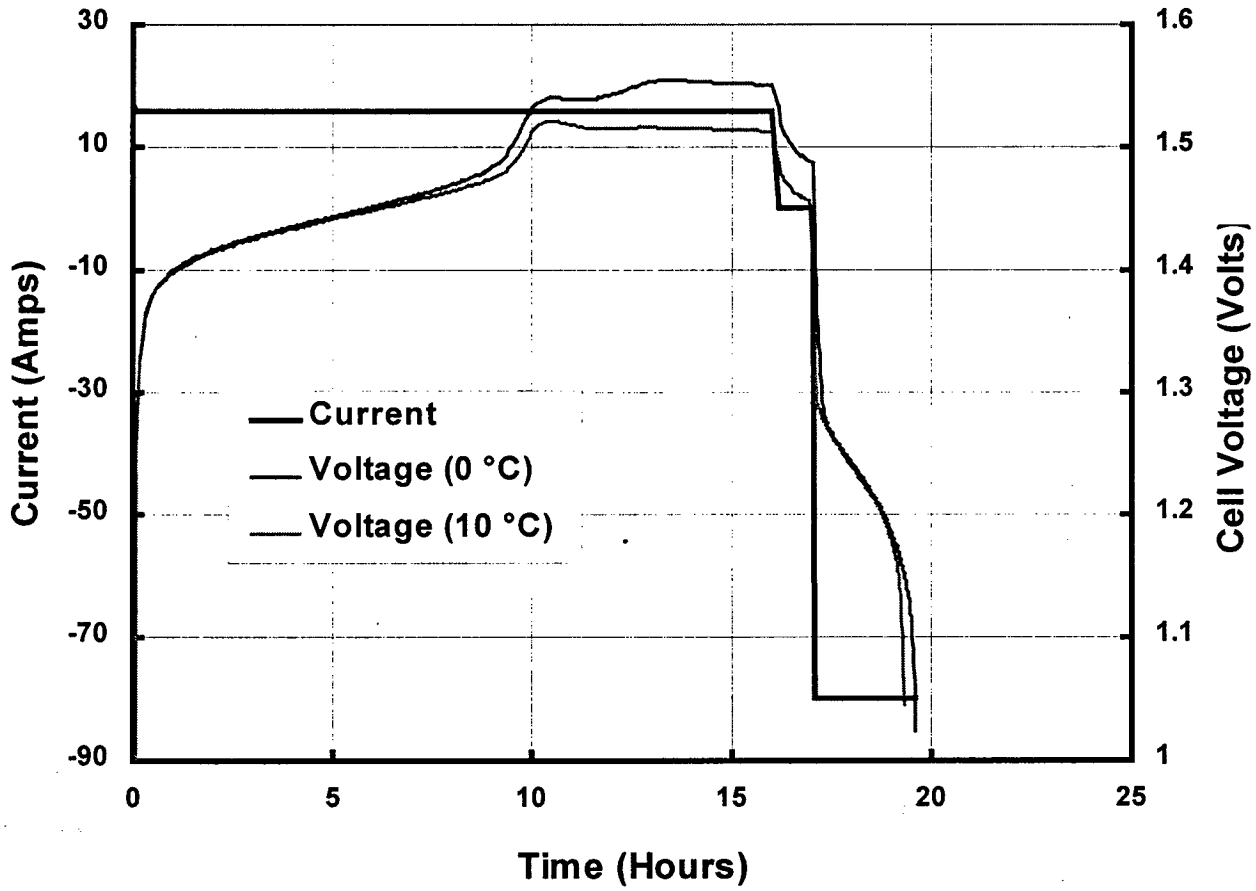

Cell Capacity Comparison
(Nameplate Capacity = 160 Ah)

TRW

	TRW		Eagle-Picher
Temp	ATP	Life Test	ATP
20 Deg C	162.6		146.9
10 Deg C	184.0	186.7	170.4
0 Deg C	202.8	200.1	186.9

EOS Life Test
Current - Voltage Curve

TRW

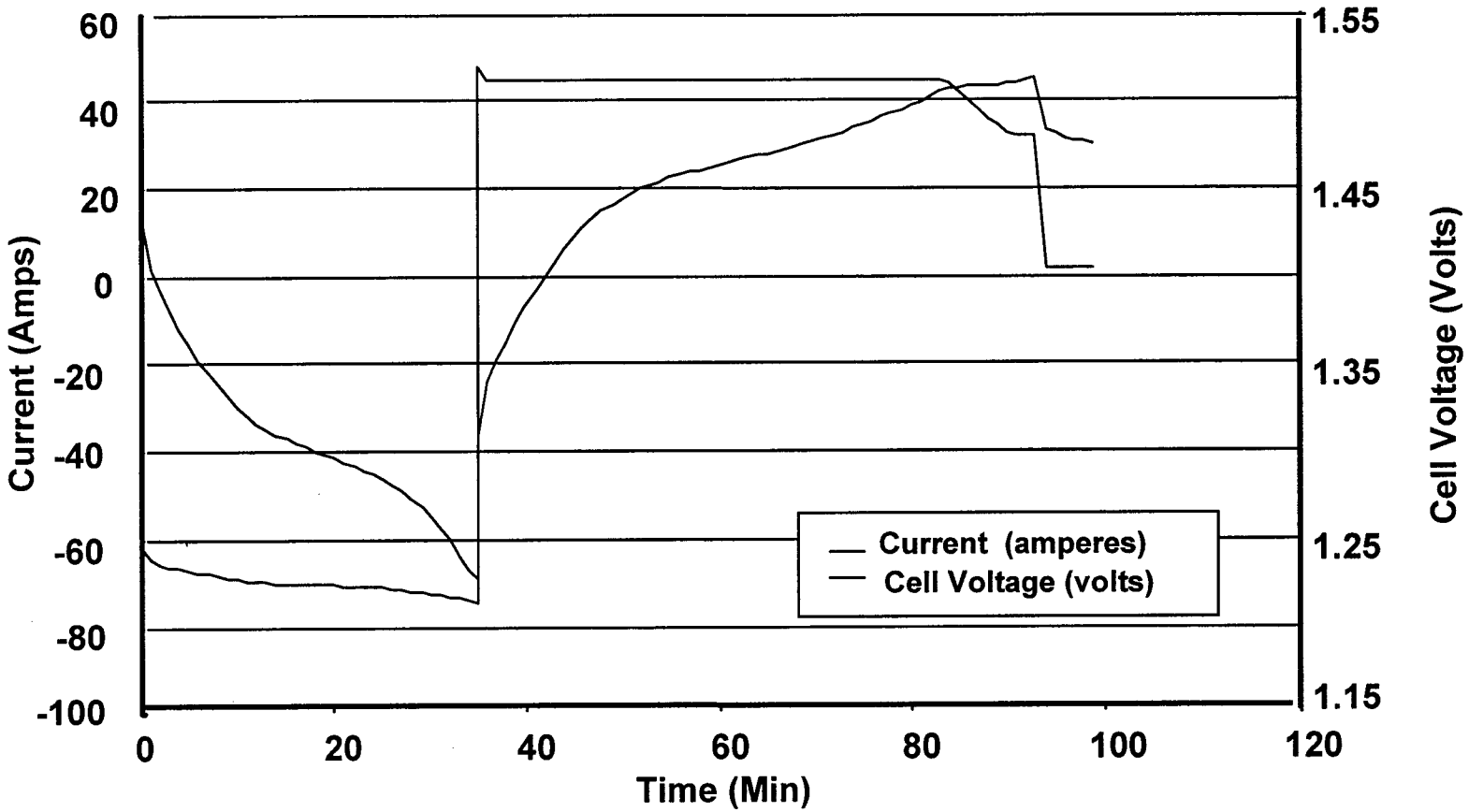

Pack Voltage vs. Cycle

TRW

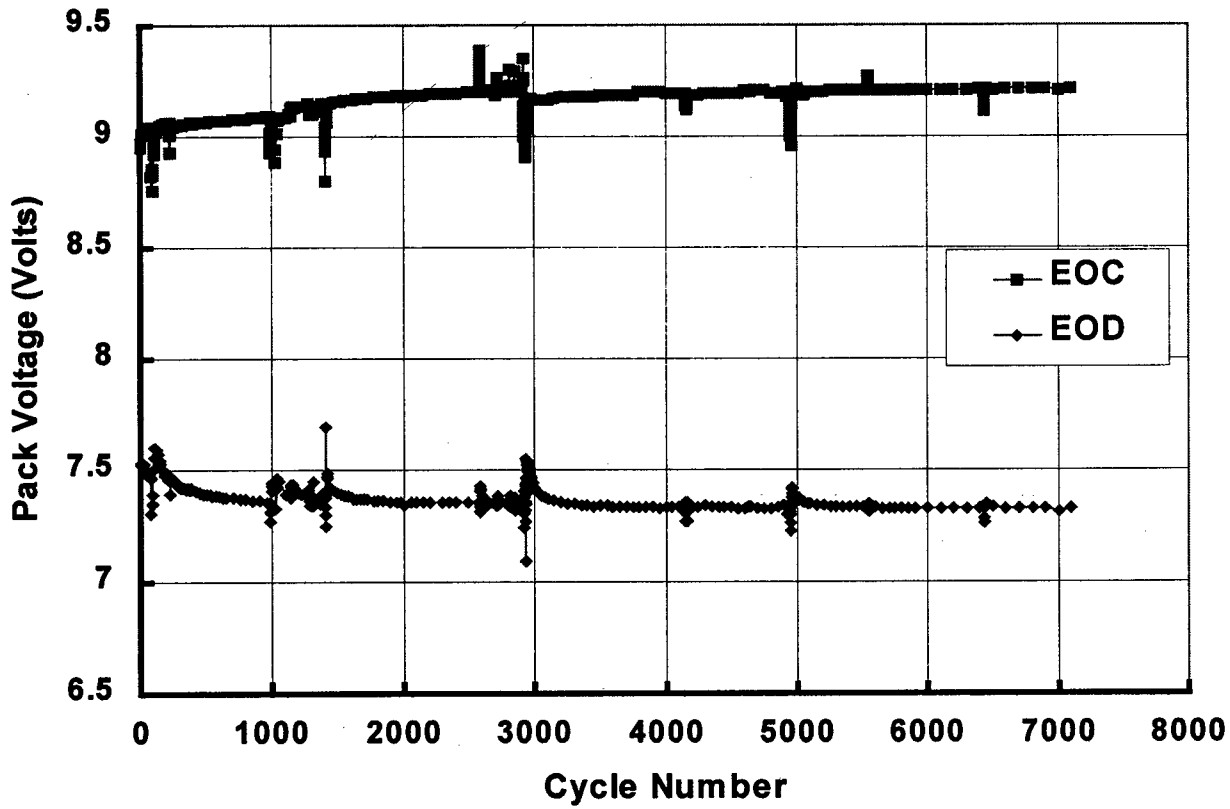

Discharge Voltage vs. Cycle

TRW

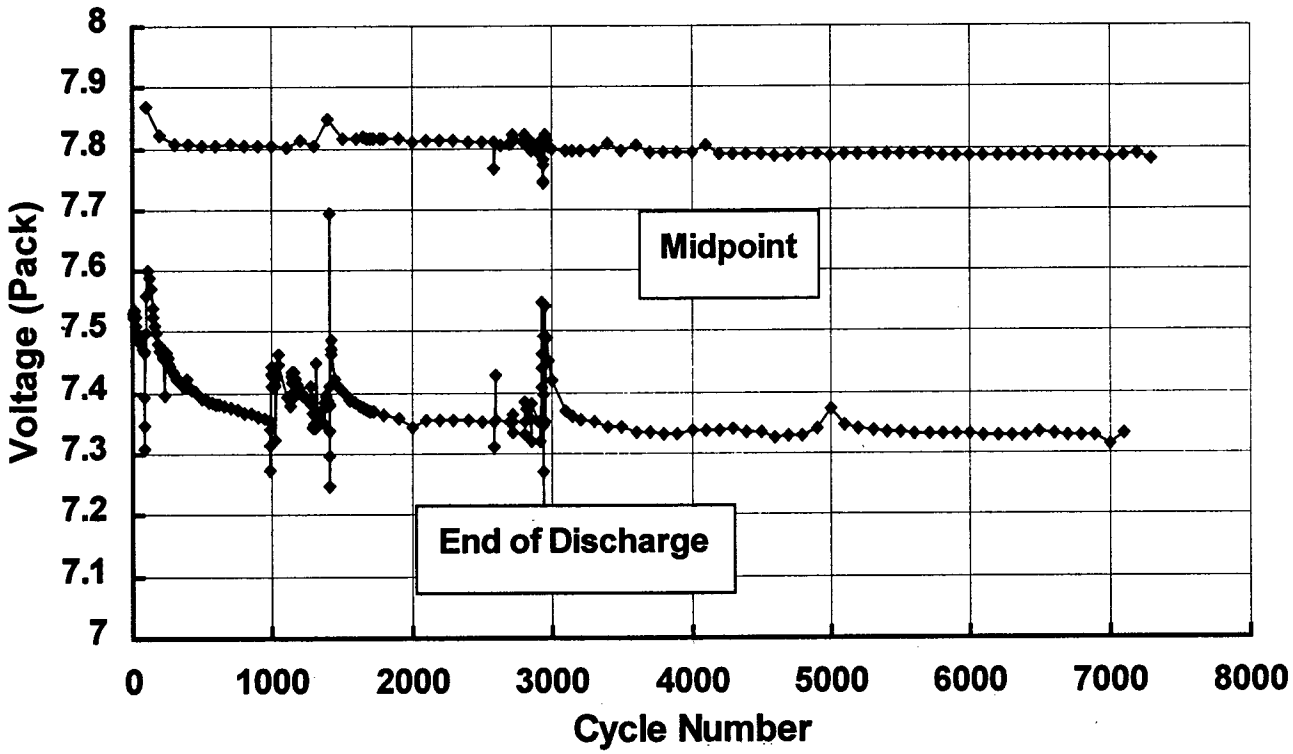

Pressure vs. Cycle

TRW

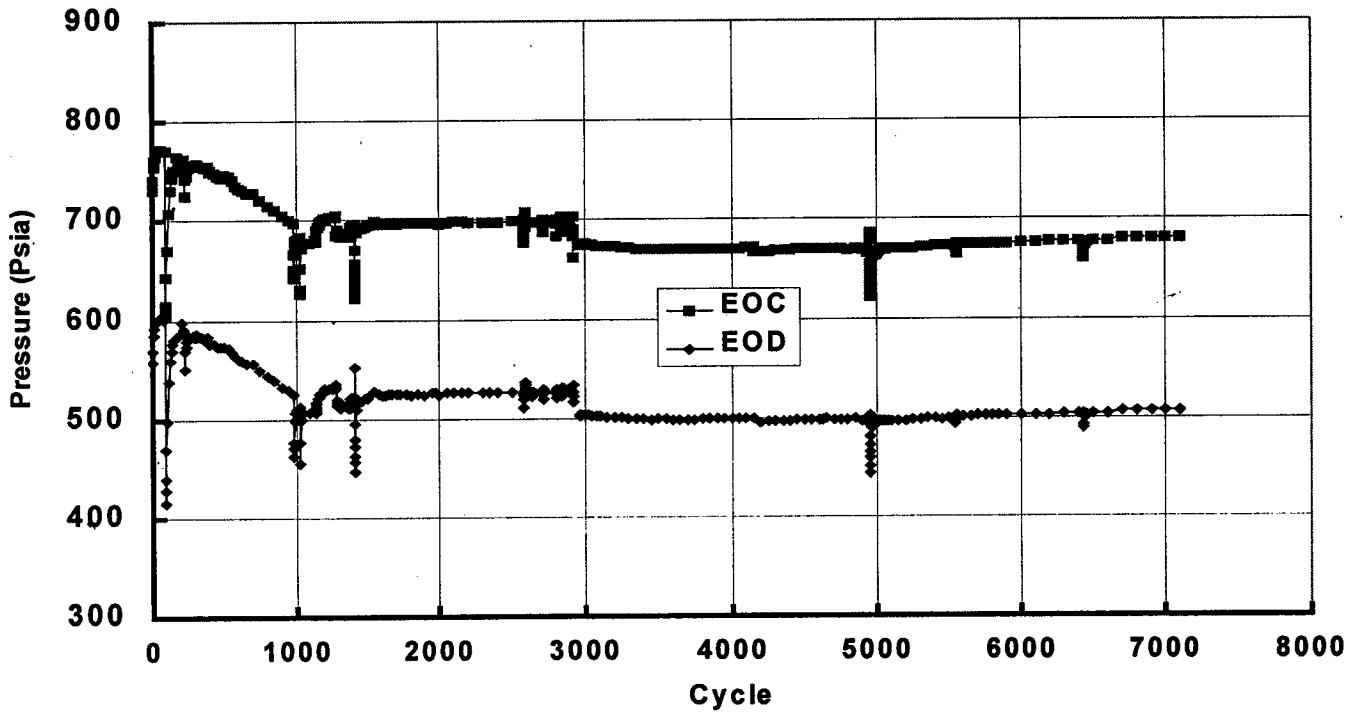

Recharge Ratio & Pressure vs. Cycle

TRW

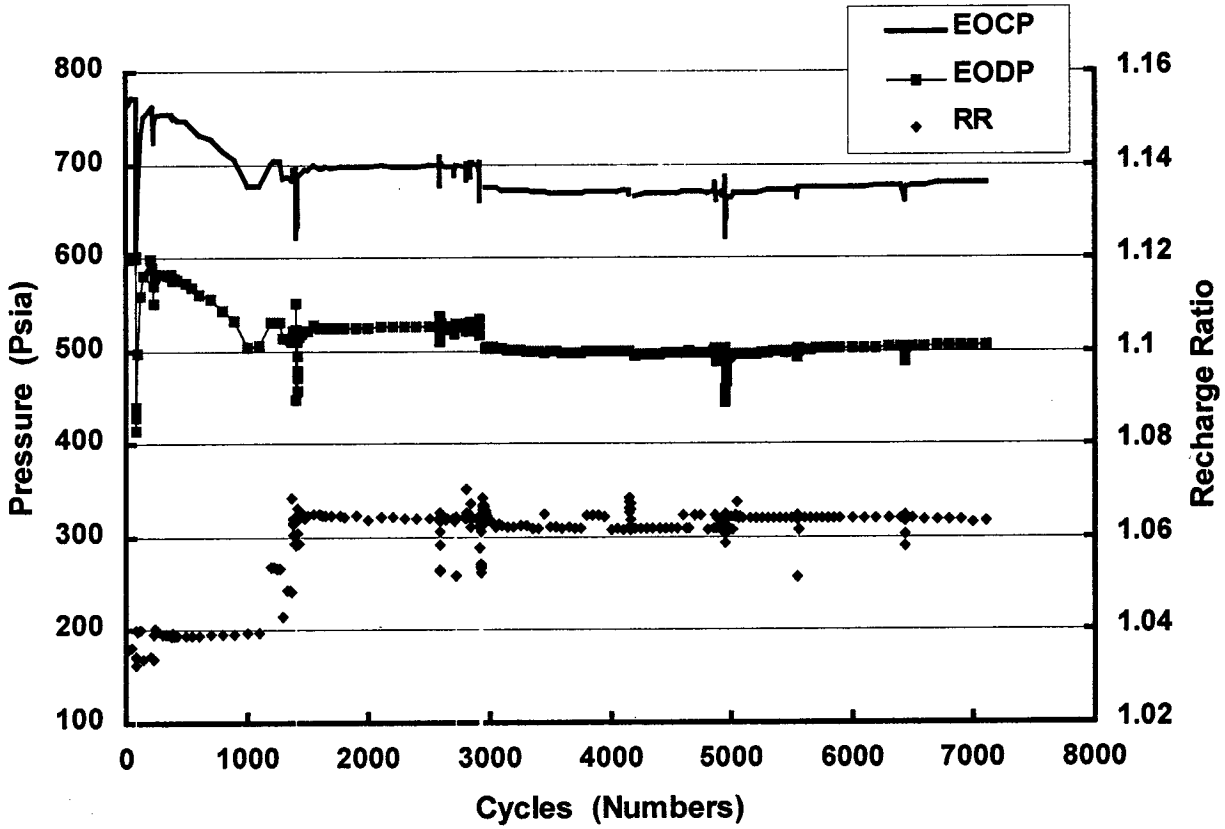

Summary

TRW

- Cells have completed 7100 cycles as of 10/11/99
- End of discharge pressure and end of charge pressure decreased initially but stabilized after the RR was increased from 1.04 to 1.06
- End of discharge voltage stabilized at approximately 1000 cycles after the RR was raised
- End of charge voltage is still increasing slightly with cycles

EAGLE PICHER
Eagle-Picher Technologies, LLC

POWER Subsystems

High Cond[illegible]posite Sleeves for N[illegible]en Cells

K.C. Snyder
Eagle-Picher Technologies, LLC
Joplin, MO

EAGLE PICHER
Eagle-Picher Technologies, LLC

POWER Subsystems

Composite Battery Program Overview

- Composite Battery Sleeve

Baseline: Aluminum Sleeves .030"- .100" Thick
Function: Sleeve Provides Structural Load and Thermal Path to Baseplate

- **Approach**
  - **Systematic Flowdown of Requirements to Design, Fabricate, and Test K1100 Battery Sleeves**

- Objective
  - Design, Fabricate, and Test Protoflight High Conductivity Composite Battery Sleeves for Rechargeable Nickel-Hydrogen Batteries
  - Qualify and Transition Composite Battery Sleeve into a Near-Term DoD/NASA Spacecraft

- **Payoffs**
  - **30- 60% Reduction in Mass vs. Aluminum**
  - **Improved Thermal Performance (Reduced ΔT Along the Length and Between Cell to Cell)**
  - **Insertion of High Conductivity K800 and K1100 into the Battery Sleeve Market. Potential application for thousands of cells per year**

EAGLE PICHER
Eagle-Picher Technologies, LLC

POWER Subsystems

Assembly Sequence

- Assembly
- Thermal-Vac Tests
- Vibration Tests
- DC Isolation Tests

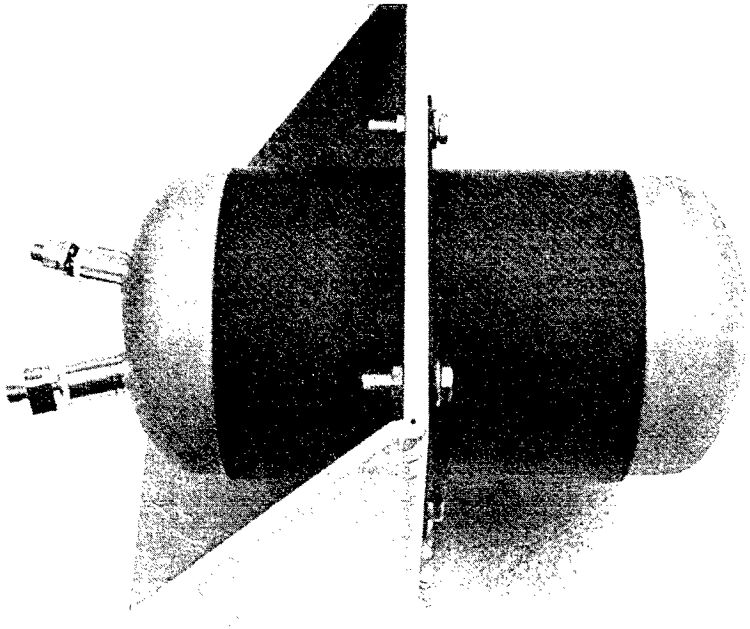

EAGLE PICHER
Eagle-Picher Technologies, LLC

POWER Subsystems

k_{axial} = 350+ W/m*K (overall)

σ = .06 lb/in^3

vs.

k = 180.0 W/m*K

σ = .10 lb/in^3

for 6061-T6 Al

Fiber orientation varies between layers for better strength

Plies bonded with cyanide-ester type resin

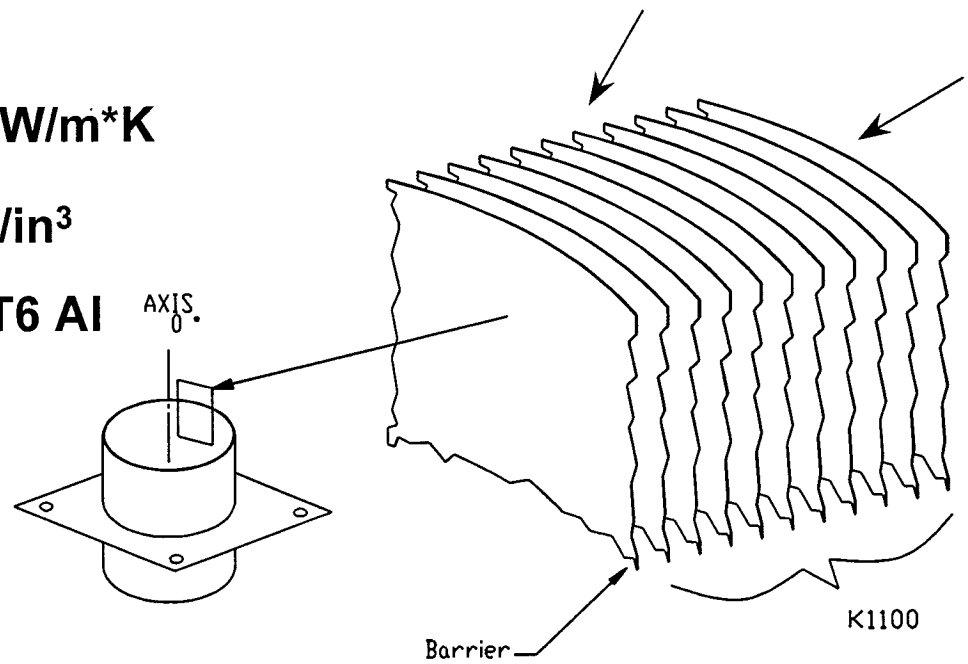

EAGLE PICHER
Eagle-Picher Technologies, LLC

POWER Subsystems

Back[illegible] Battery

- "End-mount" type sleeve
- K1100 trade study presented at Reno in January 1999
- Baseline:
  - 3.5" x 8.5" x .100" 6061-T6 Aluminum
- Replaced by:
  - 3.5" x 8.5" x .060" K1100 with Aluminum Collar (shown below)
  - Weight savings of 330 g/sleeve, or 7 kg/battery (10%)

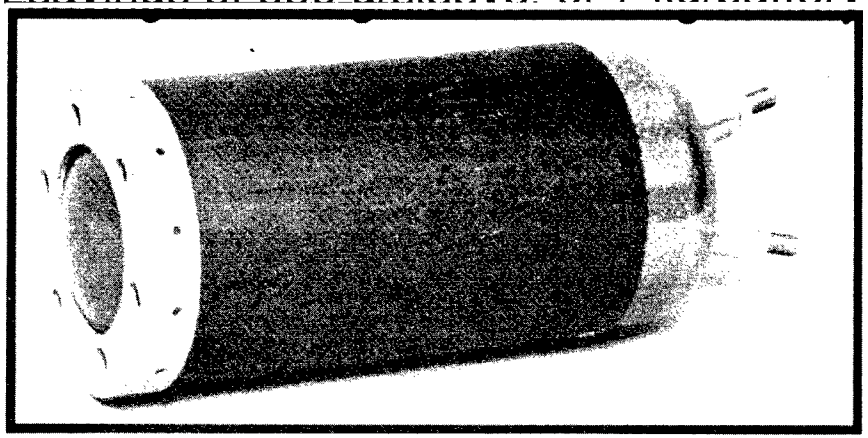

EAGLE PICHER
Eagle-Picher Technologies, LLC

POWER Subsystems

Test Articles [illegible] and 6061-T6 Al

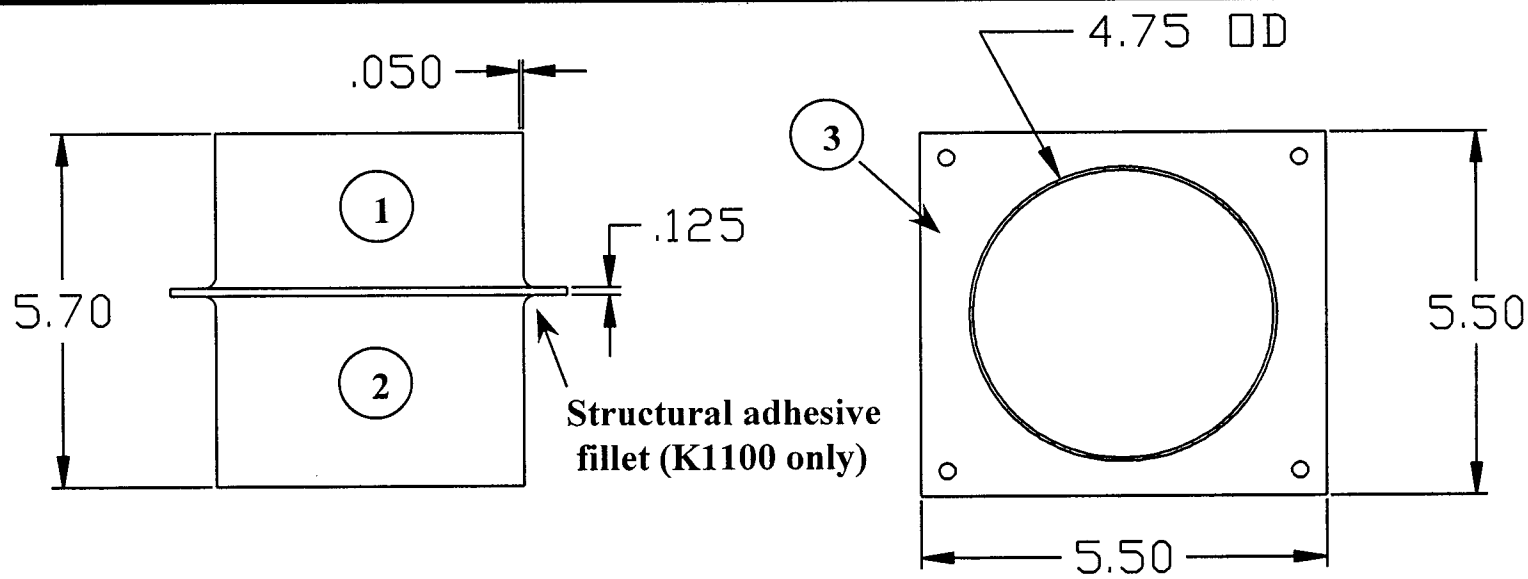

- 1-piece machined Aluminum (220 g)

  vs.

- 3-piece K1100 assembly (150 g)

- Weight savings of 33% with same dimensions
- Weight savings for a 22-cell battery: 1.5+ kg

EAGLE PICHER
Eagle-Picher Technologies, LLC

POWER Subsystems

Cell Sleeve Procedure

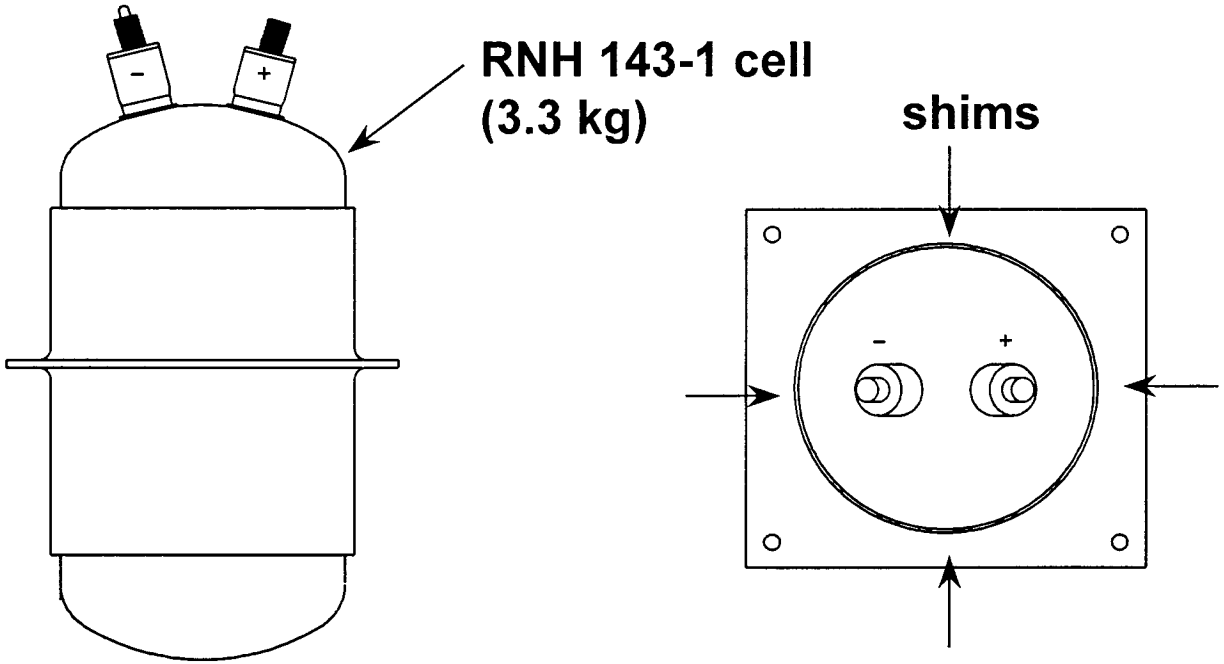

Cell centered in sleeve with Kapton shims at 90° increments and potted with red RTV-566

EAGLE PICHER
Eagle-Picher Technologies, LLC

POWER Subsystems

Cells connected in series, discharged until 1st cell reaches 0.7 volts

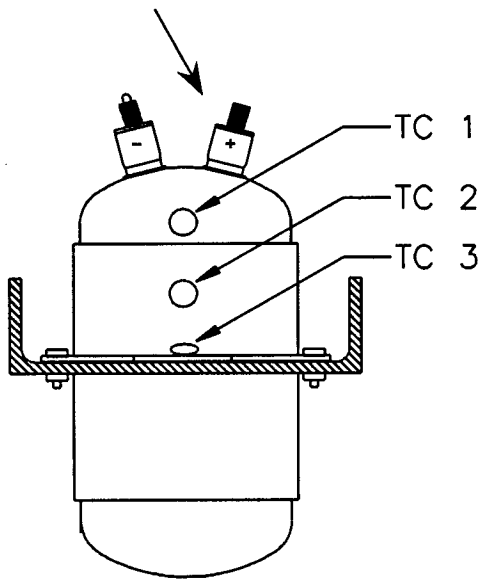

Individual cells isolated by MLI blanket in TVAC

TC 4: Controlled at 0°C
TC 1 - TC 3: Response

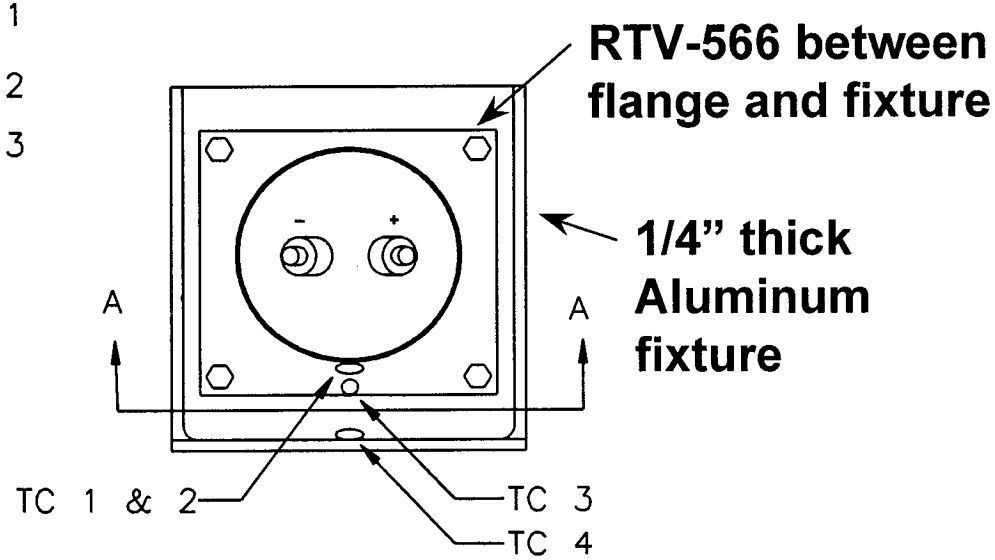

EAGLE PICHER

Eagle-Picher Technologies, LLC

POWER Subsystems

T-VAC Qu[illegible]es: K1100

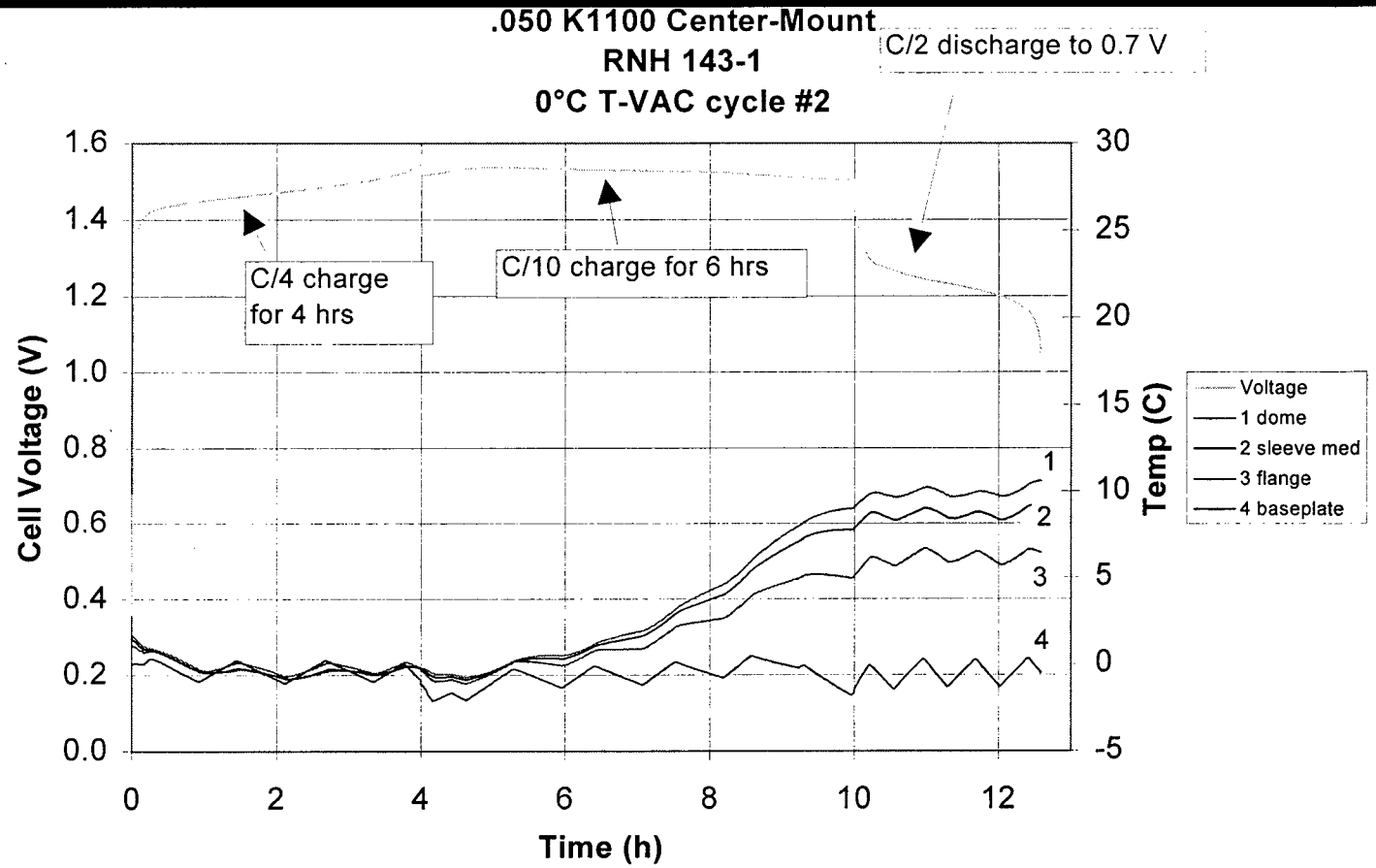

EAGLE PICHER
Eagle-Picher Technologies, LLC

POWER Subsystems

T-VAC 100

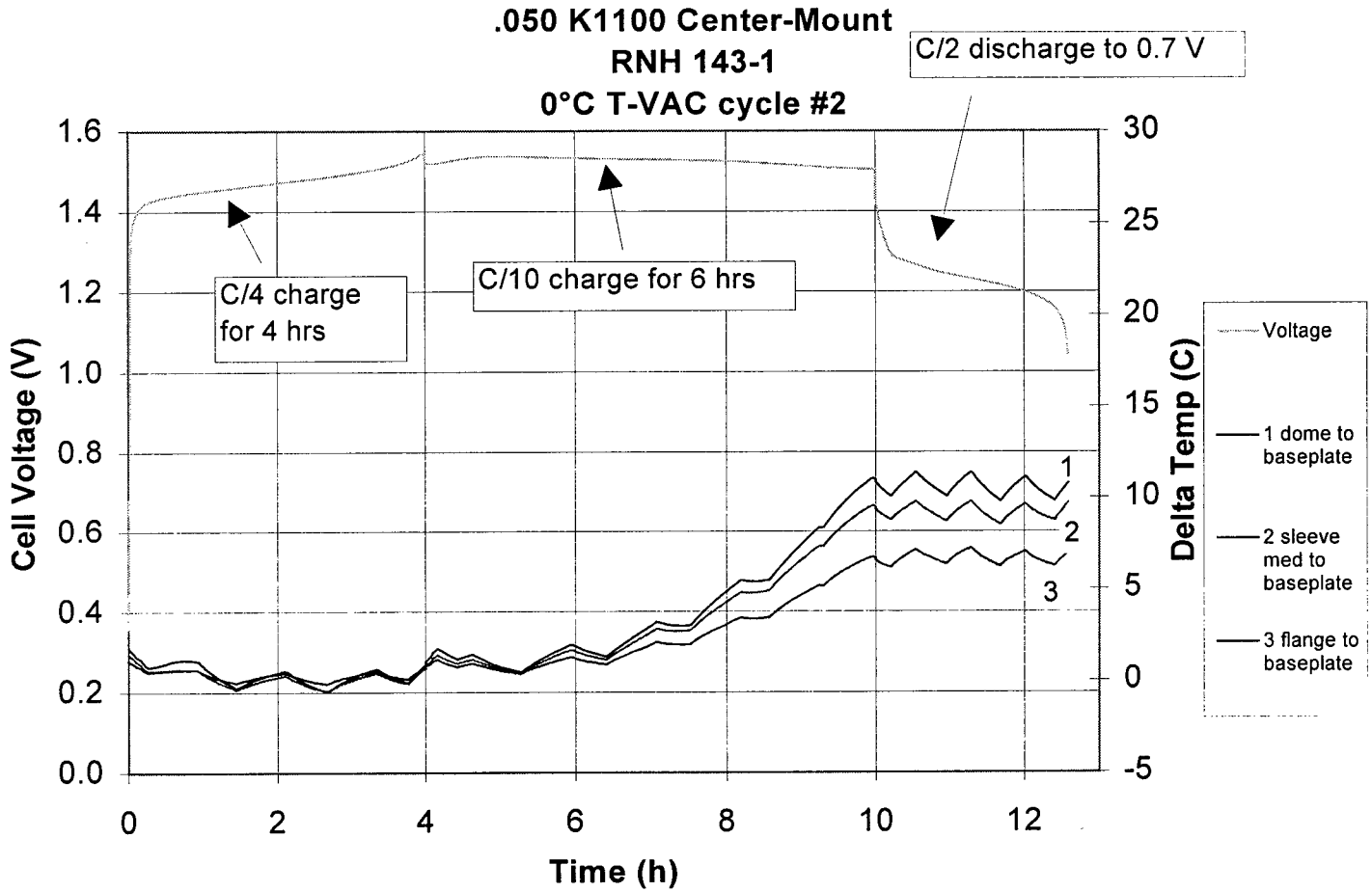

EAGLE PICHER
Eagle-Picher Technologies, LLC

POWER Subsystems

T-VAC Outp[illegible] [illegible]est Aluminum

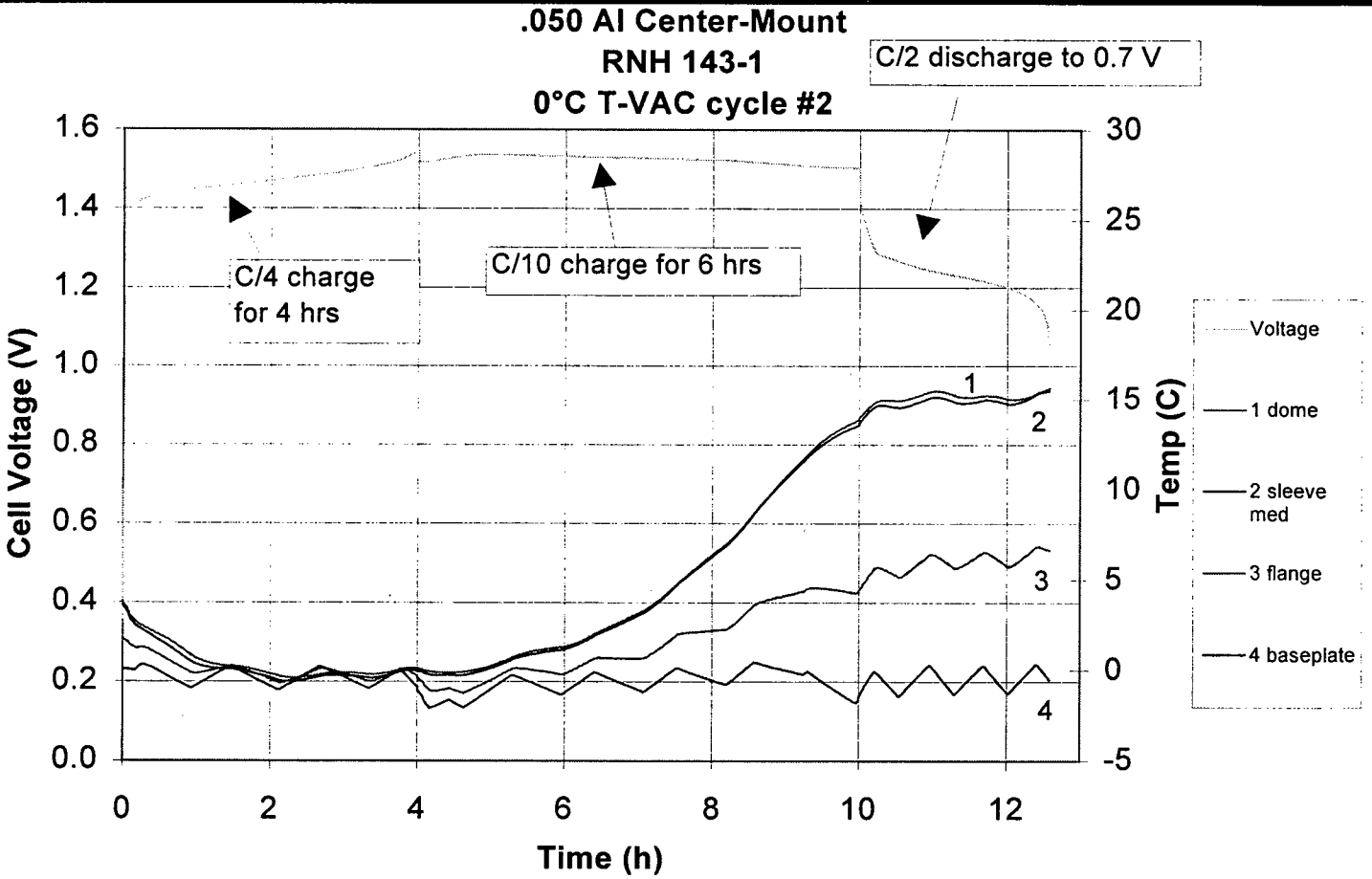

EAGLE PICHER
Eagle-Picher Technologies, LLC

POWER Subsystems

T-VAC Outp[illegible] as: Aluminum

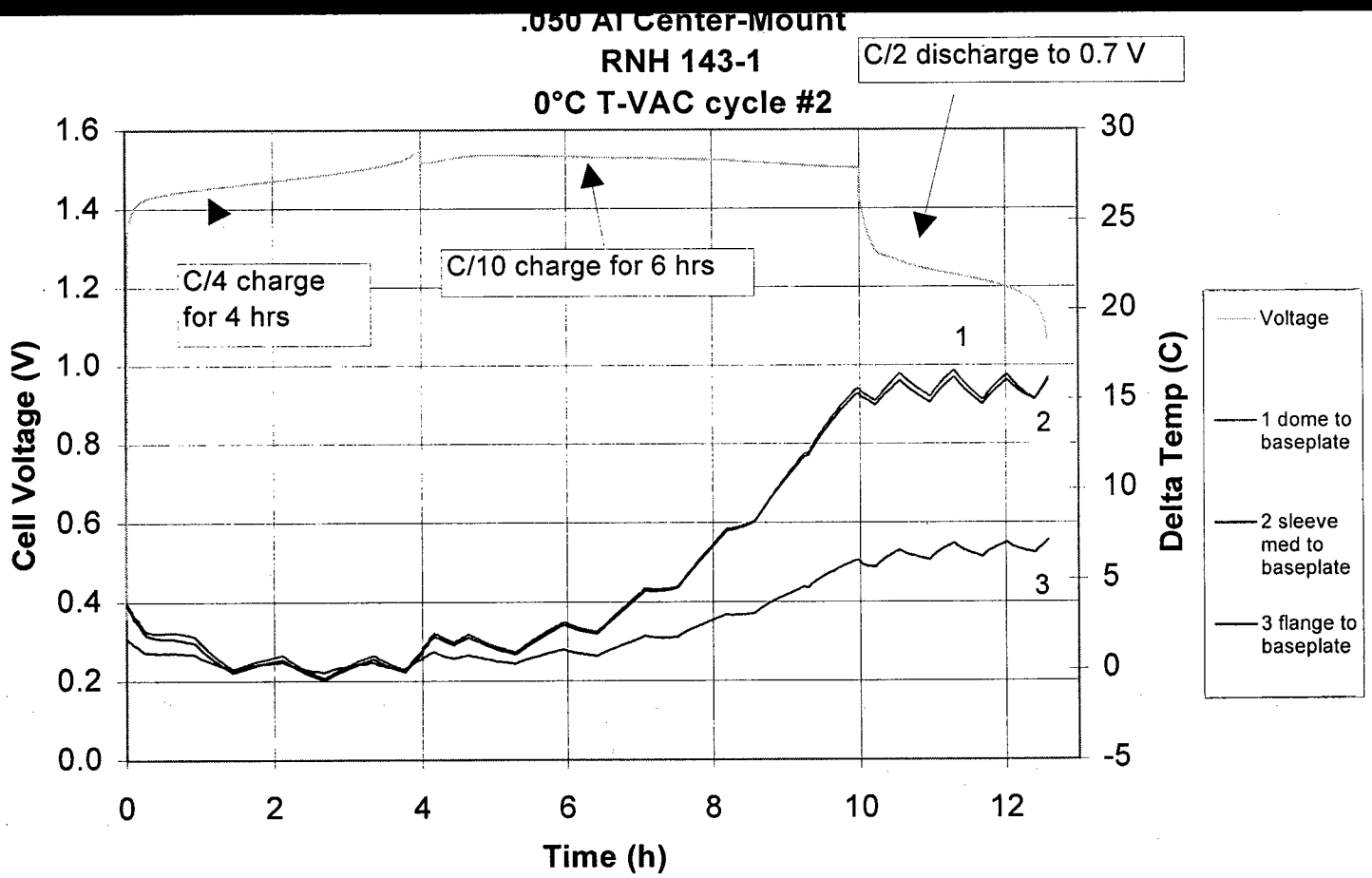

Vibration Setup

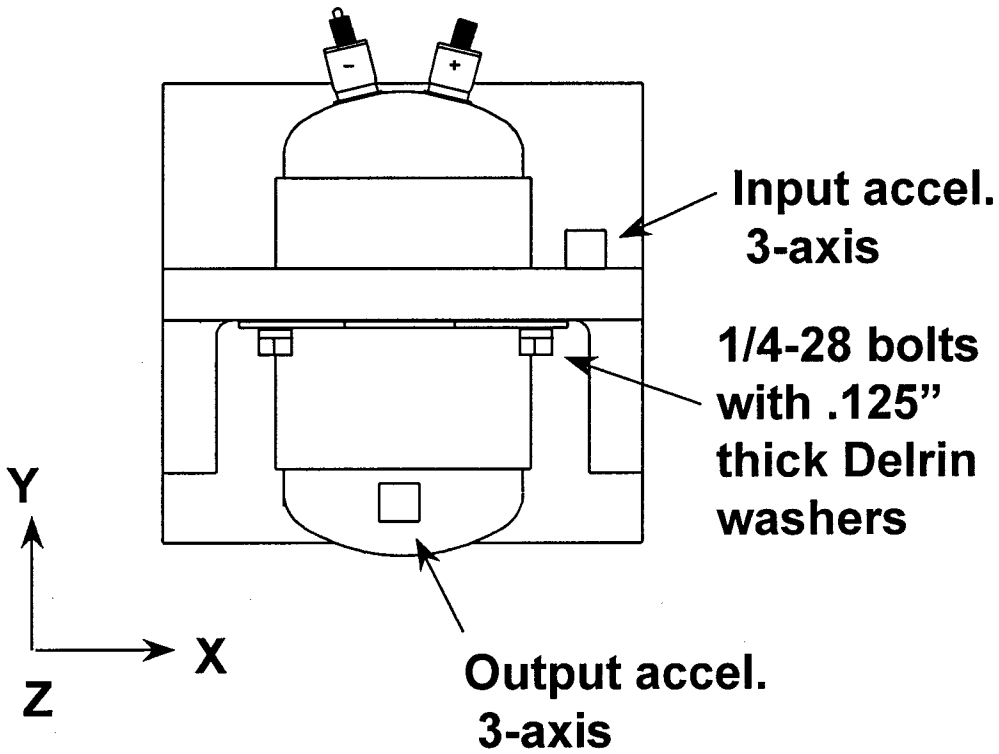

Tested in X, Y & Z axes

3 Random Vibe levels per axis:

- 10.5 grms
- 16
- 20

1/2 G Sine Sweep before and after each axis to check for shifts in 1st mode

EAGLE PICHER
Eagle-Picher Technologies, LLC

POWER Subsystems

Vibration Summary

K1100

Sleeve Type	Axis	Low Sine Pretest 1st mode (Hz)	Random Vibration input (grms) 10.5 Gain Q	16 Gain Q	20 Gain Q	Low Sine Post-test 1st mode (Hz)
K1100 Comp SN 143	X	1750	2.0	2.0	2.0	1750
	Y	1310	1.3	1.3	1.2	1280
	Z	1695	1.6	1.7	1.8	1695

Aluminum

Sleeve Type	Axis	Low Sine Pretest 1st mode (Hz)	Random Vibration input (grms) 10.5 Gain Q	16 Gain Q	20 Gain Q	Low Sine Post-test 1st mode (Hz)
6061-T6 Al SN 162	X	1953	3.3	3.0	2.6	1863
	Y	none*	1.2	1.3	1.3	none*
	Z	1695	2.7	3.1	3.8	1695

* No apparent 1st mode was found in 10-2000 Hz range.

EAGLE PICHER

Eagle-Picher Technologies, LLC

POWER Subsystems

Random Vibe[illegible] K1100 @ 20 G

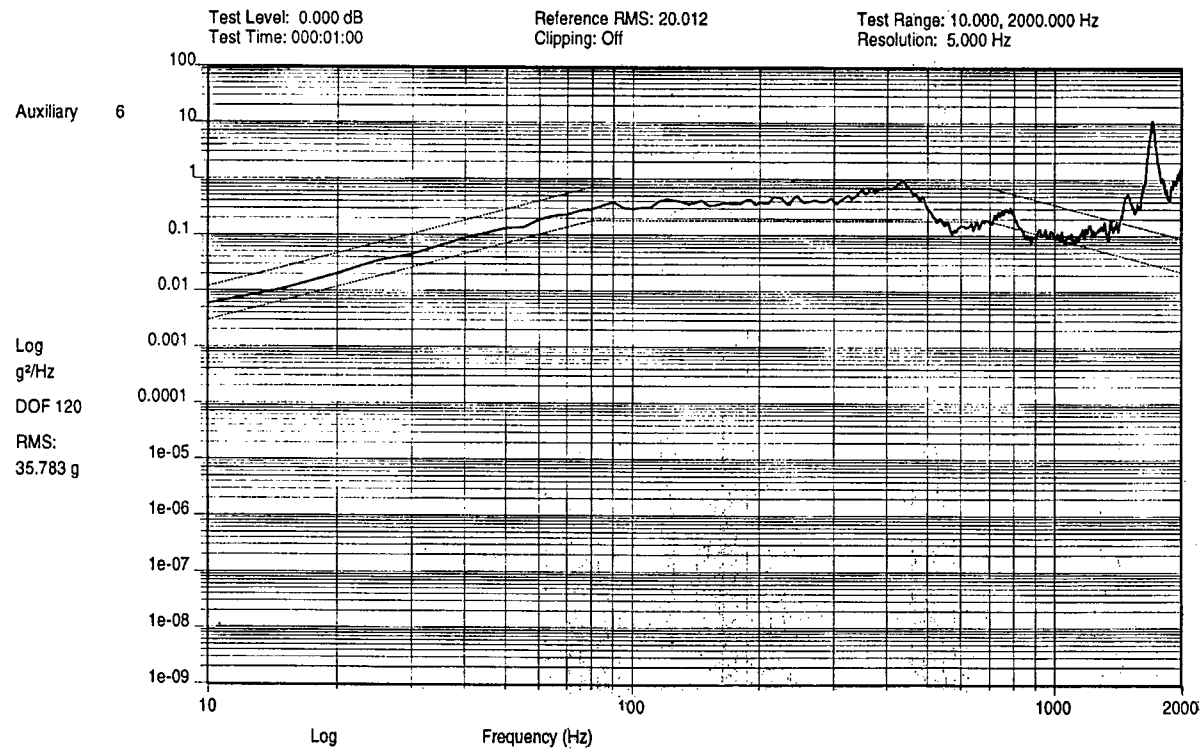

Q = 1.8

09:00:58
02-Sep-1999

RNH-350 4.5 INCH CENTER-MOUNT SLEEVE
SN 143 COMP AXIS (Z) LEVEL 3
Test Name: RNH-350-1_CELL-AXIS-20GRMS.007

2 Z RESPONSE CELL

EAGLE PICHER
Eagle-Picher Technologies, LLC

POWER Subsystems

Random Vib[illegible]minum @ 20 G

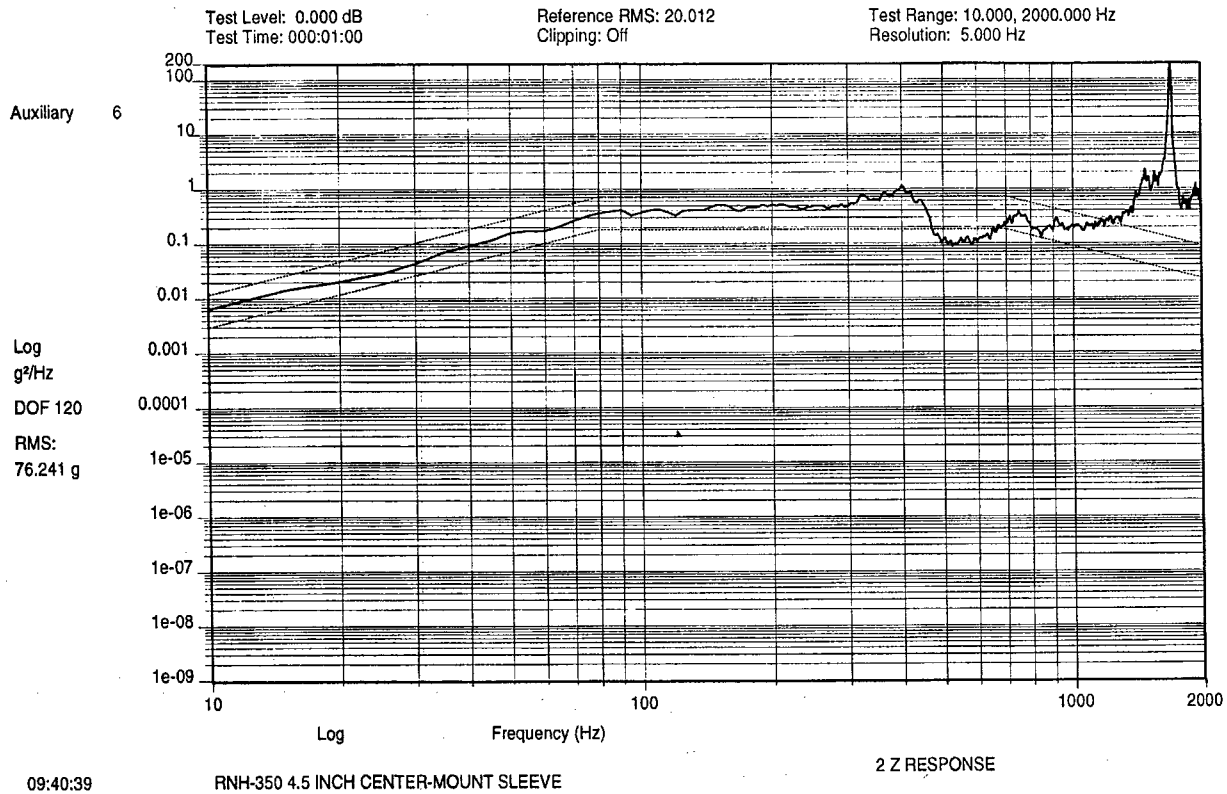

Q = 3.8

09:40:39
02-Sep-1999

RNH-350 4.5 INCH CENTER-MOUNT SLEEVE
SN 162 COMP AXIS (Z) LEVEL 3
Test Name: RNH-350-1_CELL-AXIS-20GRMS.008

EAGLE PICHER
Eagle-Picher Technologies, LLC

POWER Subsystems

Resonan[illegible]ch: K1100

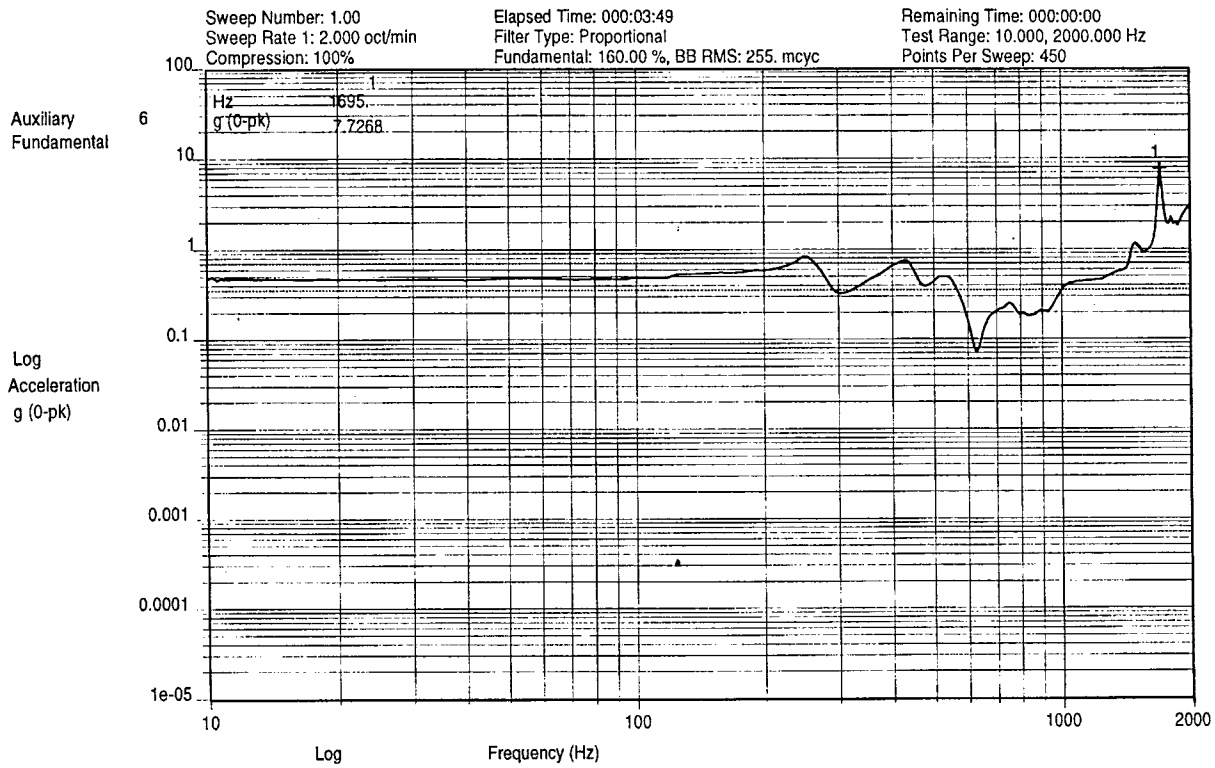

1695 Hz

2 Z RESPONSE CELL

09:09:10
02-Sep-1999

RNH-350 4.5 INCH CENTER-MOUNT SLEEVE
CELL AXIS (Z) SN 143 AFTER LEVEL 3
Sine Test Name: RNH-350_1CELL.010

EAGLE PICHER
Eagle-Picher Technologies, LLC

POWER Subsystems

Resonant Freq[illegible]ch - Aluminum

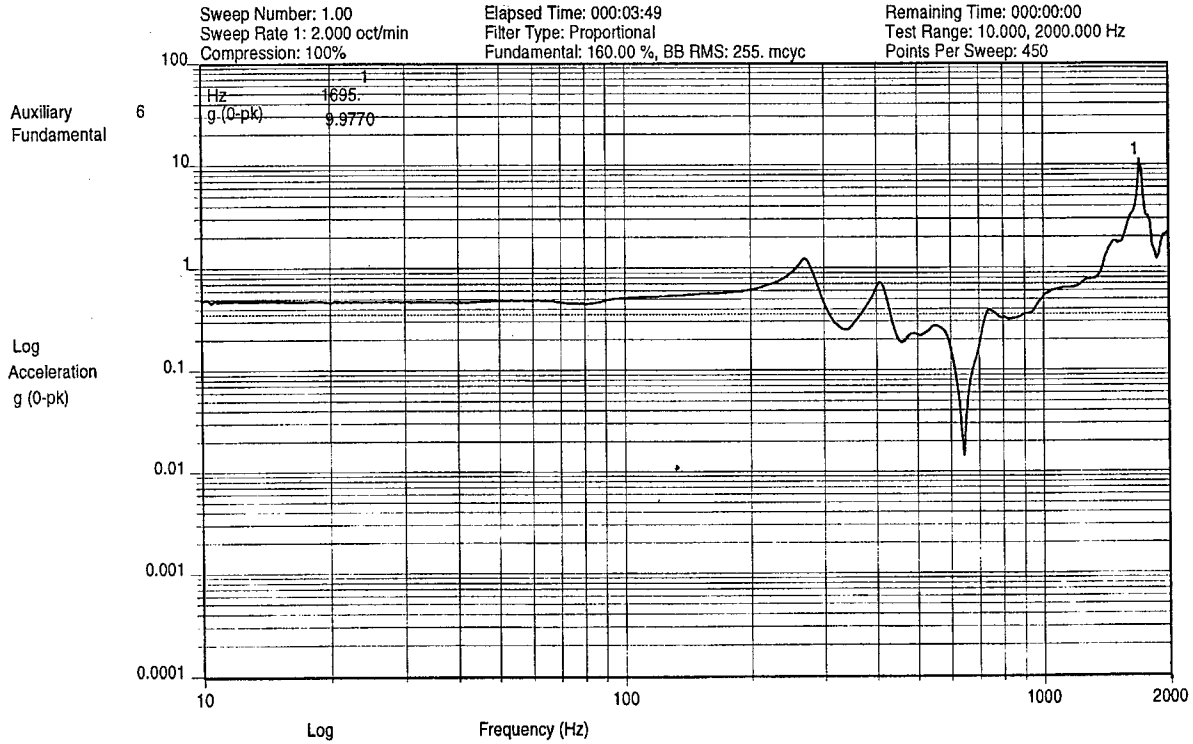

1695 Hz

2 Z RESPONSE CELL

09:52:08
02-Sep-1999

RNH-350 4.5 INCH CENTER-MOUNT SLEEVE
CELL AXIS (Z) SN 162 AFTER 3RD LEVEL
Sine Test Name: RNH-350_1CELL.014

- K1100 vs. 6061-T6 Aluminum:
- Weight Savings of 1.5 to 7.0 kg/battery
  - $60,000 to $280,000 reduced launch cost @ $40,000/kg
  - Additional hardware cost of $25,000/battery can be justified
- Reduced Δ T along cell length
  - up to 5°C cooler for "center-mount" configuration
  - up to 10°C cooler for "end-mount" configuration
- Reduced Δ T between cells on battery
  - improved battery life and performance
- Same or better structural characteristics
  - reduced vibration transmitted to cell
  - similar resonant frequencies in each axis

Acknowledgments

- Jeff Dermott, Eagle-Picher (design/testing)
- Mike Humble, R-Cubed Composites (design/test article)
- YLA, Inc (K1100 raw material)

EAGLE PICHER
Eagle-Picher Technologies, LLC

POWER Subsystems

PROGRESS IN DEVELOPMENT OF 5.5 INCH NICKEL-HYDROGEN BATTERY

JACK N. BRILL
ROBERT BROWN
FRED SILL

EAGLE PICHER
Eagle-Picher Technologies, LLC

POWER Subsystems

- Eagle-Picher Has Developed a Series of Cells Ranging From a Diameter of 2.5 Inch (4 AH) to 4.5 Inch (200AH).
- Interest of Late Has Created a Need for Cells up to 400 AH.
- Eagle-Picher Began a Development of 5.5 Inch Diameter Cells to Meet This Interest.
- Cells Having This Diameter Will Deliver Capacities Between 200 AH to 400 AH.

EAGLE PICHER
Eagle-Picher Technologies, LLC

POWER Subsystems

NIH_2 CELLS IN16 AH TO 400 [illegible] RANGE (2.5 IN. TO 5.5 IN. DIA.)

- Cells Have a Common Heritage of Electrodes Separator and Internal Meterials With Each Design.
- Each Cell Retains a Common Thermal Cross-Section Across the Electrode Stack.
- Presure Vessels All Satisfy MIL-STD 1522 Safety and Life Requirements.

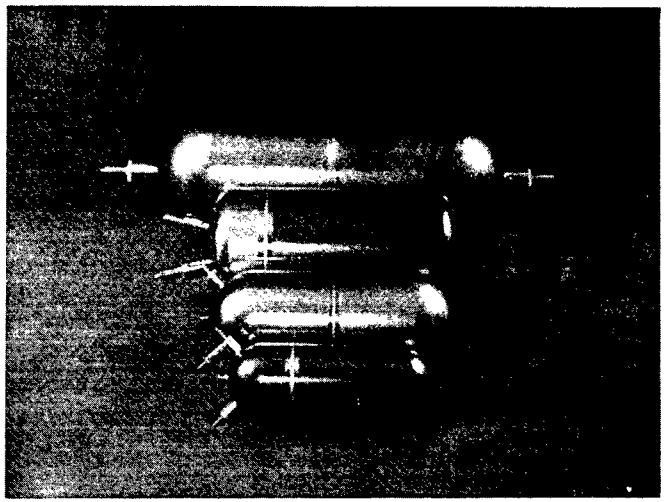

This Depicts The Progression of Cells Having Diameters of 2.5, 3.5, 4.5 And 5.5 Inches.

EAGLE PICHER
Eagle-Picher Technologies, LLC

POWER Subsystems

5.5 INCH DIAMETER CELL MANUFACTURE

- Cells Have Been Assembled and Placed on Test in Three Distinct Manufacturing Groups.
  - Initial cells:
    - 200 AH IPV Cells (1.25 volts) — 10 each
    - 100 AH CPV Cells (2.50 volts) — 10 each
  - Second Generation Cells:
    - 350 AH IPV Cells (1.25 volts) — 10 each
    - 350 AH IPV Cells, Strain Gage (1.25 volts) — 5 each
  - Third Generation Cells:
    - 350 AH IPV Cells, LEO Design (1.25 volts) — 5 each
    - 350 AH IPV Cells, GEO Design (1.25 volts) — 5 each
    - 147 AH CPV Cells, LEO Design (2.50 volts) — 5 each

- Pressure Vessel
  - Inconel 718
  - Burst Pressure - >2.5:1
- All Materials Have Flight Heritage.
  - Aqueous Impregnated, Slurry Sinter
  - ZIRCAR
  - Polysulfone
- Distance From Inner Diameter to Outer Diameter of the Positive Electrode Essentially the Same As for 3.5 In. And 4.5 In. Cells.

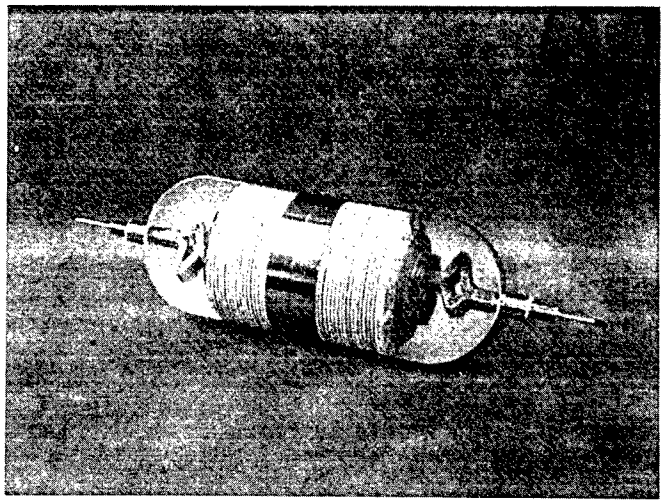

A 350 AH IPV Cell Is Shown. The 5.5 Inch Diameter Can Accommodate Capacities From 200 AH to 500 AH.

EAGLE PICHER

Eagle-Picher Technologies, LLC

POWER Subsystems

PHYSICAL CHARACTERISTICS

	Cell Group 1 (1997)		Cell Group 2 (1998)		Cell Group 3 (1999)		
	RNH 200-A IPV	RNHC 100-A CPV	RNH 350-A IPV	RNH 350-B IPV	RNH 350-C IPV	RNH 350-D IPV	RNHC 147-A CPV
Cell Voltage (volts)	1.25	2.50	1.25	1.25	1.25	1.25	2.50
Rated Capacity (AH)	200	100	350	350	350	350	147
Operating Pressure (psig)	800	825	940	940	900	900	1000
Actual Capacity @ C/2, 10°C (AH)	205	101	371	367	355*	355*	155
Cell Length w/o Terminals (in.)	10.5	10.5	15.3	15.3	15.3	14.6	13.2
Cell Length w/Terminals (in.)	15.5	15.5	20.3	20.3	20.3	19.6	18.2
Cell Diameter (in.)	5.71	5.71	5.71	5.71	5.71	5.71	5.71
Weight (grams)	5450	5550	8592	8592	7764	7420	7041
Specific Energy (WHr/kg)	47.8	46.2	54.8	54.2	58.1	60.8	55.9
Energy Density (WHr/liter)	72.2	71.1	83.8	82.9	80.2	84.6	83.0

ACC[illegible] TEST

	Cell Group 1		Cell Group 2		Cell Group 3
	RNH 200-A IPV	RNHC 100-A CPV	RNH 350-A IPV	RNH 350-B IPV	RNHC 147-A CPV
20°C (AH)	185	88	323	338	138
10°C (AH)	205	101	371	367	155
10°C, 72 hr Retention (AH)	180	85	326	324	135
0°C (AH)	212	105	388	390	165

Each Capacity Measurement Is Made From a 16 Hour C/10 Charge and a C/2 Discharge to Either 1.00 Or 2.00 Volts (Depending on IPV or CPV).

EAGLE PICHER
Eagle-Picher Technologies, LLC

POWER Subsystems

TYPICAL IPV 10°C CHARGE AND DISCHARGE CURVES

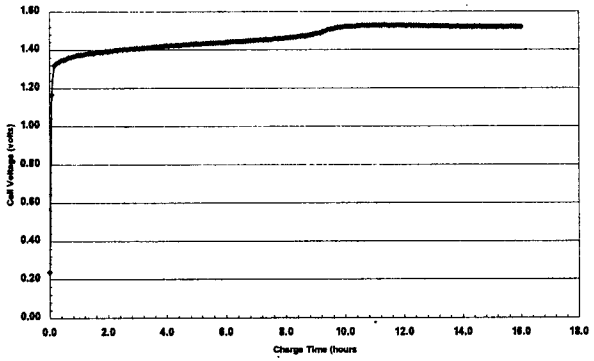

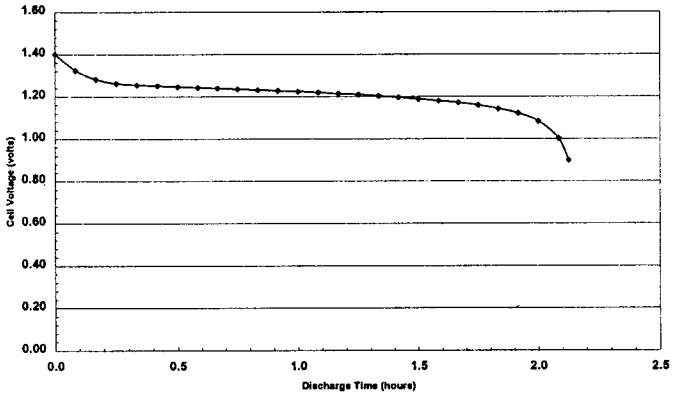

The Curves for the IPV Cells Have the Same Basic Roll Over During Charge and Fall off at the End of Discharge. At 10°C the Maximum Charge Voltage at the C/10 Rate Was Approximately 1.57 Volts.

EAGLE PICHER
Eagle-Picher Technologies, LLC

POWER Subsystems

TYPICAL CPV 10°C C[illegible] DISCHARGE CURVES

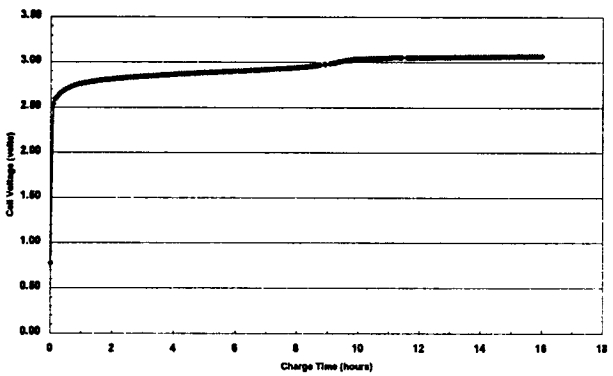

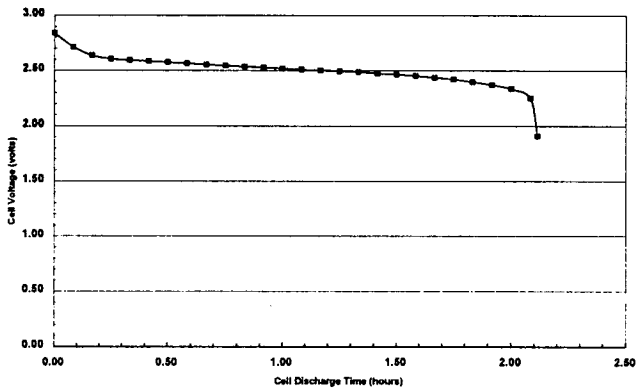

The Curves for the 5.5 Inch Diameter CPV Cells Have the Same Roll Over During Charge and a Similar Drop off in Voltage at End of Discharge. The Maximum Charge Voltage Was Approximately 3.1 Volts at 10°C.

QUALIFICATION TEST

- A 350 AH Cell Was Subjected to Vibration.
- The Vibration Level Selected Was a Qualification Level Used on an Existing Battery Program.
- The Test Sequence Was As Follows:
  - 10°C Standard Capacity
  - Vibration Test
  - 10°C Standard Capacity
- Voltage and Capacities Were Normal Before and After Vibration
- No Physical Damage

QUALIF[illegible] (Cont'd)

Vibration Levels

Axial	
10 - 80 Hz	+6 db/Oct
80 - 700 Hz	0.1g^2/Hz
700 - 2000 Hz	-6 db/oct
Overall 10.5 Grms	

Radial	
10 - 80 Hz	+4 db/oct
80 -1000 Hz	0.05 g^2/hz
1000 - 2000 Hz	-3 db/oct
Overall 9 Grms	

These Are the Qualification Vibration Levels Used in the Test for the 350 AH, 5.5 Inch Diameter Cell.

LIFE TESTING

- Life Tests Are Ongoing at Eagle-Picher With 100 AH CPV, 200 AH IPV and 350 AH IPV Cells.
- All Tests Are 90 Minute Cycles (35 Minute Discharge/55 Minute Charge) With a Recharge Ratio of 1.04.
- Depth of Discharge Is 40% Based on Nameplate for All Cycles.
- All Tests Are Being Conducted at 5°C.

EAGLE PICHER
Eagle-Picher Technologies, LLC

POWER Subsystems

LIFE CYCLE TESTING (Cont'd)

Cell	Quantity	Rated Capacity (AH)	DOD %	R.R.	Number of Cycles
RNH 200-A	10	200	40	1.04	9268
RNHC 100-A	10	100	40	1.04	6524
RNH 350-A	10	375	40	1.04	6182

CONTIN[illegible]PMENT

- The 147 AH CPV Cells Are in Acceptance Testing and Will Soon Be Placed on Life Test.
- The 350 AH Cells in the LEO Design Will Complete Activation in December, 1999.
- The 350 AH Cells in the GEO Design Will Complete Activation in December, 1999.
- All Cells Will Be on Life Test by Early 2000.

- IPV Cells Have Been Manufactured at Capacities Ranging From 200 AH to 350 AH.
- CPV Cells Have Been Manufactured at Capacities of 100 AH and 147 AH.
- A 350 AH Cell Has Been Tested to a Vibration Level of 10.5 Grms.
- Cycling at 40% DOD, 5°C, Has Been Demonstrated to 9268 Cycles.

FUTURE [illegible]MENT

4Th Generation Cells

- 250 Ah, 1.25 Volt - Leo Design
  - Expected Capacity - 270 Ah at C/2, 10°C
  - Weight Goal - 5400 Grams
- 250 Ah, 1.25 Volt - Geo Design
  - Expected Capacity - 270 Ah at C/2, 10°C
  - Weight Goal - 5200 Grams
- 125 Ah, 1.25 Volt - Leo Design
  - Expected Capacity - 135 Ah at C/2, 10°C
  - Weight Goal - 5400 Grams

✦ Completion Date - November, 2000

Lithium-Ion Session I

Dependence of Positive Plate Design and Temperature on the Performance of Nickel-Hydrogen Cells

Hari Vaidyanathan

NASA Aerospace Battery Workshop

Huntsville, Al, November 17, 1999

10/99-990338 -1

COMSAT LABORATORIES

Experimental

- Flight model cells fabricated for the INTELSAT VI, VII and VIIA program
- Cycled cells in the GEO regime
- Capacity determinations, overcharge tests, analysis of positives for swelling, absorbency, and active material utilization

COMSAT LABORATORIES

10/99-990338 -2

Figure 1

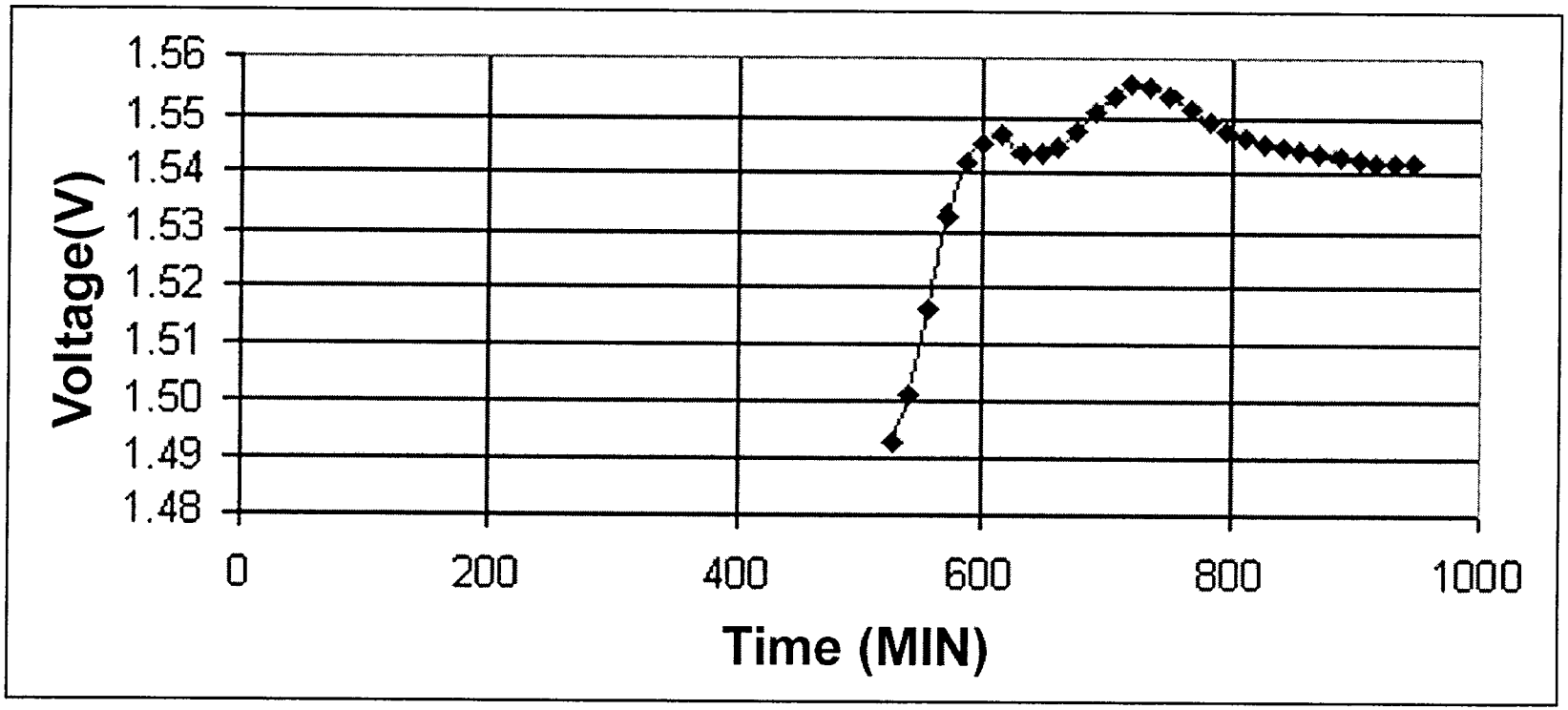

Fig. 1 Voltage Profile in the Overcharge Region.

Table 1

ID	Plate Type	Av. Weight (g)	Av. Thickness Area (mm)	Area (cm^2)	Mass $Ni(OH)^2$ (%, g)	Mass $Co(OH)^2$ (%, g)	$Co(OH)^2$ (% of active)	Mass Sinter (%, g)	Mass Substrate (%, g)	Porosity Sinter (%)	Porosity Plaque (%)	Active Ni (g/cm^3)	Total (g/cm^3)	Coeff. Utilization		Waviness in Overcharge Occurs at
														Plate (%)	Cell (%)	
EXP1	Wet slurry	15.62	0.97	50.44	34.58 5.4	2.19 0.34	5.92	48.43 7.56	10.98 1.71	81.6	78.0	1.43	1.68	119.8	123.8	0°C
EXP2	Wet slurry	23.22	0.812	83.31	34.61 8.03	2.08 0.48	5.64	47.08 10.93	14.39 3.34	80.6	75.6	1.57	1.75	145.0	124.3	0°C
INTELSAT VI	Dry sinter	13.01	0.881	50.44	35.69 4.68	4.63 0.61	11.5	43.46 5.7	13.08	84.09	80.25	1.38	1.68	141.0	117.8	-10°C
INTELSAT VIIA	Dry sinter	24.71	0.982	82.5	35.5 8.68	2.52 0.62	6.67	47.8 11.72	14.3	82.8	78.2	1.37	1.47	151.5	120.7	-10°C

Table 1. Positive Plate Analysis Comparison

COMSAT LABORATORIES

10/99-990338 -4

Voltage Rollover and Waviness

- Waviness in the voltage profile in the overcharge region
- Waviness occurs in: Both slurry and dry powder positives, plates of different Co contents, sinter porosity of 80-84% and plaque porosity of 76-80%
- Waviness appears during overcharge at -10°C

10/99-990338 -5

COMSAT LABORATORIES

Table 2

Program	Cell Design	Temp.	Capacity (Ah to 1V)	Capacity (Ah to 0.1V)	Mid-discharge Voltage (V)
INTELSAT VI	3.5 in. dia, recirc, 2-zircar alcohol positives	10°C	59.8	61.5	1.261
INTELSAT VI	3.5 in. dia, recirc, 2-zircar alcohol positives	0°C	65.6	67.3	1.254
INTELSAT VI	3.5 in. dia, recirc, 2-zircar alcohol positives	-20°C	76.0	77.2	1.245
INTELSAT VII	3.5 in. dia, back-to-back 2-zircar, aq. positives	10°C	96.75	98.18	1.253
INTELSAT VII	3.5 in. dia, back-to-back 2-zircar, aq. positives	0°C	104.8	105.5	1.25
INTELSAT VII	3.5 in. dia, back-to-back 2-zircar, aq. positives	-20°C	114.8	117.1	1.228
INTELSAT VIIA	4.5 in. dia, back-to-back 2-zircar, aq. positives	10°C	124.7	157.0	1.248
INTELSAT VIIA	4.5 in. dia, back-to-back 2-zircar, aq. positives	0°C	138.6	140.0	1.242
INTELSAT VIIA	4.5 in. dia, back-to-back 2-zircar, aq. positives	-20°C	150.9	156.0	1.212

Table 2. Capacity and Voltage at Low Temperatures.

COMSAT LABORATORIES

10/99-990338 -6

Table 4

Charge Technique	Capacity (Ah to 1V)	Capacity (Ah to 0.1V)	End of Charge Pressure (psi)	Mid-discharge Voltage (V)
1) C/10 for 18 hr at 10°C	53.6	57.2	850	1.296
2) C/10 for 18 hr at 10°C and C/10 at 50°C for 702 hr	77.0	77.8	1,190	1.226
3) C/10 at 10°C for 18 hr	58.7	60.52	870	1.275
4) C/10 for 741 hr at 10°C	67.7	70.7	996	1.241

Table 4. Capacity Obtained at C/2 Discharge at 10ºC.

COMSAT LABORATORIES

10/99-990338 -7

Figure 2

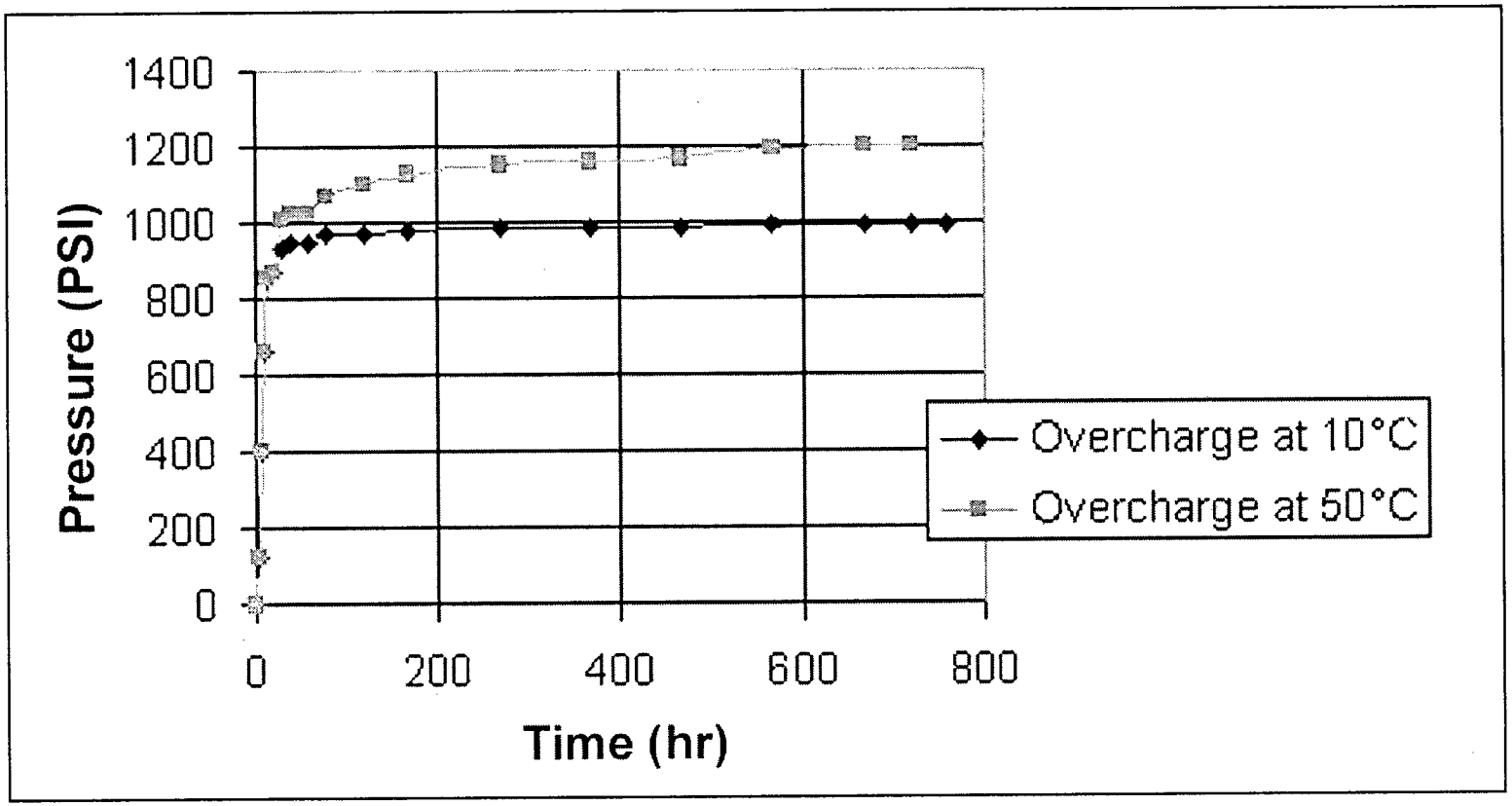

Fig. 2 Pressure Profiles During Extended Charge at C/10.

COMSAT LABORATORIES

10/99-990338 -8

Table 3

Cell ID	Temp.	Capacity (Ah to 1V)	Final Capacity (Ah to 1V)	Loss in Capacity (%)
L1004	10°C	124.4	117.5	5.5
L1004	-20°C	148.9	135.5	9.0
L1018	10°C	124.7	118.2	5.2
L1018	-20°C	150.3	138.7	7.7

Table 3. Capacity Maintenance.

COMSAT LABORATORIES

10/99-990338 -9

High Capacity and High Utilization

- In 1990 INTELSAT VI cells with alcohol positives showed 27% increase in capacity when operated at -20°C as opposed to 10°C
- High Capacity observed for aqueous positive plates when used at -20°C
- Cells containing alcohol positives also showed a capacity increase of 43% when overcharged at C/10 for 702 hours at 50°C
- Pressure increases indicating increase in the state-of-charge

COMSAT LABORATORIES

10/99-990338 -10

High Capacity

- Lower mid-discharge voltage at -20°C is attributable to hydrogen electrode polarization
- The additional capacity is less stable with cycling
- Additional capacity is attributed to Ni (+4)

Figure 3

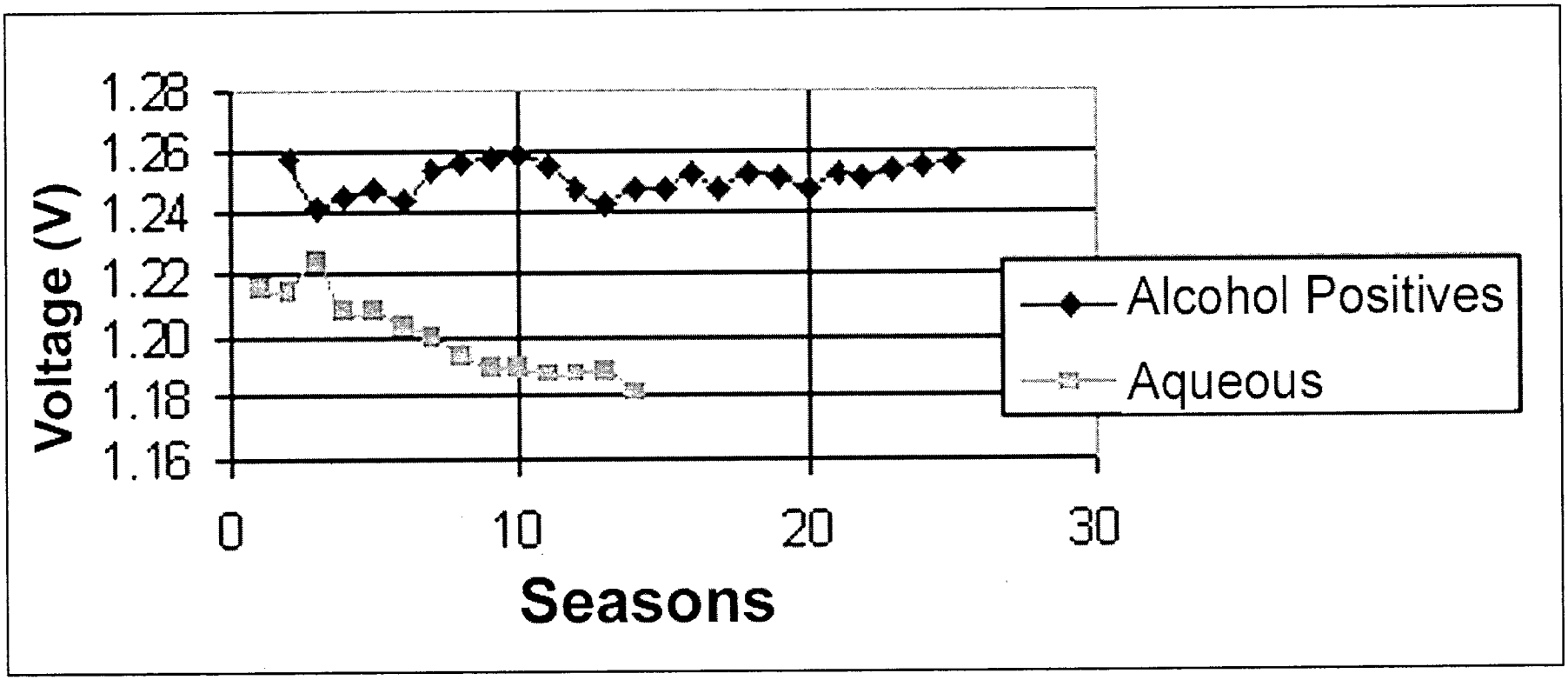

Fig. 3 Variation in End-of-Discharge Voltage.

COMSAT LABORATORIES

Figure 4

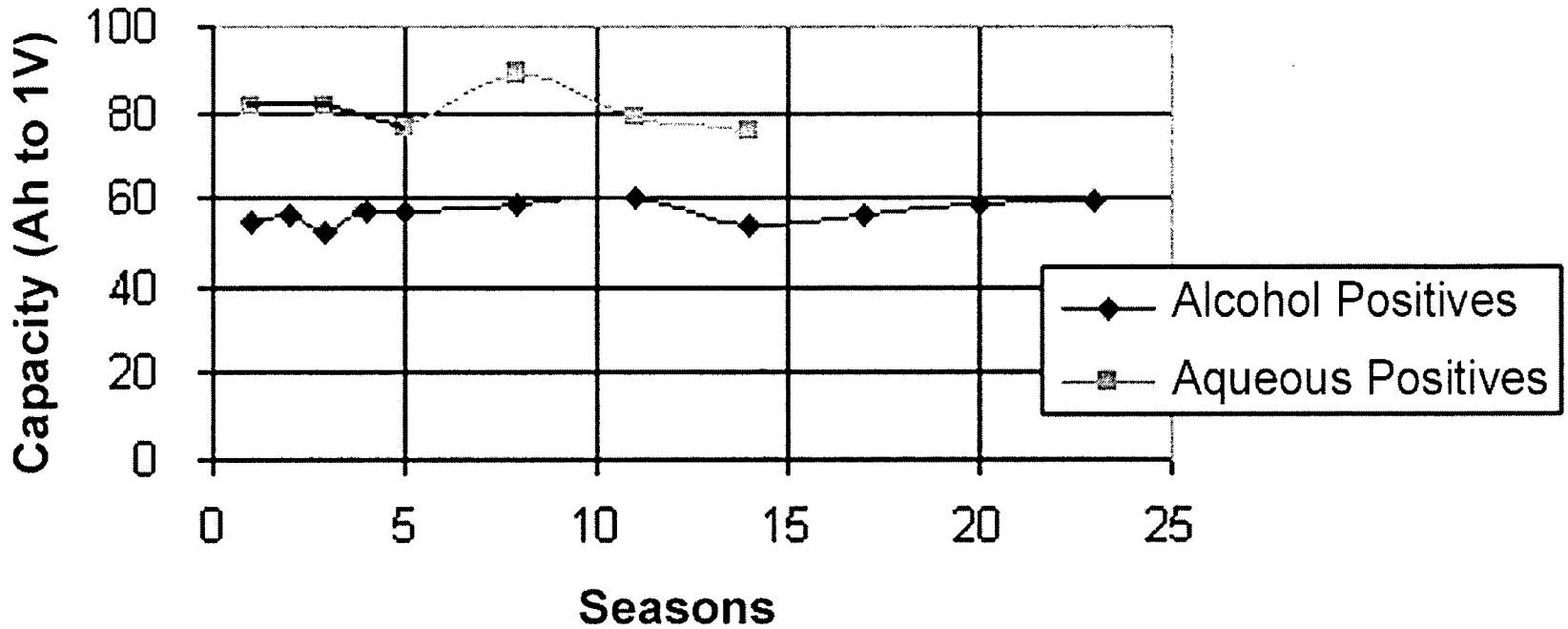

Fig. 4 Capacity Variation with Cycling.

COMSAT LABORATORIES

10/99-990338 -13

Table 5

Cell History	EOD (V)	EOC (V)	Swelling (%)	KOH Absorbed by Pos. (g)	KOH Absorbed by Separator (g)	Popping Damage
4.5-in-dia cell after 5 GEO seasons (Cell 1 - 32)	1.11	1.542	12.0	0.24	0.94	Extrusion, pinholes, melted gas screens, pos. plate delamination, melting of the center core.
4.5-in-dia cell after 9 seasons (Cell 4 - 20)	1.175	1.513	7.70	0.198	1.05	Pinholes, extrusion, delamination of Teflon backing.
3.5-in-dia cell after 13 seasons (Cell 4 - 51)	1.189	1.512	6.0	0.2	1.22	Areas of blowout in the mid-stack, melted gas screen, blackening of the separator.

Table 5. Swelling, KOH Absorbed and Performance.

COMSAT LABORATORIES

10/99-990338 -14

Figure 5

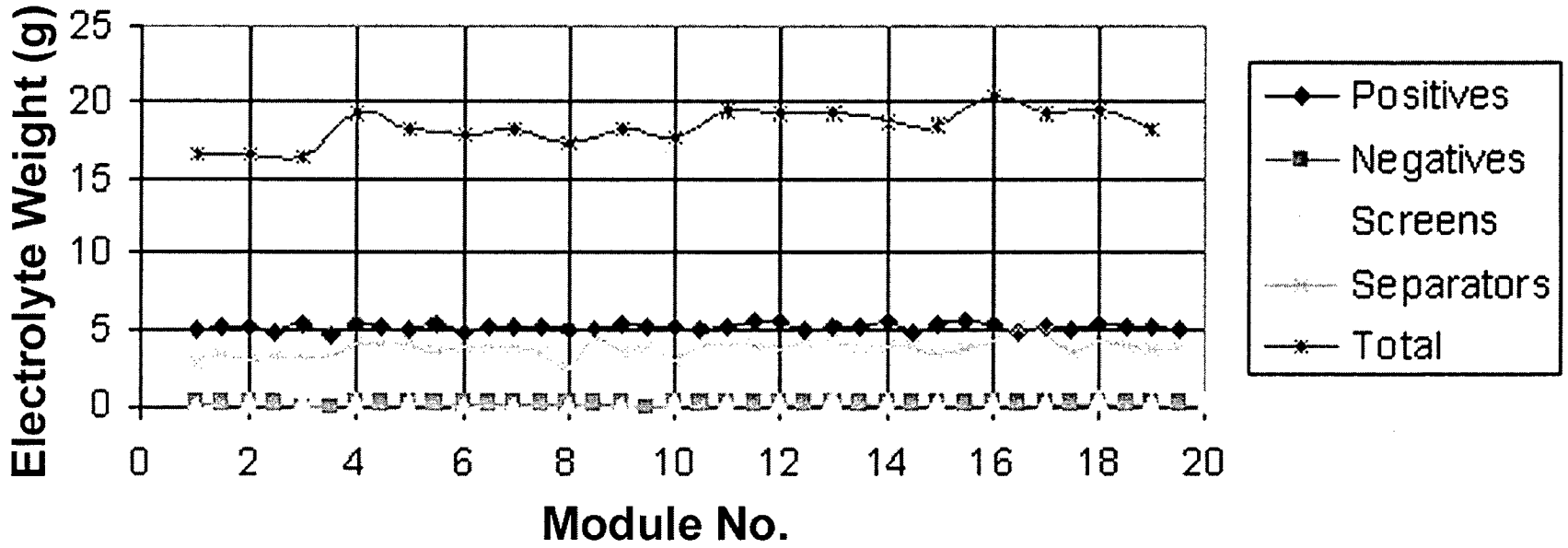

Fig. 5 Swelling, KOH Absorbed and Performance.

Popping, Swelling and Electrolyte Content

- Electrolyte absorbed is proportional to stack compression and thickness of positive and separator
- Scale-up to 4.5 in. dia. resulted in increased swelling in the INTELSAT cells
- Swelling results in increased electrolyte absorption, extrusion of active material and reduction in the gap between positives
- Swelling promotes popping

COMSAT LABORATORIES

10/99-990338 -16

Conclusions

- Occurrence of waviness and increased capacity point to the formation of Ni(+4)
- Increased capacity can be achieved by charging at very low temperatures or extensive overcharge at high temperature
- Additional capacity is less stable when cycled
- Swelling and increased electrolyte absorption by the positive result in lower voltage

COMSAT LABORATORIES

1999 NASA Aerospace Workshop
17 November 1999
Huntsville, Alabama

NAVSEA
CRANE

Comparison of Separation Performance for Four Variables in Rechargeable Silver/Zinc Cells

Harlan Lewis
Norris Caldwell
NSWC Crane Division

Albert Himy
J.J. McMullen Associates

NAVSEA CRANE

Comparison of Separation Performance for Four Variables in Rechargeable Silver/Zinc Cells

Introduction -

- Scope
  - Cycle and Wet Life Evaluations of Model Rechargeable Ag/Zn Cell Separations
- Intent:
  - Evaluate Four Parameters:
    1. Split vs. Standard Separation Wrap
    2. PVA Film for Silver Migration Barrier
    3. PVA Coating for Silver Migration Barrier
    4. Zircar as a Substitute for Asbestos as a Fire Retardant
- Background
  - Two Cell Set Studies as Conceived by Mr. Al Himy of J.J. McMullen Associates

Comparison of Separation Performance for Four Variables in Rechargeable Silver/Zinc Cells

Experimental -

Total of Thirteen Cell Sets at 28 Ah (nominal) Model Cells With the Configurations:

Set Std. - Positive/ 1X2-mil Webril, 6X3-mil Flexel// 1X4.2-mil Viskon/Negative

The five Separation Combinations Selected for the First Five Cell Sets Were as Follows:

Set 1 - Positive/1X2-mil Webril, 1X3-mil Flexel, 1X2-mil PVA, 4X3-mil Flexel// 1X4.2-mil Viskon/Negative

Set 2 - Positive/1X2-mil Webril, 1X7.2-mil SG, 1X2-mil PVA, 2X7.2-mil SG// 1X4.2-mil Viskon/Negative

Set 3 - Positive/1X2-mil Webril, 3X3-mil Flexel//3X3-mil Flexel, 1X4.2-mil Viskon/Negative

Set 4- Positive/1X2-mil Webril, 1X6-mil Asbestos, 4X3-mil Flexel// 1X4.2-mil Viskon/Negative

Set 5 - Positive/1X2-mil Webril, 1X6-mil Zircar, 4X3-mil Flexel// 1X4.2-mil Viskon/Negative

Comparison of Separation Performance for Four Variables in Rechargeable Silver/Zinc Cells

NAVSEA CRANE

Experimental -

The Second Group of Seven Cell Sets Had the Following Separations:

Set 6 - Positive/1X3-mil Pellon, 6X3-mil Flexel// 1X3-mil Pellon/Negative

Set 7 - Positive/1X3-mil Pellon, 3X3-mil Flexel// 3X3-mil Flexel,1X3-mil Pellon/Negative

Set 8 - Positive/1X3-mil Pellon, 1X2-mil PVA, 5X3-mil Flexel// 1X3-mil Pellon/Negative

Set 9 - Positive/1X3-mil Pellon, 6X3-mil PVA-coated Flexel// 1X3-mil Pellon/Negative

Set 10 - Positive/1X3-mil Pellon, 3X7.2-mil PVA-coated SC// 1X3-mil Pellon/Negative

Set 11 - Positive/1X3-mil Pellon, 1X6-mil Asbestos, 4X3-mil Flexel// 1X3-mil Pellon/Negative

Set 12 - Positive/1X3-mil Pellon, 1X6-mil Zircar, 4X3-mil Flexel// 1X3-mil Pellon/Negative

Comparison of Separation Performance for Four Variables in Rechargeable Silver/Zinc Cells

* Notes

Flexel is a cellophane film derived from wood pulp. SC is sausage casing, also derived from wood pulp, in tubular form, which was split on the length and wrapped around the plates in a manner similar to cellophane film. PVA is a film made from polyvinyl alcohol. Webril and Pellon are non-woven polypropylene films, and Viskon is a paper fibre mat. Zircar is a zirconium oxide derived mat. The layers of separation were selected to provide the same total wet thickness for the cell packs, regardless of the type of separation. In this way, the internal cell stack pressure was identical from one cell separation type to the next. This was additional insurance that the only variable from one cell set to the next was the type of separation used. N.B. All separation thicknesses are wet (45% KOH) data values.

The cells were built by Eagle-Picher Industries (EPI) of Joplin, MO. The first five sets of thirteen cells each were shipped dry and uncharged (green). The next seven sets of six cells each were filled at EPI with 45% KOH and taken through one formation cycle, then discharged and shipped in the filled, discharged state.

NAVSEA CRANE

Comparison of Separation Performance for Four Variables in Rechargeable Silver/Zinc Cells

Results and Discussion -

- All Cells in Both Cycle Life and Wet Life Were Discharged to 100% DoD on Every Cycle. Discharge Rate Was C/5
- Discharge Capacity and Silver Migration Rates

1. Standard vs. Split Wrap (Figs 1-3)
2. PVA Film Insertion (Figs 4-7, Table 1)
3. PVA Coated Film and Casing (Figs 8-10, Table 2)
4. Zircar Substitution for Asbestos (Figs 11-14)

Comparison of Separation Performance for Four Variables in Rechargeable Silver/Zinc Cells

Conclusions -

- Standard Wrap vs. Split Wrap Design
  - Discharge capacity and silver migration rates are not significantly improved by splitting the cellophane wrap over the anode and cathode
- Inclusion of a PVA Film Layer as a Silver Migration Barrier
  - The PVA causes a significant reduction in lifetime discharge capacity while simultaneously extending the cell life
- Use of PVA-Coated Separation
  - Provides some increase in barrier properties to silver migration while not affecting the discharge capacity. However, there was not a significant increase in cycle life

NAVSEA CRANE

Comparison of Separation Performance for Four Variables in Rechargeable Silver/Zinc Cells

Conclusions -

- Substitution of Zircar for Asbestos
  - A slight reduction in discharge capacity over the cell life but also reduces silver migration rate, resulting in longer cell life
- Cell Storage
  - It was noted that cells which stand in a wet, discharged state after initial formation undergo substantial silver migration while in storage

NAVSEA CRANE

Comparison of Separation Performance for Four Variables in Rechargeable Silver/Zinc Cells

Acknowledgements -

The work of Mr. Larry Hammersley in determining the silver migration data and of Mr. Carl Lenn in setting up and monitoring the cycle and wet life testing are gratefully acknowledged. This work was supported in part by NAVSEA 03Z and by SPECWARCOM NS.

NAVSEA CRANE

Comparison of Separation Performance for Four Variables in Rechargeable Silver/Zinc Cells

Figure 1 - Discharge capacity data from first study. Data exhibit scatter. Split wrap cells failed early in cycle life. Zn shedding through bottom of open anode separation penetrated cathode separation permitting hard short formation.

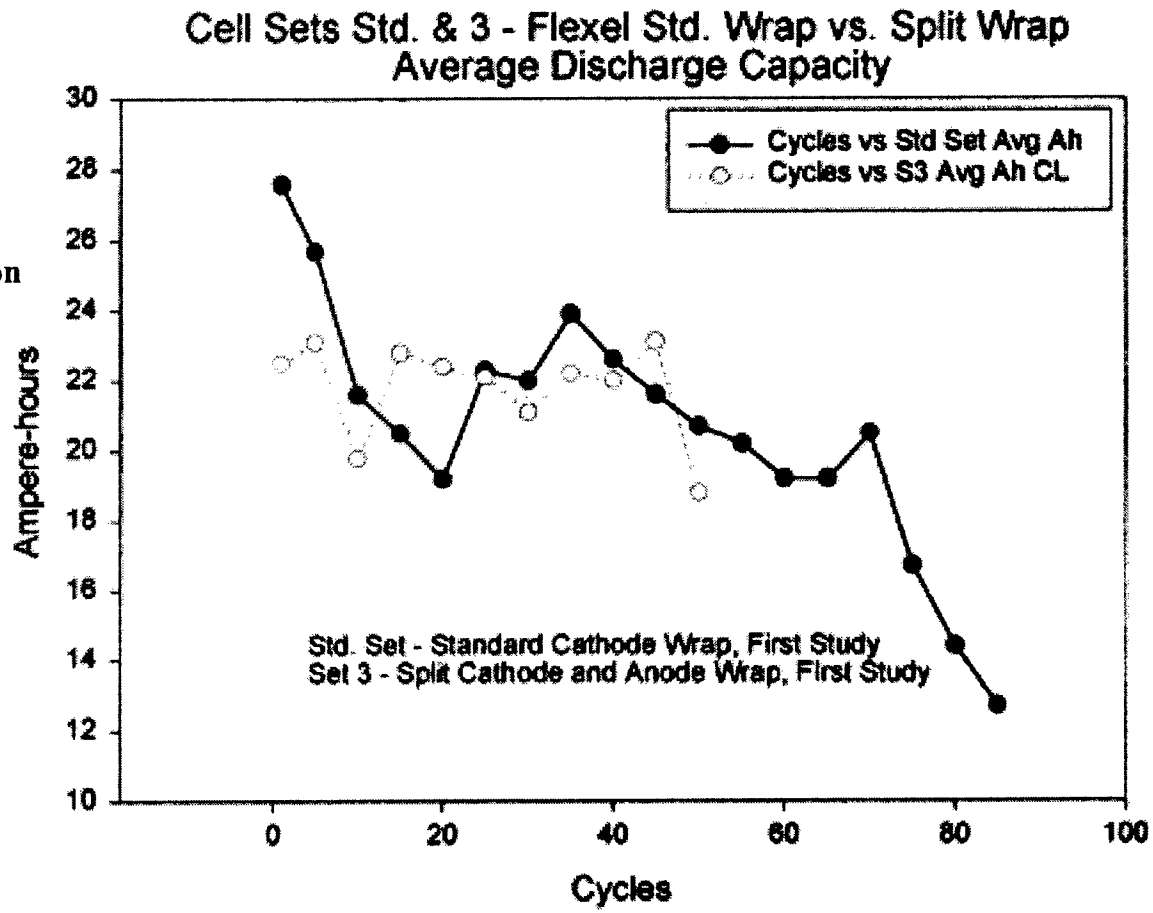

Figure 1.

NAVSEA CRANE

Comparison of Separation Performance for Four Variables in Rechargeable Silver/Zinc Cells

Figure 2 - Discharge capacity data from second study. Split wrap set had anode bottoms wrapped. Two cell sets performed almost identically with a slight capacity advantage to the split wrap.

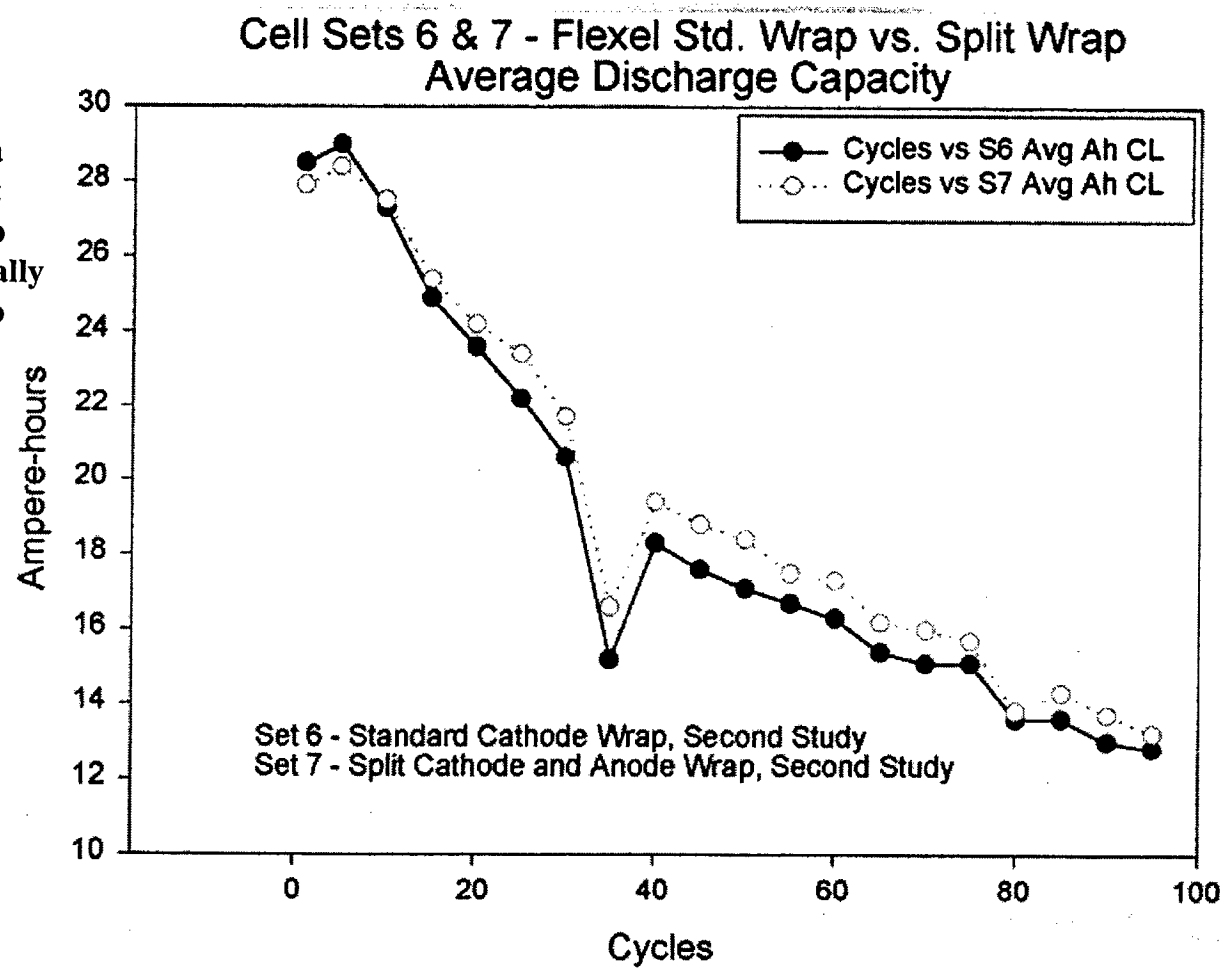

Figure 2.

Comparison of Separation Performance for Four Variables in Rechargeable Silver/Zinc Cells

Figure 3 - Silver migration data from second study for split wrap vs. standard wrap, which shows that there is no advantage to splitting the cellophane wrap in terms of preventing silver migration.

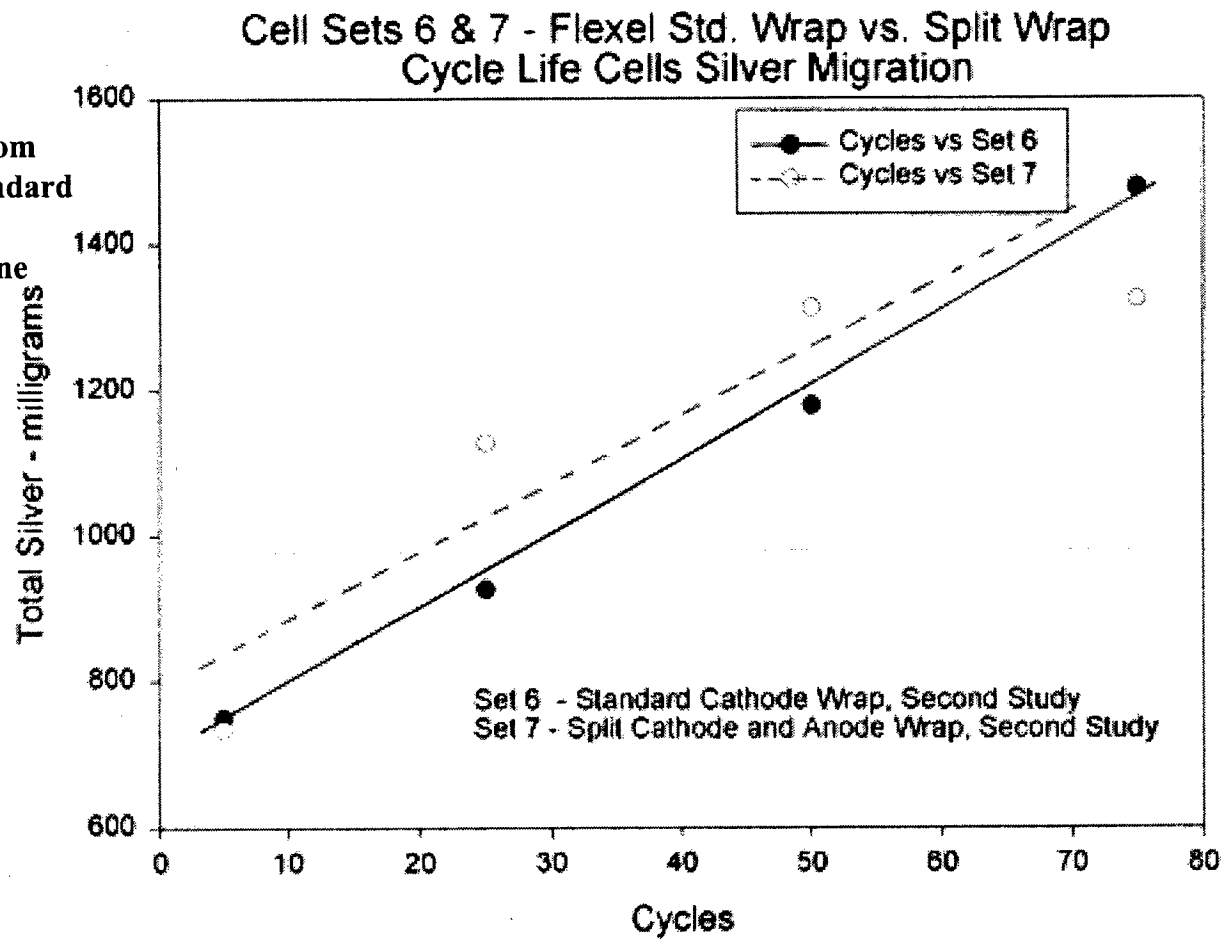

Figure 3.

NAVSEA CRANE

Comparison of Separation Performance for Four Variables in Rechargeable Silver/Zinc Cells

Figure 4 - Discharge capacity data from first study. For both cell sets with an added layer of PVA film, the performance data were inferior to the standard cellophane wrap without PVA.

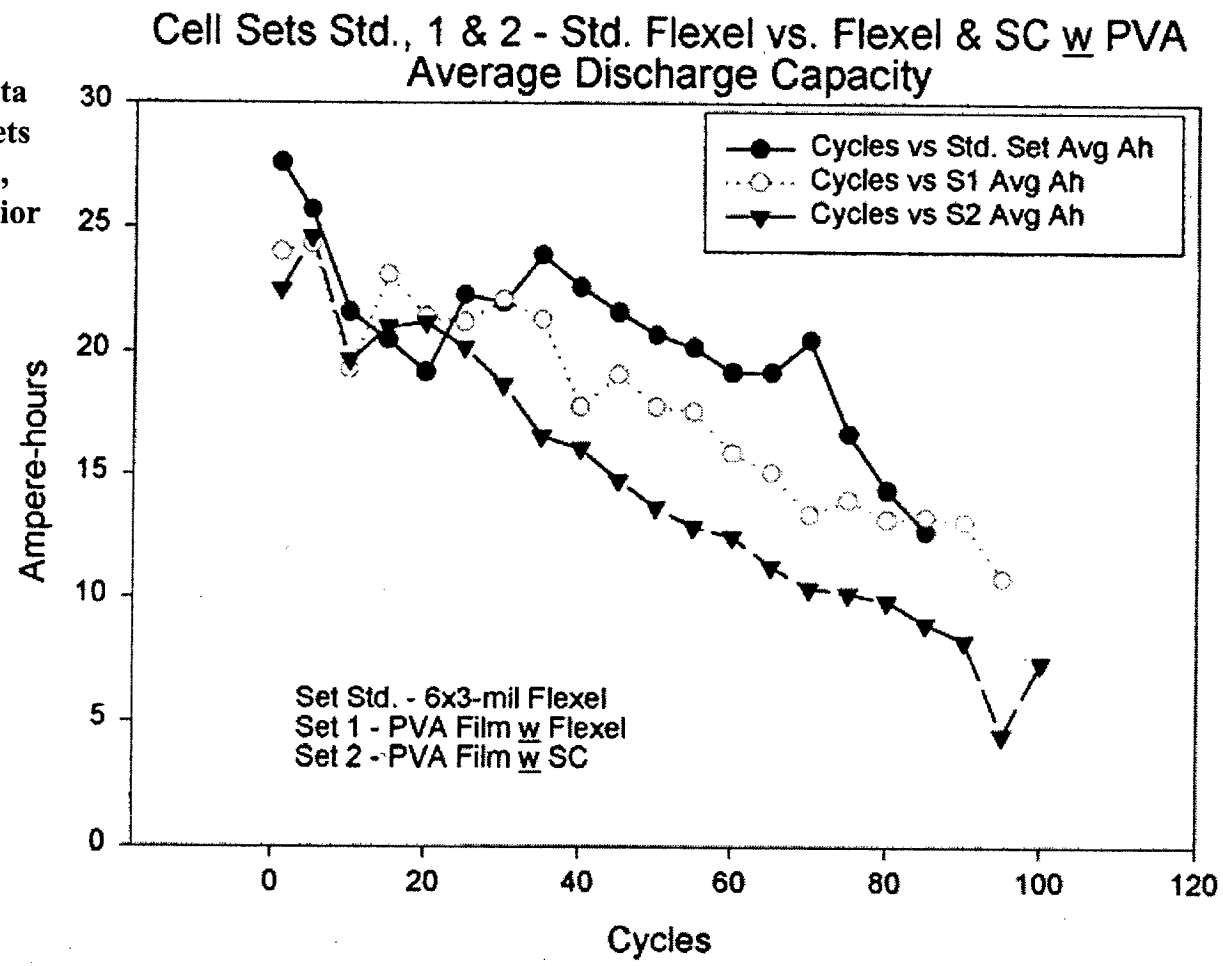

Figure 4.

Comparison of Separation Performance for Four Variables in Rechargeable Silver/Zinc Cells

Figure 5 - Discharge capacity data from the second study. Again the data indicate a performance disadvantage for cells with a layer of PVA film vs. the standard set.

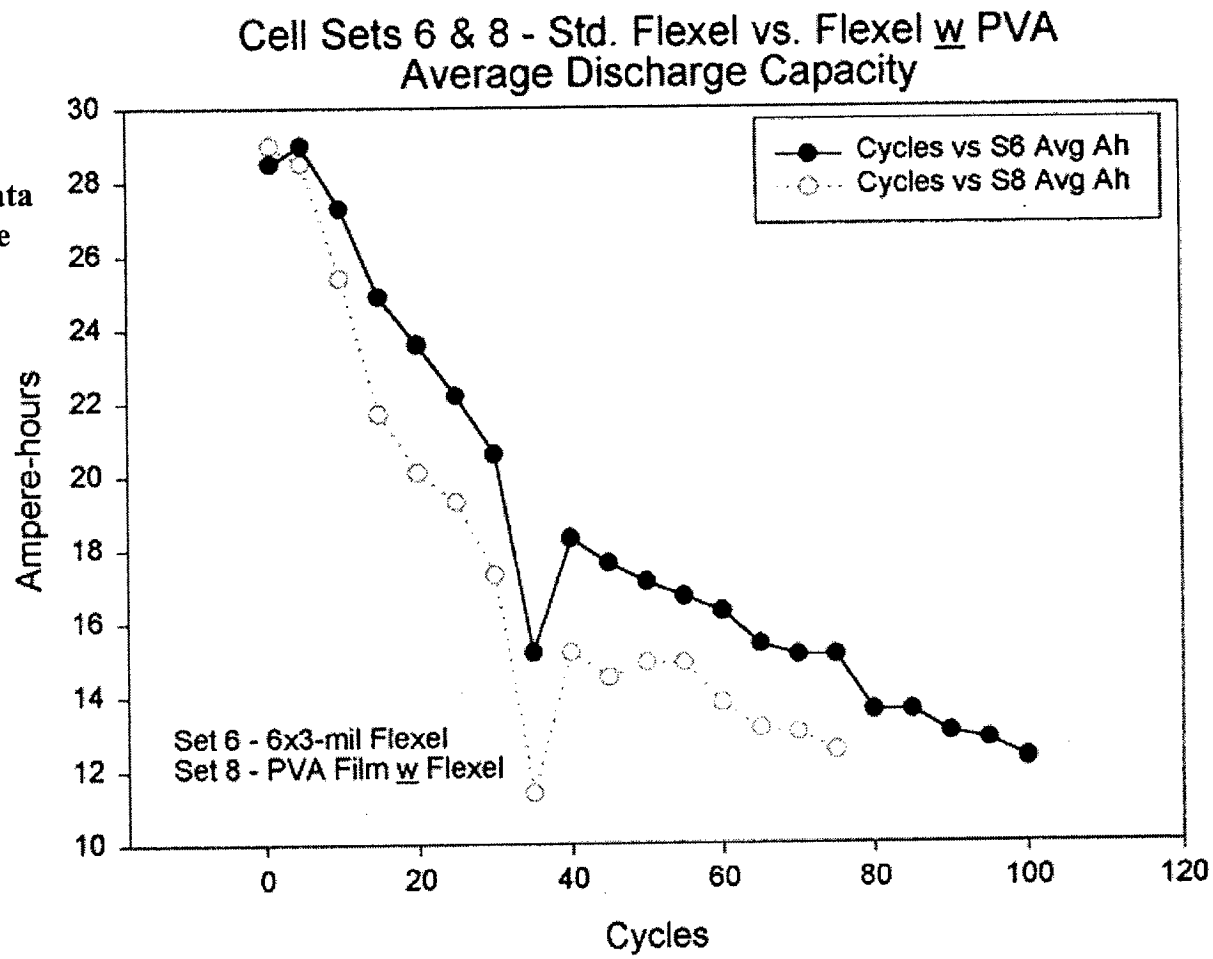

Figure 5.

NAVSEA CRANE

Comparison of Separation Performance for Four Variables in Rechargeable Silver/Zinc Cells

Figure 6 - Discharge capacity data from first study for wet life cells. Data again show a performance disadvantage for cells with a PVA film layer.

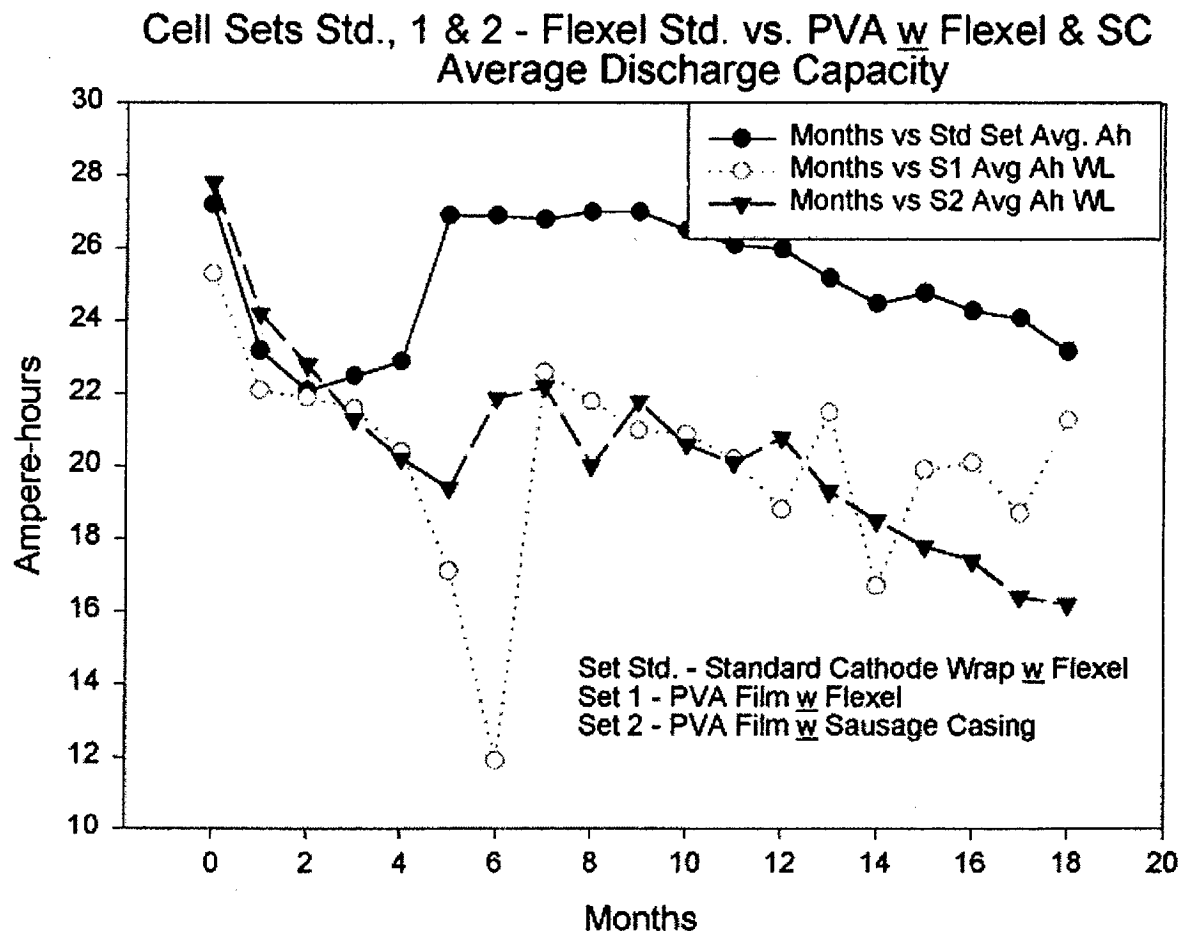

Figure 6.

NAVSEA
CRANE

Comparison of Separation Performance for Four Variables in Rechargeable Silver/Zinc Cells

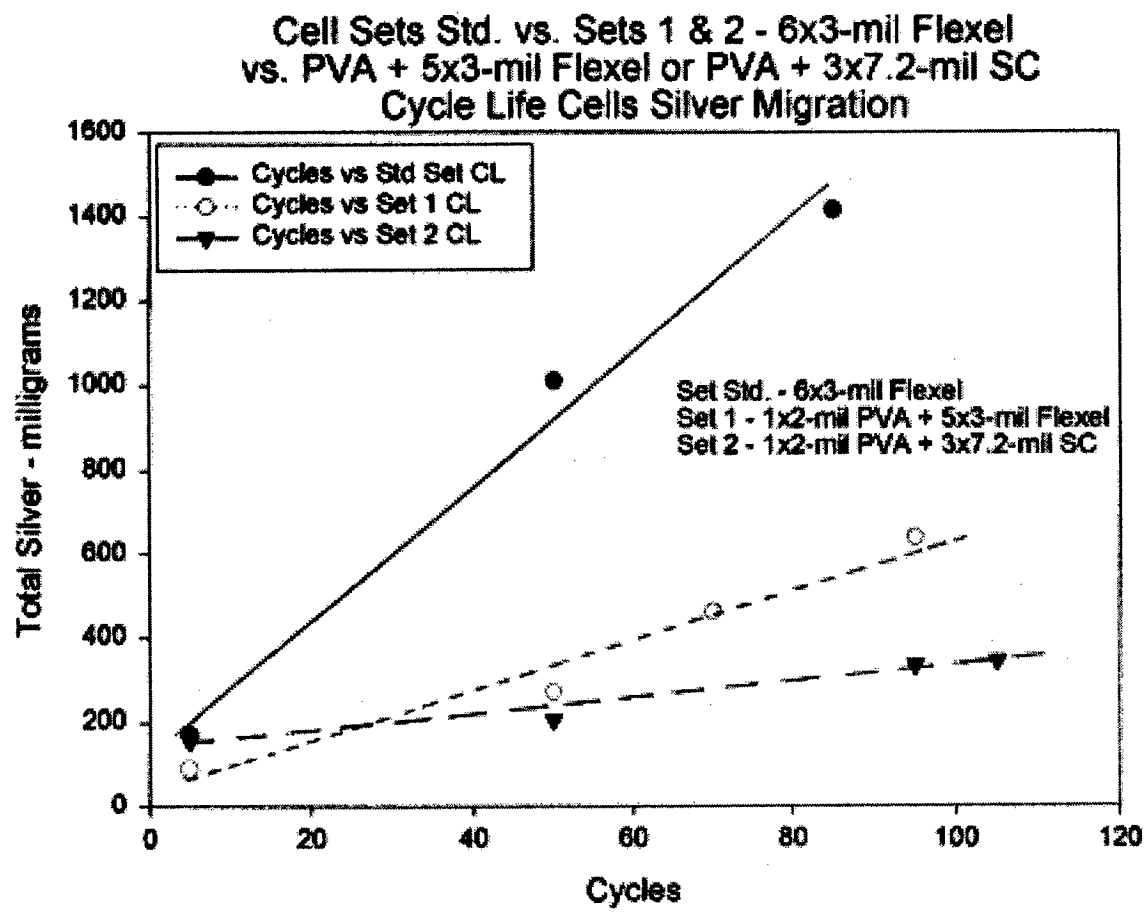

Figure 7.

Figure 7 - Silver migration data from first study, which indicate a definite reduction in rate of silver migration when a layer of PVA film is present in the cathode wrap.

Comparison of Separation Performance for Four Variables in Rechargeable Silver/Zinc Cells

Figure 8 - Discharge capacity data from second study for PVA-coated film and sausage casing separations, which show no performance disadvantage vs. a standard cellophane wrap.

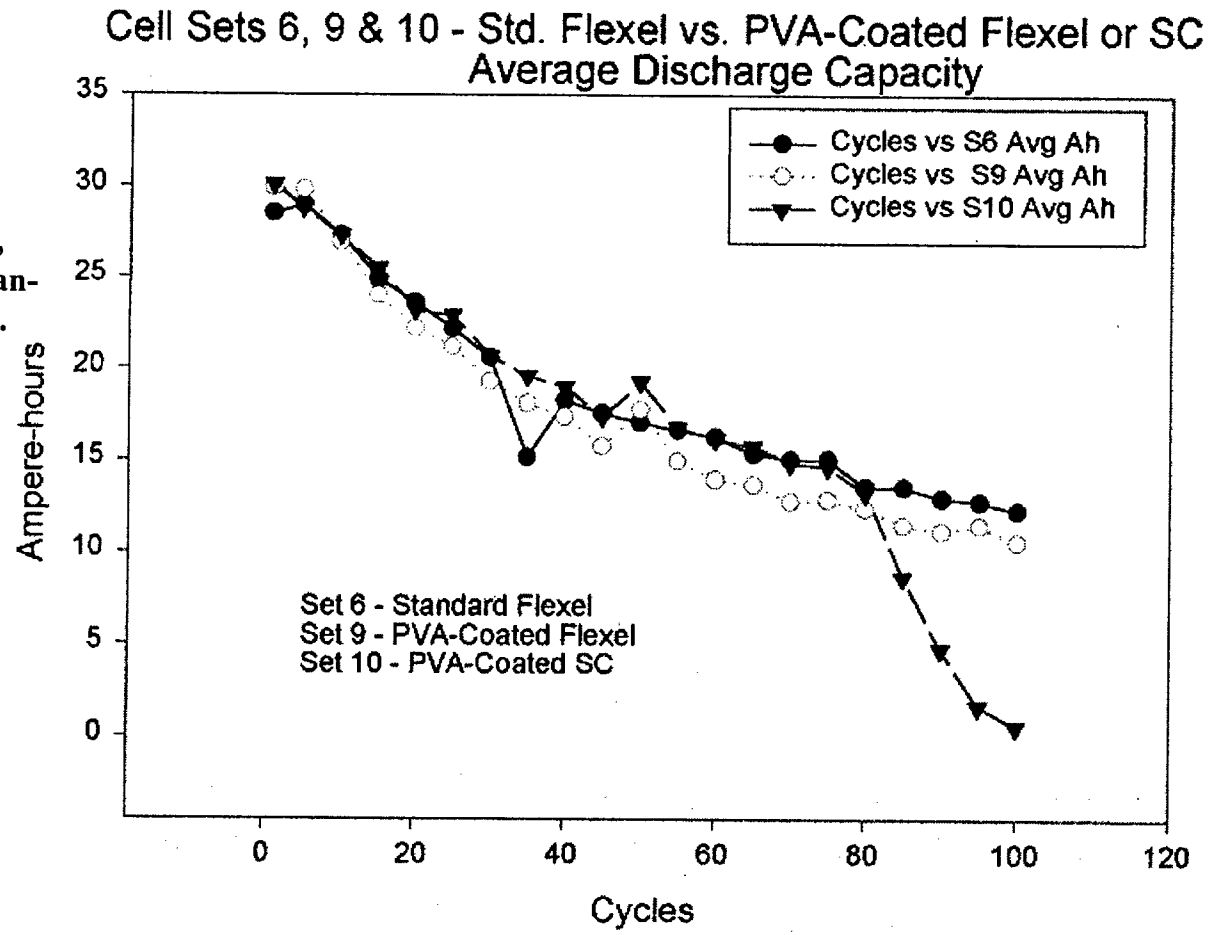

Figure 8.

Comparison of Separation Performance for Four Variables in Rechargeable Silver/Zinc Cells

Figure 9 - Discharge capacity data from second study for PVA film layer vs. PVA-coated film which show the performance disadvantage for the film layer when compared to PVA-coated separation.

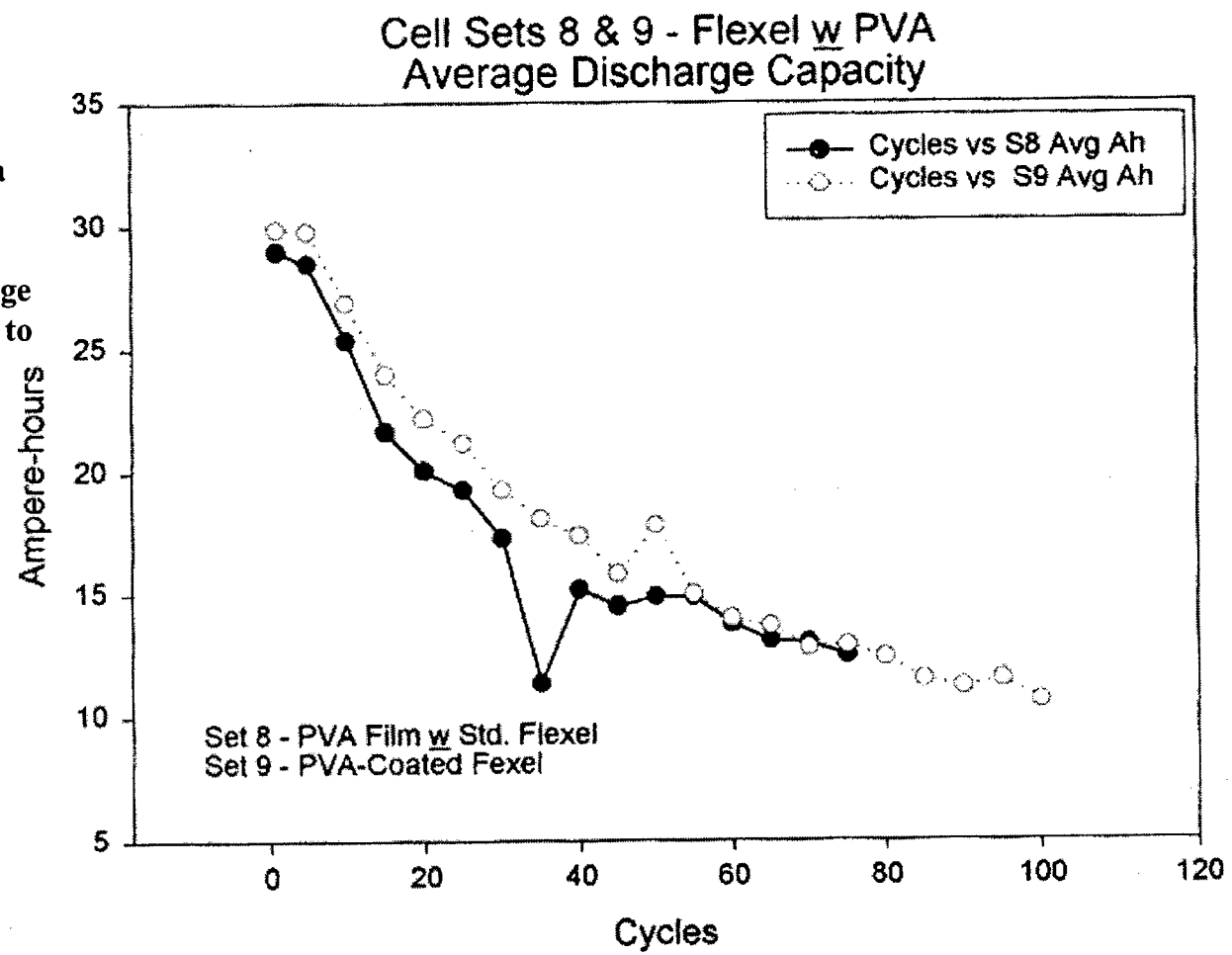

Figure 9.

Comparison of Separation Performance for Four Variables in Rechargeable Silver/Zinc Cells

Figure 10 - Discharge capacity data from first and second studies for PVA film layer with sausage casing vs. PVA-coated sausage casing which show the performance disadvantage for the film layer cell set.

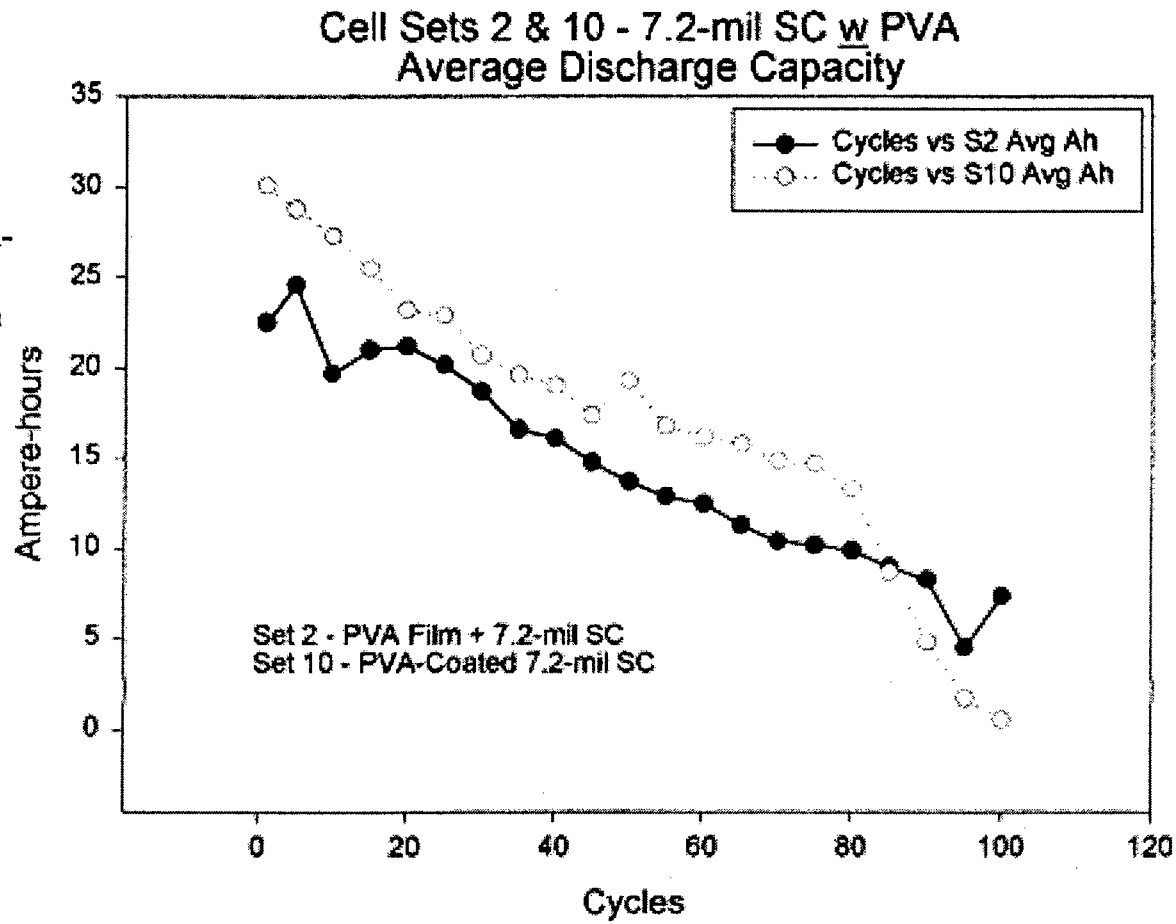

Figure 10.

NAVSEA CRANE

Comparison of Separation Performance for Four Variables in Rechargeable Silver/Zinc Cells

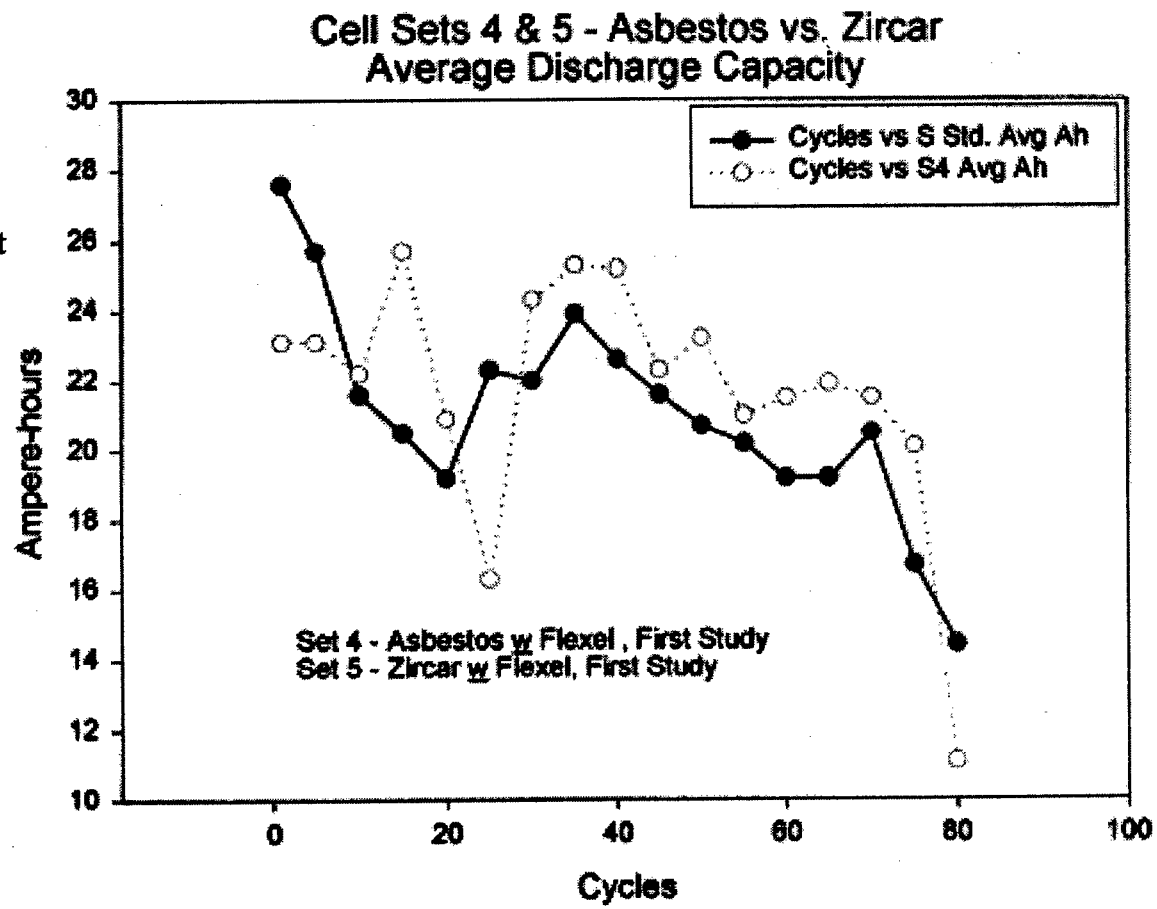

Figure 11.

Figure 11 - Discharge capacity data from first study for substitution of Zircar for asbestos as a fire retardant layer of separation. Scatter in data prevent a definitive analysis, but the indication is that the two separation configurations performed about the same.

Comparison of Separation Performance for Four Variables in Rechargeable Silver/Zinc Cells

Figure 12 - Discharge capacity data from second study for Zircar as a replacement for asbestos. These data indicate that there is no significant performance difference between the two materials.

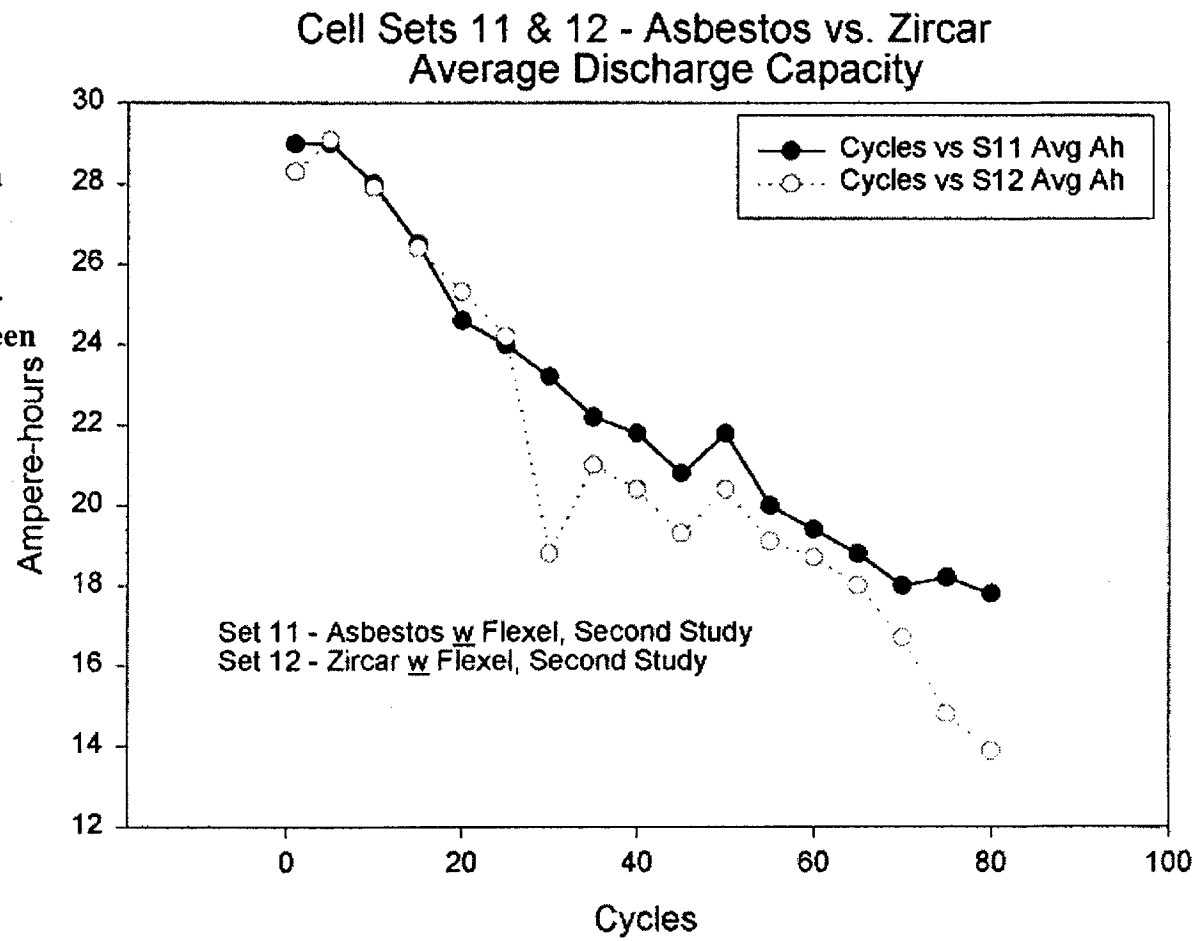

Figure 12.

NAVSEA CRANE

Comparison of Separation Performance for Four Variables in Rechargeable Silver/Zinc Cells

Figure 13 - Silver migration data from first study for Zircar and asbestos vs. the standard cellophane wrap without a fire retardant layer. The data show the retardant layers also act as a silver barrier, but that one is about as effective as the other.

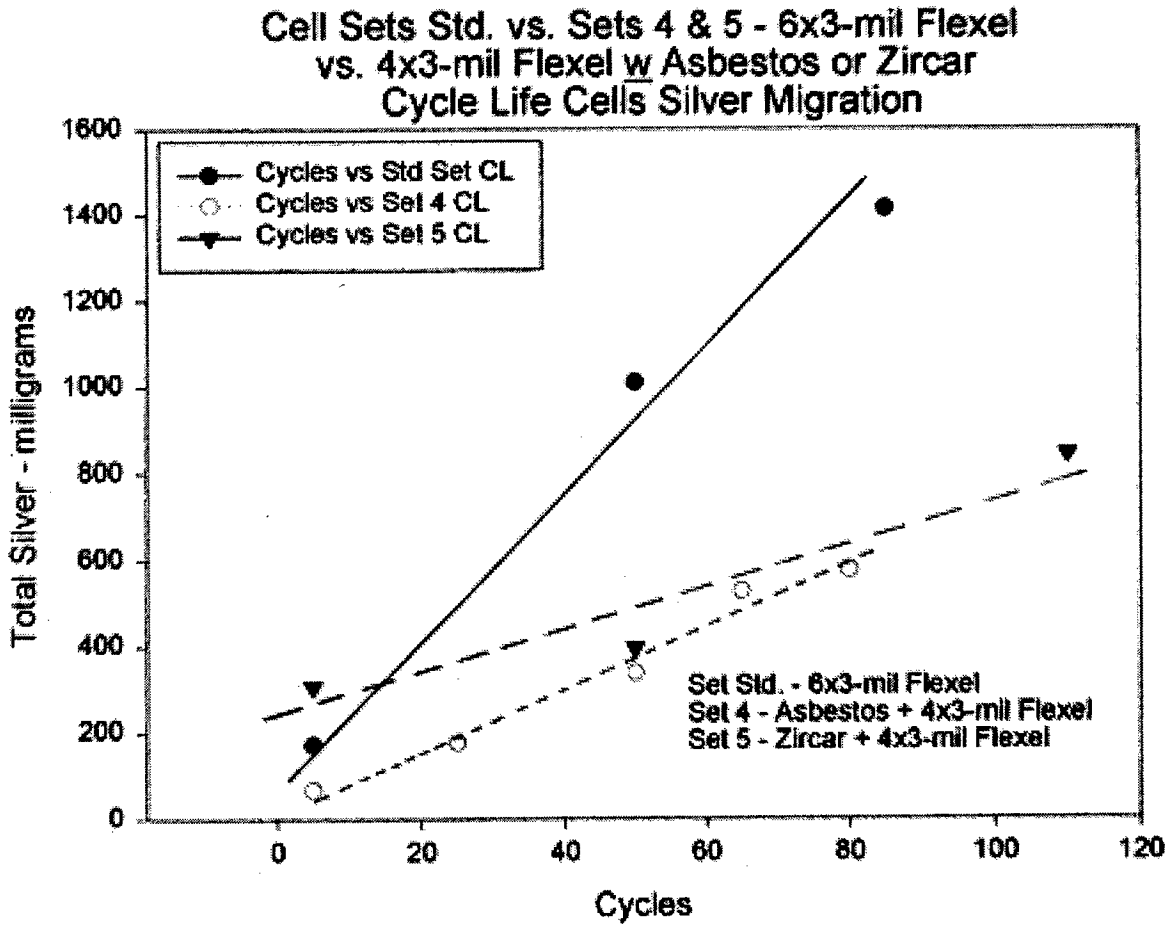

Figure 13.

Comparison of Separation Performance for Four Variables in Rechargeable Silver/Zinc Cells

Figure 14 - Silver migration data from second study, and again the data show barrier properties for the two fire retardant layers with no particular advantage for either one.

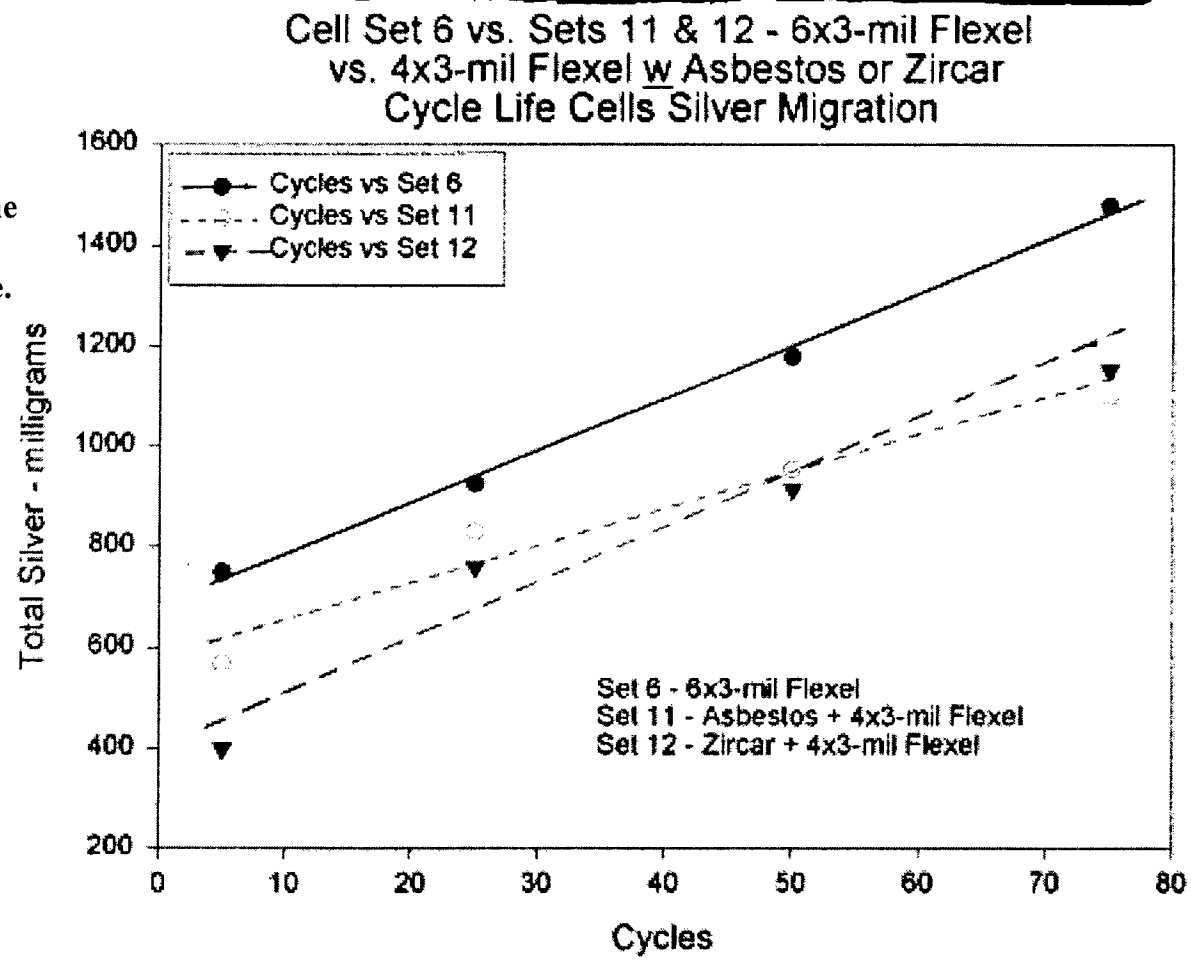

Figure 14.

NAVSEA CRANE

Comparison of Separation Performance for Four Variables in Rechargeable Silver/Zinc Cells

TABLE 1

Silver migration data by separation layer for cells with standard wrap vs. cells with a PVA film layer.

Cell Designation	Cycles	Ag Migration (ICP/Titr'n) - mg/sq cm							
		Fiber/Pellon	Layer 1	Layer 2	Layer 3	Layer 4	Layer 5	Layer 6	Total
Set Std. 6x3-mil Flexel	5	0.143	0.766	01.38	0.016	0	0	0	1.062
Set 1- PVA + 5x3-mil Flexel	5	0.110	0.362	0.138 - PVA	0.131	0	0	0	0.741
Set 2 - PVA + 3x7.2-mil SC	5	0.111	0.783	0.06 - PVA	0.08	0	N/A	N/A	0.908
Set 6 - Std. 6x1-mil Flexel	5	0.529	3.792	0.674	0.109	0	0	0	5.104
Set 8 - PVA + 5x3-mil Flexel	5	0.838	3.986 - PVA	0.002	0	0	0	0	4.826
Set 6 - Std. 6x1-mil Flexel	25	0.396	4.287	1.215	0.277	0.032	0	0	6.207
Set 8 - PVA + 5x3-mil Flexel	25	1.585	8.156 - PVA	0.037	0	0	0	0	9.778
Set Std. 6x3-mil Flexel	50	0.186	3.652	1.369	0.282	0	0	0	5.489
Set 1- PVA + 5x3-mil Flexel	50	0.209	0.892	0.620 - PVA	0.004	0.004	0	0	1.730
Set 2 - PVA + 3x7.2-mil SC	50	0.224	0.747	0.110 - PVA	0.122	0	N/A	N/A	1.204
Set 6 - Std. 6x1-mil Flexel	50	0.675	5.219	1.746	0.443	0.047	0	0	8.129
Set 8 - PVA + 5x3-mil Flexel	50	2.066	10.272 - PVA	0.007	0	0	0	0	12.345
Set Std. 6x3-mil Flexel	88	0.408	5.337	2.564	1.100	0.390	0.031	0.020	9.810
Set 1- PVA + 5x3-mil Flexel	97	0.248	1.685	1.326 - PVA	0.344	0	0	0	3.602
Set 2 - PVA + 3x7.2-mil SC	210	0.194	3.371	0.303 - PVA	0.144	0.03	N/A	N/A	3.949
Set 6 - Std. 6x1-mil Flexel	75	0.509	6.234	2.367	0.660	0.106	0.013	0	9.889
Set 8 - PVA + 5x3-mil Flexel	75	2.137	11.940 - PVA	0.022	0	0	0	0	14.099

NAVSEA CRANE

Comparison of Separation Performance for Four Variables in Rechargeable Silver/Zinc Cells

TABLE 2

Silver migration data by separation layer for cells with standard wrap vs. cells with PVA-coated wrap.

Cell Designation	Cycles	Ag Migration (ICP/Titr'n) - mg/sq cm							
Set 6 - Std. 6x1-mil Flexel	5	0.529	3.792	0.674	0.109	0	0	0	5.104
Set 9 - 6x3-mil PVA-Coated Flexel	5	0.679	3.684	0.570	0.100	0	0	0	4.946
Set 10 - 3x7.2-mil PVA-Coated SC	5	0.631	5.635	0	N/A	N/A	N/A	N/A	6.266
Set 6 - Std. 6x1-mil Flexel	25	0.396	4.287	1.215	0.277	0.032	0	0	6.207
Set 9 - 6x3-mil PVA-Coated Flexel	25	0.718	5.465	1.080	0.144	0	0	0	7.406
Set 10 - 3x7.2-mil PVA-Coated SC	25	0.486	6.605	0	N/A	N/A	N/A	N/A	7.091
Set 6 - Std. 6x1-mil Flexel	50	0.675	5.219	1.746	0.443	0.047	0	0	8.129
Set 9 - 6x3-mil PVA-Coated Flexel	50	0.597	7.249	1.900	0.305	0	0	0	10.051
Set 10 - 3x7.2-mil PVA-Coated SC	50	0.986	8.627	0.155	N/A	N/A	N/A	N/A	9.768
Set 6 - Std. 6x1-mil Flexel	75	0.509	6.234	2.367	0.660	0.106	0.013	0	9.889
Set 9 - 6x3-mil PVA-Coated Flexel	75	0.843	7.894	2.477	0.539	0.037	0	0	11.790
Set 10 - 3x7.2-mil PVA-Coated SC	75	0.916	10.331	0.246	N/A	N/A	N/A	N/A	11.493

THERMAL ASPECTS OF LITHIUM ION CELLS

H.Frank, P.Shakkottai, R. Bugga, M.Smart, C.K.Huang, P.Timmerman, and S.Surampudi

Jet Propulsion Laboratory
Pasadena, CA

1999 NASA BATTERY WORKSHOP
17 November, 1999

OBJECTIVE

Develop thermal model of Li-Ion cells in terms of heat generation, thermal mass, and thermal resistance. Intended for incorporation into battery model.

APPROACH

Heat Generation:

-Estimate rates with semi-theoretical model

-Check accuracy with efficiency measurements

Thermal Mass:

-Compute from component weights and specific heats

Thermal Resistance:

-Compute from component dimensions & conductivities

METHOD FOR ESTIMATING HEAT GENERATION RATE

$Q = I (V_{oc} - V)$

where:

Q	=	instantaneous cell heat generation at given current (I), temperature (T), and state-of-charge (SOC)
I	=	Cell current , amps
V_{oc}	=	open circuit voltage (V) at given T, and SOC, volts
V	=	operating voltage at given I, T, and SOC, volts

INPUT DATA OBTAINED EXPERIMENTALLY

V_{oc} as a function of SOC and T

V as a function of SOC, I, and T

Properties of components

Cylindrical lithium battery						
length, Lx or height	0.192	m				
diameter	0.047	m				
Conductivities						
kpara along x	57	W/mK				
keff=kz in the normal directio	1.73	W/mK				
RESISTANCES						
Rperp_whole cell, Rz	1.82	K/W				
Rx, along length	1.9425	K/W				
Ral_tab	77.7	K/W				
mass and thermal properties						
	mass,kg	cp,J/kg K	density,kg/m3	k, W/mK	mass*cp, J/oK	
can stainless	0.126	502.8	7800	16.3	63.3528	
A_coating	0.112	838	1800	5	93.856	
C_coating	0.318	838	1800	5	266.484	
Copper substrate	0.064	385.48	8900	381.29	24.67072	
Al substrate	0.043	905.04	2700	201.12	38.91672	
separator	0.027	1676	900	0.2	45.252	
electrolyte	0.227	2514	1200	0.1676	570.678	
TOTAL	0.917				**1103.2**	**thermal mass**

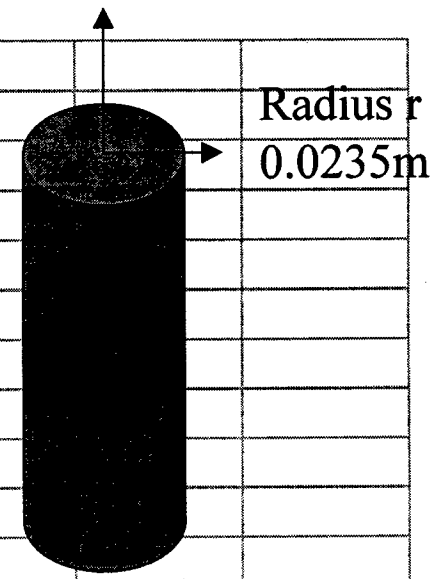

Component Properties

Prismatic lithium cell						
length, Lx	0.118	m				
width, Ly	0.091	m				
thickness,Lz	0.027	m				
area	0.010738	m2				
Conductivities						
kpara along x or y	26.69	W/mK				
keff=kz in the normal directio	1.848	W/mK				
RESISTANCES						
Rperp_whole cell, Rz	1.379	K/W				
Rx, along length	1.778	K/W				
Ry, along width	1.049	K/W				
Ral_tab	21.14	K/W				
R_all_tabs	0.128	K/W				
mass and thermal properties						
	mass,kg	cp,J/kg K	density,kg/m3	k, W/mK	mass*cp J/K	
can stainless	0.169	502.8	7800	16.3	84.9732	
A_coating	0.184	838	1800	5	154.192	
C_coating	0.228	838	1800	5	191.064	
Copper substrate	0.077	385.48	8900	381.29	29.68196	
Al substrate	0.043	905.04	2700	201.12	38.91672	
separator	0.02	1676	900	0.2	33.52	
electrolyte	0.146	2514	1200	0.1676	367.044	
TOTAL	0.867				**899.39188**	**thermal mass**

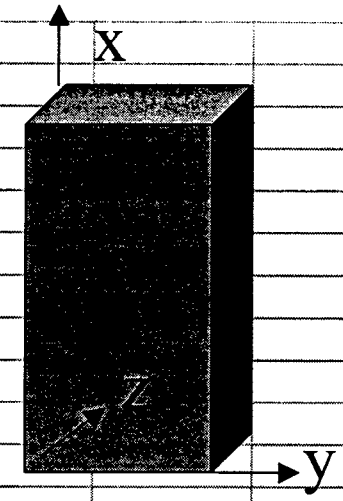

CONCLUSIONS

25 AH Li-ION CELL

HEAT GENERATION

- Developed heat generation rate model as function of I, V, & SOC
- Heat proportional to I for C & D
- Heat increases with decrease in T
- Heat is relatively independent of SOC
- Typical Heat @ 5A, 0°C, & 50%DOD: 1.5W(D), 0.5W(C)
- Support for model shown by agreement of predicted heat (by integrating calculated values) and indirectly measured heat (from electrical efficiency data) for a complete cycle

CONCLUSIONS

(cont'd)

THERMAL MASS

Prismatic Cell.....900 J/°K

Cylindrical Cell.....1103 J/°K

THERMAL RESISTANCE

Prismatic (Perpendicular to plates).....1.4°K/W

Prismatic (Parallel to plates,).....1.0-1.8 °K/W

Cylindrical (Perpendicular to plates, radial).....1.8°K/W

Cylindrical (Parallel to plates, along height).....1.9°K/W

Open-circuit Curves of Prismatic Li Ion cells

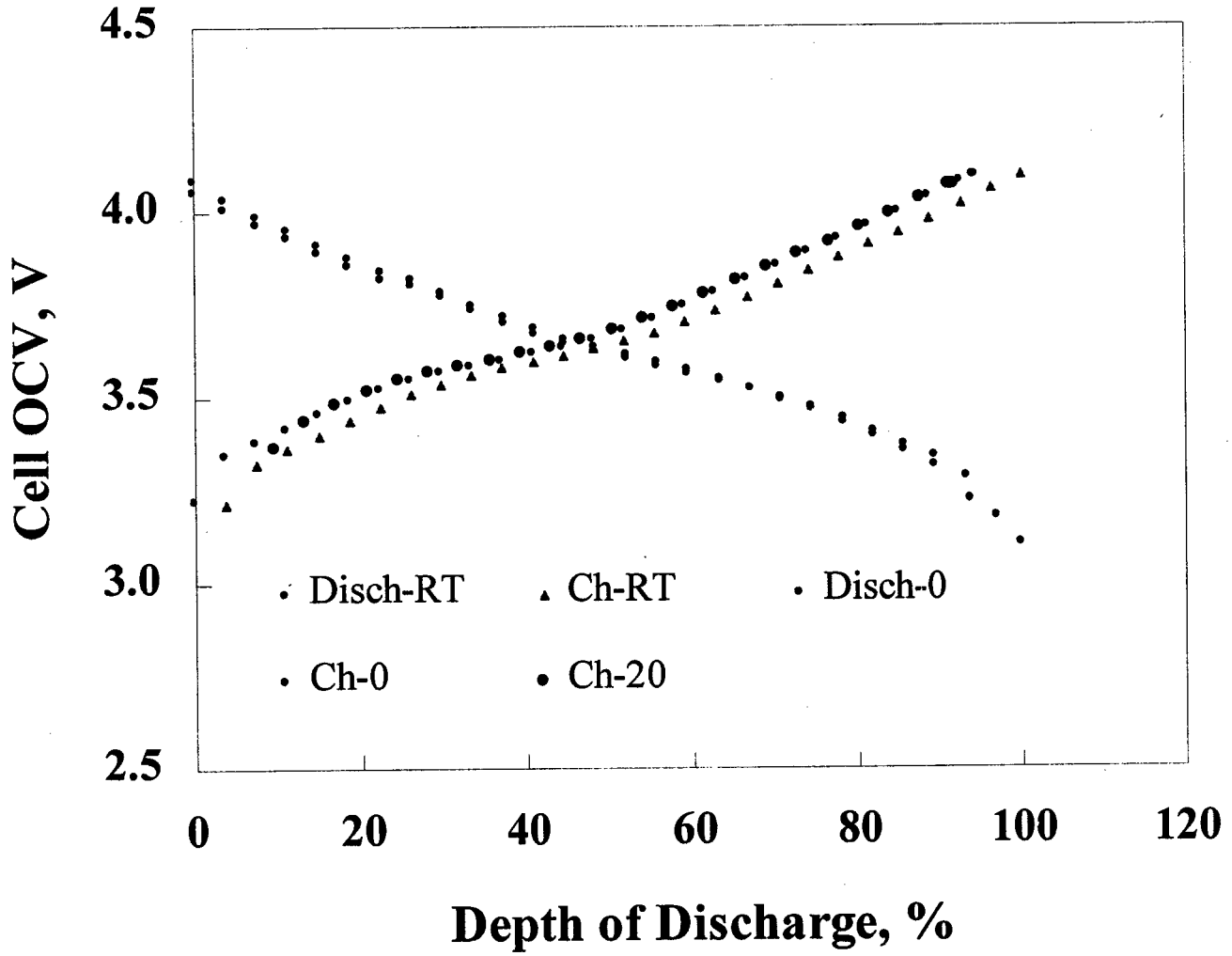

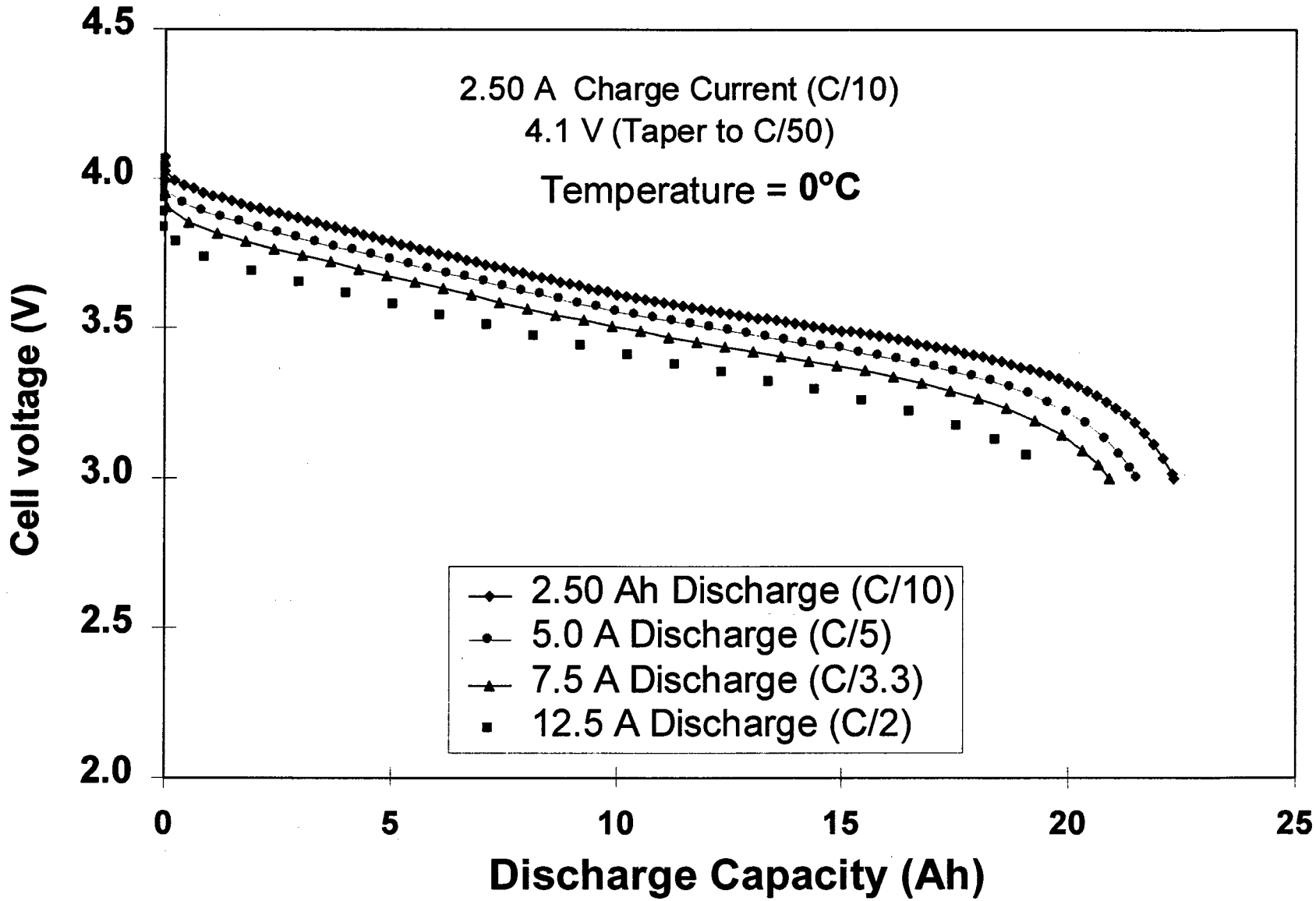
2.50 A Charge Current (C/10)
4.1 V (Taper to C/50)
Temperature = 0°C
2.50 Ah Discharge (C/10)
5.0 A Discharge (C/5)
7.5 A Discharge (C/3.3)
12.5 A Discharge (C/2)
Cell voltage (V)
4.5
4.0
3.5
3.0
2.5
2.0
0
5
10
15
20
25
Discharge Capacity (Ah)

Heat Evolution During Discharge of Prismatic Cells

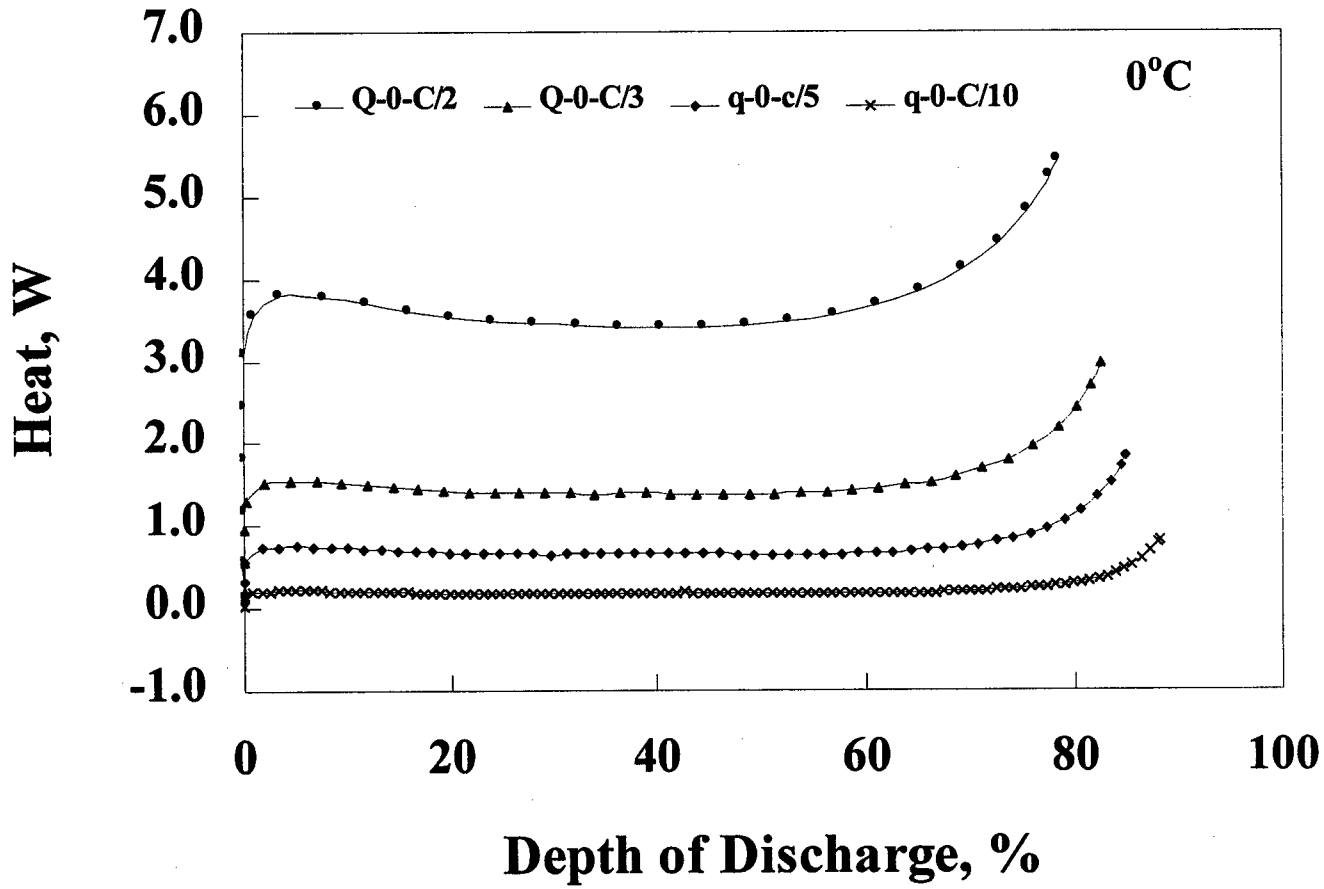

Heat Evolution During Charge of Prismatic Cells

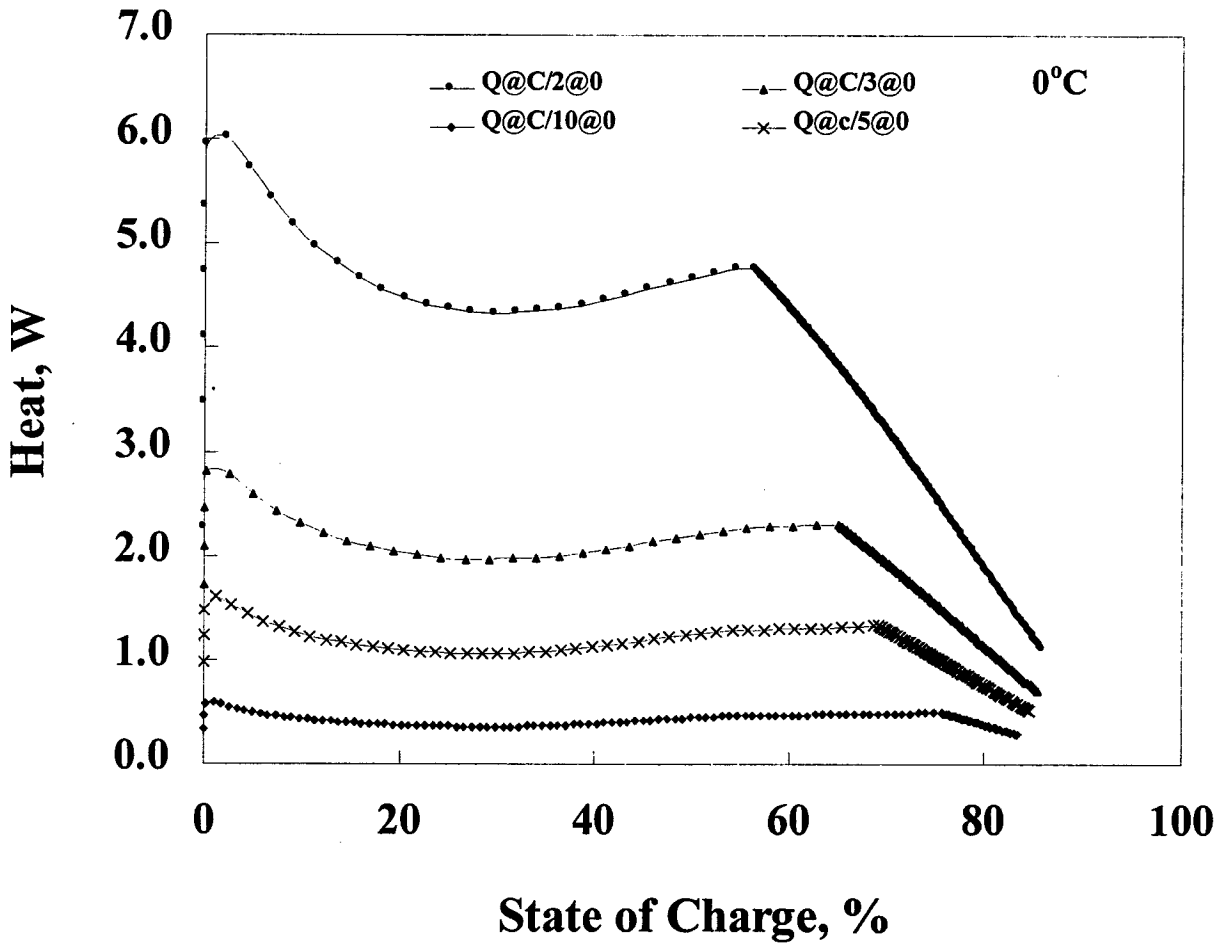

Heat Evolution During Discharge of Prismatic Cells

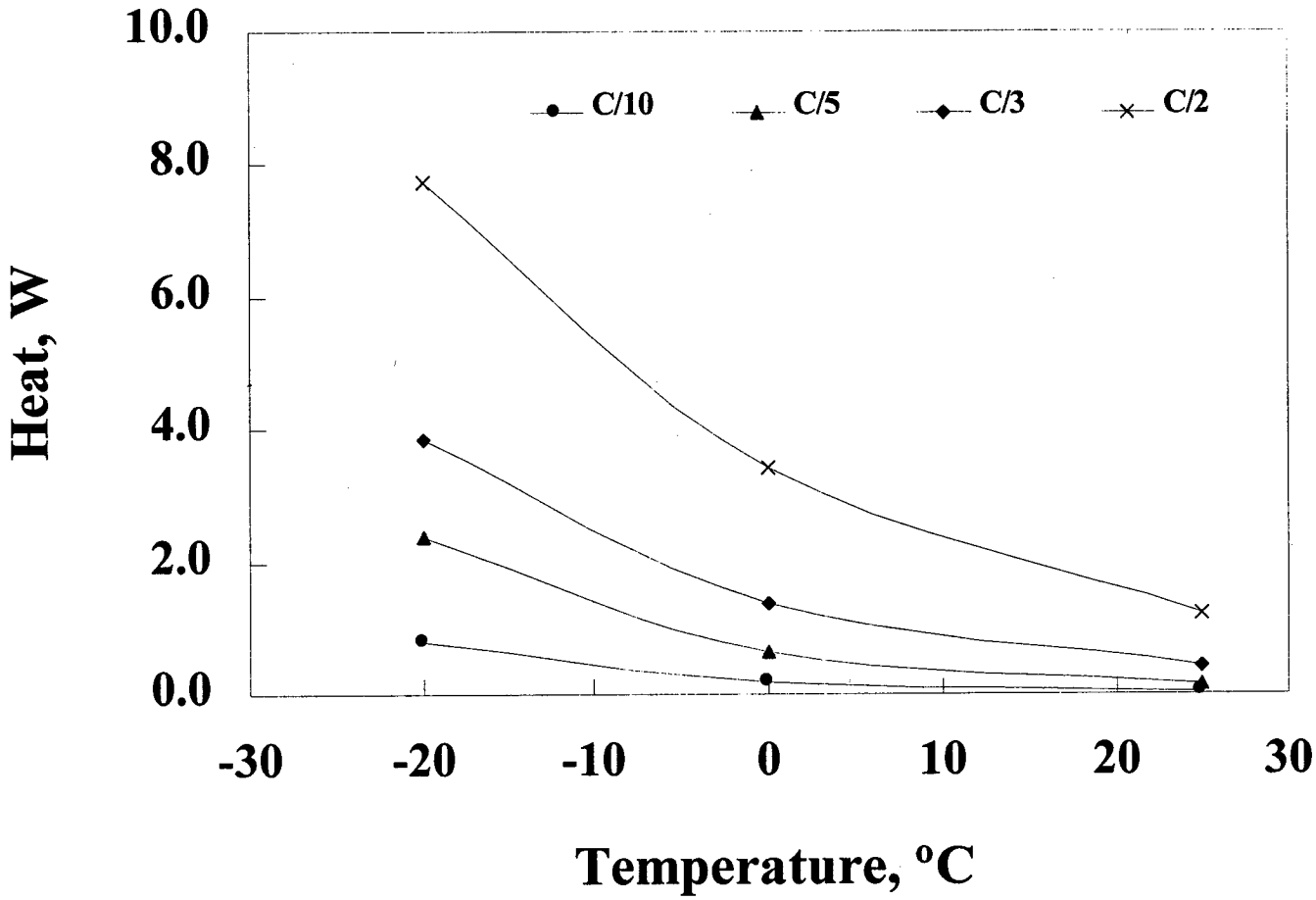

EAGLE PICHER Technologies, LLC

Pulse Testing of the Eagle-Picher Lithium-Ion System

Chad Kelly & Beth Parmley

Advanced Electrochemical Systems Operation
Eagle-Picher Technologies, LLC
3220 Industrial Drive
Joplin, Missouri 64801

POWER Subsystems

EAGLE PICHER Technologies, LLC

Pulse Test Goals

- Demonstrate pulse capabilities of EPT lithium-ion system
- Compare pulse results of small cells to those of medium cells
- Evaluate ultrasonic weld versus pop rivet

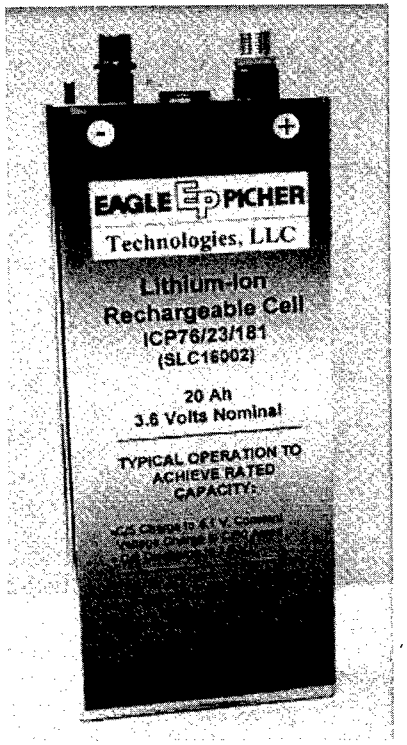

SLC-16002 (20 Ah)

POWER Subsystems

EAGLE PICHER Technologies, LLC

Completed Tests

- **250 mAh cell**
  - May 1999
  - Maccor test system
  - 5 states-of-charge
  - 10 current densities
  - 5 pulse durations
- **20 Ah cell (ultrasonic weld)**
  - October 1999
  - EPT custom test console (NiH_2)
  - 5 states-of-charge
  - 6 current densities
  - 1 pulse duration
- **20 Ah cell (ultrasonic weld & pop rivet)**
  - November 1999
  - Maccor test system
  - 1 state-of-charge
  - 3 current densities
  - 1 pulse duration

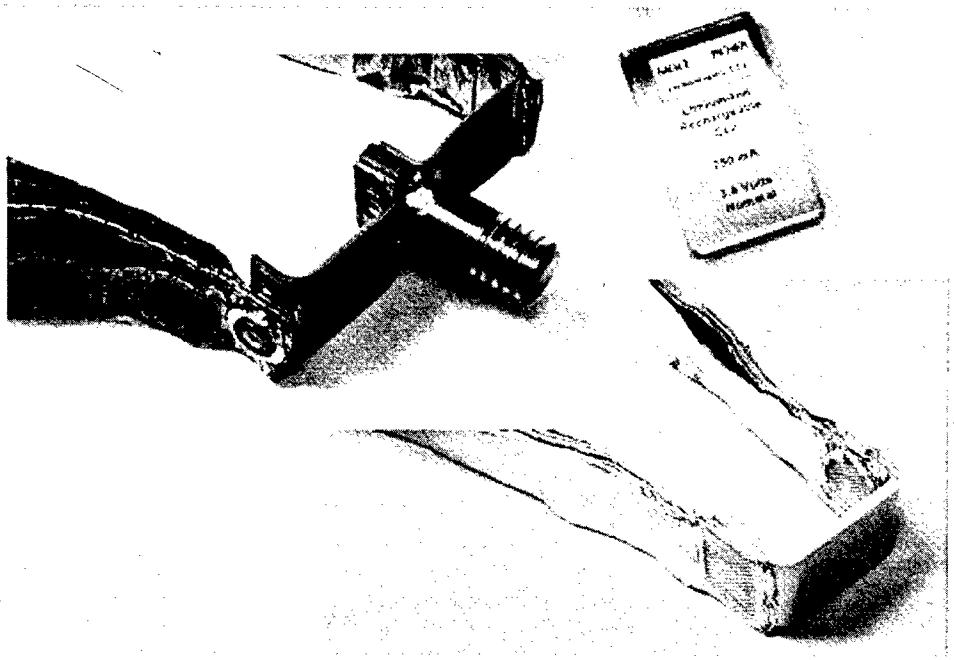

POWER Subsystems

EAGLE PICHER Technologies, LLC

Pulse Voltage - 250 mAh

- SLC-16014B, 250 mAh cell
- 66%, 53%, 39%, 26%, and 13% state of charge
- 100 ms, 500 ms, 1 sec, 5 sec, and 30 sec duration
- 10 minutes between pulses
- 21 mA, 42 mA, 72 mA, 106 mA, 179 mA, 435 mA, 870 mA, 1306 mA, 2600 mA, and 3000 mA currents

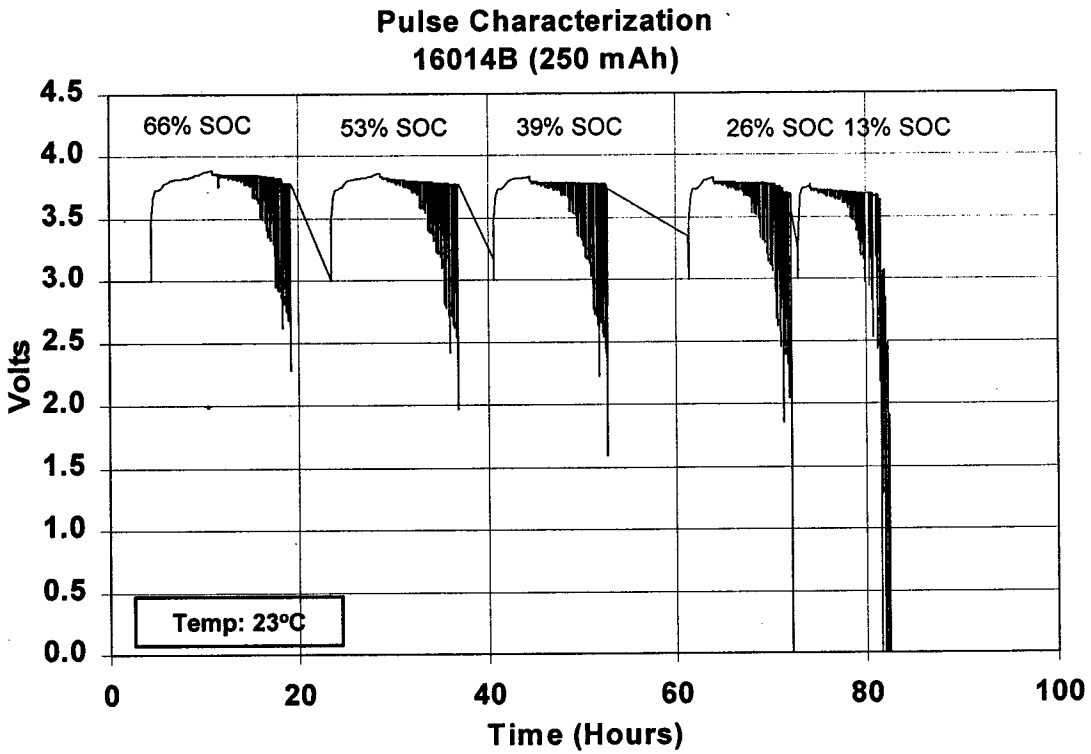

POWER Subsystems

EAGLE PICHER Technologies, LLC

Pulse Characterization 250 mAh

- Cells were tested using 5 durations, 10 rates, and 5 states of charge
- 500 msec duration test on SLC-16014B, 250 mAh cell @ 23°C
- Cell maintains > 3V at 4.6 C for SOC's > 25%
- Voltage drop increases nonlinearly at lower SOC (13% and 26%)

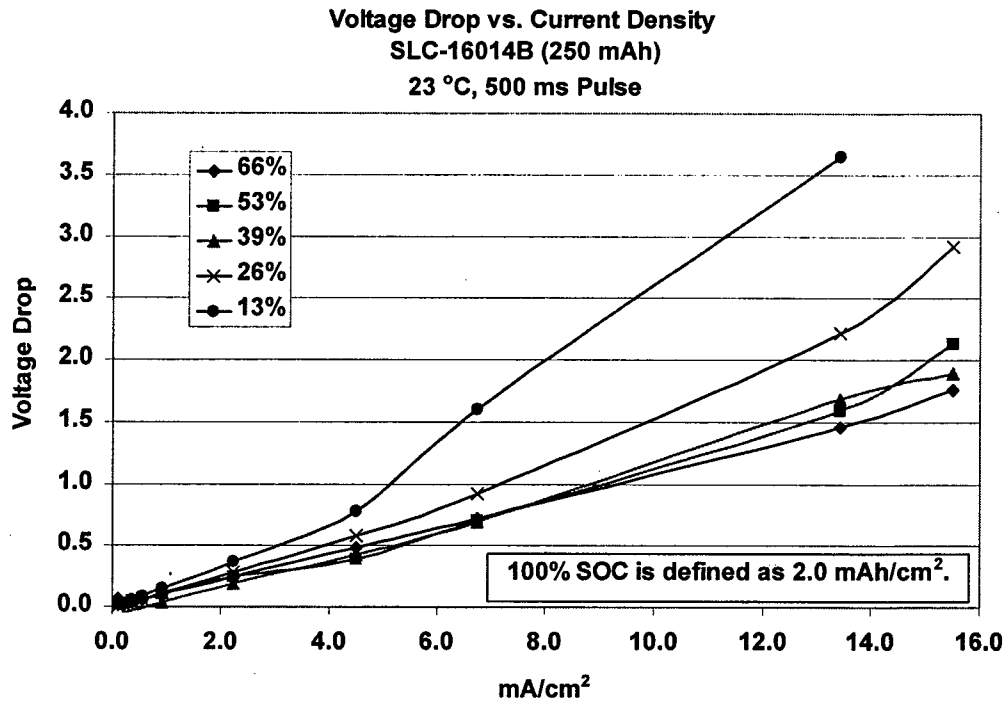

1.3 mA/cm² ≅ 1C

POWER Subsystems

EAGLE PICHER Technologies, LLC

Pulse Voltage Response 250 mAh

- Voltage response for 500 ms, 2.55 A pulse
- SLC-16014B, 250 mAh cell
- 66% state-of-charge @ 23°C
- 390 mΩ calculated impedance (ΔV/ΔI)

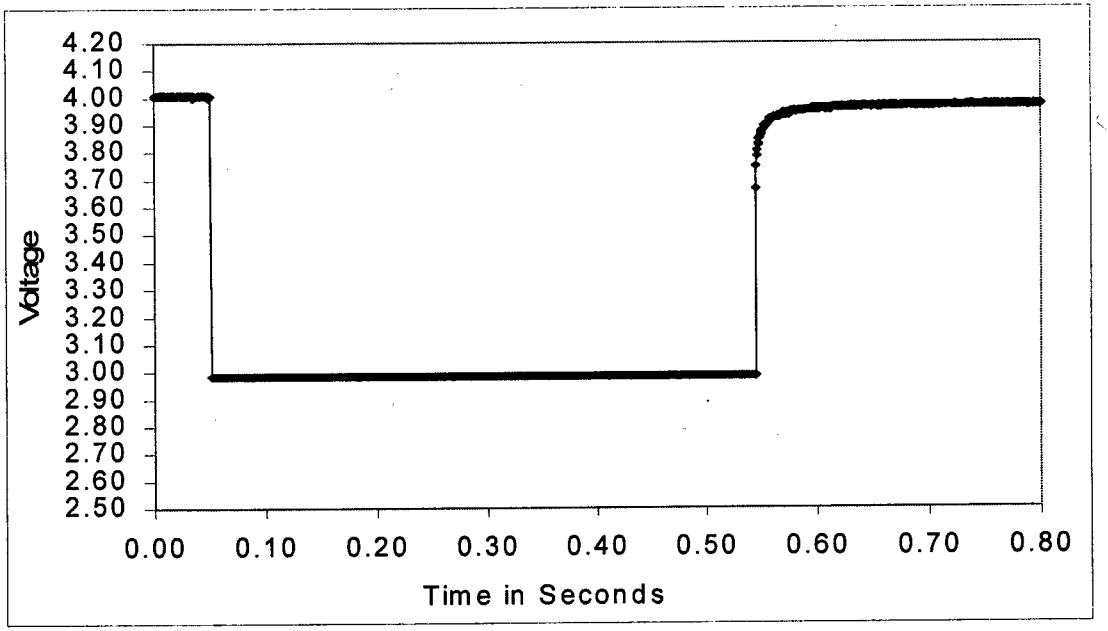

POWER Subsystems

EAGLE PICHER Technologies, LLC

Pulse Voltage - 20 Ah

- SLC-16002, 20 Ah cell
- 100%, 80%, 60%, 40% and 20% state of charge
- Three capacity cycles between each SOC
- 10-second pulses at 20A, 40A, 80A, 100A, 120A, and 140A
- 10 minutes between pulses

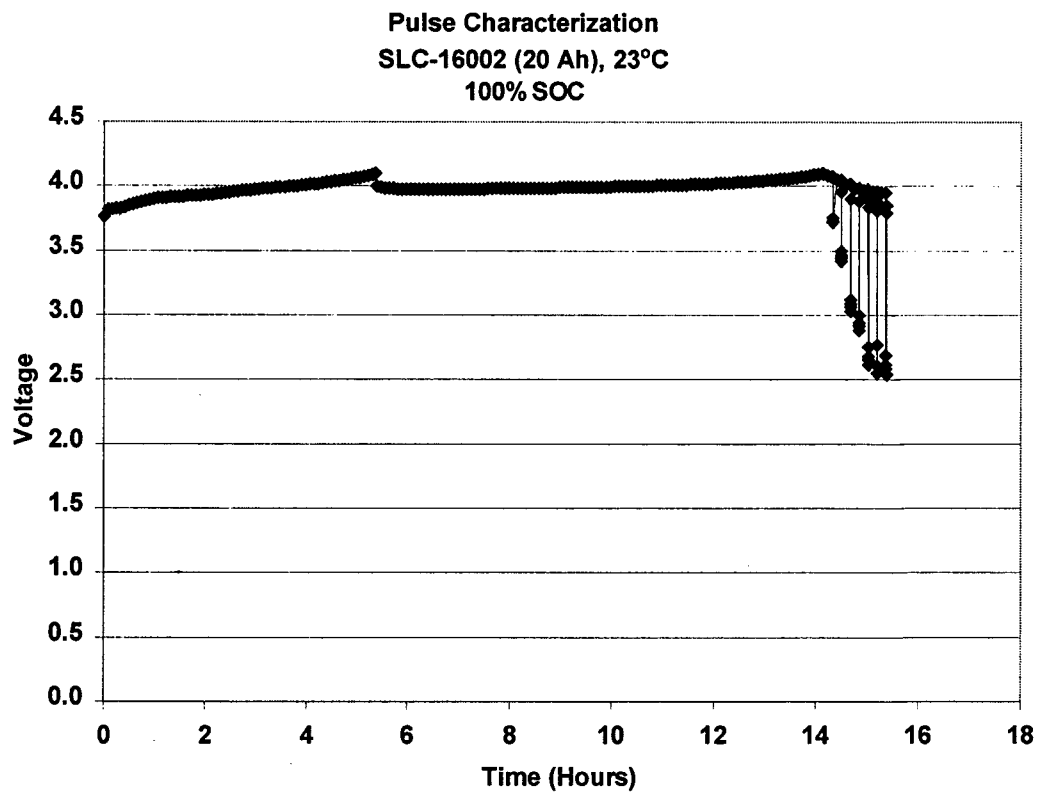

POWER Subsystems

EAGLE PICHER Technologies, LLC

Charge Regime 20 Ah

- Charge at 4 A to 4.1 V
- Rest 1 minute
- Charge at 0.4 A to 4.1 V
- Rest 10 minutes
- Discharge 4 A
  - 80% SOC - 1 hour
  - 60% SOC - 2 hours
  - 40% SOC - 3 hours
  - 20% SOC - 4 hours

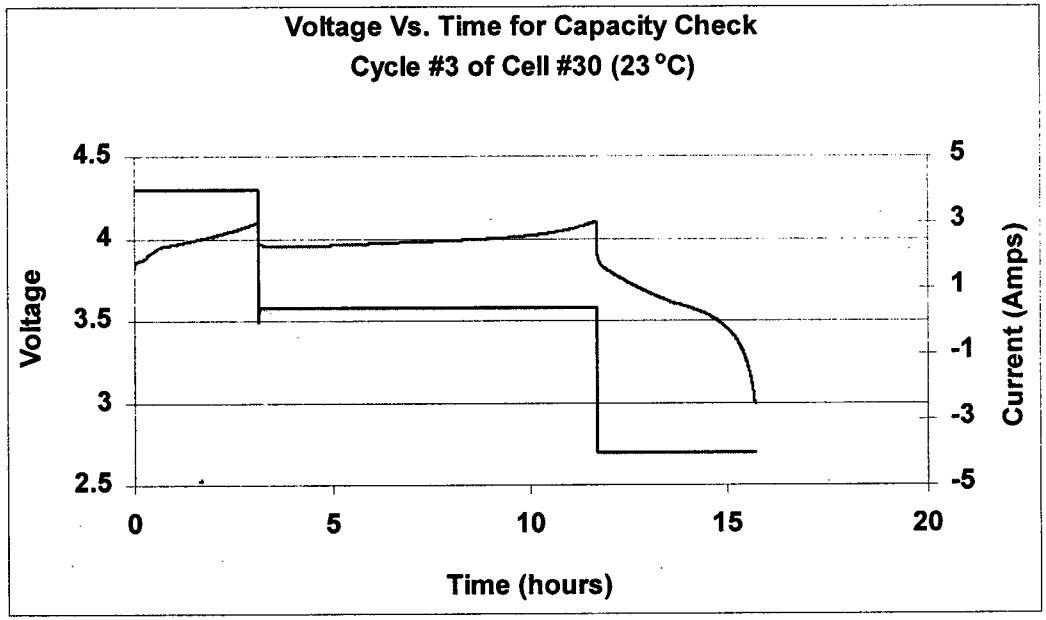

POWER Subsystems

EAGLE PICHER Technologies, LLC

Pulse Characterization 20 Ah

- Cells were tested using 6 rates and 5 states-of-charge
- 10 sec pulse on SLC-16002, 20 Ah ultrasonic weld cell at 23°C
- Delta voltage at various rates and states-of-charge
- More change in voltage drop due to SOC than 250 mAh cells

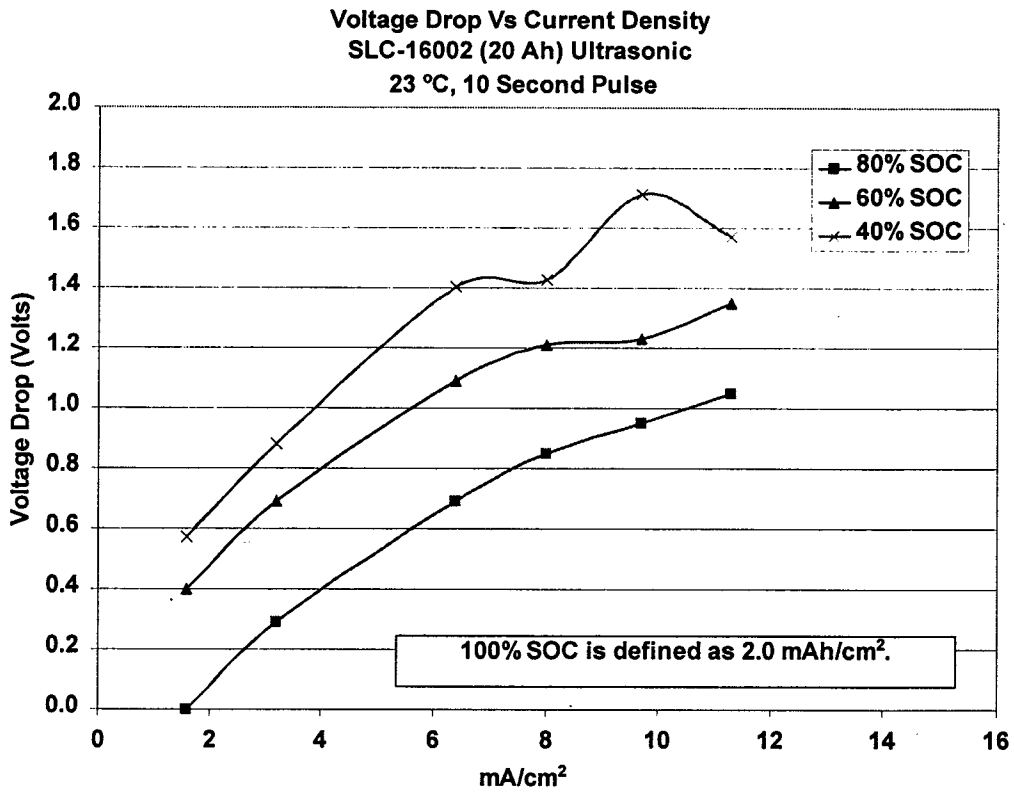

POWER Subsystems

EAGLE PICHER Technologies, LLC

Pulse Voltage Response 20 Ah

- Voltage response for 10 sec, 100 A pulse
- SLC-16002, 20 Ah cell
- 60% state-of-charge @ 23°C
- 12 mΩ calculated impedance (ΔV/ΔI)

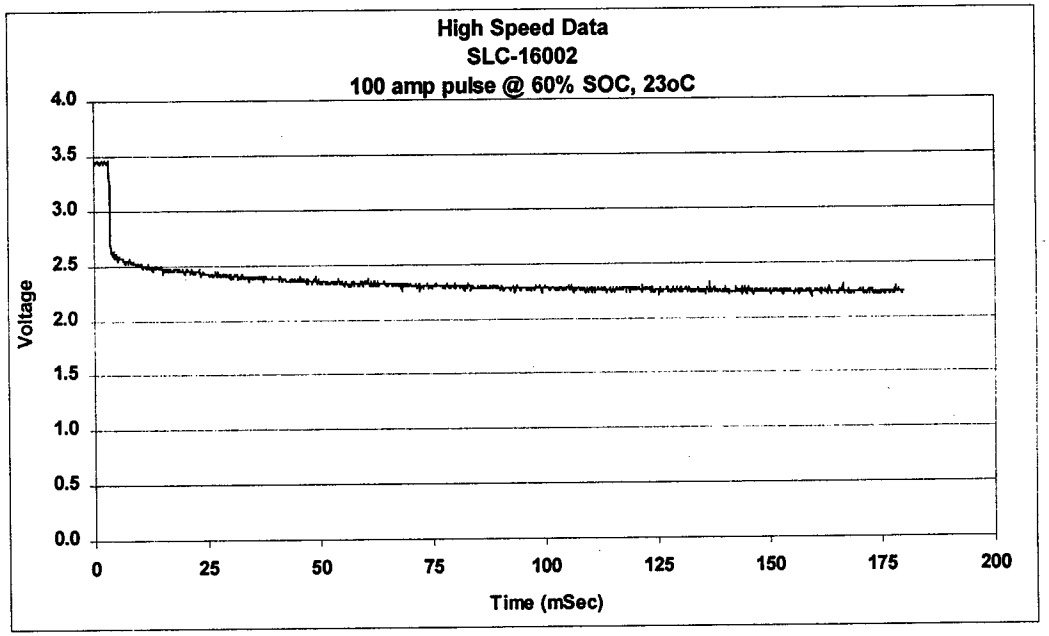

POWER Subsystems

EAGLE PICHER Technologies, LLC

250 mAh vs. 20 Ah

- The voltage drop difference between these two cells is minimal given the fact there is a factor of 60 times increased surface area from the 250mAh to the 20Ah
- The tab weld is proportionally smaller for the 20Ah cell thus causing a larger voltage drop during high current pulses

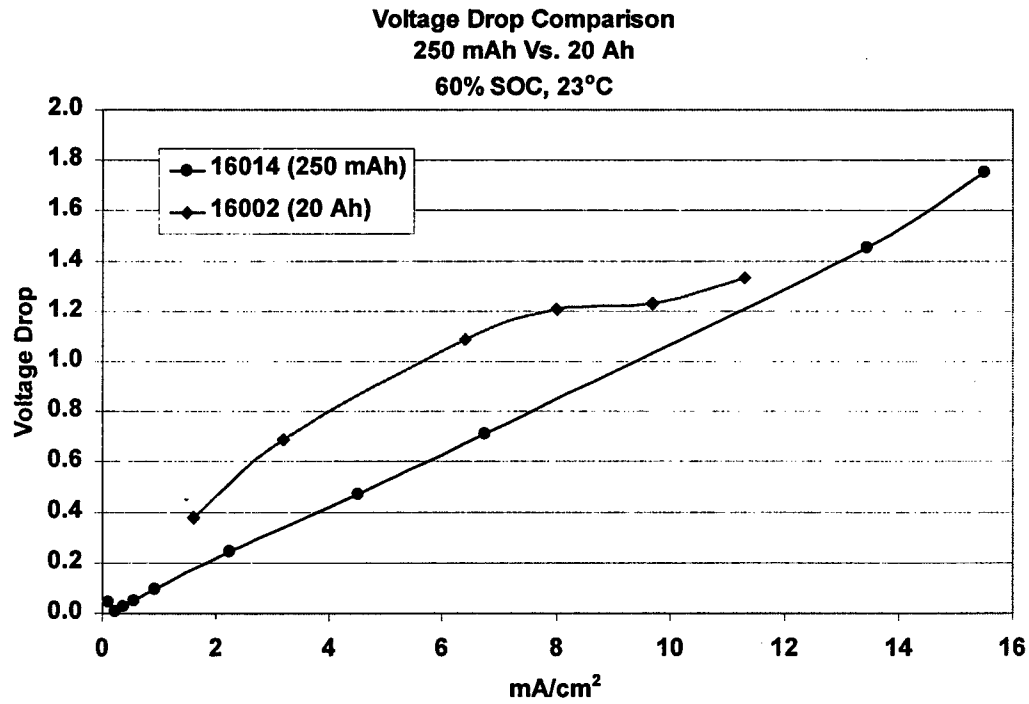

POWER Subsystems

EAGLE PICHER Technologies, LLC

EIS Comparison

- EIS performed after pulse test
- Shows order of magnitude difference

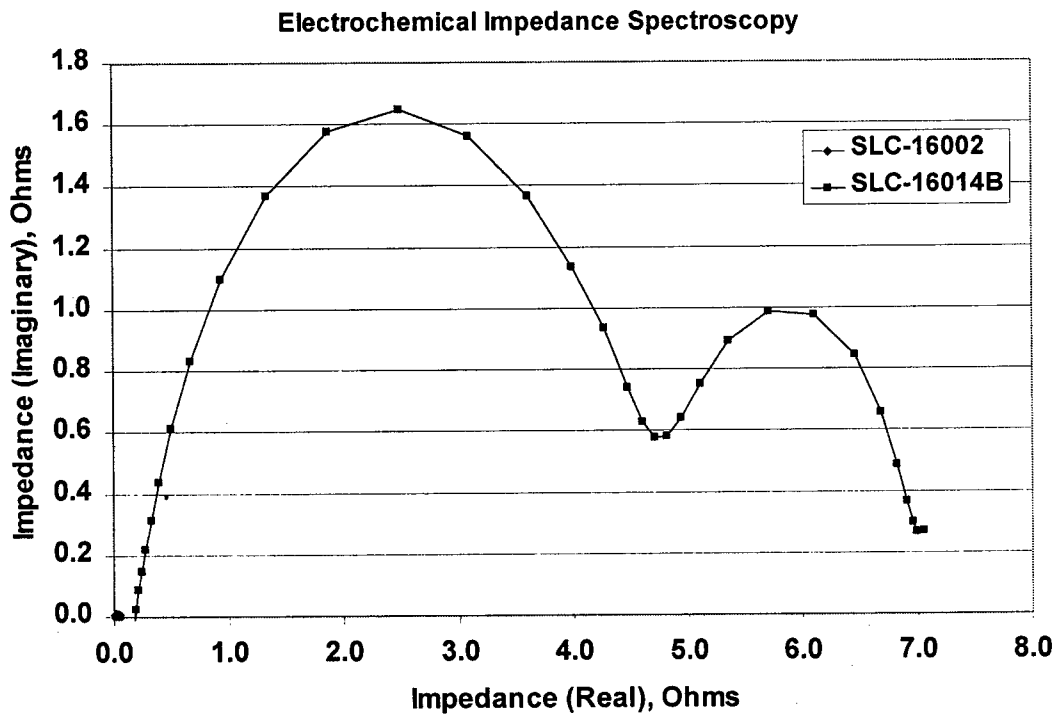

POWER Subsystems

EAGLE PICHER Technologies, LLC

EIS Evaluation

- ✦ **Both cell sizes exhibit typical EIS profiles**
- ✦ **EIS verifies calculated impedance values**
  - 20 Ah: 8 mΩ
  - 250 mAh: 200 mΩ

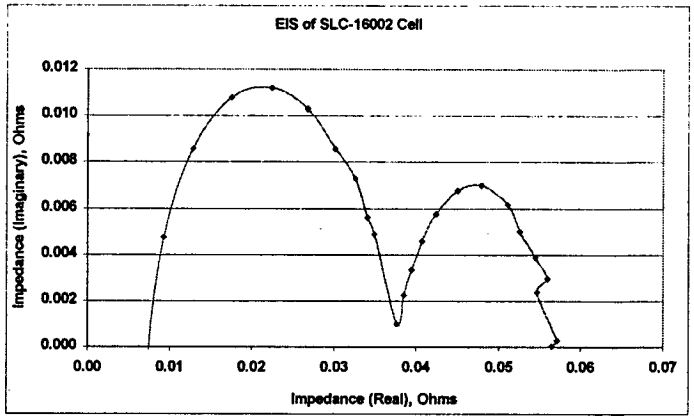

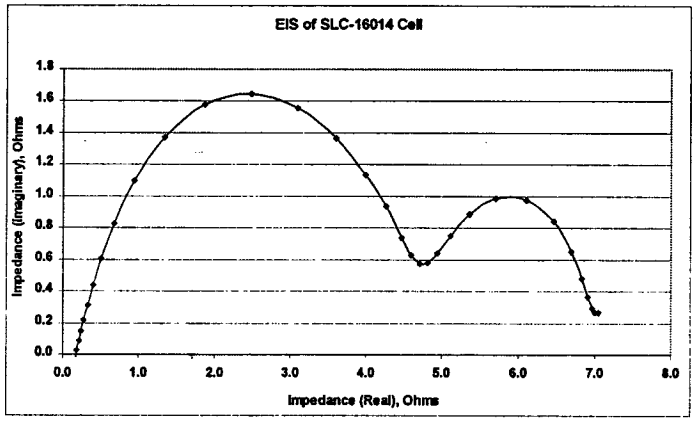

POWER Subsystems

EAGLE PICHER Technologies, LLC

Pop Rivet vs. Ultrasonic

- **Voltage drop is lower during pulses on pop riveted cells**
  - Rivet joint is slightly larger than weld joint
- **Both SCL-16002 (20 AH) cells show good performance even at high pulse rates**

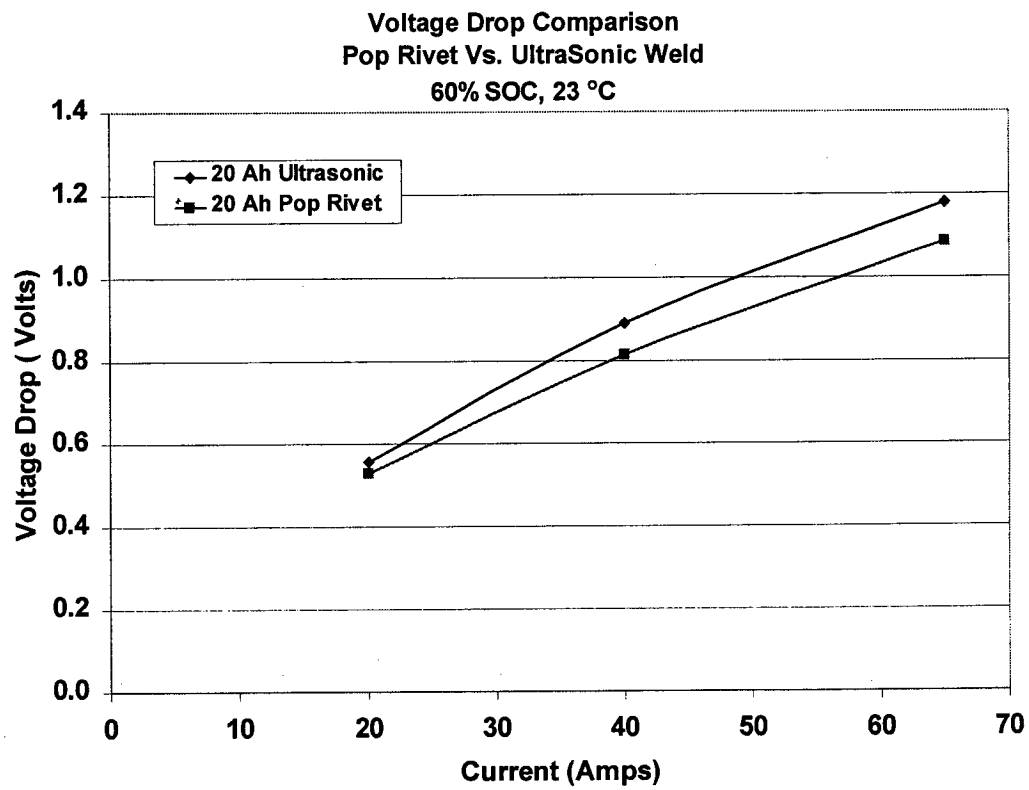

POWER Subsystems

EAGLE PICHER Technologies, LLC

Conclusion

- Lithium ion cells are very well suited to pulsing type loads
- Medium size cells (20 Ah) have overall lower resistance than small cells (250 mAh), but their resistance is more sensitive to SOC
- Pop riveted and ultrasonic welded cells perform similarly under pulse loads

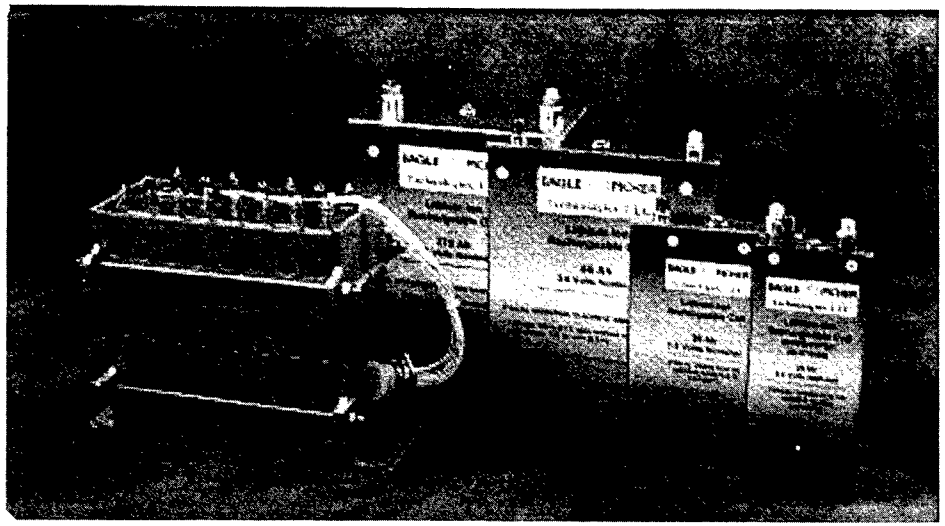

POWER Subsystems

Lithium-Ion Cell Storage Study

Leonine Lee
Gopalkrishna M. Rao
Power Systems Branch, Code 563
Electrical Systems Center
Applied Engineering and Technology Directorate
NASA/Goddard Space Flight Center
Greenbelt, MD 20771

Objective of Storage Study

- To establish a best long term storage for the lithium ion cells
- To determine the preferred solstice condition for the lithium ion chemistry (polymer and liquid electrolyte)
- To compare voltage clamped with trickle charge storage

Experimental

- Three levels of testing were performed
  - Cell characterization
  - Test parameter evaluation
  - Storage testing
- Cells used in study
  - 2 SAFT 4Ah - liquid electrolyte
  - 2 Wilson Greatbatch 1.5Ah - liquid electrolyte
  - 1 Lithium Technology 8Ah - polymer

Cell Characterization

- Capacity at ~20°C
  - C/10 Charge for 12 hours with voltage clamp at 4V
  - Discharge to 2.7V
- 72 hour charge retention
  - C/10 Charge for 12 hours with voltage clamp at 4V
  - Open circuit for 72 hours
  - Discharge to 2.7V

WGB 1.5Ah
Characterization Test Results

	Cell#1	Cell#2
Capacity In at 20°C	1.30Ah	1.25Ah
Capacity Out at 20°C	to 3.0V 1.26Ah to 2.7V 1.27Ah	to 3.0V 1.24Ah to 2.7V 1.25Ah
72 Hr Charge Retention	3.96V to 3.0V 1.18Ah to 2.7V 1.18Ah	3.99V to 3.0V 1.23Ah to 2.7V 1.23Ah
Retention Percent	to 3.0V 93.7 to 2.7V 92.9	to 3.0V 99.2 to 2.7V 98.4

SAFT 4Ah
Characterization Test Results

	Cell#1	Cell#2
Capacity In at 20°C	3.56Ah	3.58Ah
Capacity Out at 20°C	to 3.0V 3.49Ah to 2.7V 3.57Ah	to 3.0V 3.50Ah to 2.7V 3.60Ah
72 Hr Charge Retention	3.98V to 3.0V 3.44Ah to 2.7V 3.55Ah	3.98V to 3.0V 3.47Ah to 2.7V 3.57Ah
Retention Percent	to 3.0V 98.6 to 2.7V 99.4	to 3.0V 99.1 to 2.7V 99.2

LTC 8Ah
Characterization Test Results

	Cell#1
Capacity In at 20°C	7.07Ah
Capacity Out at 20°C	to 3.0V 7.01Ah to 2.7V 7.12Ah
72 Hr Charge Retention	3.99V to 3.0V 6.94Ah to 2.7V 7.03Ah
Retention Percent	to 3.0V 99.0 to 2.7V 98.7

Test Parameter Evaluation

- Determine the best voltage clamp and trickle charge current for storage testing
- SAFT cells selected
  - Well matched
  - Convenient for existing charger/discharger unit

Test Parameter Evaluation

- Cell #1 left open circuit for 6 weeks
  - Performed to determine how much charge might be lost during 6 weeks open circuit storage
- Cell #2 trickle charged at C/500
  - Performed to determine the time it would take to reach a voltage clamp set at 4.1V

Test Parameter Evaluation Results

- Cell #1
  - 3.97V after 6 weeks open circuit
  - Residual capacity found to be 3.40Ah (3.54Ah)
  - Capacity test performed after open circuit test found 3.44Ah at 3.0V and 3.57Ah at 2.7V.
- Cell #2
  - 4.1V voltage clamp reached in 4 days
  - Residual capacity found to be 3.84Ah (4.01Ah)
  - Capacity test performed after trickle charge storage test found 3.48Ah at 3.0V and 3.60Ah at 2.7V.

Storage Test

- Storage Conditions
  - Stored in 0°C for 4 weeks
  - Trickle charge with a 4.1 voltage clamp
- Capacity tests at 20°C after storage period

Storage Test
Trickle Charge Current

Cell	Trickle Charge Current
SAFT 4Ah	0.002Amp
SAFT 4Ah	0.004Amp
WGB 1.5Ah	0.002Amp
WGB 1.5Ah	0.003Amp
LTC 8Ah	0.004Amp

Storage Test Results

	SAFT Cell#1	SAFT Cell#2	WGB Cell#1	WGB Cell#2	LTC Cell#1
Residual capacity	3.67Ah 3.83Ah	3.77Ah 3.94Ah	1.18Ah 1.21Ah	1.24Ah 1.27Ah	7.38Ah 7.49Ah
Standard Capacity Test	3.40Ah 3.54Ah	3.44Ah 3.56Ah	1.18Ah 1.21Ah	1.02Ah 1.17Ah	6.74Ah 6.86Ah

Conclusions

- Voltage clamped storage at cold temperatures up to 6 weeks appears to be beneficial over trickle charged storage
  - Coulombic losses at 0°C is neglible
  - Voltage clamp eventually reached
  - Trickle charge storage may still be an option in larger capacity cells where charge rates may be relatively smaller
- Future work
  - Short term study at temperatures around 10°C and 20°C
  - Long term study for extended storage
  - Study a lower voltage clamp

LOCKHEED MARTIN

ENGINEERING AND ABUSE TESTING OF PANASONIC LITHIUM-ION BATTERY AND CELLS

1999 NASA AEROSPACE BATTERY WORKSHOP

Judith A. Jeevarajan

Lockheed Martin/NASA-JSC

Bobby J. Bragg

NASA-JSC

Panasonic Lithium-ion Battery in the IBM Thinkpad

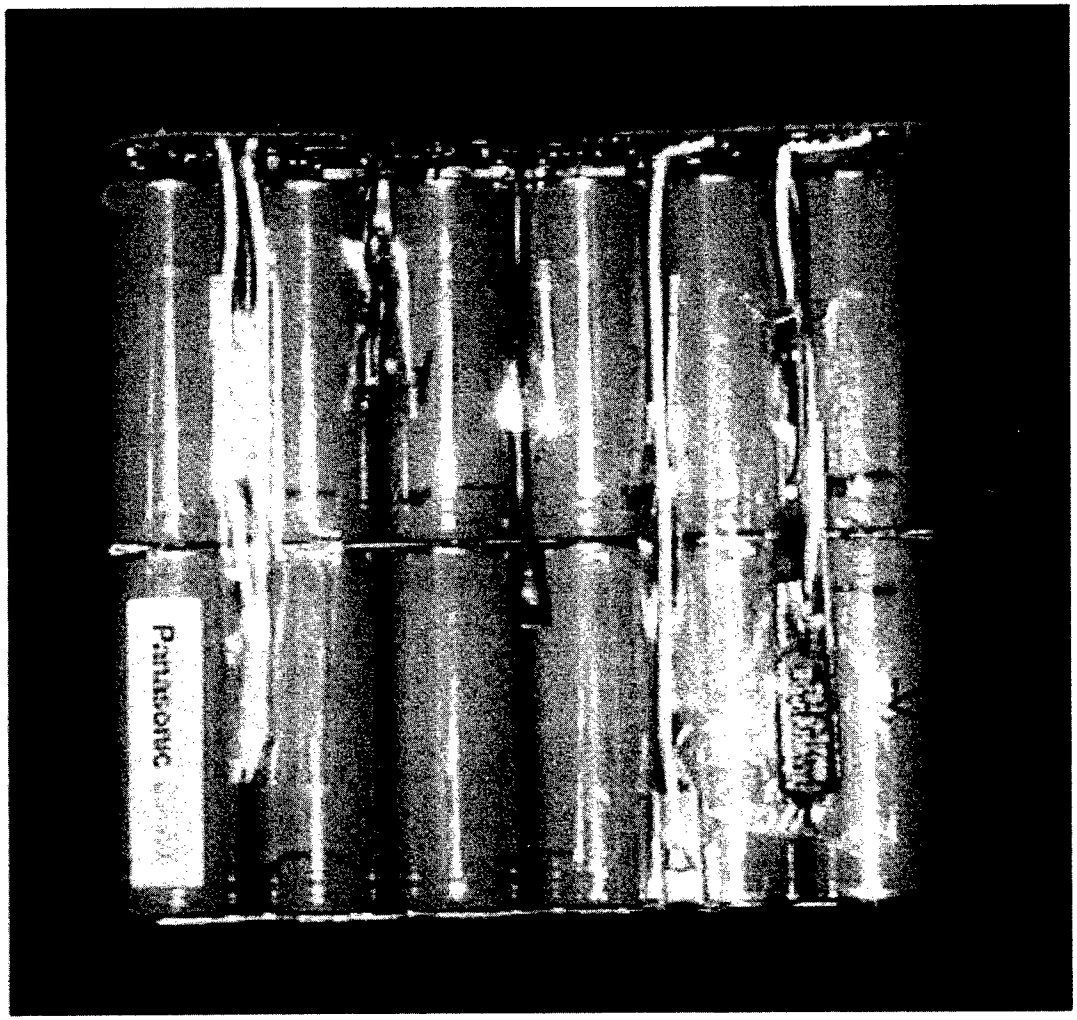

Panasonic 17500 Lithium-ion Cells

Physical Characteristics

Weight: 24.43 ± 0.6 g
Diameter: 16.399 ± 0.4 mm
Length: 49.648 ± 1.2 mm

Electrochemical Characteristics

Open Circuit Voltage: 3.9 V

Capacity (room temperature): 0.81 Ah

Charge/Discharge Curves for Panasonic 17500 Li-ion Cell

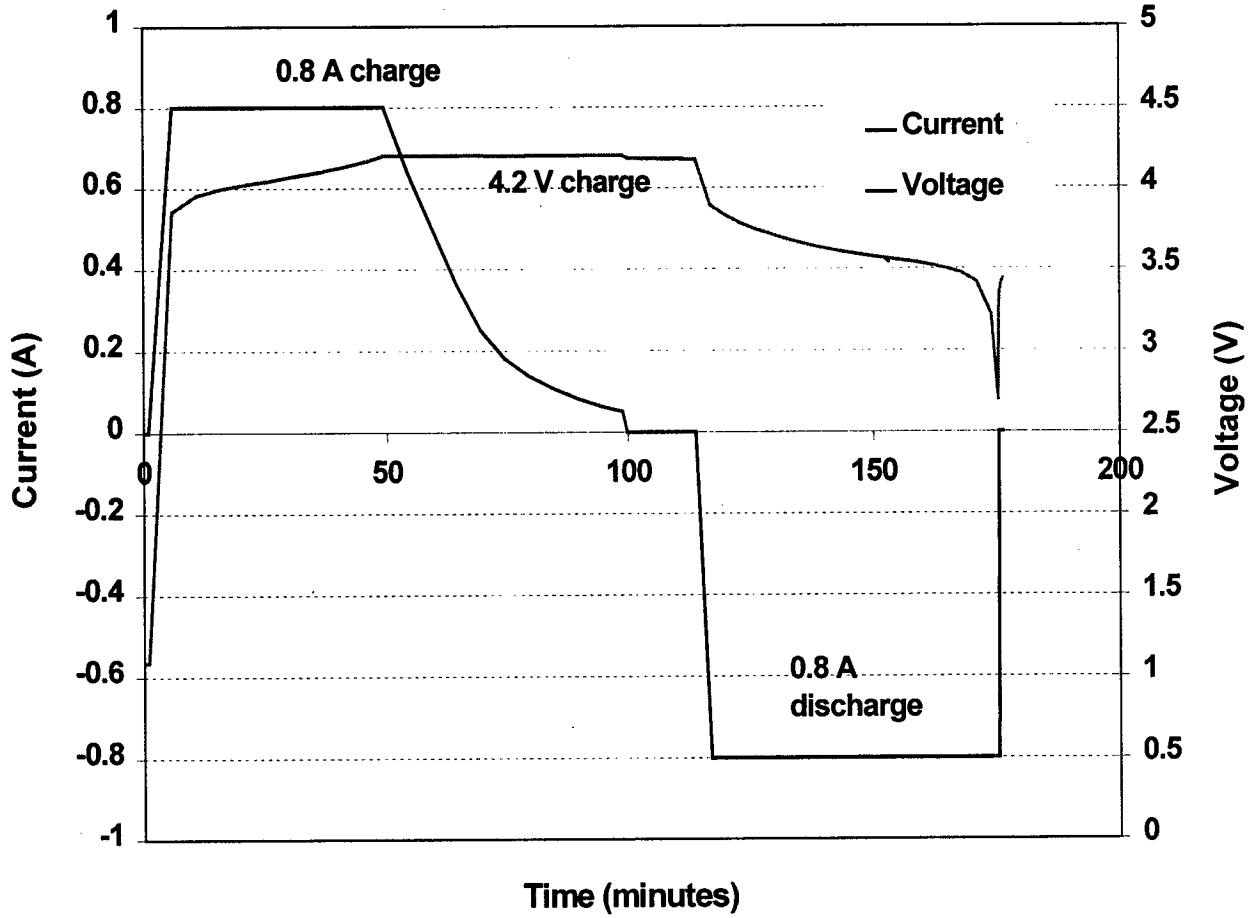

Rate Capability of Panasonic 17500 Lithium-ion Cells Under Different Conditions of Charge and Discharge

Cycle Number	1.0 C Charge			0.5 C Charge		
	1 C Discharge	0.5 C Discharge	0.25 C Discharge	1 C Discharge	0.5 C Discharge	0.25 C Discharge
1	0.816	0.837	0.828	0.824	0.837	0.840
5	0.810	0.832	0.827	0.817	0.835	0.838
25	0.801	0.820	0.816	0.802	0.826	0.832
50	0.788	0.809	0.804	0.799	0.822	0.826
100	0.774	0.794	0.792	0.792	0.819	0.822
CDR* Ah/Cycle	0.00038	0.00039	0.00037	0.00027	0.00017	0.00018

* CDR stands for Capacity Decay Rate. The shaded cell values were used to calculate the CDR. $CDR=(C_5-C_{100})/95$, C_5 and C_{100} are the capacities at cycle # 5 and 100, respectively.

At 1 C Charge/ Discharge, Capacity Decay is 4%

At 0.5 C Charge/Discharge, Cacpacity Decay is 1.9 %

Discharge Capacity for the Panasonic cells at 0.5C Rate of Discharge and Different Rates of Charge

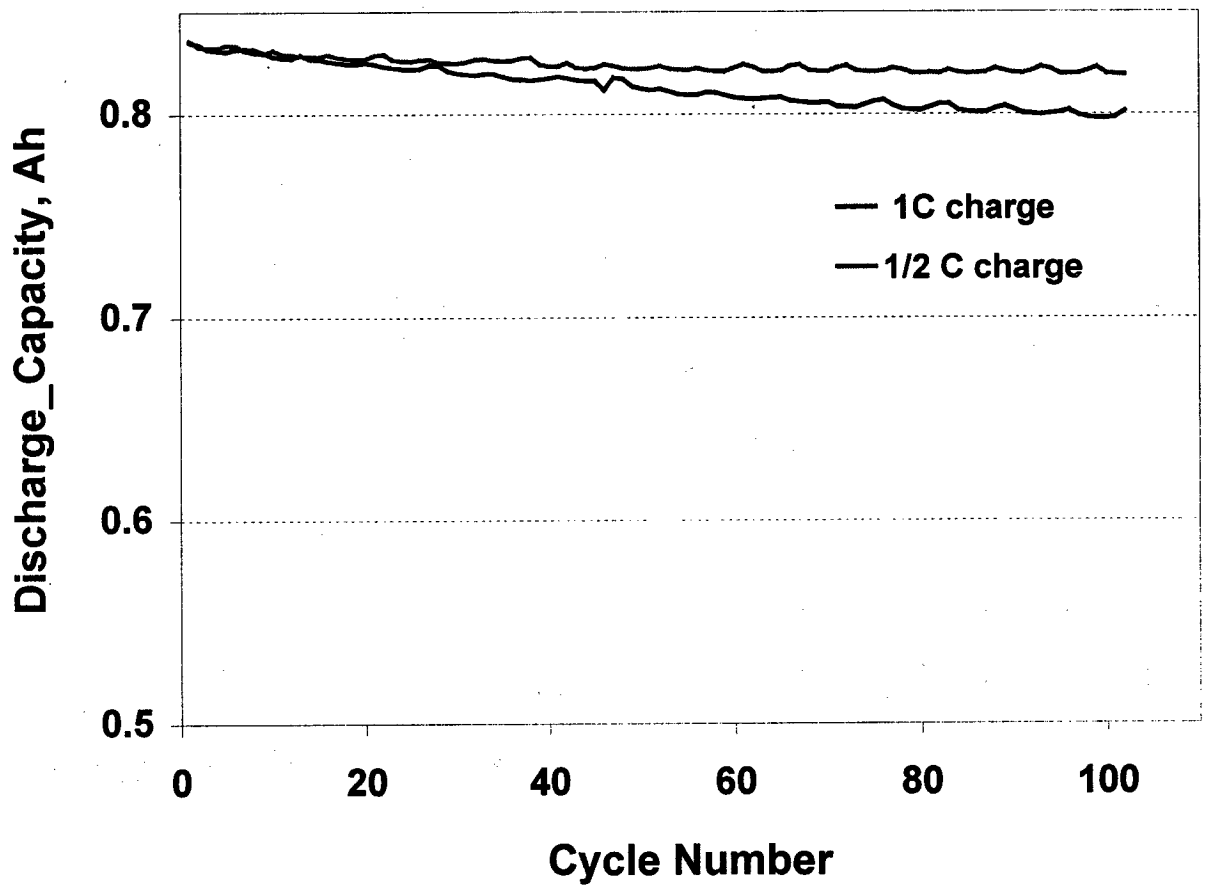

Discharge Capacities versus Temperature for the Panasonic 17500 Lithium-ion Cells

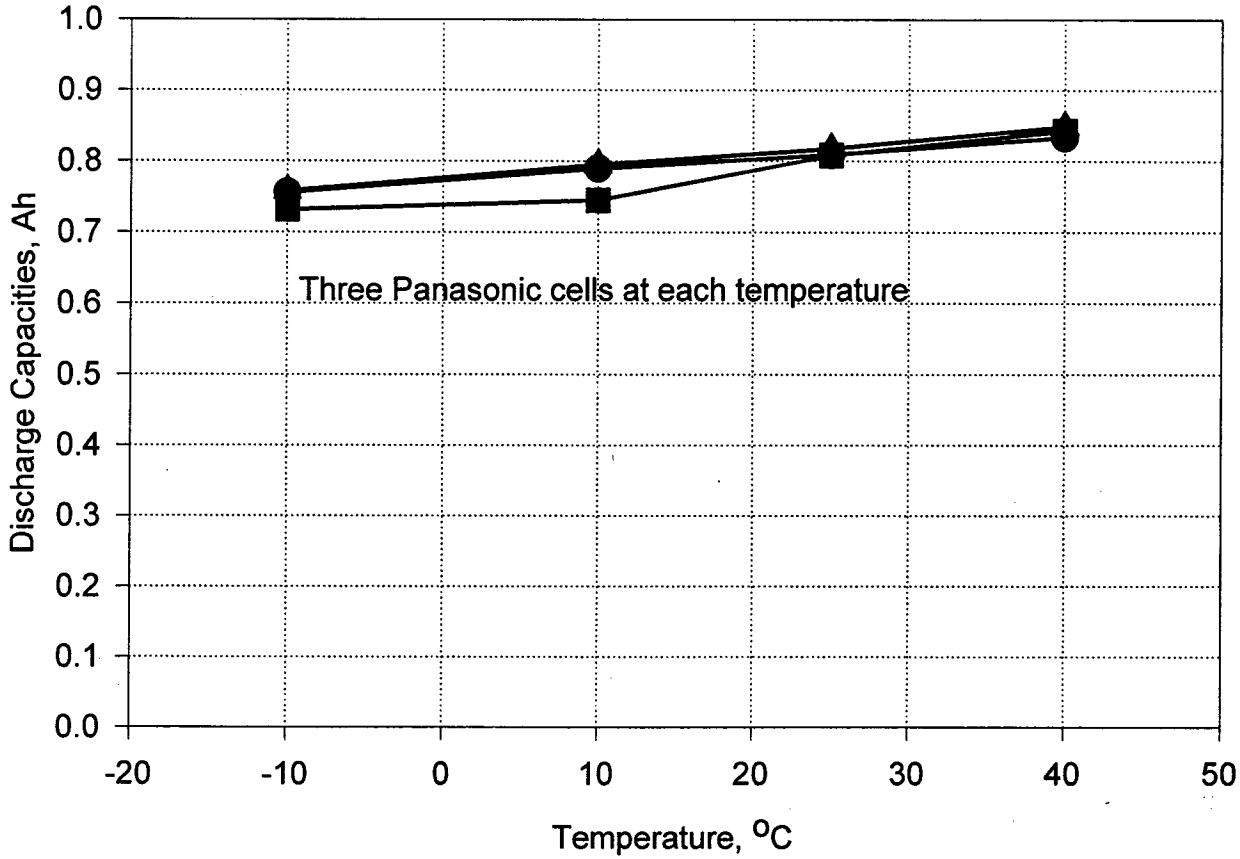

Effective Internal Resistance for the Panasonic Lithium-ion cells

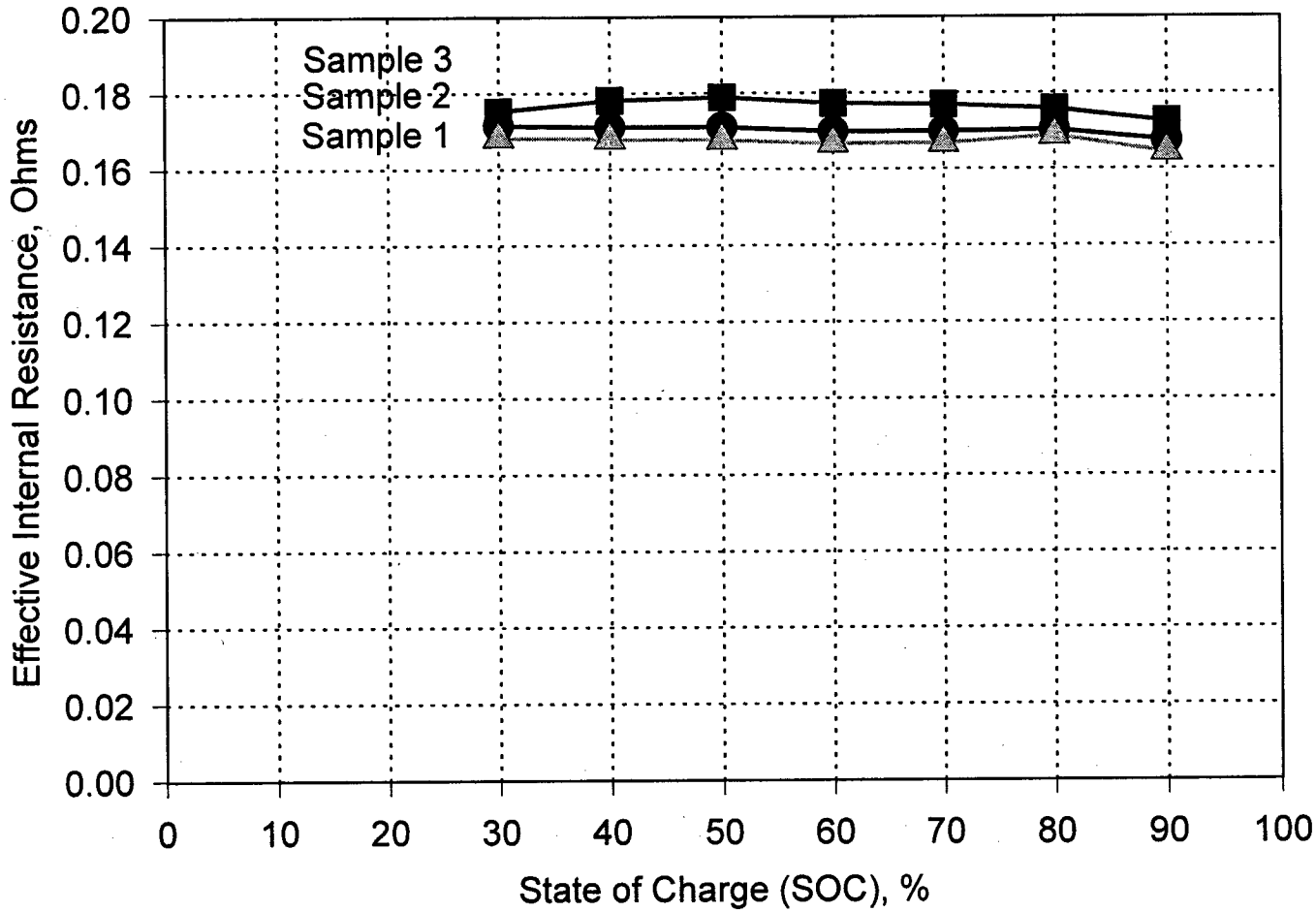

Minimum Voltages Obtained During the Discharge Pulse of the Internal Resistance Test

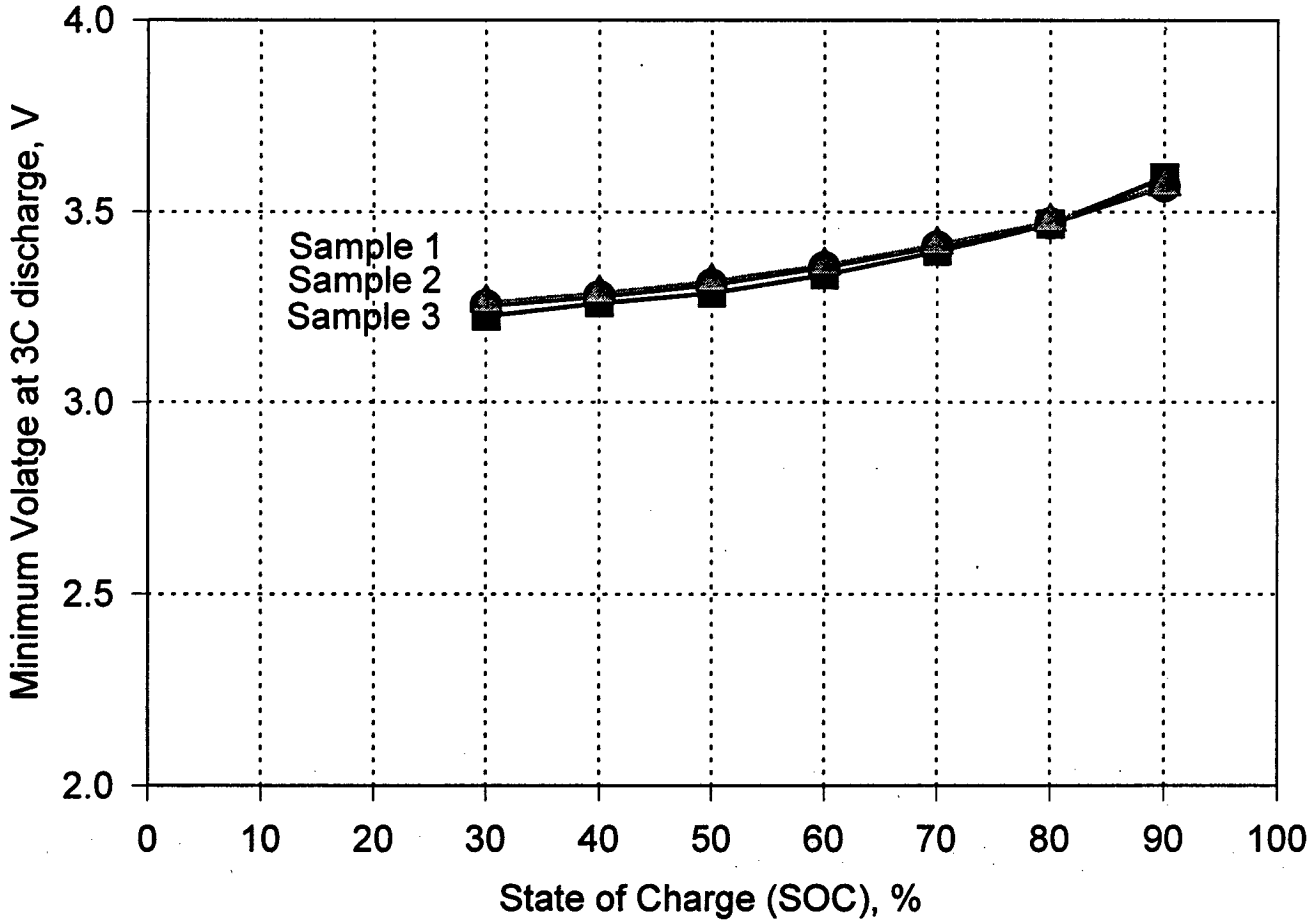

Charge Discharge Curve for Charge at 3C Rate to 4.2 V and Discharge with 1C Current to 2.7 V

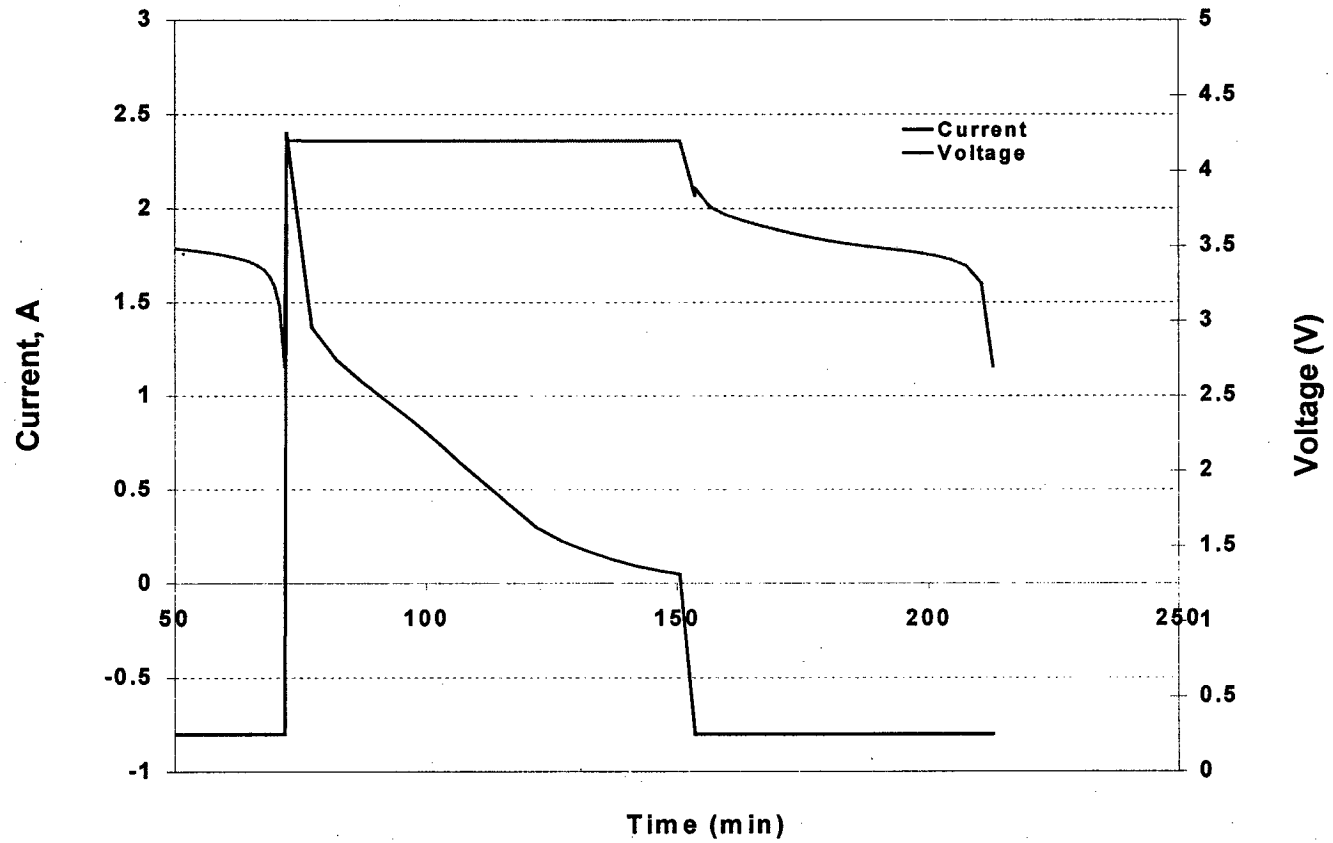

Charge-Discharge Curve for Charge to 5.0 V with a 1 C Current and Discharge to 2.7 V with 1C Current

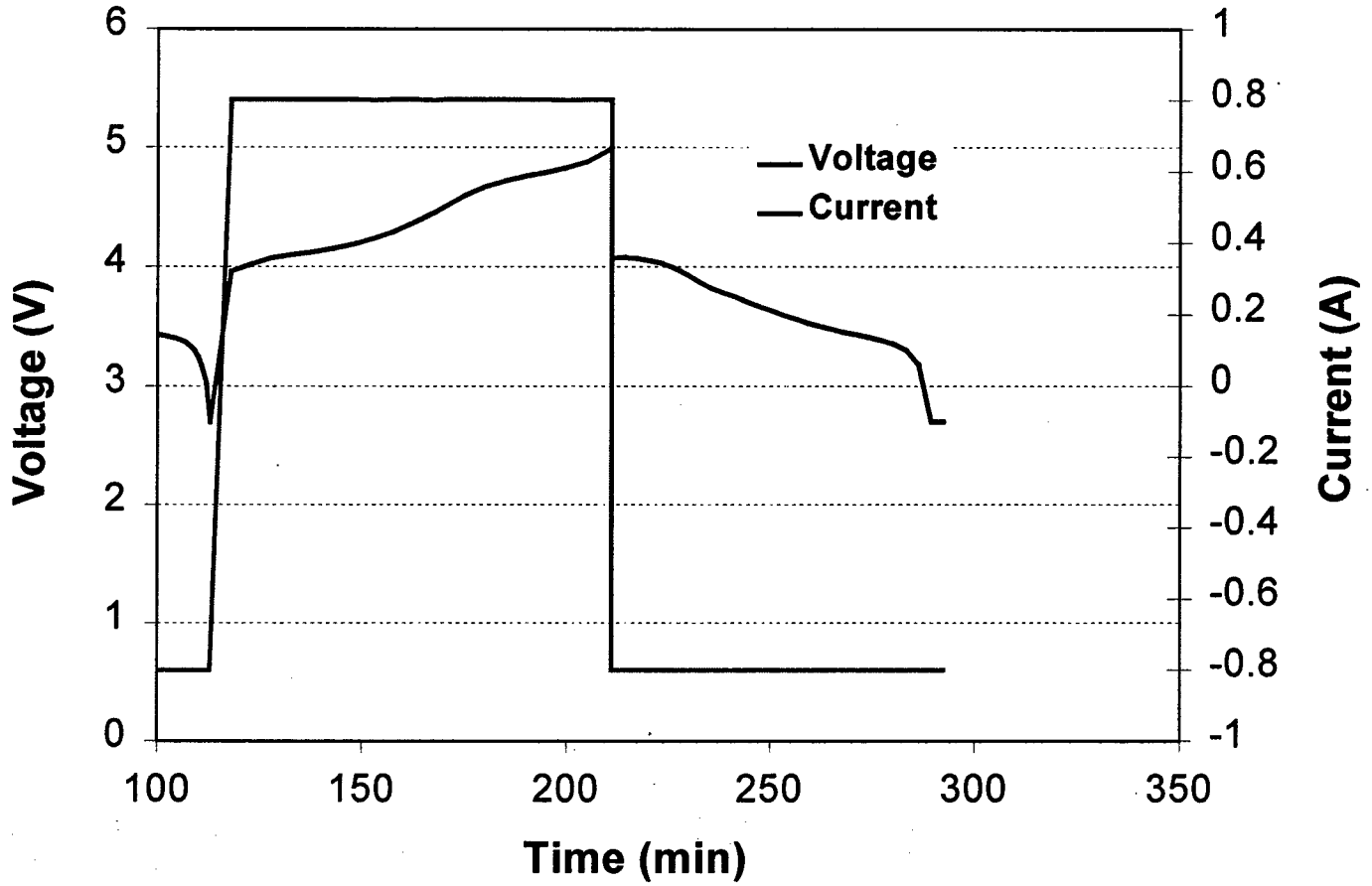

Overcharge Test Using a 3C Current to 12 V

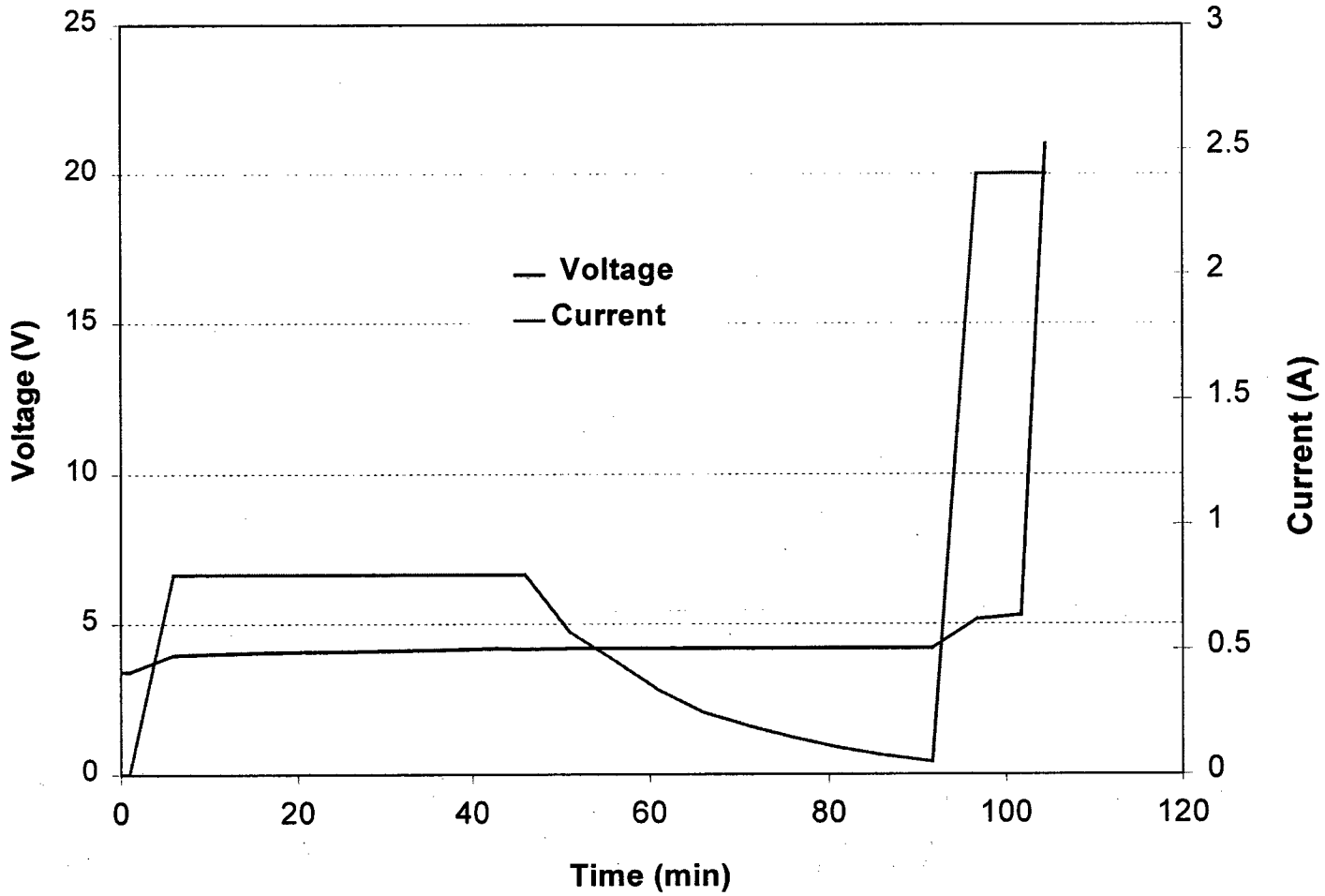

Current and Temperature Changes During a High Rate Overcharge (3C current) to 12 V

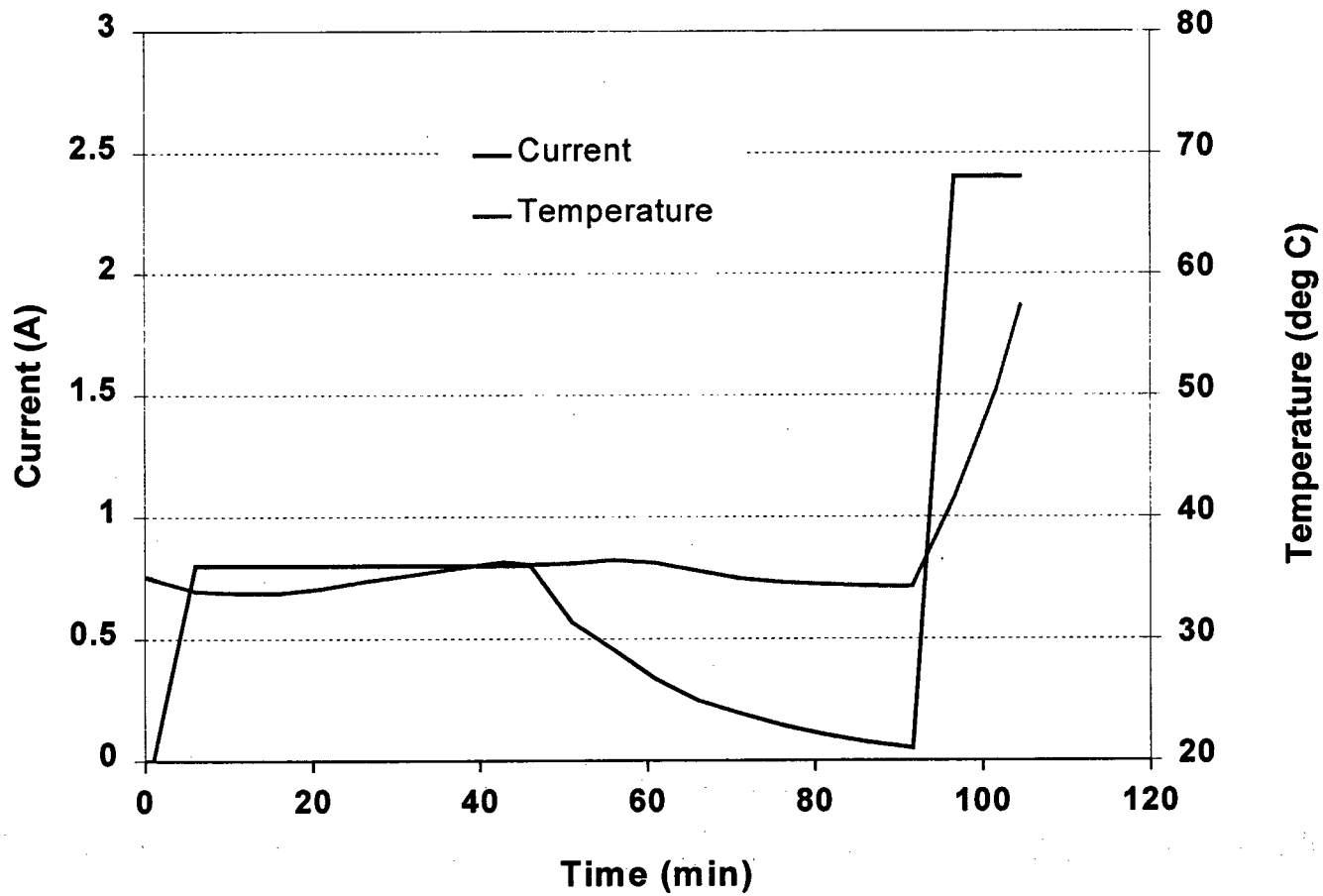

Discharge of Panasonic 17500 Lithium-ion Cells Using 3C Current

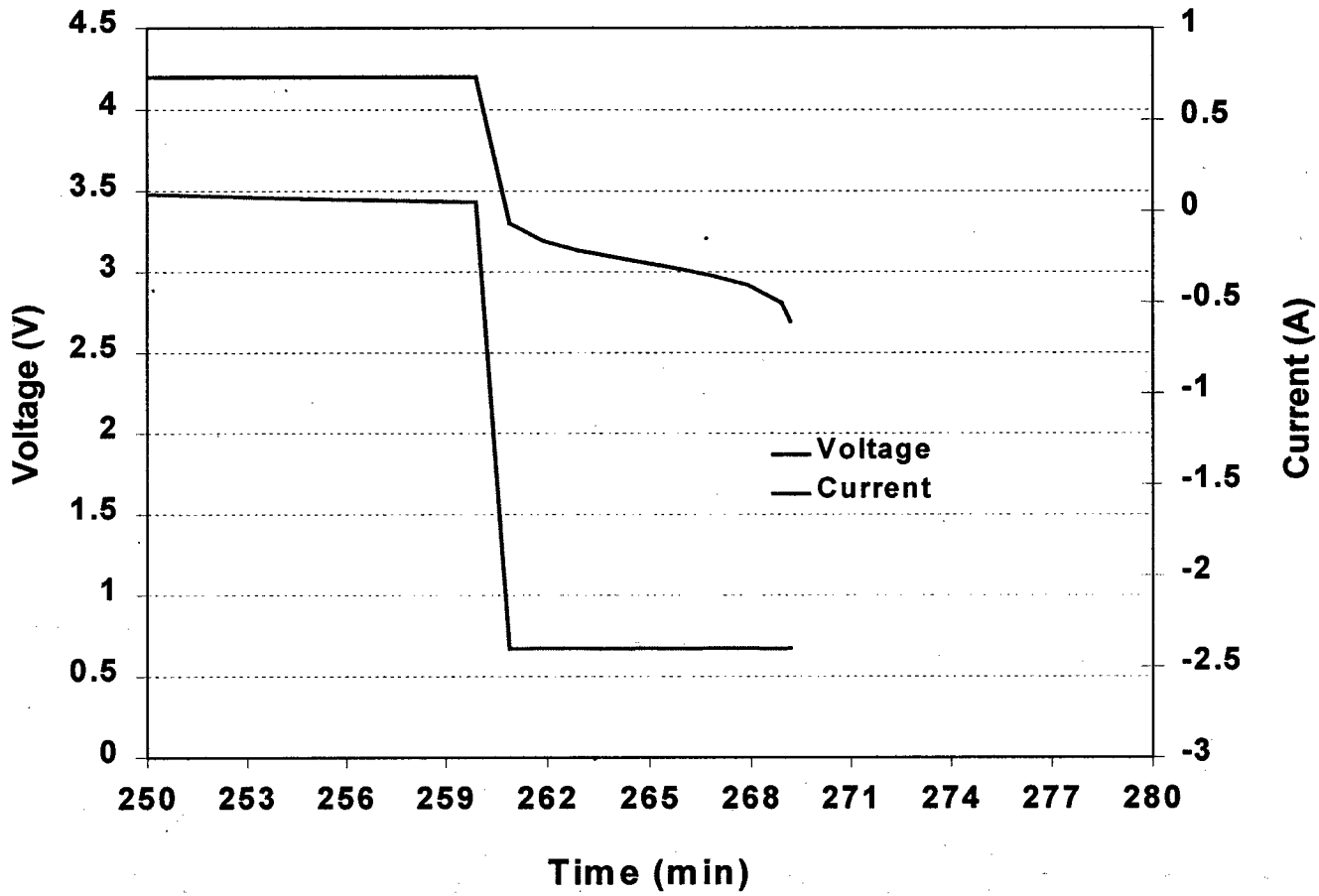

Current and Voltage Characteristics During Discharge into Reversal of Panasonic 17500 Lithium-ion Cells with 1C Current

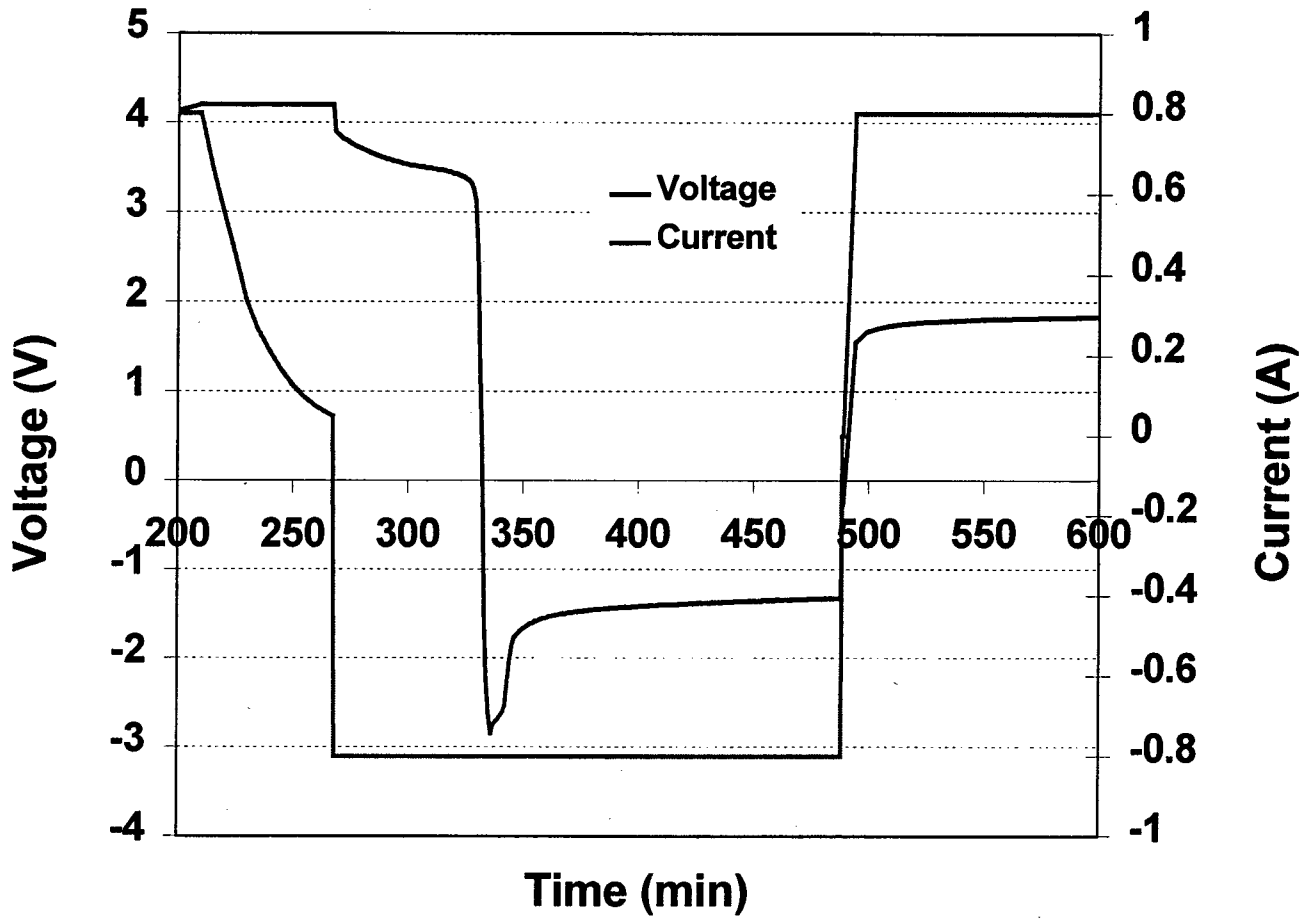

Heat-to-Vent of Panasonic 17500 Lithium-ion Cells

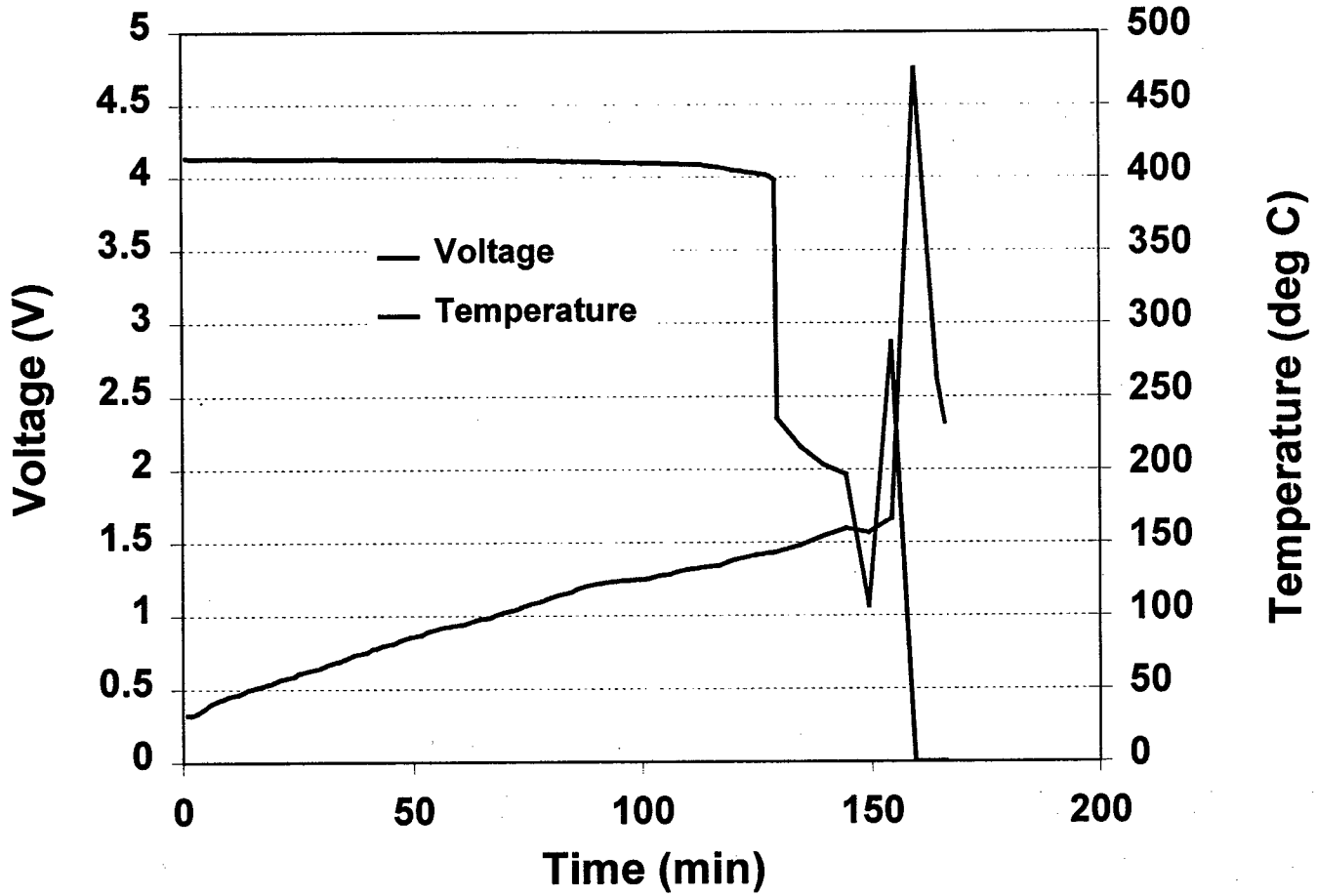

Voltage and Temperature Profile During a Soft Internal Short

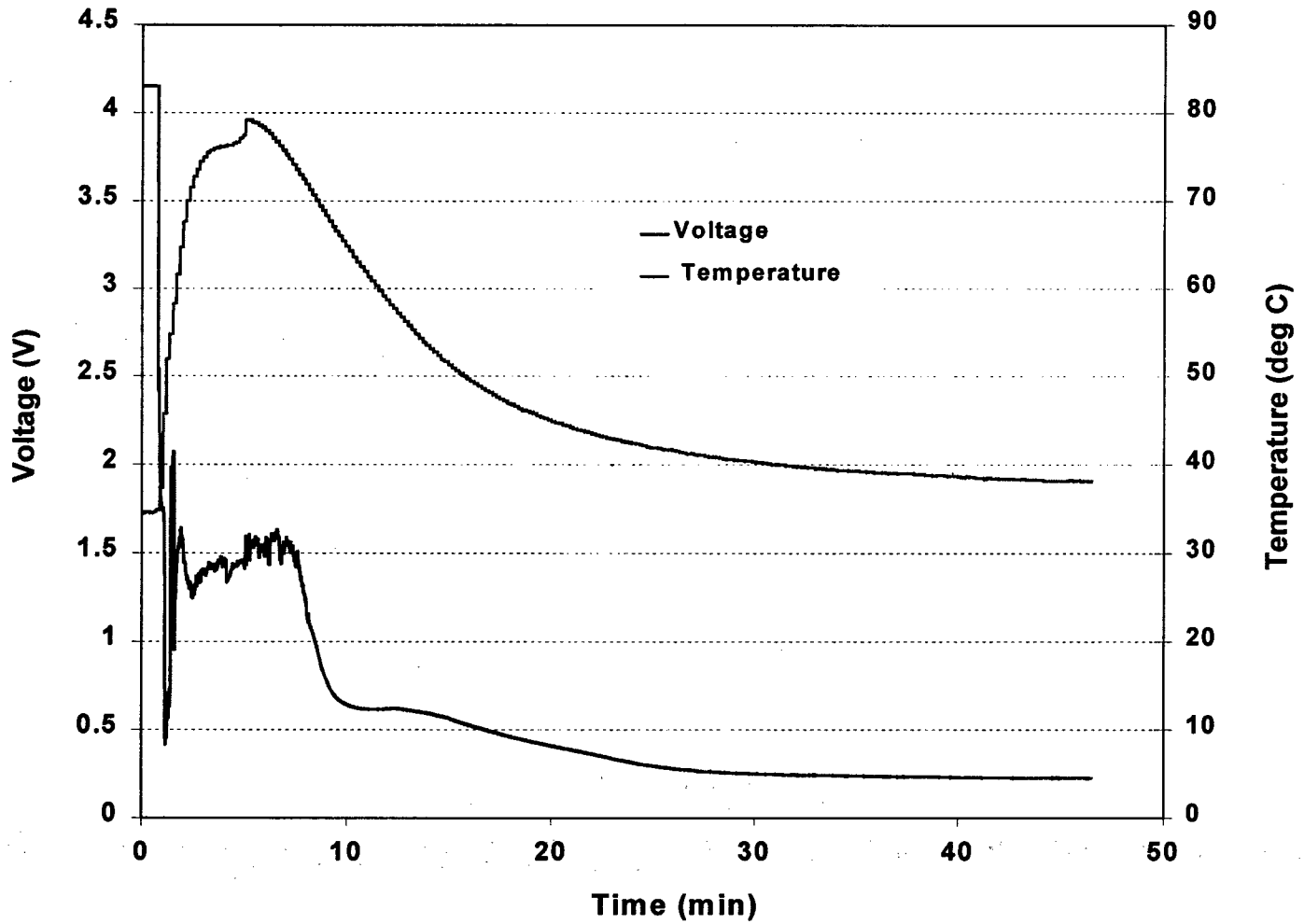

Voltage and Temperature Characteristics During a Hard Internal Short

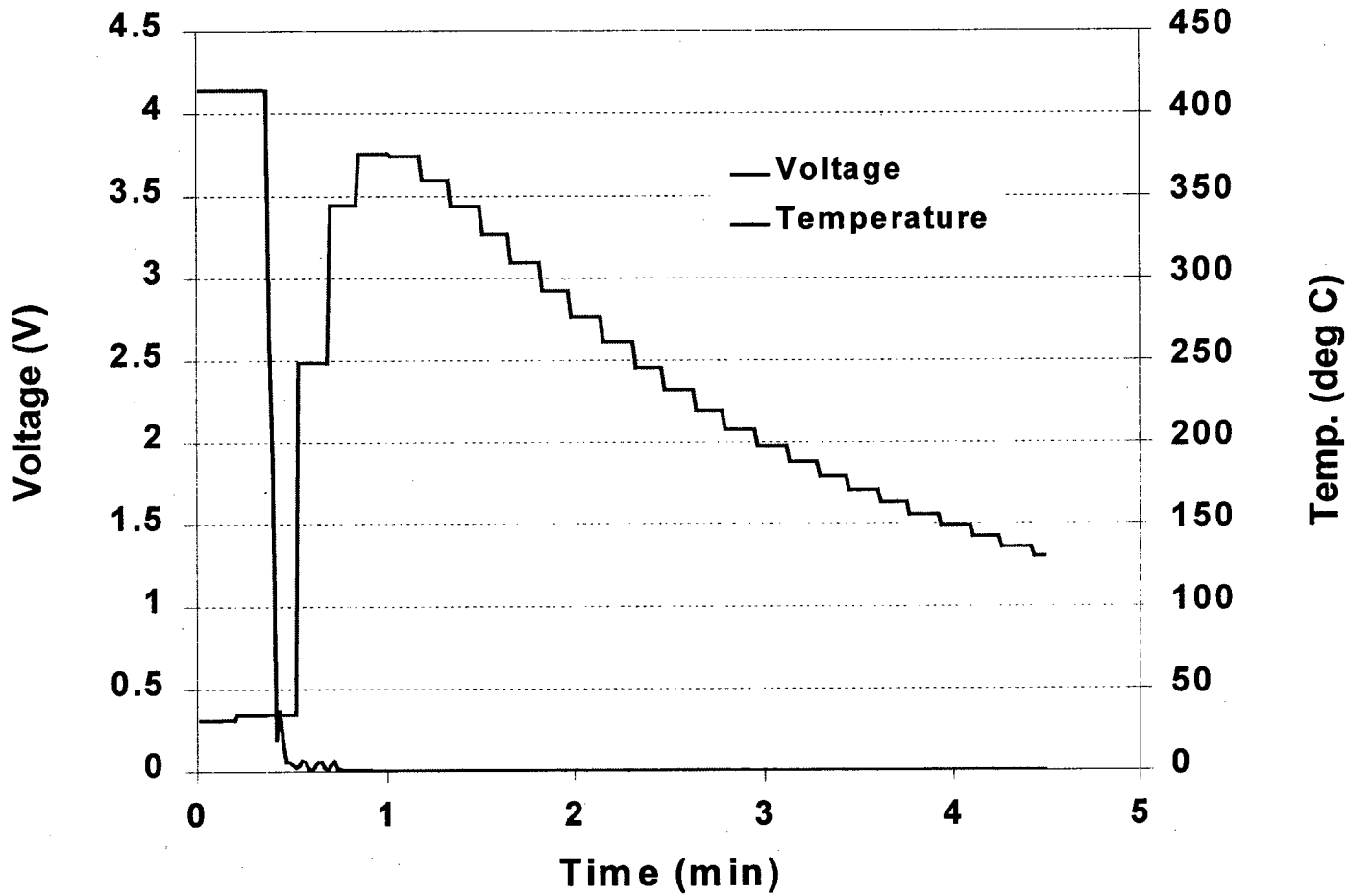

Current and Temperature Characteristics During An External Short Test Using 40 mohm Load

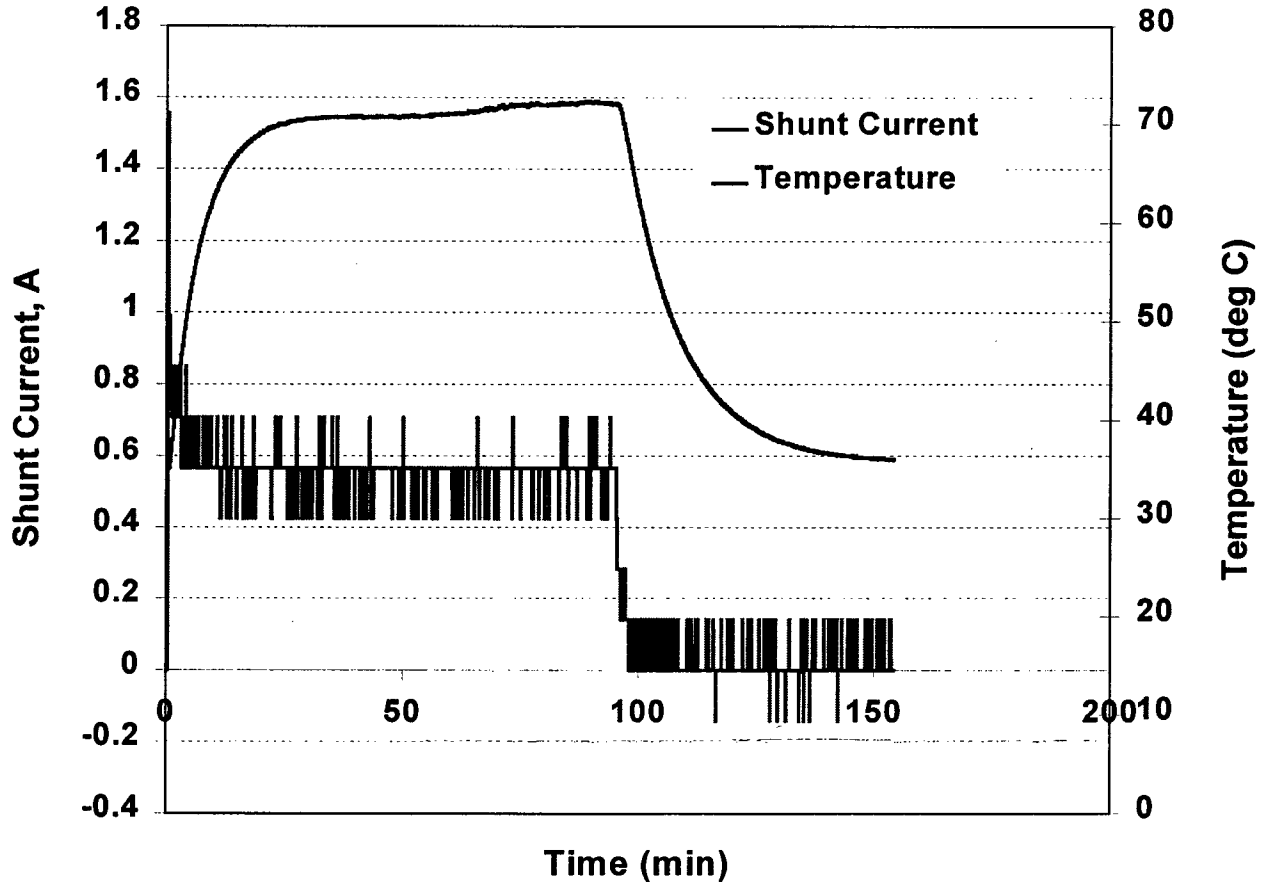

Electrolyte Analysis of Panasonic 17500 lithium-ion cell

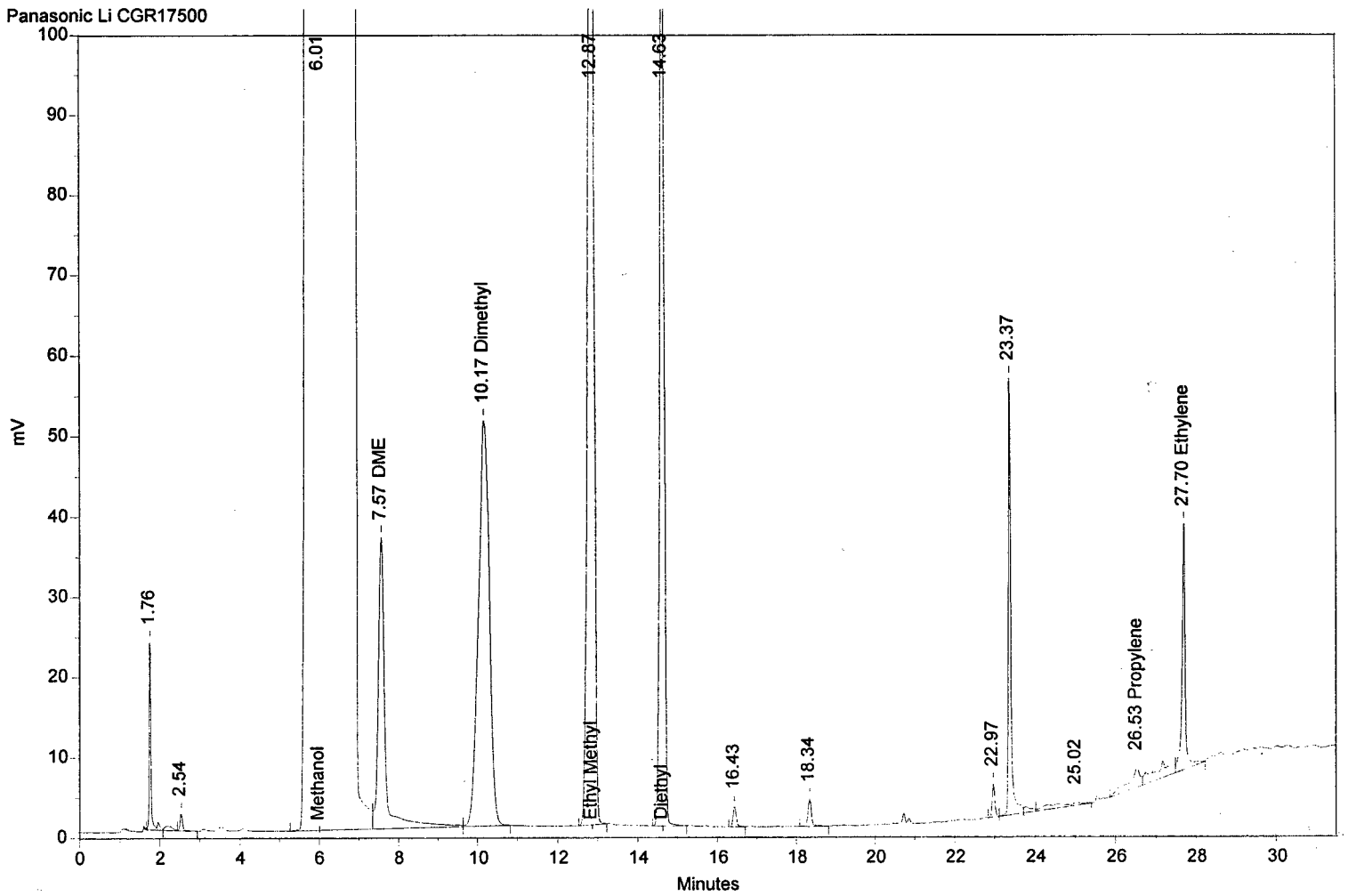

Panasonic Lithium-ion IBM Thinkpad Battery

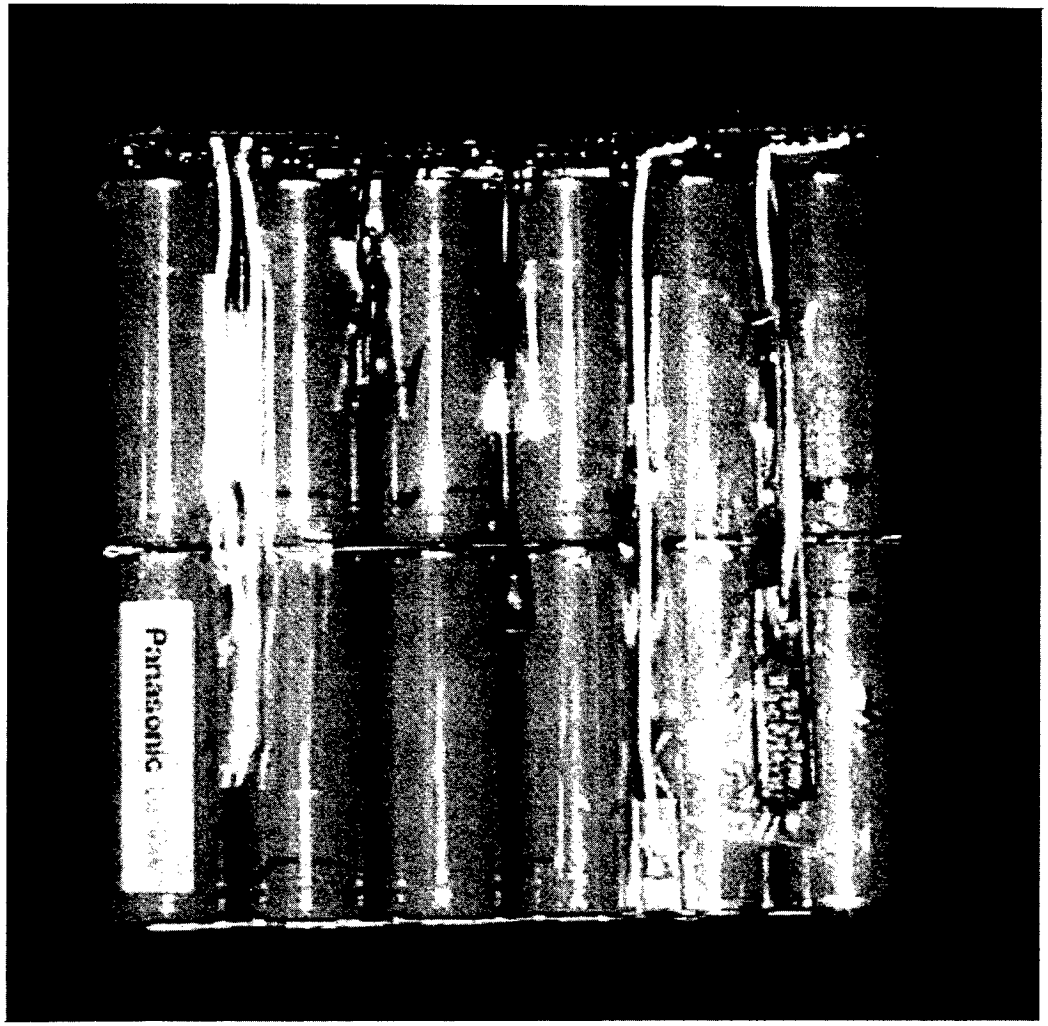

Weight: 366 g
Dimensions: 4'X 4.5'
Voltage: 10.8 V
Capacity: 3.0 Ah
Configuration: 4P3S (12 cells)

Circuit Board in the Panasonic Thinkpad Lithium-ion Battery

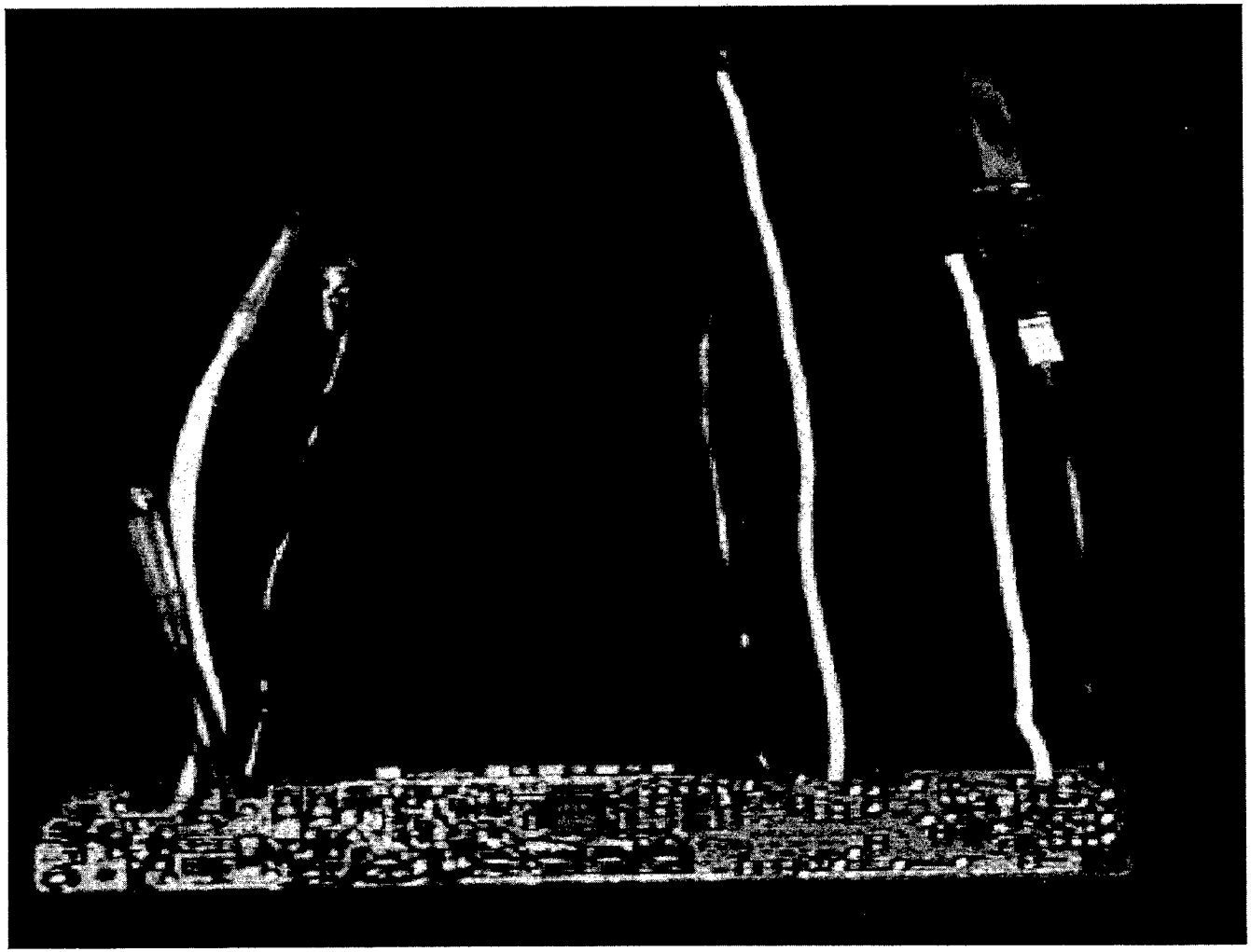

Circuit Board in the Panasonic Lithium-ion Battery

- Decisions about turning off charge and discharge switches based on cell bank voltages and current are made by firmware in microcontroller.
- Protective circuit performs capacity gauge function.
- Protective circuit can balance cell bank states-of-charge by putting small (15 mA) discharge currents on individual cell banks.

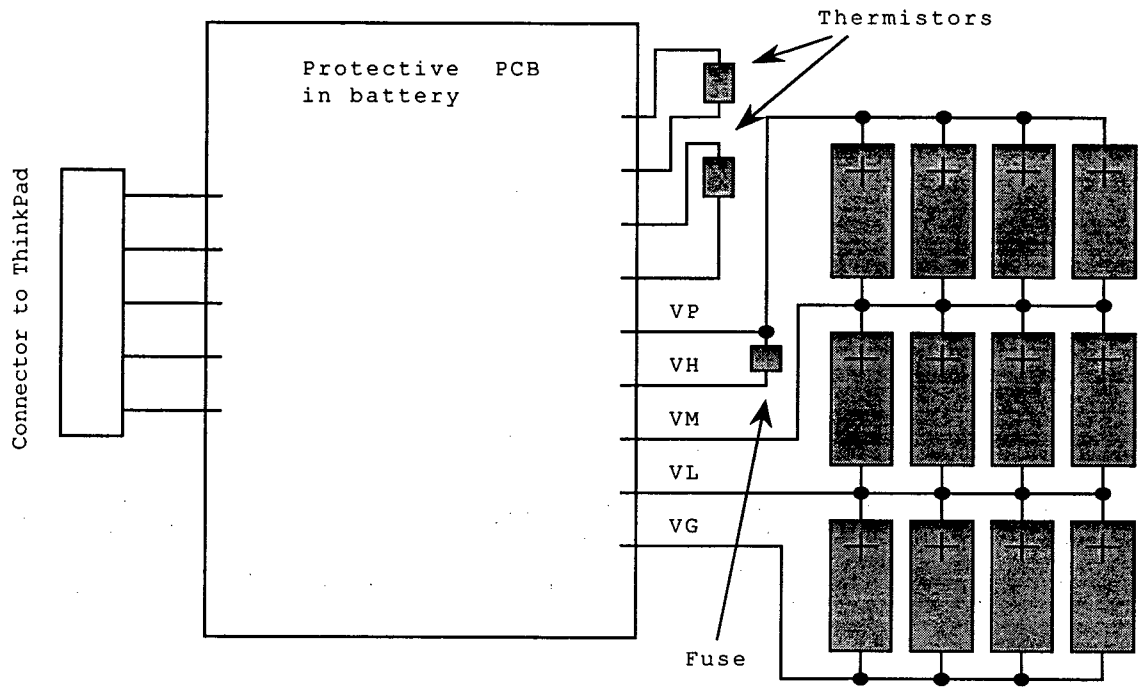

Current and Voltage During the Charging of a Panasonic Lithium-ion Battery Using the IBM Thinkpad Charger

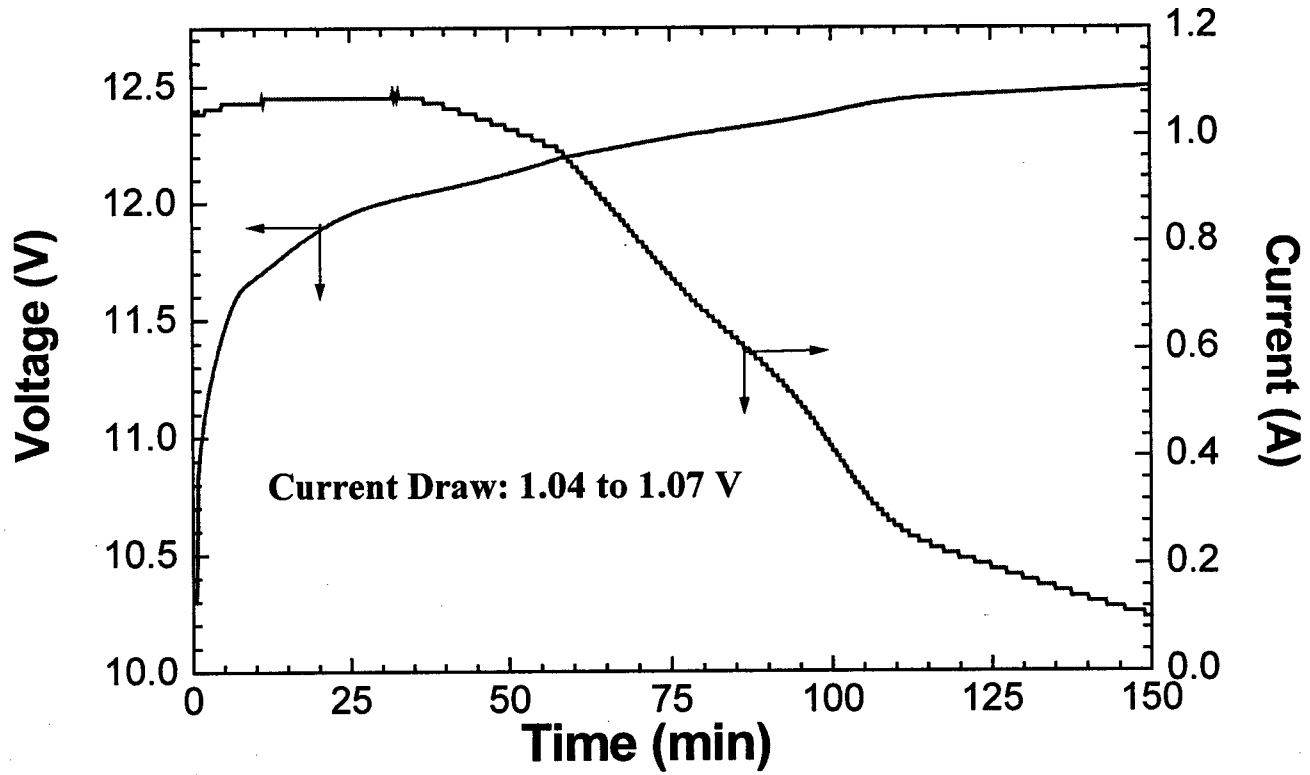

Discharge Characteristics of the Panasonic Lithium-ion Battery with No Programs Running

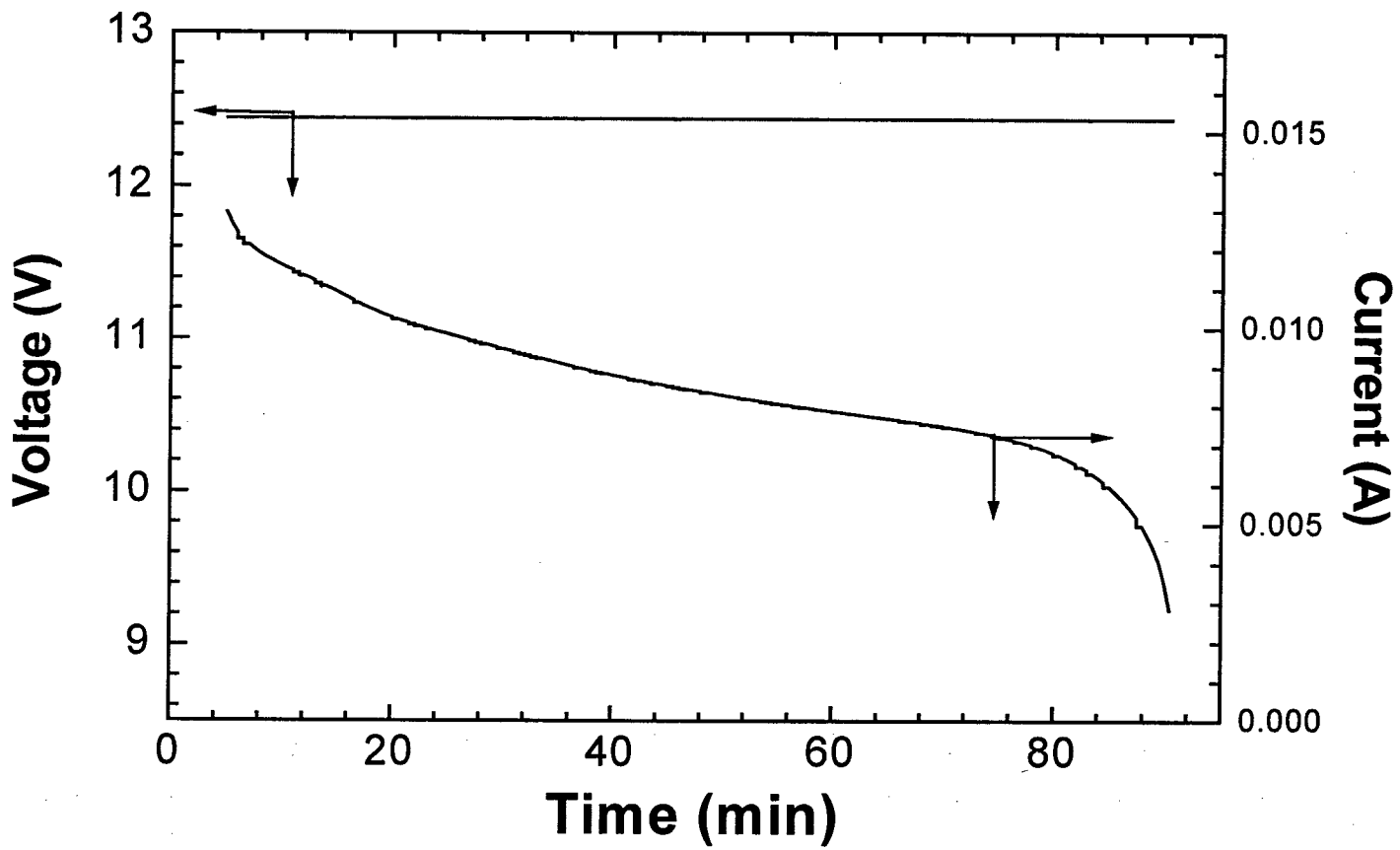

Discharge Characteristics of the Panasonic Lithium-ion Battery with the Program Running

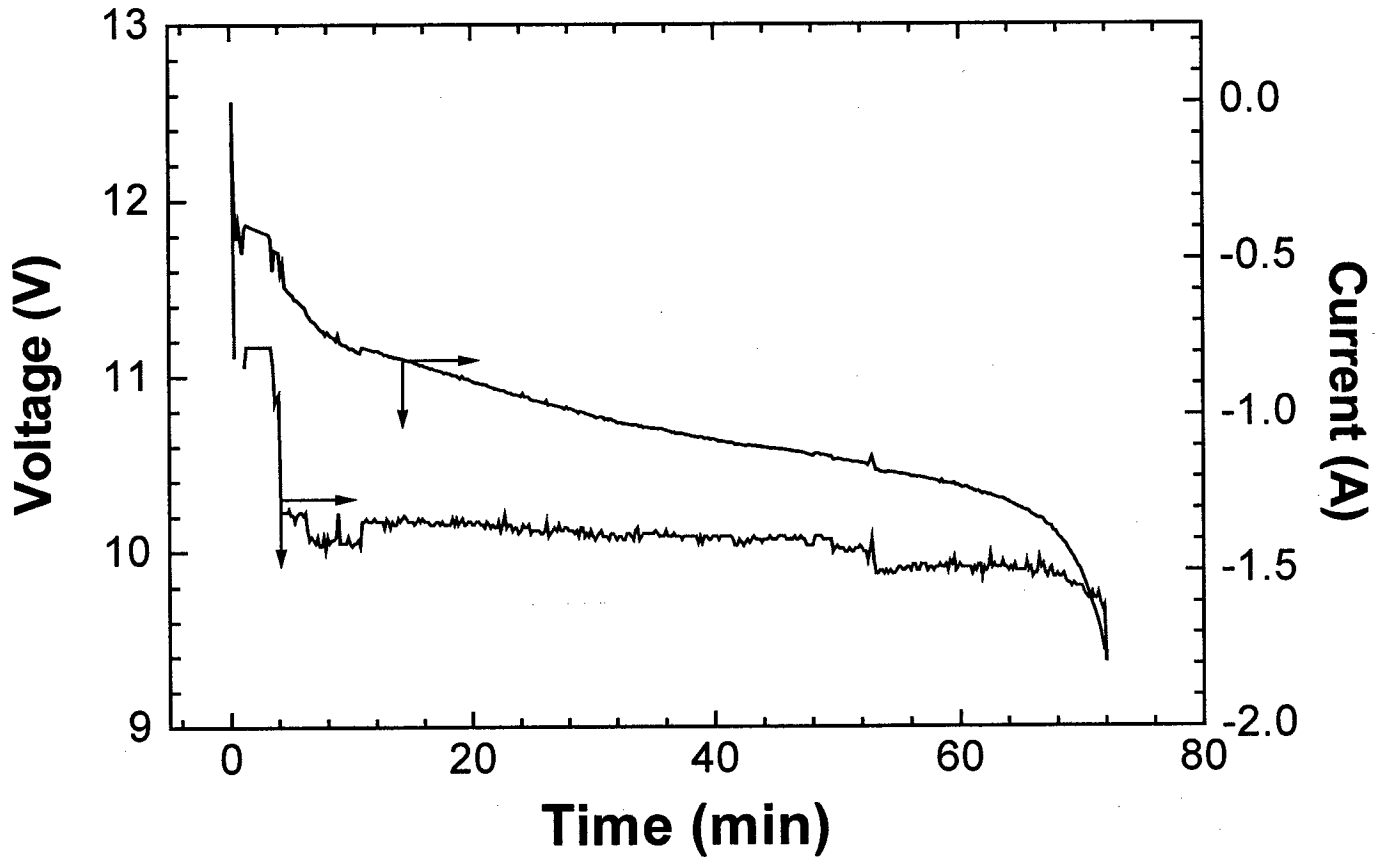

FORM SEAT 076 (08/26/1997)

Voltage Profile of Individual Cell Banks During Overdischarge of Top Cell Bank

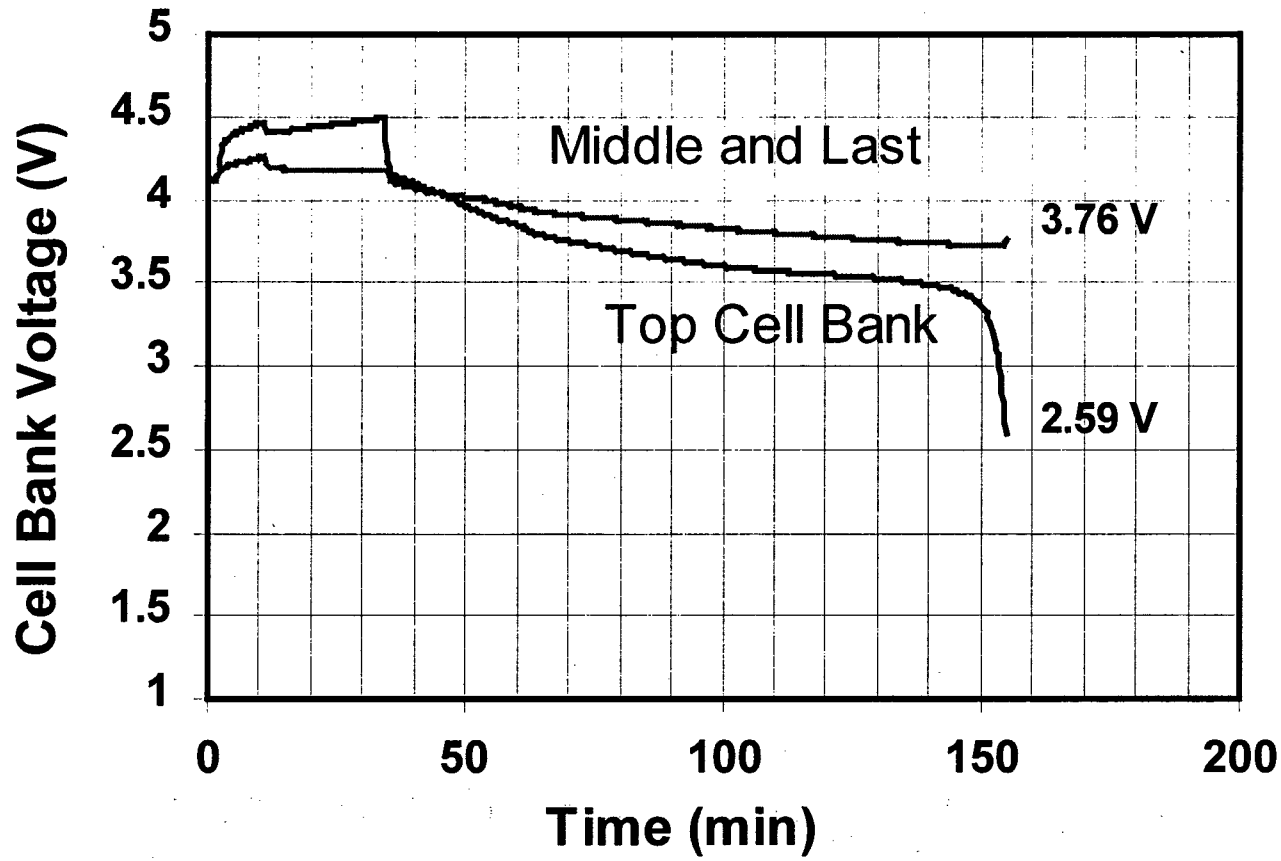

Load Current for Top Cell Bank : 2 A; For Other Two Cell Banks: 1 A

Voltage Profile of Individual Cell Banks During Overdischarge of Middle Cell Bank

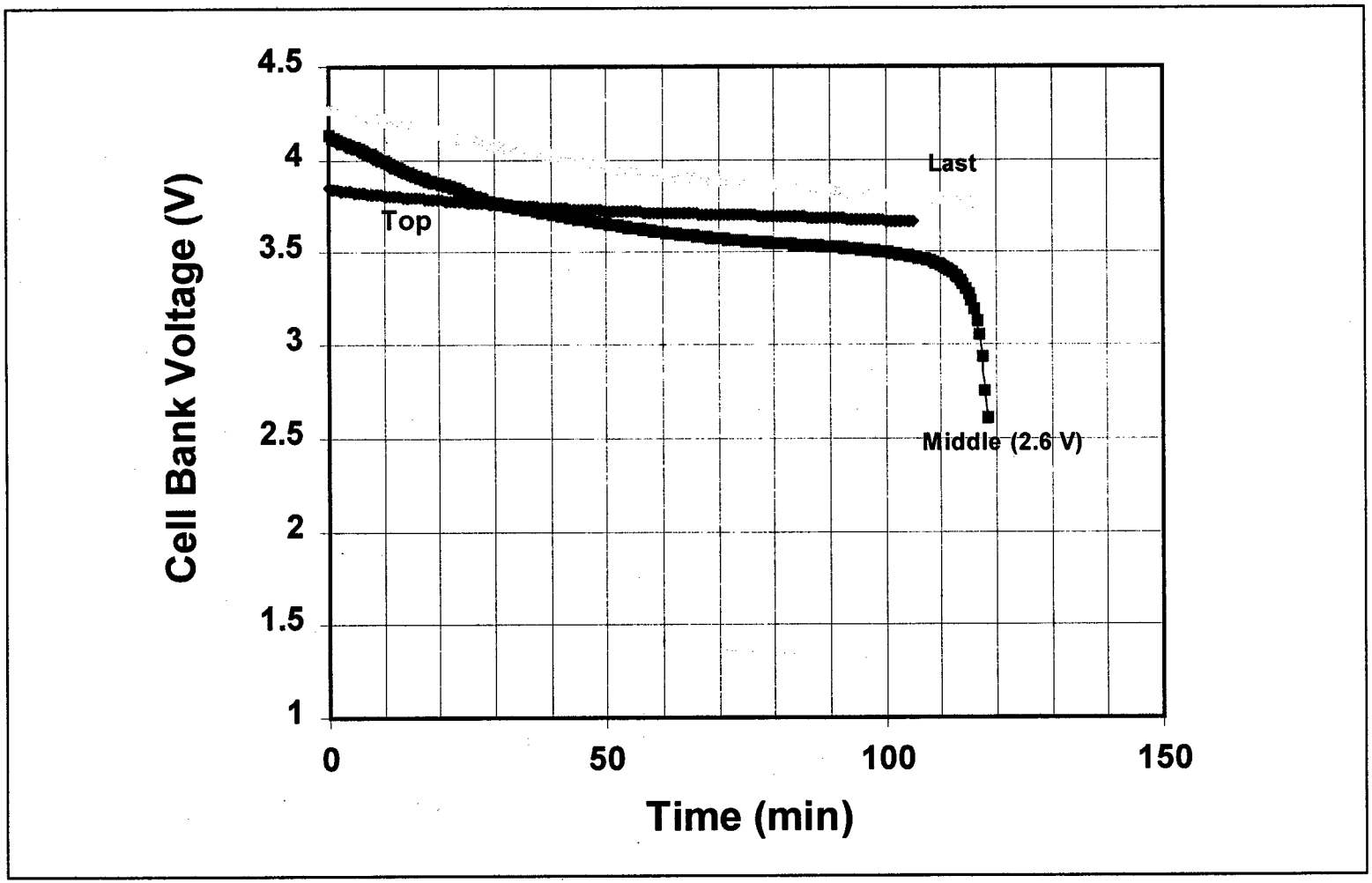

Voltage Profile During Reset of Last Cell Bank after an Overdischarge

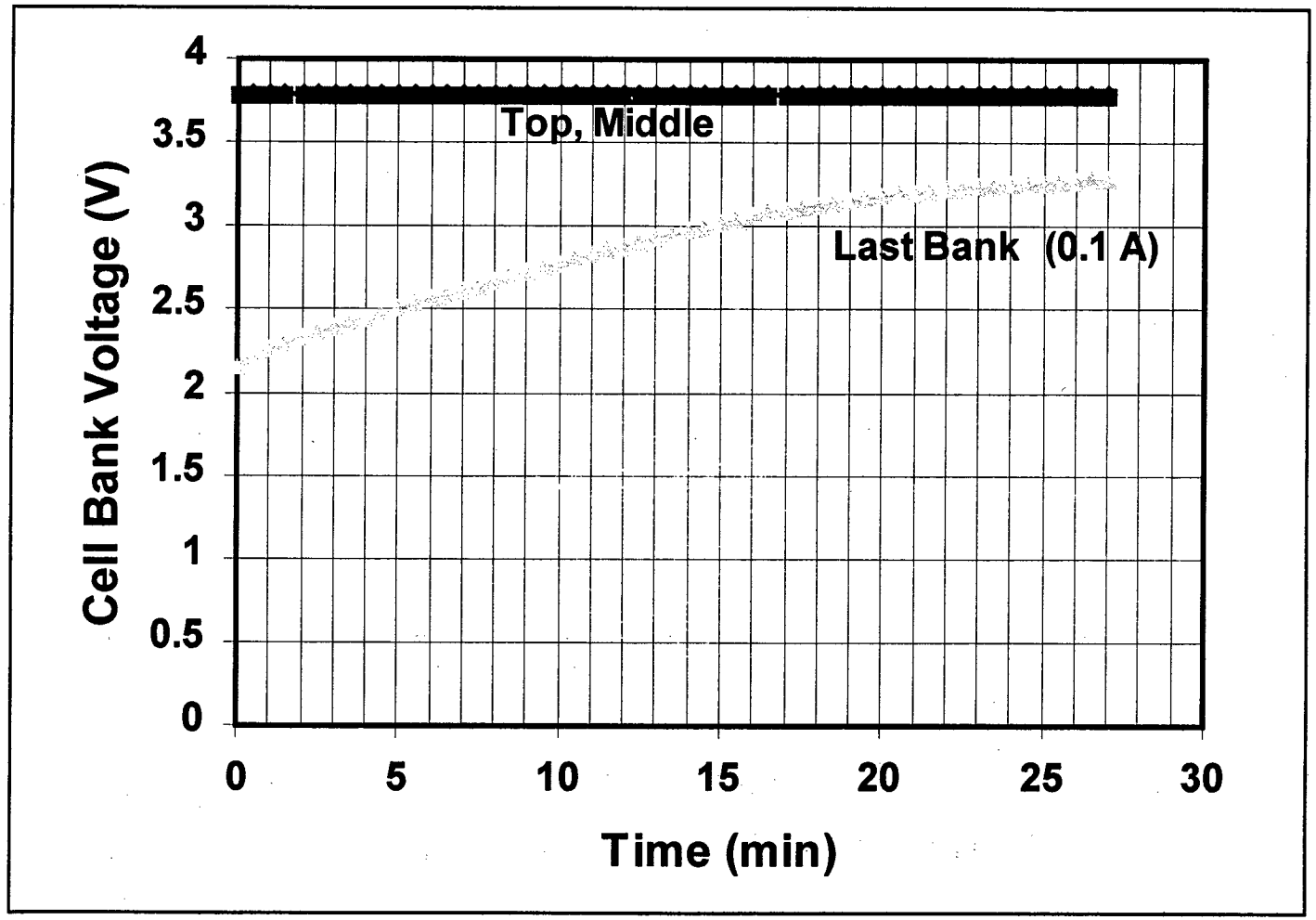

Current and Voltage Profile During An Overcharge of the Whole Battery using a 2 A Current

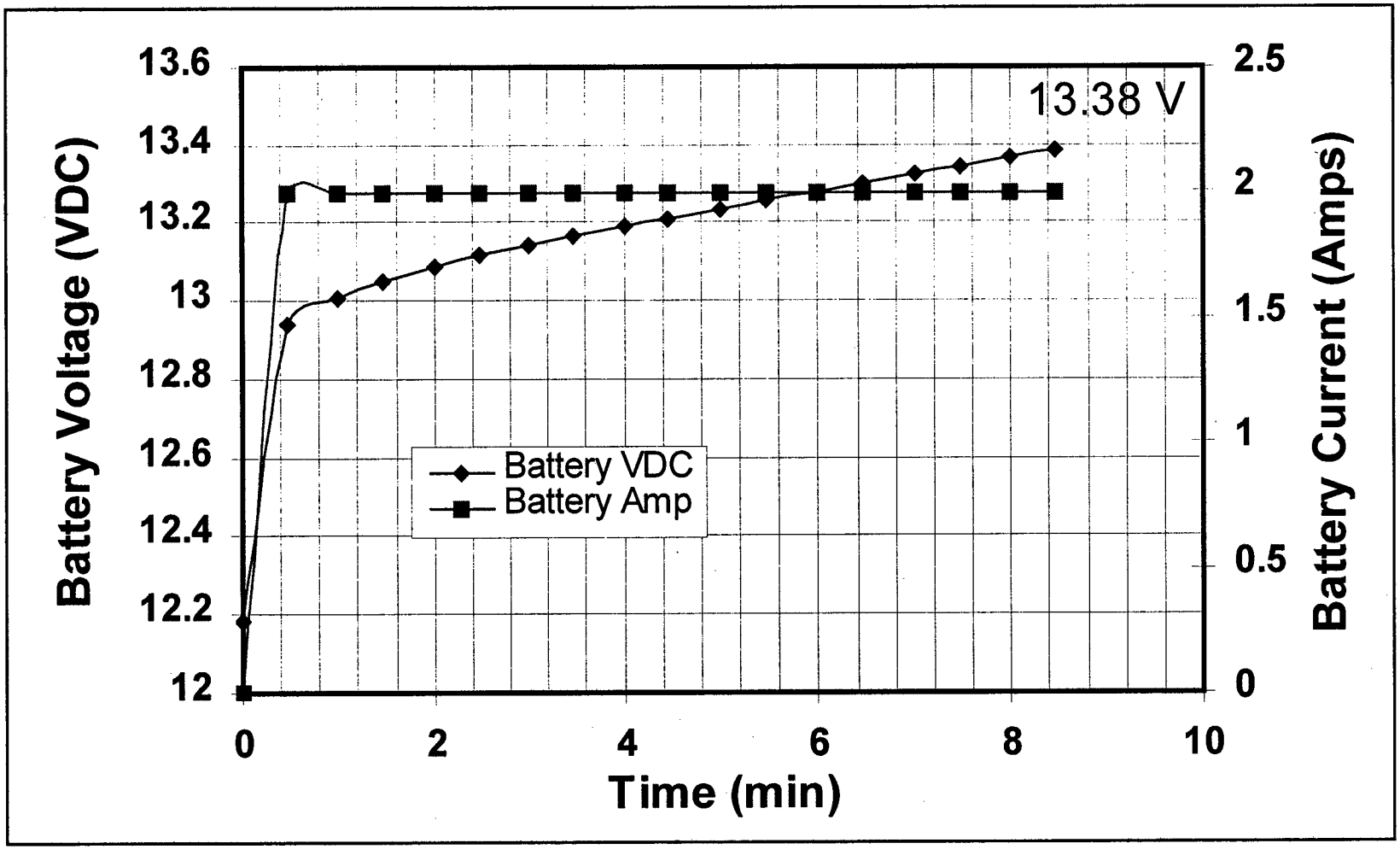

CONCLUSIONS

- Performance of the cells under different conditions of charge and discharge shows that the 0.5 C rate of charge and discharge might be the ideal condition for long term cycling.
- Overcharge and Overdischarge: The cells and the battery have adequate protection under both conditions to prevent any catastrophic occurrences.
- Temperatures above 150 °C are required to vent the cells or cause a thermal runaway. This situation is non-credible in the cabin of the Space Shuttle or ISS.
- Internal crushes can give different results depending on the nature of the crush. Soft shorts do not exhibit high temperatures or thermal runaway whereas hard internal shorts can exhibit temperatures above 400 °C and expel can contents.
- All batteries will be screened using a vibration test (0.067 g^2/Hz for one minute) for internal short before flight.

ACKNOWLEDGMENT

Dr. Wenlin Zhang - Schlumberger, Rosharon, TX
Frank Davies- Hernandez Engineering/NASA-JSC
Gerald Steward- NASA-JSC
Gwen Gilliam- Lockheed Martin/NASA-JSC
Anita Thomas- Lockheed Martin/NASA-JSC

Lithium-Ion Session II

Characterization and Simulated LEO Cycling of STRV Lithium-Ion Battery Modules

Chuck Lurie and Philip Johnson
TRW Space and Electronics Group
Redondo Beach, California 90278

The 1999 NASA Aerospace Battery Workshop
The Huntsville Hilton
Huntsville, Alabama
November 16 - 18, 1999

Wksp9901.ppt

Scope

- Lithium-ion battery modules, similar to the modules to be flown on the STRV spacecraft, are being tested.
- The modules, designed and assembled by AEA Technology plc, each contain twelve Sony 26650 cells.
- The testing reported here includes
  - Characterization to evaluate charge acceptance and cell resistance
  - Simulated LEO cycling

Test Articles

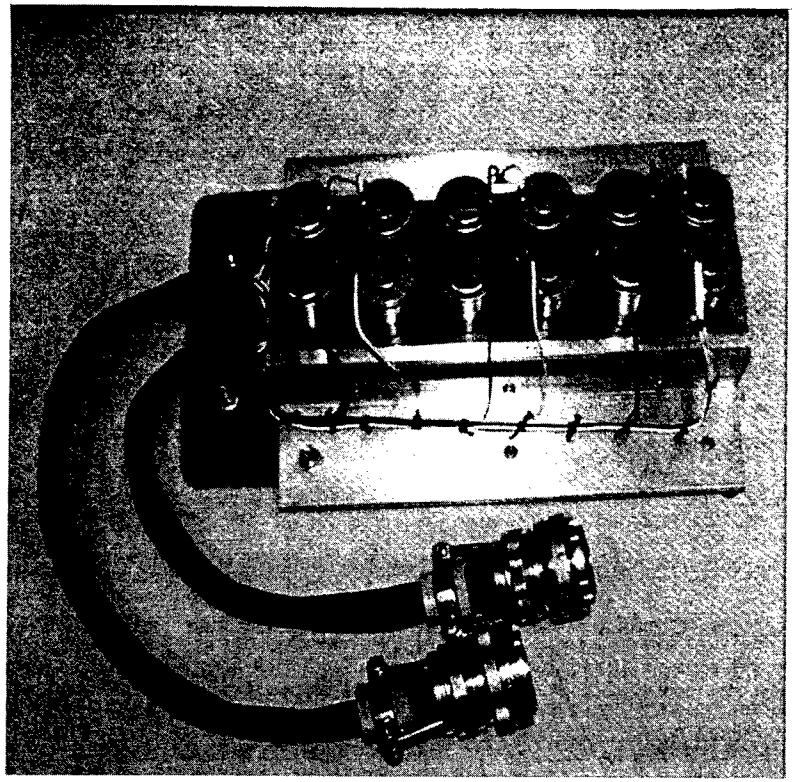

- STRV modules consist of two 6-cell strings of Sony 26650 cells.
- Test modules were reconfigured
  - one 6-cell string
  - two 2-cell strings
  - two individual cells
- Each cell is equipped with a thermocouple at its midpoint.

Wksp9901.ppt

Test Plan

Characterization: Charge Acceptance, Cell Resistance

- Charge Acceptance: determined as a function of charge voltage limit (CVL) and temperature
  - Charge at 0.2C to a CVL; Taper charge until current is < C/100
  - Discharge at 0.2C to 3.0 volts
- Cell Resistance: determined as a function of SOC, during charge and discharge
  - Impose 10% current pulses during 0.2C charge and discharge
  - determine cell resistance as dE/dI
- Two modules were tested; one at 25°C and one at 15°C

Wksp9901.ppt

Test Plan

Simulated Leo Cycling

- Depth of Discharge: 25% (basis 2.7 Ah nameplate capacity)
- Orbit: 100 minutes with 36 minute eclipse periods
- Charge regime: 0.5C to CVL; taper until eclipse discharge
- Charge management: Pack level, e.g.,
  - 6-cell average voltage for the 6-cell packs
  - 2-cell average voltage for the 2-cell packs
  - individual cell control for the single cells
- Discharge: 0.42C (36 minutes)
- Two modules were tested; one at 25°C and one at 15°C

Wksp9901.ppt

Test Setup

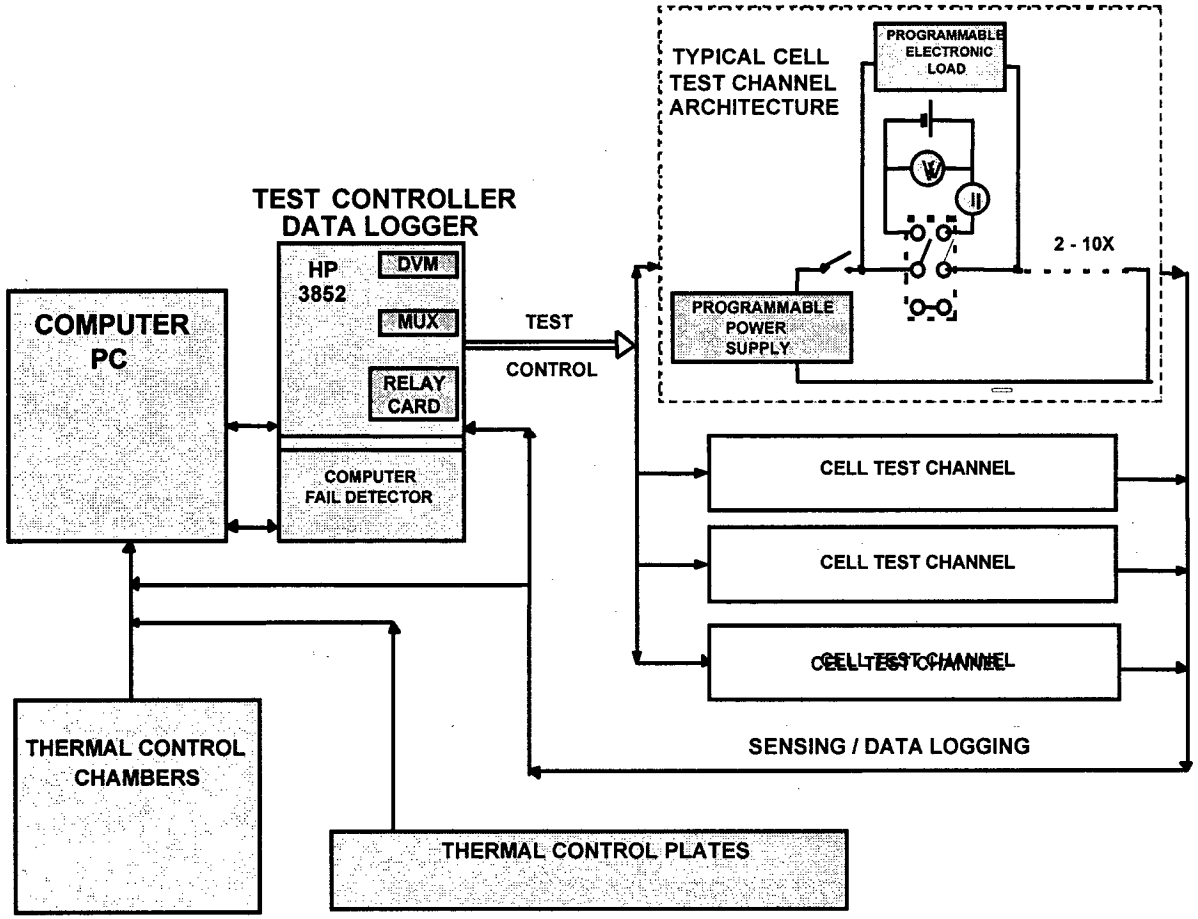

Wksp9901.ppt

Characterization

Charge Acceptance Results

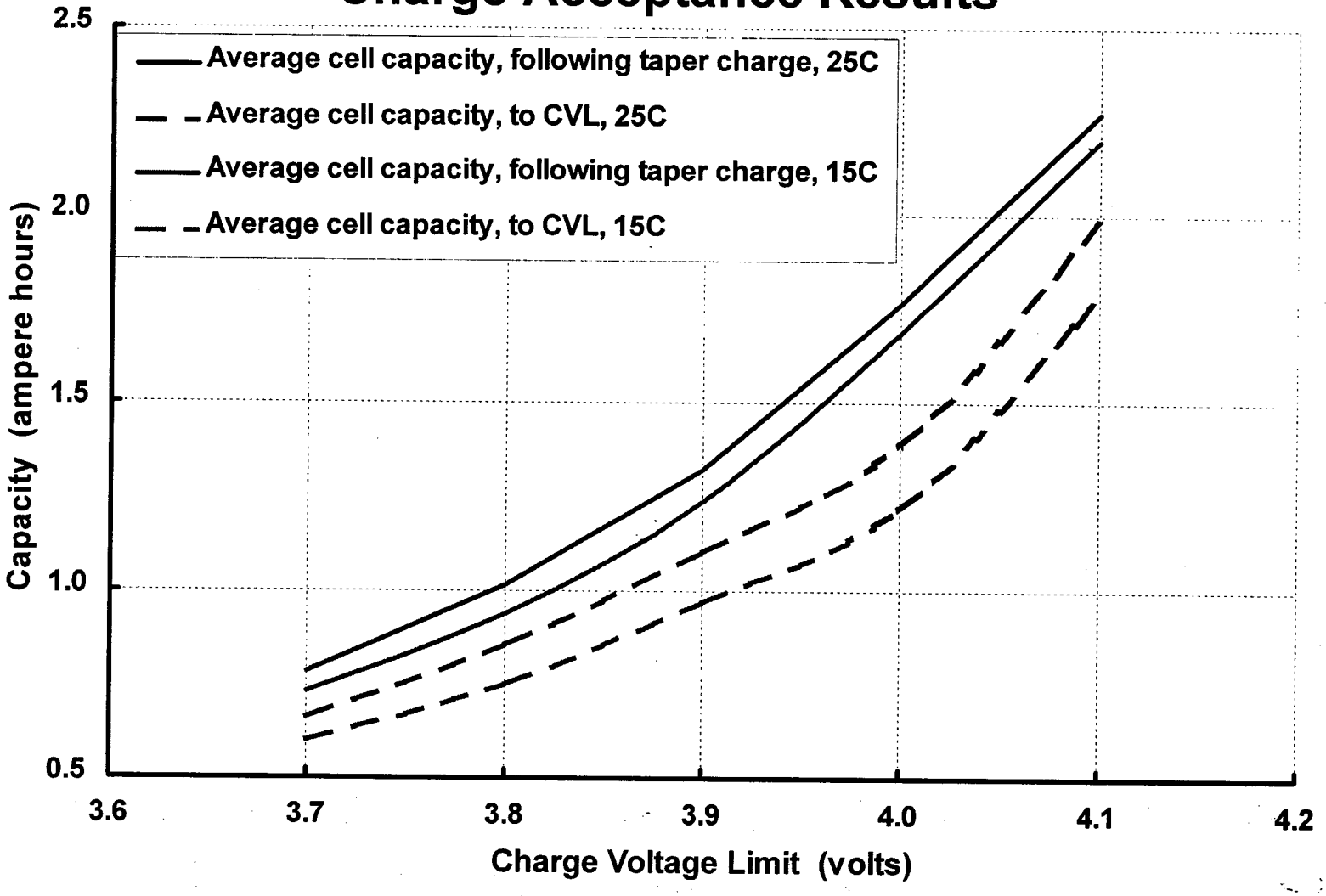

Wksp9901.ppt

Characterization

Internal Resistance as a Function of State of Charge

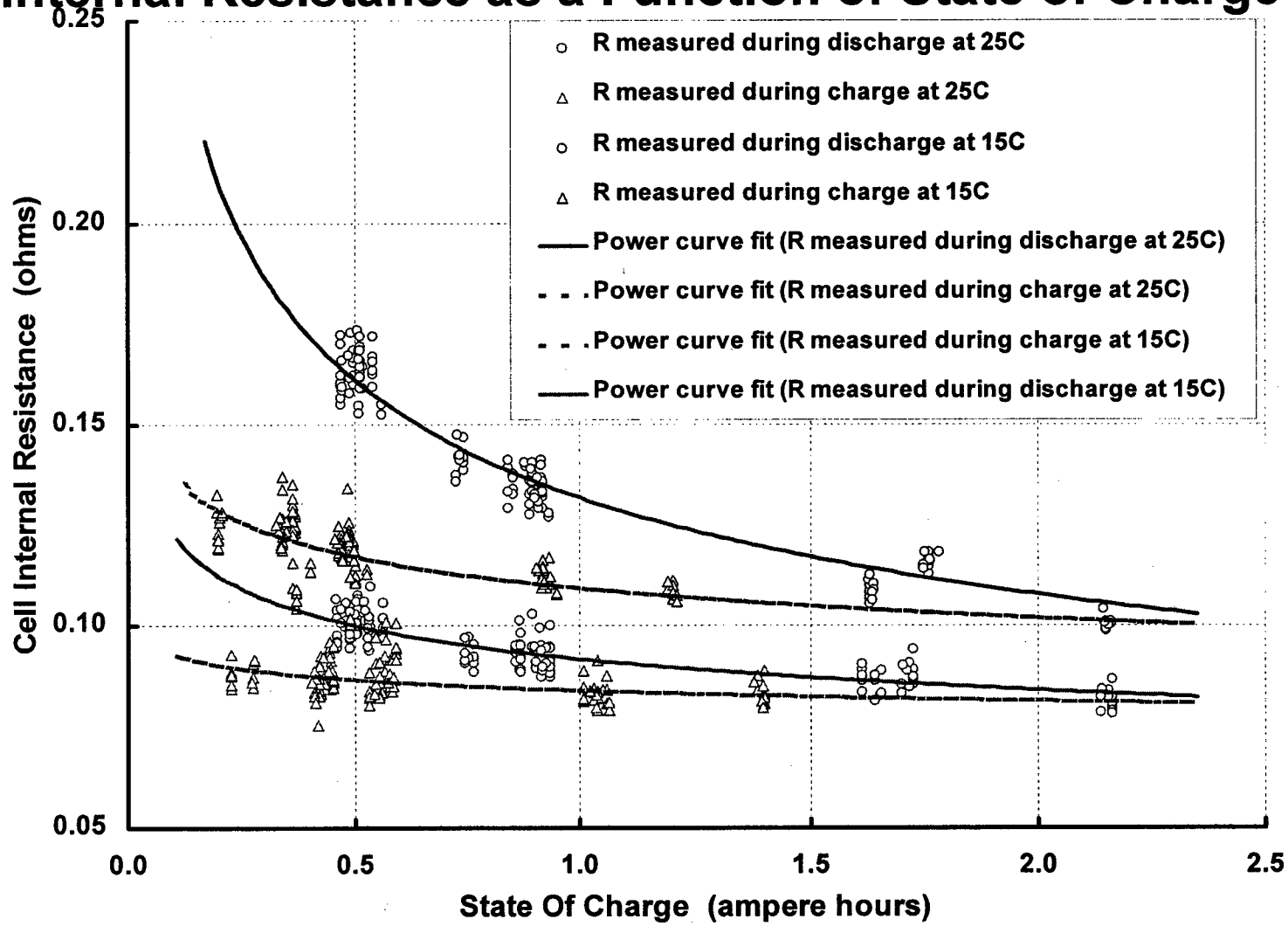

Wksp9901.ppt

Simulated LEO Cycling Results

- 25°C End of Discharge Voltage trend charts
  - 6-cell Pack
  - 2-cell pack (typical of two)
  - single cells (both cells on one plot)
- 15°C End of Discharge Voltage trend charts
  - 6-cell Pack
  - 2-cell pack (typical of two)
  - single cells (both cells on one plot)
- 6-cell pack dispersion analysis

25% DOD LEO Cycling at 25 Deg C -- 6-Cell Pack

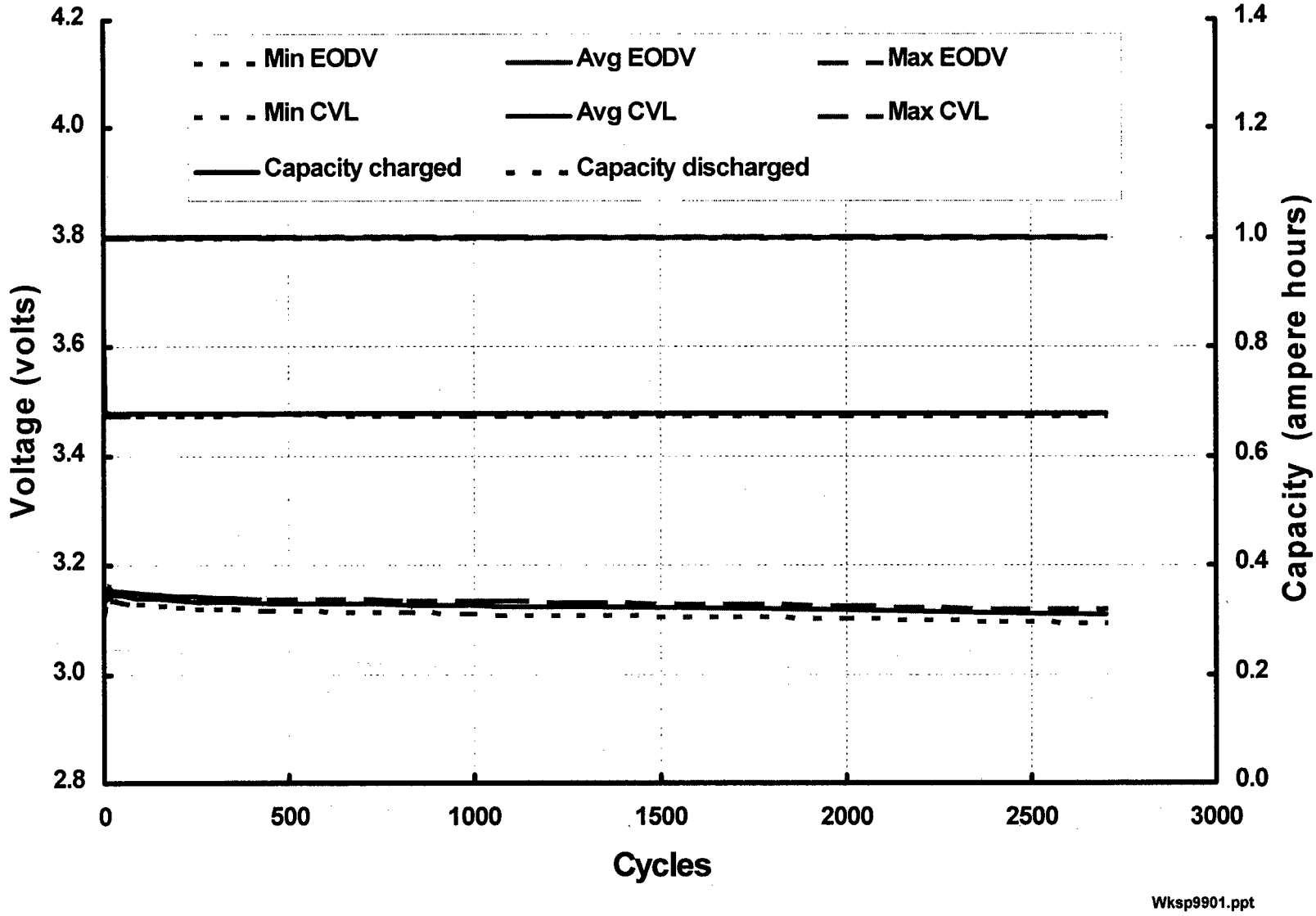

25% DOD LEO Cycling at 25 Deg C -- 2-Cell Pack

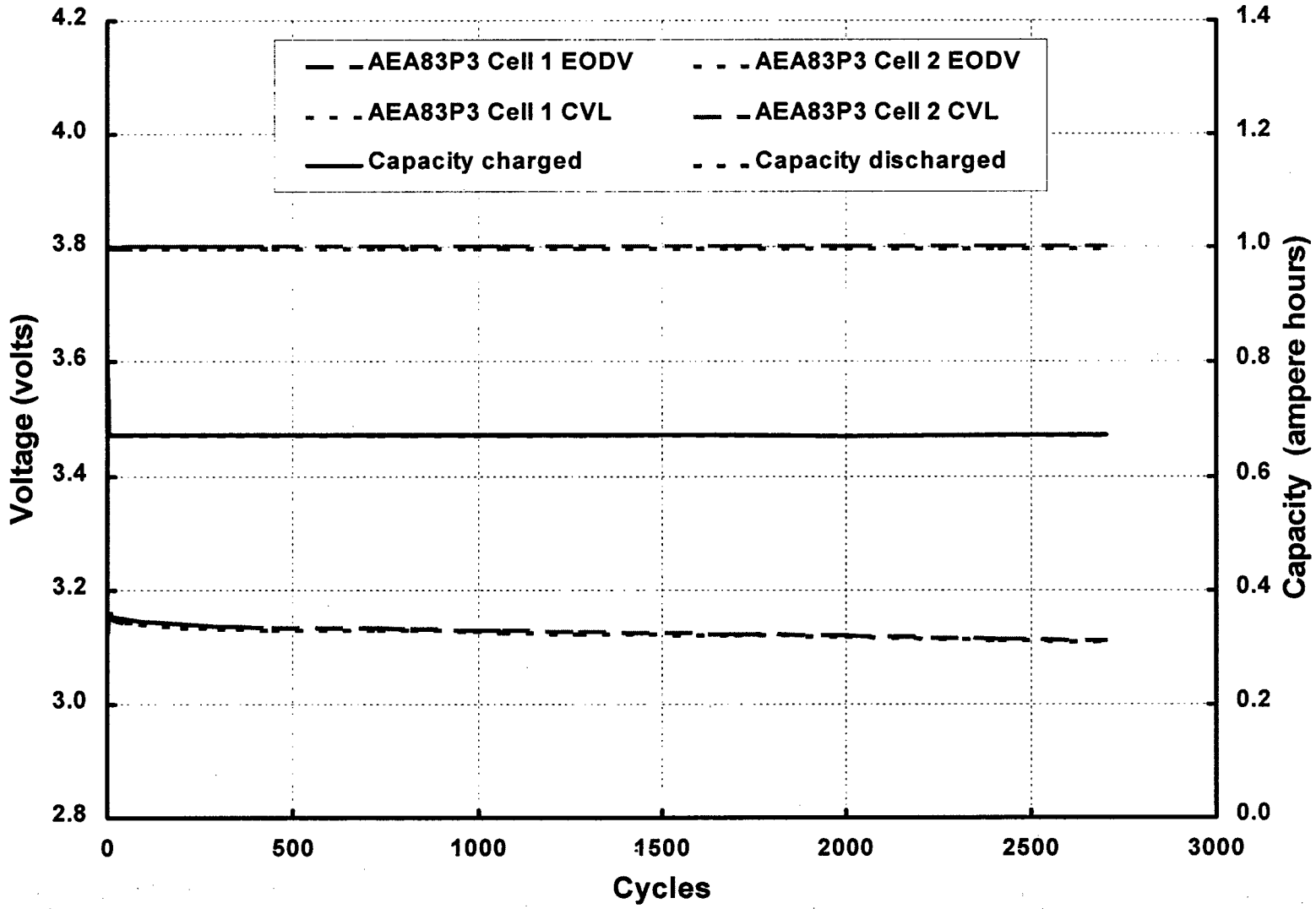

Wksp9901.ppt

25% DOD LEO Cycling at 25 Deg C -- Single Cells

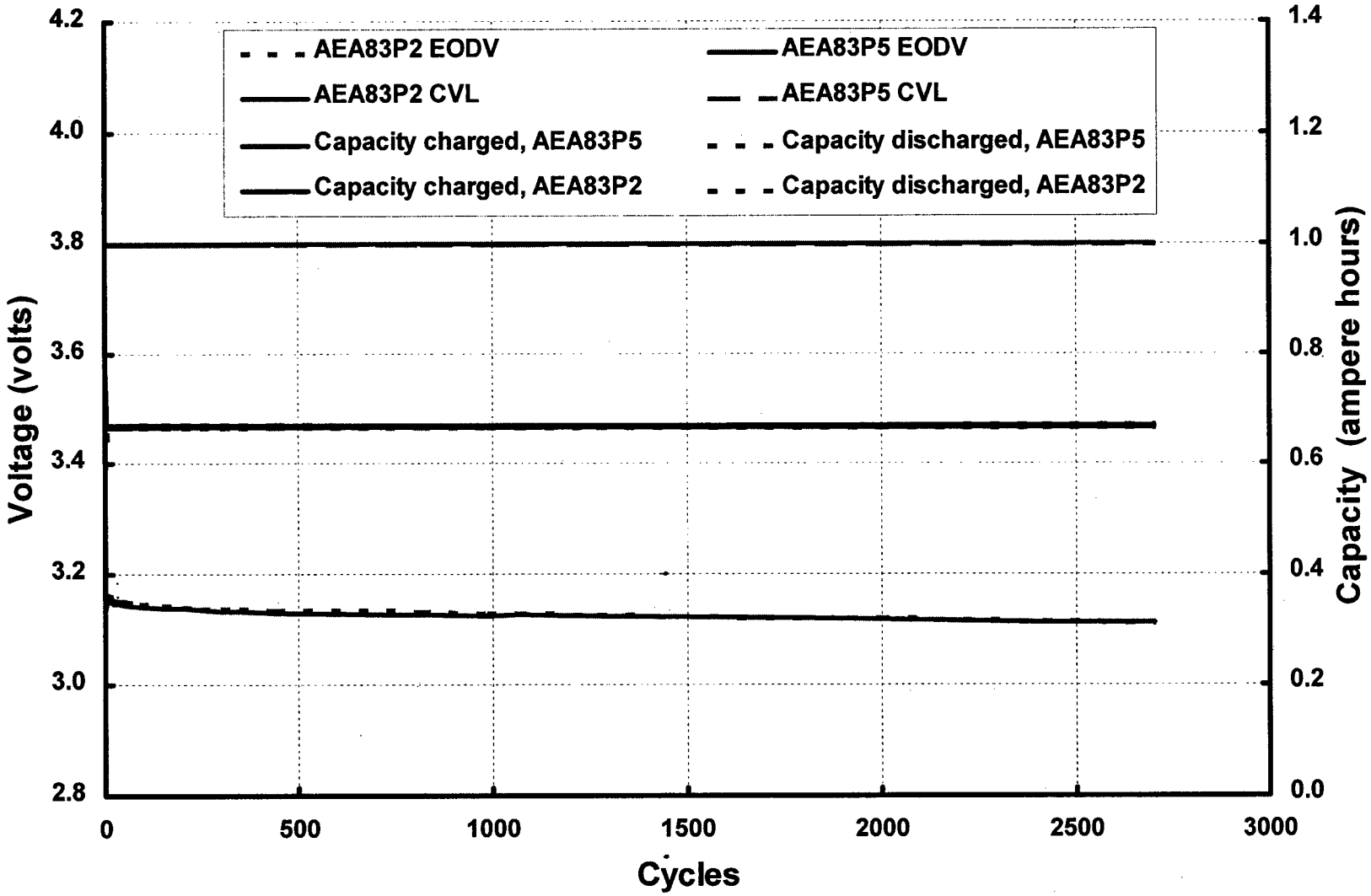

Wksp9901.ppt

25% DOD LEO Cycling at 15 Deg C -- 6-Cell Pack

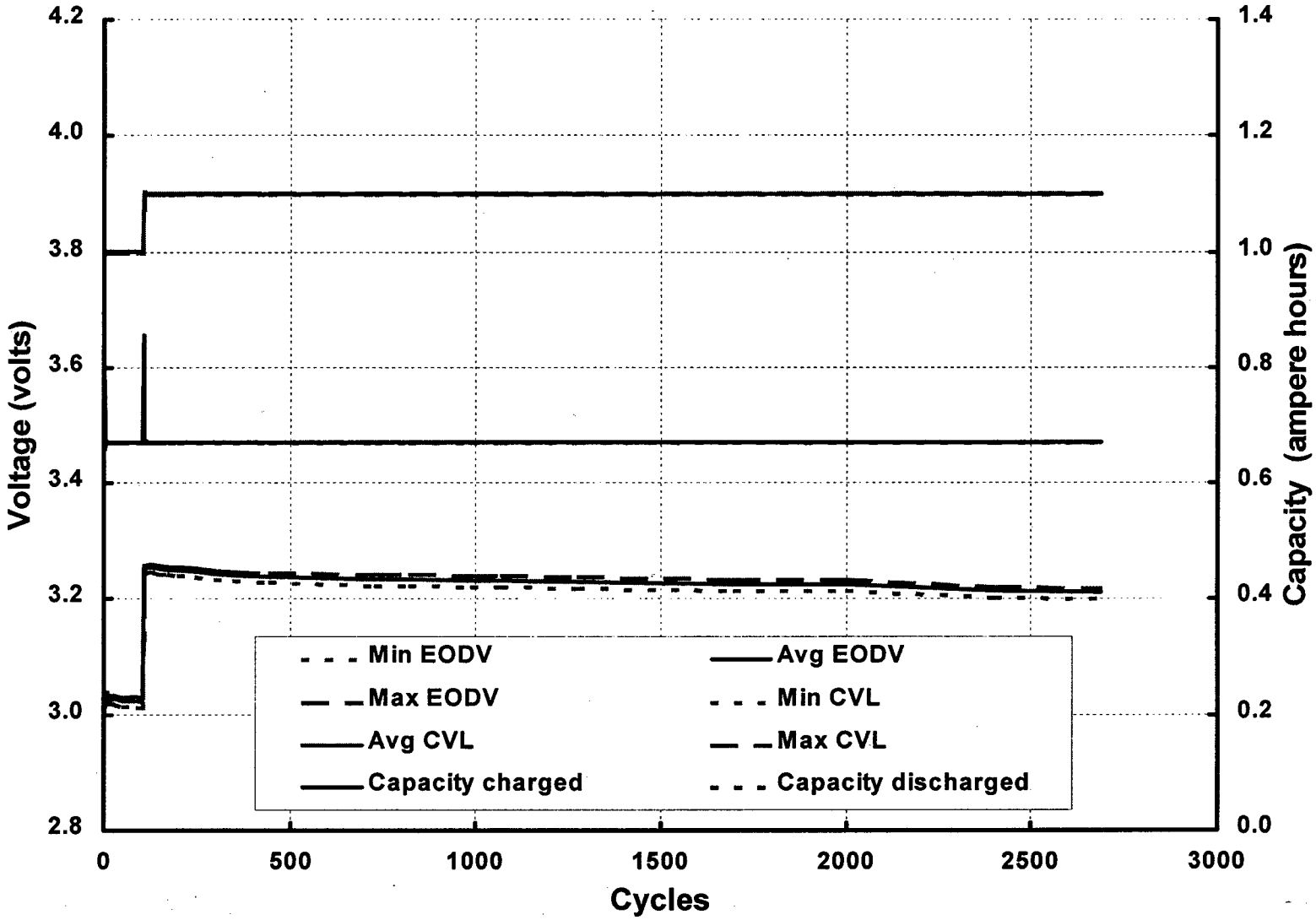

Wksp9901.ppt

25% DOD LEO Cycling at 15 Deg C -- 2-Cell Pack

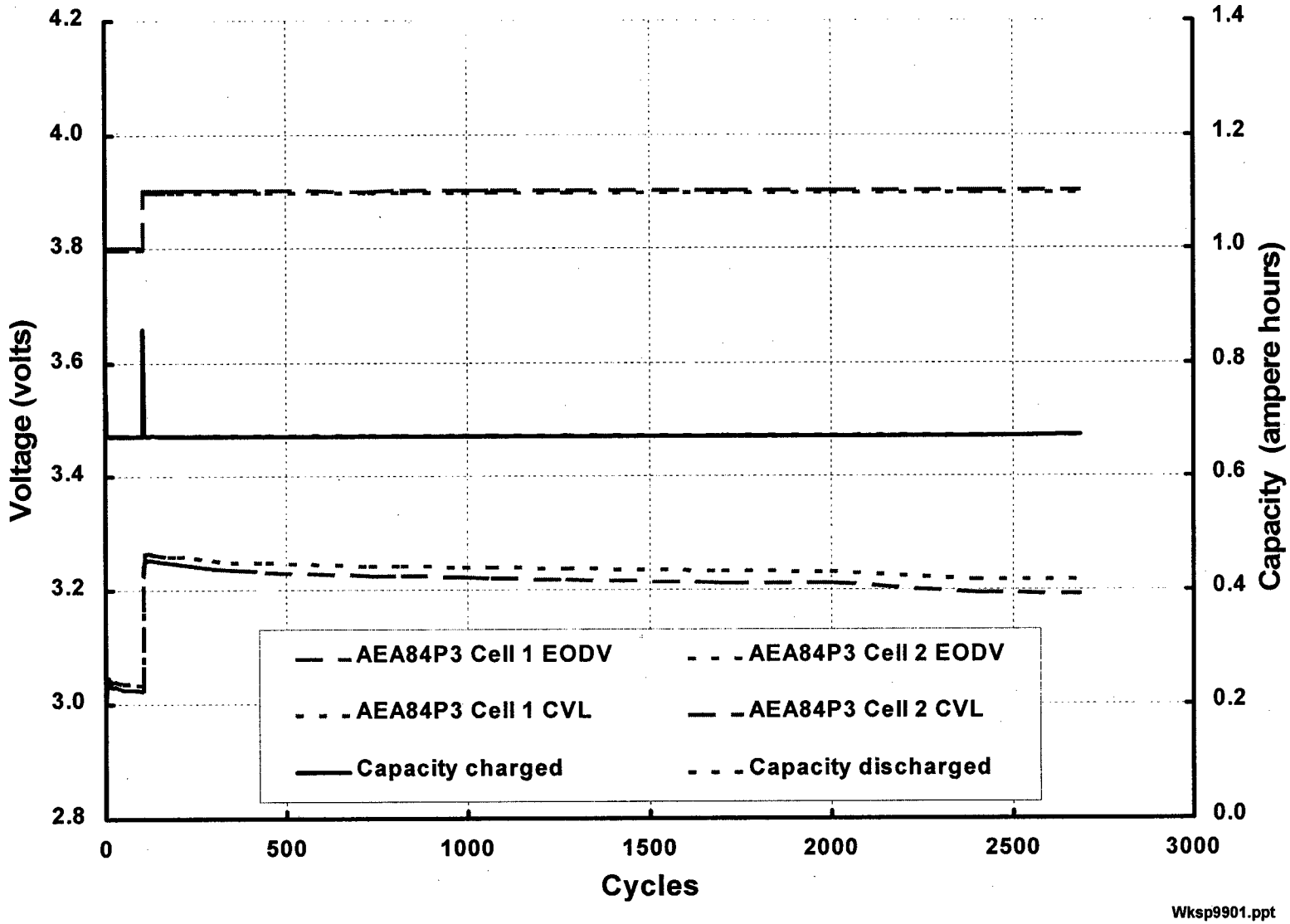

Wksp9901.ppt

25% DOD LEO Cycling at 15 Deg C -- Single Cells

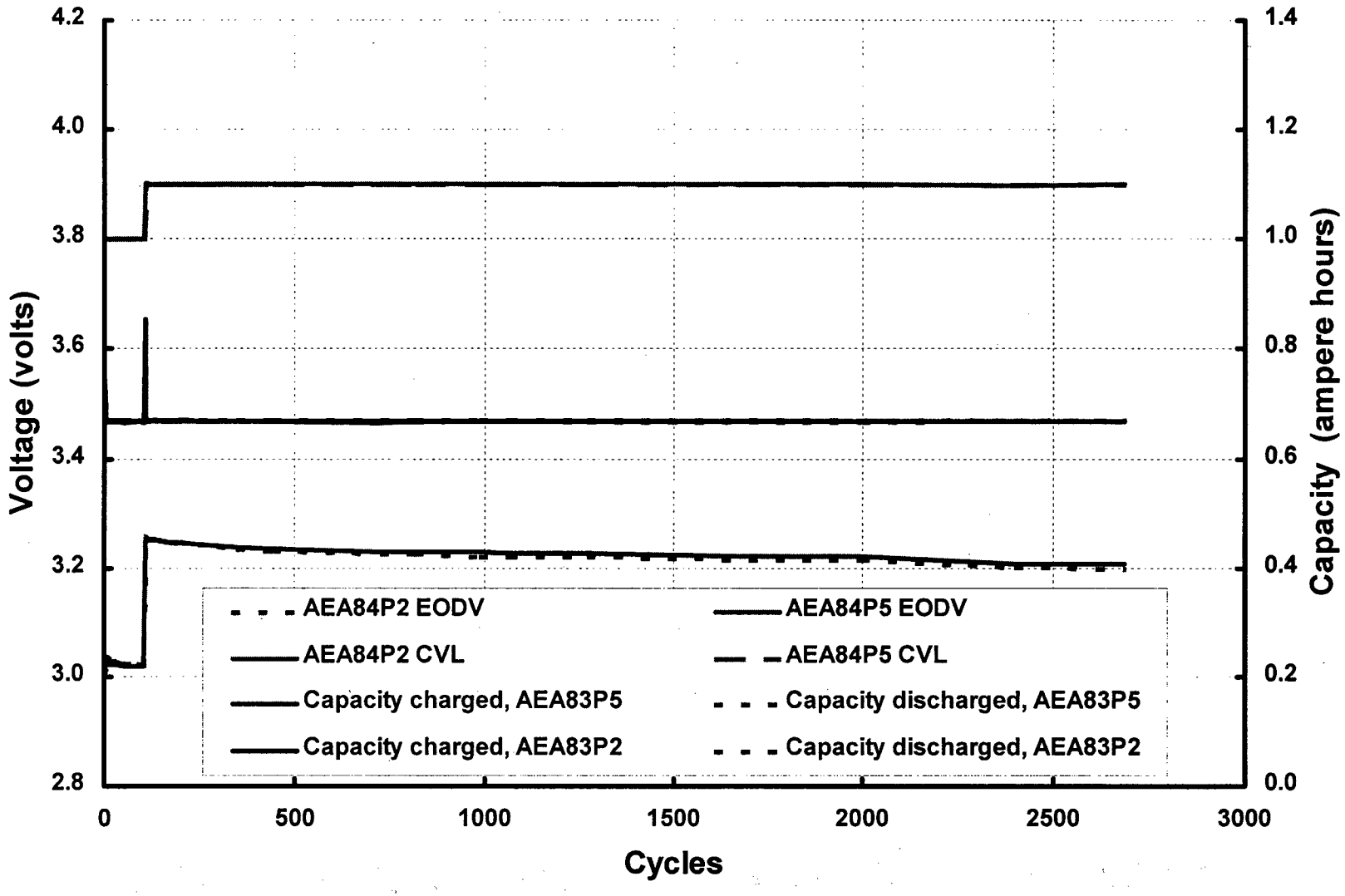

Wksp9901.ppt

6-Cell Pack EODV Dispersion Analysis

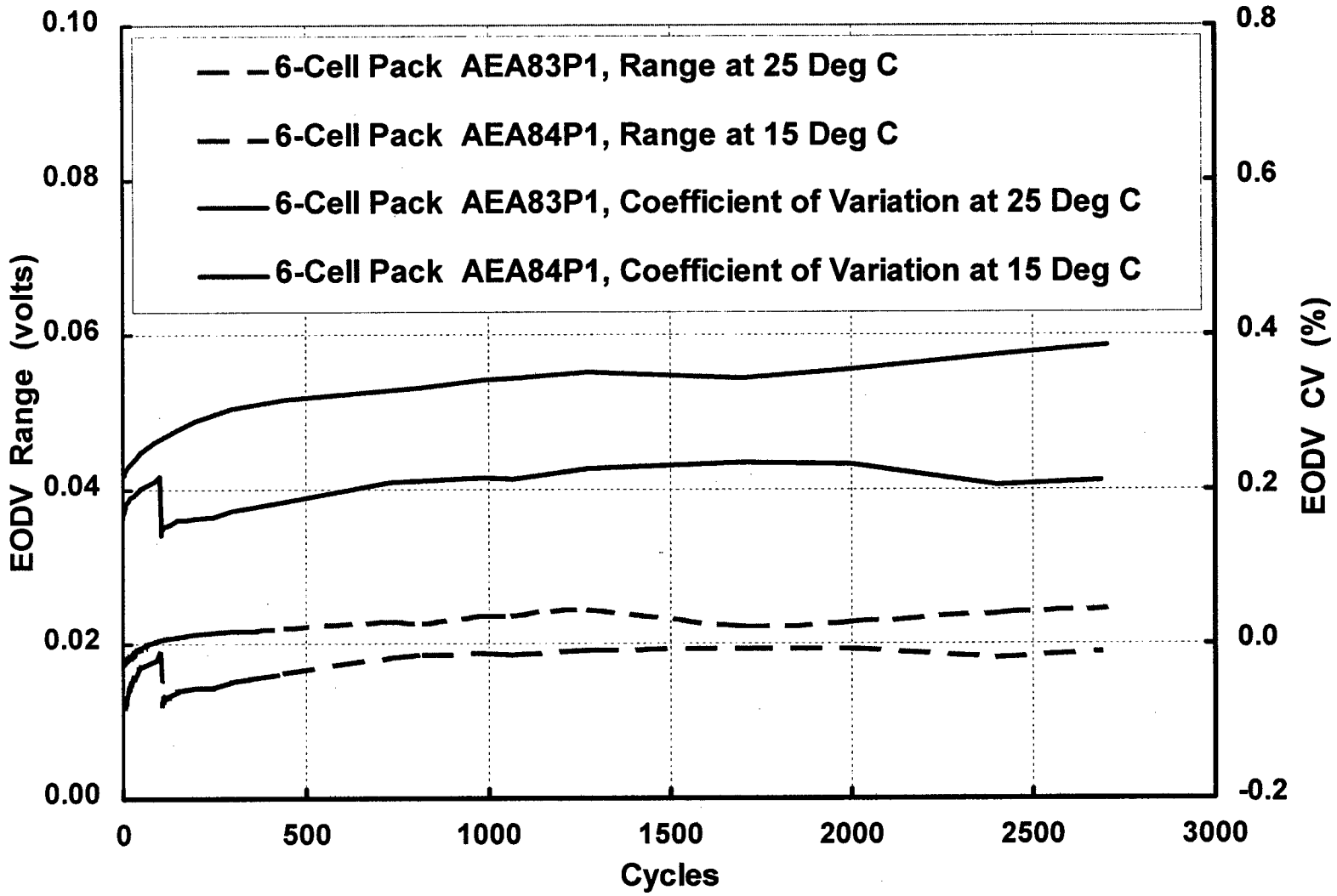

Wksp9901.ppt

Summary

- AEA STRV battery modules are on test.
- The STRV "two 6-cell strings" configuration was modified to provide 6-cell strings, 2-cell strings and individual cells.
- Charge control is at the pack level.
- Initial characterization to evaluate charge acceptance and cell resistance is complete.
- Simulated 25% DOD cycling is in progress. Greater than 2000 cycles have been completed without incident.
- EODV voltage dispersion (in the absence of cell level balancing) is acceptable and is not increasing.

Wksp9901.ppt

SAFT

SAFT SPACE Li-Ion

DEVELOPMENT STATUS

Dr Yannick BORTHOMIEU
SAFT Defense and Space Division

File : O/st/ppt/s2774-99.ppt

1999 Nasa Aerospace Battery Workshop, Nov 16-18,1999

SAFT

Li-Ion FOR SPACE APPLICATIONS

▼AGENDA

- ❑Space Cell Development
- ❑Synthesis of Tests in Progress
- ❑Calendar and Fading Parameters

SAFT

SAFT Development Context

- Saft Industrial Space Cell is issued from to the EV Cell Development.

- The Space Cell is identical to the EV cell with space specific design for the negative terminal feed through.
  - Hermiticity
  - Vibrations

SAFT

Main Development Steps

FROM PROTOTYPE TO INDUSTRIAL CELL

Phases	Objectives	Date
Prototype	Cyclability,	1996
	Winded Cell	
Stentor	GEO Cell Qualification	1997
	Battery Development	
	Cyclability Improvement	
Industrial Cell	**Industrial Design**	**1999**
	Calendar Life Time Improvement	

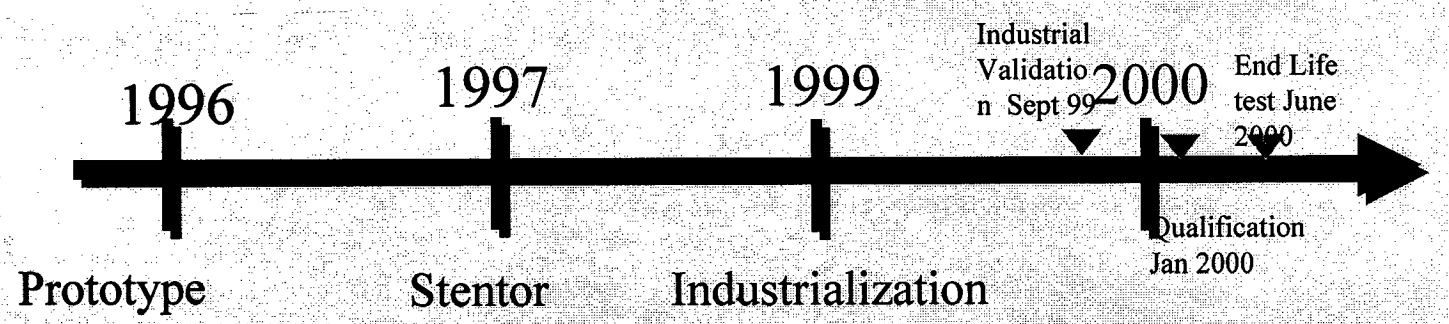

SAFT

Prototype Cell Development

- Objectives :
  - Demonstrate that the design fits with the Satellites requirements
  - Demonstrate the cyclability of the Saft Electrochemistry
- Cell developed in Cockeysville (Research Center) :
  - Use the first electrochemistry generation
  - LEO cycling on Prototype cells

SAFT

Prototype Cell Development (Cont'd)

- Demonstration of the cyclability :
  - For LEO :
    - > 35.000 cycles at 10 % DOD
    - > 17.500 cycles at 20 % DOD
    - > 10.000 cycles at 30 % DOD
  - For GEO :
    - 1159 cycles at 60 % (Fading 8 %)

SAFT

STENTOR Development Project

- European Pathfinder GEO Satellites with innovative technologies and products
- Launch Date End 2000
- Key Objectives for Li-Ion :
  - Qualification of the cell and the battery
  - GEO Life test
  - Flight demonstration

SAFT

STENTOR Development Status

- Cell qualification achieved : March 99
- Completed Life tests : End of Oct 99
  - 9 years with Electrical Propulsion+ Solstice simulation
- Battery qualification under completion : January 2000

SAFT

Batterie STENTOR EQM

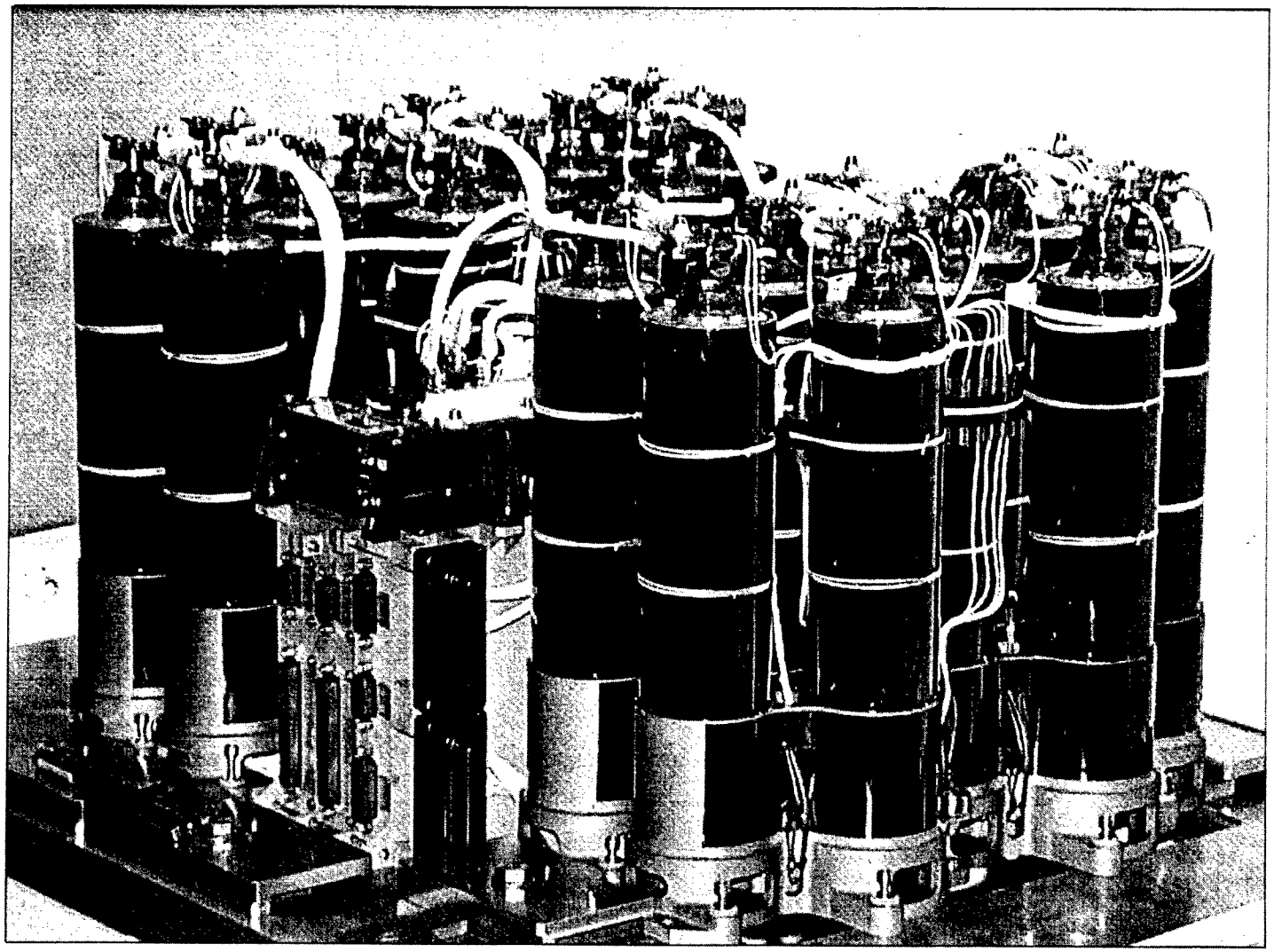

SAFT

Industrial Cell Development

- Objectives : qualification of an industrial cell for GEO and LEO missions with :
  - industrial processes : > 30.000 cells/year
  - improved cyclability performances .
- Key Dates :
  - PDR : Dec 98
  - CDR : Jul 99
  - QR : Jan 2000

SAFT

Evolution Justification

- Mains evolutions from Stentor to industrial design
  - Same mechanical interfaces and feed through
  - Negative Mix in order to get process improvement at coating level
  - Positive alloy in order to improve both alloy process and cell internal resistance stability
  - Electrode loading in order to improve cell cyclability

SAFT

Industrial Line

- Able to produce more than 30.000 cells per year
- More than 2.000 Industrial EV cells (250 space cells) built since July 99
- Complete line validation achieved by end 99, processes already qualified
- Cell qualification batch has been produced on this line :
  - BOL qualification performed:
    - (electrical and thermal characterizations, vibrations)
    - Overcharge, overdischarge and short circuit
  - Life test on module (2P3S) : june 2000

SAFT Li-Ion INDUSTRIAL SPACE CELL DEVELOPMENT

- Mains performances:
  - guaranteed capacity : 38.6 Ah @ 4.1V
  - mean discharge voltage : 3.6 V
  - Max Weight : 1.13 kg
  - Impedance 2.5 mOhms
  - **Total energy : 139 Wh (4.1V EOCV)**
  - Specific energy : 125 Wh/kg at 4.1V
  - Energy efficiency > 94%
  - **Thermal Dissipation : 3 to 4 times less than the NiH_2**

SAFT Li-Ion INDUSTRIAL SPACE CELL DEVELOPMENT

▼ Energy = f(Current and EOCV)

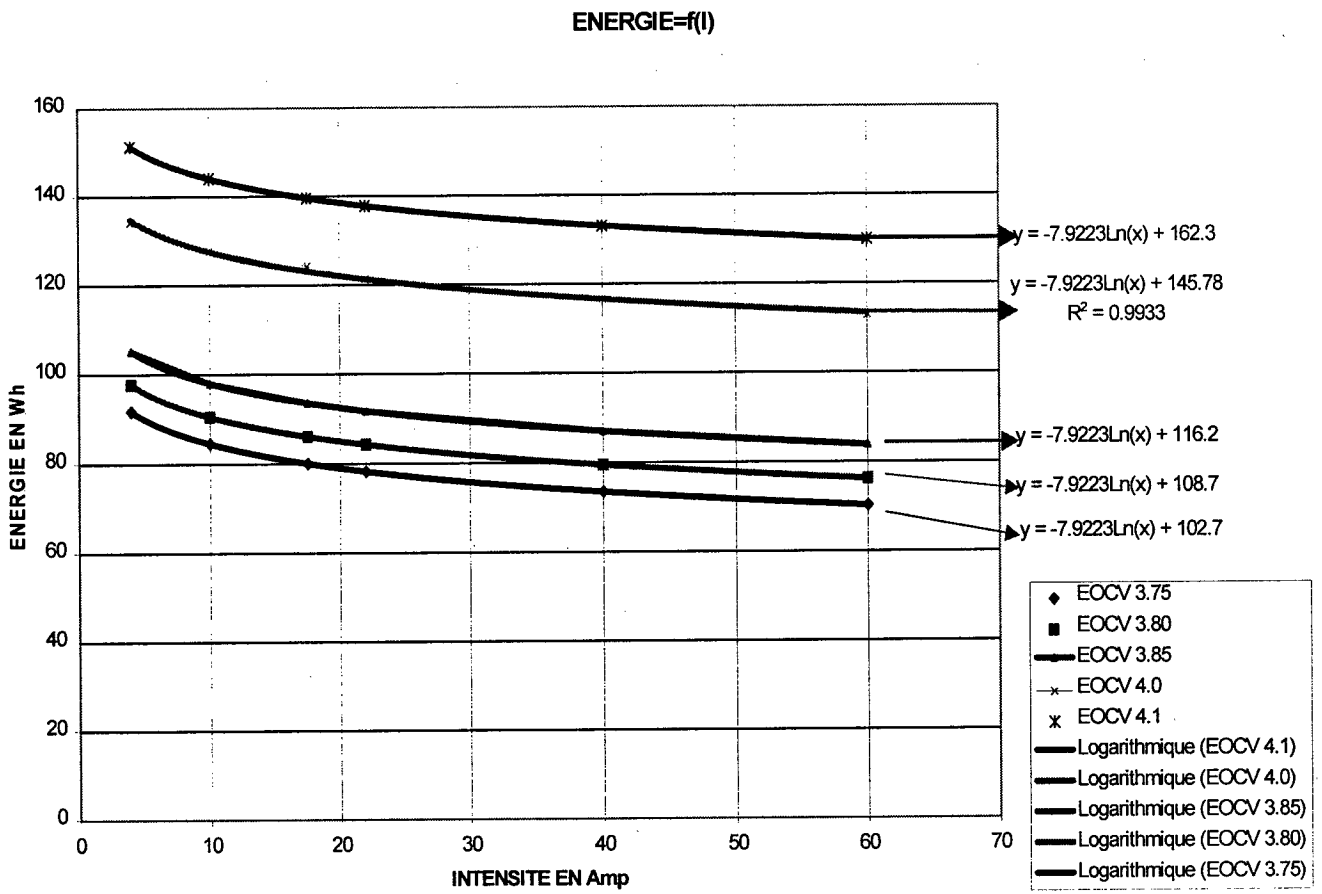

SAFT Li-Ion INDUSTRIAL SPACE CELL DEVELOPMENT

▼ Energy = f(Current and Temp)

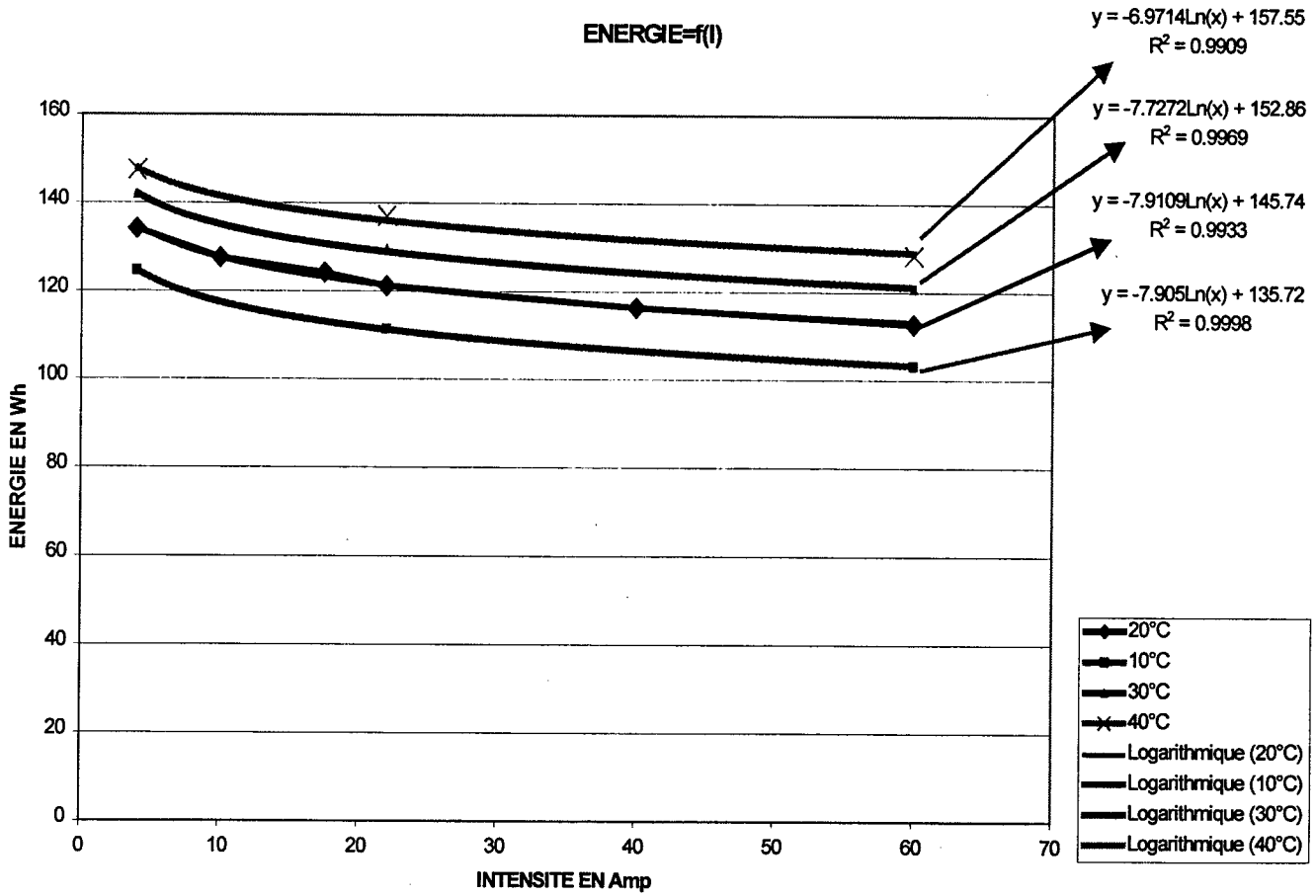

File : O/st/ppt/s2774-99.ppt

1999 Nasa Aerospace Battery Workshop, Nov 16-18,1999

SAFT

SYNTHESIS OF TESTS IN PROGRESS

SAFT

Accelerated LEO test

- 20 % DOD (10 to 30 % tested)
- EOCV : 3.8 V
- Charge 35 A (C/1.15), Discharge 60 A (1.5 C)
- > 40 cycles per day
- Diagnostic every 500 cycles

Data provided by Dr B.Staniewicz
(R and D Center Cockeysville)

SAFT

Accelerated LEO test

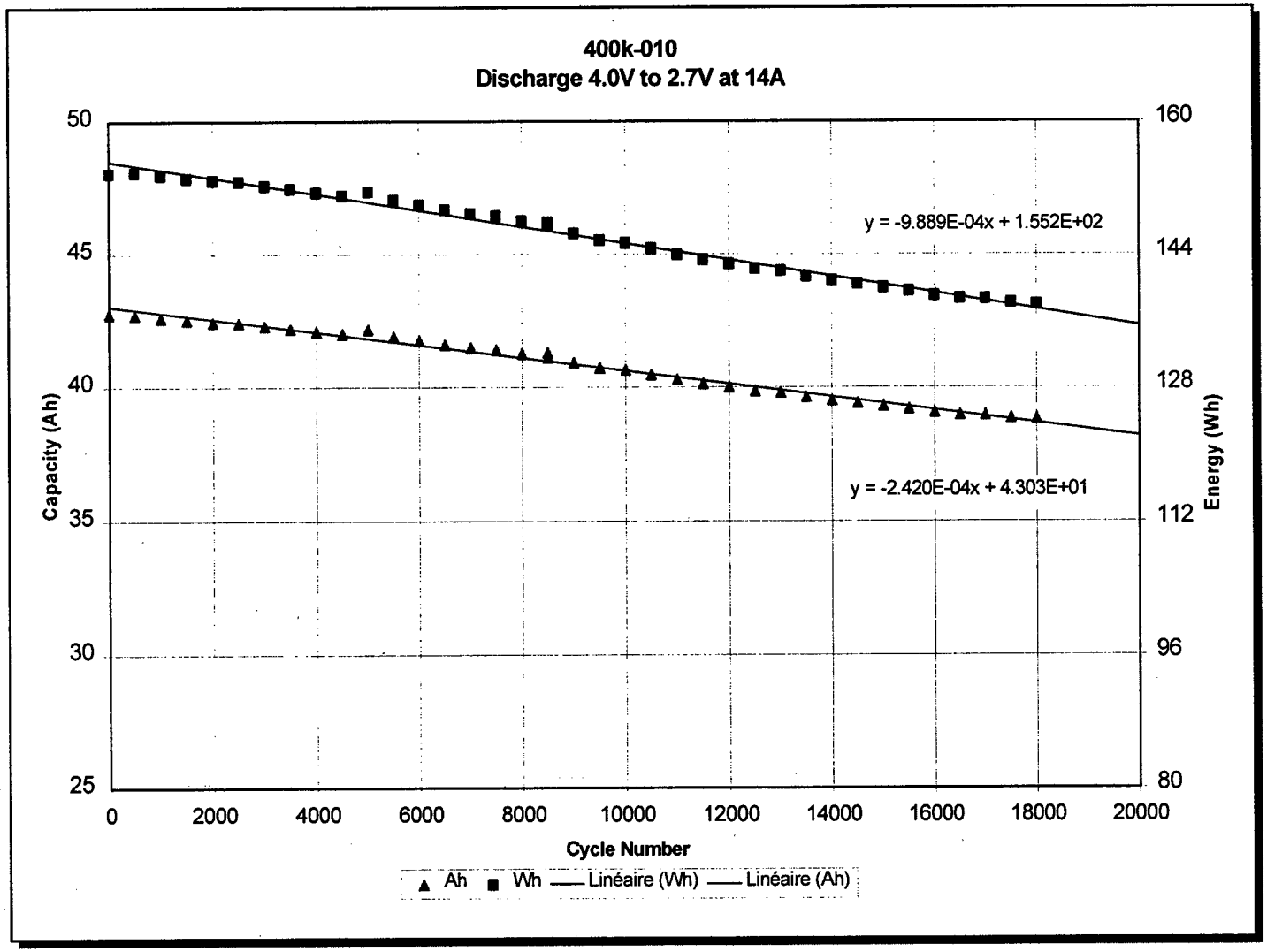

SAFT

GEO STENTOR Cycling

(Started Nov 97 and July 98)

- 2 Batteries of 6 Cells (1P6S) with Electronic (EOCV : 3.9 V equinox, 3.8 V solstice)
- 2 First years : 44 % DOD, 7 Last years : 34 % DOD
- Ionic propulsion (2 cycle/day @ 25 % DOD during equinox, 1 cycle/day @ 35 % DOD during solstice)
- Solstice : 92 Cycles, duration : 15 days
- **9 years=18 Seasons Performed**
- **3 % of capacity loss**

SAFT

GEO STENTOR Cycling

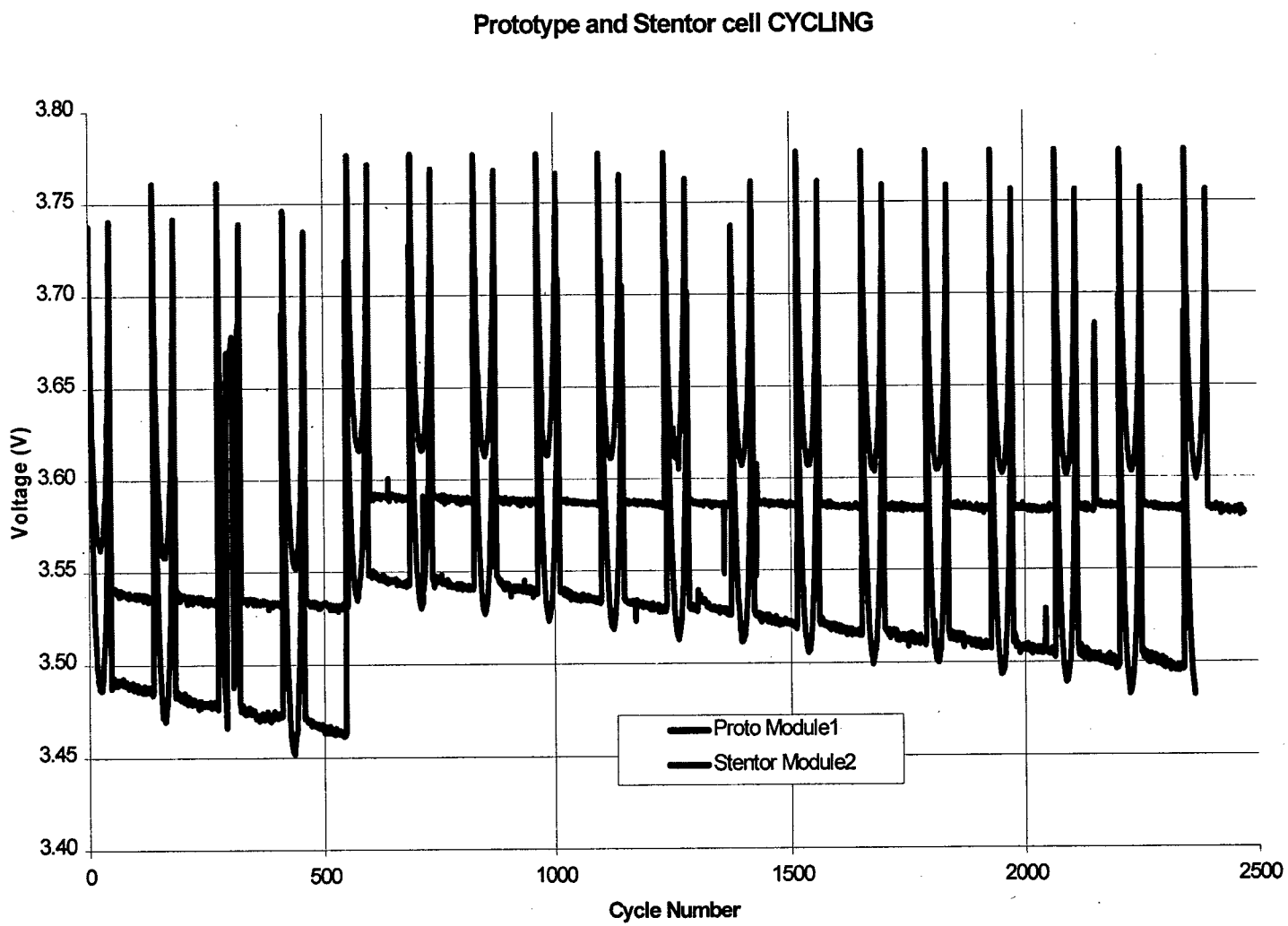

SAFT

80 % DOD on STENTOR Cells

- 2P2S Module with Electronic management
- Max DOD = 80 % (eclipse profile)
- EOCV= 3.9 V and 3.95 V EOL
- Semi-accelerated conditions : 1season=1 week
  - charge C/3 and Discharge C/1.5
- **15 years =30 Seasons Performed**
- **10 % of capacity loss after 30 seasons (15 years)**

SAFT

80 % DOD on STENTOR Cells

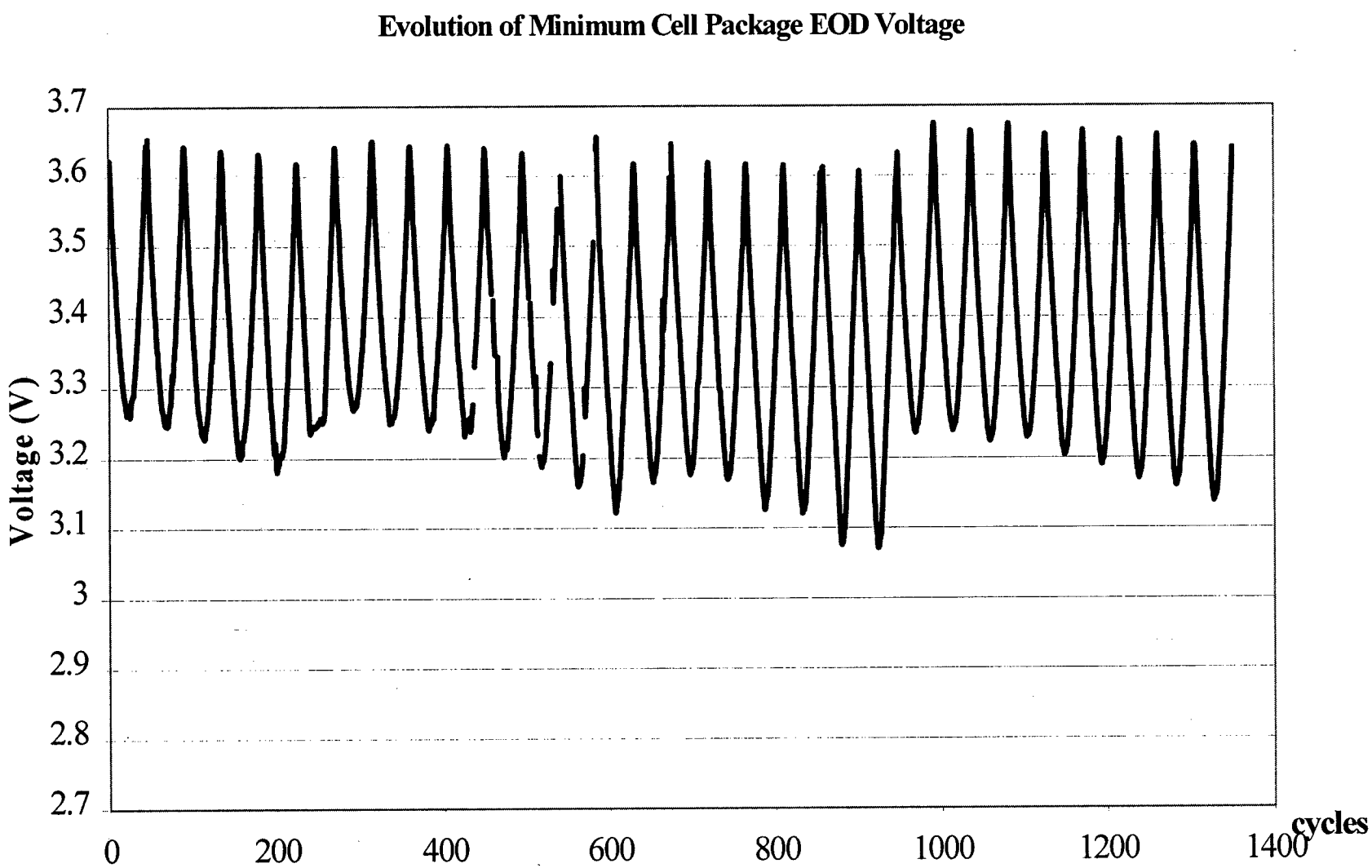

File : O/st/ppt/s2774-99.ppt

1999 Nasa Aerospace Battery Workshop, Nov 16-18,1999

SAFT

100 % DOD Industrial Cell

- Cycling comparison on generations of cells
- Charge C/5; Discharge C/2 up to 2.7 V
- Continuous 100 % DOD
- **550 cycles Performed**
- **3 % of capacity loss**

SAFT

100 % DOD on Industrial cell

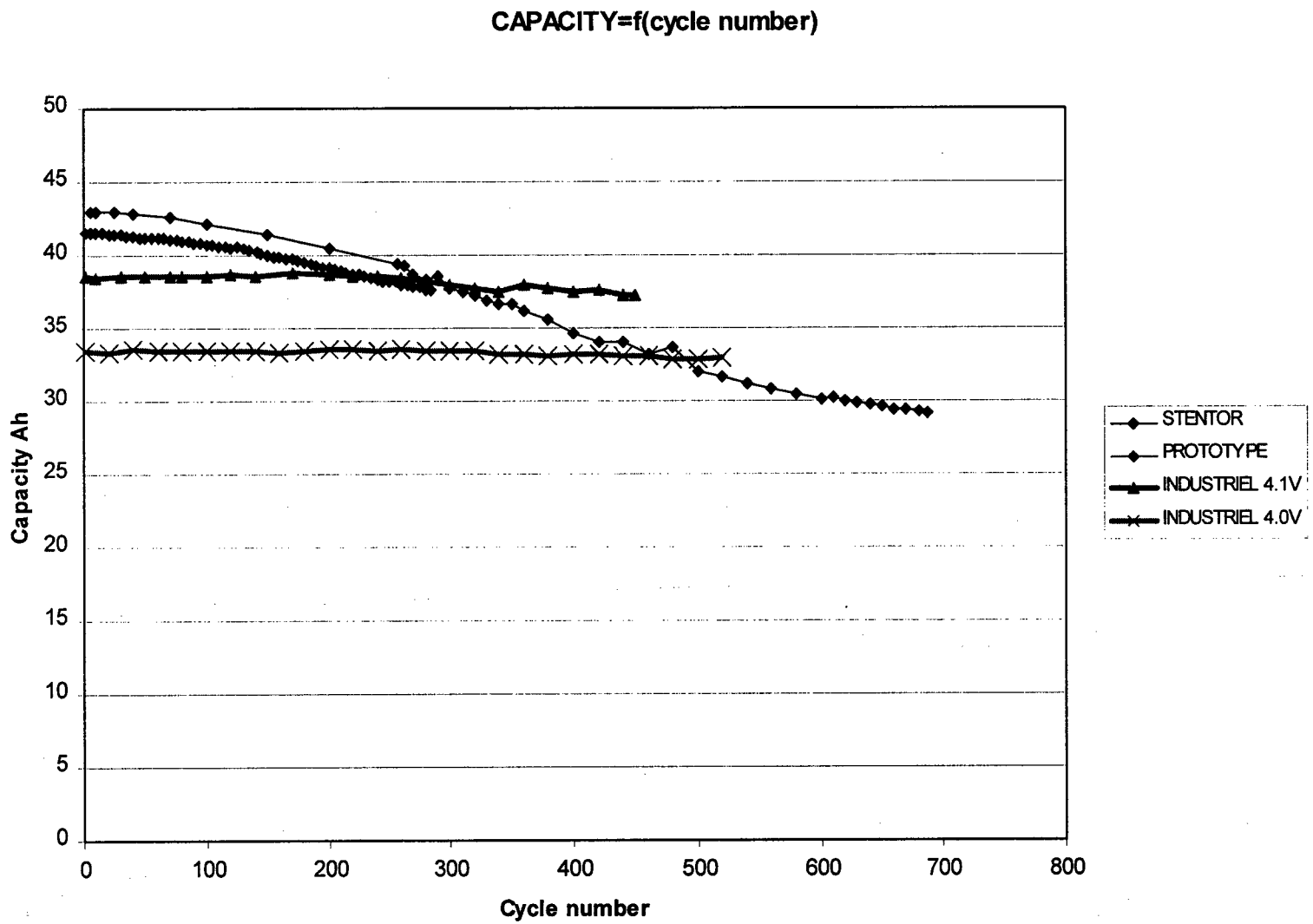

SAFT

FADING AND CALENDAR PARAMETERS

SAFT

LiION first cycle

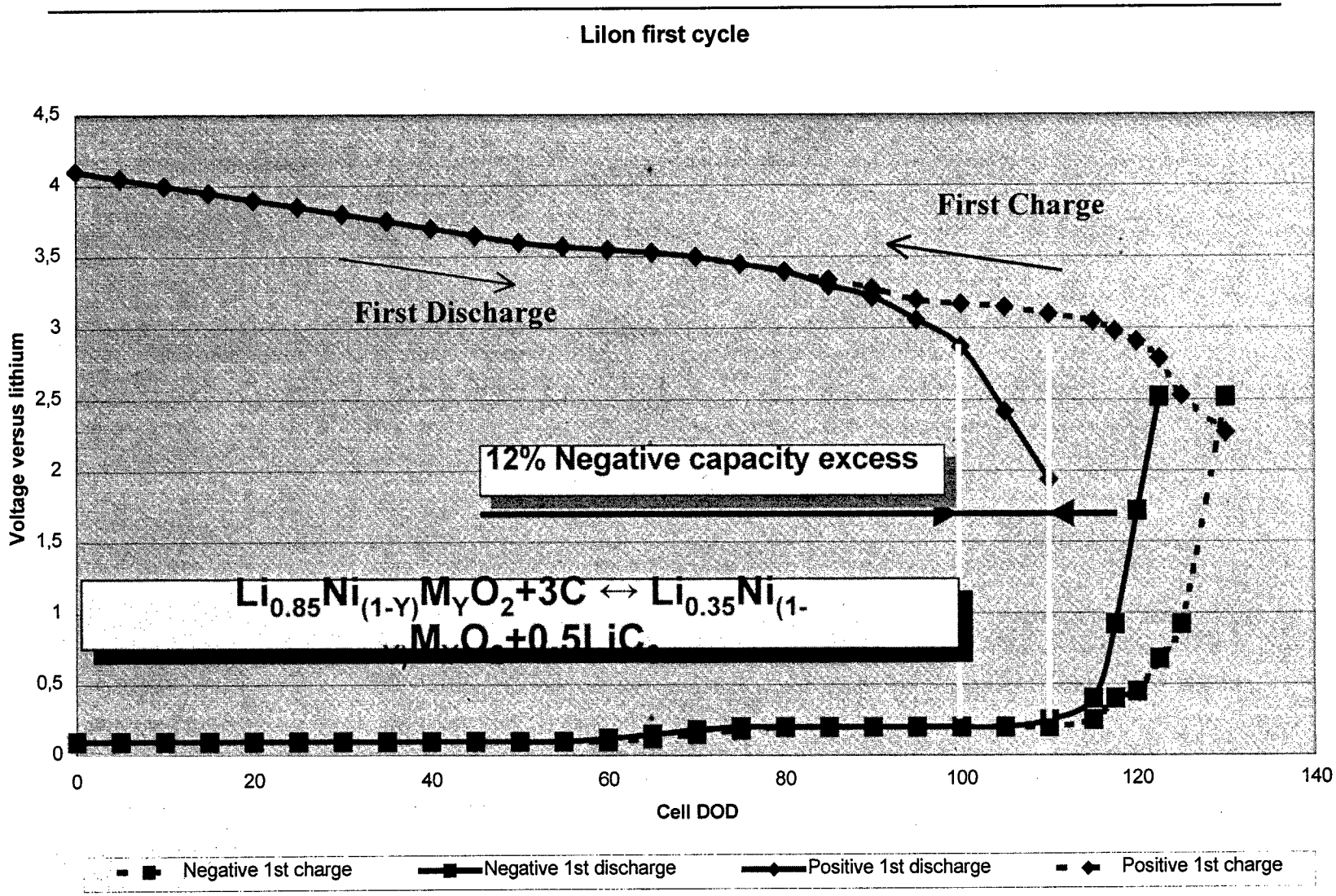

SAFT

Specificity of SAFT Design

▼ Ni based positive material :

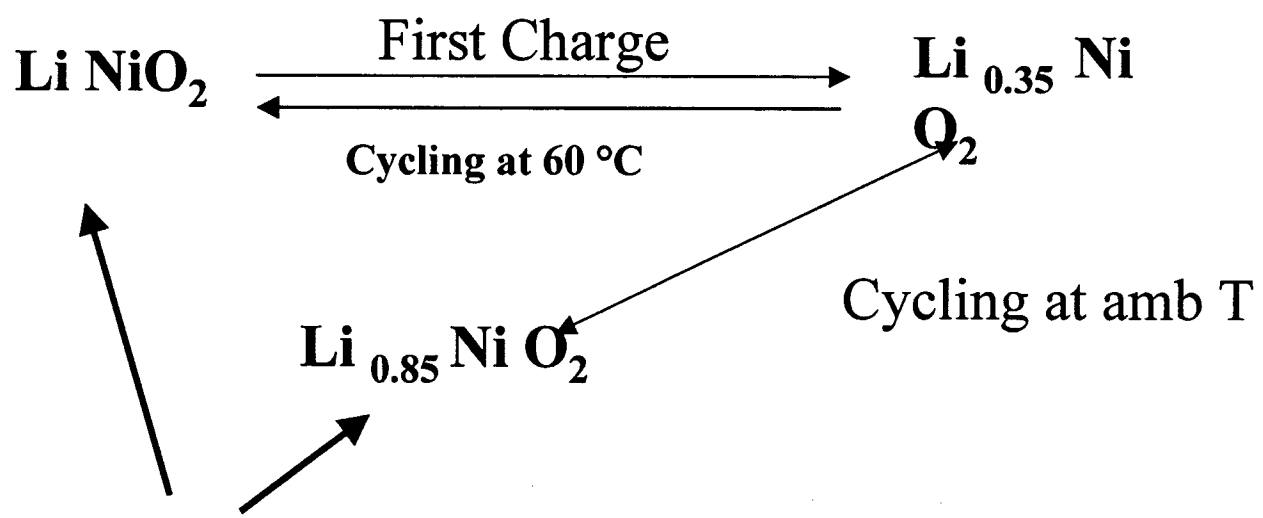

Lithium Excess = 12 % in the negative

▼ AT 60°C: Increase of Li Intercalation up to 97 %

Measurement of Li excess

SAFT

Cell voltage

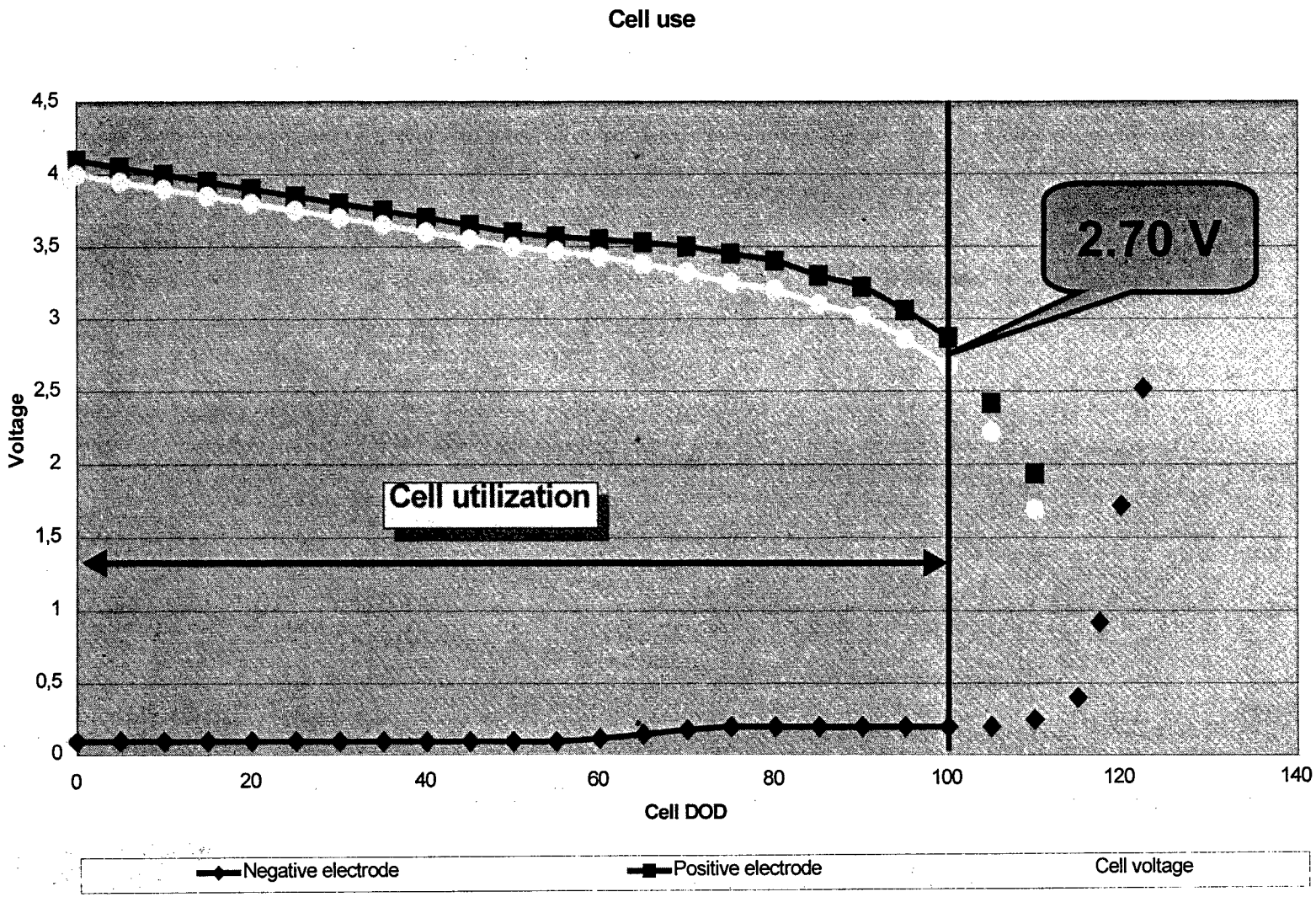

SAFT

Negative capacity loss impact

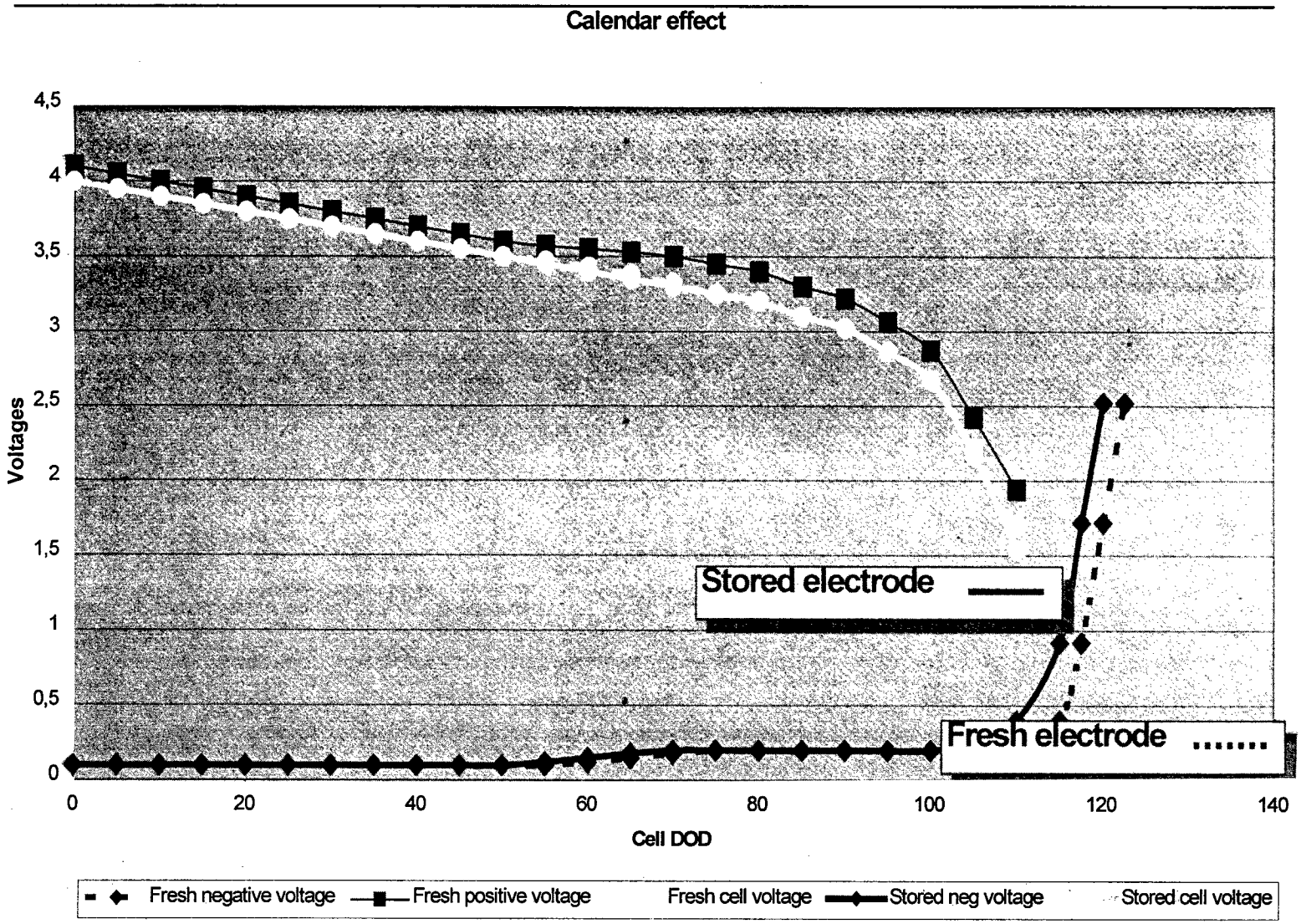

SAFT

Negative capacity loss impact

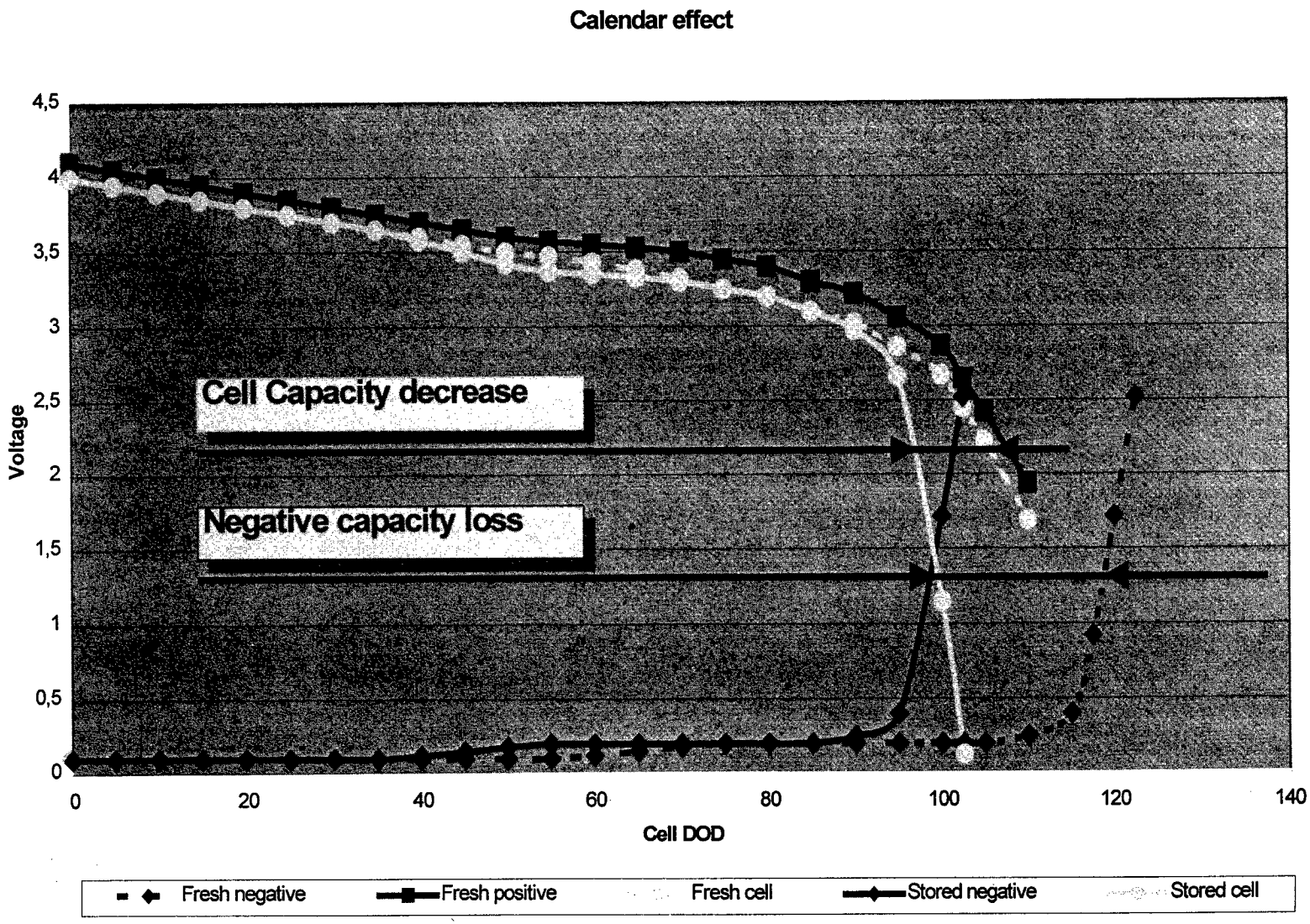

SAFT

Internal resistance increase impact

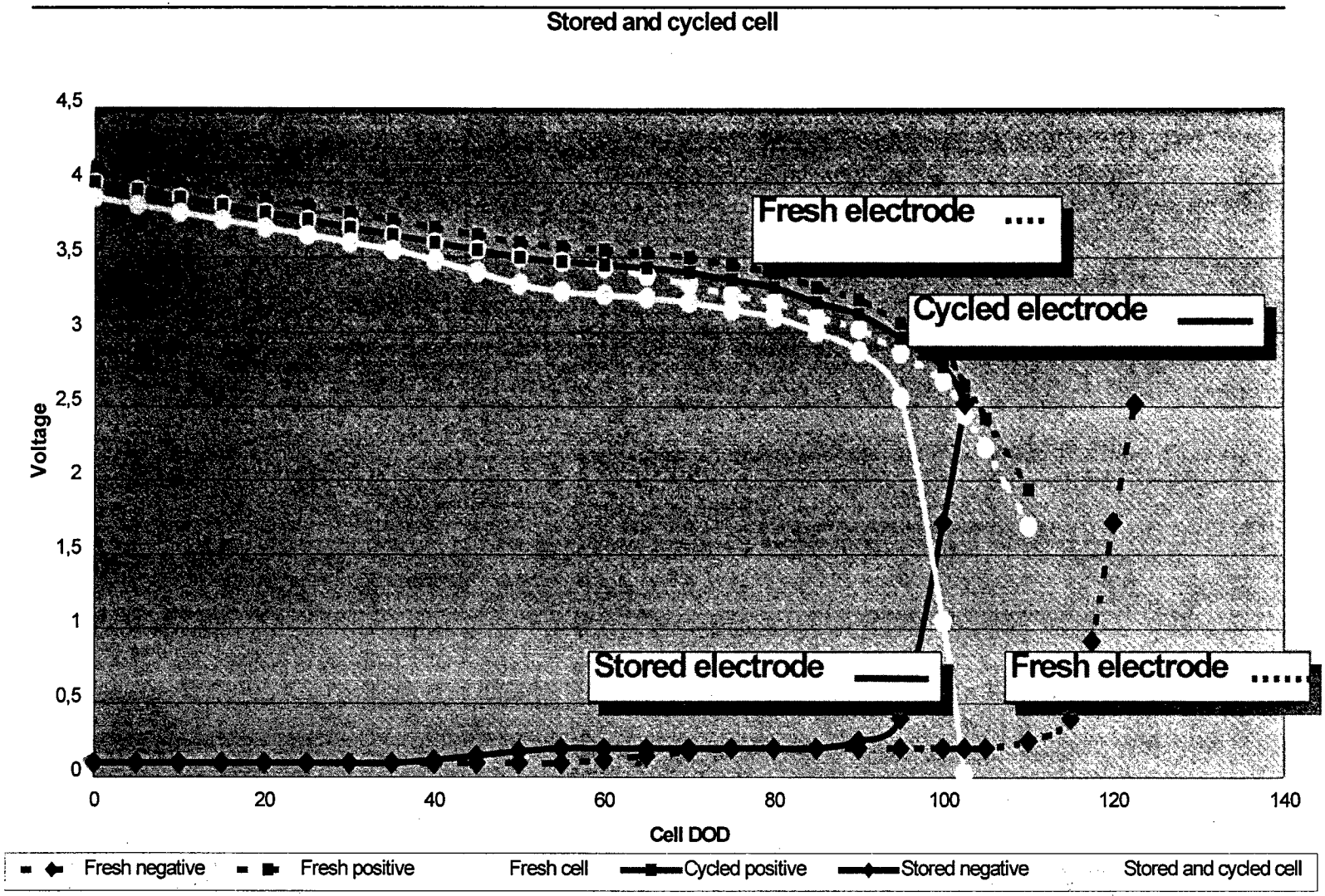

SAFT

Cycling Laws

- Mathematical law based on experimental values :

$$N=1.65*10^{6}\ Exp^{(-0.0846*DOD)}$$

- At 15 years, 80 % DOD :

  2000 cycles > 1.44 margin factor

SAFT

Life Time Evaluation

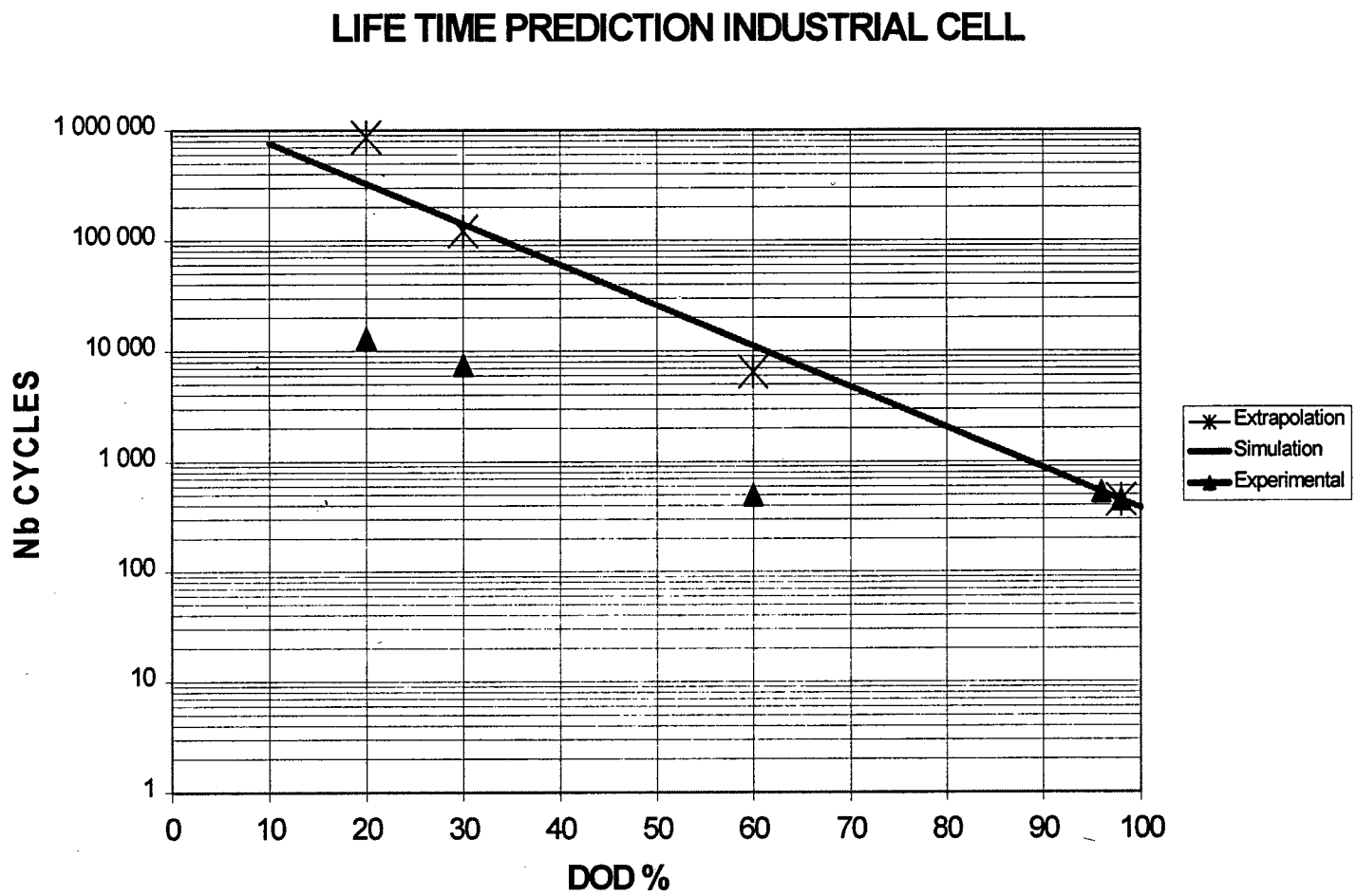

SAFT

Calendar Effects

- Cell capacity decrease due to lithium loss :
  - Corrosion of Li is due to a parasitic reaction occurring between the lithium inserted in the carbon and the electrolyte.
  - Slow reduction of electrolyte on lithiated carbon, forming soluble and insoluble side products, consuming lithium (negative capacity)
  - Insoluble products (mainly Li2CO3) keep lithium in the passivation layer, induce irreversible capacity loss, but very limited resistance increase.
- Main driven Parameters :
  - The conductance of the passivation interface layer (Solid Electrolyte Interface)
  - The temperature, but not the voltage for graphite materials

SAFT

Calendar Effect Law

- Lithium loss based on theoretical model using diffusion and Arrhenius law (coefficients determined with experimental data) :

$$t=e^{(6680/T-20.24)}\,x^2+e^{(6989/T-20.59)}\,x$$

x=%Li loss, t = duration in day, T= temperature °K

If x<12% no capacity loss at 20°C

If x>12 % Capacity loss= x -12 % at 20°C

SAFT

Model Results (1)

Capacity Loss due to Calendar Effect vs Temperature

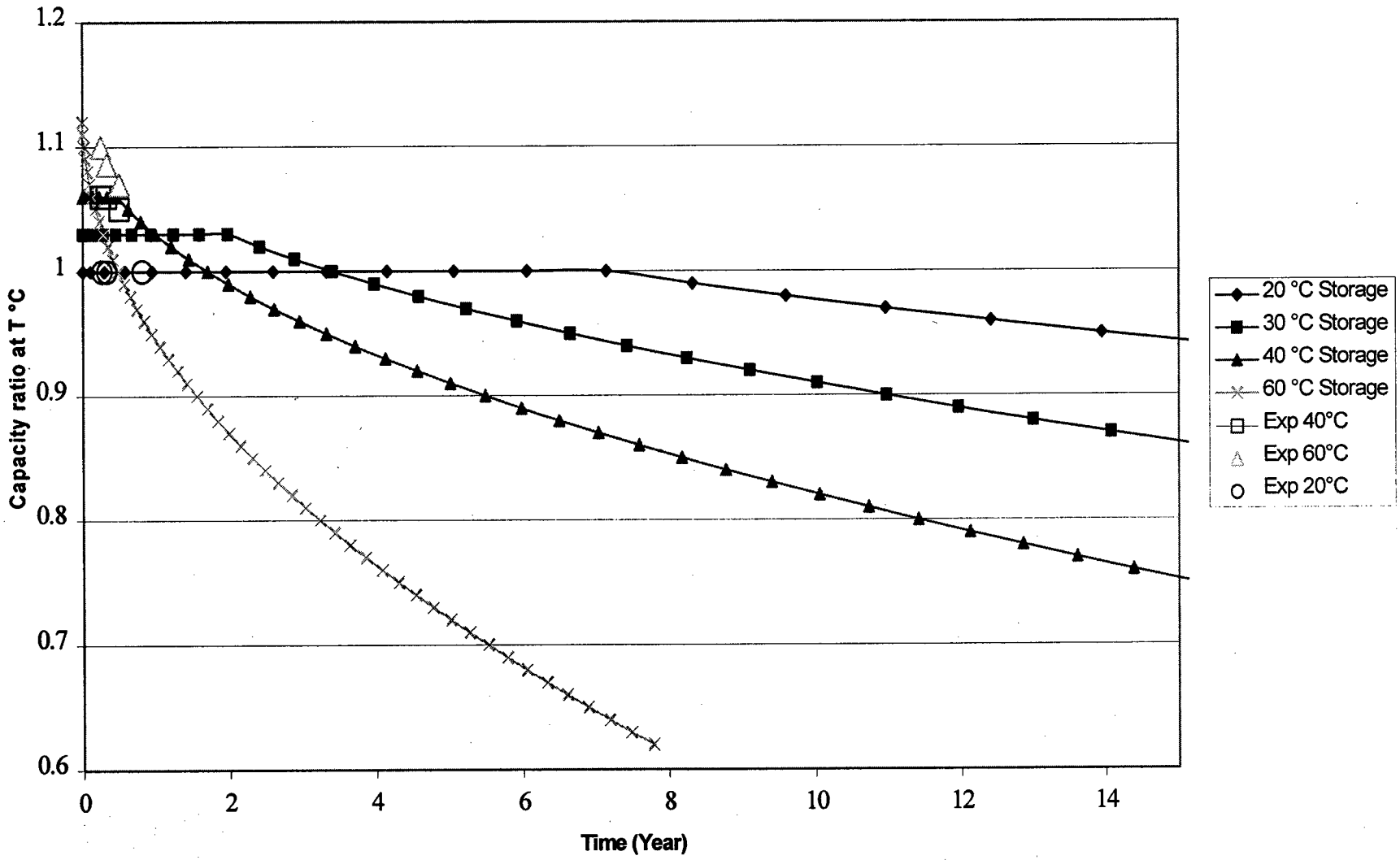

SAFT

Model Results (2)

Capacity Loss due to Calendar Effect vs Temperature

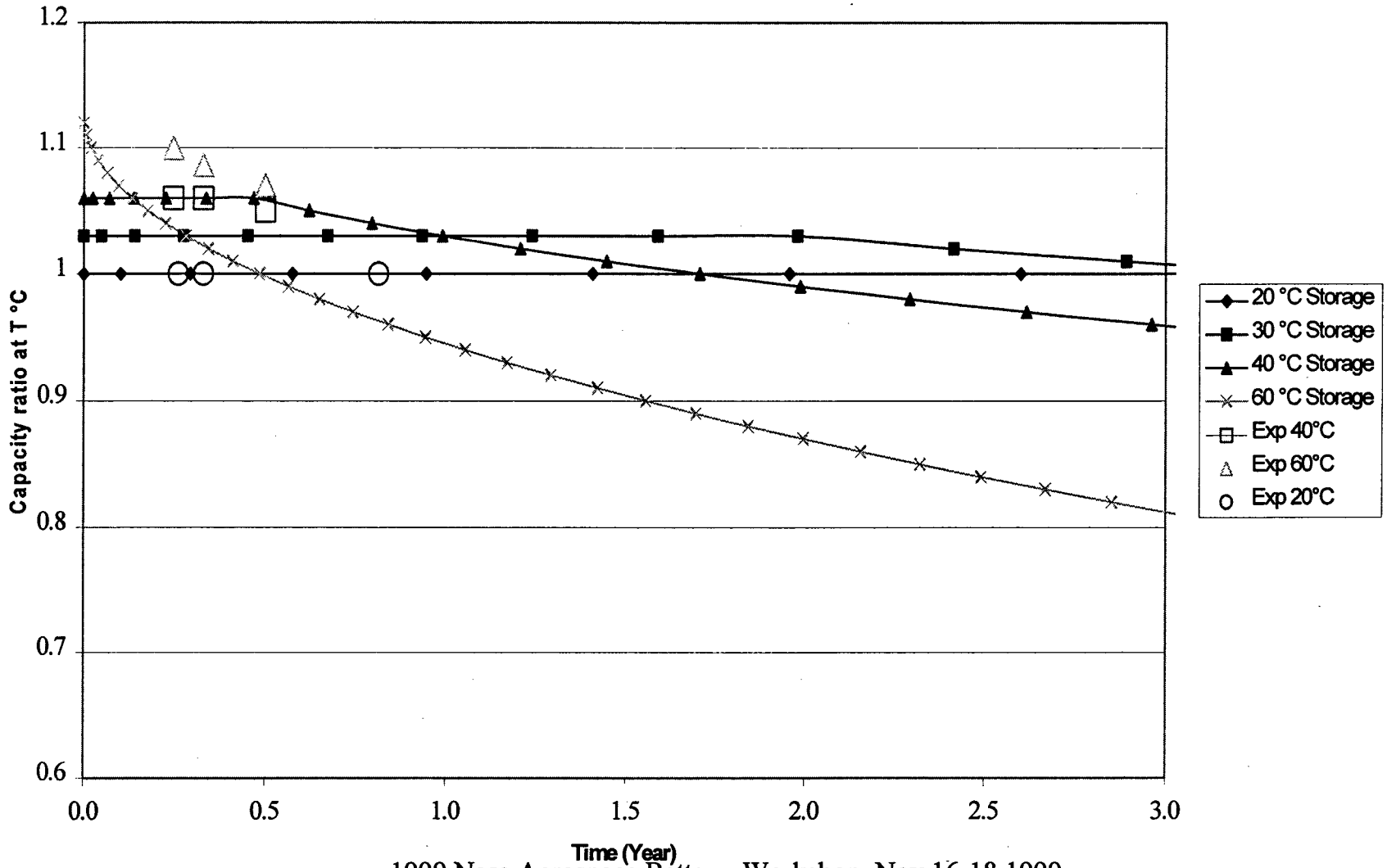

File : O/st/ppt/s2774-99.ppt

1999 Nasa Aerospace Battery Workshop, Nov 16-18,1999

SAFT

GEO DESIGN RULES

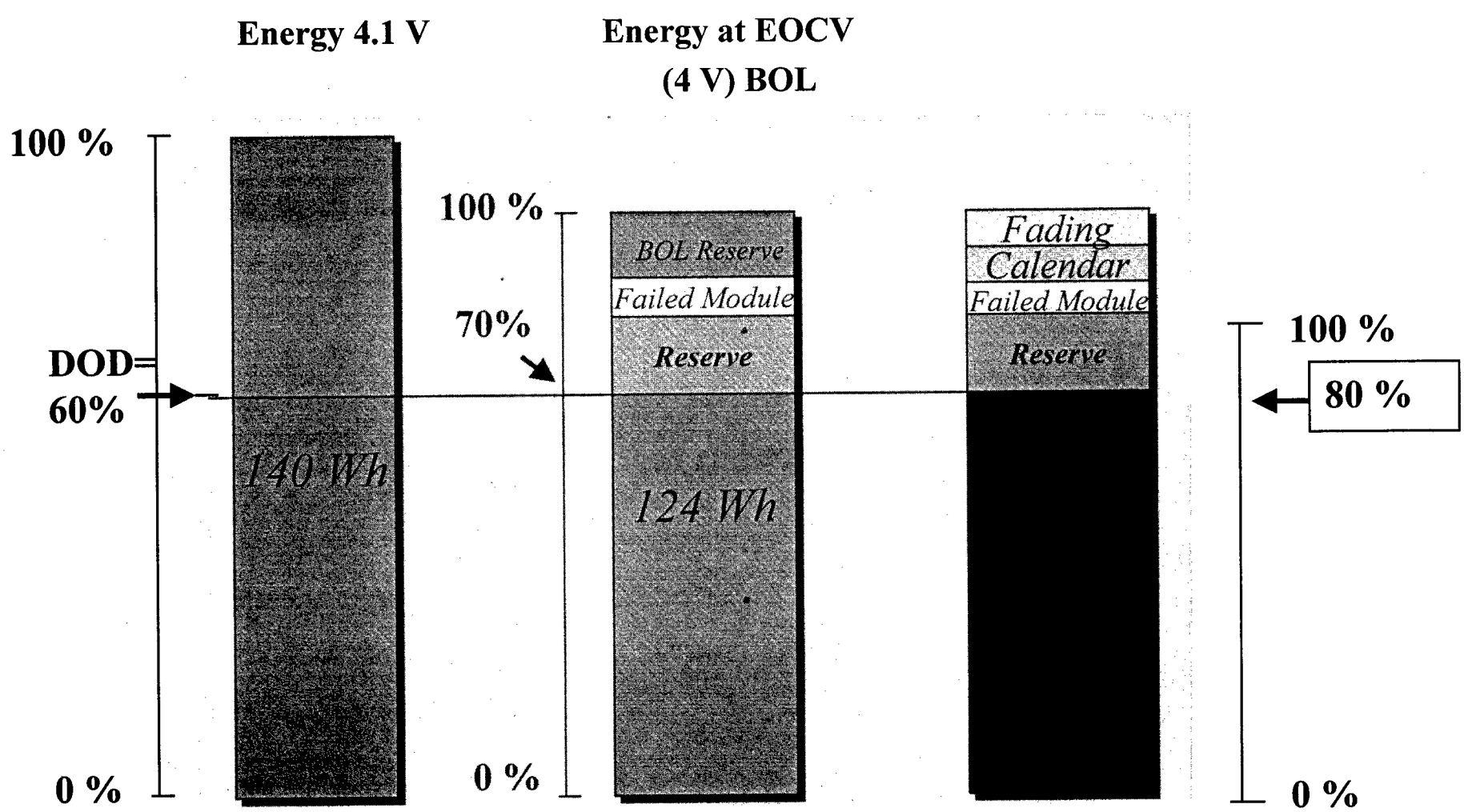

SAFT

Battery Design Rules

- GEO Satellites
  - 60-70 % Max DOD

For 15 kW battery : 150 kg saved over 500 kg for NiH_2 at battery level

(other system impacts : radiators, heat pipes, solar panels)

- LEO Satellites
  - 20-30 % Max DOD and EOCV= 3.85 V

For 3 kW battery : 25 kg saved over 100 kg for NiH_2

SAFT

Li-Ion SPACE BATTERY DEVELOPMENT

- Design qualified in the frame of Stentor
  - Based on one cell size
  - Modularity using parallel and series connections
  - Voltage range : from 6 to 32 S (21 V to 112 V with 3.5 Volt Step)
  - Capacity : from 1P to 16 P (40 to 640 Ah with 40 Ah Step)
  - Integrated electronic
  - Non dissipative by-pass system

SAFT

CONCLUSION

- SAFT Li-Ion technology is ready for Space
  - Saft presents an industrial and performing cell and battery design
- 2000 SAFT Objectives :
  - Fly in 2000 (with Stentor)
  - Achieve the GEO life test on the Industrial Cell (15 years)
  - Develop a battery range 12-25 kW

2000 WILL BE THE Li-ION YEAR FOR SPACE

Performance Characteristics of Lithium-Ion Prototype Batteries for Mars Surveyor Program 2001 Lander

M. C. Smart, B. V. Ratnakumar, L. Whitcanack and S. Surampudi
Jet Propulsion Laboratory, Pasadena, California

J. Byers
Lockheed Martin Astronautics Corporation, Denver, CO, and

R. A. Marsh
Wright-Patterson Air Force Base, Dayton, OH

JPL

Supported by Mars 2001 Surveyor and NASA Code S Battery Programs

NASA Battery Workshop, Huntsville, Alabama., Nov. 17, 1999

Lithium-Ion Cells for Mars Surveyor 2001 Lander

Outline

- Introduction
- Cell Performance and Battery Requirements
- Overview of Performance Evaluation Tests
- Cycle Life Performance Tests
- Low Temperature Performance Tests
- Cell Charge Characteristics
- Cell Storage Characteristics
- Summary and Conclusions

Mars Surveyor 2001 Lander- Scientific Payload

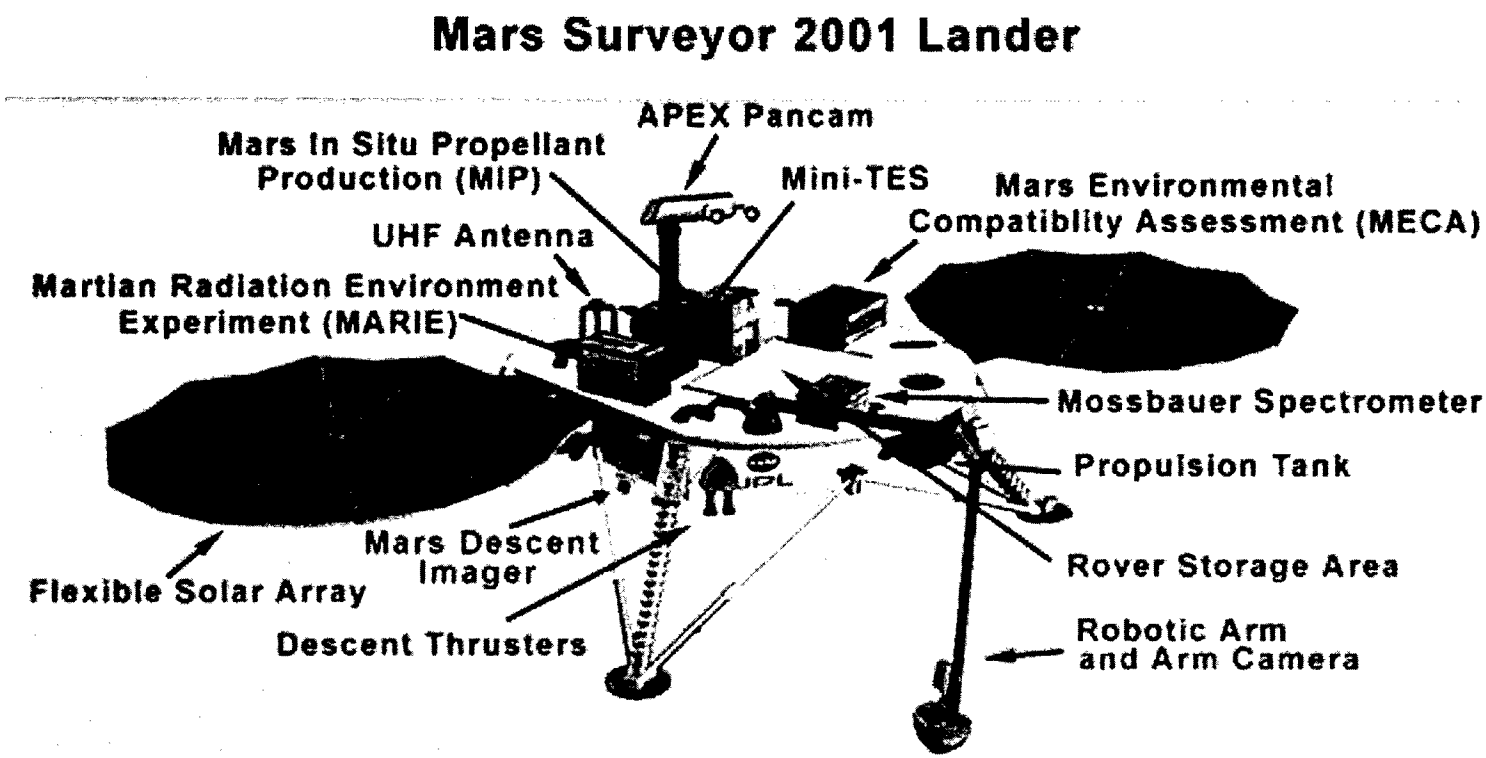

Mars Surveyor 2001 Lander

- Scheduled launch date April 10, 2001; Expected landing Jan 22, 2002.
- Lander has an imager to picture the surrounding terrain of the landing site during rocket-assisted descent.
- Platform for instruments and technology experiments designed to provide key insights to decisions regarding human missions to Mars.
- In-situ demonstration test of rocket propellant production.
- Martial soil properties and surface radiation environment

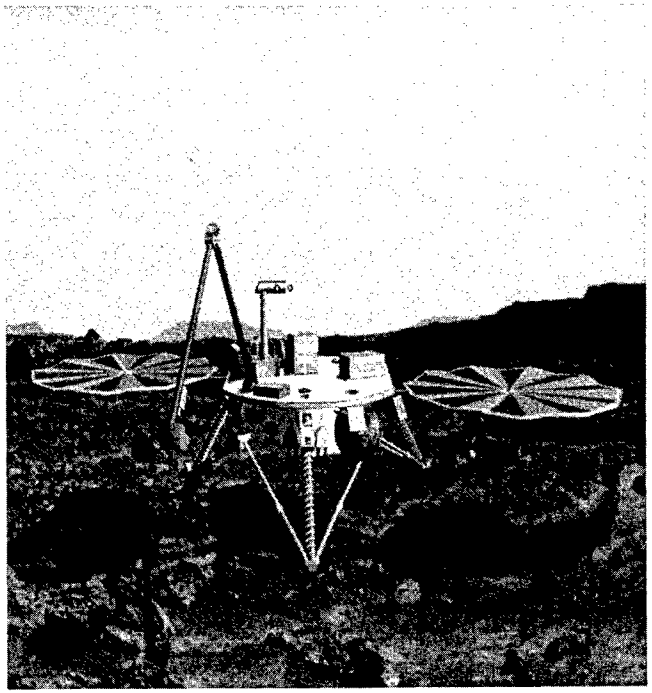

Mars Surveyor 2001 Lander- Components

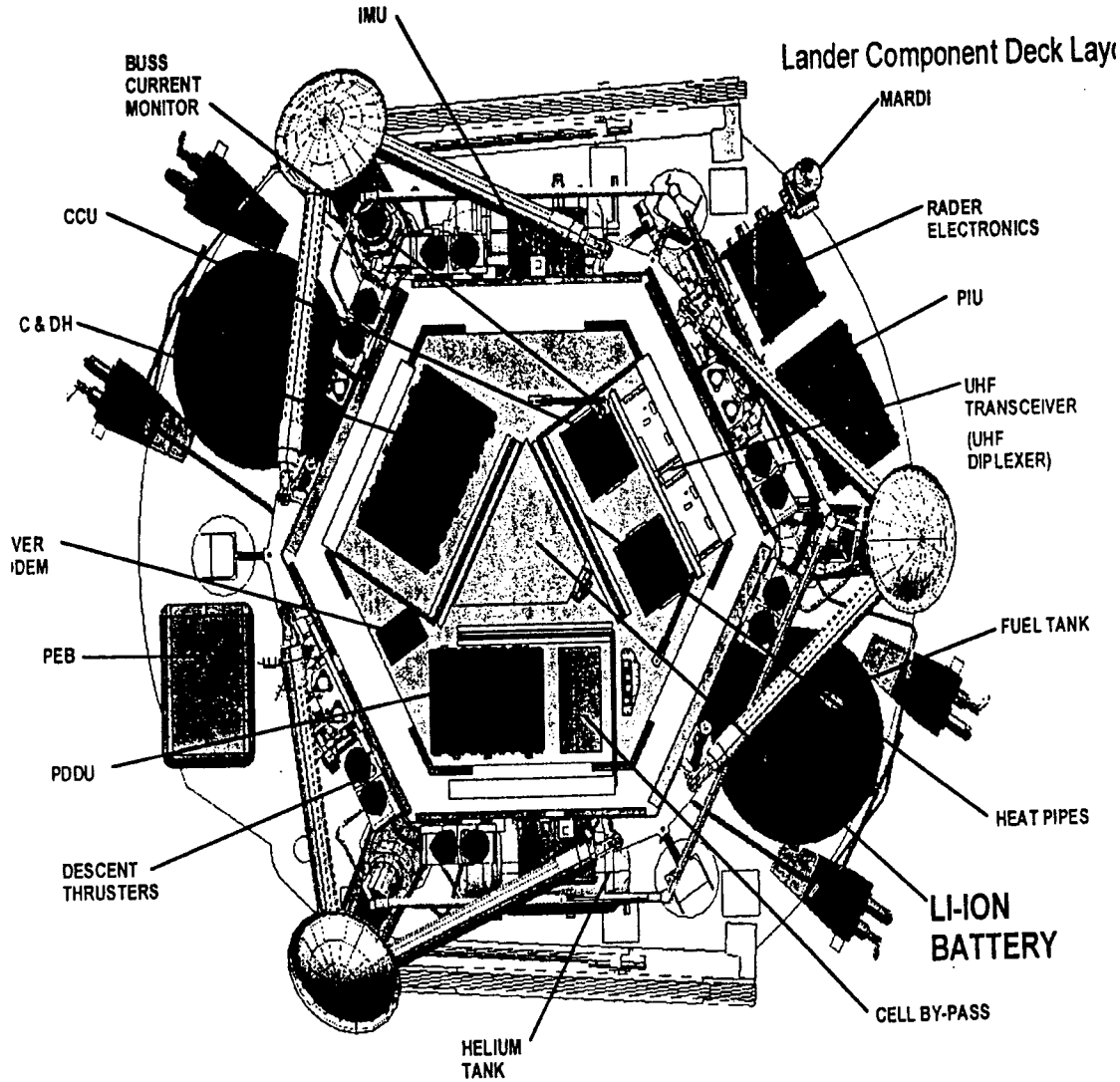

MSP 2001 Lander Battery

- Two 25 Ah, 8-Cell Li Ion Batteries (N+1)
- Individual Cell Monitoring and control via Cell Bypass Unit (CBU) to prevent overcharge
- Individual Charge Control Unit (CCU)
- Constant Voltage Charging at - 32.8 Vdc
- 16 Selectable V/T curves.
- Amp Hour Integration.

Battery Envelope

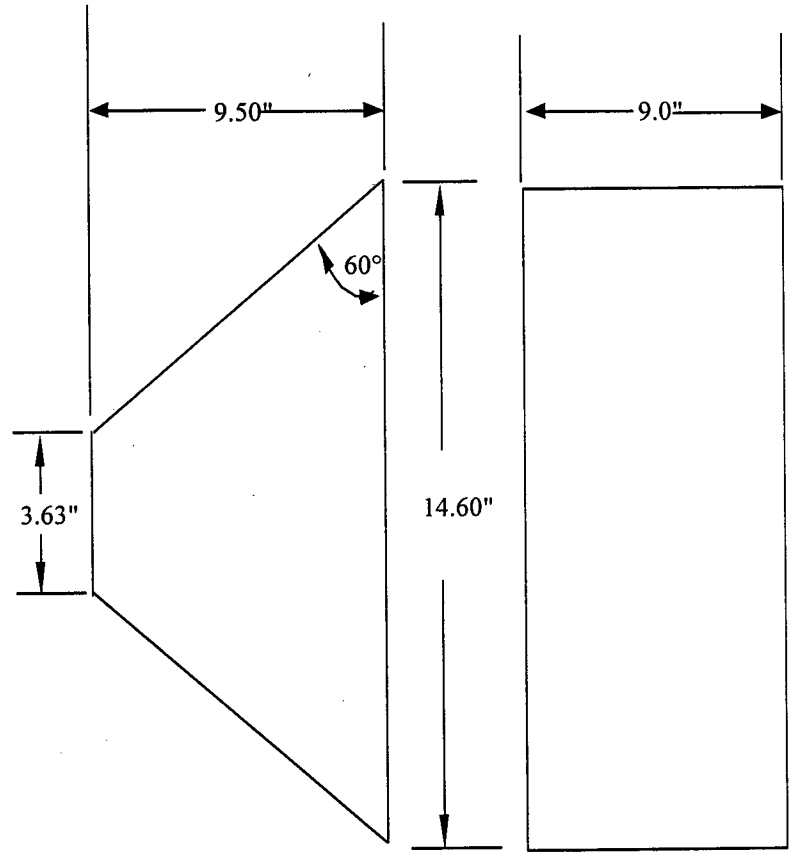

MSP 2001 Lander Power System Battery Challenges

- *High specific Energy*
  - 800 Wh in 7.94 Kg (100 Wh/kg)
- *Low Temperature Performance*
  - Op. Temperature : -20 to +40°C
  - Capacity of 25 Ah -20°C at C/5
- *Good Cycle Life*
  - 200 Cycles @ 70%
- *Long Calendar Life*
  - Two years of storage (1 year cruise) before battery operation
  - Low temperature performance after storage (final phase of the mission)

NASA-DOD Interagency Li-Ion Program

Objectives

- DEVELOP HIGH SPECIFIC ENERGY AND LONG CYCLE LIFE Li -ION BATTERIES
- ESTABLISH U.S. PRODUCTION SOURCES
- DEMONSTRATE TECHNOLOGY READINESS
  - LANDERS BY 2001
  - ROVERS BY2003
  - GEO MISSIONS BY 2003
  - AVIATION/UAV's BY 2001
  - MILITARY TERRESTRIAL APPLNS's BY 2001
  - LEO MISSIONS BY 2003

Technology Drivers

Mission	Technology Driver
Lander Rover	Low Temperature Operation High rate Pulse Capability
GEO S/C	10-20 Year Operating life Large Capacity cells (50-200 Ah)
LEO PlanetaryS/C	Long Cycle life(30,000) Medium Capacity Cells (50 Ah
Aircraft	Low temperature Operation High Voltage Batteries (270 V)
UAV	Large Capacity cells (200 Ah) High Voltage Batteries (100V)

Lithium-Ion Cells for Mars Surveyor 2001 Lander
Program Objectives

- Assess viability of using lithium-ion technology for future Aerospace applications.

- Demonstrate applicability of using lithium-ion technology for the MSP 2001 Lander application.

JPL

Lithium-Ion Cells for Mars Surveyor 2001 Lander

Performance Evaluation Tests

- **Cycle Life Performance**
  - Room temperature cycle life (23° +/- 2°C)
  - Low temperature cycle life (-20°C)
  - High temperature cycling (40°C)
  - Variable temperature cycling
- **Electrical Performance Characterization**
  - Range of charge and discharge rates (C/2, C/3.3, C/5 and C/10)
  - Range of temperatures (-30, -20, 0, 23, 40°C)
  - Pulse capability (40 and 60A)
  - Impedance measurements
- **Storage Characteristics**
  - * 2 Month storage test (0 and 40°C, 50 and 100% SOC)
  - * Accelerated storage test: at different SOC (50, 70,100% SOC), temperatures (25, 40, 55°C), and storage conditions.
- **Quality Control**
  - Reproducibility of cell results
  - Cell to cell performance performance variations

ELECTROCHEMICAL TECHNOLOGIES GROUP

Cycle Life Performance Tests

Requirement **: Deliver > 200 cycles on surface of Mars**

- **100% DOD cycling (3.0-4.1V, C/5-C/10)**
- **Wide temperature range (-20°C to 40°C)**
- **At end of life should deliver 25 Ah**

***Approach*:**

100 % DOD cycling @ 23°C (C/5 charge, C/5 discharge)
100 % DOD cycling @ -20°C (C/10 charge, C/5 discharge)
100 % DOD cycling @ 40°C (C/5 charge, C/5 discharge)
Variable temperature cycling (temperature extremes)
Mission simulation cycling

***Possible Evaluation Criteria*:**

Initial capacity (must exceed 25 Ah)
Capacity after 200 cycles (Ah)
Capacity fade rates
Capacity delivered over range of temperatures

Lithium-Ion Cells for Mars Surveyor 2001 Lander

Room Temperature Cycle Life Performance
Comparison of Different Cell Designs and Sizes

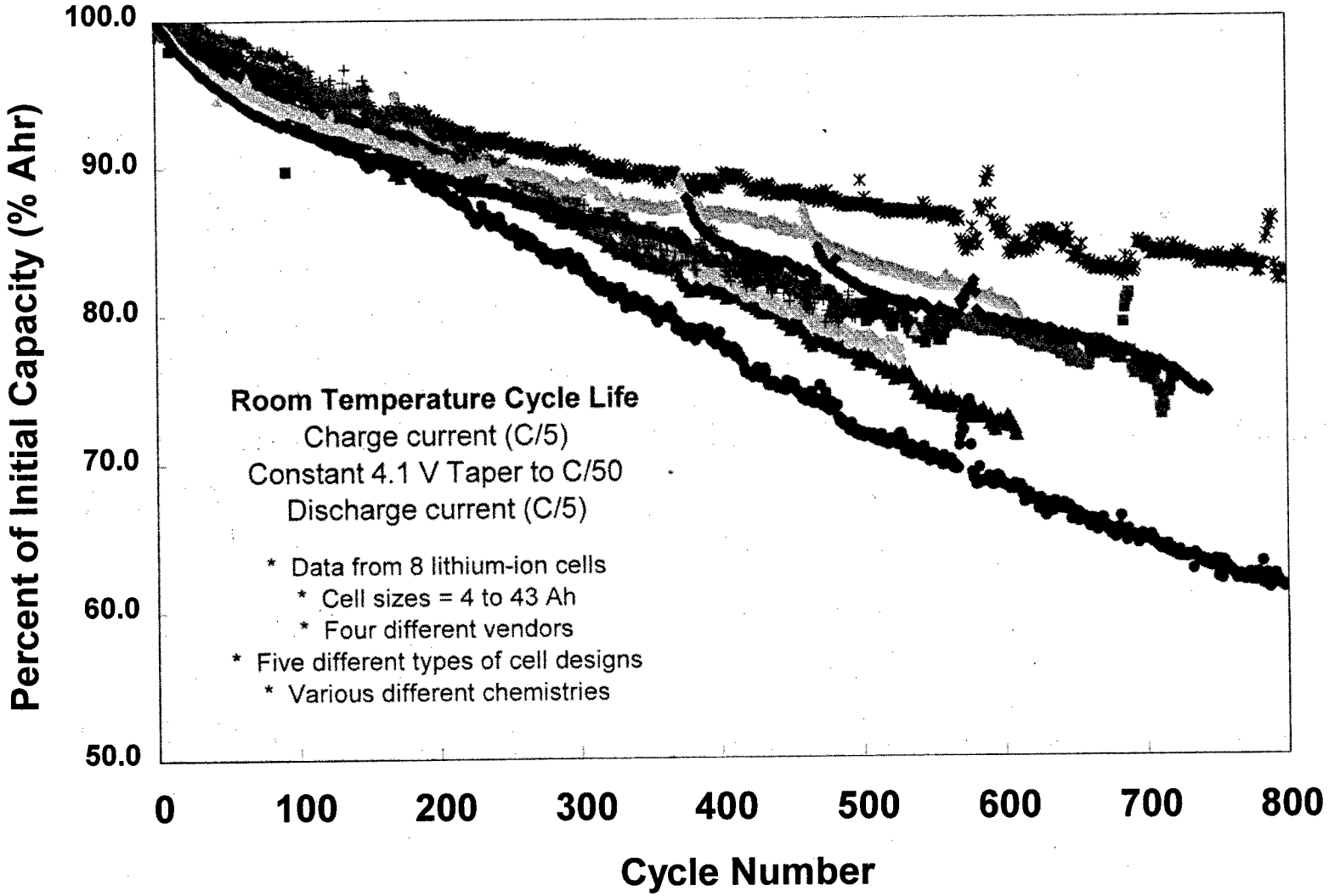

Lithium-Ion Cells for Mars Surveyor 2001 Lander

Cycle Life Performance at Different Temperatures

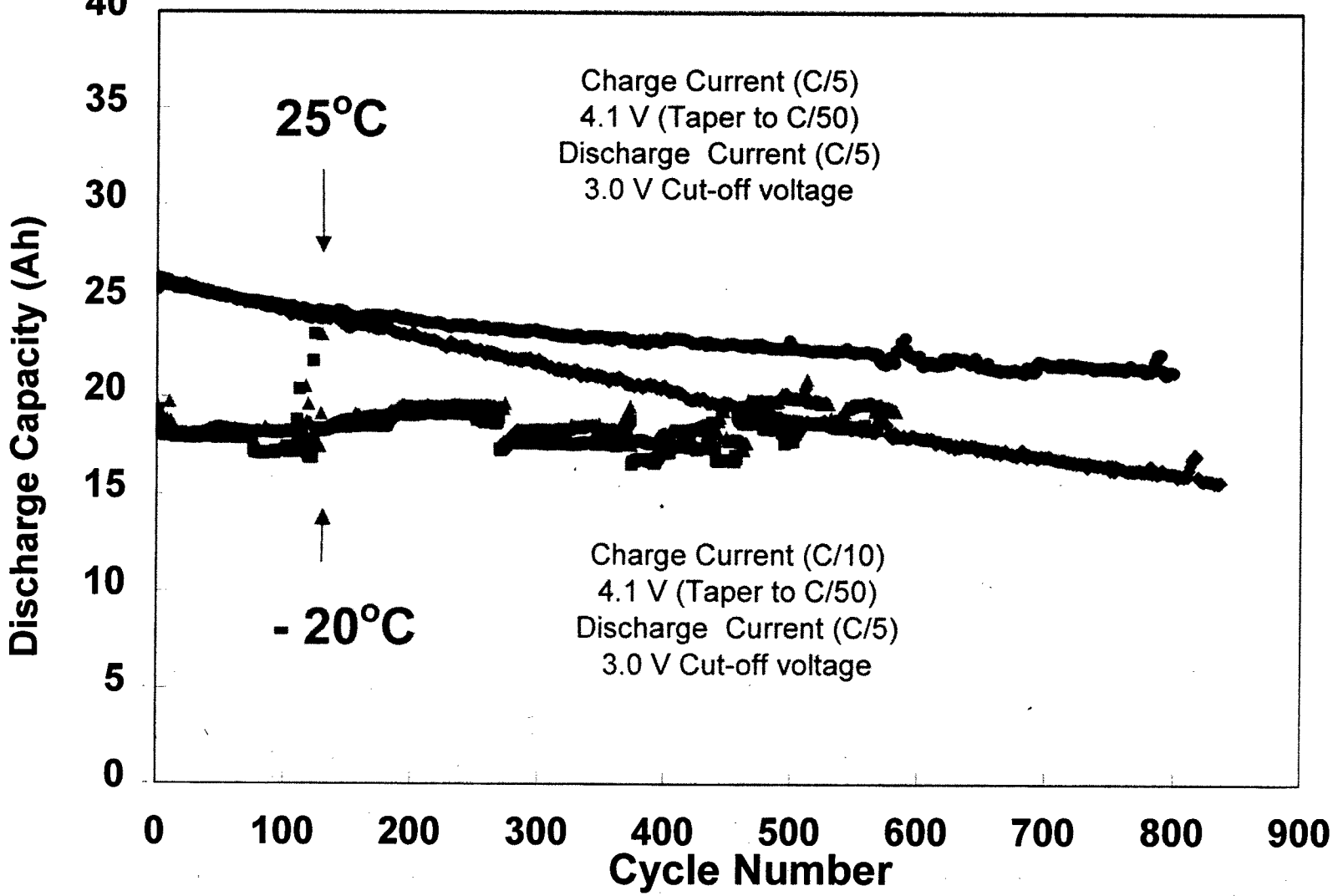

Lithium-Ion Cells for Mars Surveyor 2001 Lander

Cycle Life Performance at Varying Temperatures

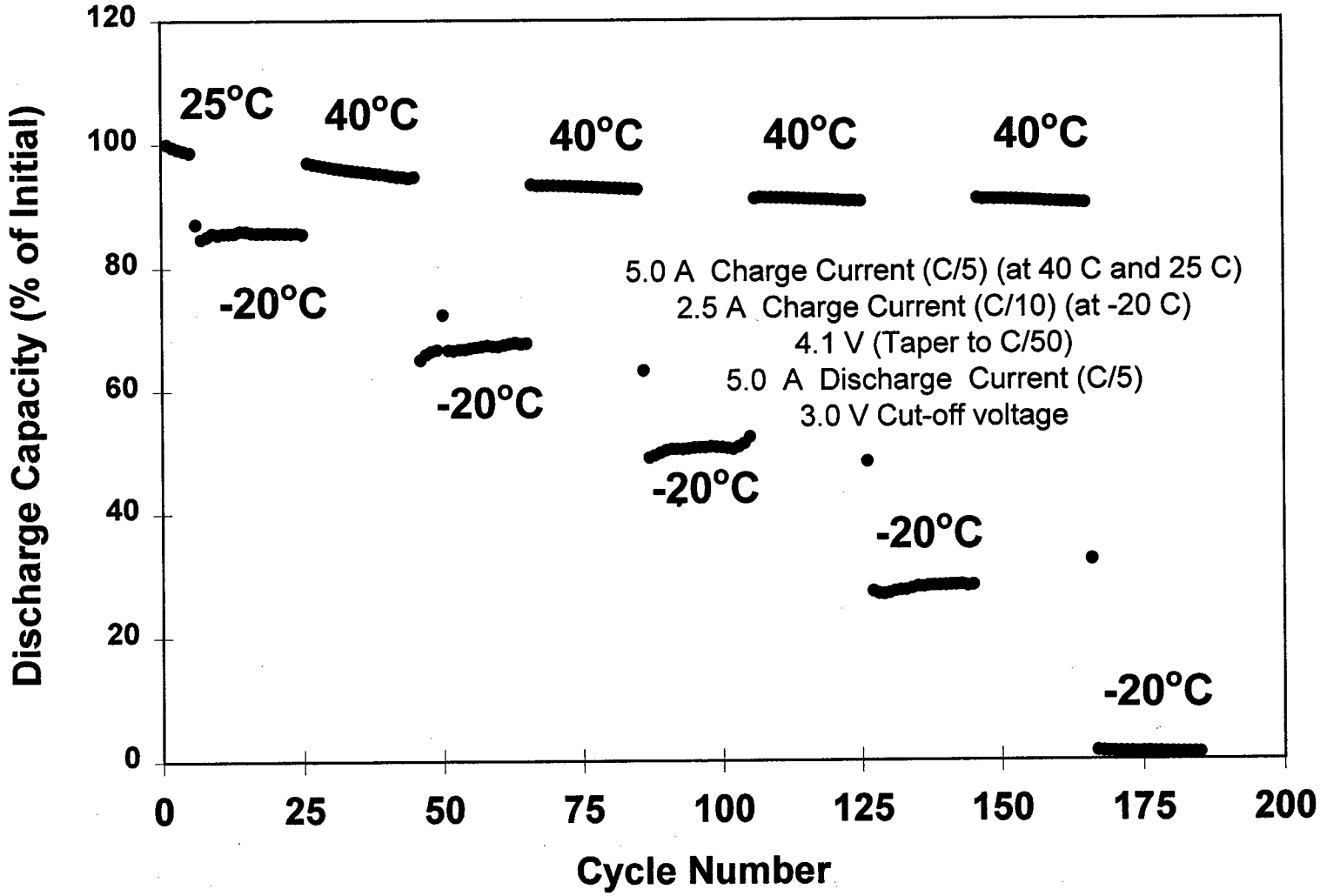

Lithium-Ion Cells for Mars Surveyor 2001 Lander

Cycle Life Performance at Varying Temperatures

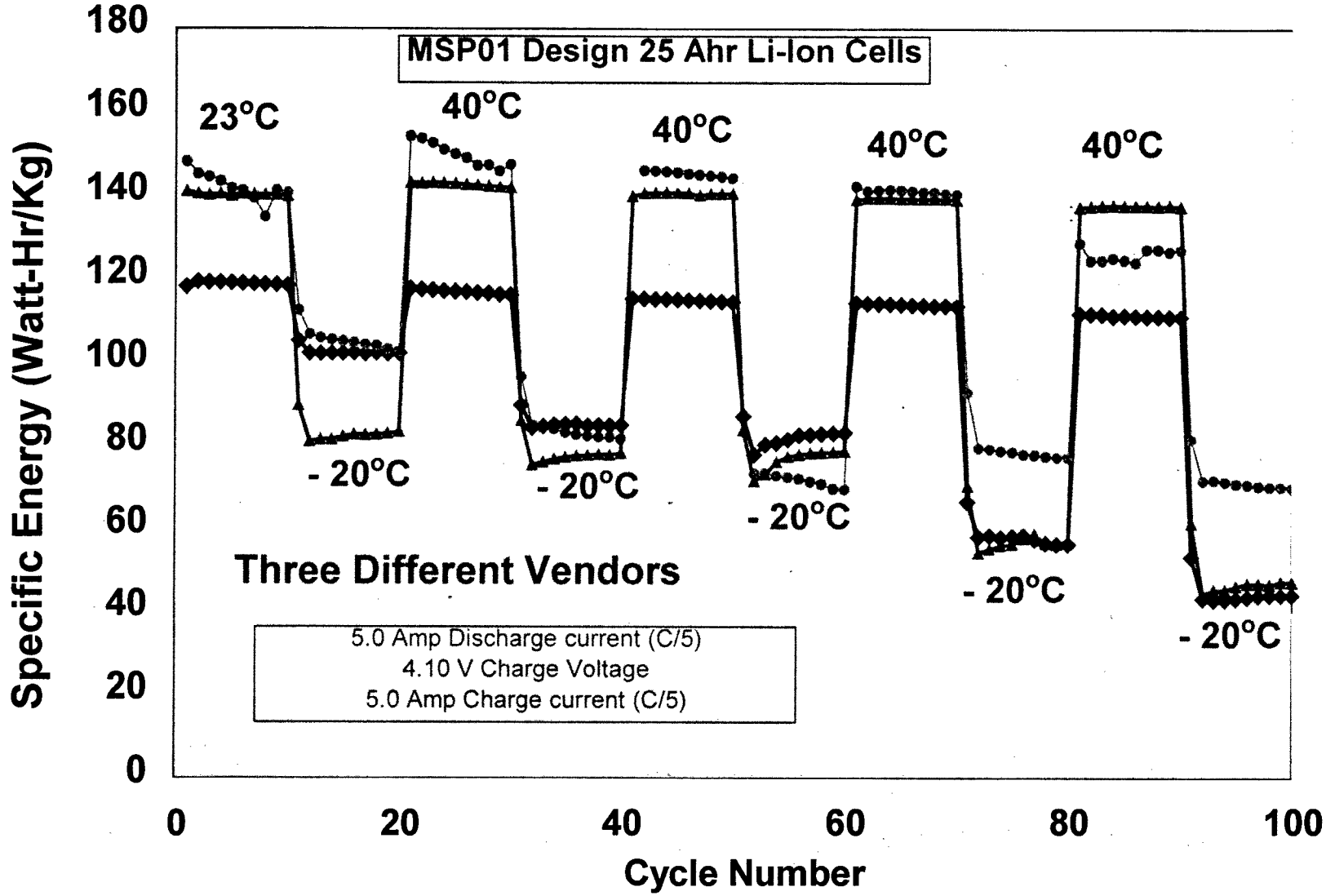

Lithium-Ion Cells for Mars Surveyor 2001 Lander

Cycle Life Performance at Different Temperatures

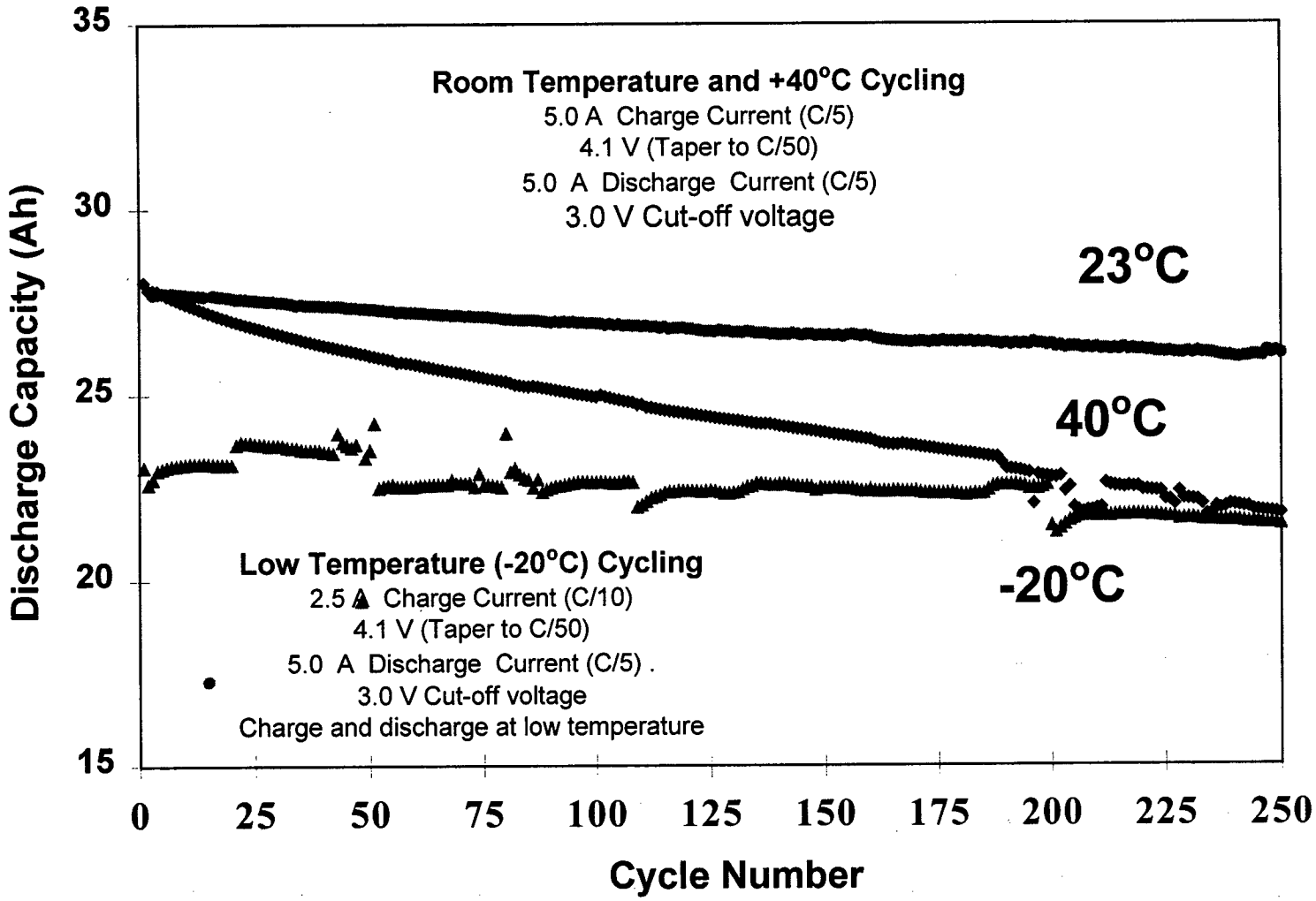

Lithium-Ion Cells for Mars Surveyor 2001 Lander

Low Temperature Performance Evaluation

Requirement :

- Provide 25 Ah over wide range of temperatures (-20°C to 40°C)
- Provide 25 Ah at C/2 rate - C/10 rate
- Should be capable of meeting mission profile

Approach:

Rate characterization at various temperatures (-20, 0, 20 and 40°C)
Range of charge and discharge rates (C/2, C/3.3, C/5 and C/10)

Possible Evaluation Criteria:

Low temperature discharge capacity (@ -20°C)
Low temperature charge characteristics
Capacity delivered over range of temperatures
Discharge energy (Wh/Kg)
Watt-hour efficiency (round-trip efficiency)
Heat generation
Effect of cell history upon rate capability

Lithium-Ion Cells for Mars Surveyor 2001 Lander

Rate Capability at Different Temperatures

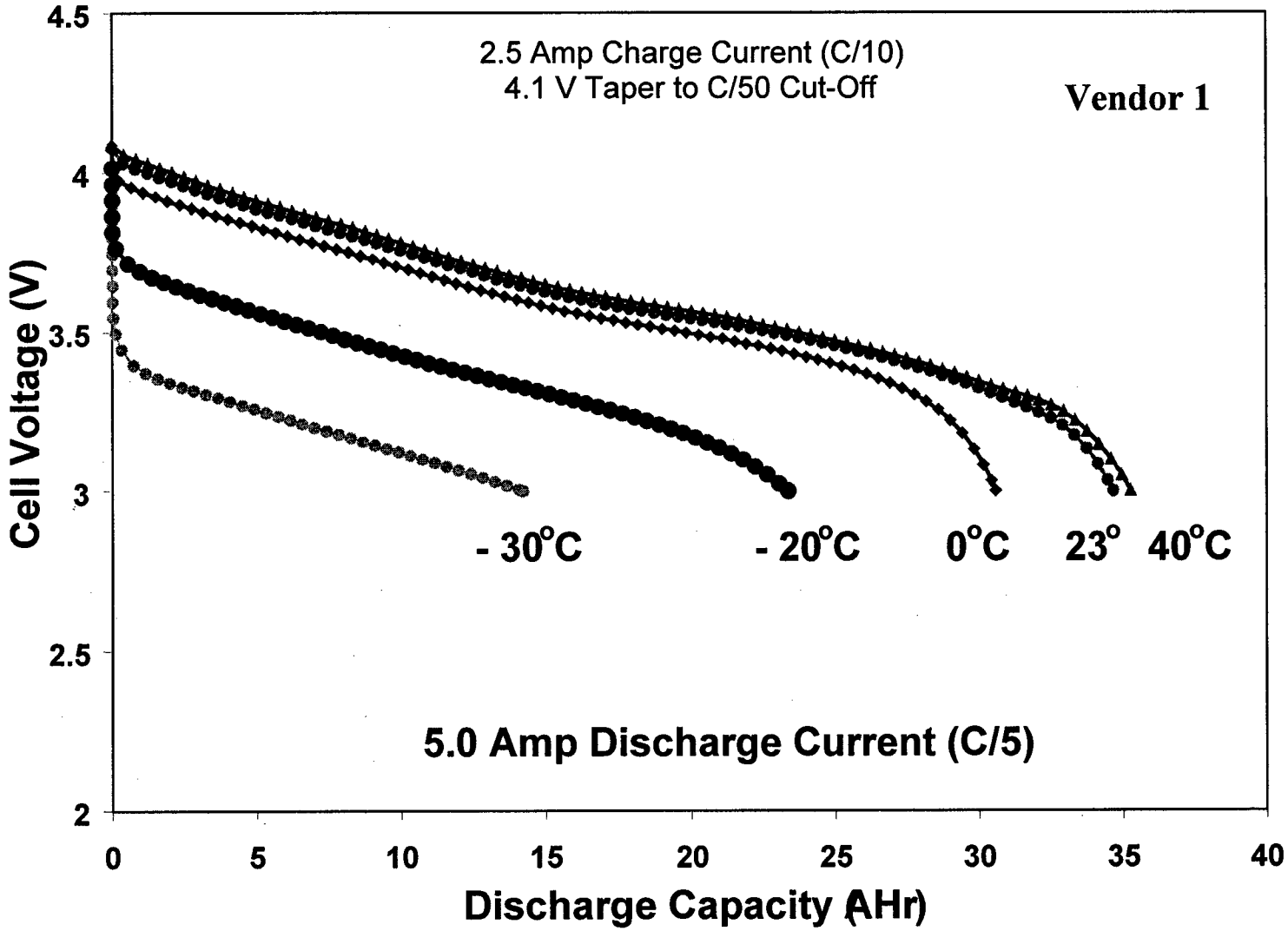

Lithium-Ion Cells for Mars Surveyor 2001 Lander

Rate Capability at Different Temperatures

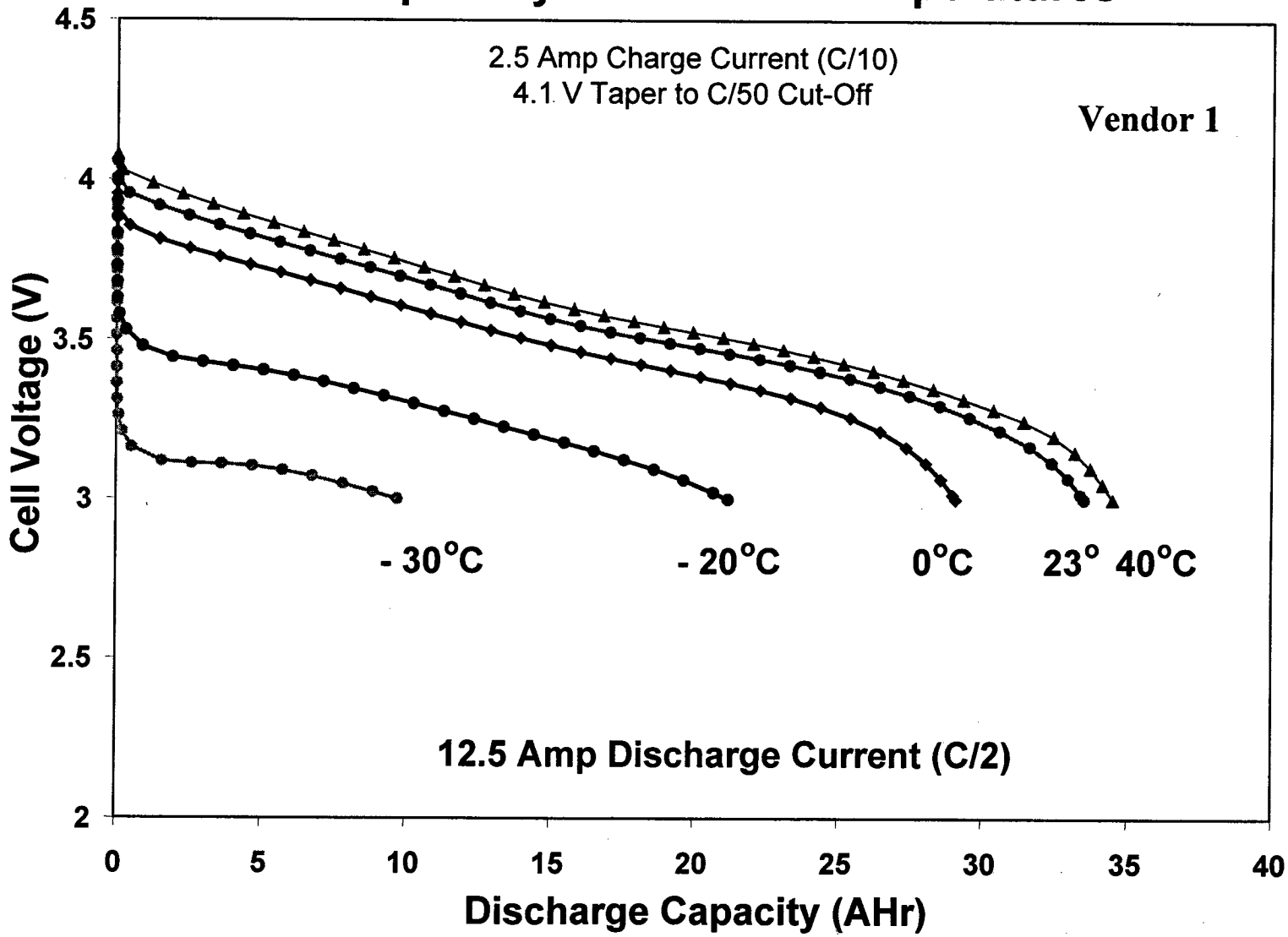

JPL

Lithium-Ion Cells for Mars Surveyor 2001 Lander

Cell Specific Energy as a Function of Temperature

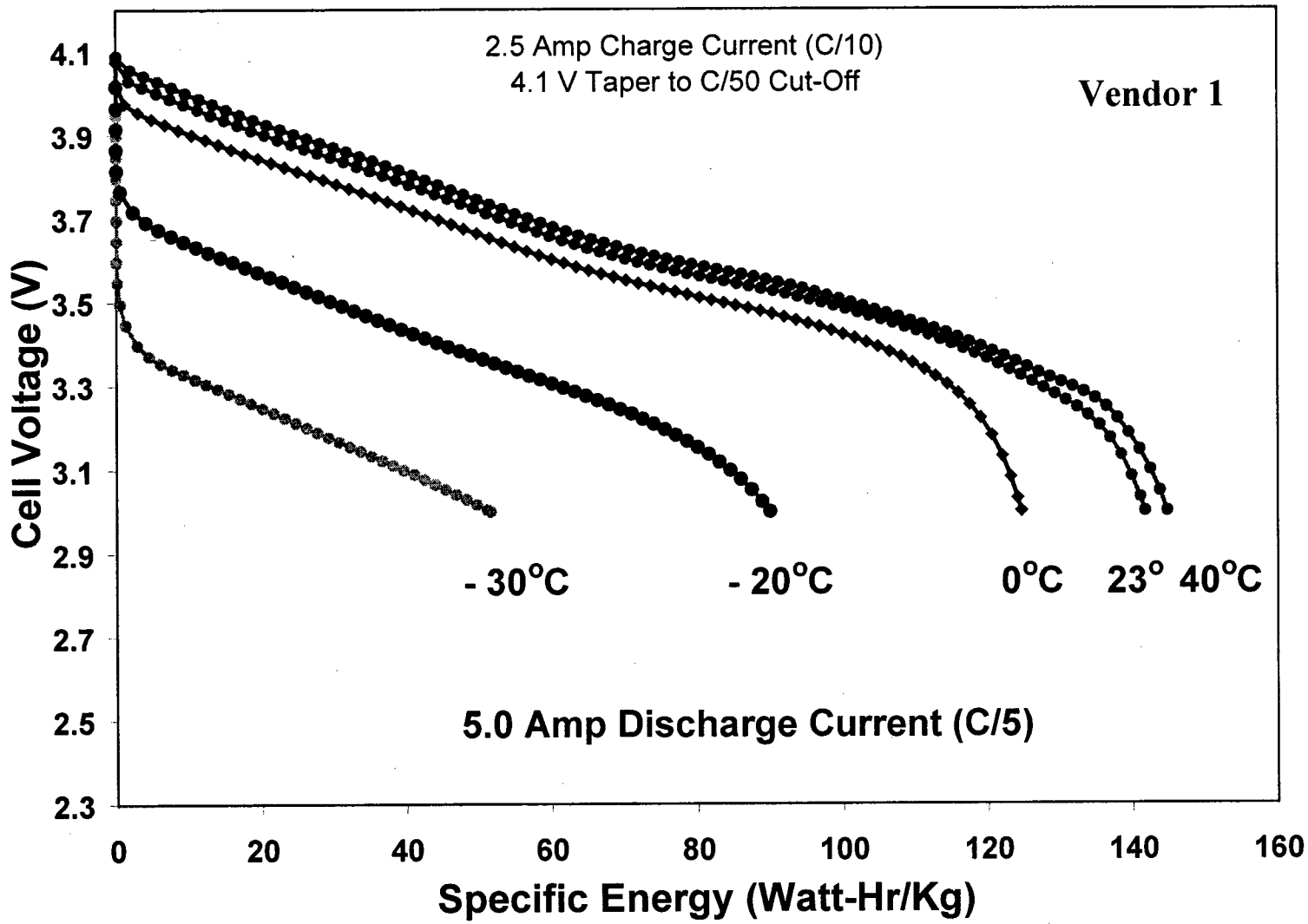

Lithium-Ion Cells for Mars Surveyor 2001 Lander Rate Capability at Different Temperatures

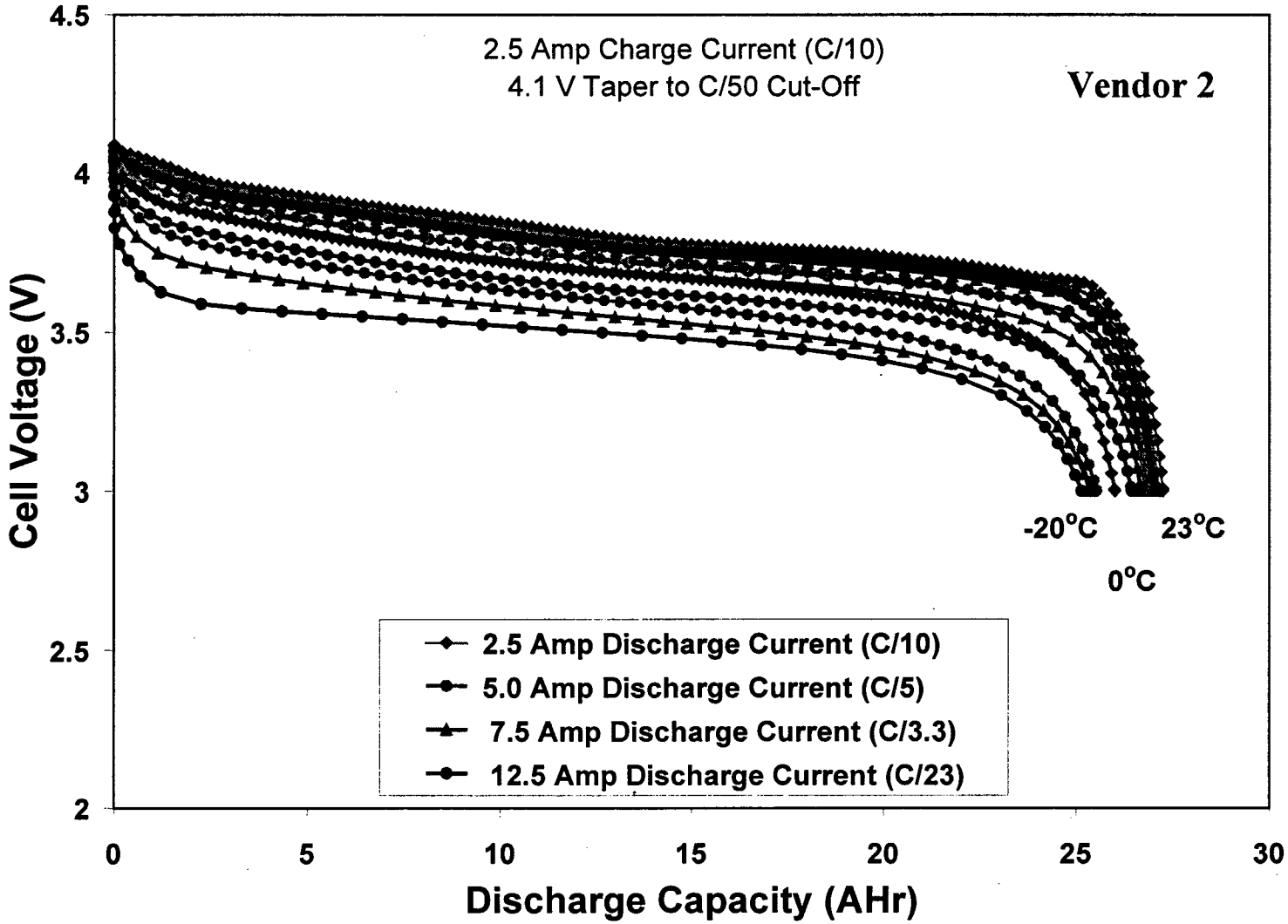

ELECTROCHEMICAL TECHNOLOGIES GROUP

Lithium-Ion Cells for Mars Surveyor 2001 Lander Discharge Rate Capability at Different Temperatures

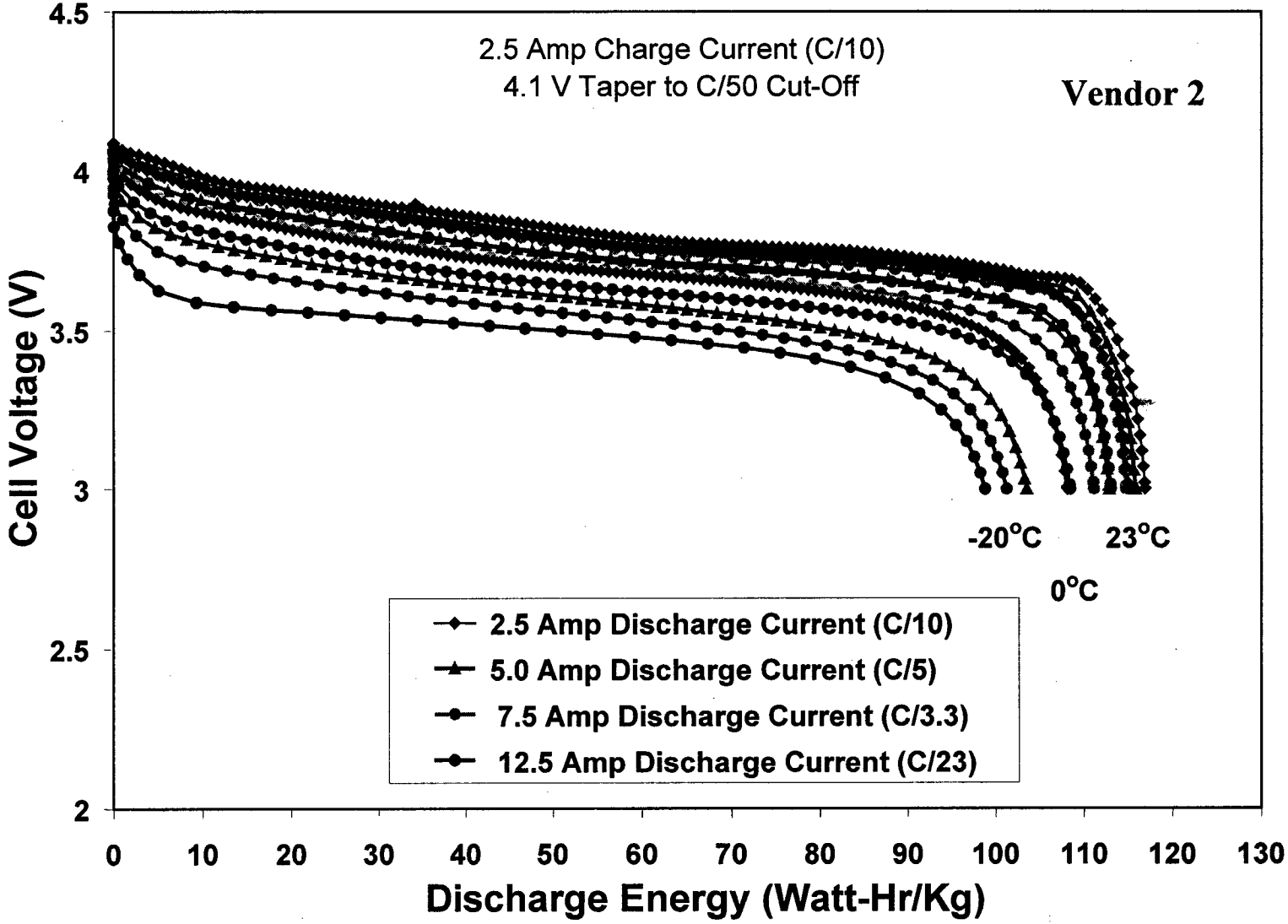

Cell Charge Characteristics

- Charge acceptance at various rates and temperatures
- Effect of cycle life upon charge characteristics
- Effect of charge voltage upon cell performance
  - V/T characterization
- Effect of charge methodology

Lithium-Ion Cells for Mars Surveyor 2001 Lander Low Temperature Charge Characteristics

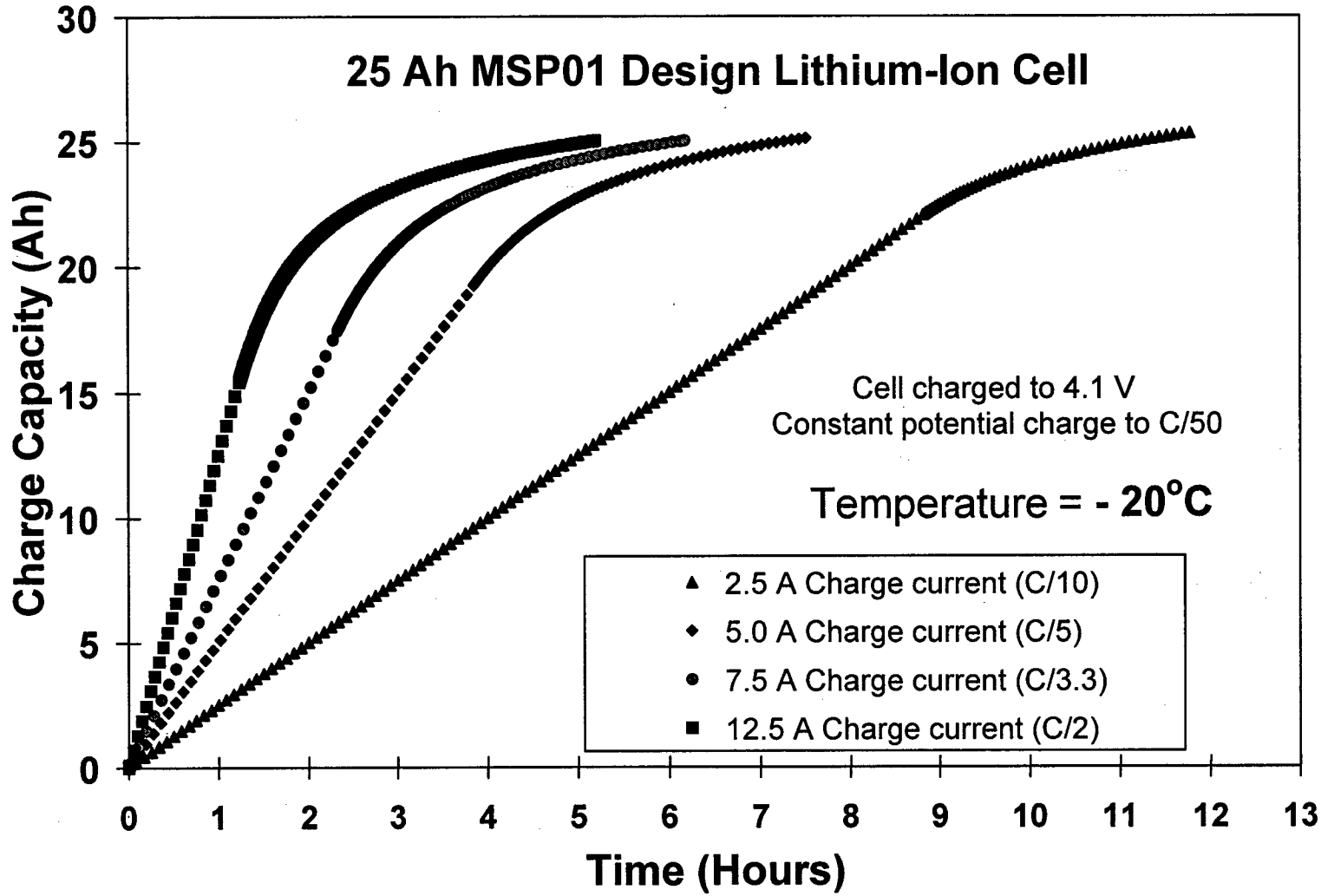

Lithium-Ion Cells for Mars Surveyor 2001 Lander Room Temperature Charge Characteristics

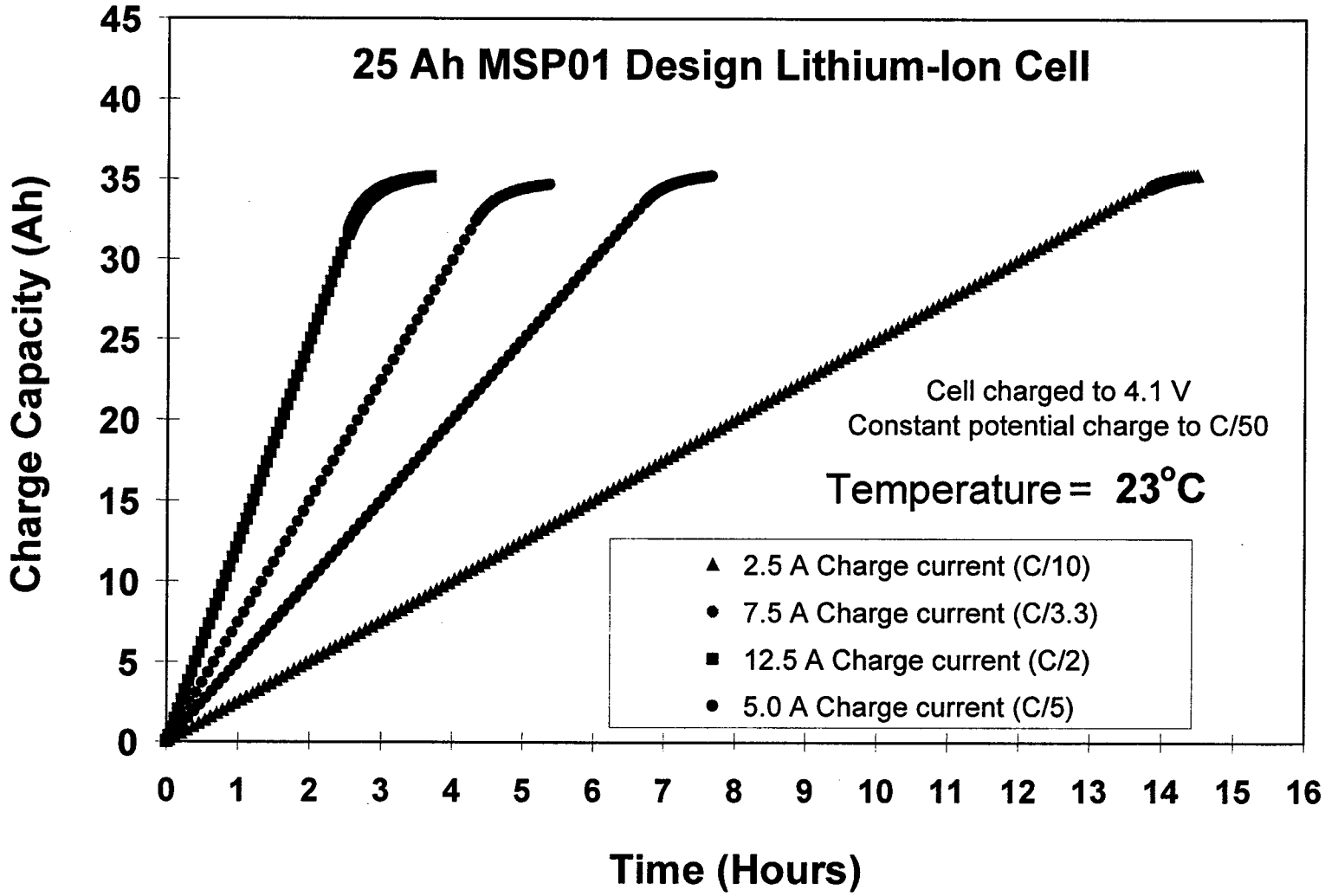

Lithium-Ion Cells for Mars Surveyor 2001 Lander Charge Characteristics

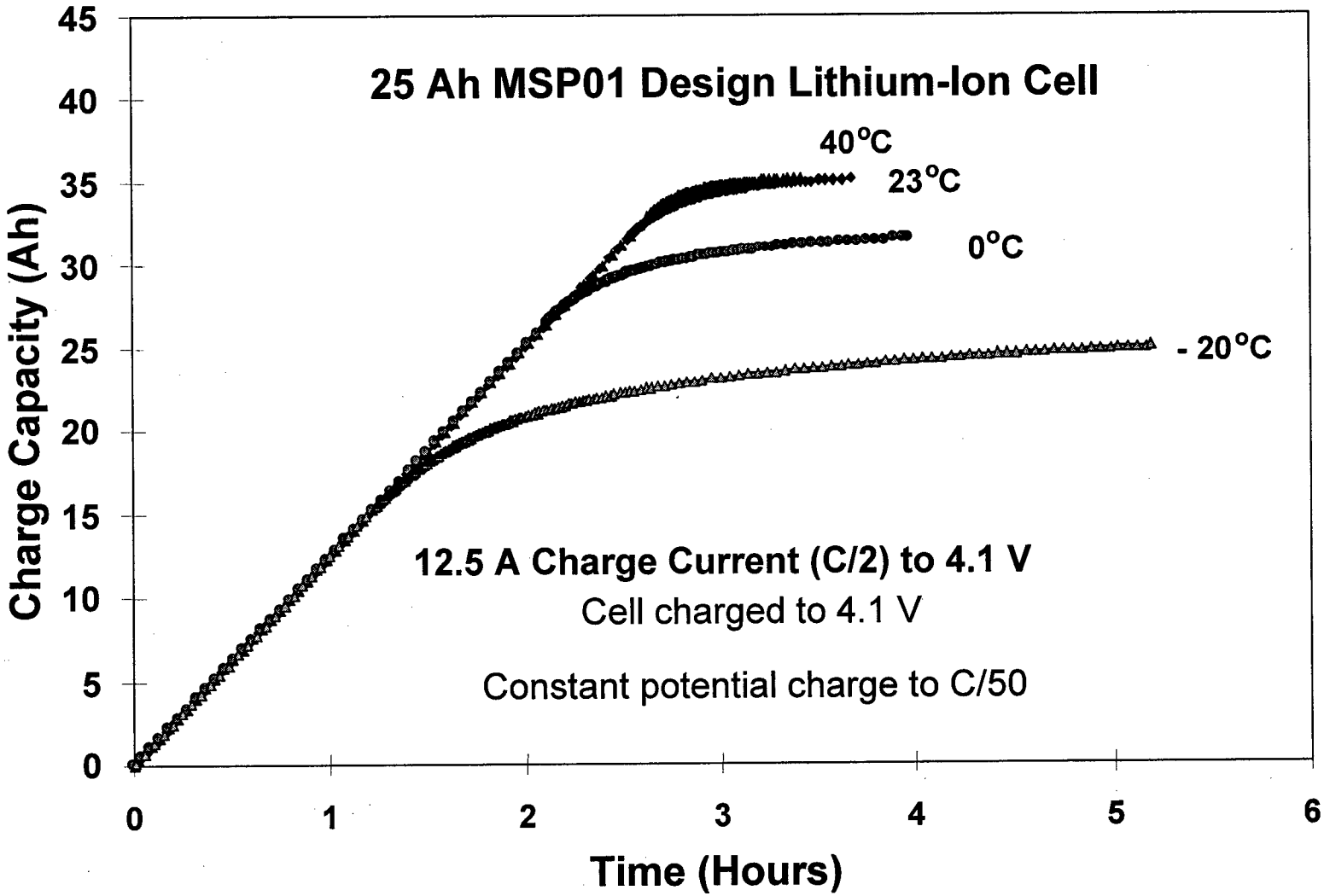

Lithium-Ion Cells for Mars Surveyor 2001 Lander Charge Characteristics

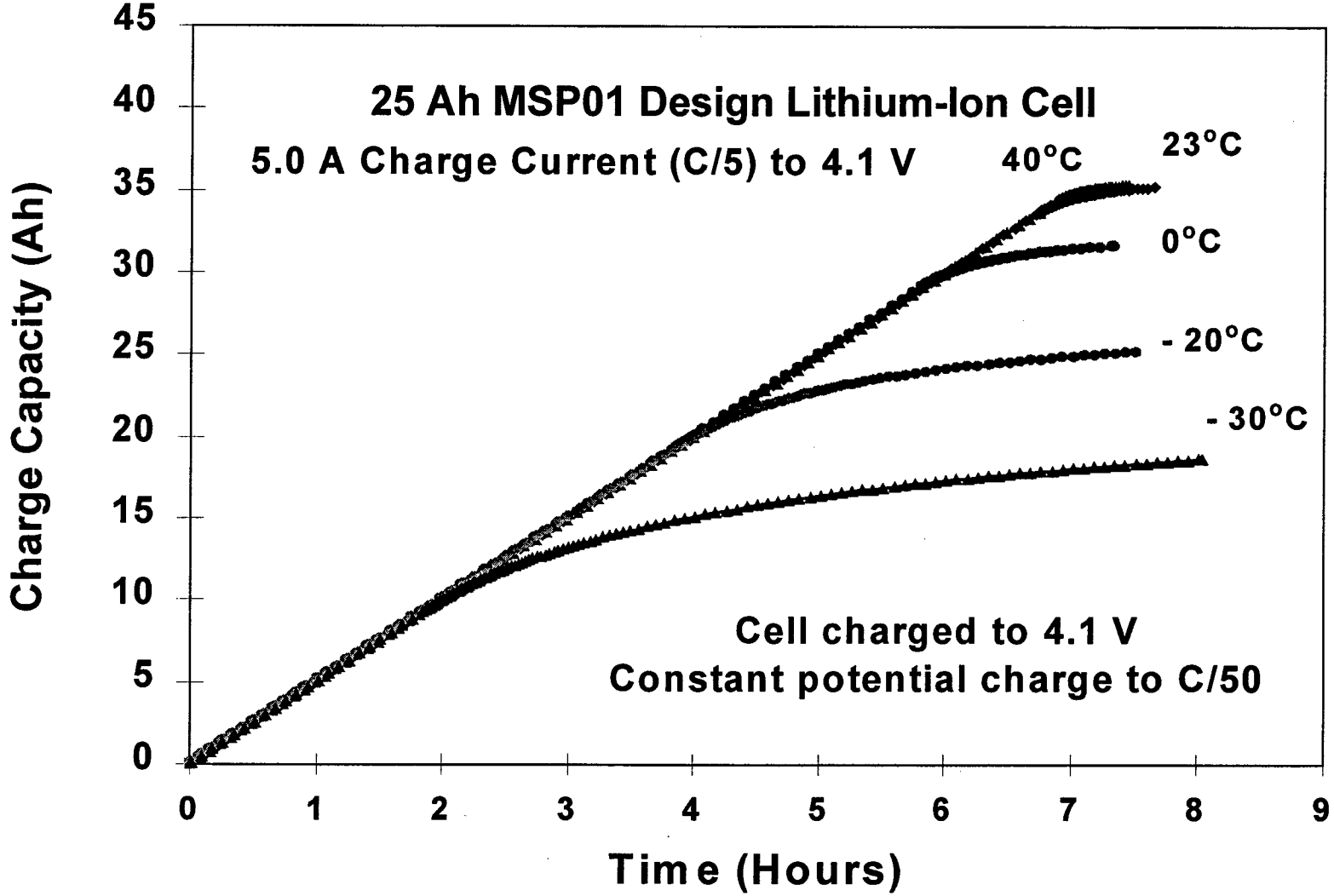

Large Capacity Lithium-Ion Cells for Mars Lander Applications
Room Temperature Charge Characteristics

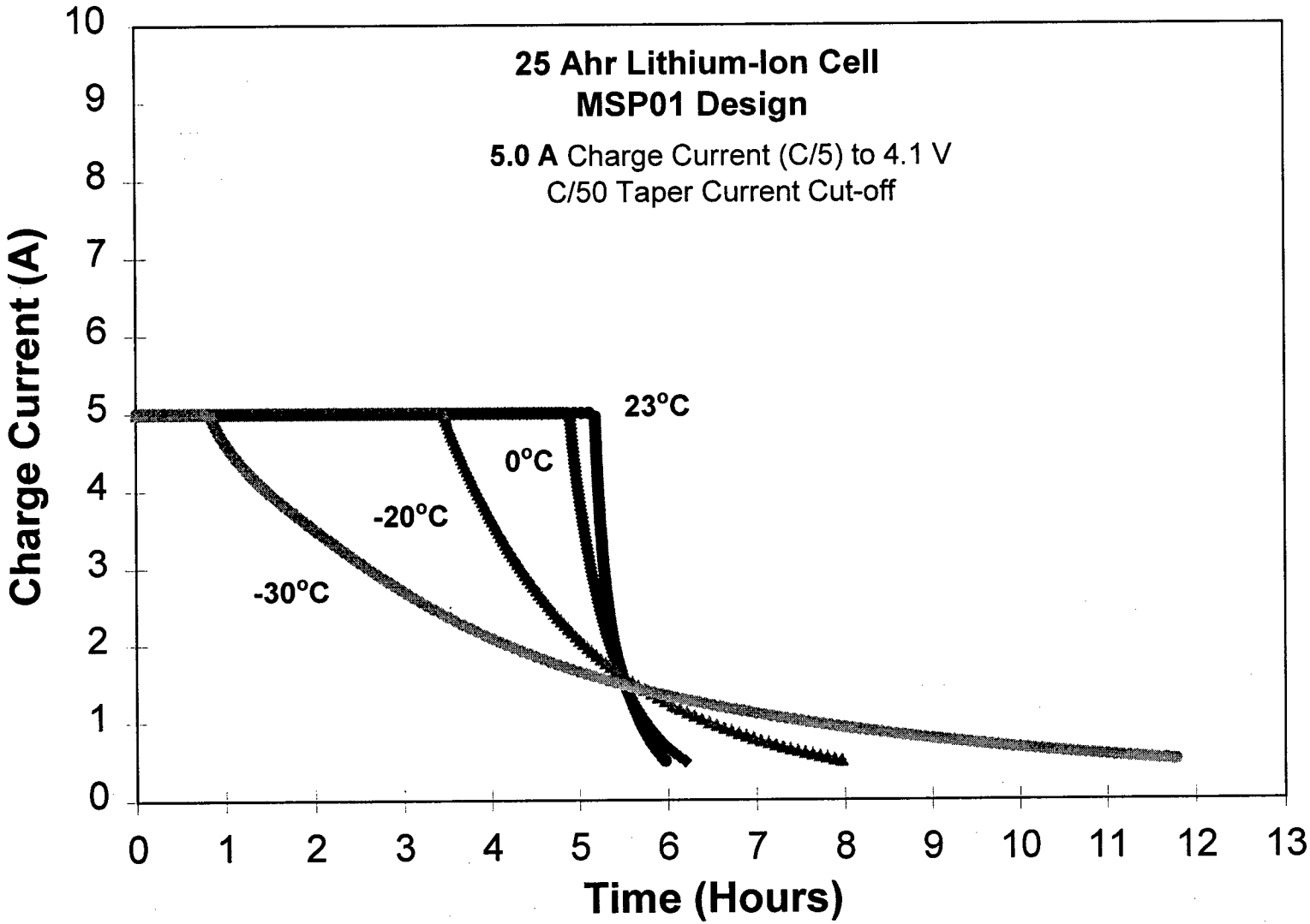

Lithium-Ion Cells for Mars Surveyor 2001 Lander
Effect of Cycle Life on Charge Characteristics

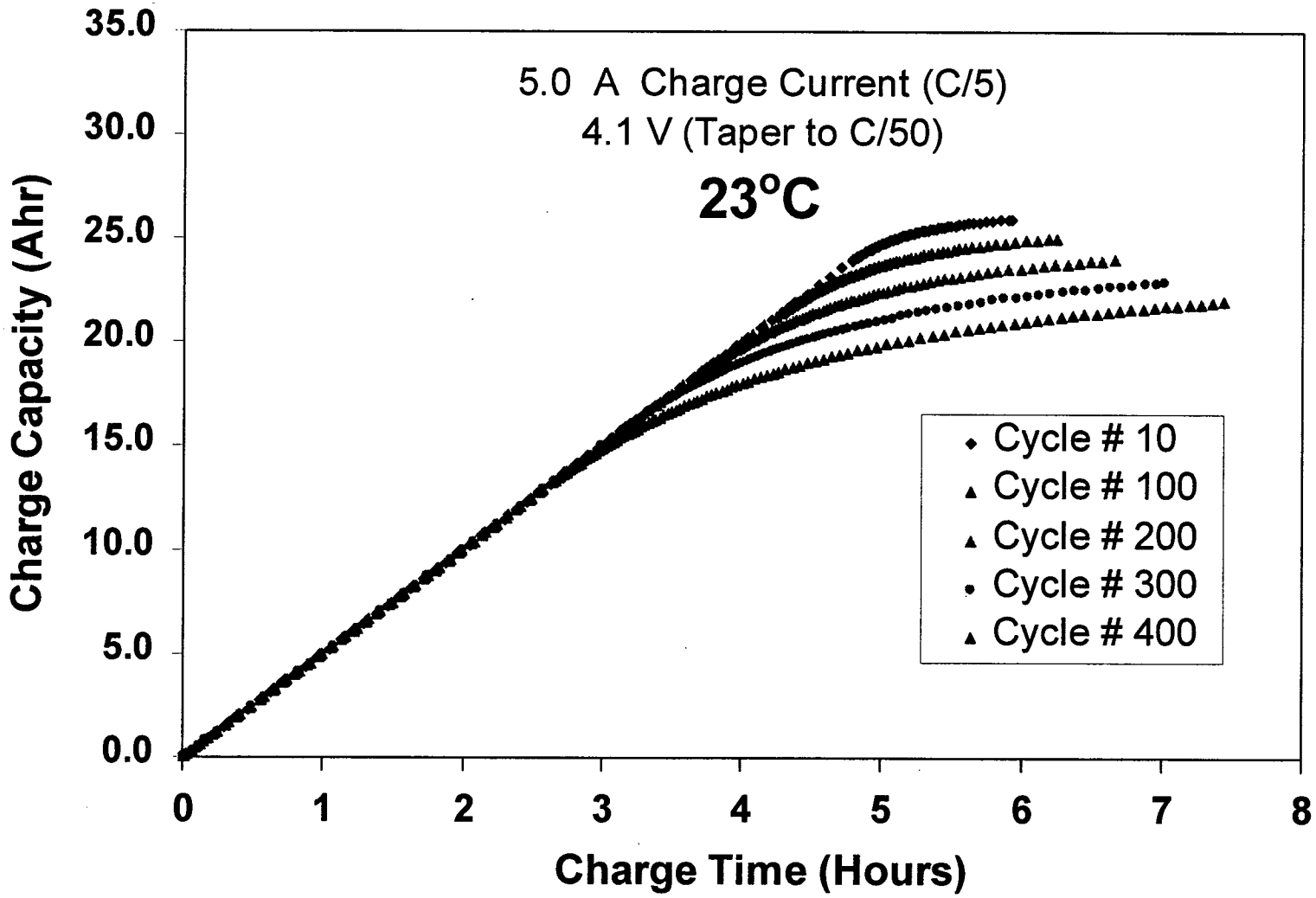

JPL

Lithium-Ion Cells for Mars Surveyor 2001 Lander
Effect of Cycle Life on Charge Characteristics

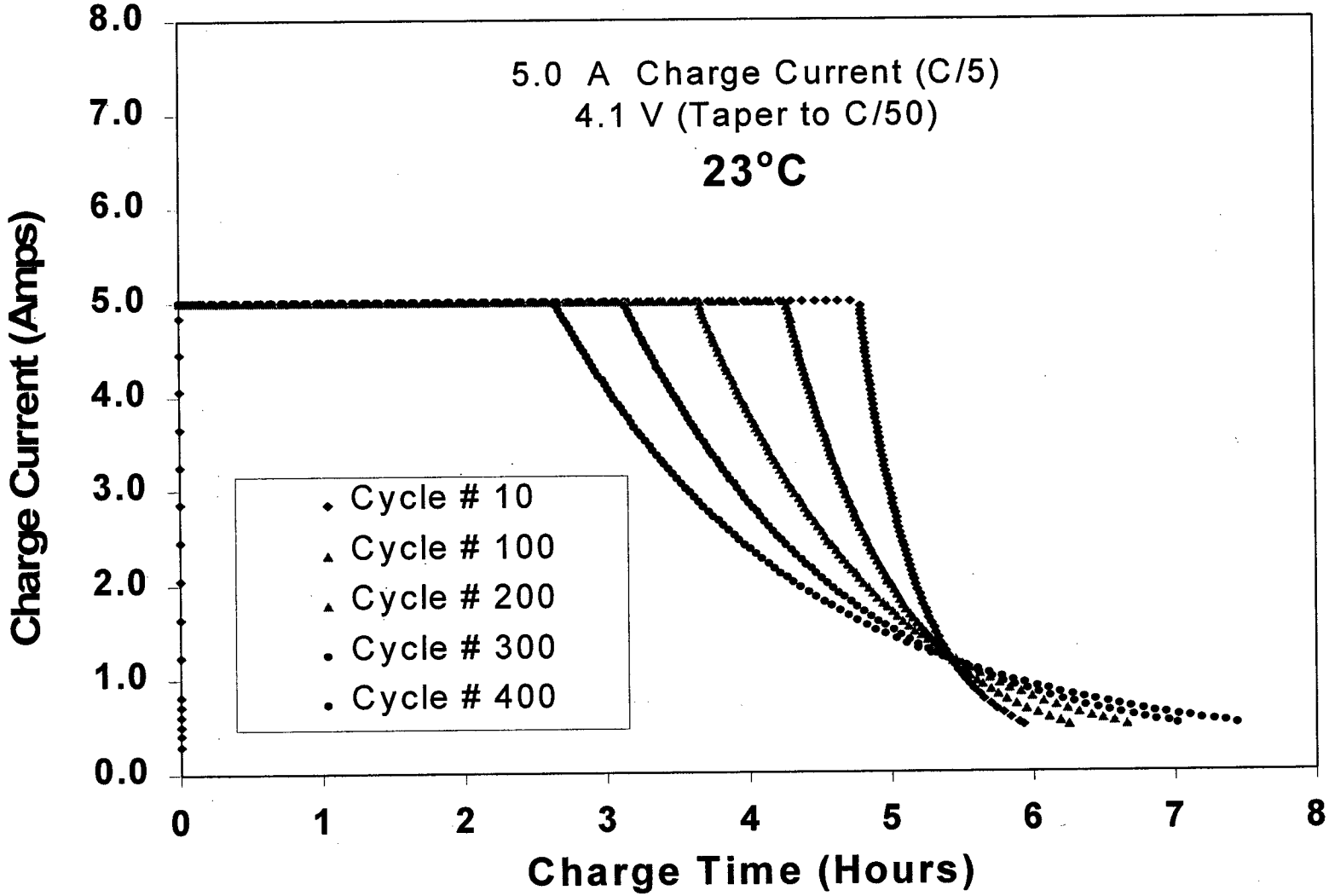

Lithium-Ion Cells for Mars Surveyor 2001 Lander
Effect of Cell Life Upon Charge Characteristics

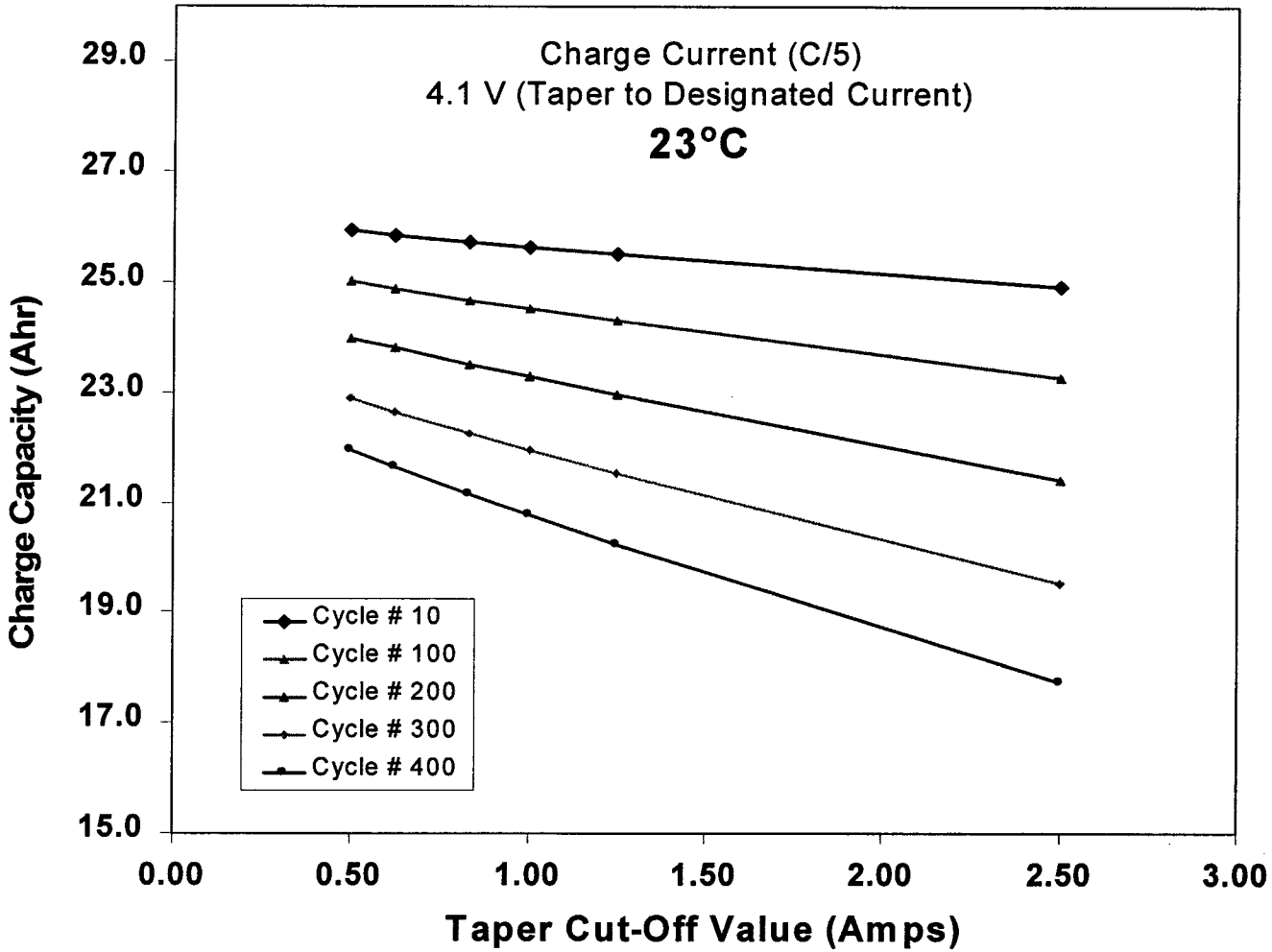

Lithium-Ion Cells for Mars Surveyor 2001 Lander
Effect of Taper Current Upon Charge Characteristics

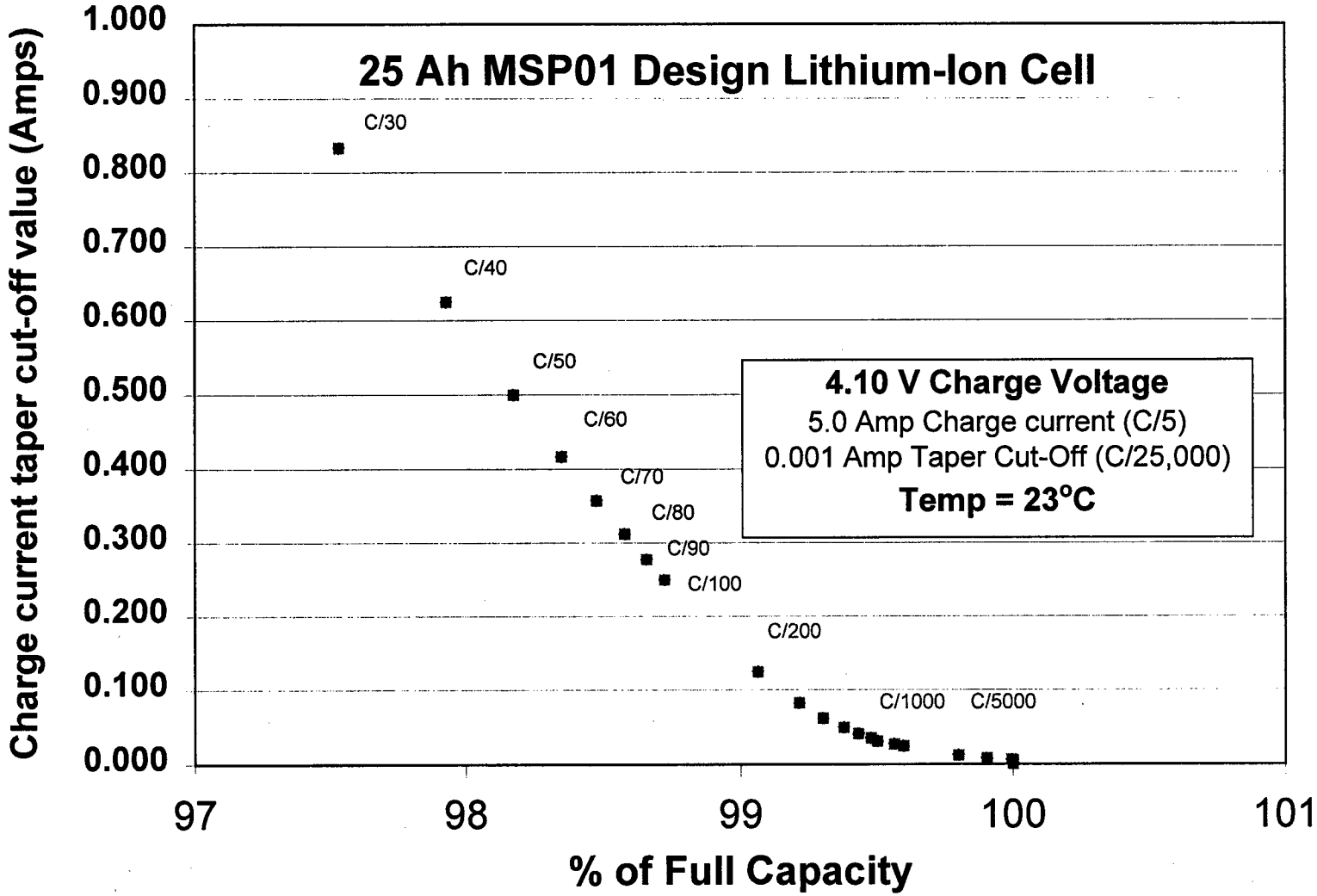

Lithium-Ion Cells for Mars Surveyor 2001 Lander
Effect of Taper Current Upon Charge Characteristics

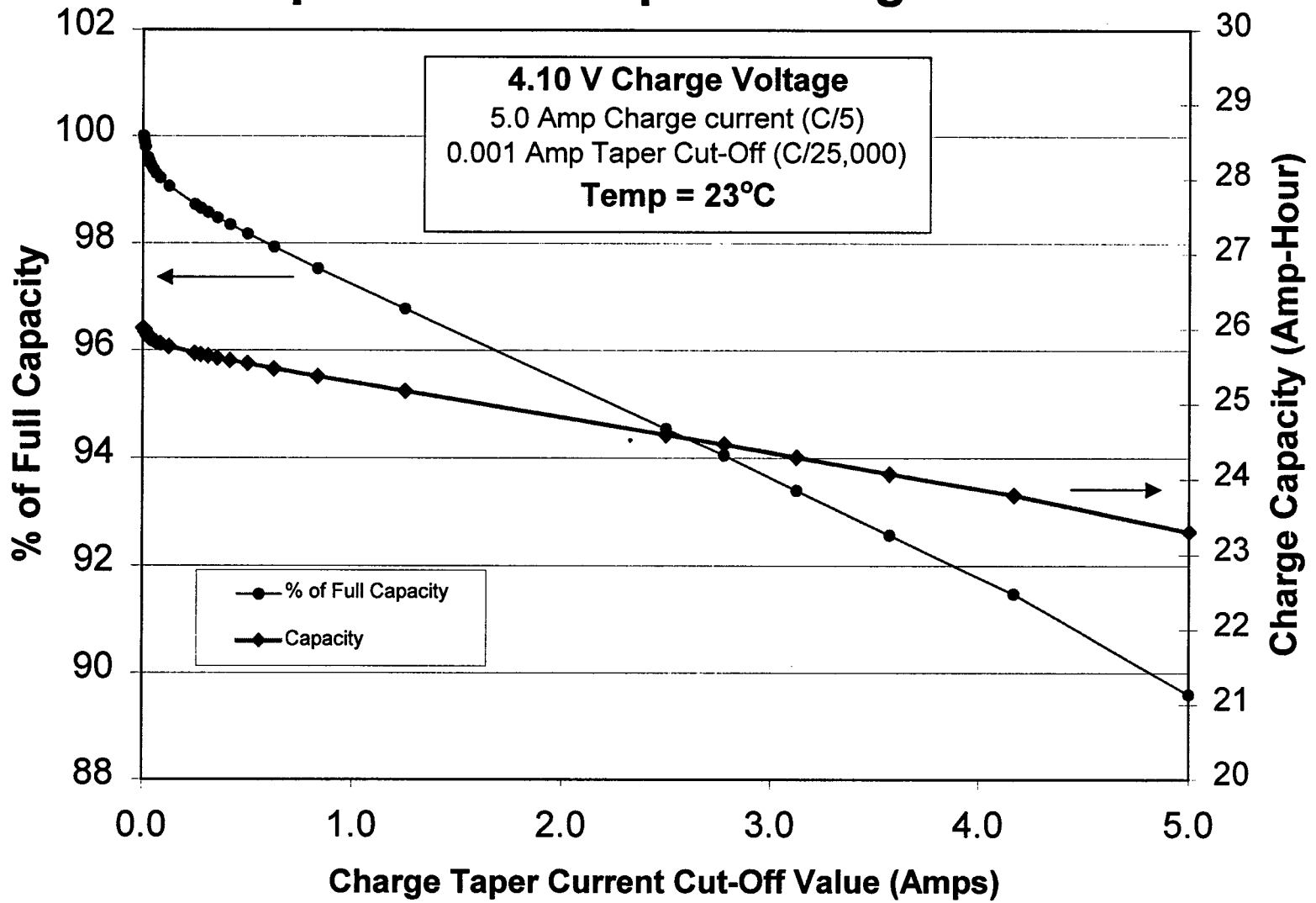

Lithium-Ion Cells for Mars Surveyor 2001 Lander
Effect of Charge Voltage Upon Cycle Life Characteristics

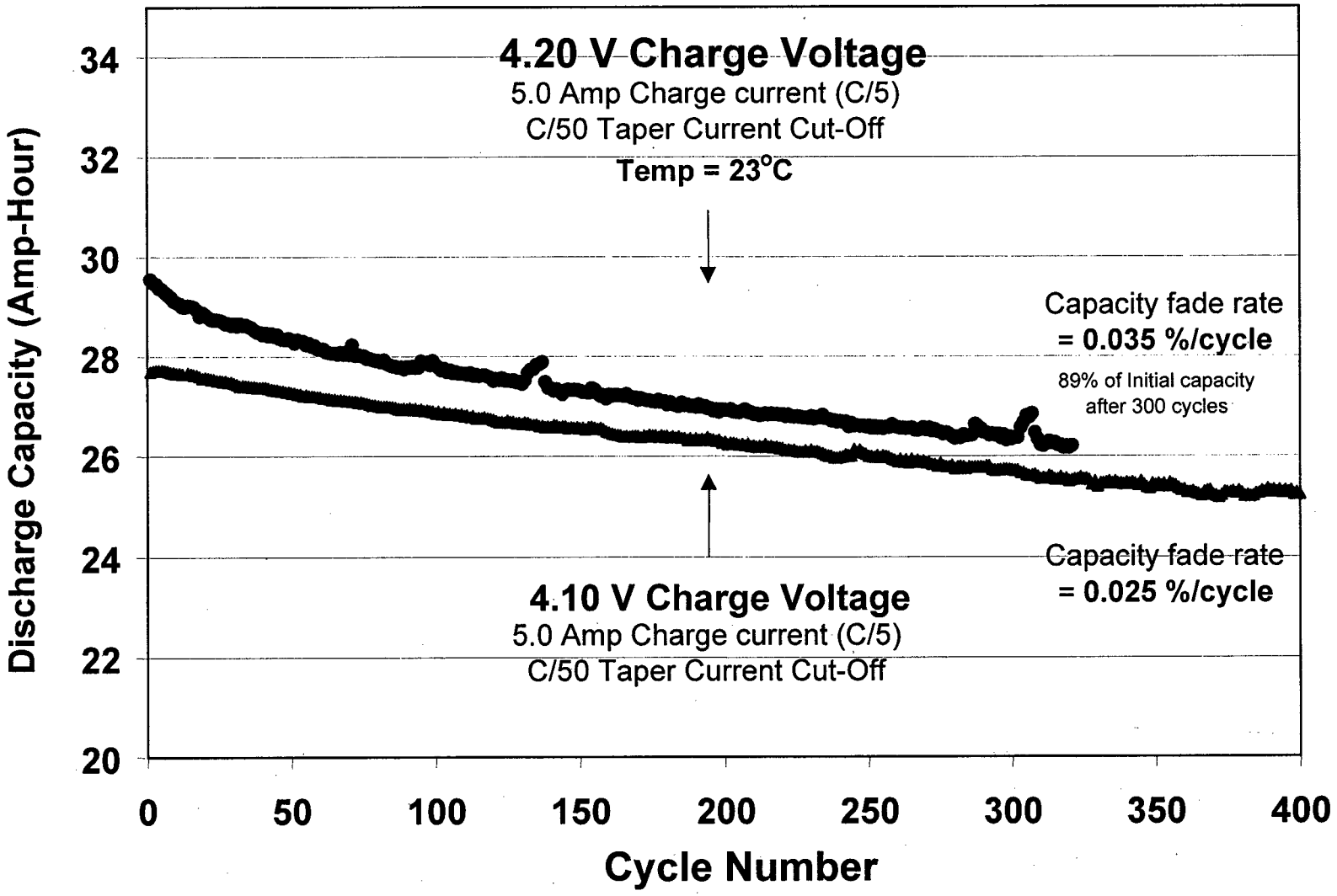

V/T Curves of Li Ion Cells

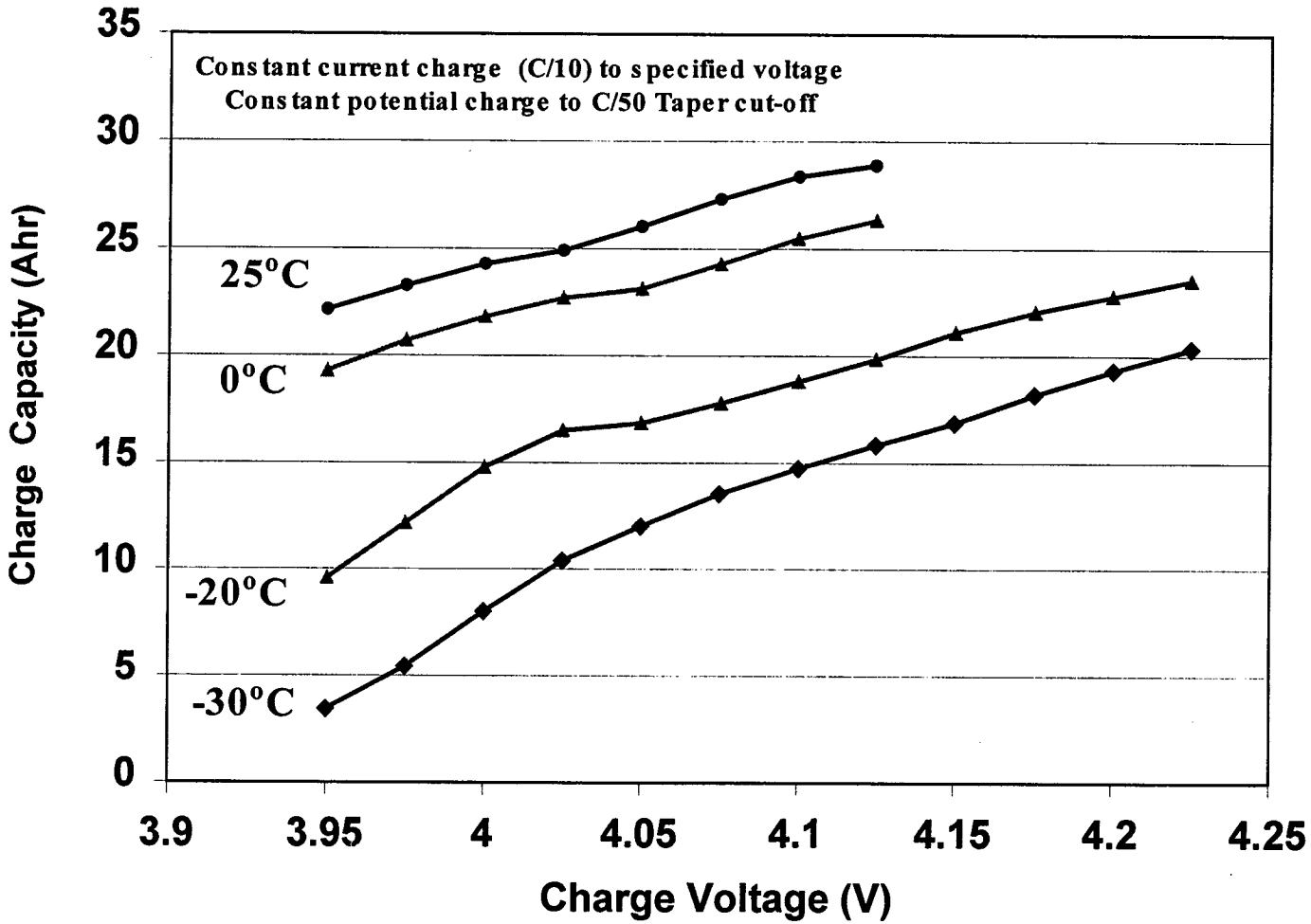

- Are higher charge voltages justified at lower temperature ?
- Need to define specific conditions under which lithium plating can occur (rate and system dependent).

Lithium-Ion Cells for Mars Surveyor 2001 Lander Capacity Retention Characterization Tests

Requirement :

- Should be capable of meeting all other requirements after prolonged storage period (>10 months)

Approach:

- Identify optimum storage conditions
- Quantify performance degradation due to storage
  - 2 Month storage test (0 and 40°C, 50 and 100% SOC)
  - 10 Month storage test (0 and 40°C, 50 and 100% SOC)
  - Accelerated storage test: (at different SOC (50, 70,100% SOC), temperatures (0, 25, 40, 50°C), and storage conditions.

Possible Evaluation Criteria:

- Self-discharge of stored capacity
- Permanent loss of reversible capacity
- Impact upon low temperature performance

Lithium-Ion Cells for Mars Surveyor 2001 Lander

Storage Characteristics - Capacity Retention

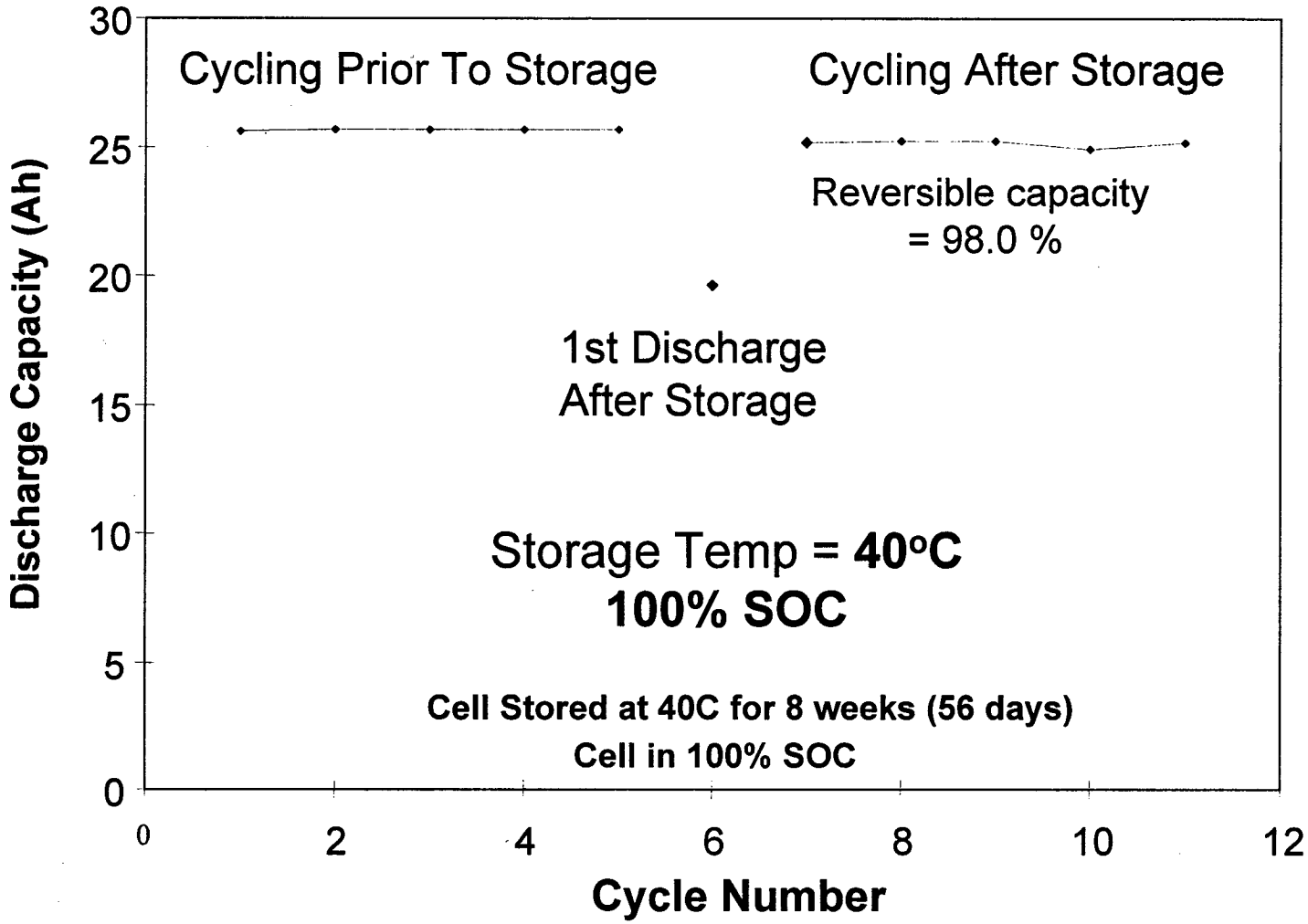

Lithium-Ion Cells for Mars Surveyor 2001 Lander Self Discharge Characteristics

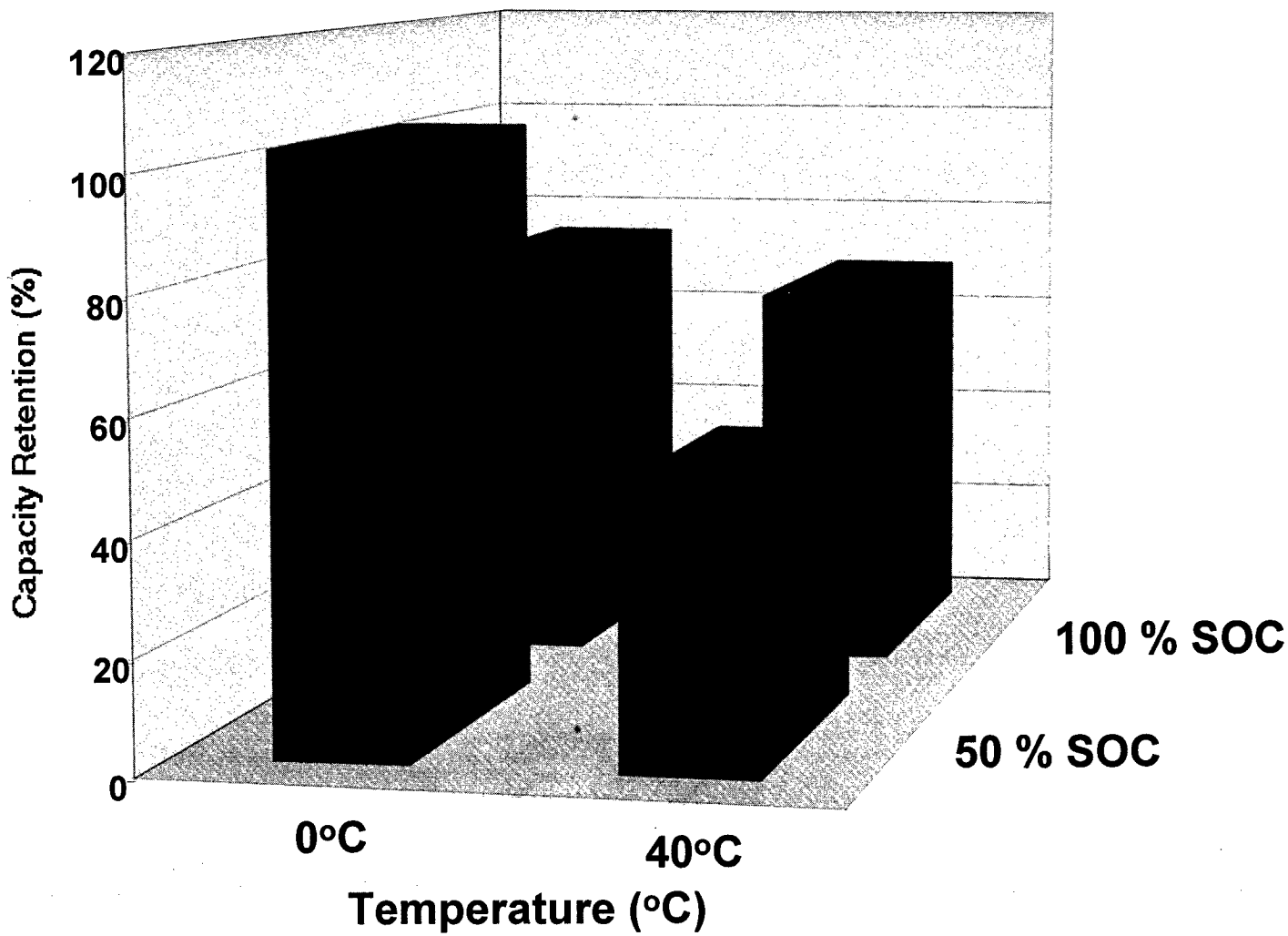

Lithium-Ion Cells for Mars Surveyor 2001 Lander Storage Characteristics

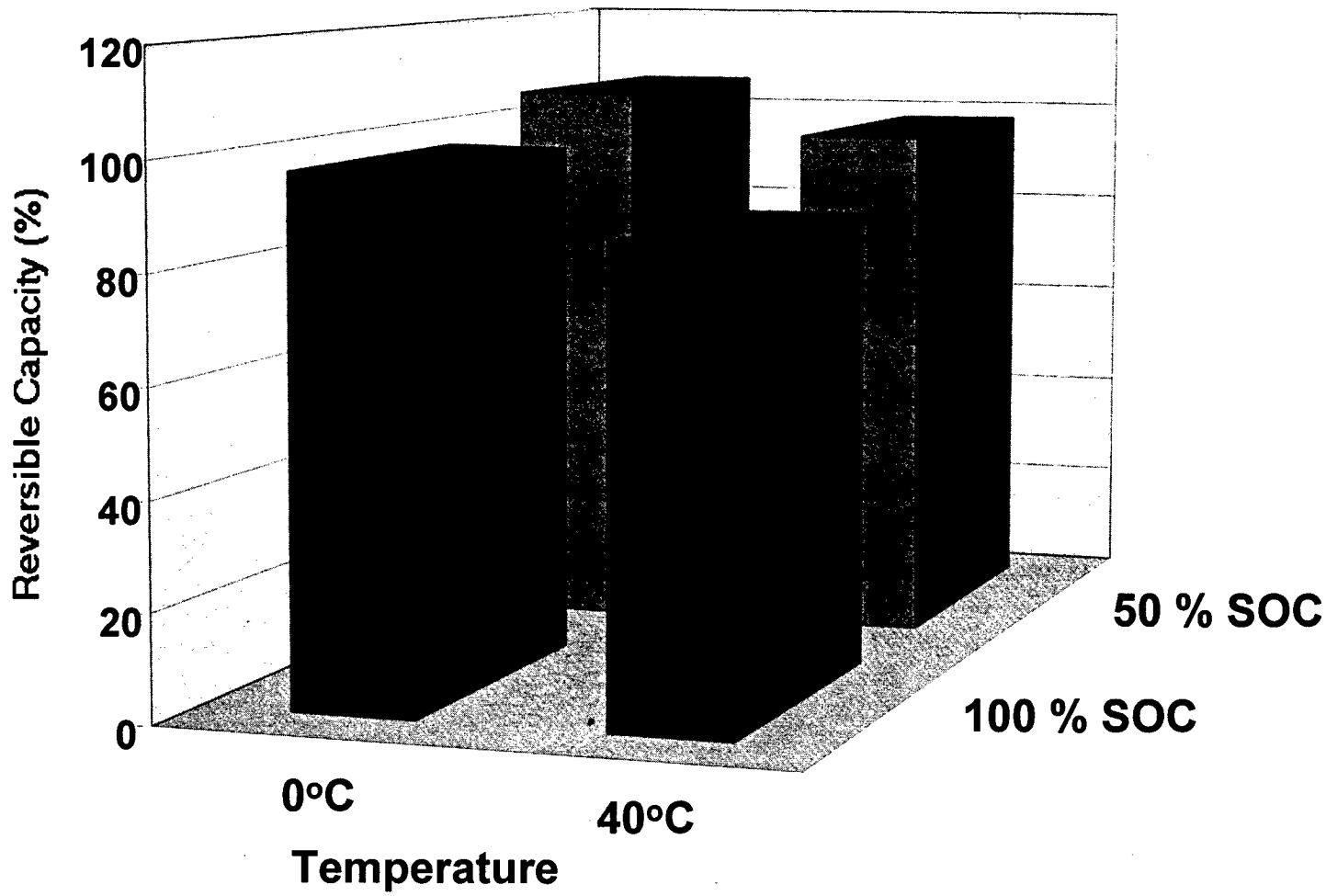

Lithium-Ion Cells for Mars Surveyor 2001 Lander Storage Characteristics - Capacity Retention 25 Ah Prototype Cells

Storage Temp (°C)	State of Charge	Capacity Loss (Ah)	Reversible Capacity
0	50 %	12.03 Ah	98.4 %
0	100 %	6.10 Ah	97.1 %
40	50 %	14.00 Ah	99.4 %
40	100 %	2.37 Ah	98.0 %

Lithium-Ion Cells for Mars Surveyor 2001 Lander

Design Experiments for Cruise Conditions

Experiment #	Storage time, weeks	Storage Temp	State of charge	Storage condition
1	2	25	50	Open Circuit
2	2	40	70	On Buss
3	2	55	100	Cycling
4	4	25	70	Cycling
5	4	40	100	Open Circuit
6	4	55	50	On Buss
7	6	25	100	On Buss
8	6	40	50	Cycling
9	6	55	70	Open Circuit

Parametric Storage Studies

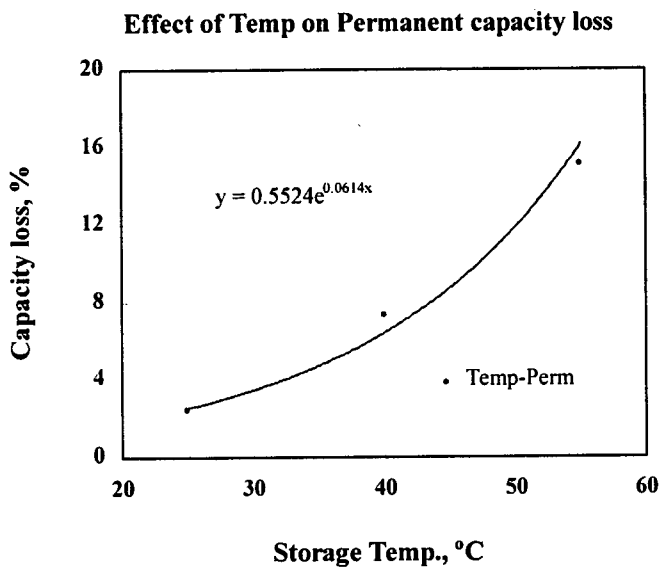

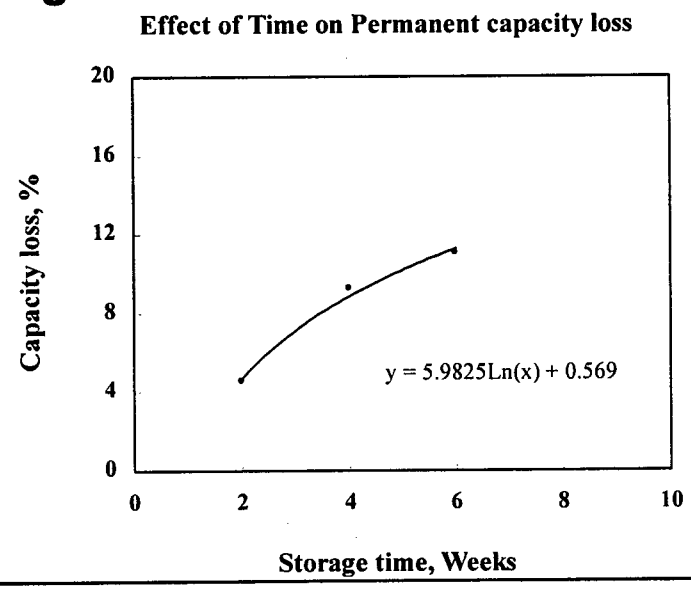

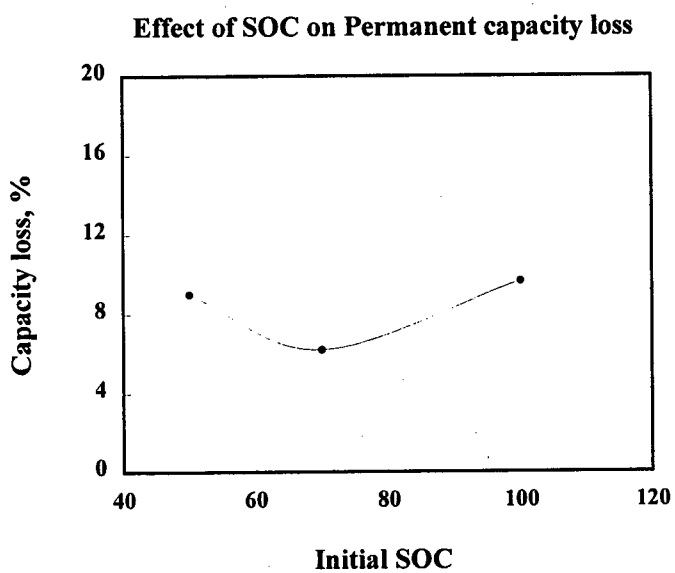

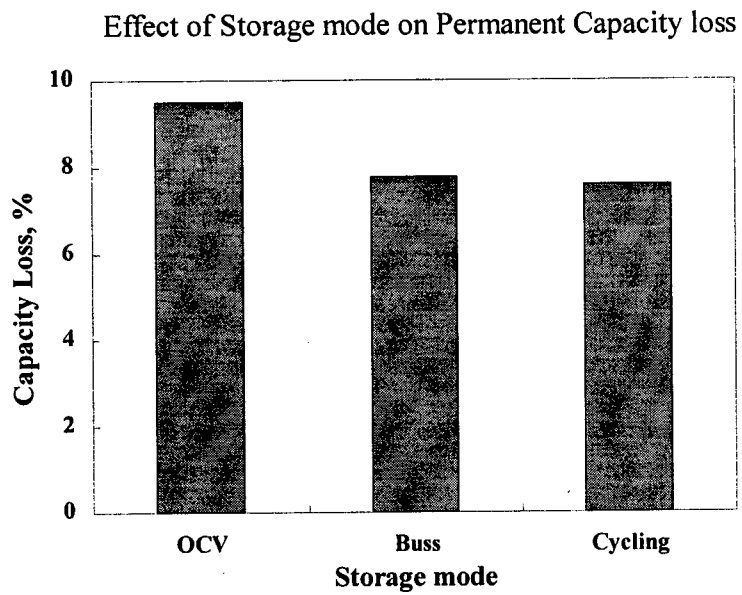

SUMMARY

- *Li Ion cells meet the MSP 2001 Lander mission requirements in*
  - *Cycle Life Performance*
    - Room Temperature = Excellent (>90% @ 200 cycles)
    - Low Temperature (-20) = Sufficient
    - High Temperature (40°C) = Sufficient (>70% @ 200 cycles)
  - *Discharge Rate Capability at Various Temperatures*
    - Room Temperature = Excellent
    - Low Temperature (-20) = Sufficient (~ 24 Ah @ C/5 rate)
    - High Temperature (40°C) = Excellent
  - *Storage Characteristics*
    - Demonstrated minimal reversible capacity loss (2 months)
    - Identified temperature as most crucial storage parameter
    - Demonstrated efficacy of storage "on the buss"
  - *Mission simulation (Variable Temperature Cycling)*
    - Identified potential performance limiting conditions (worst case)
    - Implemented characterization test to quantify behavior

Acknowledgments

The work described here was carried out at the Jet Propulsion Laboratory (JPL), California Institute of Technology, for the **Mars 2001 Surveyor and NASA Code S Battery Programs** under contract with the National Aeronautics and Space Administration (NASA).

Performance Characteristics of Lithium Ion Prototype Cells for 2003 Mars Sample Return Athena Rover

B. V. Ratnakumar, M. C. Smart, R. Ewell and S. Surampudi
Jet propulsion Laboratory, Pasadena, California
and
R. Marsh
Wright-Patterson Air Force Base, Dayton, OH

JPL

Supported by MSR 2003 Rover and NASA Code S Battery Programs

NASA Battery Workshop, Huntsville, AL, Nov. 16-18,1999

2003 MSR Athena Rover

Mission Objectives

To determine the geologic and climatic history of Martian site with conditions favorable to possible life

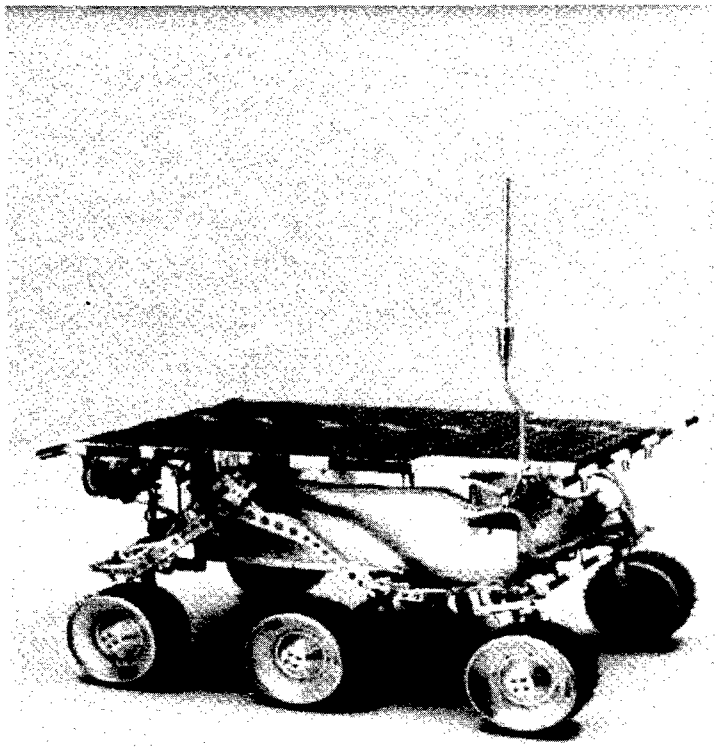

- **Specific objective include**
  - taking color stereo images of the Martian surface
  - determining elemental and mineralogical compositions
  - obtaining microscopic images of rocks
  - Collecting samples with evidence of ancient environmental conditions and possible life
- **Payloads Elements**
  - Pancam for stereo imaging
  - alpha proton X-ray spectrometer
  - Mossbauer, Mine TES and Raman spectrometers for mineralogical composition
  - microscopic imager and
  - mini-corer

2003 MSR Athena Rover

Power Subsystem

- Primary Source : Ga-As solar array
- Auxiliary Power Sources : Li ion Battery
- Li Ion Battery Characteristics
  - 16 V, 150 Wh
  - Mass 3 kg (max) and Volume 2 lit (max)
  - Three (N+1) parallel batteries of four cells each
  - EOL (200 cycles) performance
    - 5 Ah @ 0°C at C/2
    - 3.5 Ah @ -20°C at C/2
  - Calendar life : 2 years
  - Cylindrical or prismatic
  - In-house charger
    - individual cell monitoring and cell balancing

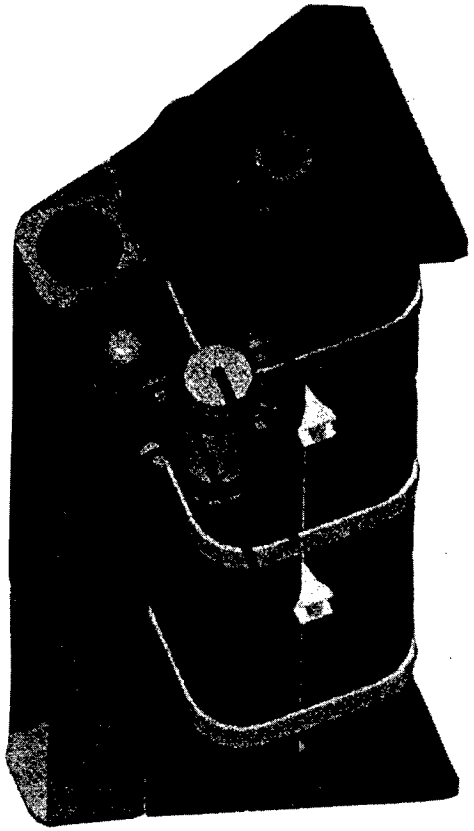

NASA-DOD Interagency Li Ion Program

Objectives

- DEVELOP HIGH SPECIFIC ENERGY AND LONG CYCLE LIFE Li -ION BATTERIES
- ESTABLISH U.S. PRODUCTION SOURCES
- DEMONSTRATE TECHNOLOGY READINESS
  - LANDERS BY 2001
  - ROVERS BY2003
  - GEO MISSIONS BY 2003
  - AVIATION/UAV's BY 2001
  - MILITARY TERRESTRIAL APPLNS's BY 2001
  - LEO MISSIONS BY 2003

Technology Drivers

Mission	Technology Driver
Lander Rover	Low Temperature Operation High rate Pulse Capability
GEO S/C	10-20 Year Operating life Large Capacity cells (50-200 Ah)
LEO PlanetaryS/C	Long Cycle life(30,000) Medium Capacity Cells (50 Ah)
Aircraft	Low temperature Operation High Voltage Batteries (270 V)
UAV	Large Capacity cells (200 Ah) High Voltage Batteries (100V)

Lithium-Ion Cells for 2003 MSR Athena Rover

Program Objectives

- Assess viability of using lithium-ion technology for future Aerospace applications.
- Demonstrate applicability of using lithium-ion technology for future 2003 Mars Sample Return Athena Rover applications.

Lithium-Ion Cells for 2003 MSR Athena Rover

Evaluation Tests On-Going at JPL

- Cycle life performance at room temperature (25°C)
- Cycle life performance at low temperature (-20°C)
- Cycle life at alternating temperatures (40 and -20°C)
- Discharge rate characterization (at 40, 25, 0, and -20°C)
- Charge rate characterization (at 40, 25, 0, and -20°C)
- Capacity retention
- Storage characterization tests (cruise conditions)
- VT charge characterization tests
- Electrical characterization by a.c. impedance
- Thermal characterization

Lithium-Ion Cells for 2003 MSR Athena Rover

Cycle Life Performance Tests

Requirement **: Deliver > 200 cycles on surface of Mars**

- **100% DOD cycling (3.0-4.1V, C/5-C/10)**
- **Wide temperature range (-20°C to 40°C)**
- **At end of life should deliver 5 Ah @ 0°C**

***Approach*:**

100 % DOD cycling @ 23°C (C/5 charge, C/5 discharge)
100 % DOD cycling @ -20°C (C/10 charge, C/5 discharge.)
100 % DOD cycling @ 40°C (C/5 charge, C/5 discharge)
Variable temperature cycling (temperature extremes)
Mission simulation cycling

***Possible Evaluation Criteria*:**

Initial capacity (must exceed 5 Ah)
Capacity after 200 cycles (Ah)
Capacity fade rates
Capacity delivered over range of temperatures

JPL

Lithium-Ion Cells for 2003 MSR Athena Rover

Cycling at 25°C and -20°C

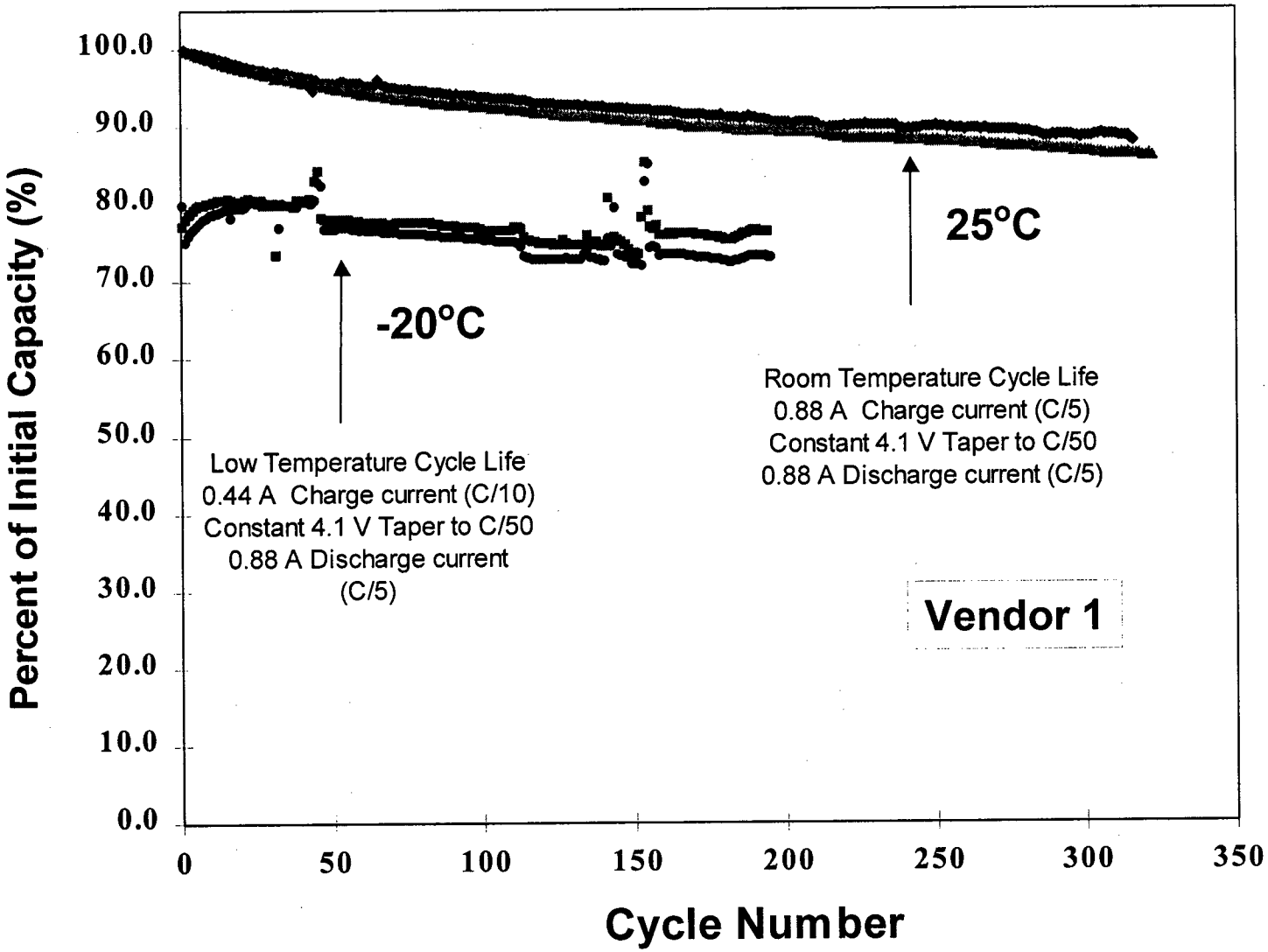

Lithium-Ion Cells for 2003 MSR Athena Rover

OCV During Cycling at 25°C and -20°C

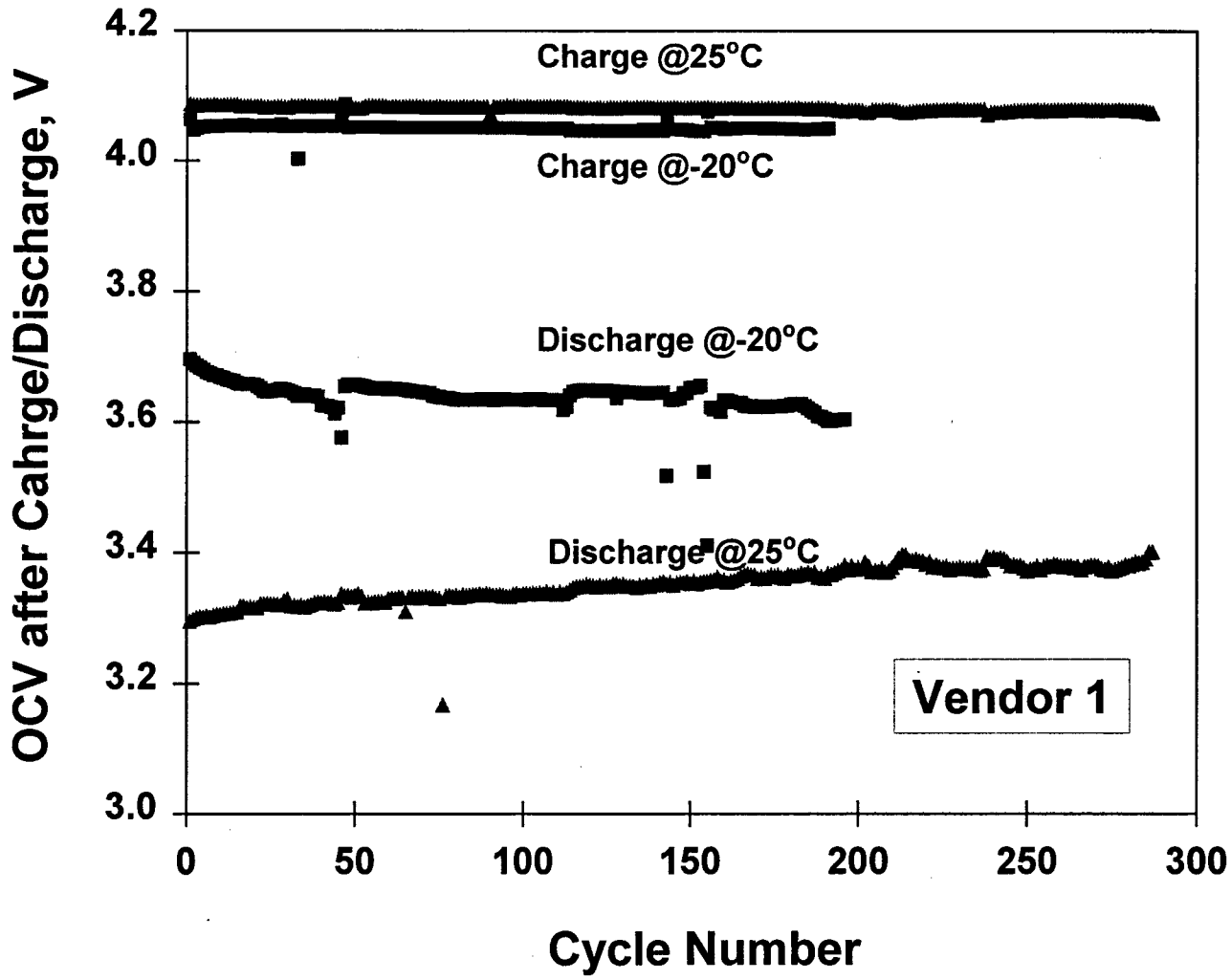

Lithium-Ion Cells (D-Size) for Mars Rover Applications
Characteristics of Conditioning Cycles

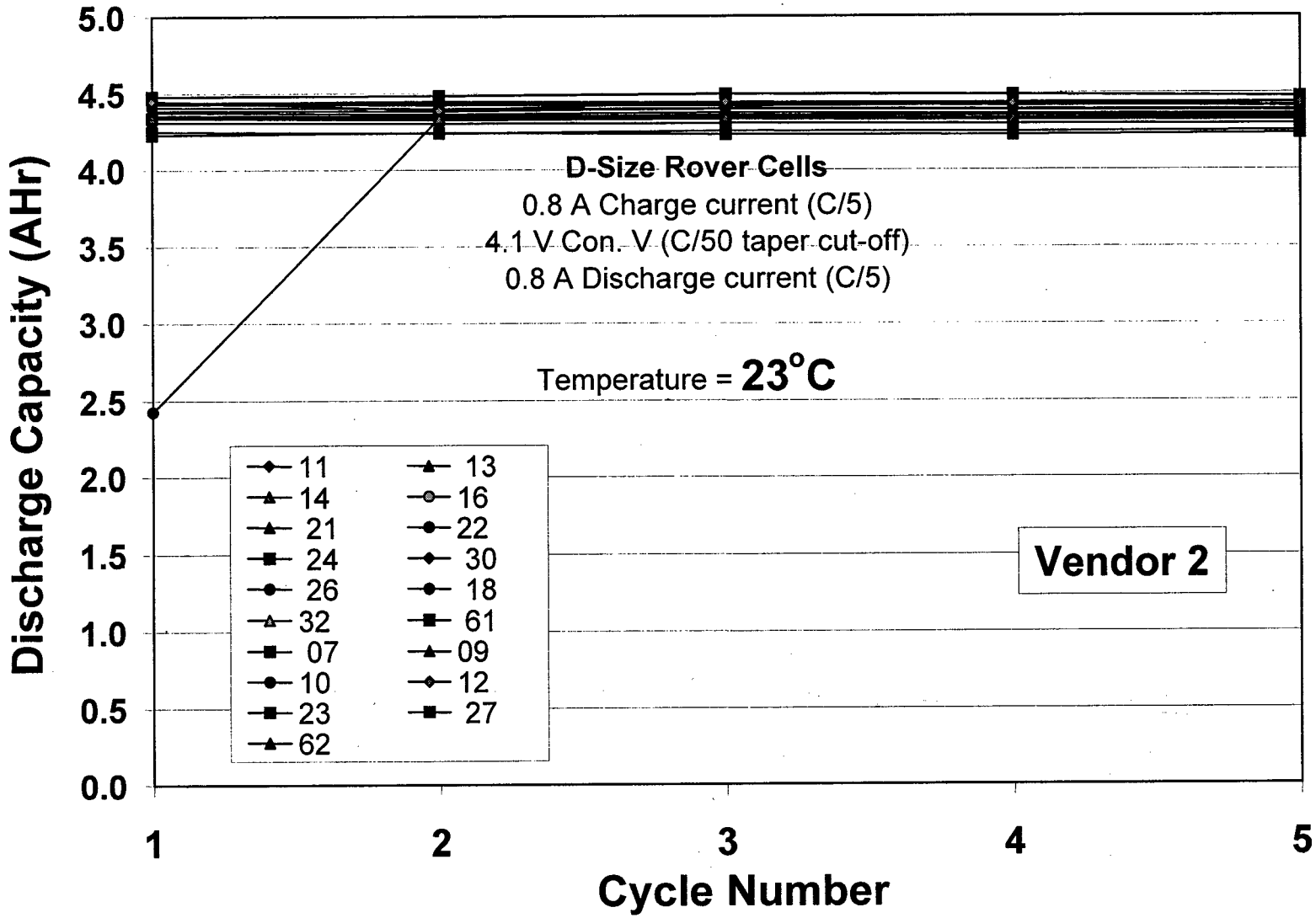

Lithium-Ion Cells (D-Size) for Mars Rover Applications Cycle Life Performance at Different Temperatures

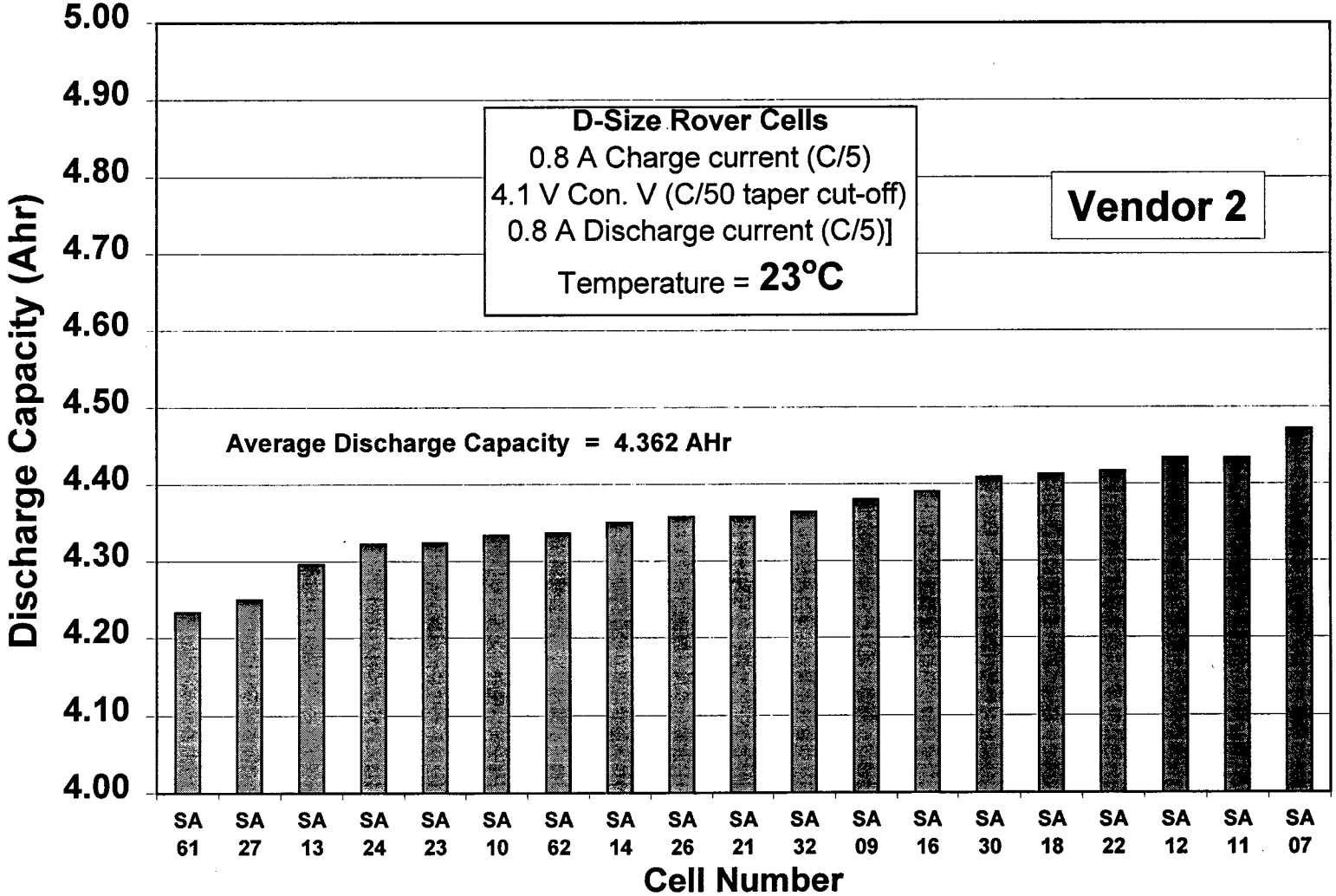

Lithium-Ion Cells (D-Size) for Mars Rover Applications
EIS Measurements of Cells After Conditioning Cycles

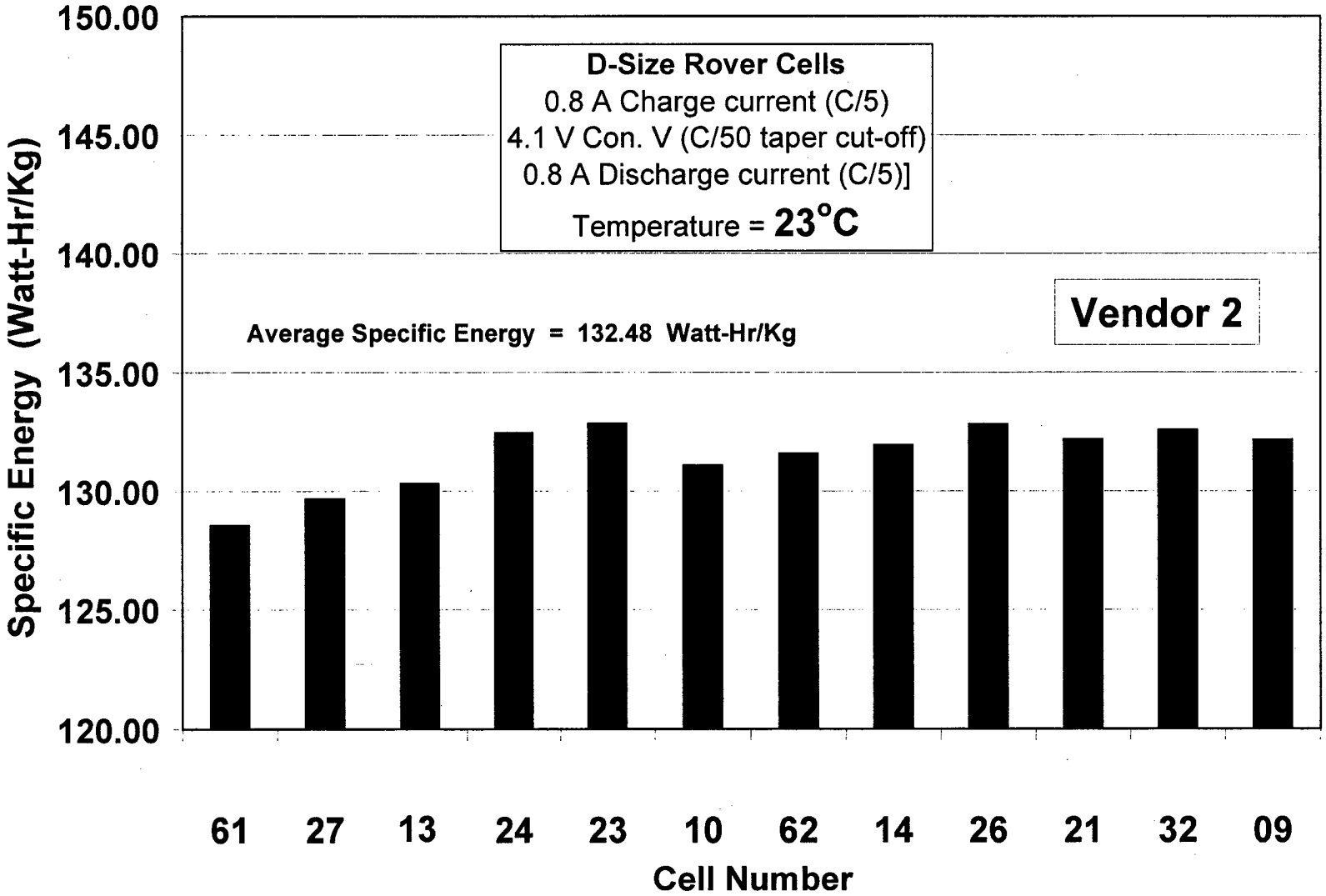

Lithium-Ion Cells (D-Size) for Mars Rover Applications
EIS Measurements of Cells After Conditioning Cycles

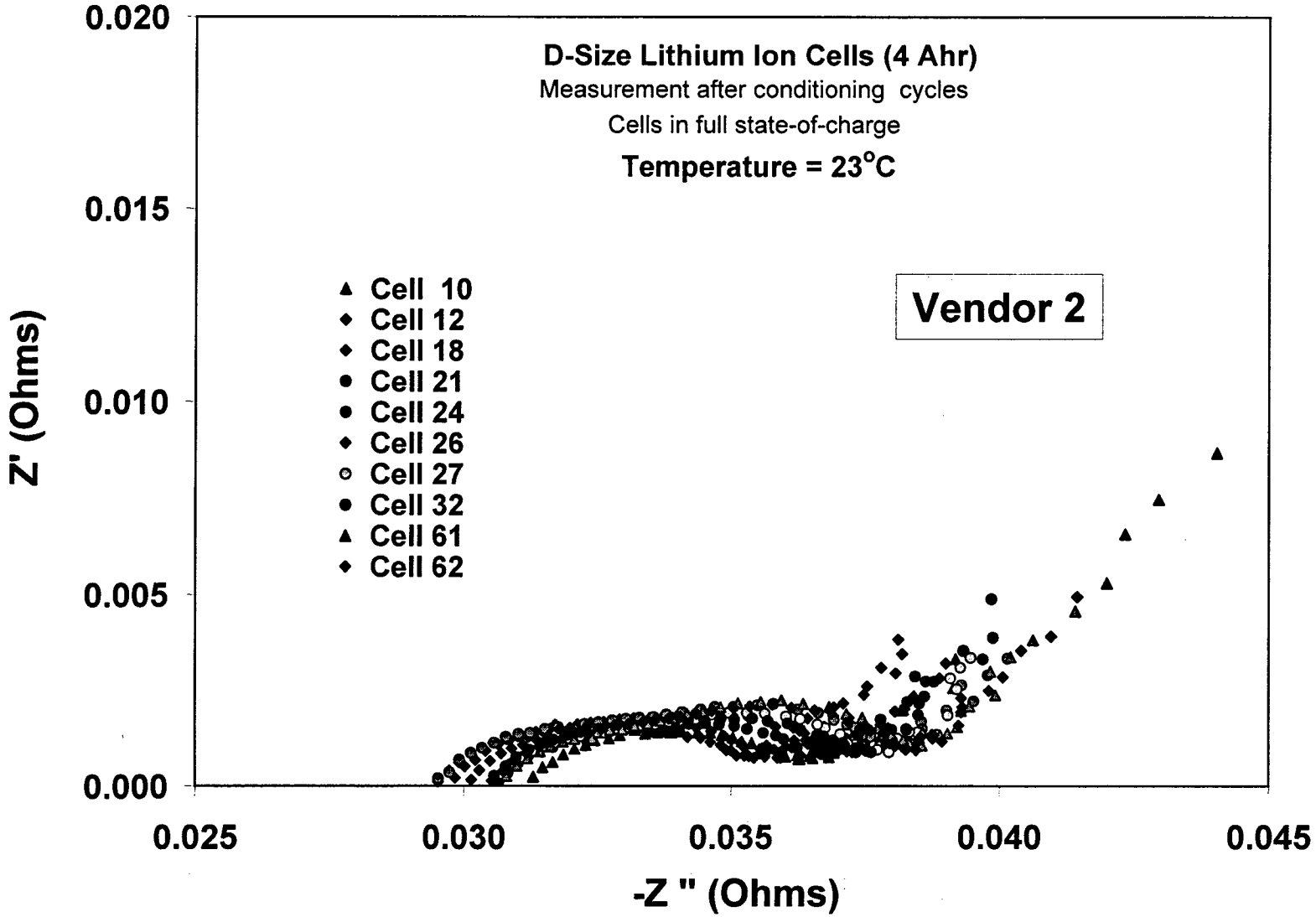

JPL

Lithium-Ion Cells (D-Size) for Mars Rover Applications
Cycle Life Performance at Different Temperatures

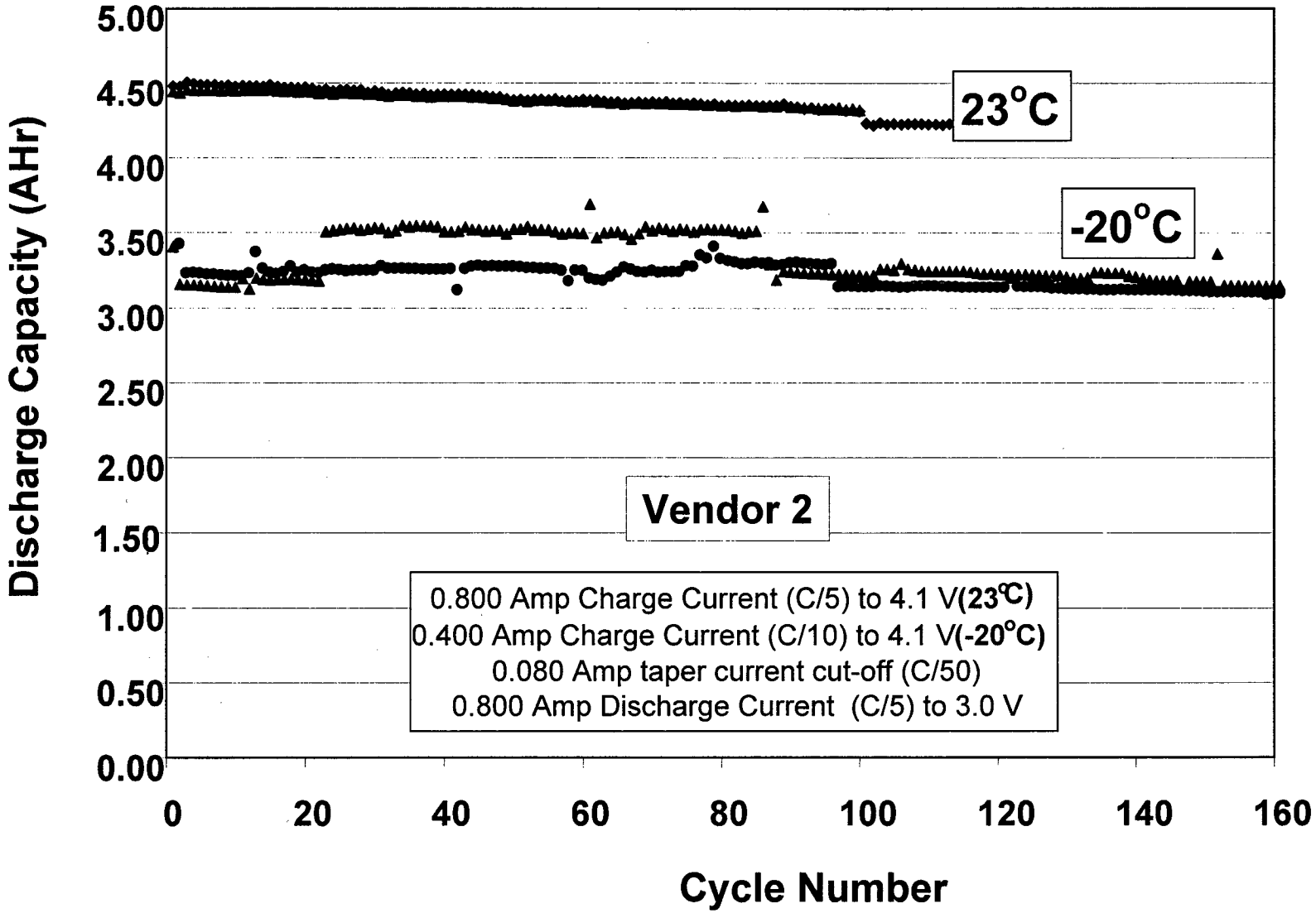

Lithium-Ion Cells (D-Size) for Mars Rover Applications
Cycle Life Performance at Different Temperatures

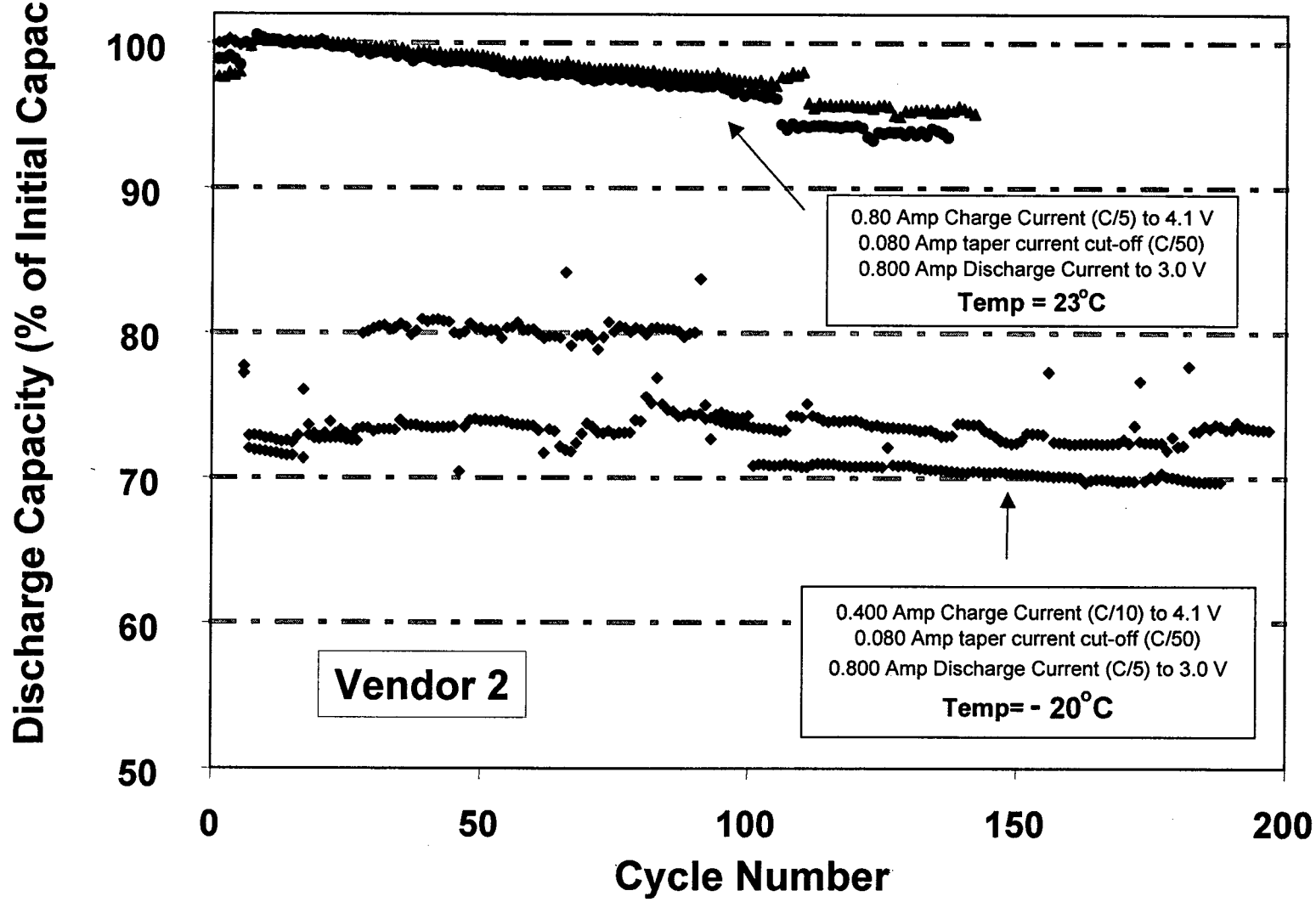

Lithium-Ion Cells (D-Size) for Mars Rover Applications
Cycle Life Performance at Different Temperatures

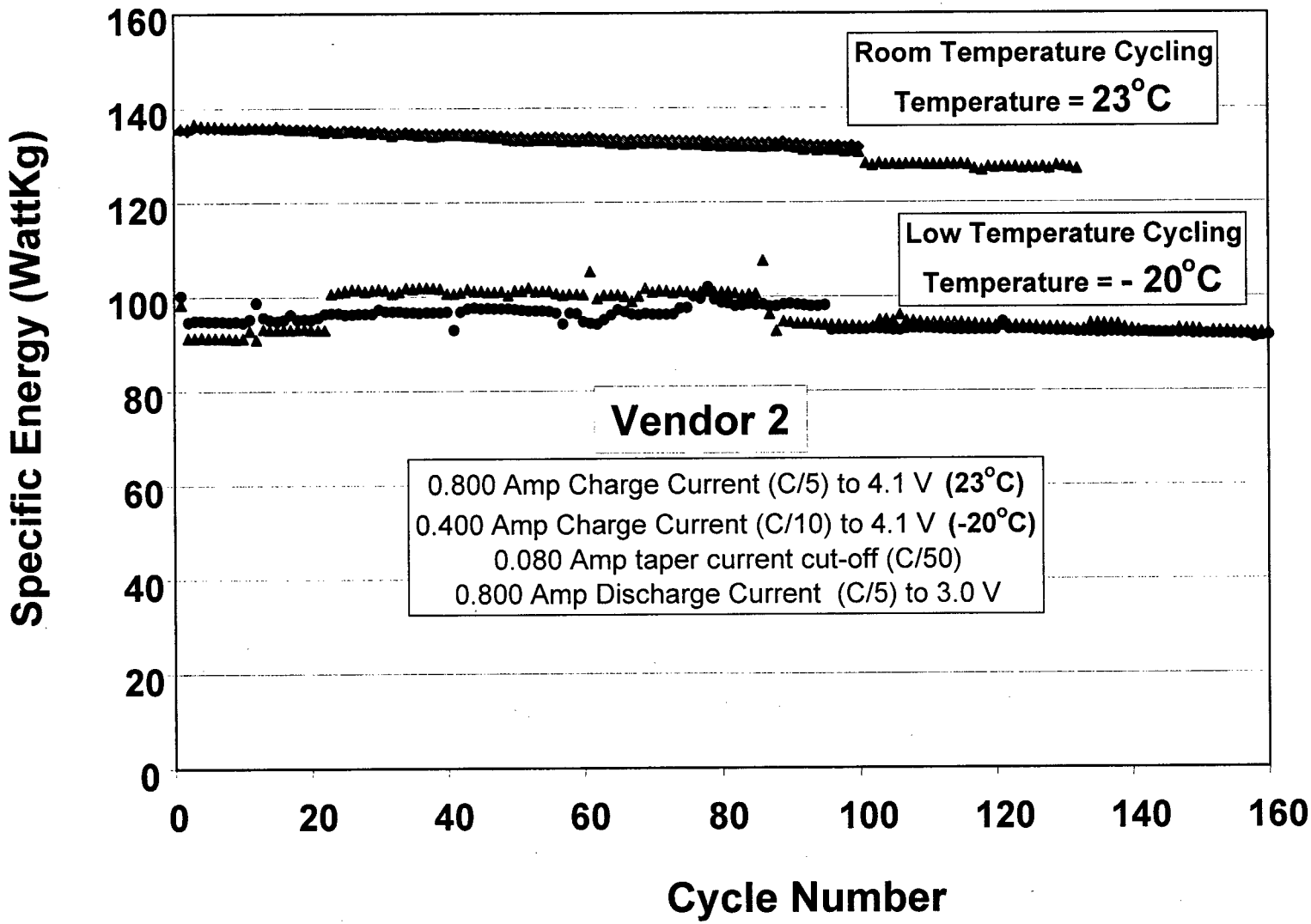

Lithium-Ion Cells (D-Size) for Mars Rover Applications
Cycle Life Performance at Different Temperatures

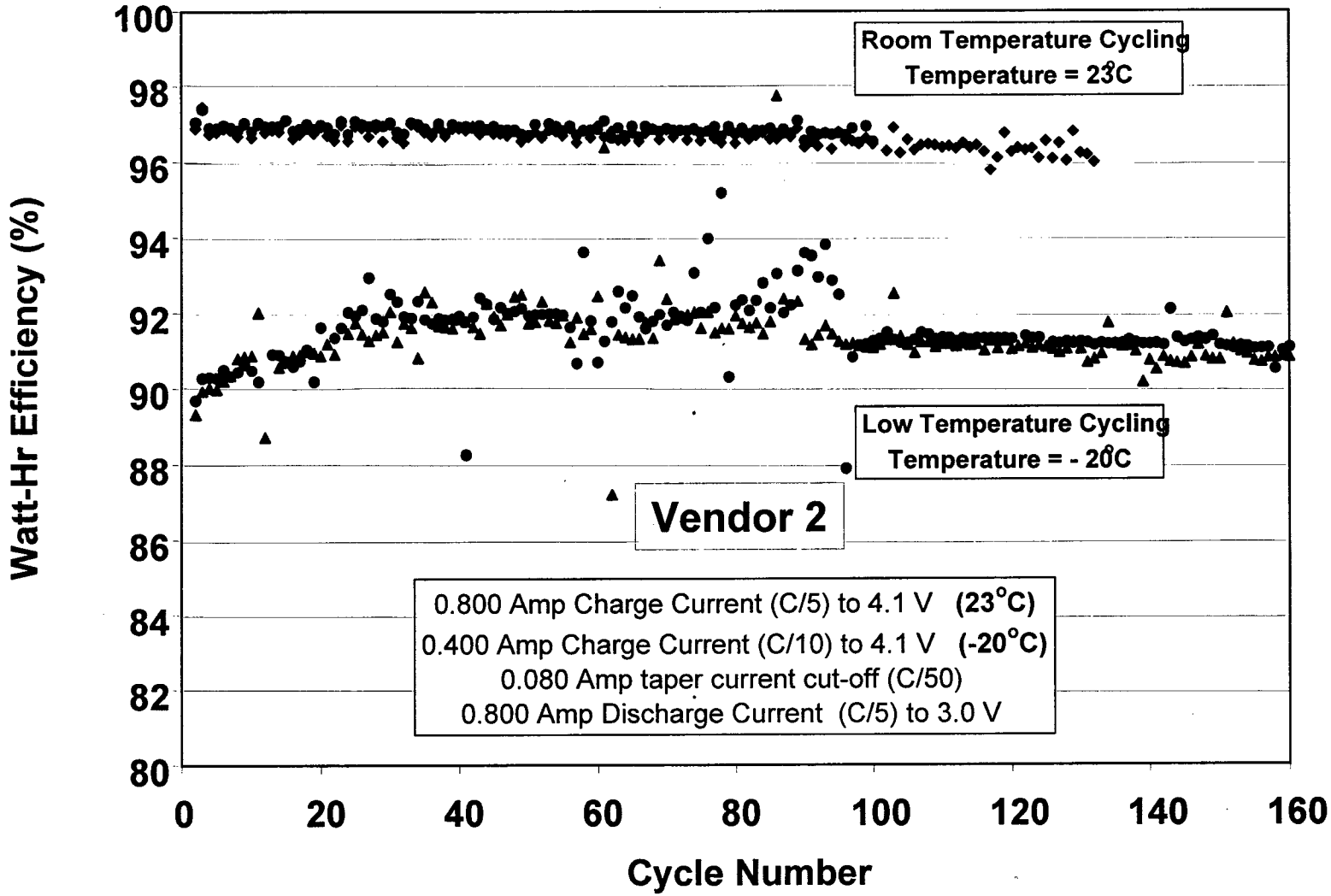

Lithium-Ion Cells (D-Size) for Mars Rover Applications Cycle Life Performance at Different Temperatures

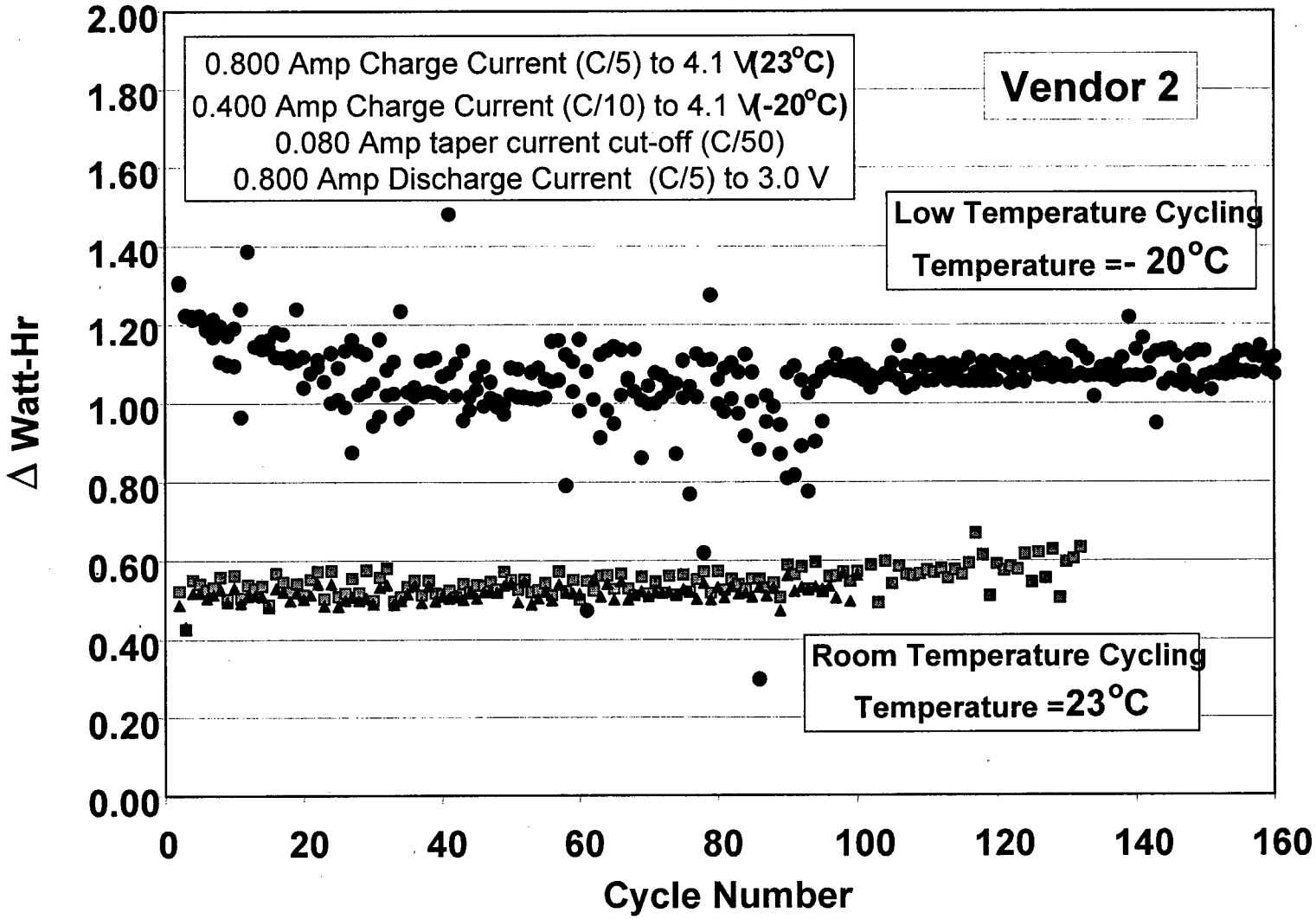

Prismatic Lithium-Ion Cells (5Ahr) for Mars Rover Applications
Cycle Life Performance at Different Temperatures

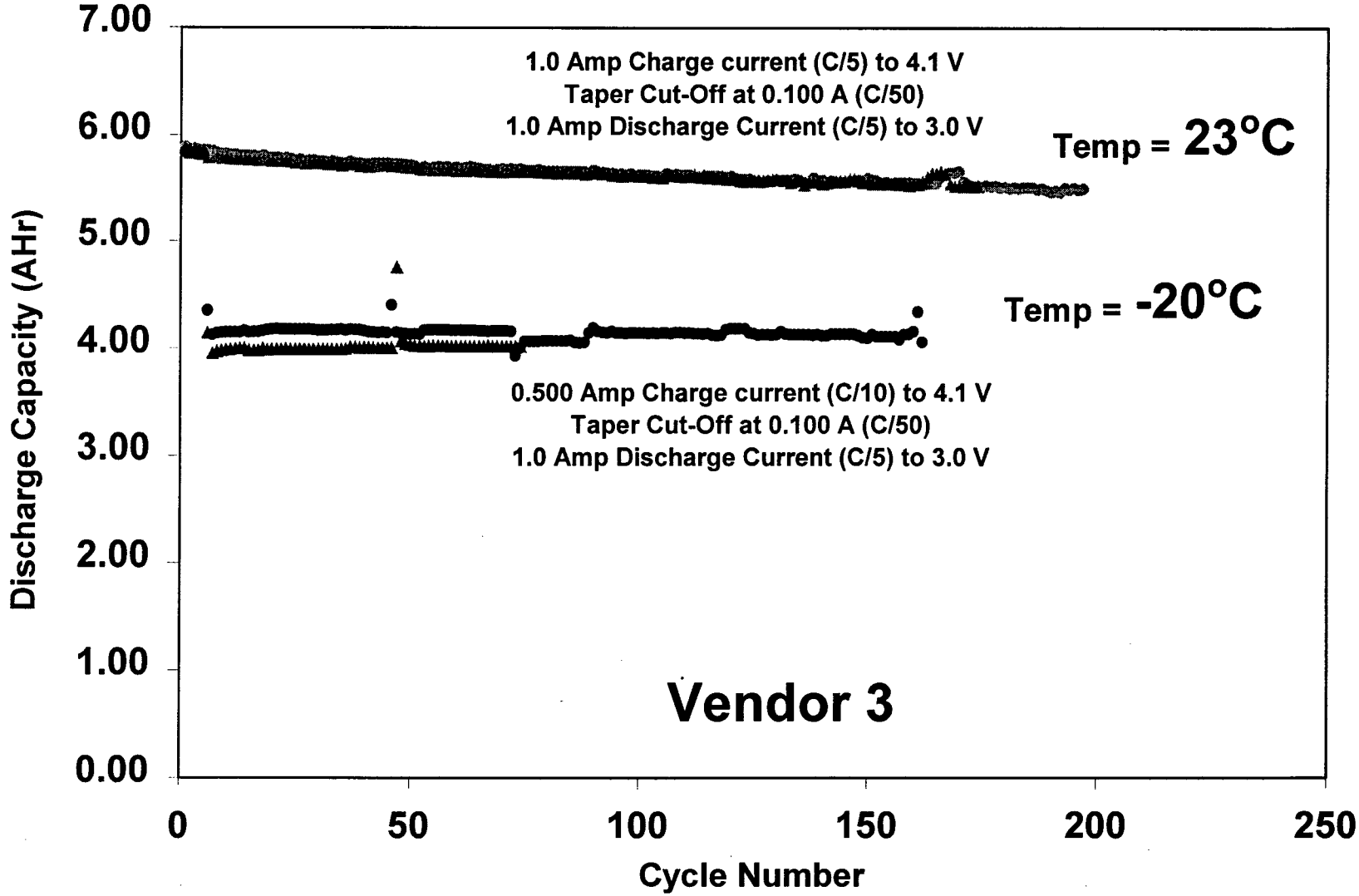

Prismatic Lithium-Ion Cells (5Ah) for Mars Rover Applications
Cycle Life Performance at Different Temperatures

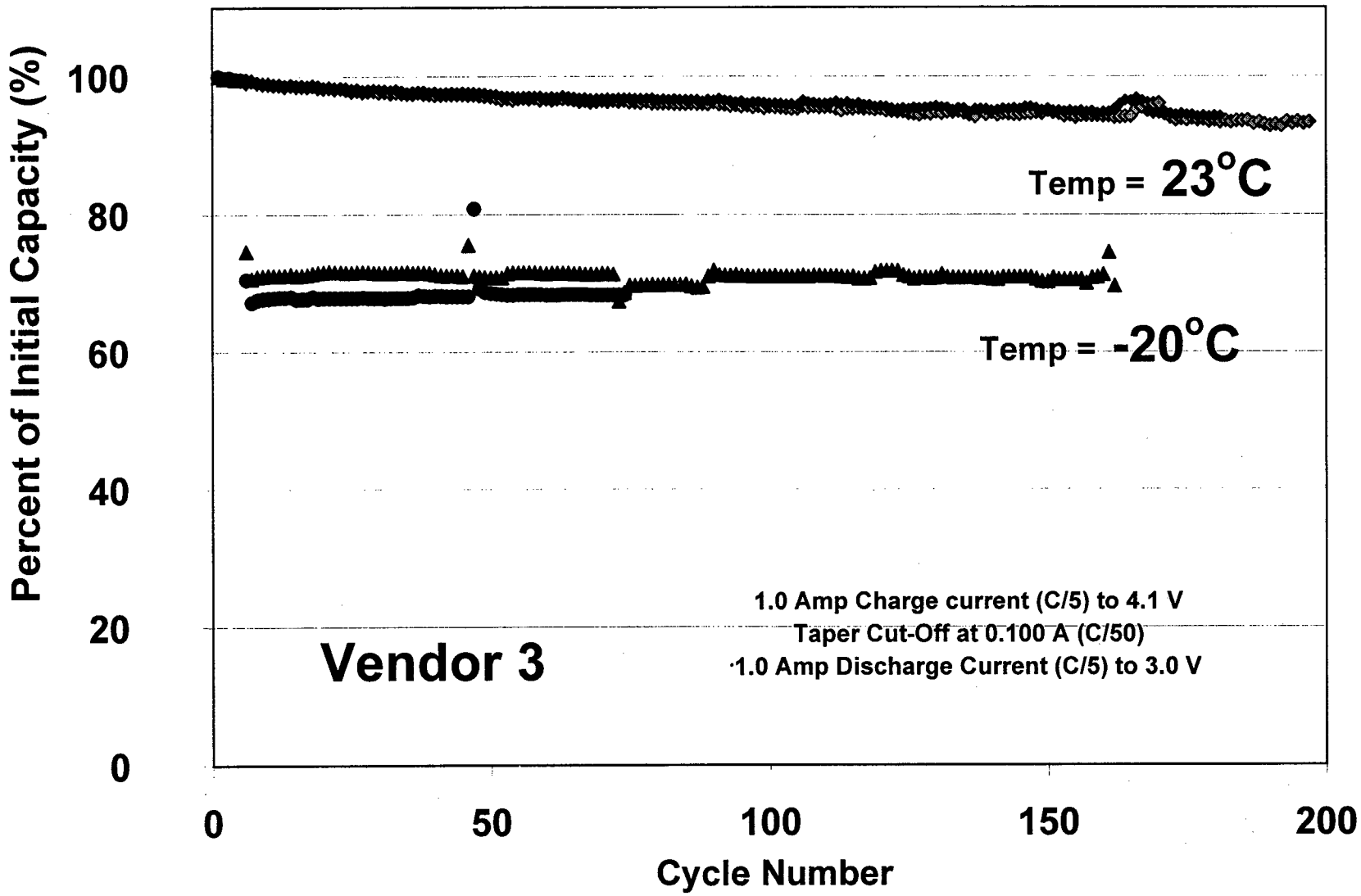

Prismatic Lithium-Ion Cells (5Ah) for Mars Rover Applications
Cycle Life Performance at Different Temperatures

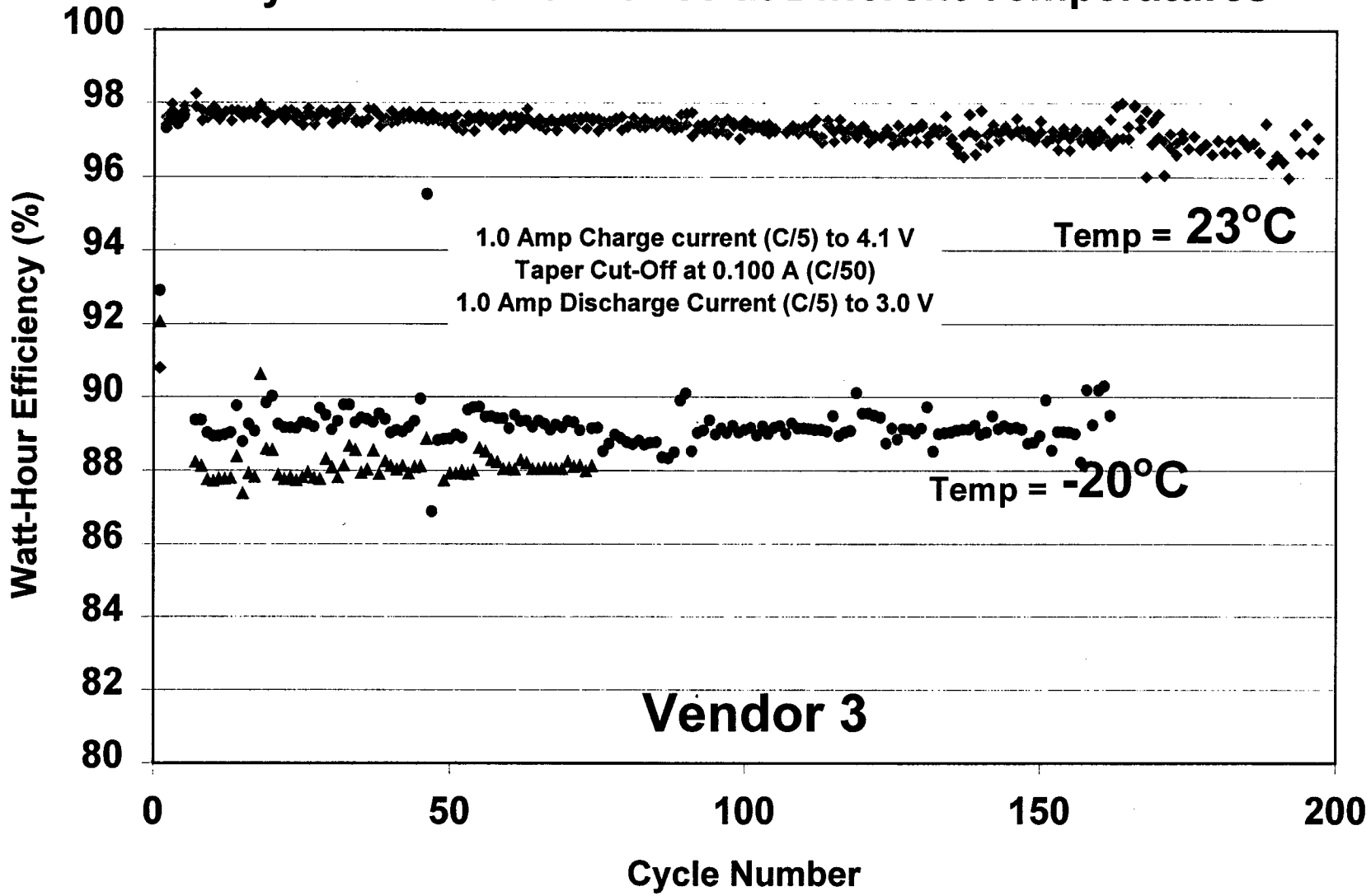

Prismatic Lithium-Ion Cells (5Ahr) for Mars Rover Applications
Cycle Life Characteristics at Different Temperatures

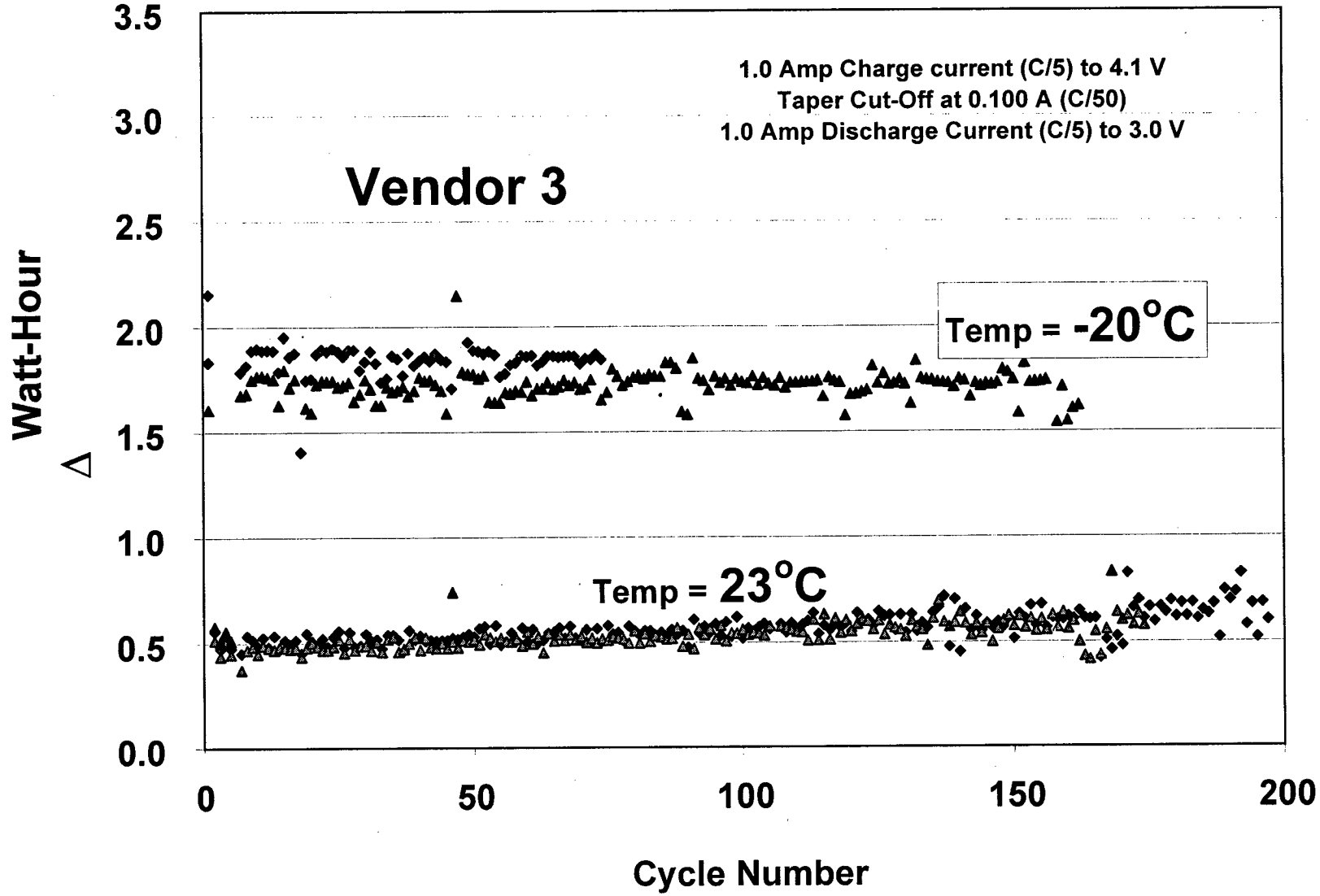

Prismatic Lithium-Ion Cells (5Ahr) for Mars Rover Applications
Cycle Life Characteristics

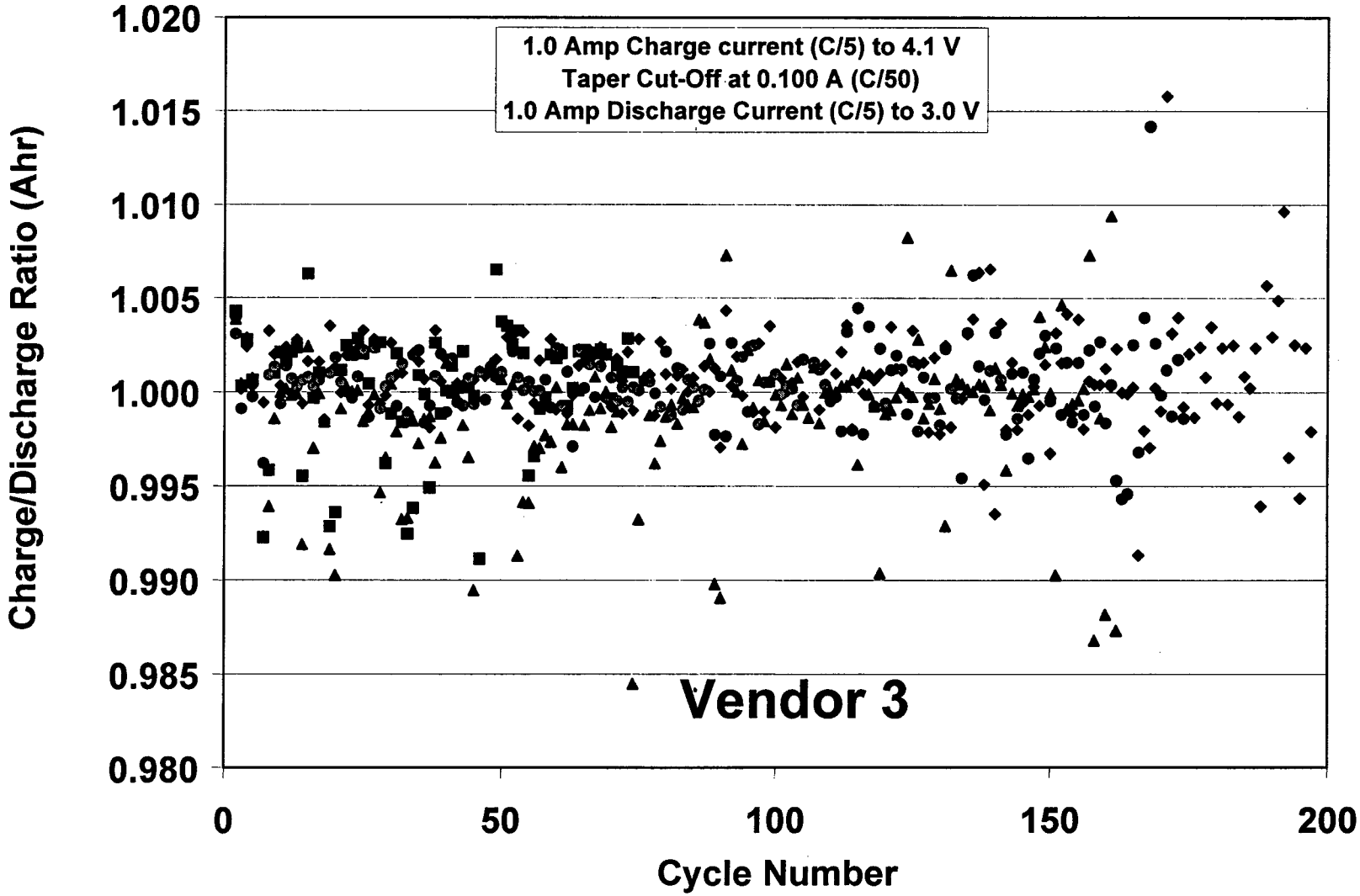

DD-Size Lithium-Ion Cells for Mars Rover Applications
Cycle Life Characteristics at Different Temperature (Gen I)

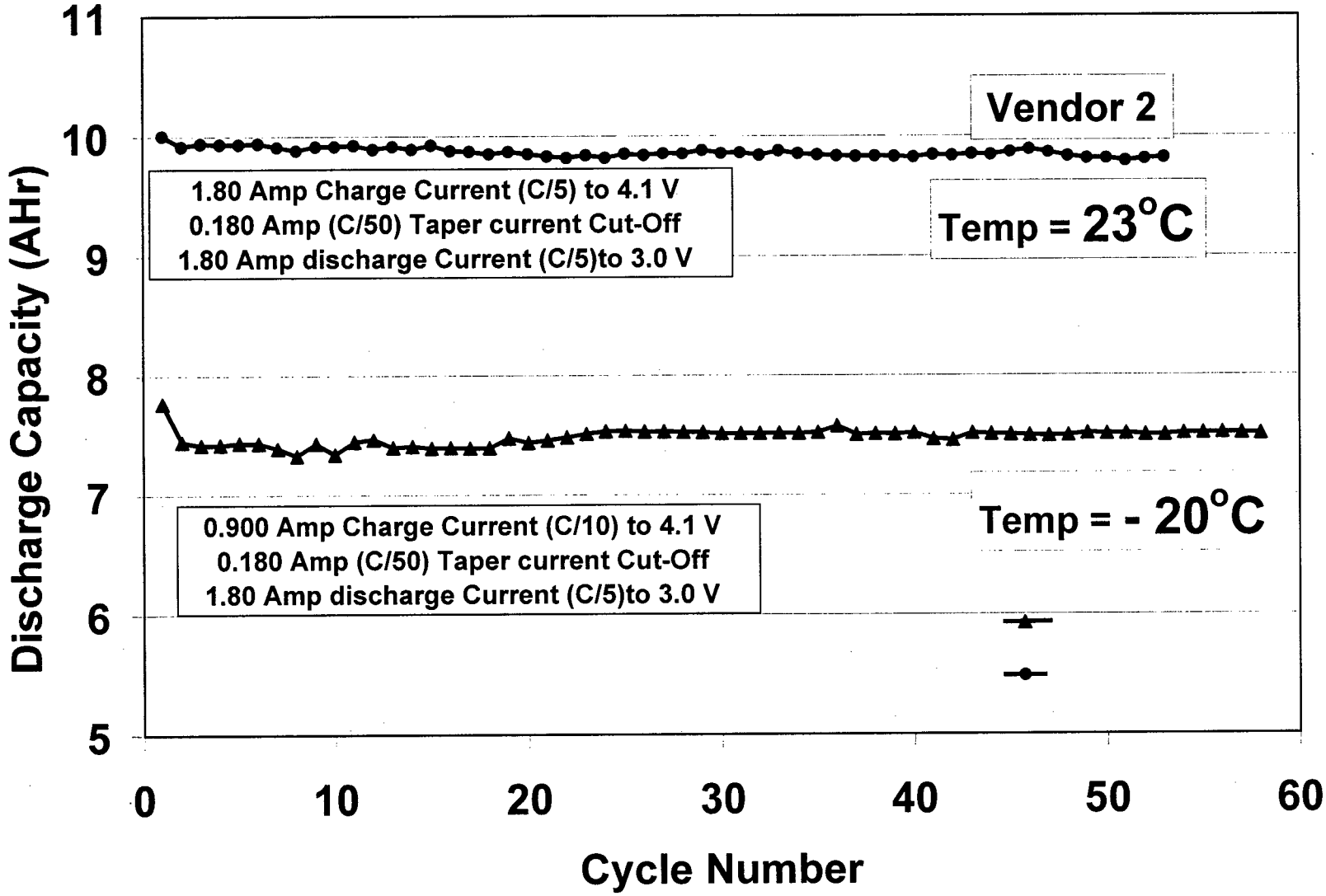

Rate Characterization Tests

Approach:

- Range of charge and discharge rates (C/2, C/3.3, C/5 and C/10)
- Range of temperatures investigated (-20, 0, 23, 40°C)
- Pulse capability (40 and 60A)

Cell Performance Aspects

- Discharge/charge capacity (Ah)
- Discharge energy (Wh/Kg)
- Watt-hour efficiency (round-trip efficiency)
- Heat generation
- Effect of cell history upon rate capability

Lithium-Ion Cells (D-Size) for Mars Rover Applications
Discharge Capacity at Various Temperatures (C/10 Rate)

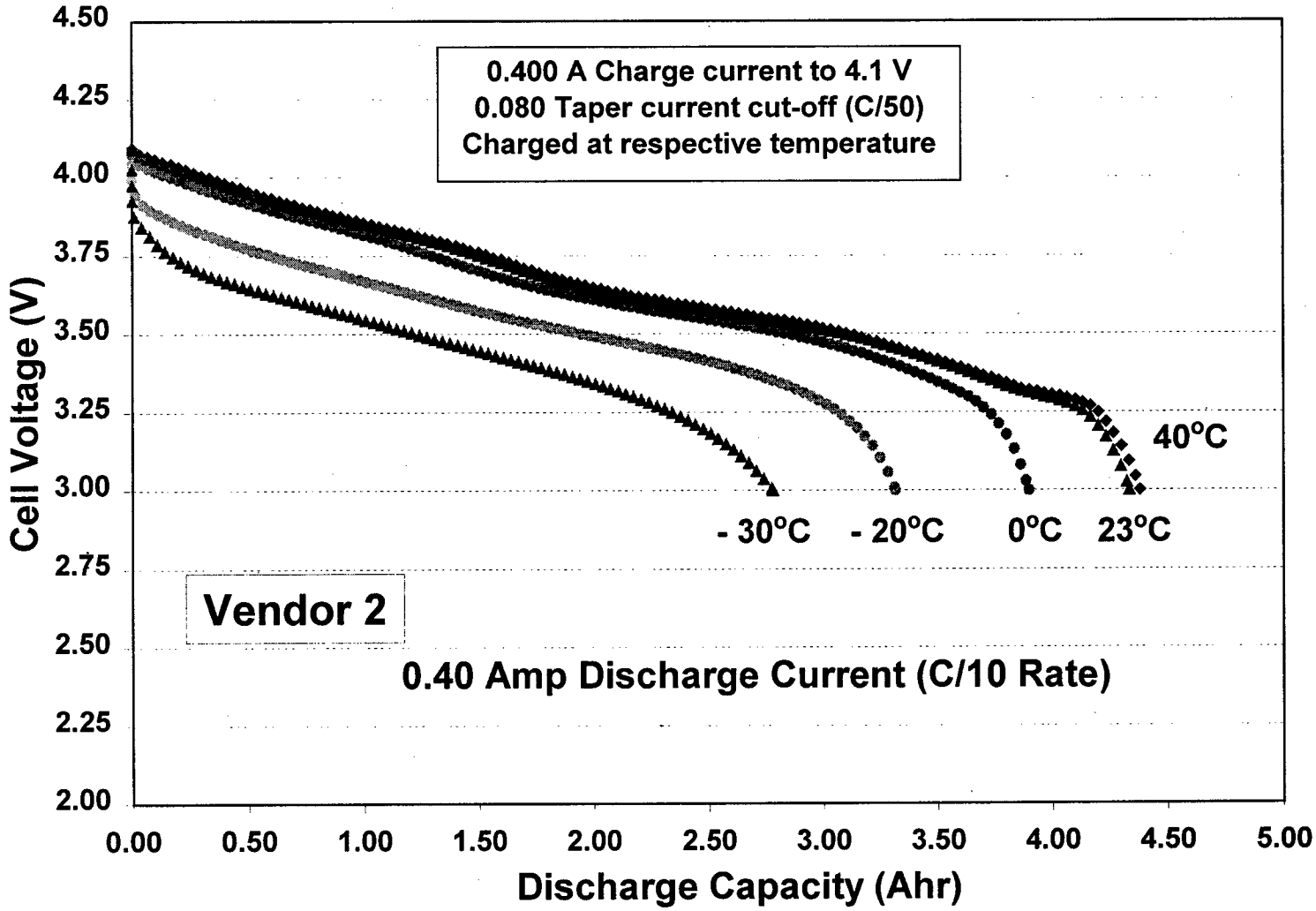

Lithium-Ion Cells (D-Size) for Mars Rover Applications
Discharge Capacity at Various Temperatures (C/2 Rate)

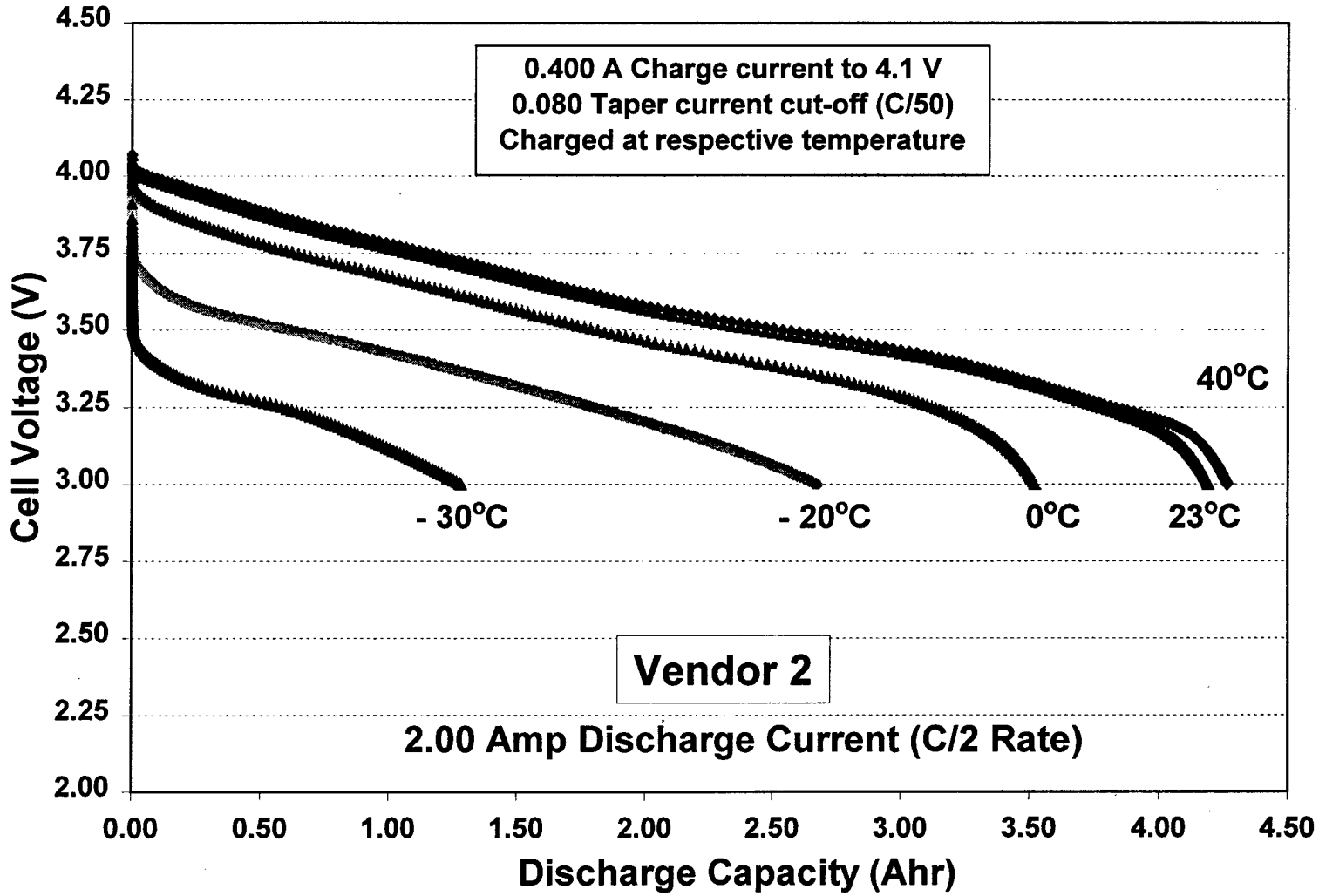

Lithium-Ion Cells (D-Size) for Mars Rover Applications
Discharge Behavior as a Function of Temperature

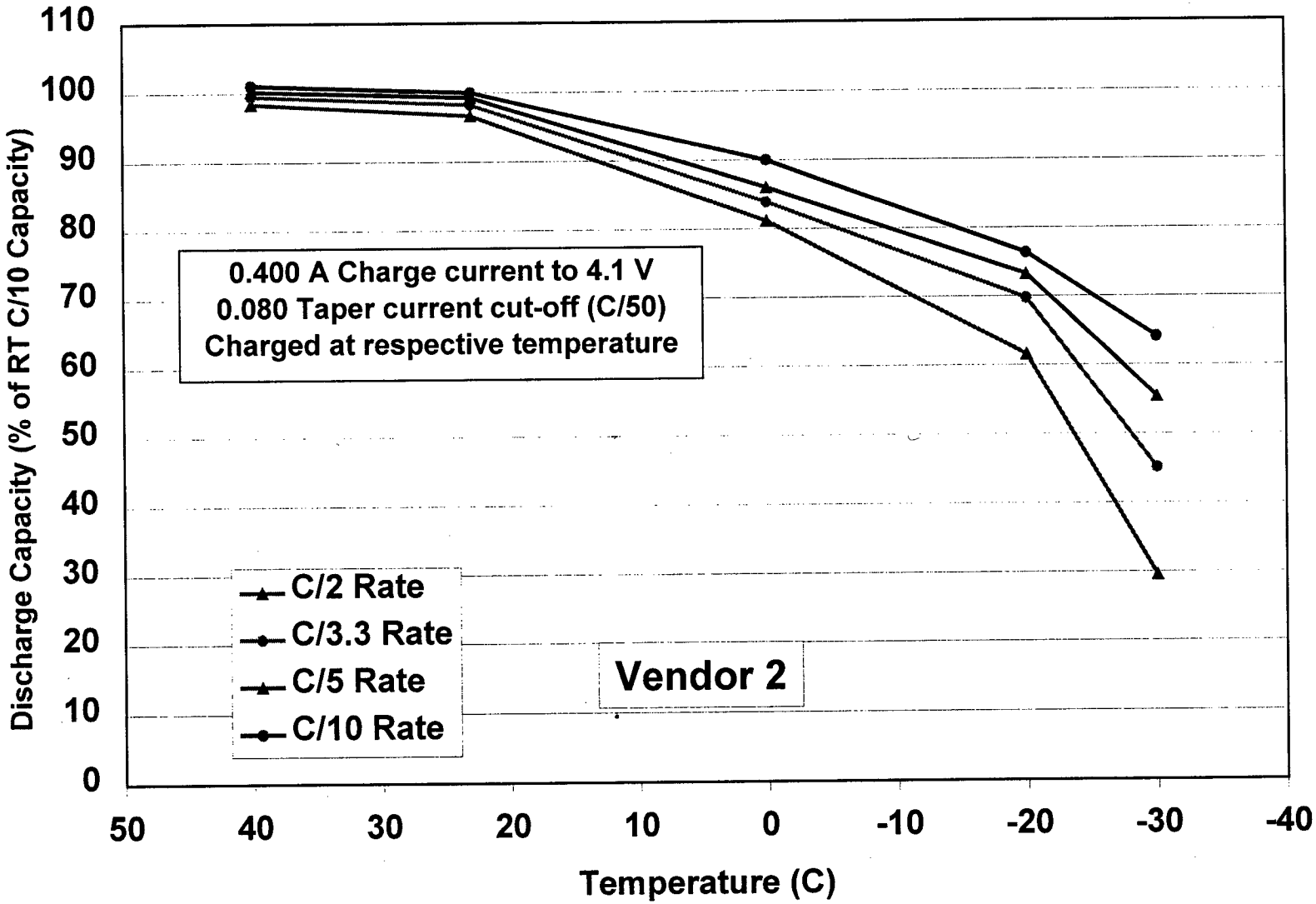

Lithium-Ion Cells (D-Size) for Mars Rover Applications
Specific Energy at Room Temperature

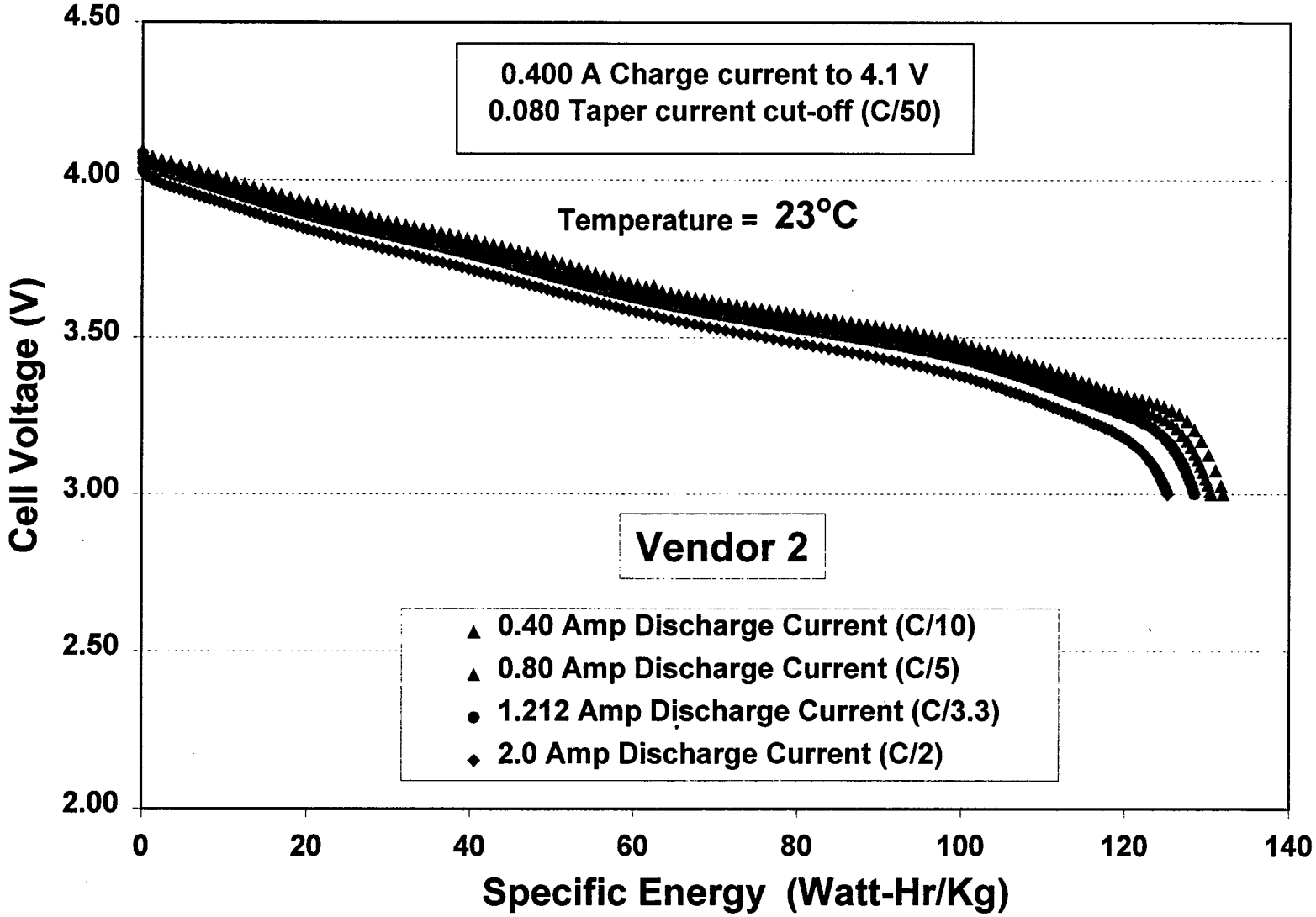

Lithium-Ion Cells (D-Size) for Mars Rover Applications
Specific Energy at High Temperature (40°C)

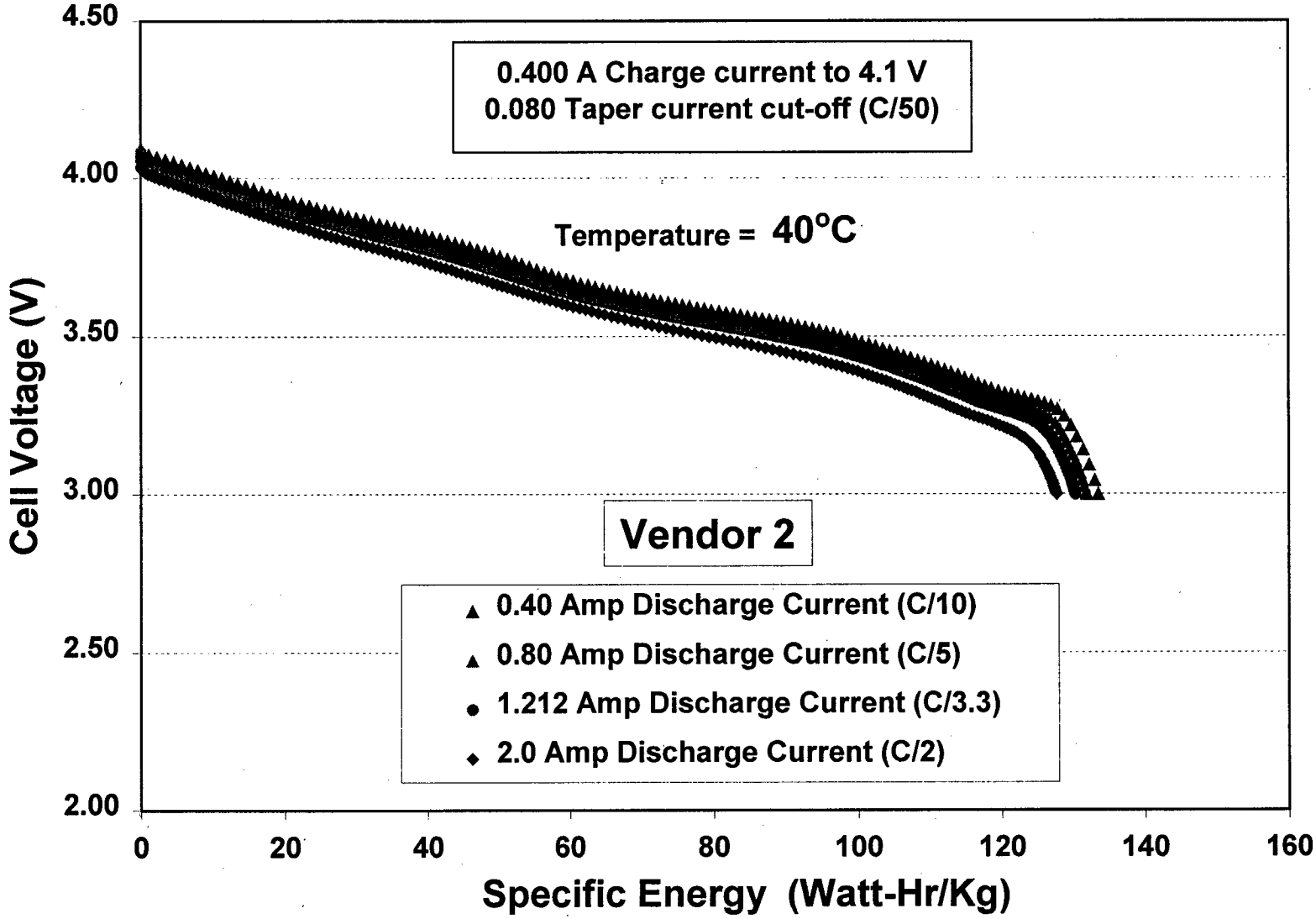

Lithium-Ion Cells (D-Size) for Mars Rover Applications
Discharge Characteristics at Low Temperature (-20°C)

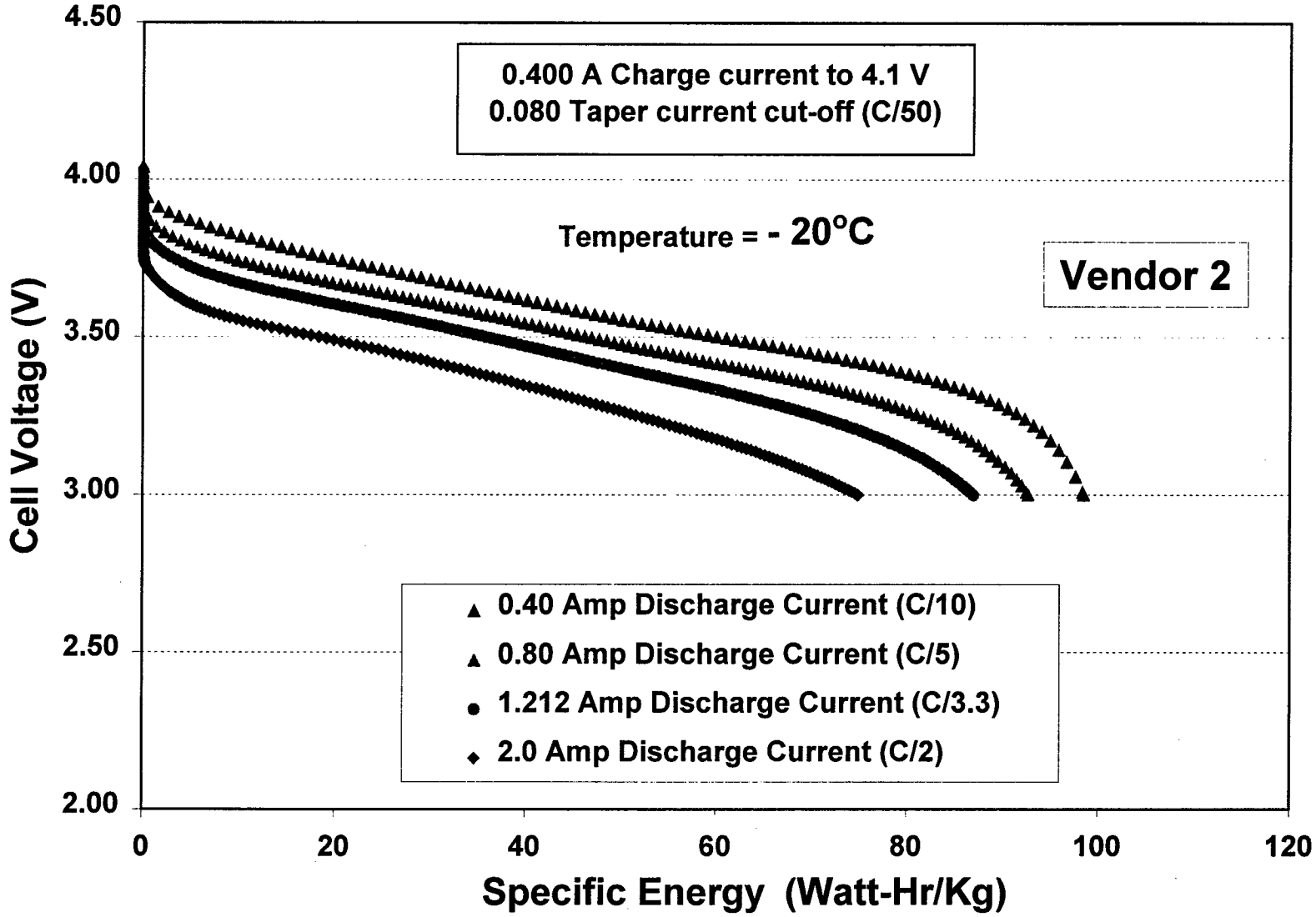

Lithium-Ion Cells (D-Size) for Mars Rover Applications Discharge Characteristics at Low Temperature (-30°C)

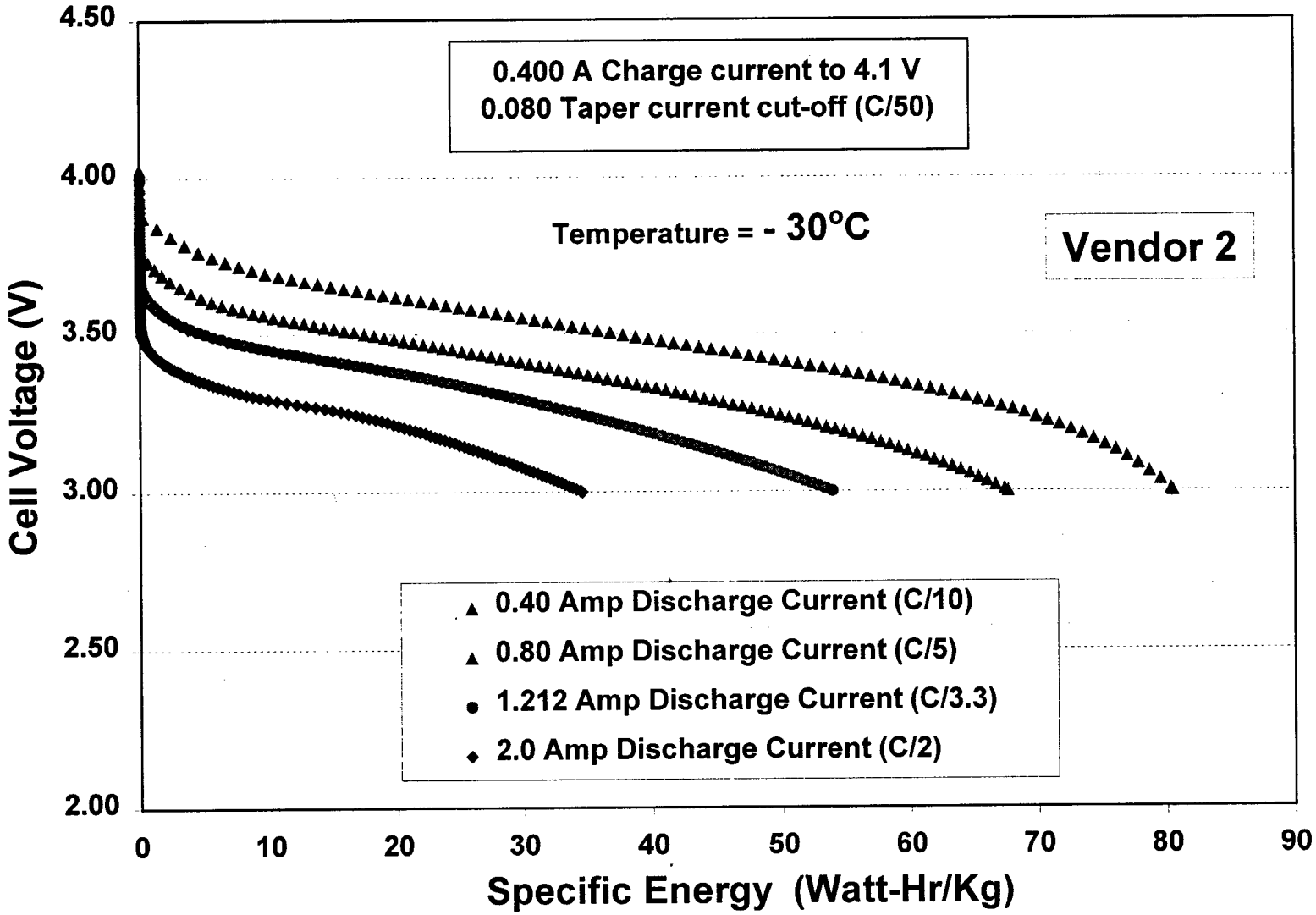

Lithium-Ion Cells (D-Size) for Mars Rover Applications
Charge Characteristics at Room Temperature

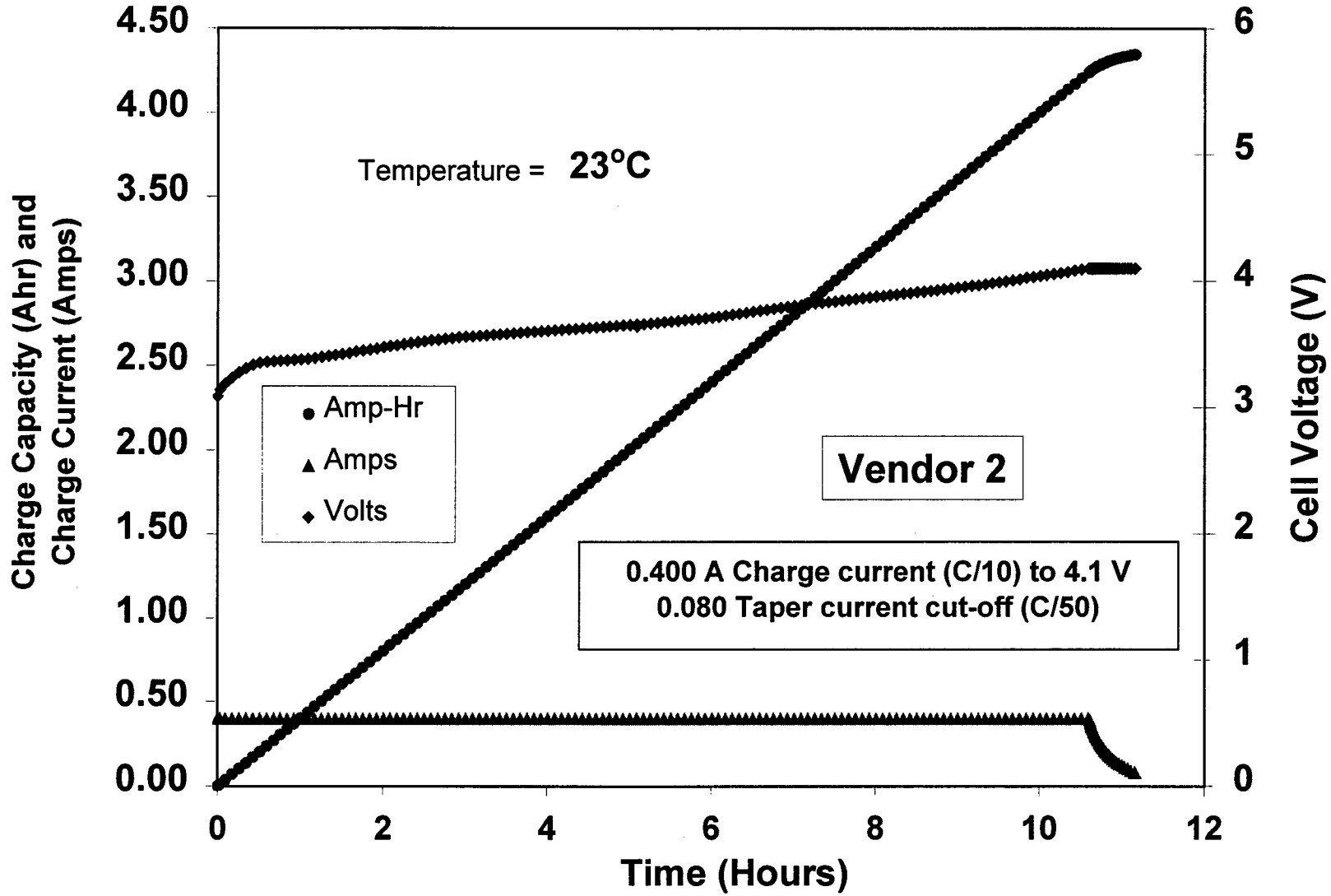

Lithium-Ion Cells (D-Size) for Mars Rover Applications
Charge Characteristics at Low Temperature (-20°C)

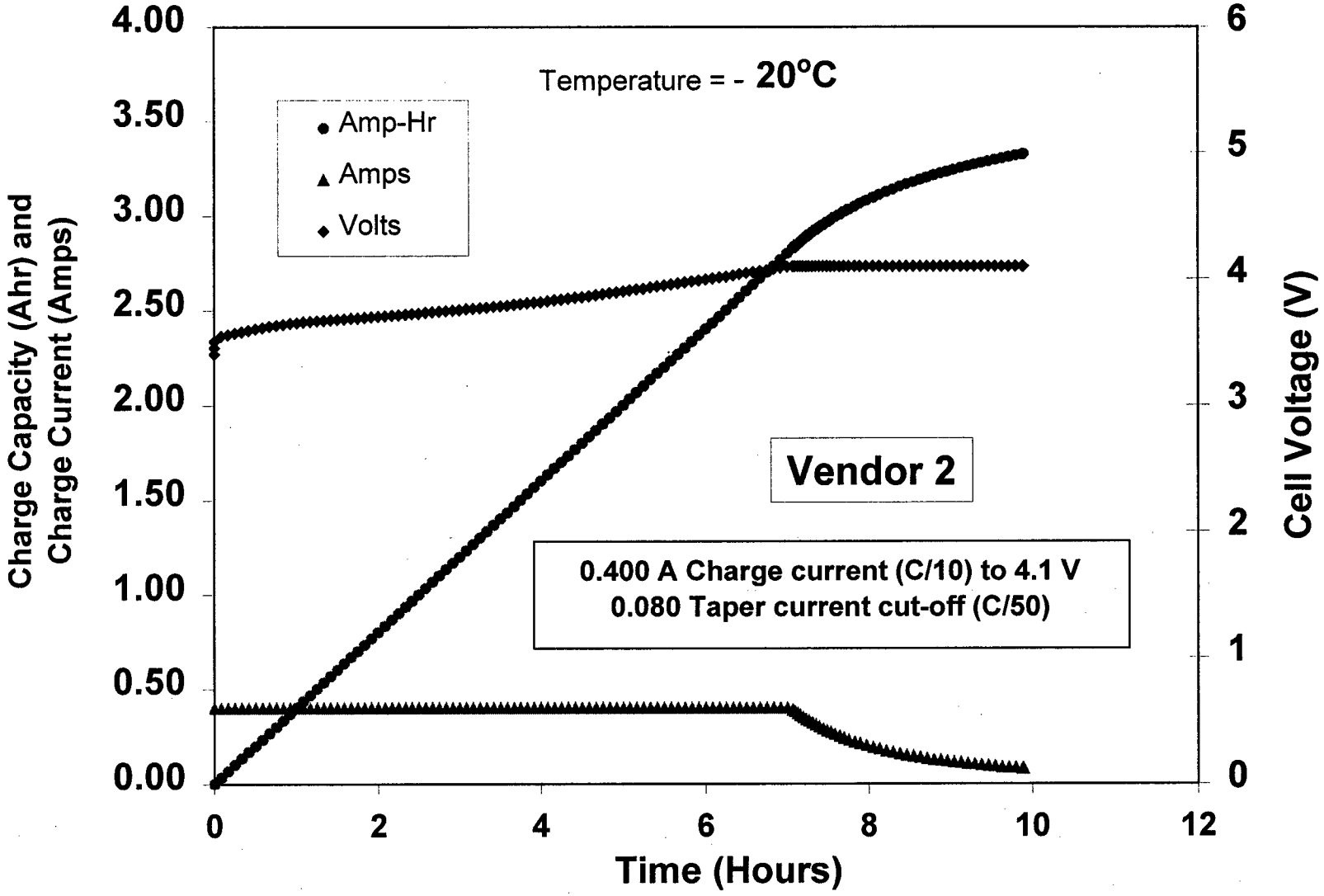

Lithium-Ion Cells (D-Size) for Mars Rover Applications
Charge Characteristics at Low Temperature (-30°C)

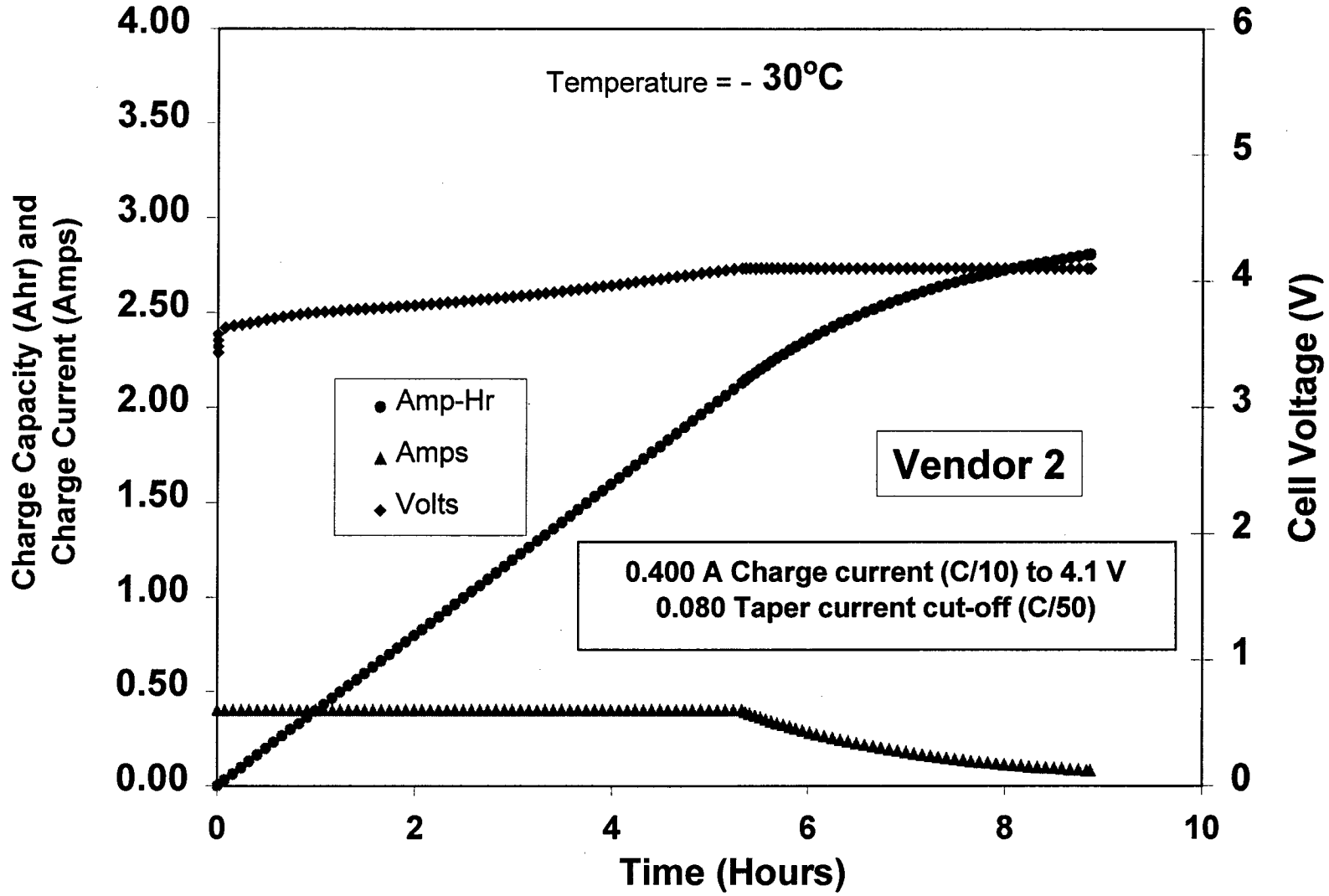

Lithium-Ion Cells for 2003 MSR Athena Rover

Capacity Retention Characterization Tests

Approach:

- Identify optimum storage conditions
- Quantify performance degradation due to storage
  - 2 Month storage test (0 and 40°C, 50 and 100% SOC)
  - 10 Month storage test (0 and 40°C, 50 and 100% SOC)

Performance Evaluation Criteria:

- Permanent loss of reversible capacity
- Self-Discharge of stored capacity
- Impact upon low temperature performance

Lithium-Ion Cells for Mars Surveyor 2001 Lander

Design Experiments for Cruise Conditions

Experiment #	Storage time, weeks	Storage Temp	State of charge	Storage condition
1	2	25	50	Open Circuit
2	2	40	70	On Buss
3	2	55	100	Cycling
4	4	25	70	Cycling
5	4	40	100	Open Circuit
6	4	55	50	On Buss
7	6	25	100	On Buss
8	6	40	50	Cycling
9	6	55	70	Open Circuit

JPL

Parametric Storage Studies

Effect of Temp on Permanent capacity loss

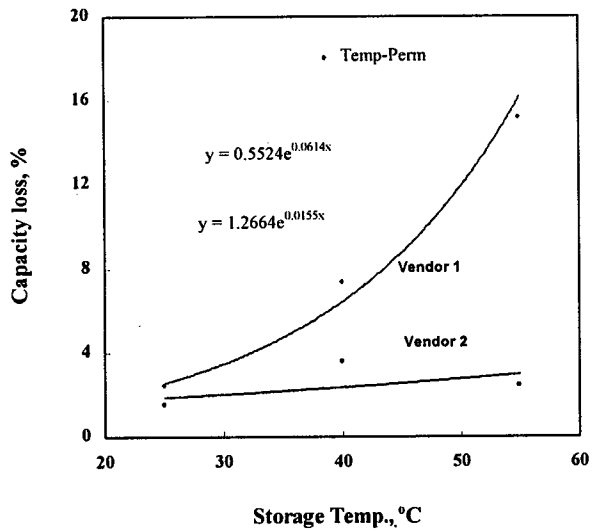

Effect of Time on Permanent capacity loss

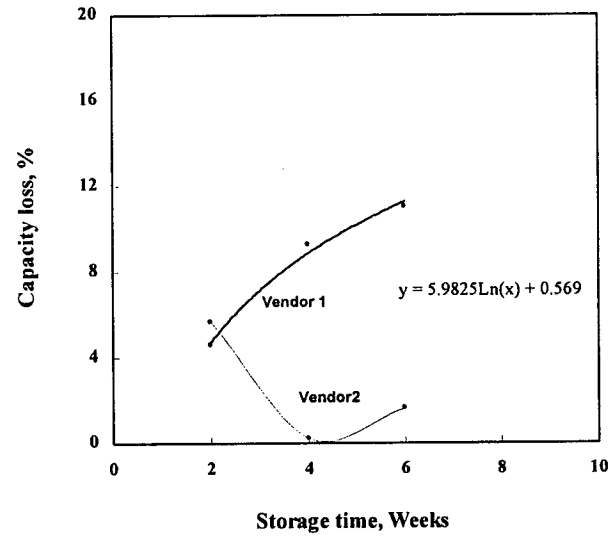

Effect of SOC on Permanent capacity loss

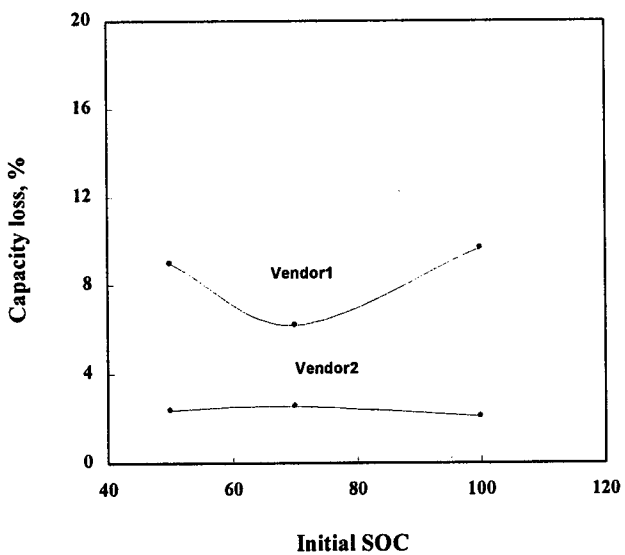

Effect of Storage mode on Permanent Capacity loss

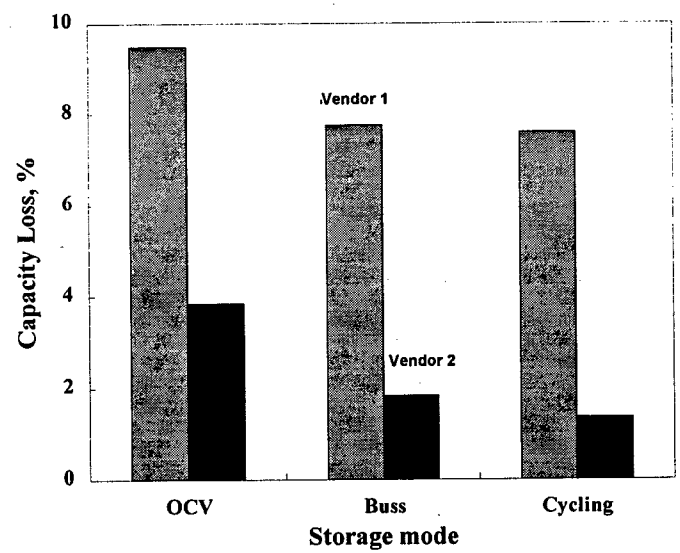

SUMMARY

- **Lithium ion cells of capacity 4-7 Ah, fabricated in U.S and being tested for 2003 Mars Rover mission at JPL under the NASA-DoD joint effort have shown**
  - **Excellent cycling characteristics at RT and LT**
  - **Improved low temperature performance and**
  - **Good storage characteristics during cruise**
- **Low temperature performance after frequent exposure to high temperatures and long storage is yet to be established.**
- **Optimum storage conditions for battery during cruise needs to be identified.**

Acknowledgments

The work described here was carried out at the Jet Propulsion Laboratory (JPL), California Institute of Technology, for the 2003 **Mars Sample Return Athena Rover and NASA Code S Battery Programs** under contract with the National Aeronautics and Space Administration (NASA).

EAGLE PICHER Technologies, LLC

Development of a 70 Ah Li-ion Cell for Aerospace Applications

Jim DeGruson
Advanced Electrochemical Systems Operation
Eagle-Picher Technologies, LLC
3220 Industrial Drive
Joplin, Missouri 64801

POWER Subsystems

EAGLE PICHER Technologies, LLC

Li-Ion Technology Center Joplin, Missouri

- 20,000 ft^2 Total
- 15,000 ft^2 Mfg.
- 5,000 ft^2 Office
- Stand-alone Facility

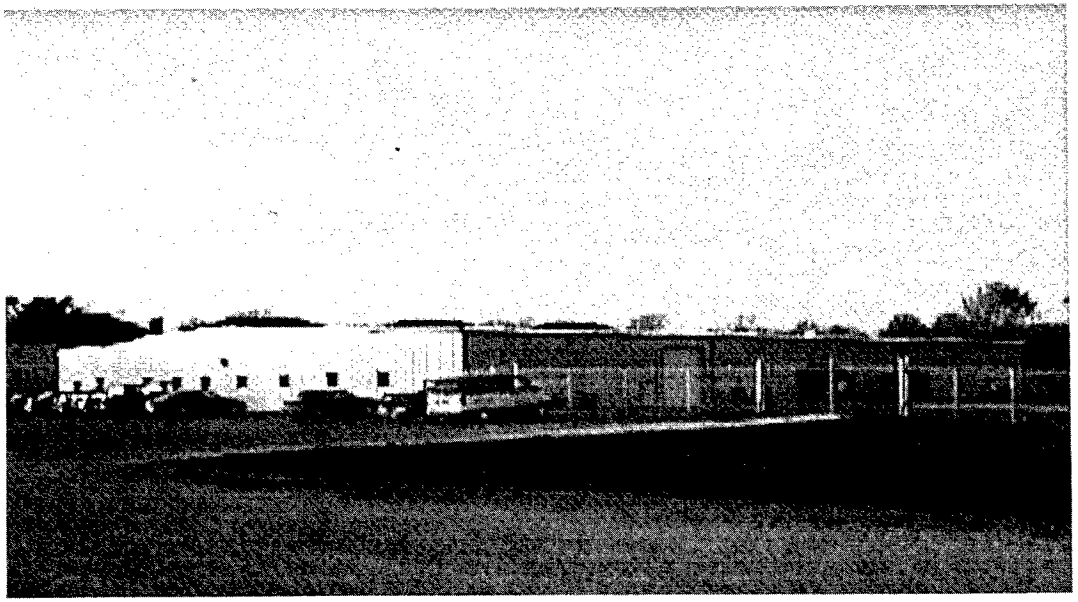

POWER Subsystems

EAGLE PICHER Technologies, LLC

Lithium-Ion Test Area

- 300 cell capability
- 35 battery capability
- 200 amps
- 40 volts
- - 65°C to + 85°C

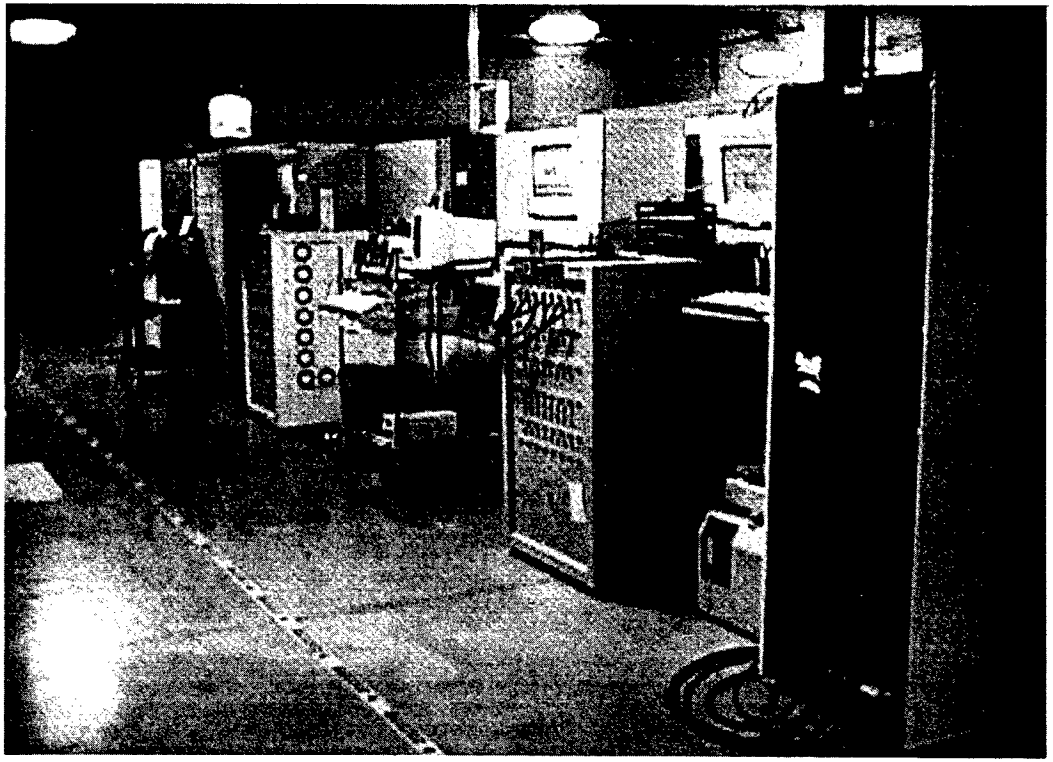

POWER Subsystems

EAGLE PICHER Technologies, LLC

LEO Test Regime

- **Charge: 35 A - 60 min.**
  - No Taper Charge
  - Cut-off of 4.1 volts
- **Discharge: 70 A- 30 min.**
  - Cut-off of 3.0 volts
- **Temp. Stabilization**
  - 5 temperatures
  - 20 cycles/temperature
- **Pulse Tests**
  - ±10A, ±20A, & ±40A

POWER Subsystems

EAGLE PICHER Technologies, LLC

Li-Ion Aerospace Design

- SLC-16020 cell
- 66 Ah nameplate
- Size: 6.69" x 8.63" x 1.06"
- 3 cells in initial group
- 2 cells @ temperature range, 1 cell as control unit

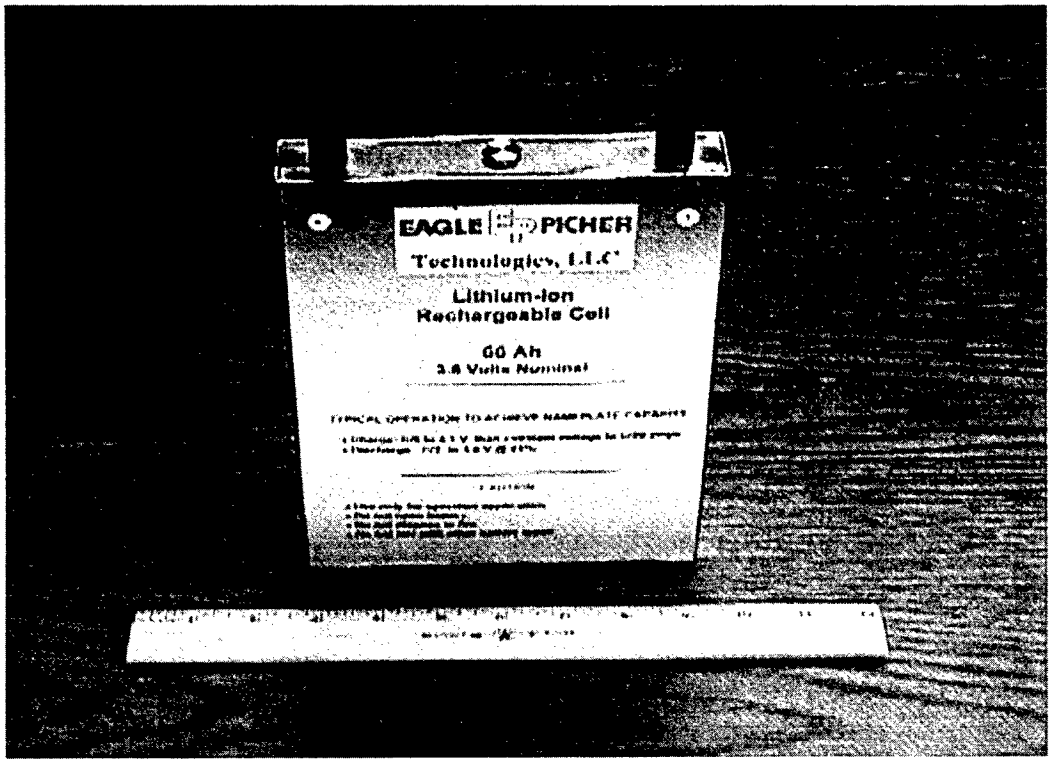

POWER Subsystems

EAGLE PICHER Technologies, LLC

Cell Construction

- Riveted header/tab
- 6 3/8" by 7 1/2" electrodes
- Ambient temperature electrolyte
- Conservative approach

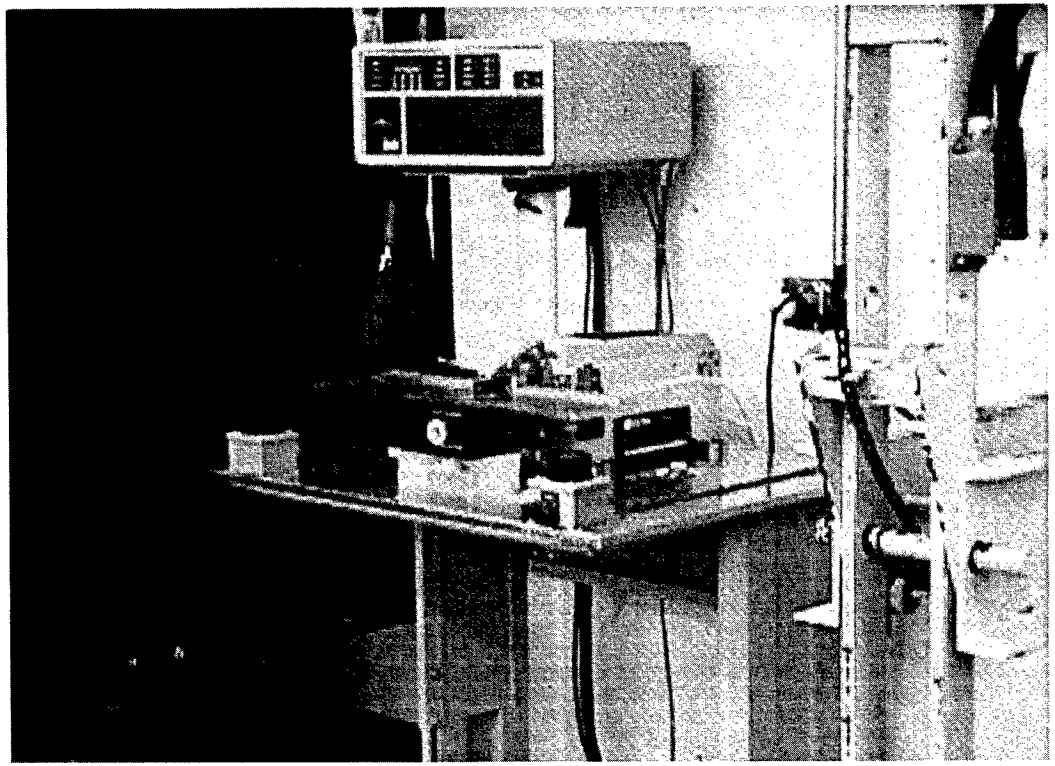

EAGLE PICHER Technologies, LLC

Typical Charge/Discharge @ + 23°C

- **23°C Performance**
  - Charge Capacity: 35.01 Ah
  - Discharge Capacity: 34.90 Ah
  - Full capacity achieved on LEO cycle

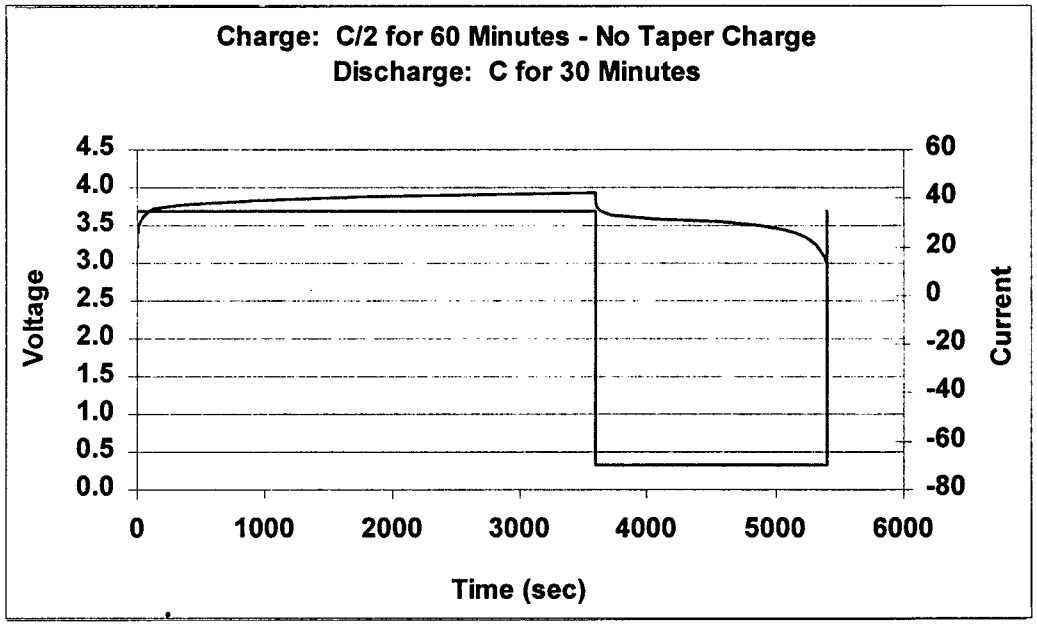

POWER Subsystems

EAGLE PICHER Technologies, LLC

Typical Charge/Discharge @ + 10°C

- **10°C Performance**
  - Charge Capacity: 35.01 Ah
  - Discharge Capacity: 34.83 Ah
  - Achieved full capacity on LEO cycle

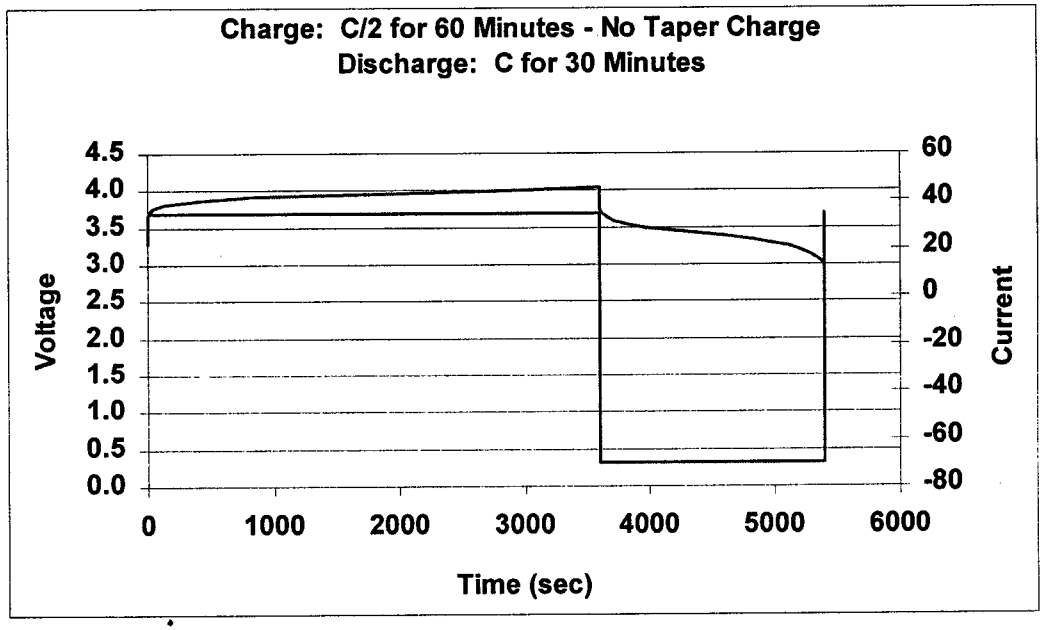

POWER Subsystems

EAGLE PICHER Technologies, LLC

Pulse Test Data @ 10°C

- Impedance measurement conducted during charge and discharge

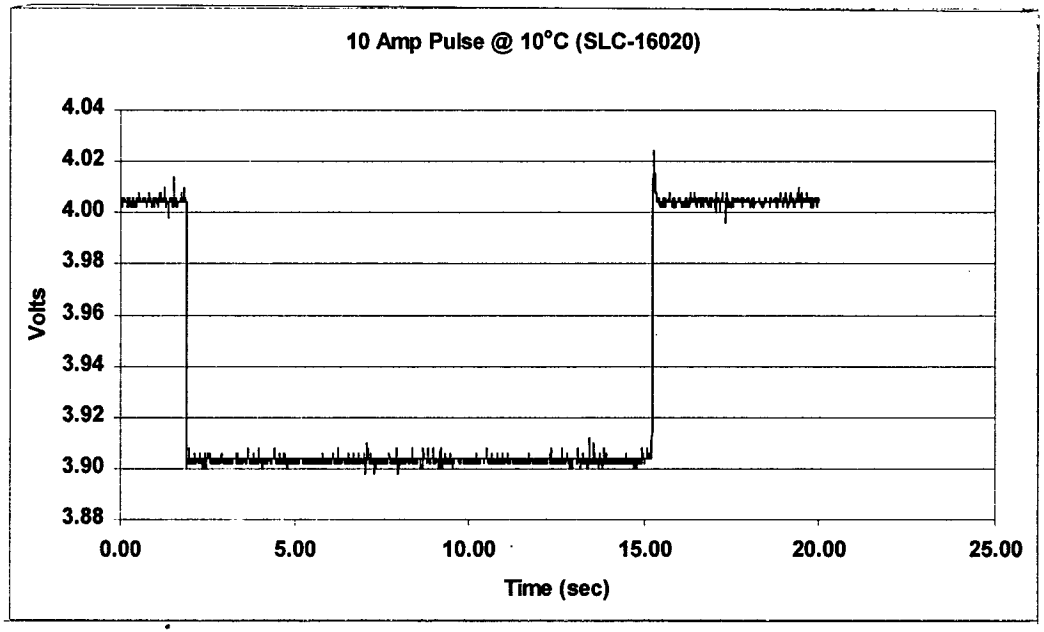

POWER Subsystems

EAGLE PICHER Technologies, LLC

Pulse Test Data @ 10°C

- 10 amp pulse
- Rise time approx. 0.00004

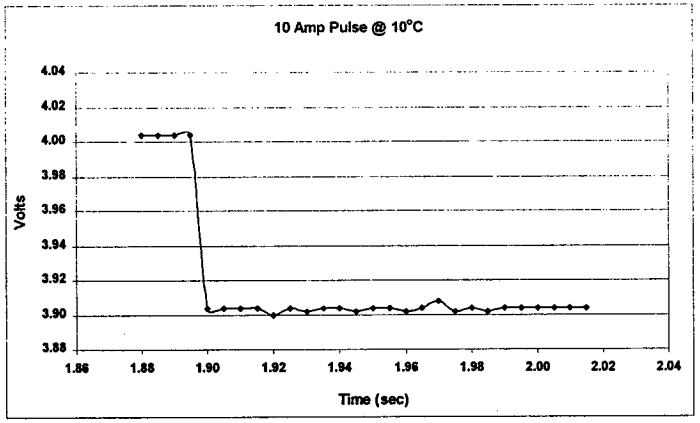

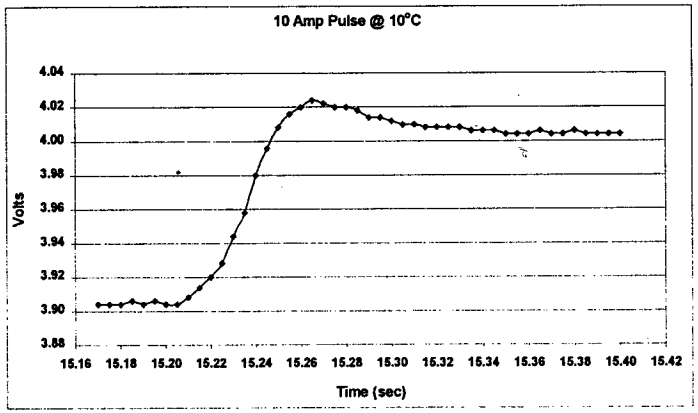

POWER Subsystems

EAGLE PICHER Technologies, LLC

Typical Charge/Discharge @ + 5°C

- **5°C Performance**
  - Charge Capacity: 16.22 Ah
  - Discharge Capacity: 16.06 Ah
  - Discharge/Charge Efficiency > 99%
  - Achieved 25% Depth of Discharge

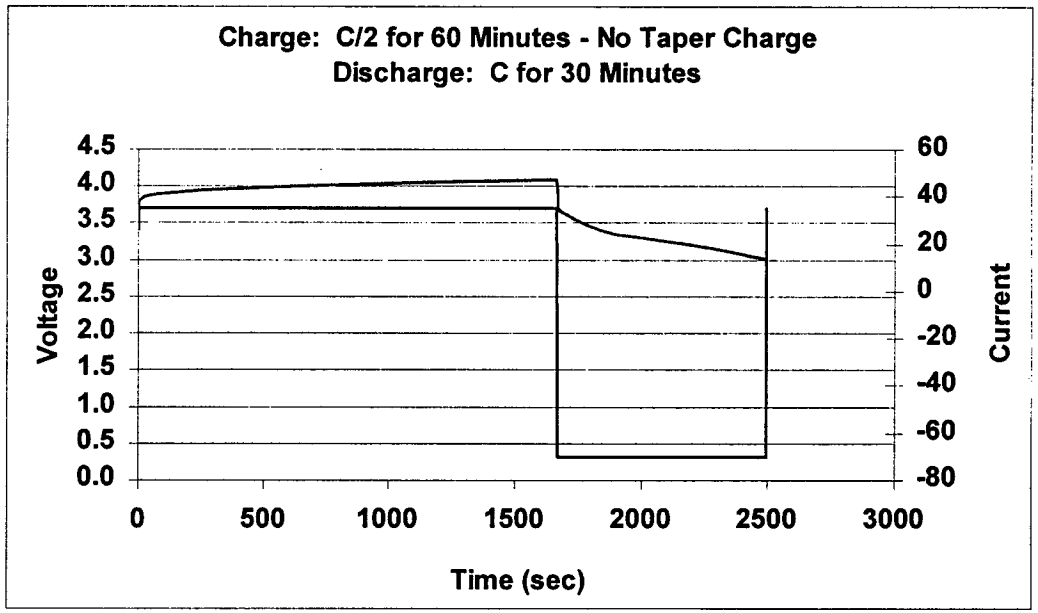

POWER Subsystems

EAGLE PICHER Technologies, LLC

Typical Charge/Discharge @ 0°C

- **0°C Performance**
  - Charge Capacity: 17.20 Ah
  - Discharge Capacity: 16.97 Ah
  - Performance same as 5°C Data:
    - Efficiency >99%
    - Achieved 25% DOD

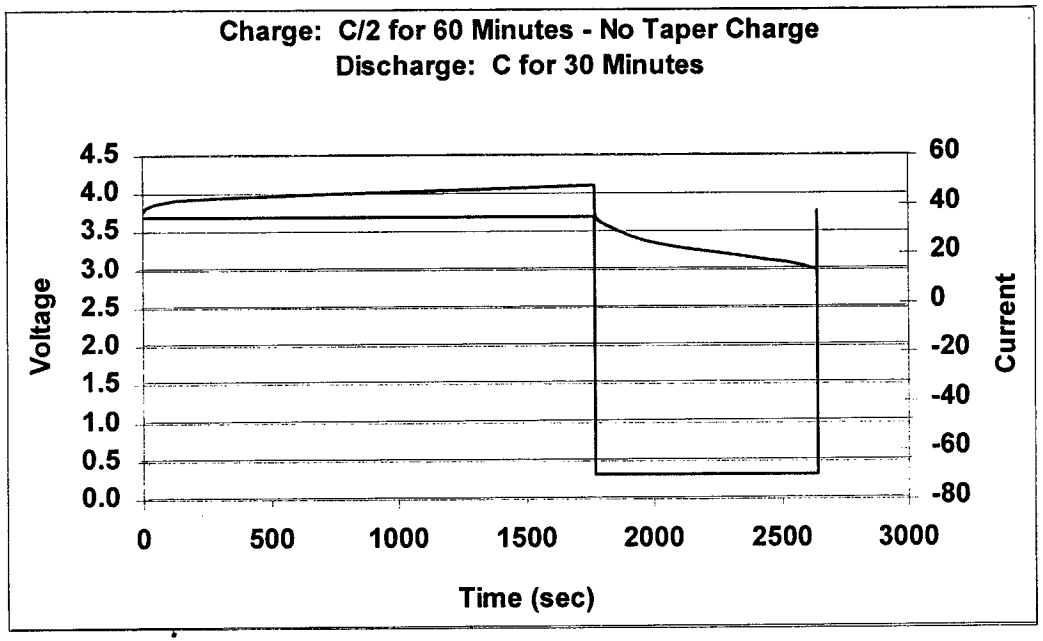

POWER Subsystems

EAGLE PICHER Technologies, LLC

Typical Charge/Discharge @ - 5°C

- **-5°C Performance**
  - Charge Capacity: 17.71 Ah
  - Discharge Capacity: 17.52 Ah
  - Met requirements of LEO test regime

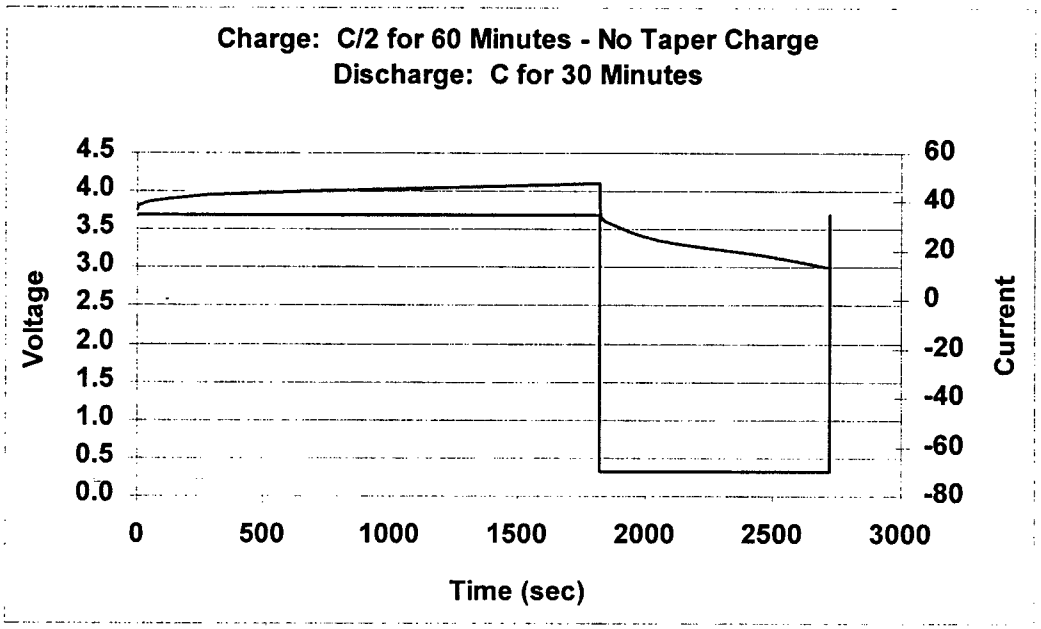

POWER Subsystems

EAGLE PICHER Technologies, LLC

Calculated Impedance

- Control cell 661-002 was subjected to same cycling tests as cells 001 and 003 at a constant temperature of 23°C
- Control cell showed no increase in impedance

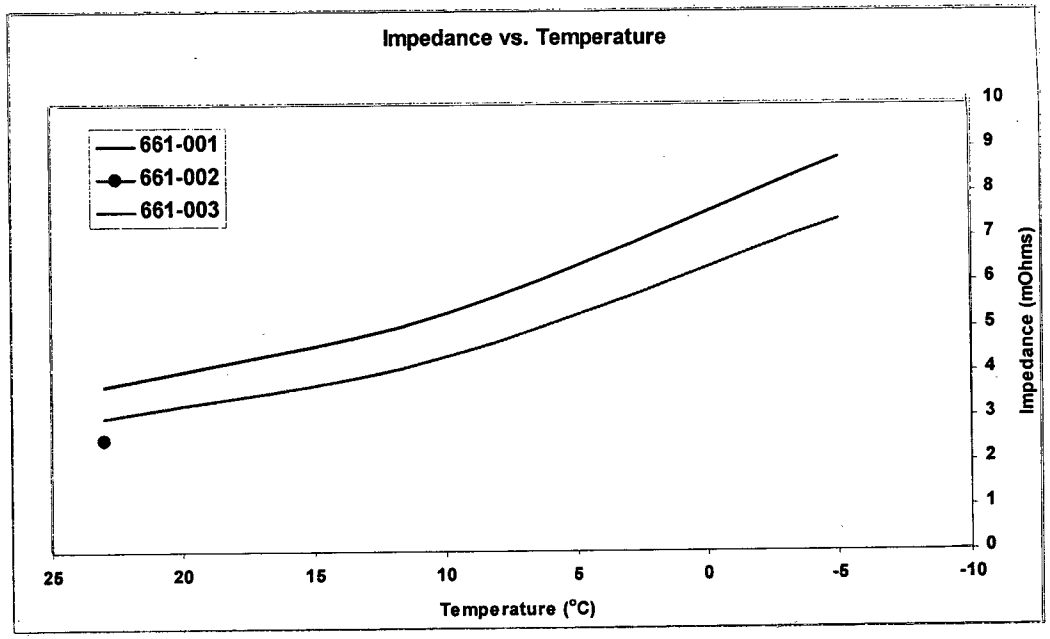

POWER Subsystems

EAGLE PICHER Technologies, LLC

Typical Charge/Discharge for Cell #003 from -5°C to +23°C

- Effects of temperature on cell performance
- From 10°C to 23°C full capacity (50% DOD) at C rate
- From -5°C to +5°C, 25% DOD achieved at C rate

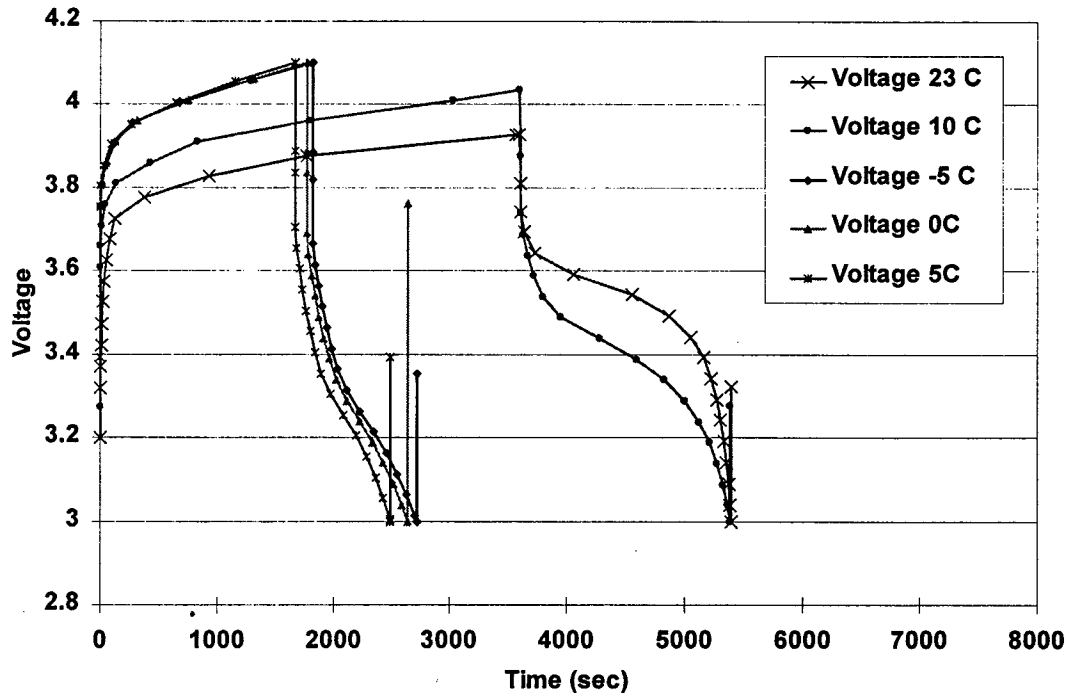

POWER Subsystems

EAGLE PICHER Technologies, LLC

Typical Charge/Discharge @ 23°C (C/2 Charge & C/2 Discharge)

- **23°C Performance after 120 cycles over temperature range**
  - Charge Capacity: 35.01 Ah
  - Discharge Capacity: 34.93 Ah

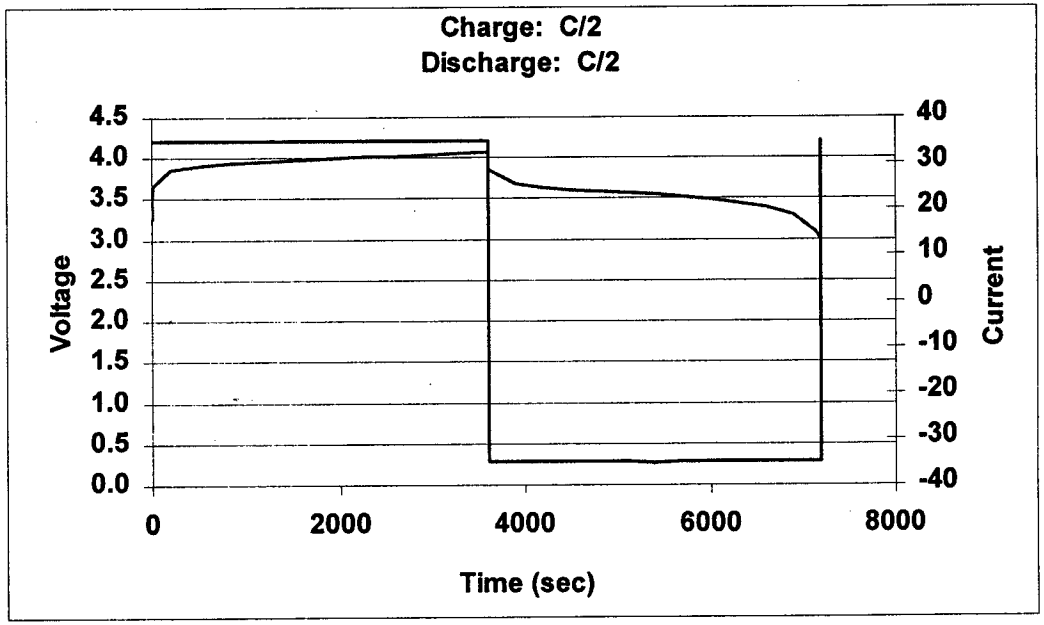

POWER Subsystems

EAGLE PICHER Technologies, LLC

Typical Charge/Discharge of Control Cell @ 23°C

- **Cycles 1-100:**
  - C/2 Charge (35 A)
  - C Discharge (70 A)
- **Consistent @ 23°C**

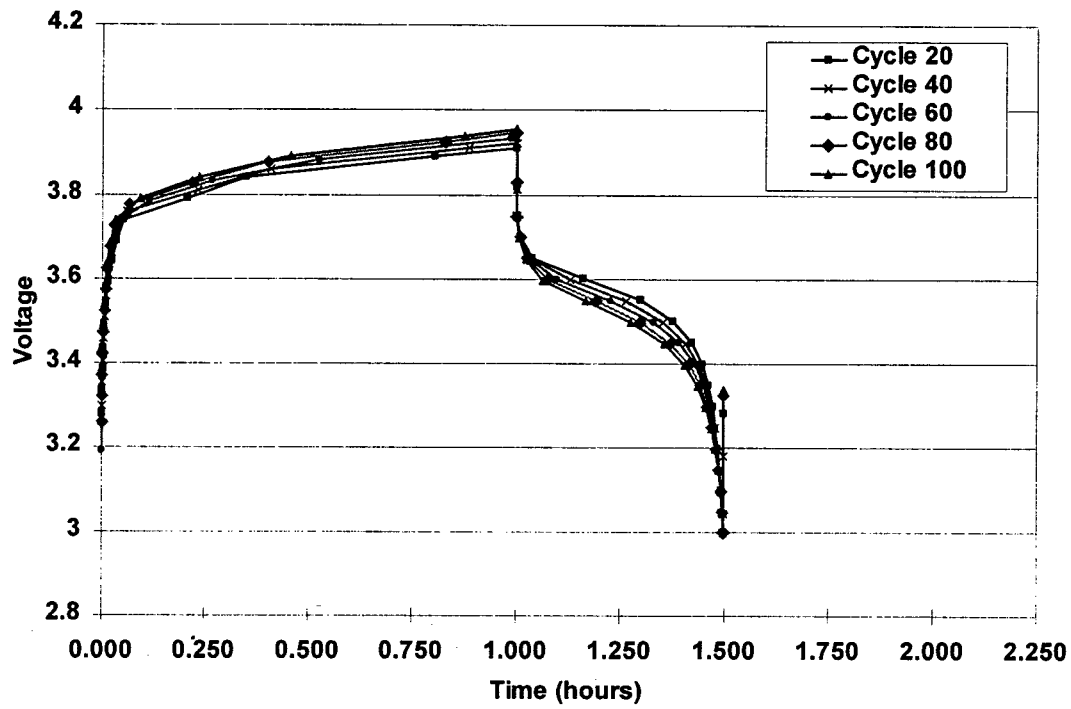

POWER Subsystems

EAGLE PICHER Technologies, LLC

Conclusion

- Initial cell group performance very good
- Demonstrated LEO rates to 50% DOD
- Demonstrated -5°C to +23°C performance
- Demonstrated C discharge and C/2 charge
- Demonstrated 99+% efficiency at LEO rates
- Demonstrated low impedance

POWER Subsystems

EAGLE PICHER Technologies, LLC

Near Future Activities

- Ultrasonic weld header/tab connection
- Incorporate alternate electrolyte
- Reduce number of electrodes
- Optimize anode and cathode
- Conduct cycle life tests

POWER Subsystems

EAGLE PICHER Technologies, LLC

Acknowledgements

- Air Force & NASA & government organizations for financial support & technical guidance

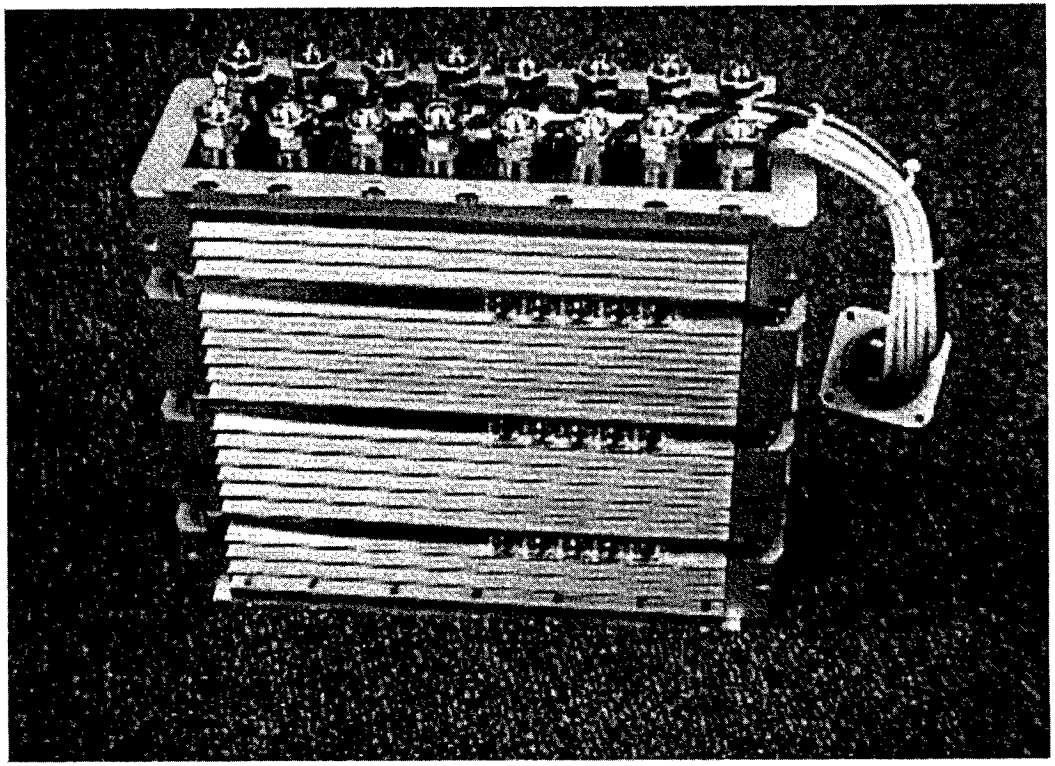

POWER Subsystems

Nickel-Hydrogen Session II

Computational Fluid Dynamics Modeling of Nickel Hydrogen Batteries

R. Cullion, W.B. Gu, C.Y. Wang
GATE Center for Advanced Energy Storage
Department of Mechanical and Nuclear Engineering
Pennsylvania State University
University Park, PA 16802

P. Timmerman
Jet Propulsion Laboratory
Pasadena, CA 91109

Abstract

An electrochemical Ni-H_2 battery model has been expanded to include thermal effects. A thermal energy conservation equation was derived from first principles. An electrochemical and thermal coupled model was created by the addition of this equation to an existing multiphase, electrochemical model. Charging at various rates was investigated and the results validated against experimental data. Reaction currents, pressure changes, temperature profiles, and concentration variations within the cell are predicted numerically and compared with available data and theory.

Introduction

The nickel hydrogen battery provides an important form of energy storage. This battery has applications in both the aerospace and the electric vehicle industries. Nickel hydrogen batteries are used in these fields due to their ability to provide long cycle lifetimes, high specific energy, high power density, and high tolerance to overcharge.

Demands by industry have made mathematical modeling of these batteries crucial, in particular, thermal modeling has become essential. Temperature variations within the battery influence the performance, life, and reliability of the power source. At low temperatures there are capacity losses due to high internal resistance within the battery and at high temperatures the capacity is compromised by fast self-discharge. Use of the active material must be balanced in order to maximize battery life. To do this a uniform temperature profile is necessary. Modeling provides a way to monitor the temperature profiles, and a way to test improvements without running lengthy and expensive experiments. Another very important reason thermal modeling is essential is safety. Side reactions occurring within the battery often result in temperature increases, which could lead to thermal runaway. Modeling would allow the runaway to be predicted.

The cell electrochemical behavior is described by electrochemical reactions that are affected by temperature-dependent electrochemical and transport properties. This interrelation of the electrochemical reactions and temperature-dependent properties makes it necessary to couple the electrochemical and thermal models of the Ni-H_2 cell into a single comprehensive model. Incorporating the thermal energy conservation

equation, in which the local heat generation rate is determined by the electrochemical processes, into the model achieves the coupling.

A one-dimensional, thermal and electrochemical model has been developed by DeVidt et. Al [2]. The transport phenomena of the gaseous species and electrolyte within the cell were described using concentrated solution theory and the volume averaging technique. A pseudo-second dimension was used to model the proton diffusion inside the active material. Three reactions in the nickel electrode were considered. The main reaction was the oxidation/reduction of the nickel species into the solid active material, and the side reactions were oxygen evolution/reduction and oxidation of dissolved hydrogen. The present work provides a two-dimensional, fully coupled, thermal and electrochemical model. It also makes use of the volume averaging technique and concentrated solution theory [8]. Unlike the model developed by DeVidt et. al. [2], the present work employs a multiphase reaction scheme. At the nickel electrode two main reactions are considered. Oxidation/reduction reactions of the nickel species in both the beta and gamma phases are considered. The side reactions, oxygen evolution/reduction and oxidation of dissolved hydrogen, are also included. The gamma phase is less stable than the beta phase and occurs mainly during overcharge [6]. Adding both the beta and gamma phase reactions to the model allows for more accurate prediction of the discharge/charge behavior as was demonstrated by Timmerman [7].

DeVidt's work [2] considers the cell to be isothermal spatially. An adiabatic case and an isothermal case were investigated. The focus of this study is to create an axisymmetric, multidimensional, thermal and electrochemical coupled model. The multidimensional nature of the present model is necessary because temperature gradients in the Ni-H_2 cell are present mainly in the radial direction due to heat dissipation through the battery wall, while the electrochemical and ion transport processes occur in the axial direction. Temperature gradients within the cell will be determined by this model due to their importance in predicting cell performance, making improvements, and for safety purposes. The energy equation of the two-dimensional model will include a heat generation term that incorporates the heat effects due to electrochemical reactions, joule heating, and phase changes of non-electrochemical nature. Also, as mentioned earlier, DeVidt's model [2] considered two extreme boundary conditions, an adiabatic case and an isothermal case. This model allows for a general convective boundary condition.

Thermal-Electrochemical Model

A single Ni-H_2 cell consists of an aluminum current collector, a nickel electrode, a separator, a hydrogen electrode (which has a micro-porous Teflon membrane backing permeable only to gas), a nickel current collector, and a gas diffusion screen, as shown schematically in Fig. 1. A concentrated KOH aqueous solution serves as the electrolyte. The Ni-H_2 battery is composed of a stack of these disk-shaped cells housed within a pressure vessel [3]. The cells are center aligned within the vessel. There is an outer gap between the wall of the pressure vessel and the circumference of the cell stack to ensure electric insulation between the cell stack and the pressure vessel and to provide a path for hydrogen gas to diffuse from the external reservoir into the cell stack. It is important to note the cell is axisymmetric, therefore although only the radial and axial directions will be examined the results will be the same as those found for a three-dimensional case.

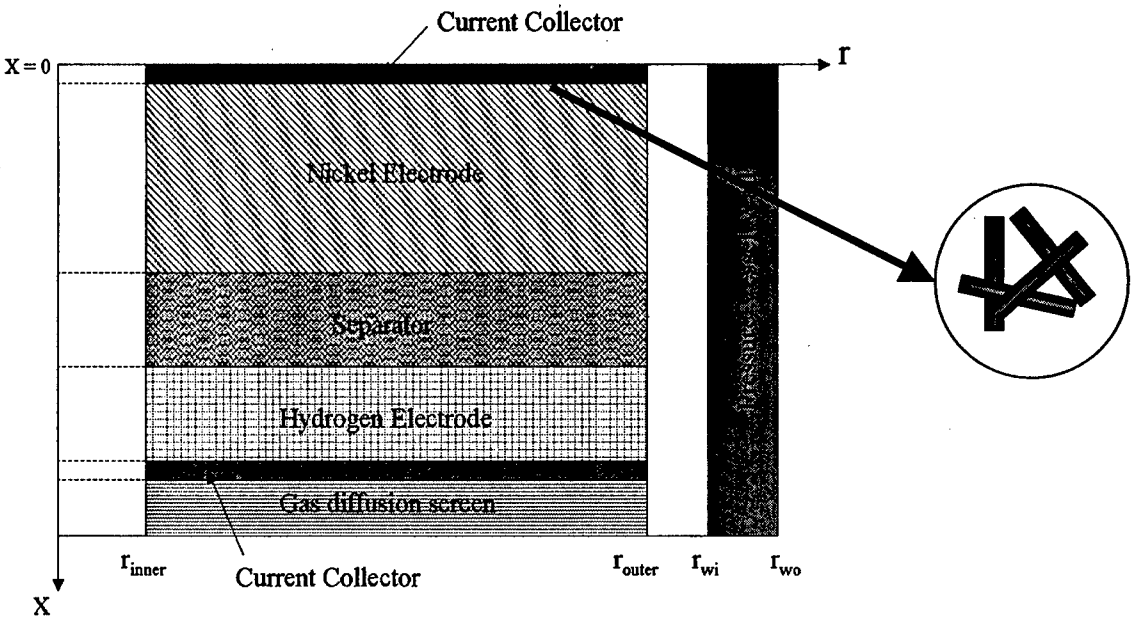

Figure 1. Schematic Representation of a Ni-H_2 Cell

Assumptions

The present work is based on the following assumptions. This problem is considered to be axisymmetric. The convection effect between the outer edge of the cell and the pressure vessel wall, important when the temperature difference between the two is large, is ignored for simplicity. As a result, in this space the species transport is by diffusion and migration only and the heat transfer is by conduction only. The nickel electrode consists of composite cylindrical needles with a substrate inside (see Fig. 1). The active material film is assumed to be a mixture of multiple phases with a constant diffusion coefficient for the protons. Furthermore, the α and γ phases are treated as a single phase [7]. The electrode porosities are considered to be constant. There is a continuous gas-pore network throughout the cell with a uniform constant volume fraction. The gas, a mixture of hydrogen, oxygen, and water vapor, is ideal. Its composition varies with time but does not change with position [1]. The solid phase is assumed to be completely wetted by the electrolyte film. Interfacial chemical equilibrium exists in the liquid phase for all species other than the dissolved oxygen that has a small value of mass diffusivity in the liquid electrolyte. Electrical equilibrium exists in the liquid phase due to the large value of ionic conductivity of the electrolyte. Finally it can be said that the combined thickness of the current collector and the Ni electrode is much smaller than the diameter of the cell, therefore ϕ_{sub} is considered to be constant along x but to vary with r.

Model Equations

At the nickel electrode the following main reactions occur:

β phase reaction:

$$NiOOH_{\beta} + H_2O + e^- \Leftrightarrow Ni(OH)_{2,\beta} + OH^- \tag{1a}$$

γ phase reaction:

$$NiOOH_{\gamma} + H_2O + ne^- \Leftrightarrow Ni(OH)_{2,\alpha} + OH^- \tag{1b}$$

γ phase production:

$$NiOOH_{\beta} + ne^- + K^+ \rightarrow NiOOH_{\gamma} + OH^- \tag{1c}$$

α phase reconversion:

$$Ni(OH)_{2,\alpha} \rightarrow Ni(OH)_{2,\beta} \tag{1d}$$

Oxygen evolution/reduction and the oxidation of dissolved hydrogen also occur at the nickel electrode and are considered to be side reactions:

$$\frac{1}{2}O_2 + H_2O + 2e^- \Leftrightarrow 2OH^- \tag{2}$$

$$2H_2O + 2e^- \leftarrow H_2 + 2OH^- \tag{3}$$

Two reactions occur at the hydrogen electrode, the main reaction:

$$H_2 + 2OH^- \Leftrightarrow 2H_2O + 2e^- \tag{4}$$

and the side reaction is:

$$2OH^- \leftarrow \frac{1}{2}O_2 + H_2O + 2e^- \tag{5}$$

The general Butler-Volmer equation is used to determine the rates at which these reactions occur. The equations are written with respect to a specified reference state, namely a temperature of 10°C and an electrolyte concentration of 7.1d-3 mol/cm^3.

$$\bar{i}_{n1a} = i_{o1a,ref}\left[\left(\frac{c^{OH}}{c^{OH}_{ref}}\right)\left(\frac{c^{-H}_{\beta}}{c^{H}_{\beta ref}}\right)\exp\left(\frac{\alpha_{a1a}F}{RT}\eta_{1a}\right) - \left(\frac{c^{H}_{\beta\max} - c^{-H}_{\beta}}{c^{H}_{\beta\max} - c^{H}_{\beta ref}}\right)\exp\left(-\frac{\alpha_{c1a}F}{RT}\eta_{1a}\right)\right] \tag{6}$$

$$\bar{i}_{n1b} = i_{o1b,ref}\left[\left(\frac{c^{OH}}{c^{OH}_{ref}}\right)\left(\frac{c^{-H}_{\gamma}}{c^{H}_{\gamma ref}}\right)\exp\left(\frac{\alpha_{a1b}F}{RT}\eta_{1b}\right) - \left(\frac{c^{H}_{\gamma\max} - c^{-H}_{\gamma}}{c^{H}_{\gamma\max} - c^{H}_{\gamma ref}}\right)\exp\left(-\frac{\alpha_{c1b}F}{RT}\eta_{1b}\right)\right] \tag{7}$$

$$\bar{i}_{n1c} = 2i_{o1c,ref}\left[1 - \left(\frac{c^{-H}_{\beta}}{c^{H}_{\beta\max}}\right)\exp\left(-\frac{\alpha_{c1c}F}{RT}\eta_{1c}\right)\right] \tag{8}$$

$$\bar{i}_{n2} = i_{o2,ref}\left[\left(\frac{c^{OH}}{c^{OH}_{ref}}\right)^2 \exp\left(\frac{\alpha_{a2}F}{RT}\eta_2\right) - \left(\frac{c_e^{-O_2}}{c^{O_2}_{eref}}\right)\exp\left(-\frac{\alpha_{c2}F}{RT}\eta_2\right)\right] \tag{9}$$

$$\bar{i}_{n3} = i_{o3,ref}\left[\left(\frac{c^{OH}}{c^{OH}_{ref}}\right)^2\left(\frac{c_e^{-H_2}}{c^{H_2}_{eref}}\right)\exp\left(\frac{\alpha_{a3}F}{RT}\eta_3\right) - \exp\left(-\frac{\alpha_{c3}F}{RT}\eta_3\right)\right] \tag{10}$$

$$\bar{i}_{n4} = i_{o4,ref}\left[\left(\frac{c^{OH}}{c^{OH}_{ref}}\right)^2\left(\frac{c_e^{-H_2}}{c^{H_2}_{eref}}\right)\exp\left(\frac{\alpha_{a4}F}{RT}\eta_4\right) - \exp\left(-\frac{\alpha_{c4}F}{RT}\eta_4\right)\right] \tag{11}$$

$$\bar{i}_{n5} = i_{o5,ref}\left[\left(\frac{c^{OH}}{c^{OH}_{ref}}\right)^2 \exp\left(\frac{\alpha_{a5}F}{RT}\eta_5\right) - \left(\frac{c_e^{O_2}}{c^{O_2}_{eref}}\right)\exp\left(-\frac{\alpha_{c5}F}{RT}\eta_5\right)\right] \tag{12}$$

The subscripts in the above equations; 1a, 1b, 1c, 2, 3, 4, 5 refer to the reactions labeled with the respective equation number.

The overpotential of a given reaction j, η_j, is given by [4]:

$$\eta_j = \phi_{se} - \phi_e - \left(U_{j,ref} + \left(T - T_{ref}\right)\left(\frac{\partial U}{\partial T} - \frac{\partial U_{ref}}{\partial T}\right)\right) \tag{13}$$

The temperature dependency of the overpotential is considered in the above equation. The reference overpotentials for the nickel electrode are calculated using the following equations [7]:

$$U_{1\bullet,ref} = U^o_{1\bullet} - \frac{RT}{F}\ln\left(\frac{c^H_{sref}}{c^H_{s\max} - c^H_{sref}}\right) + \frac{RT}{F}k\left(2\theta_s - 1\right) \tag{14}$$

$$U_{1c,ref} = U^o_{1c} \tag{15}$$

and the reference overpotentials for the oxygen and hydrogen reactions are [1]:

$$U_{3,ref} = U_{4,ref} = -0.9263 - \frac{RT}{2F}\ln\left(p^{H_2}_{ref}\right) \tag{16}$$

$$U_{2,ref} = U_{5,ref} = 0.3027 + \frac{RT}{4F}\ln\left(p^{O_2}_{ref}\right) \tag{17}$$

k in equation 14 is an intercalation constant used to describe the interaction between species in a solid solution.

The conservation of OH species in the liquid phase is represented by the following equation [7]:

$$\frac{\partial\left(\varepsilon_e c^{OH}\right)}{\partial t} = \nabla\left(D^{OH}_{eff}\nabla c^{OH}\right) + \frac{t^o_- - 1}{F}j^{OH} \tag{18}$$

where t^o_ is the transference number of OH^- with respect to the velocity of the solvent. j^{OH} is the total transfer current from all electrochemical reactions that generate or consume OH at the electrode/electrolyte interface:

$$j^{OH} = \begin{cases} j_b^{OH} + j_g^{OH} & \text{in the nickel electrode} \\ 0 & \text{in the separator} \\ a_H(\bar{i}_{n4} + \bar{i}_{n5}) & \text{in the hydrogen electrode} \end{cases} \tag{19}$$

where

$$j^{OH}_{\beta} = a_{Ni}(1 - X_\gamma)[\bar{i}_{n1a} + (\bar{i}_{n2} + \bar{i}_{n3})_\beta] \tag{20}$$

$$j_\gamma^{OH} = a_{Ni}X_\gamma[\bar{i}_{n1b} + (\bar{i}_{n2} + \bar{i}_{n3})_\gamma]$$

Similarly, $j^H{}_2$ and $j^O{}_2$ are the transfer currents associated with the generation or consumption of hydrogen and oxygen respectively:

$$j^{H2} = \begin{cases} a_{Ni}\bar{i}_{n3} & \text{in the nickel electrode} \\ 0 & \text{in the separator} \\ a_H\bar{i}_{n4} & \text{in the hydrogen electrode} \end{cases} \tag{21}$$

$$j^{O2} = \begin{cases} a_{Ni}\bar{i}_{n2} & \text{in the nickel electrode} \\ 0 & \text{in the separator} \\ a_H\bar{i}_{n5} & \text{in the hydrogen electrode} \end{cases} \tag{22}$$

Conservation of H_2 species in the liquid phase is given by [7]:

$$\frac{\partial\left(\varepsilon_e C_e^{H_2}\right)}{\partial t} = \nabla\left(D_{eff}^{H_2}\nabla c_e^{H_2}\right) + \frac{1}{2F}j^{H_2} + J_{eg}^{H_2} \tag{23}$$

O_2 species conservation in the liquid phase is [7]:

$$\frac{\partial\left(\varepsilon_e c_e^{O_2}\right)}{\partial t} = \nabla\left(D_{eff}^{O_2}\nabla c_e^{O_2}\right) + \frac{1}{4F}j^{O_2} + J_{eg}^{O_2} \tag{24}$$

The interfacial mass transfer rate of the hydrogen or oxygen from the liquid to the gas phase is expressed as:

$$J^{i}_{eg} = K^{i}\left(\frac{H^{i}}{RT}c^{i}_{g} - c^{i}_{e}\right) \qquad i = H_2 \text{ and } O_2 \tag{25}$$

Conservation of species in the gas phase is given as [7]:

$$\frac{\partial\left(c^{i}_{g}\right)}{\partial t} = \frac{-1}{V_g}\int_{v} J^{i}_{eg}\,dV \tag{26}$$

Conservation of species in the solid phase [7]:

$$\frac{\partial\left(\varepsilon_e c^{H}_{s}\right)}{\partial t} = \frac{j^{H}_{s}}{F} \tag{27}$$

where

$$j^{H}_{s} = \begin{cases} a_{Ni}(1 - X_g)\bar{i}_{n1a} & \text{for } s = b \\ a_{Ni}X_g\bar{i}_{n1b} & \text{for } s = g \end{cases} \tag{28}$$

Conservation of charge in the liquid phase is represented by [7]:

$$\nabla\cdot\left(k^{eff}\nabla\phi_e\right) + \nabla\left(k^{eff}_{d}\nabla\ln c^{OH}\right) + j^{OH} = 0 \tag{29}$$

Conservation of charge in the solid phase is given [7]:

$$\nabla\left(\sigma^{eff}_{s}\nabla\phi_s\right) - j^{OH}_{s} + a_{sb}\frac{\bar{\phi}_{sb} - \phi_s}{R_{sb}} = 0 \tag{30}$$

The energy conservation equation is written in the following form [4]:

$$\rho C_p\frac{\partial T}{\partial t} = \nabla\lambda\nabla T + q''' \tag{31}$$

where

$$\rho C_p = \varepsilon_e\rho_e C_p + \varepsilon_s\rho_s C_p + \varepsilon_g\rho_g C_p \tag{31a}$$

$$\lambda = \varepsilon_e\lambda^{eff}_{e} + \varepsilon_s\lambda^{eff}_{s} + \varepsilon_g\lambda^{eff}_{g} \tag{31b}$$

The third term of the energy equation has three components. The first part:

$$\frac{1}{V}\int_V a_{se}\sum \bar{i}_{nj}\left(\bar{\eta}_j + \Pi_j\right)dV \tag{32}$$

represents the heat effect produced by the electrochemical reactions [4]. This component includes both the reversible heat characterized by the Peltier coefficient:

$$\Pi_j = T\frac{\partial U_j}{\partial t} \tag{33}$$

and the irreversible heat related to the surface overpotential.

The second component of the heat generation term is associated with phase changes of the non-electrochemical nature, e.g. evaporation or condensation of water within the cell [4]:

$$\sum \Delta h \cdot \Gamma = \Delta h_{\alpha\beta} r_{\alpha\beta} + \Delta h_{eg}^{H_2O} J_{eg}^{H_2O} \tag{34}$$

The third component of the heat generation term:

$$\frac{1}{V}\int_V \sum_\sigma \left(\sigma_s^{eff}\nabla\phi_s + k^{eff}\nabla\phi_e\nabla\phi_e + k_D^{eff}\nabla\ln c^{OH}\cdot\nabla\phi_e\right)dV \tag{35}$$

represents the joule heating in both the solid and liquid phases [4].

Electrochemical and transport properties that are temperature dependent are expected to follow the Arrhenius equation [4]:

$$\Phi = \Phi_o \exp\left(-\frac{E_{act}}{R}\left(\frac{1}{T} - \frac{1}{T_o}\right)\right) \tag{36}$$

where E_{act} is the activation energy corresponding to a property Φ.

The top and bottom of the cell were considered to be adiabatic. The thermal boundary condition applied to the inner edge of the cell and the outer wall of the pressure vessel was the following:

$$-k\frac{\partial T}{\partial r} = h(T - T_{environment}) \tag{37}$$

where k is the thermal conductivity of the material, and h is the heat transfer coefficient.

Results and Discussion

Cell performance under various conditions was simulated using the model described above. Physical properties and electrochemical parameters were provided from experimental work conducted at JPL and are listed in Table I. Several parameters were

not available, but found through trial and error to produce the best overall agreement with experimental charge data (these values are indicated with an asterisk).

Table 1: Parameters

Parameter	Values	References
Kinetics		
$i_{o,1a}$	3.0d-04 A/cm^2	*
$i_{o,1b}$	1.0d-04 A/cm^2	
$i_{o,1c}$	2.0d-55 A/cm^2	
$i_{o,2}$	3.0d-10 A/cm^2	*
$i_{o,3}$	2.5d-16 A/cm^2	*
$i_{o,4}$	6.5d-05 A/cm^2	*
$i_{o,5}$	1.0d-07 A/cm^2	*
α_{1a}	5.0d-01 A/cm^2	
α_{1b}	5.0d-01 A/cm^2	
α_{1c}	5.0d-01 A/cm^2	
α_2	1.0d+00 A/cm^2	
α_3	5.0d-01 A/cm^2	
α_4	5.0d-01 A/cm^2	
α_5	1.0d+00 A/cm^2	
$P_{hydrogen,ref}$	52.0 Atm	Ref 1
$P_{oxygen,ref}$	5.0e-4 Atm	Ref 1
U_{1a}	4.2d-01 V	
U_{1b}	3.35d-1 V	
U_{1c}	4.4d-01 V	
U_2	3.0d-01 V	
U_3	-9.26d-1 V	
U_4	-9.26d-1 V	
U_5	3.0d-01 V	
E_{1a}	5.0d+04 J/mol	
E_{1b}	3.0d+04 J/mol	
E_{1c}	0.0d+00 J/mol	
E_2	8.0d+04 J/mol	
E_3	0.0d+00 J/mol	
E_4	2.0d+04 J/mol	
E_5	1.2d+05 J/mol	
Thermal		
$dudt_{1a}$	-2.11d-3 V/K	
$dudt_{1b}$	-1.51d-3 V/K	
$dudt_{1c}$	0.0d+00 V/K	
$dudt_2$	-1.68d-3 V/K	
$dudt_3$	-8.36d-3 V/K	
$dudt_4$	-8.36d-3 V/K	
$dudt_5$	-1.68d-3 V/K	
initial temperature	15°C	
reference temperature	15°C	
environmental temperature	0°C	

heat transfer coefficient	5 W/m^2K	*
Cell		
electrode pairs	17	
inner pressure vessel radius	4.435 cm	
outer electrode radius	4.400 cm	
inner electrode radius	0.350 cm	
Al current collector thickness	0.0015 cm	
Ni electrode thickness	0.453 cm	
Separator thickness	0.210 cm	
Pt H_2 electrode thickness	0.400 cm	
Ni current collector thickness	0.0010 cm	
Gas screen thickness	0.0610 cm	
Porosity of substrate	0.85	
Porosity of Ni electrode	0.41	
Porosity of Pt H_2 electrode	0.85	
Porosity of separator	0.85	
Specific interfacial area of substrate	2000 cm^2/cm^3	
Specific interfacial area of nickel electrode	3919 cm^2/cm^3	
Specific interfacial area of Pt-H_2 electrode	2000 cm^2/cm^3	
H_2 reference concentration	1.461d-3 mol/cm^3	*
O_2 reference concentration	1.529d-3 mol/cm^3	*
Reference concentration	7.1d-3 mol/cm^3	*

Experimental data for charging at various rates and a constant temperature of 10°C were used to validate the present model. Figure 2 compares the experimental cell potential curves with those predicted. The general shape compared well. The quick rise during initial charging was captured, and the second plateau was reproduced. At lower rates there is an under-prediction of the potential and as the rate increases there is a slight overprediction. Because a single set of parameters was kept for all simulations the observed discrepancies were expected.

Figure 3 compares cell pressure variations measured experimentally with the present model predictions. It plots the cell's pressure against time. Excellent agreement is shown for all three charging rates. The change in cell pressure is approximately linear until the overcharge period begins. At that point the pressure rise becomes strongly non-linear.

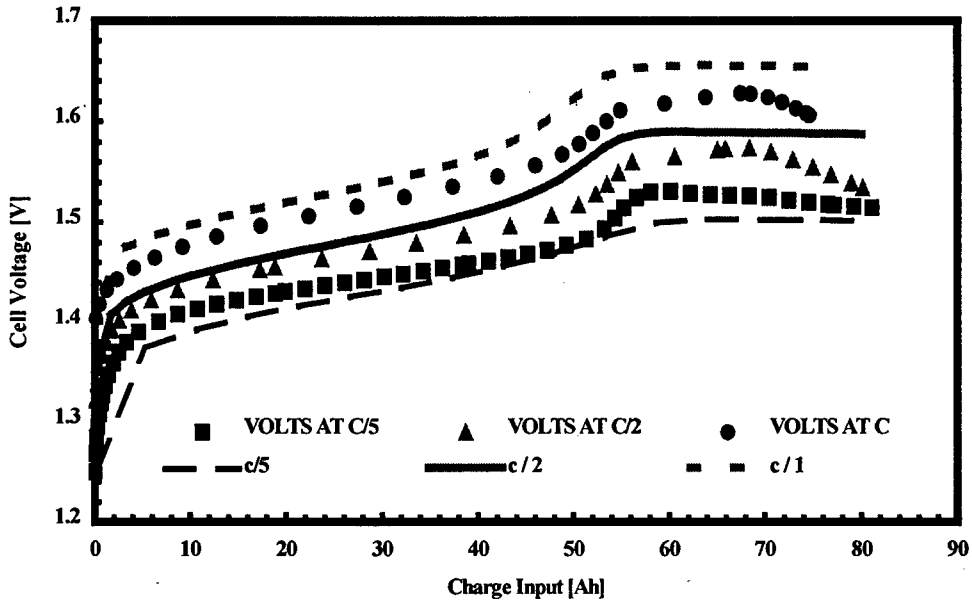

Fig. 2: Comparison of predicted and measured charge curves for a Ni-H_2 cell at different charge rates and constant 10°C. The lines are simulation results, and the symbols denote experimental data.

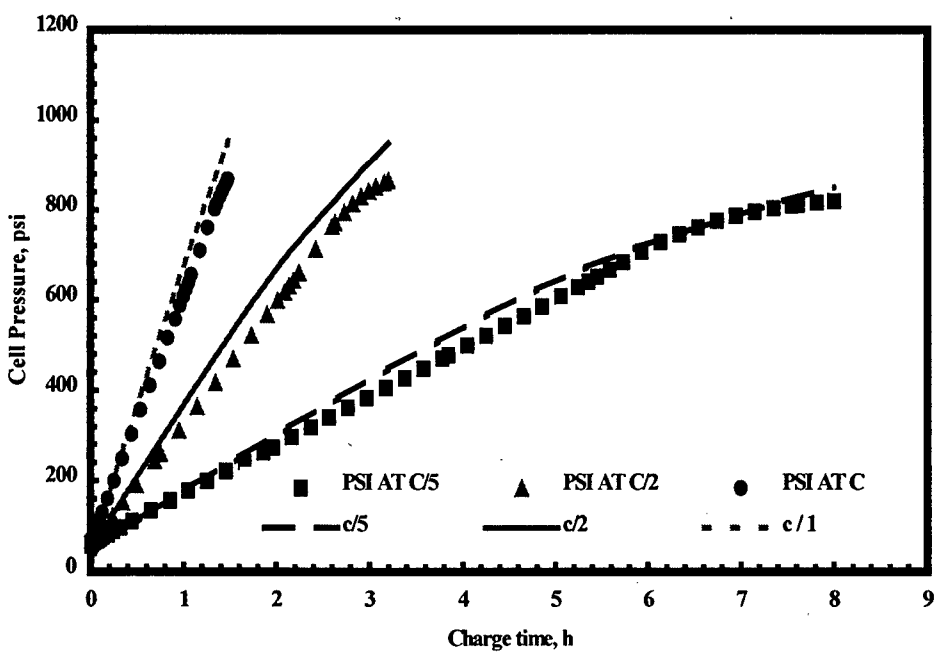

Figure 3. Comparison of experimental and simulated pressure variations for charging at various rates at 10°C.

The following results obtained from the computer simulation are intended to further reveal the internal processes of the Ni-H_2 cell during charge.

Figure 4 plots the reaction current distributions within the nickel electrode when the cell is being charged at a rate of C/1 and a constant temperature of 10°C to 50% charge input. As discussed earlier there are both primary reactions and secondary reactions that occur in the nickel electrode. Theoretically, prior to reaching 100% charge input the primary reactions are the principle reactions. Beyond 100% charge input the secondary reactions take over as the major reactions. Figure 4 clearly shows that for 50% state of charge the primary reactions, 1a and 1b, are dominant. It is also important to note that these reactions are stronger at the electrode/electrolyte interface than at the back of the electrode. Inspection of the chemical reactions, 1a and 1b, reveals that OH^- is a reactant during charging. A large supply of OH^- explains why the reaction is more intense at this location.

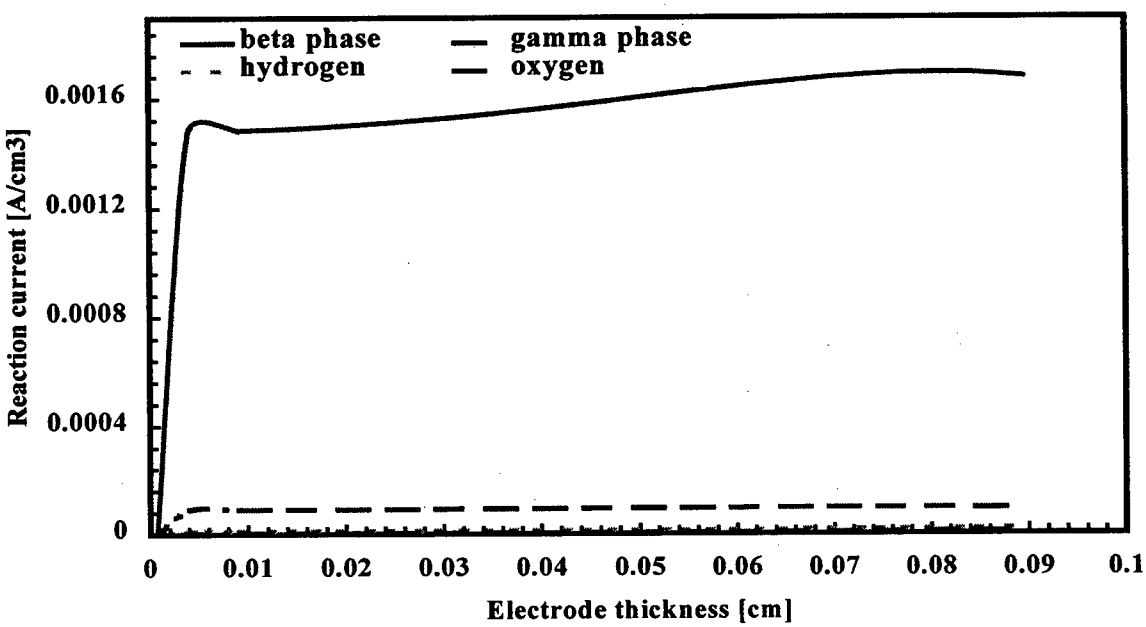

Figure 4: Reaction current distribution inside the nickel electrode for a cell charged at C/1 at constant 10°C to 50 % charge input.

Figure 5 also shows the reaction current distribution within the nickel electrode when the cell is being charged at C/1 and kept at 10°C. It is charged to 150% charge input in this case. As expected, the simulation shows that the primary reactions diminish to approximately zero and the secondary reactions develop once the battery has been charged to 100% charge input. The oxygen and hydrogen reactions, 2 and 3, become the dominant reactions once the 100% point is passed. Also, from Fig. 5 it can be noted that the secondary reaction rates are larger at the electrode/electrolyte for the same reason as stated previously.

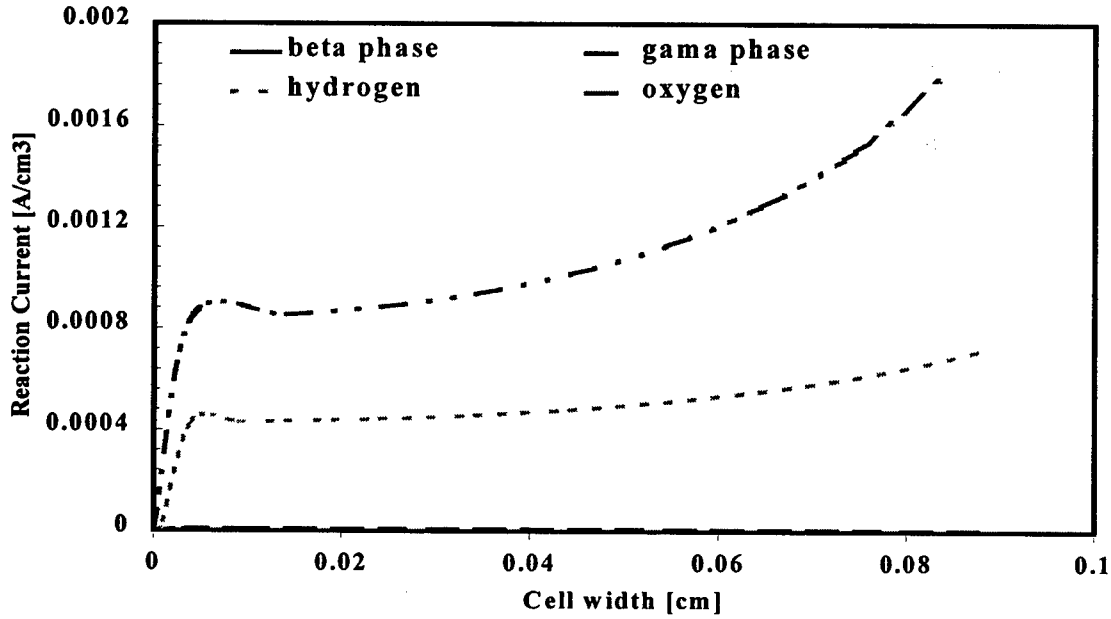

Figure 5: Reaction current distribution within the nickel electrode of a cell charged at C/1 at constant 10°C to 150 % charge input.

Figure 6 plots the reaction currents in the nickel electrode as a function of the charge input relative to the cell capacity. The primary reactions are seen to dominate until 100% charge input is reached, beyond that point the secondary reactions take over. Also to be noted is that the total current prior to and after 100% charge input remains the same.

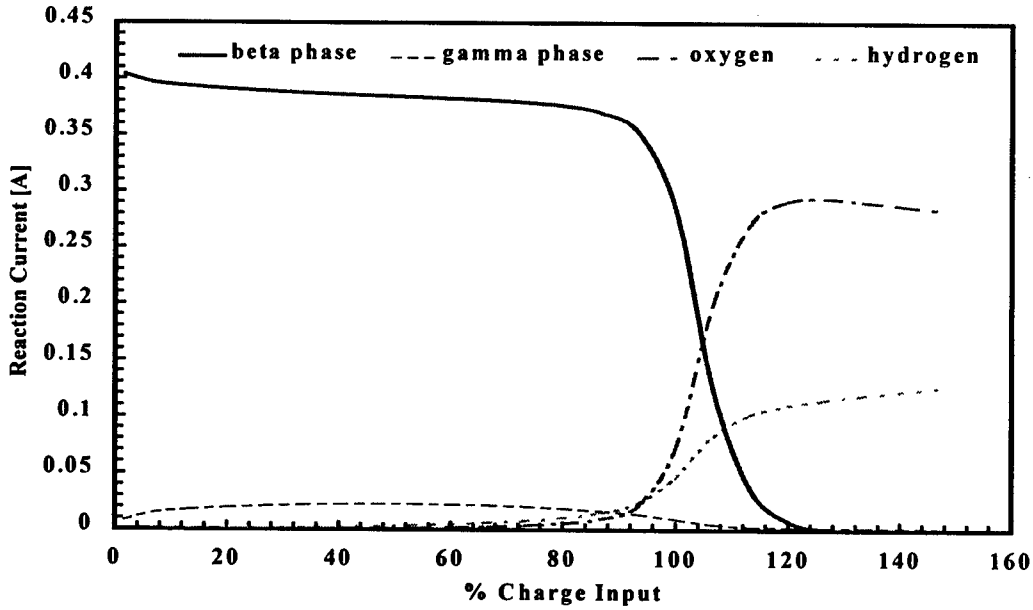

Figure 6. Reaction currents within a cell charged at C/1 and constant 10°C as a function of percent charge input.

Figure 7 plots the partial pressures of the hydrogen and oxygen within a cell charged at C/1 and 10°C. As expected, the increase of pressure due to the hydrogen reaction is dominant. The primary reaction at the hydrogen electrode is the main contributor prior to 100 % charge input, and beyond 100 % the secondary hydrogen reaction at the nickel electrode is adding to the pressure increase. Also at 100 % charge input and beyond the secondary oxygen reaction at the nickel electrode begins, producing a rise in pressure and contributing to the overall increase in pressure.

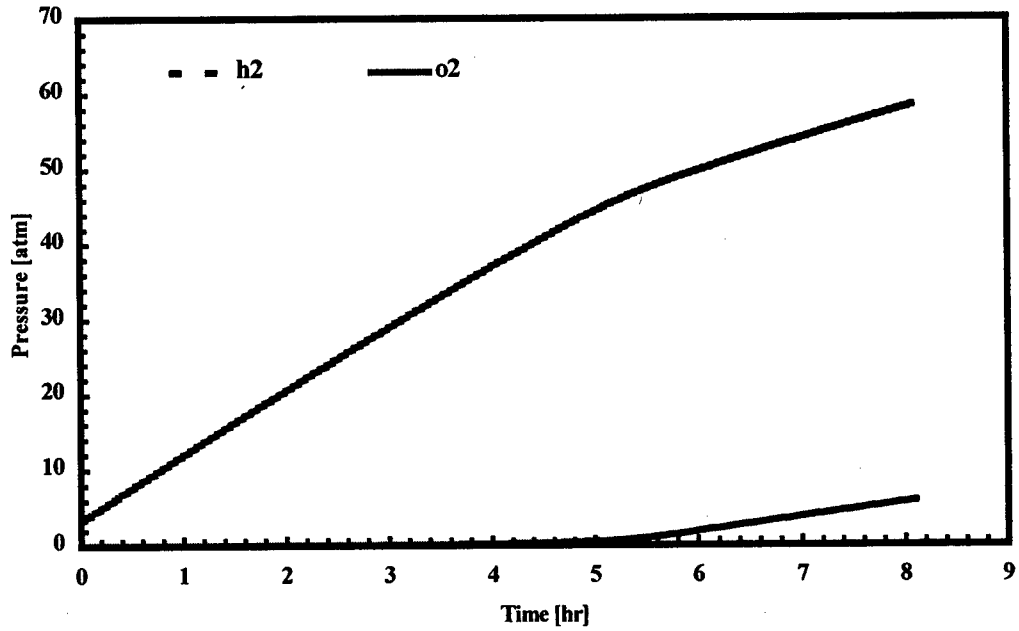

Figure 7: Partial pressures within a cell charged at C/1 and 10°C to 150% of the cell capacity as a function of time.

Figure 8 explores the thermal effects within the cell, showing the temperature profile within the cell with respect to the cell radius. As mentioned earlier the cell is shaped like a disk with a hole at its center. The cell is hottest near the inner edge of the hole and the temperature decreases as the outer diameter of the cell is approached, this is expected based on the boundary conditions. A temperature change of 3°C is seen. A temperature difference of this magnitude influences the kinetic rates of the reactions by as much as 10%.

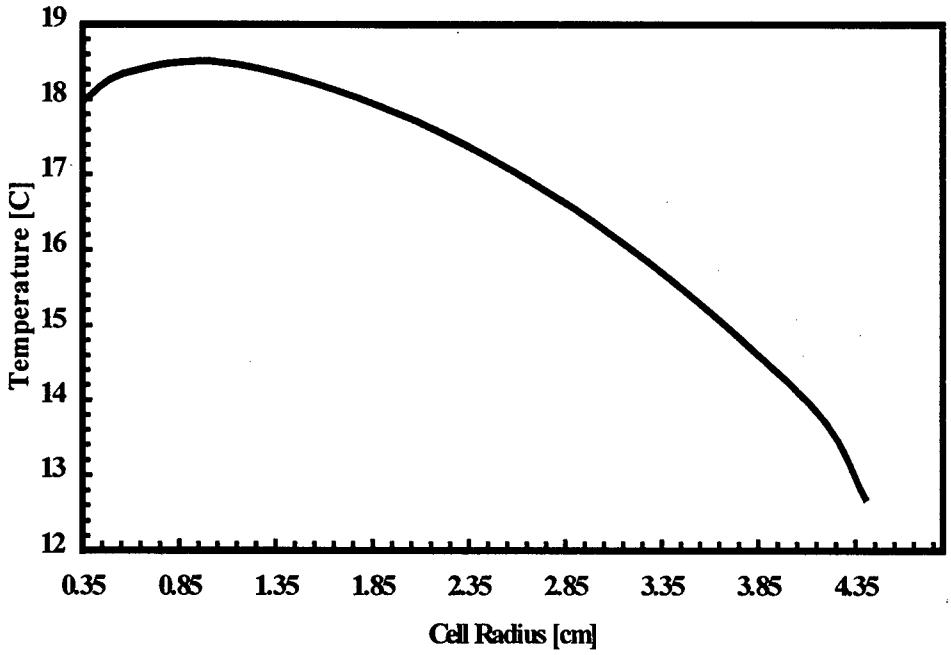

Figure 8: Average temperature of the cell charged at C/1 to 150% of its capacity as a function of the radius with h = 5 W/m^{2}K.

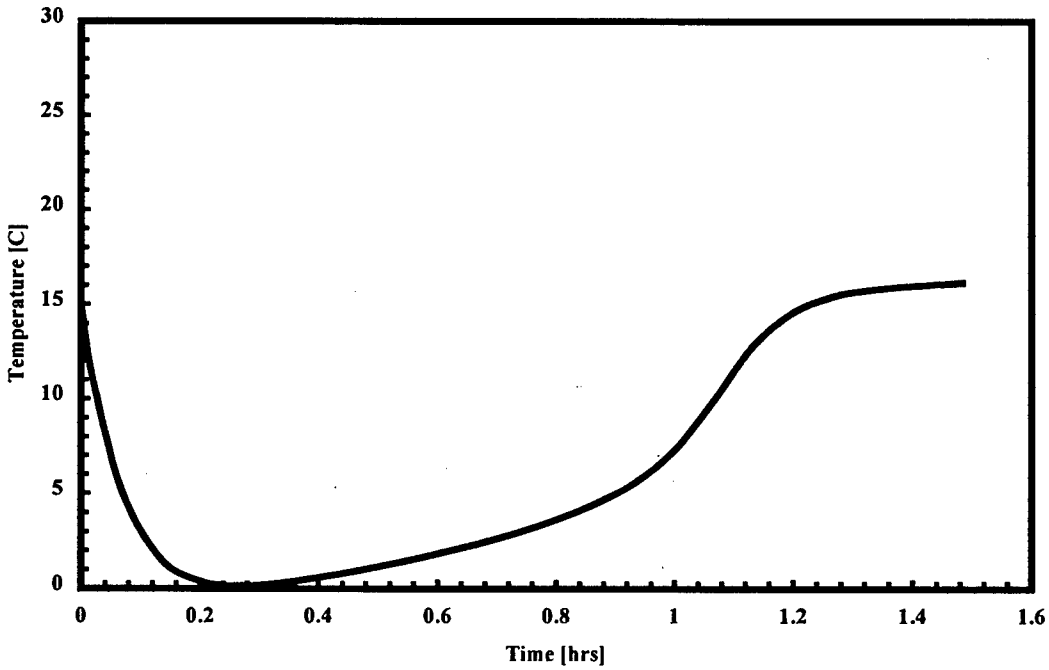

Figure 9: Average temperature of a cell charged at C/1 to 150% of its capacity as a function of time, when h = 5 W/m^{2}K and $T_{initial}$ = 15°C.

Figure 9 is a graph of the change in average cell temperature with time for a cell charged at C/1. This plot shows an initial temperature drop during the early stages and then an increase in temperature during the later times. At the end of the charging period the battery is hotter than it was initially. The primary reactions dominate when the charging time is less than one hour. It is known that the primary reactions are endothermic [5], therefore explaining the temperature drop during the beginning stages of charging. The hydrogen reaction at the hydrogen electrode is exothermic as is the hydrogen side reaction at the nickel electrode. The hydrogen reactions coupled with resistive heating cause the temperature rise as charging progresses [2].

Experimental temperature measurements were made at the pressure vessel seam. This data was then plotted versus the charging time, as shown in Figure 10. An initial drop in temperature is followed by a strong increase in temperature. Qualitatively Figure 9, the simulation results for the average temperature of the cell, demonstrates a trend very similar to the temperature profile found through external measurements as seen in Figure 10.

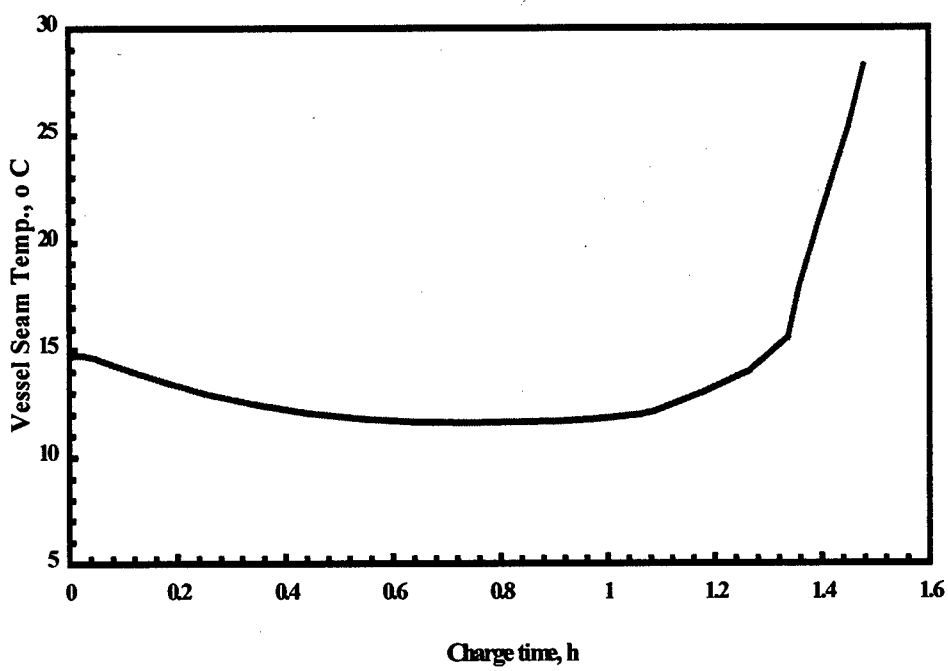

Figure 10: Experimental pressure vessel temperatures plotted as a function of the charging time for a cell charged at C/1.

Figure 11 addresses two important points. It plots the cell proton concentration contour for a cell charged at C/1 to 50 % of the cell capacity. It demonstrates the necessity of having two-dimensionality in the model. The plot shows that the proton concentration varies in both the axial and radial directions. It also shows the effect of temperature on the cell. The proton depletion is greater at the inner diameter of the cell, this is related to the higher temperatures at this location, clearly demonstrating the thermal, electrochemical link. Also, as was noted earlier, there is larger proton concentration depletion along the electrolyte interface due to the plentitude of OH^-.

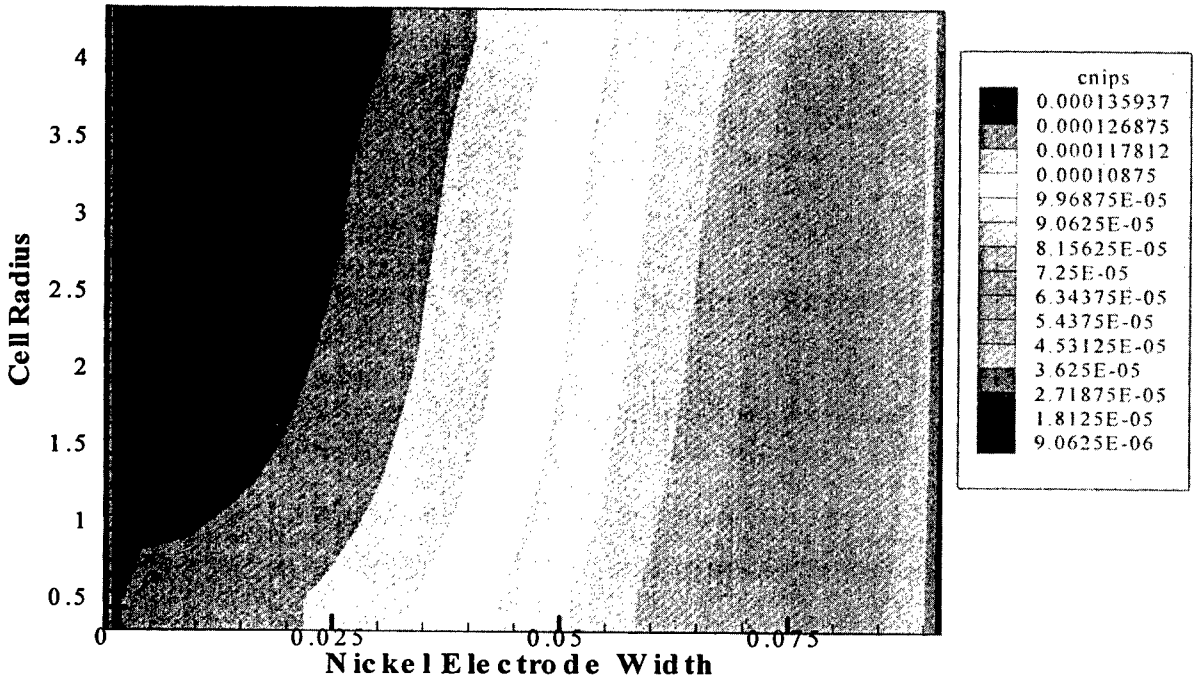

Figure 11: Proton concentration in a cell charged at C/1 to 50 % the cell capacity.

Conclusions:

A two-dimensional, fully coupled, thermal and electrochemical Ni-H_2 model has been developed. Comparison with experimental data validates the model's results. This model complements experimentation by allowing the user to understand occurrences within the cell for various conditions and for many different charging rates. Examples of the program capabilities have been given. Work is underway to expand this model to the entire cell stack, and the thermal interactions between the cells that arise due to this change will be addressed and investigated.

References

1. P. De Vidts, J. Delgado, R. White, *J. Electrochem. Soc.,* **143**, 3223 (1996).
2. P. De Vidts, J. Delgado, B. Wu, D. See, K. Kosanovich, R.E. White *J.Electrochem. Soc.,* **145**, 3874 (1998).
3. J.D. Dunlop, G.M. Rao, and T.Y. Yi, *NASA Handbook for Nickel-Hydrogen Batteries,* NASA reference publication 1314 (1993).
4. W.B. Gu and C.Y. Wang, "Thermal-Electrochemical Modeling of Battery Systems", *J. Electrochem.,* submitted for publication 1999.
5. C. F. Holmes and A.R. Landgrebe, *Batteries for Portable Applications and Electric Vehicles,* The Electrochemical Society Inc., Pennington, NJ (1997).
6. B. Ratnakumar, P. Timmerman, D. Perrone, S. Di Stefano, *Proceedings of 31st Intersociety Energy Conversion Engineering Conference,* **1**, 374 (1996).
7. P. Timmerman, R. Bugga, S. DiStefano, NASA Battery Workshop, 1996.
8. C.Y. Wang, W.B. Gu, and B.Y. Liaw, *J. Electrochem. Soc.,* **145**, 3407 (1998)

List of Symbols

a	specific interfacial area, cm^2/cm^3
c^i	volume-averaging concentration of species i over a phase, mol/cm^3
C_p	specific heat, J/g/K
D^i	diffusion coefficient of species i in a phase, cm^2/s
E_{act}	activation energy, J/mol
F	Faraday's constant, 96,487 C/mol
h	heat transfer coefficient, W/m^2K
i_{nj}	area-averaged transfer current density of reaction j, A/cm^2
$i_{oj,ref}$	exchange current density of reaction j at reference conditions, A/cm^2
j^i	reaction current density due to production or consumption of species i, A/cm^2
k	thermal conductivity, W/mK
q'''	heat generation term
R	universal gas constant, 8.3143 J/mol K
R_{sb}	electrical resistance from solid/substrate interface to the bulk of solid, $\Omega\ cm^2$
t	time, s
t^o_-	transference number of OH^- with respect to the solvent velocity
T	absolute temperature of the cell system, K
$U_{j,ref}$	open-circuit potential for reaction j at reference conditions measured with respect to a Hg/HgO reference electrode, V
V_i	volume of a phase, cm^3

Greek Symbols

α_{aj}, α_{cj}	anodic and cathodic transfer coefficients for reaction j
Δh	enthalpy change
ε_i	volume fraction of a phase in the reference volume fraction
η_j	surface overpotential of electrode reaction, j, V
Φ	general symbol representing a property at a temperature T
λ	thermal conductivity, W/m^2K
Π	Peltier coefficient
ϕ	potential in a phase, V
ρ	density of a species I, g/cm^3
σ	thermal conductivity W/m^2K

VALIDATION OF THE STATIC MODEL FOR NICKEL-HYDROGEN CELLS

By:

Lawrence H. Thaller

The Aerospace Corporation

El Segundo, CA

Presented at:

The 1999 NASA Aerospace Battery Workshop

Huntsville, AL

16-18 November 1999

Electronics Technology Center
Energy Technology Department

THE AEROSPACE CORPORATION

OUTLINE

- BASICS OF STATIC MODELS
- MODEL FOR NICKEL-HYDROGEN CELLS
- APPLICATIONS OF A VALID MODEL
  - Assess projected cycle life
  - Trades single layer vs. double layer separators
- EARLIER VALIDATION EFFORTS
- ADDITIONAL FACTORS CONSIDERED HERE
  - Density variations with DOD
  - Compressibility of components
  - Survey of available dryout information
  - A closer review of earlier partitioning studies
- CURRENT STATUS OF MODEL

Electronics Technology Center
Energy Technology Department

THE AEROSPACE CORPORATION

BASICS OF STATIC MODELS

- A SERIES OF CALCULATIONS TO DETERMINE POROUS WETTABLE VOLUME WITHIN THE CELL
  - Densities, porosities, dimensions
- INCORPORATES CHANGES DURING CYCLING
  - Cycle to cycle, start to finish
  - Electrode expansion, plaque corrosion, gamma phase formation
- DETERMINE OR PROJECT IMPACT OF CHANGES IN ELECTROLYTE PARTITIONING BETWEEN COMPONENTS

Electronics Technology Center
Energy Technology Department

THE AEROSPACE CORPORATION

A static model is one that calculates the total wettable volume of the components within a cell. By knowing the interior volume of a cell and the amount of electrolyte in the cell, an assessment can be made as to whether there is too much or too little electrolyte. The desired amount of electrolyte depends on whether the cell design is a flooded one or a starved one. It also depends on the changes that are expected to take place during the course of expected usage or cycle life. We have developed static models for nickel-cadmium, nickel-hydrogen, silver-zinc, and lithium-thionyl chloride cells. For the nickel-hydrogen model which will be addressed here, the model was set up to investigate the dryout tendencies that are caused by the natural degradation mechanisms as the cells are cycled. Expansion of the nickel electrode, corrosion of the sintered nickel plaque material, and the formation of the gamma phase of charged active material all result in reductions in the volume of electrolyte. Since the rates of these processes are partially known, information from a validated static model can be helpful in evaluating the projected cycle life of a particular cell design.

STATIC NICKEL-HYDROGEN MODEL

- FULL DESCRIPTION GIVEN AT THE 1997 IECEC MEETING
  - Details of how to construct a model for your own use
- PAPER GIVEN AT 1998 IECEC MEETING DESCRIBED DATABASE OF DIFFERENT DEGRADATION MECHANISMS
- 1999 PRESENTATION AT THE ANNUAL BATTERY CONFERENCE DESCRIBED VOLUME TOLERANCE OF CELL
- SOME FINE TUNING EFFORTS WERE STILL NEEDED

Electronics Technology Center
Energy Technology Department

THE AEROSPACE CORPORATION

A full description of the initial version of the model was presented at the 1997 IECEC meeting in Hawaii. The model consists of a spreadsheet wherein all the diameters, thicknesses, porosities, and densities are used to calculate the wettable volumes of all the components. There are only a few design-specific variables that are required to be inserted into the spreadsheet. These include the amount of plate expansion that is expected, the amount of plaque corrosion that might take place, and the amount of charged active material that will be found in the gamma phase. Of course, the amount of electrolyte added to the cell during activation is also needed. The resulting calculations will determine the amount of electrolyte that will be in each component given the expected changes that were inserted into the model.

Extensive review of life cycle testing data coupled with post test destructive physical analyses have permitted reasonable estimates to be made of the rates of plaque corrosion and electrode expansion. A summary of this ongoing study as of 1998 was presented at the 1998 IECEC meeting in Colorado Springs, CO.

More recently, a technique was developed and reported at the 1999 Annual Battery Conference held in Long Beach, CA. This technique permitted the increase in internal resistance of a nickel-hydrogen cell to be monitored as the volume of electrolyte was reduced to the point where the cell performance was unacceptably low.

Since then, other efforts have been explored in an attempt to match the results of post test analyses with results predicted by the model.

APPLICATIONS FOR A VALIDATED MODEL

- DRYOUT RESULTS IN AN INCREASE IN INTERNAL RESISTANCE
  - Gradual at first, becoming significant if diffusional limit is exceeded
- DRYOUT OCCURS DURING CYCLING
  - Aggravated by aggressive cycling conditions
- THEREFORE, MODEL HELPFUL IN ASSESSING:
  - Cycling conditions when long cycle life is required
  - Evaluation of cell designs with single layer of separator
  - Evaluation of cells that are under filled with respect to electrolyte

Electronics Technology Center
Energy Technology Department

THE AEROSPACE CORPORATION

Models of any type are developed because it is hoped that results, information, or insight can be gained that would not be obtained using other means. As with any other cell type that is classified as being a "starved" design, nickel-hydrogen cells have been known to display symptoms of having an insufficient amount of electrolyte. This situation is usually referred to as a dryout condition. Besides an increase in internal cell impedance, dryout can result in severe cases of a condition that results in a diffusion-limited current. In this situation, there are not enough ions to conduct the current through the electrolyte and the result is a sudden drop in current carrying capability.

Since the degradation mechanisms in nickel-hydrogen cells are reasonably well understood as well as the factors of temperature and recharge protocols that can exacerbate the rates of degradation, a validated model would be useful for commenting on suggested cell designs, cycling conditions, and recharge protocols.

MAJOR ASSUMPTIONS OF MODEL

- ELECTROLYTE DISTRIBUTES ITSELF ACCORDING TO THE PORE SIZE CHARACTER OF THE COMPONENTS
  - Capillary pressures are equalized
- THE SEPARATOR GIVES UP ELECTROLYTE TO THE EXPANDING NICKEL ELECTRODE
- THE EFFECTIVE DENSITIES OF THE DIFFERENT FORMS OF THE ACTIVE MATERIALS ARE AS FOLLOWS:
  - Discharged beta material - 3.97
  - Charged beta material - 4.56
  - Gamma material - 3.71

Electronics Technology Center
Energy Technology Department

THE AEROSPACE CORPORATION

Like most models, there were a few assumptions in the original model. The major one in the initial version of the model was that the wettable pores of the nickel electrode would remain filled with electrolyte at the expense of the electrolyte contained in the separator.

When two porous materials are in contact and have some amount of liquid within their pore structures, the liquid will distribute itself according to the wettability and the pore size character of the two components. This redistribution will result in equal capillary pressures between the pores of the two structures. Based on an extensive study* that was carried out earlier when the topic of pore size engineering was being developed, the pore size distribution of typical cell components were determined. For the cases where zircar was the separator, the difference in pore size distribution vs. a typical nickel electrode suggested that the nickel electrode would remain filled.

The second assumption deals with the densities of the different forms of active material within the nickel electrode. The ones used in this study are slightly different than those found in the normal handbooks. They have been derived from practical experience with nickel elecrodes.

The third assumption was related to the lack of compression that the cell components experienced while in the cell.

In this study, the first and the third assumption will be reviewed and incorporated into an upgraded version of the model.

*Abbey, K. and Briton, D. "Electrolyte Management in Porous Battery Components", NASA TM 83073

EARLIER NASA STUDIES ON DISTRIBUTION AND PARTITIONING OF ELECTROLYTE

NASA TM 83073 by Abbey and Britton - Electrolyte Management in Porous Battery Components

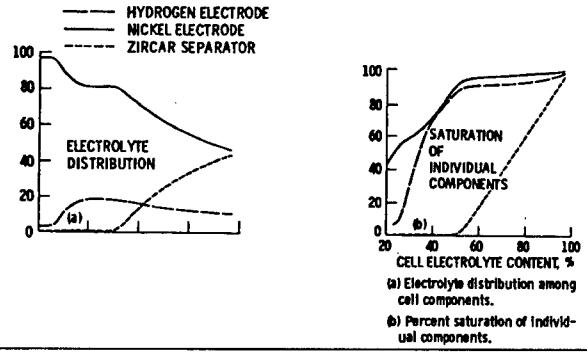

(a) Electrolyte distribution among cell components.

(b) Percent saturation of individual components.

Electronics Technology Center
Energy Technology Department

THE AEROSPACE CORPORATION

The above two figures that appeared in the referenced NASA publication. They were generated starting with the pore size distributions of the individual components of a typical nickel-hydrogen cell - single layer zircar, standard nickel electrode, and the normal hydrogen electrode. With the given pore size distribution data and the requirement to have equal capillary pressures across the three components, these two curves were developed.

The figure on the left charts how the electrolyte is partitioned across the three components as electrolyte is withdrawn from the set of parts. When the components are filled with electrolyte, about 45% of it is in the nickel electrode, another 45% in the separator, and the remainder in the hydrogen electrode. As the set dries out, a larger percentage of the electrolyte remains in the nickel electrode.

The chart on the right describes the percentage of the pore structure that is filled with electrolyte. When the cell set is completely filled, then all three components are of course filled. As the set of components begins to dryout, it is seen that the separator material preferentially loses electrolyte due to the separator's high percentage of large pores compared to the other two components. The nickel electrode and the hydrogen electrode do not stay fully saturated but do share a small amount of their liquid content with the separator.

Later, it will be shown that a cell displays dryout symptoms when the pore structure of the separator is only about 30% filled with electrolyte. At this point, the pore structure of the nickel electrode is between 90% and 95% filled.

CHECKING THE MODEL

- SET MODEL FOR EITHER FULL CHARGE OR FULL DISCHARGE
- IN THE CHARGED MODE, THE PERCENTAGE OF GAMMA PHASE IS INSERTED
- ALL KNOWN FACTORS - DIMENSIONS, THICKNESSES, ETC. ARE INSERTED
- ASSUMPTIONS RELATED TO COMPRESSION AND EXPANSION ARE INSERTED
- RESULTS ARE NOTED
  - Partitioning of electrolyte
- RESULTS ARE COMPARED WITH RESULTS FROM DPA STUDIES

Electronics Technology Center
Energy Technology Department

THE AEROSPACE CORPORATION

The model is best set up for the cell to be in the fully charged state or the fully discharged state. This permits the proper value for the density to be used for the active material. If the cell is set for the fully charged condition, one must insert a value for the percentage that is in the gamma phase. As the cell approaches a dryout condition, selecting the proper density for the active material does make a difference in the amount of electrolyte that is calculated to be in the separator.

Other factors that are known with a higher degree of certainty are then added - dimensions, thicknesses, etc.

Assumptions relating to how much the electrodes are expected to expand over the life of the test and how much each of the components are compressed due to being compressed between the end plates by the Belleville washer are next made.

The results are noted in terms of partitioning and percentage of the separator pores that are filled with electrolyte.

During the validation process, the results from the model were compared with the results from the DPA studies.

EARLY ATTEMPTS TO VALIDATE MODEL

- CELL MODIFIED AND WATER INCREMENTALLY REMOVED*
- PERFORMANCE MONITORED DURING DISCHARGE AT DIFFERENT RATES
- RISE IN INTERNAL IMPEDANCE WITH REDUCTION IN ELECTROLYTE VOLUME WAS NOTED
- AT THE POINT WHERE THE IMPEDANCE DOUBLED, THE CELL WAS DISASSEMBLED AND THE PARTITIONING WAS DETERMINED VIA TITRATION OF COMPONENTS
  - THE MODEL PREDICTED A DRYER SEPARATOR THAN THE RESULTS OF THE TITRATION ANALYSIS

*DETAILS IN 1999 ANNUAL BATTERY CONFERENCE PAPER

Electronics Technology Center
Energy Technology Department

THE AEROSPACE CORPORATION

Early attempts to validate the model consisted of developing a dryout test in which incremental amounts of water were evaporated from a known new cell (no corrosion or expansion) that had been filled with a known amount of electrolyte during its activation. As electrolyte volume was removed from the cell, the performance was monitored at several discharge rates over the course of the full discharge. The rise in internal impedance as the electrolyte volume was reduced was noted. Evidence for diffusion limiting currents were watched for, and was occasionally seen. When the internal impedance had doubled, the cell was judged to have dried out. The cell was disassembled and selected components were analysed for their electrolyte content. The results suggested that the partitioning of the electrolyte was uniform in the six locations within the cell that were examined. The initial version of the model predicted a dryer separator than was suggested by the chemical analyses.

Since I was dissatisfied with the agreement between the two sets of answers, attempts were made to bring the results and the prediction closer together. When this process was completed, the model very closely matched the post test analyses. More realistic numbers for the compression of cell components had to be determined. Out-of-cell thicknesses of expanded electrode material had to be converted to in-stack thicknesses. The assumption that the nickel electrodes were 100% full gave way to the more valid value of between 90 and 95%. Since the cell was taken apart in the discharged state, the density of the beta nickel hydroxide had to be used. The remainder of the paper will outline the steps in this process.

STEPS IN UPGRADING MODEL

- VARIABLES SET FOR THE DISCHARGED CONDITION
  - Condition when the cells were opened
- PERCENT EXPANSION IS ADJUSTED TO BEST FIT OF ELECTROLYTE PARTITIONING BASED ON DPA
- ASSUMPTION OF 100% FILL OF POSITIVE PLATES IS ADJUSTED TO ACTUAL PLATE EXPANSION
- PERCENT FILL OF POSITIVE PLATE IS COMPARED TO PREVIOUSLY GENERATED CAPILLARY PRESSURE STUDIES
- THE MODEL RESULTS ARE NOW IN VERY CLOSE AGREEMENT WITH DPA RESULTS

Electronics Technology Center
Energy Technology Department

THE AEROSPACE CORPORATION

The chart on the next page will be used to illustrate how the available data related to cell dryout was used to upgrade and validate our original version of the static model for nickel-hydrogen cells.

SOURCES OF DATA FOR THE STUDY

- RESULTS OF SPECIALLY CONDUCTED DRYOUT TESTS WHERE THE ELECTROLYTE VOLUME WAS SEQUENTIALLY REDUCED AS THE PERFORMANCE WAS MONITORED
- POST TEST ANALYSES WHERE THE PARTITIONING OF ELECTROLYTE BETWEEN THE SEPARATOR AND THE NICKEL ELECTRODE WAS DETERMINED
- POST TEST ANALYSES WHERE THE AMOUNTS OF EXPANSION OF THE NICKEL ELECTRODES WERE MEASURED WITHOUT ANY COMPRESSIVE FORCES
- RESULTS OF COMPRESSING STACKS OF TYPICAL CELL COMPONENTS

Electronics Technology Center
Energy Technology Department

THE AEROSPACE CORPORATION

We had several sources of information that we were able to use in our efforts to upgrade and validate our static model for nickel-hydrogen cells. Different pieces of the inputs that were available to us were complete in differing degrees, but they were all helpful. Information on the dryout or partitioning aspects of six different cells were used in this study. Common to all cases was an evaluation of the cell performance at the time the cell was disassembled or the dryout test was completed. The three dryout tests were ended at the point where there was a significant increase in internal impedance. Full cell capacity was always available, but at a reduced terminal voltage. In all cases, information was available on the initial amount of electrolyte that was added to the cell. Three tests were carried out where the water portion of the electrolyte was incrementally removed using our dryout technique. Three data sets were available from cycling tests that were stopped and the partitioning of the electrolyte between components was determined or estimated. The cells covered several different manufacturers, cycling conditions, electrolyte concentrations, and nickel electrode types. The compressive characteristics of representative cell components from disassembled cells were also incorporated into this study. In all cases, it was assumed that the results of post test analysis was correct and the results of the static model was required to give the same results. All six cells were treated equally and the model was expected to be equally accurate when applied to each example.

COMPONENTS STUDIED

- GAS SCREENS
- HYDROGEN ELECTRODES
- ZIRCAR SEPARATORS
- NYLON SEPARATORS*
- UNIMPREGNATED PLAQUE
- NICKEL ELECTRODES WITH DIFFERENT AMOUNT OF EXPANSION - 10%, 20%, AND 30%
- BELLEVILLE WASHERS*
- POLYSULFONE CORE PIECE*

*BASED ON AVAILABLE LITERATURE INFORMATION

Electronics Technology Center
Energy Technology Department

THE AEROSPACE CORPORATION

The above listed items are typical of nickel-hydrogen cells. Over the years, our laboratory has disassembled many different kinds of IPV nickel-hydrogen cells. We were able to select representative components that were available to us from these DPA studies. Information on different Belleville washers and the tensile characteristics of the material used for the core piece were obtained from manufacturer data sheets. Earlier SAFT cell designs used nylon-based separator felts that had been reported upon at previous NASA Battery Workshop meetings.*

Denning, C. and Jamin, T. "Polyamide Separator Behavior in NiH_2 Cells", Proceedings of the 1994 NASA Aerospace Battery Workshop

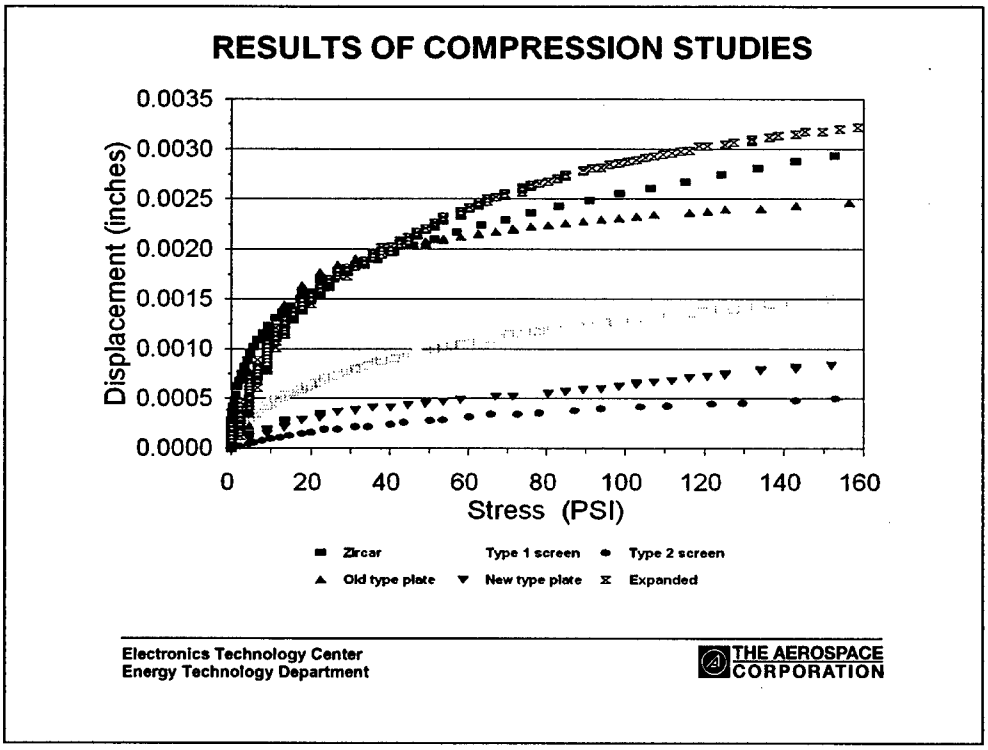

The compression studies consisted of stacking eight elements of the item under investigation and applying pressures using an Instron machine. The amount of displacement was monitored along with the compressive forces. From the plot of displacement on a per item basis, it is seen that all of the components had the same general shape as they were compressed. Some components were more resistant to the compressive forces, but they all displayed a tendency to be squeezed to a thinner dimension as pressure was applied to them. On this figure, the compressibility of three different nickel electrodes are plotted - one taken from a cell that was almost new (about 10% expansion relative to the original plaque thickness due to the activation step), one that had about a 20% increase in its electrode thickness, and another had a 30% increase in its out-of-cell thickness. These thickness variations resulted from different amounts of cycling stress.

The information in this figure is needed to help estimate the thickness of these components while they are still inside the cell under the compressive forces of the core piece and the end plates.

To be noted in the figure is the fact that when the cell is early in life where not too much expansion has taken place, the zircar separator is less resistive to compression than the nickel electrode. However, after extended cycling, the zircar separator is less compressible than the electrode that had expanded about 30%. It is not entirely trivial to estimate the thicknesses of all the components while they are still in the cell following a life cycle test.

ESTIMATING IN-STACK THICKNESSES

- DETERMINE COMPRESSION CHARACTERISTICS OF ALL COMPONENTS INCLUDING THE BELLEVILLE WASHER
- NICKEL ELECTRODES WITH DIFFERENT AMOUNTS OF EXPANSION MUST BE TESTED
- DETERMINE THE ELONGATION OF THE CORE PIECE
- BY TRIAL AND ERROR, DETERMINE WHERE THE SUM OF INCREASES EQUALS THE SUM OF THE DECREASES
- THESE DIMENSIONS ARE THEN TESTED IN THE MODEL

Electronics Technology Center
Energy Technology Department

THE AEROSPACE CORPORATION

When cells are built, the plate pack of electrodes, separators, and gas screens are compressed between endplates and one or more Belleville washers. After the proper degree of compressive forces have been applied to the plate pack, the end nut is attached to the central core piece of the cell assembly. At this point, all of the components are squeezed together. Depending on the compressive characteristics of each component, it will be somewhat thinner than it was in the uncompressed state. The Belleville washer will be compressed and the polysulfone core piece will be stretched.

As cycling proceeds, the nickel electrodes will expand depending on the amount of stress placed on them by the cycling conditions. This will result in more compressive forces on the remainder of the components. At the end of the test, the components are set free of the compressive forces and then measured for the amount of expansion they have experienced. The real question is what was their thickness when they were still in the cell. It is under the compressed condition in the plate pack that the electrolyte is distributing itself between the different components.

SUMMARY OF RESULTS

Cell Identification	Cell A	Cell B	Cell C	Cell D	Cell E	Cell F
Cell Dryout Test	Yes	Yes	No	No	Yes	Yes
Fill Concentration -%	38	31	31	31	31	26
Partitioning - by analysis						
In Separator %	20	20	37	42	N/A	N/A
In Nickel Elect. %	77	75	60	54	N/A	N/A
Partitioning - from model						
In Separator %	20	15	37	42	22	6
In Nickel Elect. %	75	79	59	54	74	90
In Hydrogen Elect. %	5	6	4	4	5	4
Fill % - Based on Model						
Overall Cell %	80	74	77	82	63	71
Separator %	45	30	56	65	27	13
Plate Expansion						
From DPA-%	12	6	20	12	12	N/A
Used in Model-%	6	0	8	5.5	6	0
Corrosion of Ni - %	0	0	6.3	5.5	0	0
% Vol. Loss at Dryout	N/A	25	N/A	N/A	20/32	28

Electronics Technology Center
Energy Technology Department

THE AEROSPACE CORPORATION

The information that was available to us was placed in the table above. The initial conditions and fill amounts were all known and the out-of-cell plate thicknesses were measured at the end of the test: Cells A through D had measurements of the partitioning between components. At this point, the static model for each of these cells was set for full discharge, the separator was assumed to be 10% compressed, the amount of corrosion was inserted, the amount of plate expansion as measured out-of-cell was inserted, and the model was solved.

If the results did not match the results of the partitioning that were obtained by chemical analysis, the amount of expansion of the nickel electrodes was adjusted so that a match occurred. This process worked for three of the four cells. Cell B would have required a net compression to bring the model results in line with the analysis data. With the exception of cell C, an adjustment of about 6% in the as-measured expansion was necessary to bring the results of the static model in line with the results from the chemical analysis.

Following this, the assumption used in the model which stated that the nickel electrode was always 100% filled was changed to be in keeping with the more accurate results of the earlier NASA pore size studies. By assuming that only 95% of the nickel electrode pores were filled with electrolyte rather than 100%, it was no longer necessary to apply any adjustments to the electrode thickness. Irrespective of what the model predicts, the evidence from the different dryout and partitioning studies demonstrate that when the separator is only about 30% filled with electrolyte, significant performance degradation results due to dryout.

SUMMARY

- THE LITERATURE HAS DOCUMENTED A FEW CASES OF CELL DRYOUT
- SPECIAL DRYOUT TESTS AND THE AVAILABLE INFORMATION RELATED TO PLATE EXPANSION AND SUBSEQUENT PARTITIONING OF ELECTROLYTE SUGGEST:
  - Dryout results in significant increases in resistance before it results in diffusion-limited currents
  - Double layer Zircar separators are almost impossible to dry out
  - Single layer Zircar designs should not be rejected out of hand
  - The original static model predicted a dryer separator than that found in DPA studies
  - Upgraded model useful for evaluating cell designs and projected cycle life based on known degradation modes

Electronics Technology Center
Energy Technology Department

THE AEROSPACE CORPORATION

There have been documented and undocumented cases of cell dryout during life cycle testing. There have also been documented and undocumented cases of excessive amounts of expansion of nickel electrodes leading to breakage of the core piece and/or failure of the threads between the core piece and the core nut. Knowledge of the impact of these phenomenon is helpful in finding ways to avoid these situations. The static cell model which has now been updated and validatied coupled with estimates for corrosion and expansion rates as affected by cycling conditions, can be used to assess either a suggested cell design or a suggested set of cycling conditions and recharge protocols.

Some cell designs use two layers of separator material, whereas others use only one. The weight savings resulting from using only one layer are significant. The model coupled with the understanding of the changes taking place during cycling can be used to evaluate the suitability of using the lighter-weight single layer cell design.

As dryout is approached, a small error in the accuracy of the model resulted in significant changes in the suggested percentage of the pores of the separator that were filled with electrolyte. For this reason, it was necessary to be as accurate as possible in terms of the assumptions that were used in the model. Further, these assumptions had to be checked against the actual data that were available following different kinds of tests that addressed the issues of cell performance and the partitioning of electrolyte between components. We now feel very comfortable with the accuracy and utility of our nickel-hydrogen model.

EAGLE PICHER
Eagle-Picher Technologies, LLC

POWER Subsystems

NICKEL-HYDROGEN LIFE MODELING

Robert A. Brown
Eagle-Picher Technologies, LLC

NASA Aerospace Battery Workshop
November 18, 1999

INTRODUCTION

- Nickel-Hydrogen system has accumulated extensive life test database
- Database can be used to accurately size batteries to meet given mission requirements & reliably predict their cycle life capabilities
- Battery users are more frequently asking battery manufacturers to recommend battery capacity given complex & variable discharge profiles

LIFE TEST DATA - DESIGN PARAMETERS

Test	Cell Designation	Positive Electrode	Separator
A	RNH 50-15	Slurry	Asbestos
B	RNH 30-1	Slurry	Asbestos
C	RNH 50-15	Slurry	Asbestos
D	RNH 65-33	Slurry	Double Zircar

EAGLE PICHER
Eagle-Picher Technologies, LLC

POWER Subsystems

LIFE TEST DATA - TEST PARAMETERS

Test	Cell Designation	Test Facility	DOD	Discharge Rate	Temp	Recharge Ratio	Test Status
A	RNH 50-15	EPT	15%	.4C	5°C	1.04	141,300 Cycles Ongoing
B	RNH 30-1	EPT	30%	.5C	5°C	1.03	78,250 Cycles Terminated
C	RNH 50-15	EPT	45%	.4C	5°C	1.04	59,300 Cycles Ongoing
D	RNH 65-33	NSWC-CRANE	60%	1C	10°C	1.05	41,600 Cycles Ongoing

EAGLE PICHER
Eagle-Picher Technologies, LLC

POWER Subsystems

60% DOD DATA

NSWC Crane Pack ID 5004L 3 cells

Voltage/pressure/Recharge EOC/EOD Trend Plot 04/20/1992 - 06/10/1999
EPI 65 AmpHr 3.5" 60% DOD 10 Deg C 31% KOH Acq. Impreg. (Cells 4-6)
× Vavg ◇ Vmax △ Vmin

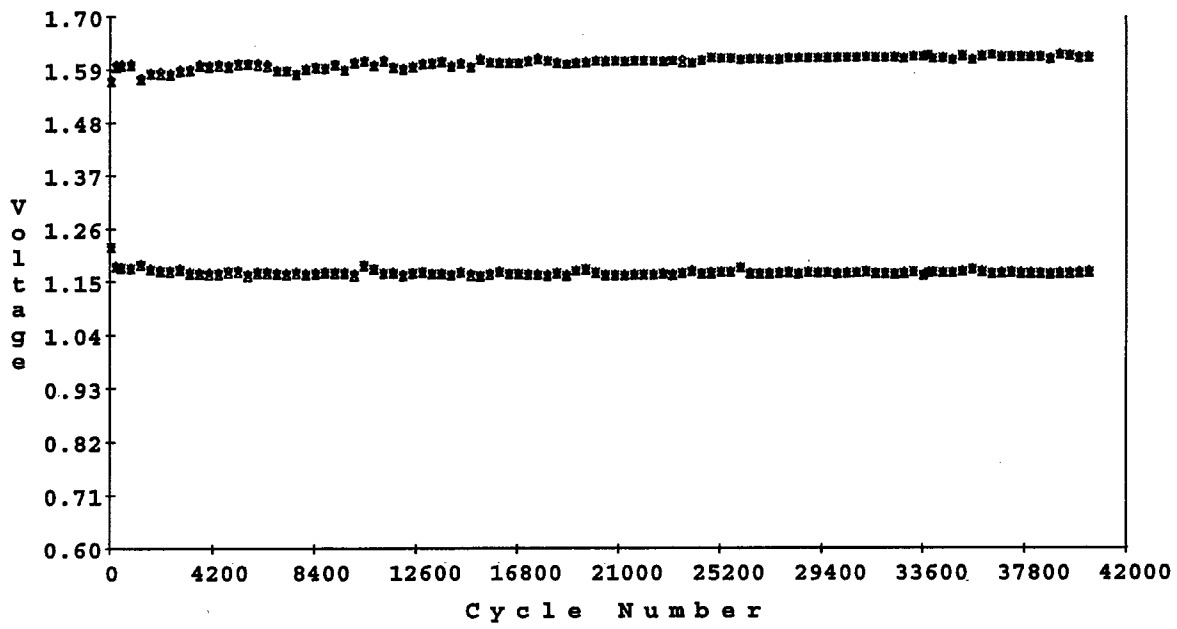

EAGLE PICHER

Eagle-Picher Technologies, LLC

POWER Subsystems

CYCLE LIFE VS DEPTH OF DISCHARGE

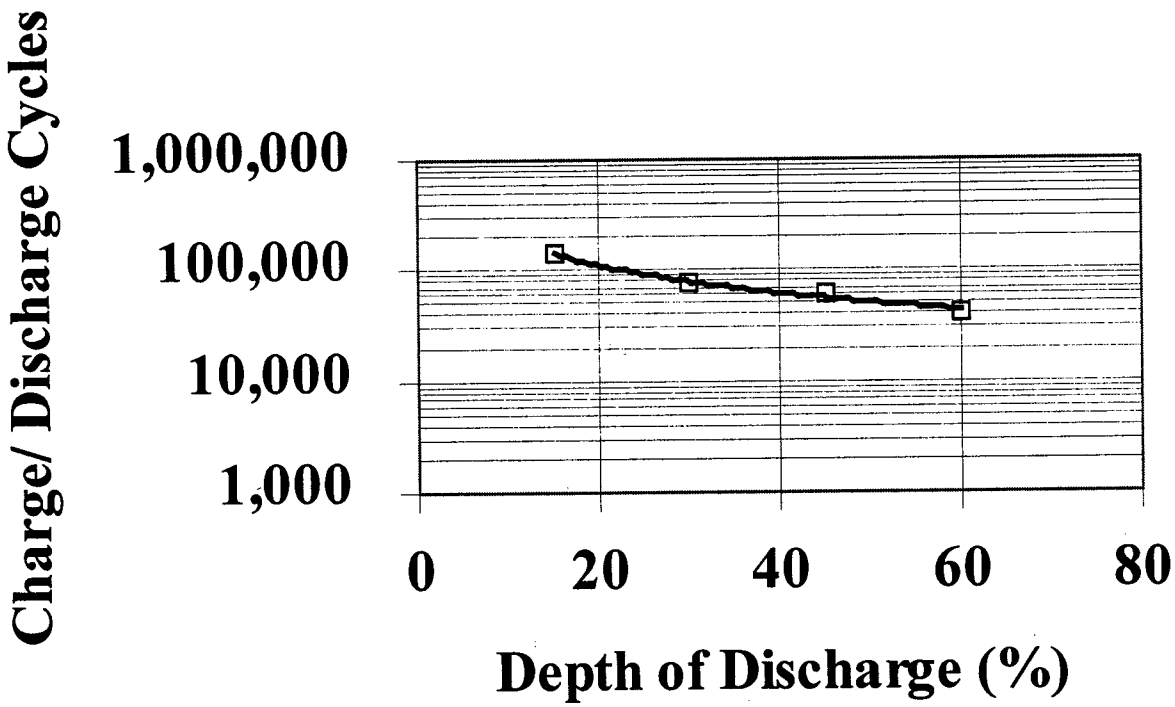

EAGLE PICHER
Eagle-Picher Technologies, LLC

POWER Subsystems

CAPACITY FADE VS CYCLE LIFE

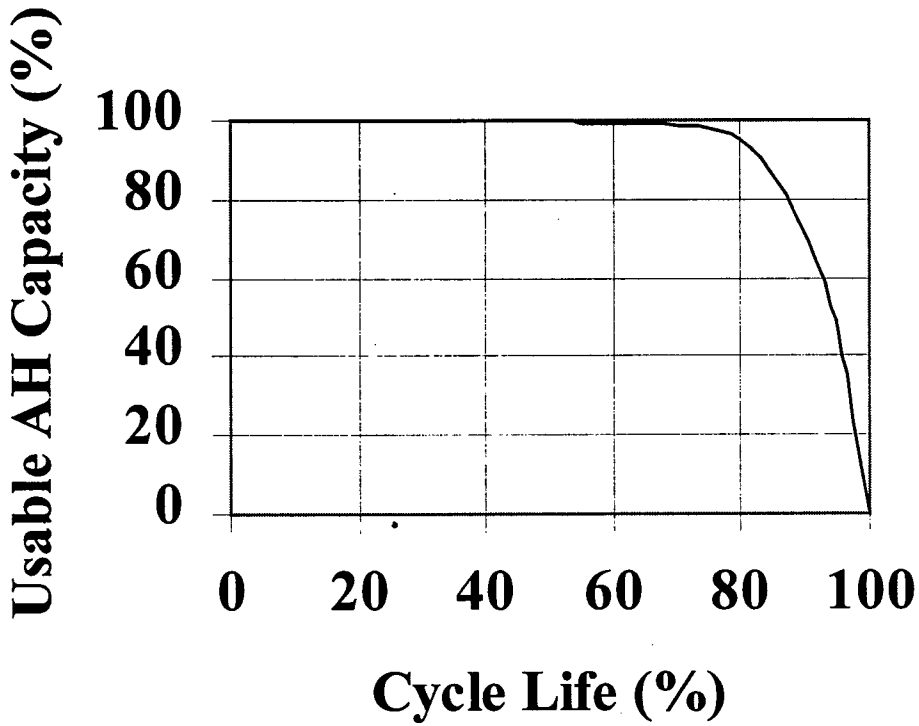

SAMPLE MISSION REQUIREMENTS

Mission Phase	Number of Cycles	Energy Per Cycle (WH)
Deployment	5	2,300
Operation	10,400	2,000
Operation	10,400	2,200
Operation	10,400	2,400
Operation	10,400	2,600
De-orbit	100	2,100

EAGLE PICHER
Eagle-Picher Technologies, LLC

POWER Subsystems

LIFE MODELING TABLE

Mission Life:	9.5
Discharge Multiplier:	1.0
Life Multiplier:	1.0

NiH_2 Parameters				
AH Capacity	Volts/ Cell	No. Cells	System Voltage	System Whr
102.2	1.25	30	37.5	3,833

Discharge Cycles/ Mission	Discharge (WHr)	Bin DOD (%)	Avg DOD (%)	Life Capability (Individual Bin)	Pct of Cycle Life	Cum Cycle Life Expended (%)	Remaining Usable Capacity (%)	Avg. DOD x BOL Capacity (AH)	Delta Usage Capacity (AH)	Total Capacity (AH)	Remaining (WHr)
5	2,300	60.0	60.0	43,188	0.01	0.01	99.8	61.3	40.8	102.1	3,830
10,400	2,000	52.2	52.2	48,948	21.2	21.3	99.7	53.3	48.7	102.0	3,827
10,400	2,200	57.4	54.8	44,943	23.1	44.4	100.2	56.0	46.3	102.3	3,835
10,400	2,400	62.6	57.4	41,573	25.0	69.4	98.8	58.7	43.0	101.7	3,813
10,400	2,600	67.8	60.0	38,697	26.9	96.3	36.3	61.3	14.8	76.2	2,856
100	2,100	54.8	60.0	46,855	0.2	96.5	34.6	61.3	14.1	75.5	2,829
41,705											

Using the cycle life vs. DOD and capacity fade characteristics, the remaining energy is calculated for each energy bin. This process takes into account the capacity degradation caused by each energy bin. The requirement is that the remaining energy must be sufficient to support the energy bin at an acceptable DOD.

EAGLE PICHER
Eagle-Picher Technologies, LLC

POWER Subsystems

RUNDOWN EFFECTS ON STATE OF CHARGE

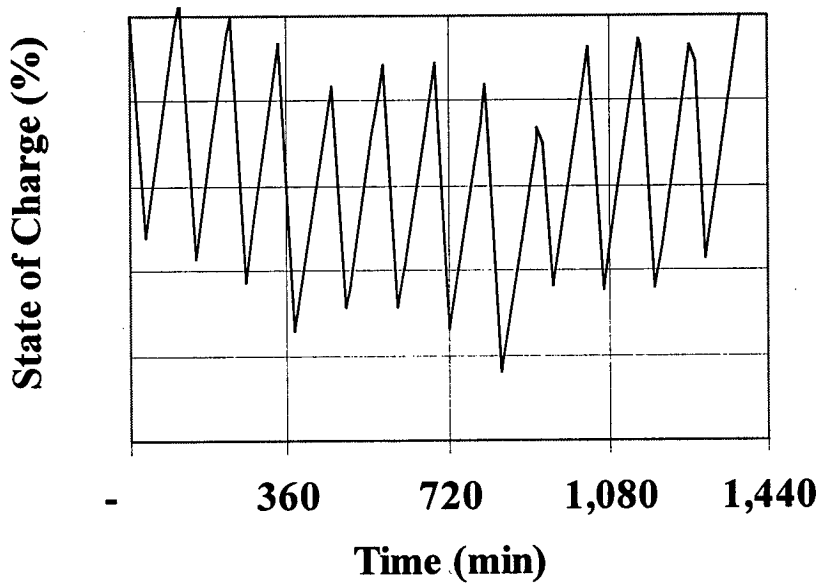

It is possible that energy balance is not achieved for each cycle.
In this case the state of charge will rundown during the orbital day.
This introduces the additional requirement that the degraded capacity must support each energy bin starting at less than full charge.

REVISED MISSION REQUIREMENTS

- Maximum Rundown Capacity = 27 AH (1012 WH)
- To support highest energy discharge from maximum rundown condition, "Adjusted" energy requirement becomes 2600 WH + 1012 WH = 3612 WH

EAGLE PICHER
Eagle-Picher Technologies, LLC

POWER Subsystems

REVISED LIFE MODELING TABLE

Mission Life:	9.5
Discharge Multiplier:	1.0
Life Multiplier:	1.0

NiH_2 Parameters				
AH Capacity	Volts/ Cell	No. Cells	System Voltage	System Whr
114.75	1.25	30	37.5	4,303

Discharge Cycles/ Mission	Discharge (WHr)	Bin DOD (%)	Avg DOD (%)	Life Capability (Individual Bin)	Pct of Cycle Life	Cum Cycle Life Expended (%)	Remaining Usable Capacity (%)	Avg. DOD x BOL Capacity (AH)	Delta Usage Capacity (AH)	Total Capacity (AH)	Remaining (WHr)
5	2,300	53.4	53.4	47,910	0.01	0.01	99.8	61.3	53.3	114.7	4,300
10,400	2,000	46.5	46.5	54,299	19.2	19.2	99.7	53.3	61.2	114.5	4,296
10,400	2,200	51.1	48.8	49,856	20.9	40.0	100.3	56.0	58.9	114.9	4,310
10,400	2,400	55.8	51.1	46,118	22.6	62.6	99.1	58.7	55.6	114.2	4,284
10,400	2,600	60.4	53.4	42,927	24.2	86.8	83.3	61.3	44.5	105.8	3,968
1	3,612	83.9	53.5	31,977	0.0	86.8	83.3	61.3	44.5	105.8	3,968
100	2,100	48.8	53.4	51,977	• 0.19	87.00	82.76	61.3	44.2	105.5	3,958
41,706											

The modeling table has been updated to incorporate an "adjusted" energy requirement to accommodate the rundown condition.

CONCLUSIONS

- Database supports using Nickel-Hydrogen system for LEO cycling at high depths of discharge (60%)
- Life models can be used to select battery capacities for complex mission requirements

Nickel-Hydrogen Cell Positive Precharge Signatures

Chuck Lurie
TRW Space and Electronics Group
Redondo Beach, California 90278

The 1999 NASA Aerospace Battery Workshop
The Huntsville Hilton
Huntsville, Alabama
November 16 - 18, 1999

Wksp9902.ppt

Positive Precharge Characterization
Outline

- What is precharge?
- Why positive precharge?
- How is precharge characterized?
- Generic characterization
- Experience base

Wksp9902.ppt

Precharge

- Cells can be designed with
  - Equal nickel and hydrogen electrode capacities
  - Excess hydrogen electrode capacity
  - Excess nickel electrode capacity
- "Balanced" designs, with equal nickel and cadmium electrode capacities, are not appropriate for most applications.
- For many years nickel-hydrogen cells were were provided with excess hydrogen, e.g., with hydrogen precharge.
- Cells with excess nickel electrode capacity, e.g., nickel precharge configuration, provide certain advantages and are being baselined for many missions.

Cell Capacity Diagrams

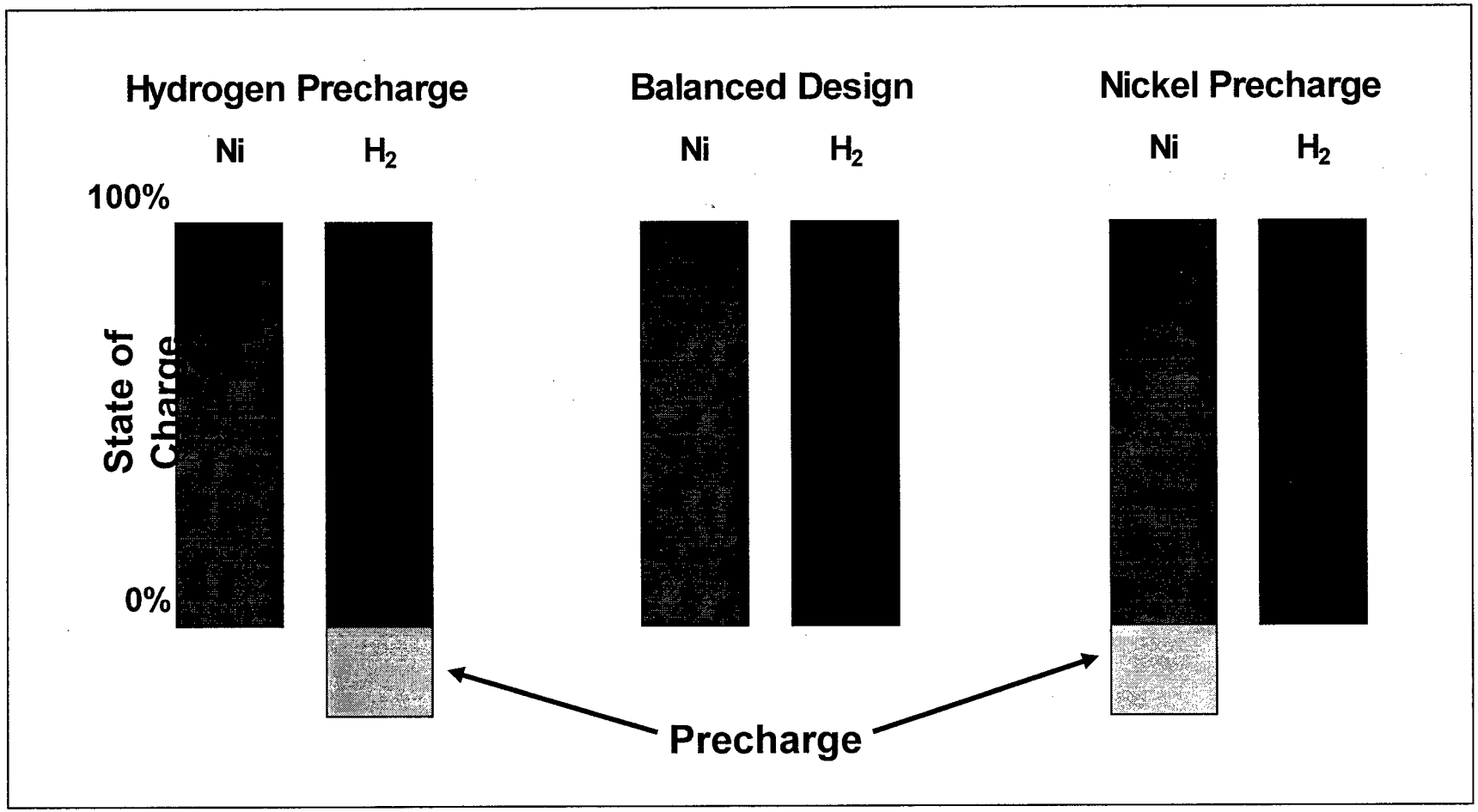

Wksp9902.ppt

NiH_2 Cell Chemistry
Discharge/Reversal

Discharge

Nickel	$2\ NiOOH + 2\ HOH + 2e \rightarrow 2\ Ni(OH)_2 + 2\ OH^-$	$E° = +0.5v$
Hydrogen	$H_2 + 2\ OH^- - 2\ e \rightarrow 2\ HOH$	$E° = +0.8v$
	$2\ NiOOH + H_2 \rightarrow Ni(OH)_2$	$E° = +1.3v$

Overdischarge (Reversal) With Hydrogen Precharge

Nickel	$2\ HOH + 2\ e \rightarrow 2\ OH^- + H_2$	$E° = -0.8v$
Hydrogen	$H_2 + 2\ OH^- - 2\ e \rightarrow 2\ HOH$	$E° = +0.8v$

No Net Reaction; H_2 Recombines

Wksp9902.ppt

NiH_2 Cell Chemistry
Overdischarge (Reversal) With Nickel Precharge

Active Nickel Precharge Present

Nickel	$2\ NiOOH + 2\ HOH + 2\ e$	$\rightarrow 2\ Ni(OH)_2 + 2\ OH^-$	$E° = +0.5v$
Hydrogen	$2\ OH^- - 2\ e$	$\rightarrow \frac{1}{2}\ O_2 + HOH$	$E° = -0.4v$
	$2\ NiOOH + HOH$	$\rightarrow 2\ Ni(OH)_2 + \frac{1}{2}\ O_2$	$E° = +0.1v$

Active Nickel Precharge Exhausted/Unavailable

Nickel	$2\ HOH + 2\ e$	$\rightarrow 2\ OH^- + H_2$	$E° = -0.8v$
Hydrogen	$2\ OH^- - 2\ e$	$\rightarrow \frac{1}{2}\ O_2 + HOH$	$E° = -0.4v$
Electrochemical	HOH	$\rightarrow \frac{1}{2}\ O_2 + H_2$	$E° = -1.2v$
Chemical	$\frac{1}{2}\ O_2 + H_2$	HOH	

Wksp9902.ppt

Verification of Nickel Precharge
Preparation for Storage

- Discharge at the C/2 rate to 1.0 volt. (10°C)
- Resistor-down to < 0.020 volt. (R = 10/C ohms)
- Charge at the C/10 rate for 16 hours.
- Immediately discharge at the C/5 rate to 0.5 volt.
- Resistor-down to 0.000 volt. (20°C)
- Discharge at the - C/30 rate (measured capacity) for 10 minutes.
- Criteria: Cell voltage shall be < - 0.30 volts at 10 minutes.

Wksp9902.ppt

Discharge into Reversal

Hydrogen Precharge -- C/2 Rate

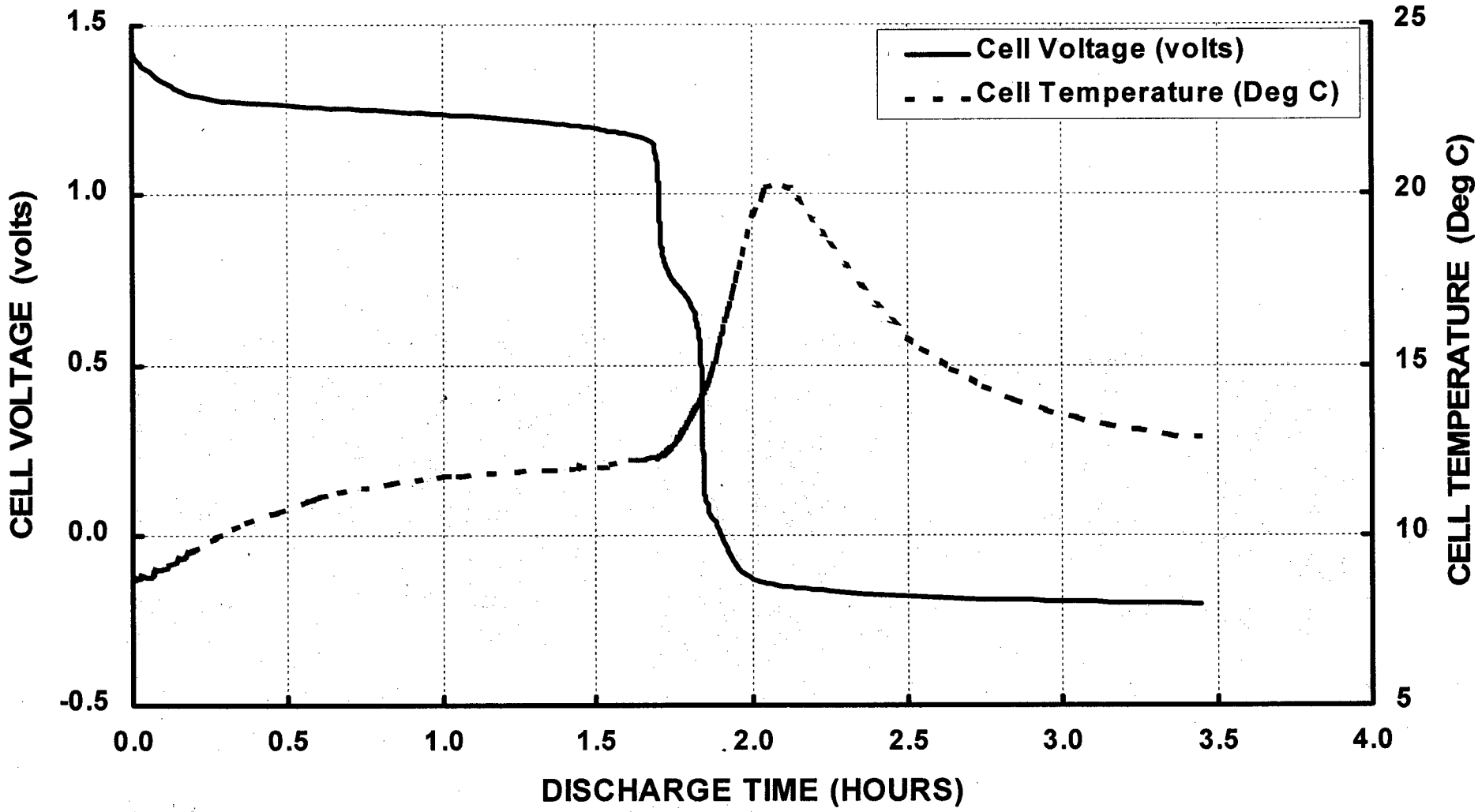

Wksp9902.ppt

Discharge into Reversal

Nickel Precharge -- C/2 Rate

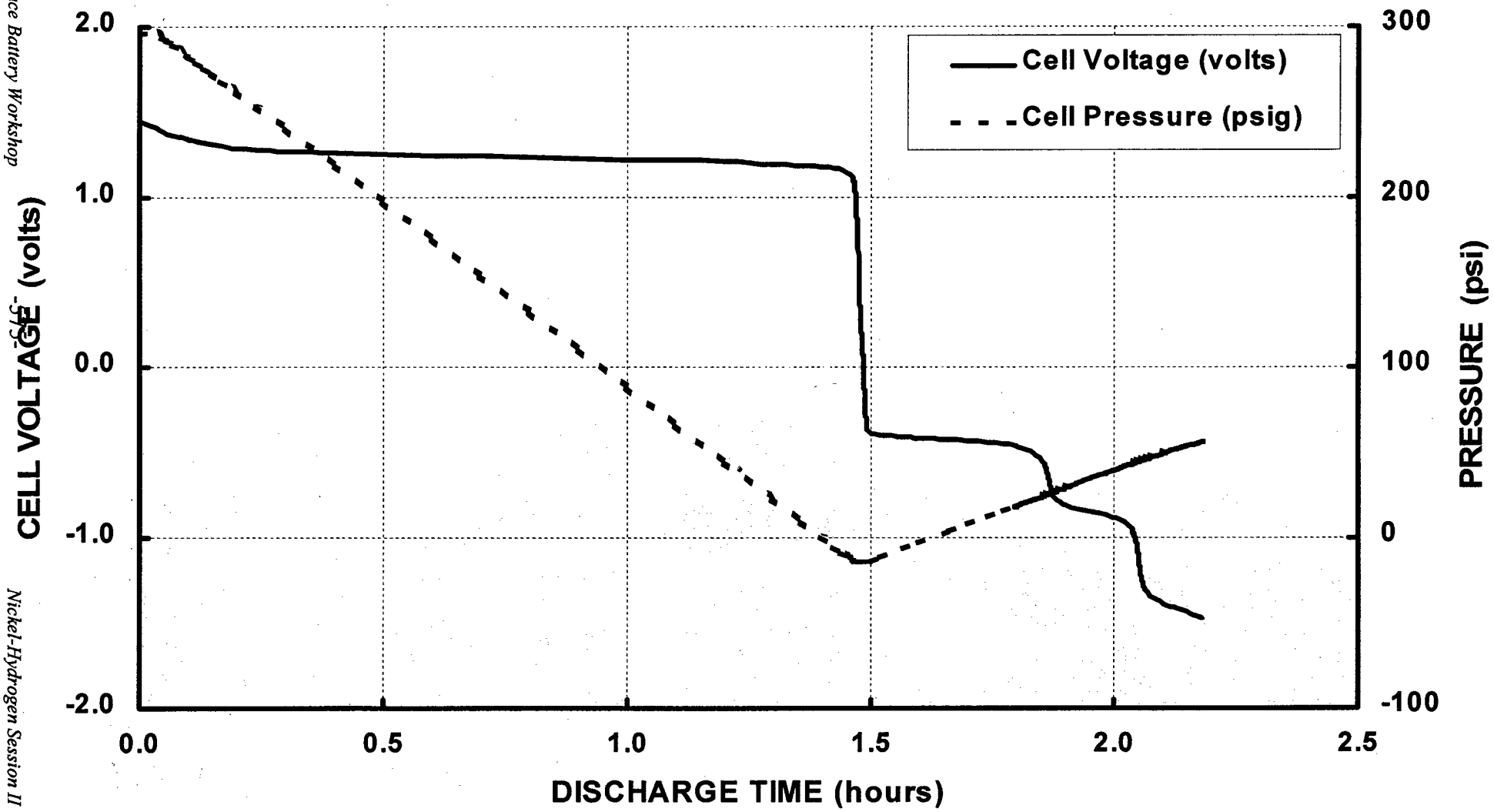

Wksp9902.ppt

Precharge Verification

Hydrogen Precharge -- Typical

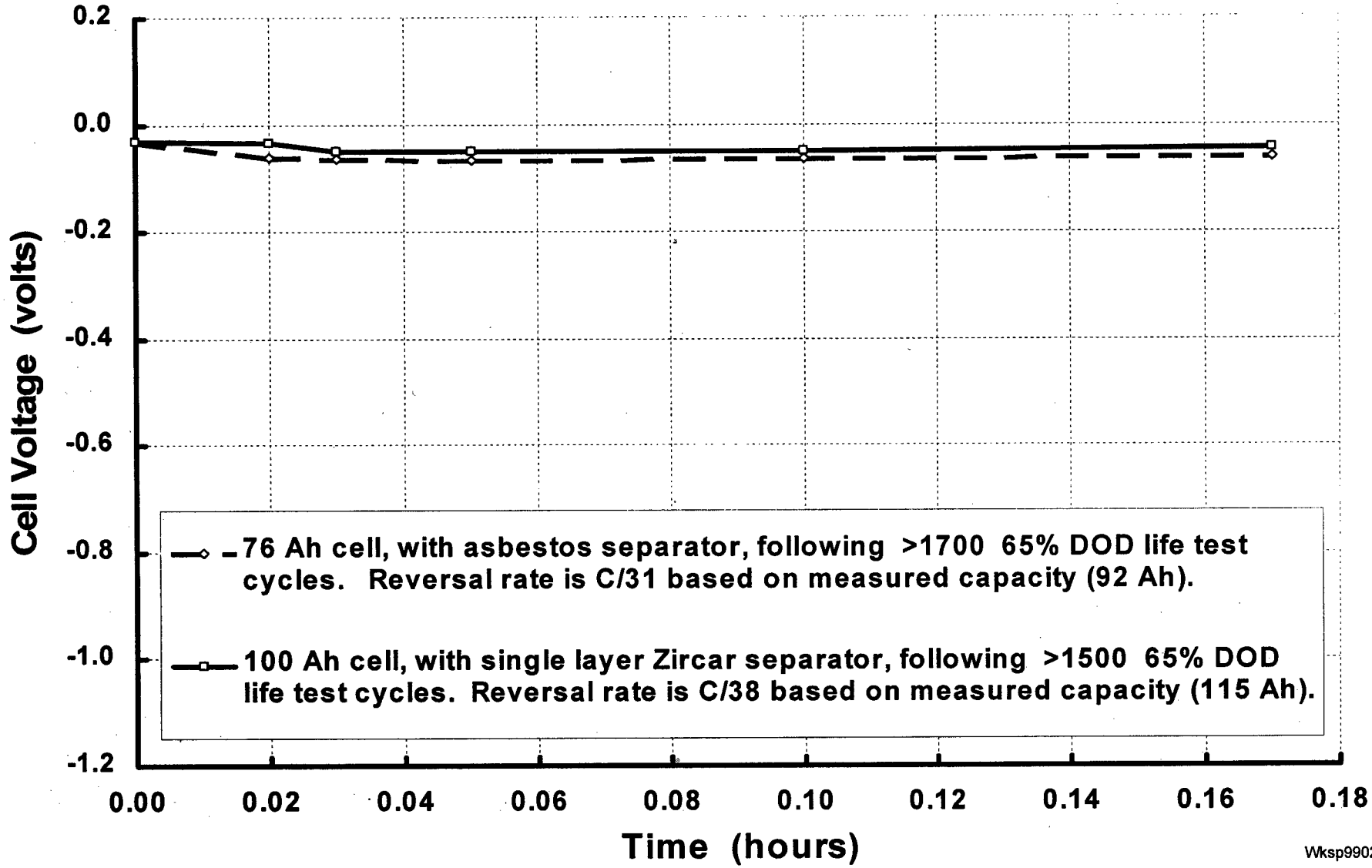

Wksp9902.ppt

Precharge Verification

Nickel Precharge -- Eagle Picher RNH60-5 Cells

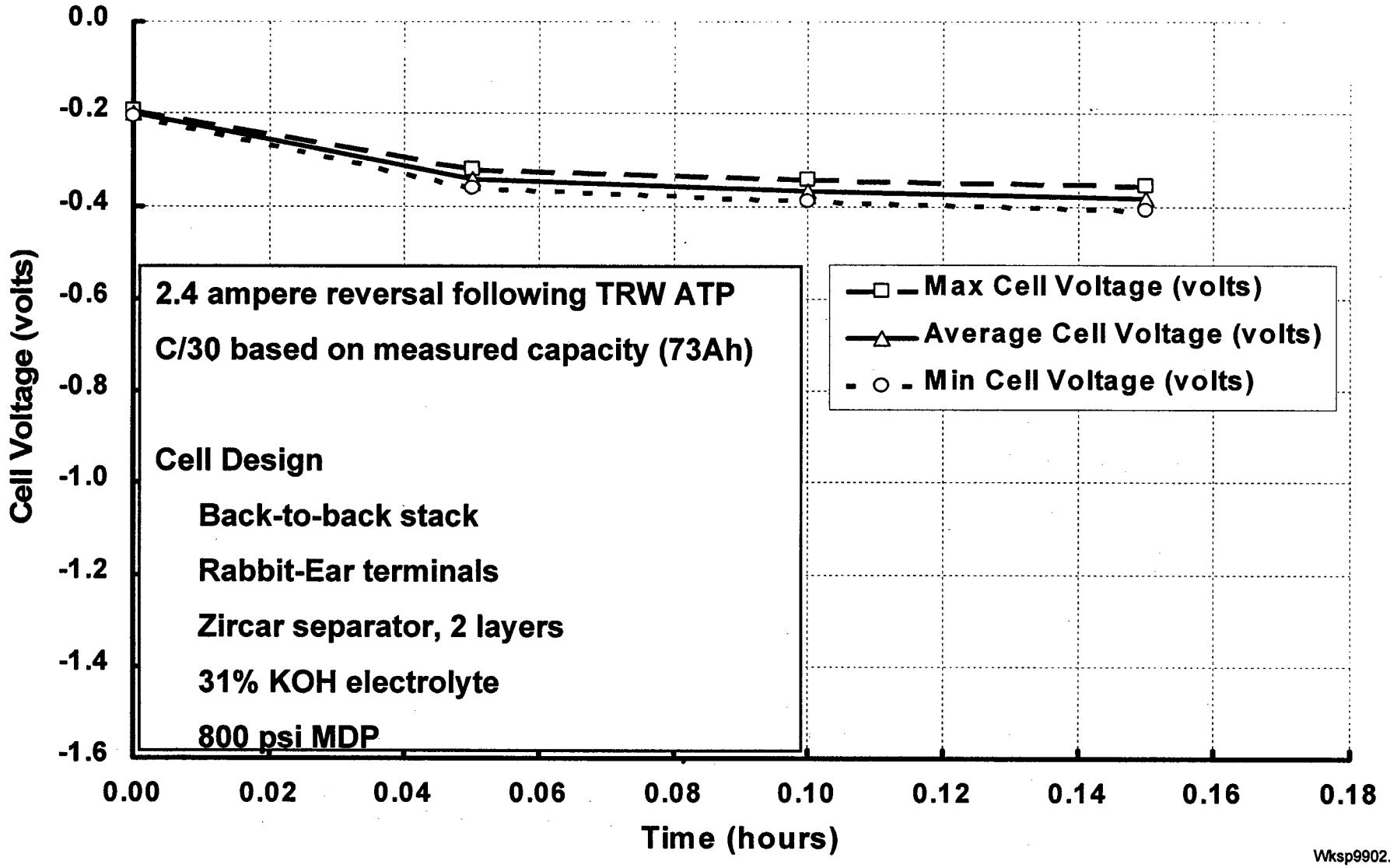

Wksp9902.ppt

Precharge Verification

Nickel Precharge -- Eagle Picher RNH160-3 Cells

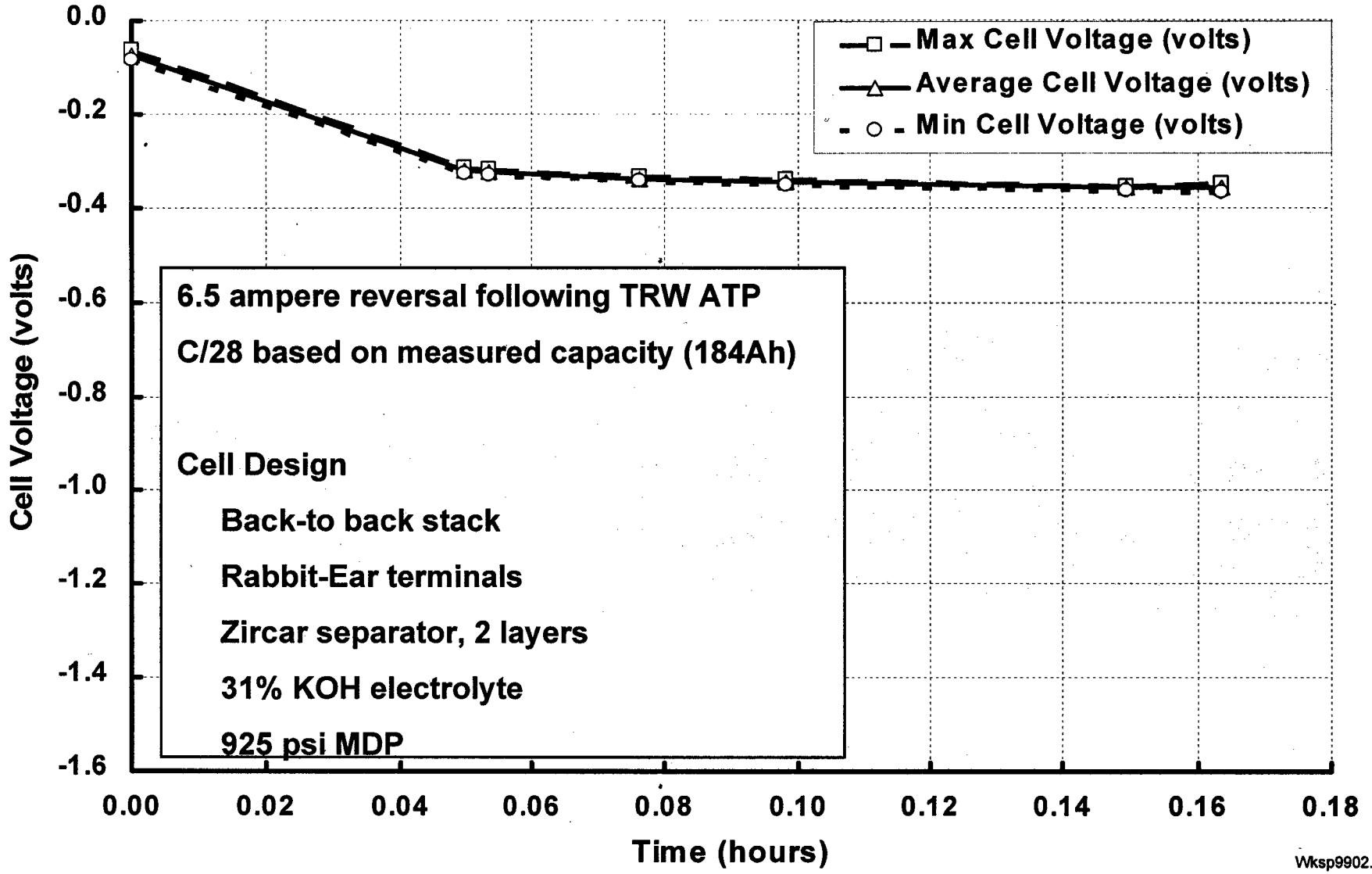

Wksp9902.ppt

Precharge Verification

Nickel Precharge -- Eagle Picher RNH86-1 Cells

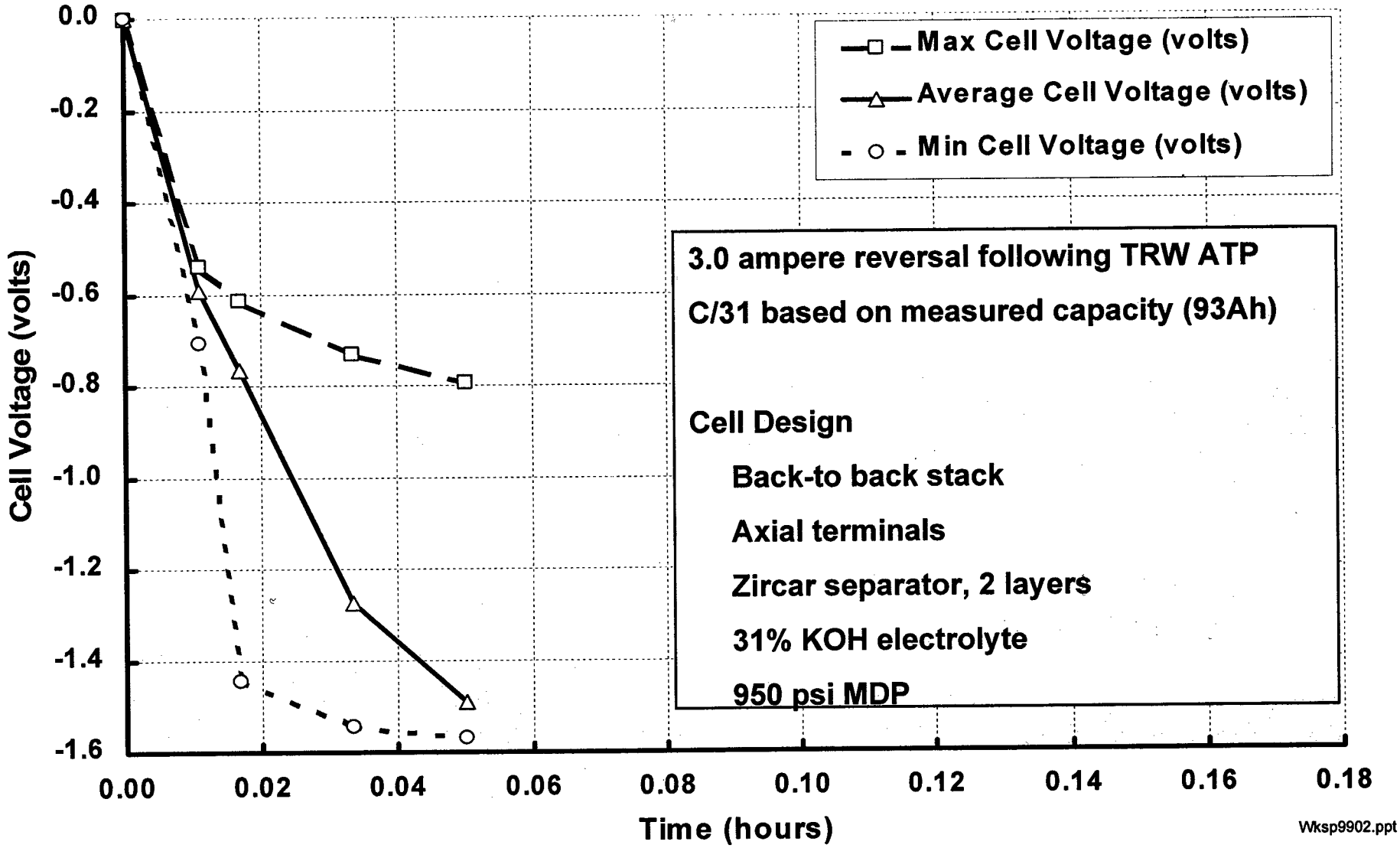

Wksp9902.ppt

Precharge Verification

Nickel Precharge -- Eagle Picher RNH86-1 Cells

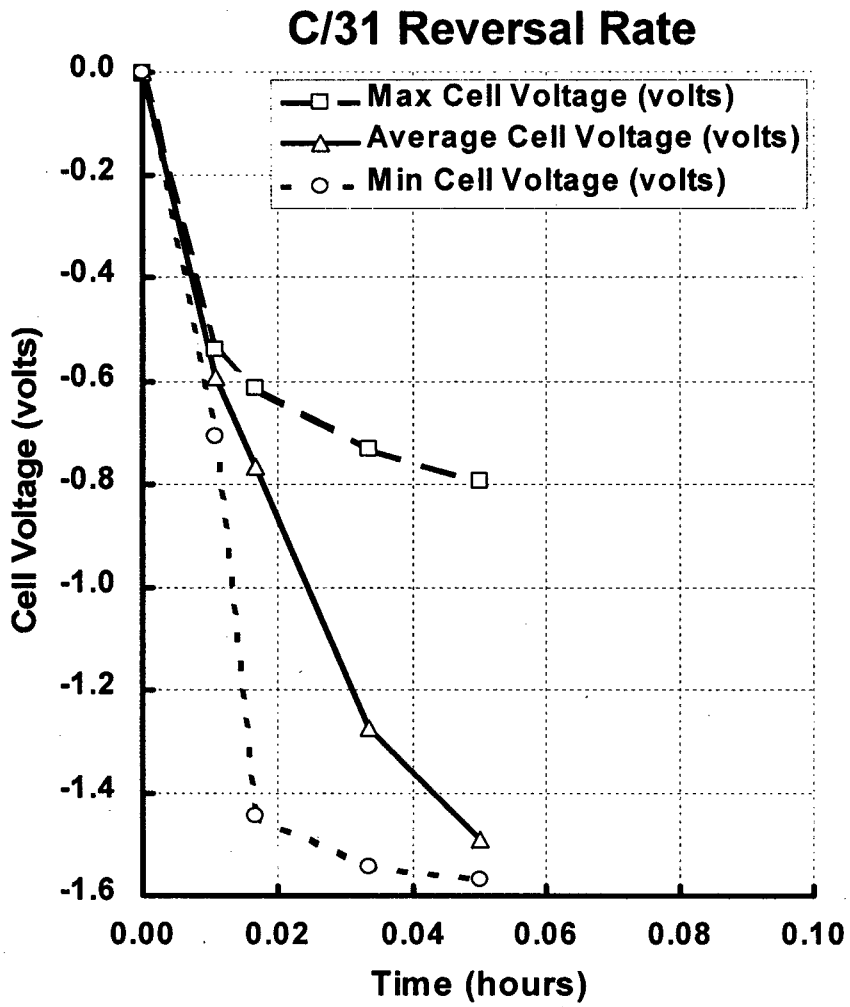

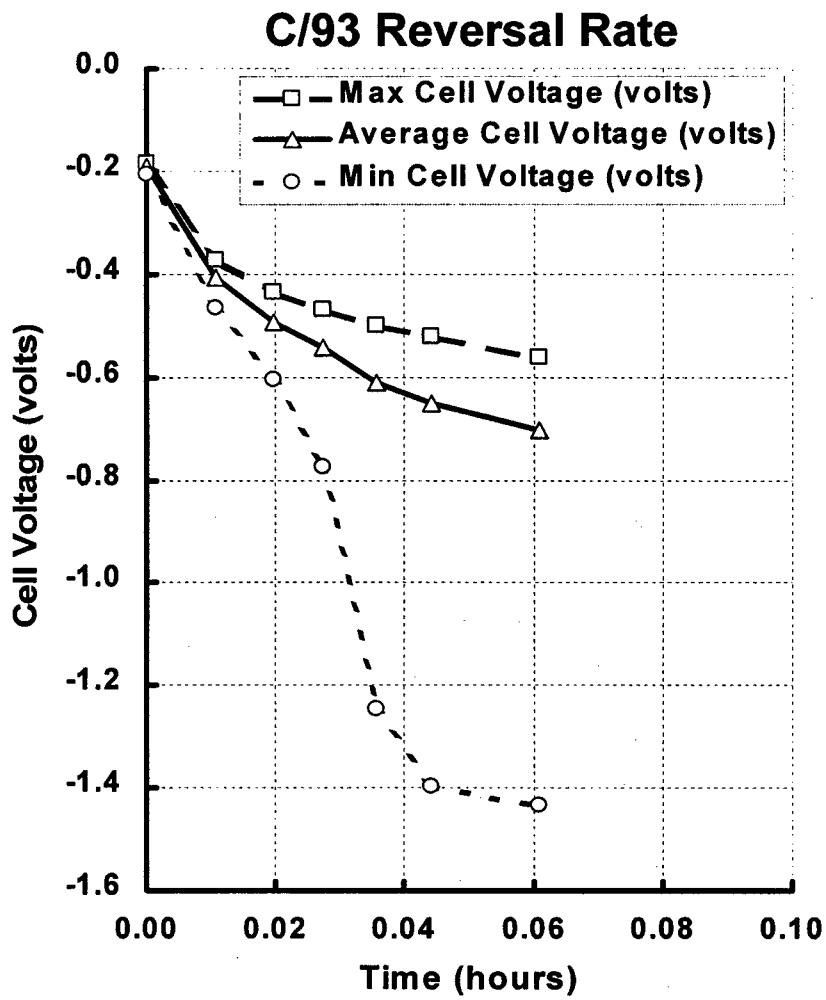

Wksp9902.ppt

Precharge Verification

Nickel Precharge -- Eagle Picher RNH98-1 Cells

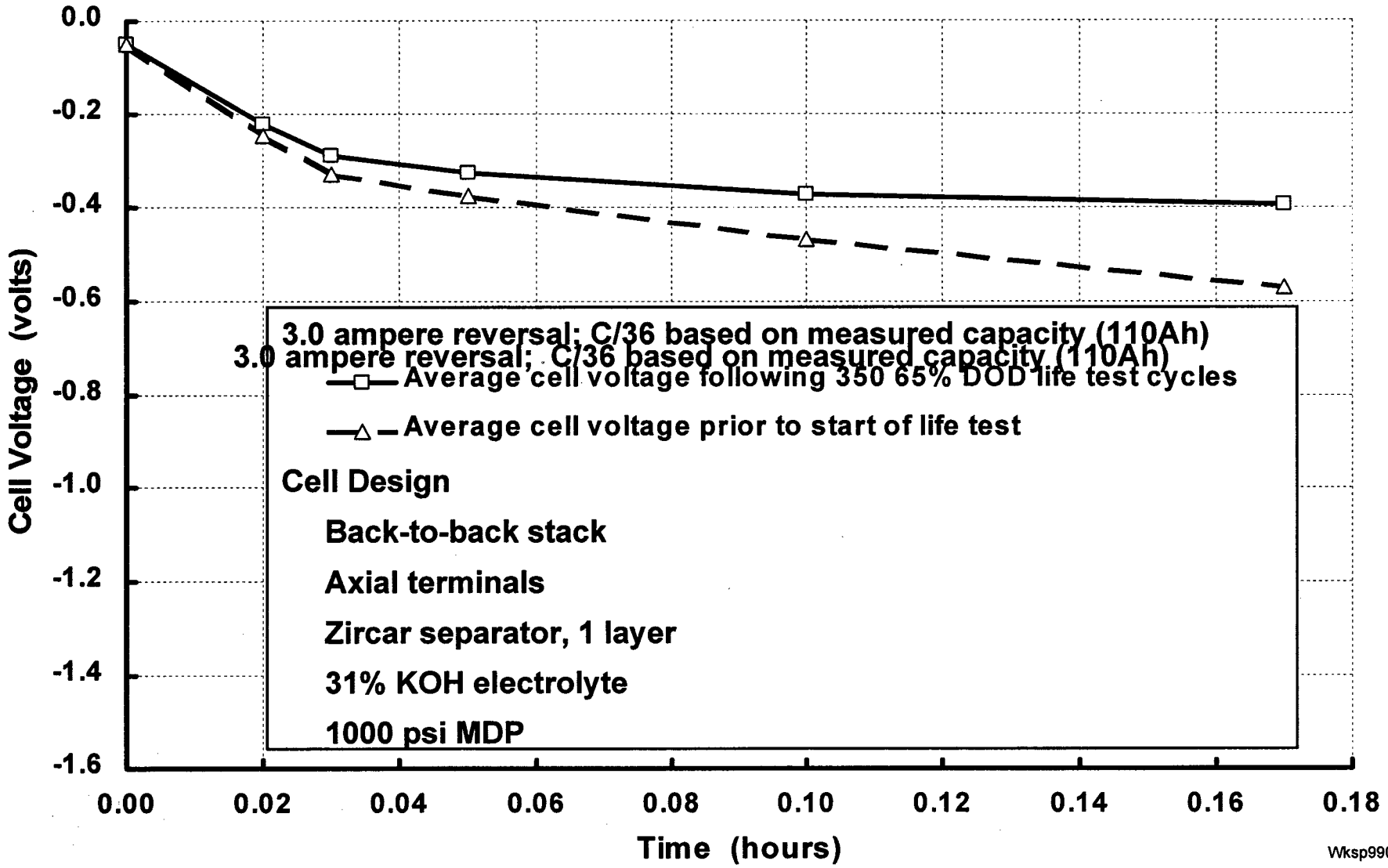

Wksp9902.ppt

Precharge Verification

Nickel Precharge -- 22-Cell 40Ah Battery

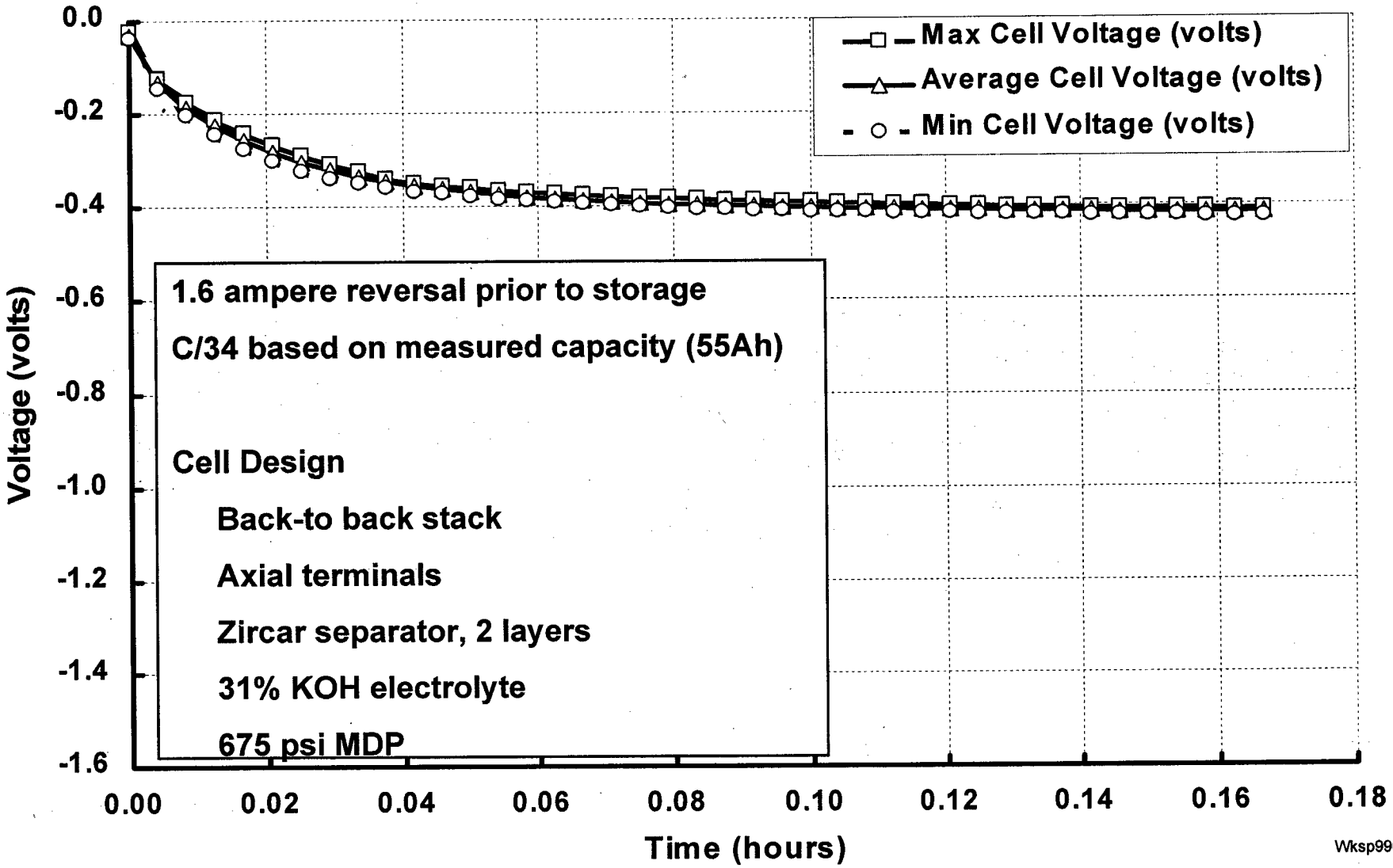

Wksp9902.ppt

22-Cell 40Ah Battery -- Precharge History

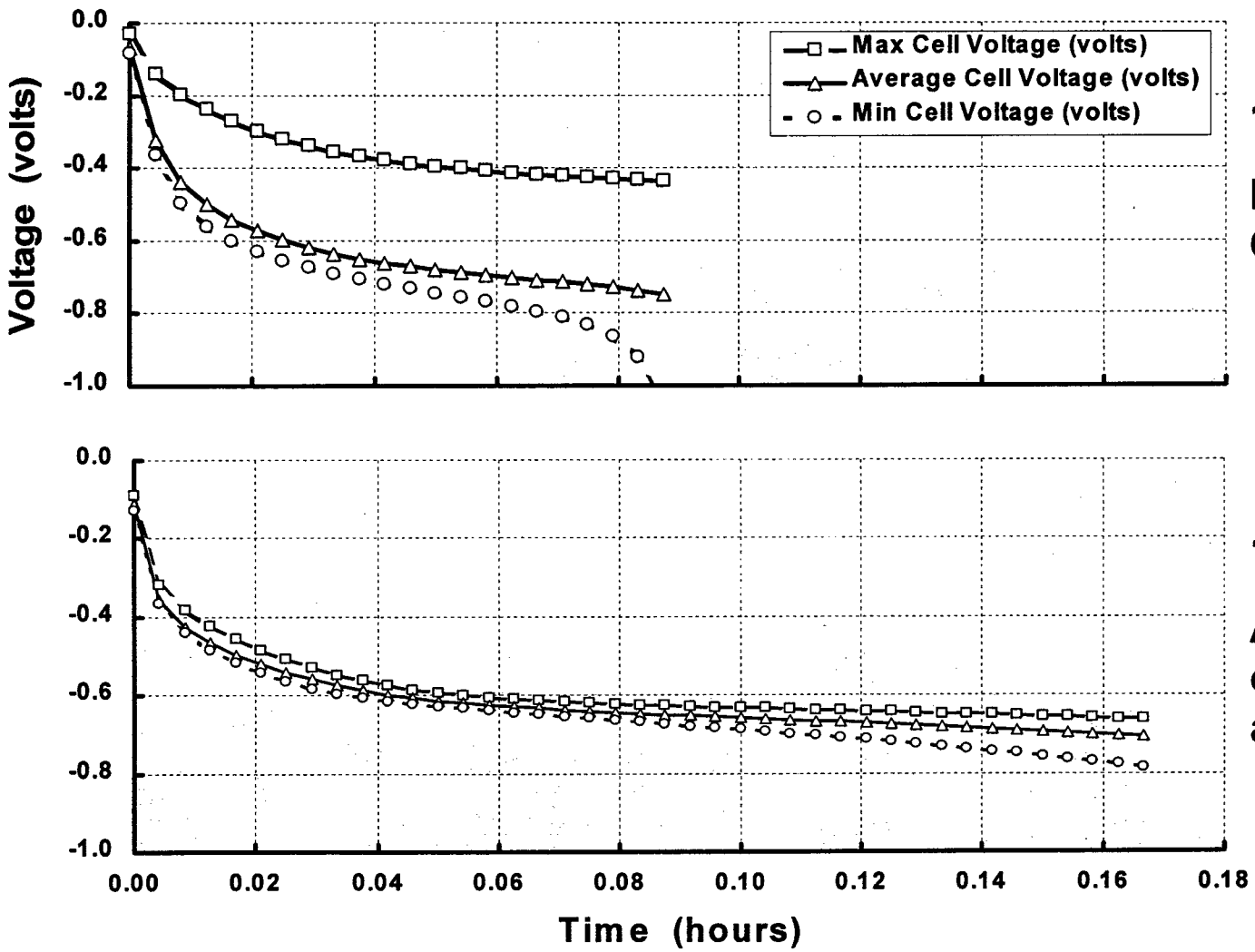

1 Oct 98

Following 6 weeks of C/500 trickle charge.

1 Apr 99

After 6 months of open circuit storage at 5 Deg C.

Wksp9902.ppt

Summary

- Nickel precharged cells are favored for many applications because they are easier to store.
- Nickel precharge degrades (mechanism unclear at present) and its presence should be verified prior to extended storage.
- A verification procedure, criteria and voltage trajectory signatures have been presented.

Strain Gage Effects and the Van der Waals' Equation

By

Dean W. Maurer

Introduction

One of the many advantages of the nickel hydrogen battery is that it provides a direct and continuous measure of its available capacity. Since hydrogen gas is the active material of the negative electrode and its pressure is a direct measure of its quantity (with certain restrictions to be discussed later), a simple measurement of the pressure and temperature can be converted to capacity available (assuming an offset for the pressure remaining at cut-off). The pressure is measured with a strain gage which is bonded to the dome of the pressure vessel and responds to the microscopic reversible bulging of the dome with pressure (the cell wall is only 0.024" thick). In addition since hydrogen gas obeys Faraday's law and well known equations of state (gas laws), measures of the rate of change of pressure can be used to derive other parameters such as power levels or currents during charge and discharge. In attempting to do this for Telstar batteries, it became apparent that the strain gage output itself varied with temperature. This paper describes methods used to determine the cell free volume and to calibrate the strain gages for temperature effects.

The Strain Gage

The strain gage consists of two stress sensitive resistors wired into the arms of a Wheatstone bridge. One of them is rigidly bonded onto the dome (active element) and the other (the dummy) is bonded along with the rest of the circuit to a piece of metal from the dome of another cell can which in turn is bonded to the dome. The other two resistors of the bridge are adjusted to create an output signal in the appropriate range (~10 mv max) when the bridge is activated with the specified excitation voltage (typically 5 to 10 volts). This use of the two stress sensitive resistors is intended to compensate for temperature effects such as metal expansion. After the cell is built, but before electrolyte addition, each strain gage is calibrated at room temperature at 4 or 5 different pressures against an external calibrated dial gage. Typically these data fall on a straight line with approximately a 0.01 mv/ psi slope and an intercept close to zero and a coefficient of correlation greater than 0.9999. **It is important to keep in mind that the strain gage measures the gage pressure not the absolute pressure.** In practice when the cell pressure falls below atmospheric pressure the strain gage output remains constant or nearly so. For calculations described here 14.7 psi must be added to the value provided by the strain gage. **Also note that when the cell is in space the gage and absolute pressures are the same.** This needs to be considered in those circumstances.

The Equations of State

The simplest equation of this type is the Ideal Gas Law:

$$PV = nRT \qquad (1)$$

Where P, V and T are the absolute pressure, volume and absolute temperature. "n" is the number of moles[1] of the gas and R is the gas constant equal to 0.082059 liter-atmospheres/ mole-^{0}K or 1206.238 cc-psia/ mole-^{o}K. In this form the molecules are considered to be point masses with no interaction other than kinetic collisions. It holds very well at low pressures and for simple molecules; for hydrogen it is good up to about 200 psia. For higher pressures the more elaborate Van der Waals' equation is required:

$$P = \frac{nRT}{(V - nb)} - a\left(\frac{n}{V}\right)^2 \qquad (2)$$

Where the variables are the same as before and the constants a and b are the Van der Waals' constants which depend on the gas. For hydrogen, a = 0.2444 liter^2-atmosphere/ mole^2 or 3592680 cc^2-psi/ mole and b = 0.02661 liters/ mole or 26.61 cc/mole. In this equation, the term with "a" is an adjustment to the pressure to account for the attraction between molecules due to their close proximity (Van der Waals' forces). This attraction is the result of electric dipoles in the molecules caused by the molecular distribution of electrons. For hydrogen this is a small effect; it would be larger with a polar molecule such as water or carbon dioxide. The term with "b" is a correction to the effective volume to account for the finite volume of the molecules themselves. The two equations give similar results below about 200 psia but gradually diverge above that pressure and are about 5% different at 800psia. This difference will be the topic of the next section. Equation (2) can be rearranged as:

$$PV^3 - n(bP + RT)V^2 + an^2V - abn^3 = 0 \qquad (3)$$

Note equation (3) is cubic in both V and n. Fortunately the numbers are such that this equation can be solved with conventional techniques and has a real root. In Excel spreadsheets the solution can easily be written as a "function macro" in Visual Basic.

The Van der Waals/ Ideal Gas Ratio or (P_i/P_v)

Using equations (1) and (2) above the P_i/P_v ratio can be calculated for specific values of V and T and a series of n's. A plot of the ratio vs. P_v results in a quadratic form. The curve fit values of sets of A's and B's for each set of particular V's and T's (the C value of the quadratic expression is 1 because at low pressure the two laws converge). By repeating this operation for the useful range of values of V and T, a series of A's and B's are obtained which can in turn be curve fit by multivariable least squares. The net result for V in the range of 900 to 1200 cc's and T in the range of 250 to 310^0 K is:

$$\begin{aligned} {}^{Pi}/_{Pv} &= 1 - \left(7.4818*10^{-9} + 8.7204*10^{-13}*V - 2.7031*10^{-11}*T\right)*Pv^2 \\ &- \left(6.4571*10^{-5} - 8.393*10^{-10}*V - 5.707*10^{-8}*T\right)*Pv \end{aligned} \qquad (4)$$

[1] A mole of a substance is a specific amount which has a weight equal to its molecular weight and is 6.023x10^{23} molecules or Avogadro's number of molecules.

In this equation the volume is in cc's and the temperature is in degrees Kelvin. This equation can also be written as function macro.
Another technique is to rearrange equation (2) above and to divide through by V, which gives:

$$\frac{(V-nb)\left(Pv+a(n/V)^2\right)}{V}=\frac{nRT}{V}=Pi \qquad (5)$$

The term to the right of the first equal sign is seen to be the ideal gas expression and equals the ideal gas pressure Pi. Equation (5) is more generally applicable than equation (4), however, in the applicable range of (4), it is more useful if it is inconvenient to use "n" whereas (5) is more useful (simpler) when "n" is available.

Faraday's Law & Graphical Techniques

In simple terms Faraday's law states that when 96,496 Coulombs or amp-seconds of charge are passed through an electrolysis cell, one equivalent of matter (Avogadro's number of electrons or charges) is reacted at each electrode. The 96,496 Coulombs is called "The Faraday" (F) and is usually rounded off to 96,500 Coulombs. This concept, using electroplating of silver under specific conditions, defines the "ampere". For the hydrogen electrode as we use it, there are essentially no parasitic reactions on discharge[2] so the relationship between charge passed and the quantity of hydrogen is considered to be exact. In units of amp-hours (AH) the Faraday is 26.3 AH/ equivalent[3]. Since for the hydrogen reaction there are two equivalents per molecule, this results in 53.6 AH/ mole of hydrogen. Thus,

$$n = At/53.6 \qquad (6)$$

where t is time in hours and A is the current in amperes. Combining equation (1) with (6), gives:

$$Pi=\frac{AtRT}{53.6V} \qquad (7)$$

Thus if Pi is plotted vs. t and the slope determined then,

$$\frac{dPi}{dt}=slope=\frac{ART}{53.6V} \qquad (8)$$

from which one of the constant terms can be determined if the others are known. In addition, if T is not constant Pi/T can be plotted and A or V determined. If the discharge is also at constant power, W/E= A (where E is the battery voltage) can be substituted into the equation so that from a plot of EPi/T vs. t, W can be determined from the slope.

The Cell Volume

The free volume of the cell can be determined by a variety of techniques but the selection is limited after the cell is sealed. One method is to use the well-controlled, constant temperature capacity tests, available in Excel, made at the supplier as part of the cell lot acceptance tests (ATP). Starting with the 20^{0}C data since the strain gages (SG's) were calibrated at room temperature, the pressure (after converting it to absolute pressure) is plotted vs. time starting from about 200 psi down to the 1.0 volt cut-off. From the slope, the volume can be estimated (equation (8)). This value has some errors associated with it which will be discussed bellow.

---

[2] Actually there is some self-discharge but this is negligible at the normal discharge rates and temperatures used. The charge reaction does have parasitic elements that are significant, namely oxygen evolution, self-discharge and the direct reaction of hydrogen with the charged nickel species on the nickel electrode.
[3] That is per electron transfer

Next from the current and discharge time a data column is generated (Table 1) providing the capacity removed at each data point. Using the volume estimate and the ideal gas law the " hydrogen equivalent capacity" (HEC) remaining at the cut-off (or any other point) can be estimated from the absolute pressure reading at that point. From this value a column of "HEC remaining" at each point in the discharge can be generated. Using a macro generated to determine

Table 1 A Sample Section of Spreadsheet Data

Discharge Time	Capacity Out	Average Temp	HEC Remaining	Supplier SG Pres.	Apparent Volume	Back Calc. SG mv	VdW Pressure
0	0	19.3	121.8	816.35	1003.76	8.53	817.07
0.167	12.52094	19.9	109.2	732.01	1000.23	7.63	729.92
1.167	87.52499	18.5	34.2	213.43	996.54	2.13	211.96
1.333	99.97621	19.4	21.8	126.08	1027.27	1.20	129.53
1.417	106.2756	18.5	15.5	87.36	1002.94	0.79	87.36
	AVE T =	19.1	15.5	= CUT OFF HYDROGEN CAP.			

the volume from cubic solution of equation (3), the calculated apparent volume at each step of the discharge is determined. An example of a plot of the data for a cell is shown in Fig 1. A trendline

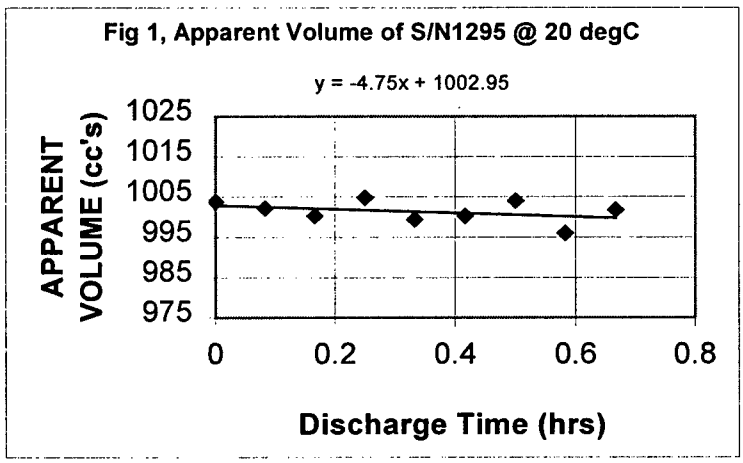

is generated and the intercept is used as the best representation of the free volume of the cell. This volume will be different from the one used earlier to determine the HEC at cut-off. These steps are repeated using the new apparent volume estimate to recalculate HEC at cut-off and recalculate the column of "HEC remaining" at each step. The apparent volume and Figure 1 is redone and a new volume determined. These steps are repeated as many times as necessary for the values to converge; usually about five times. This effectively averages a number of data points but note that the trendline has a slope. The possible causes of this slope will be discussed in the next section.

This process was repeated for the other ATP temperatures with a surprising result, namely a systematic variation of the apparent volume with temperature as shown in Fig. 2. Since changes in

the cell free volume could be caused by volume expansion of the cell components, differences in density of the active material, etc., changes of this magnitude are physically unreasonable, other possibilities were explored, namely the strain gage calibration.

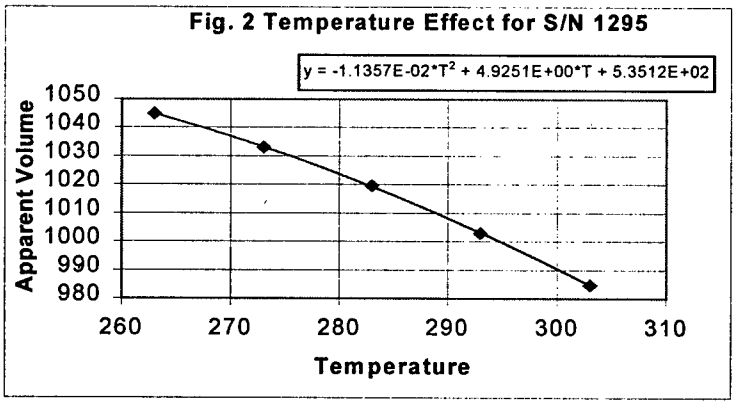

Strain Gage Temperature Calibration

Returning to the ATP data in Table 1, the column generated previously for the "HEC remaining" is used to calculate the absolute pressure with a macro based on the Van der Waals equation (2). The volume previously determined in the 20^{0}C test, is used for this calculation since the strain gages were originally calibrated at that temperature. This absolute pressure is converted to gage pressure and plotted vs. the strain gage voltages derived from the gage pressures using the original supplier calibrations. A trendline then gives the new calibration values. Figures 3 & 4 show these

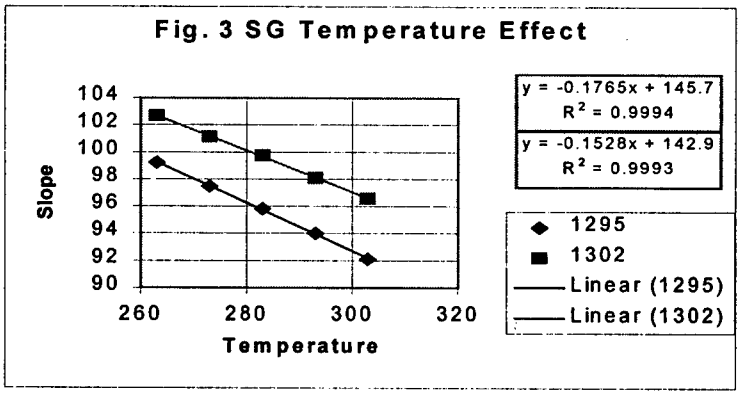

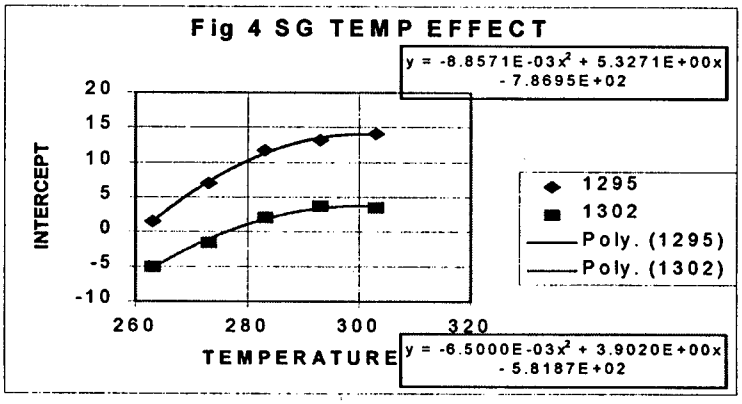

effects on both the slope and the intercept. Note that the slope changes by 8% in 40 degrees or 0.2% per degree. The intercept is non linear and varies by 15 psi in 40 degrees or the equivalent of about 2.4 AH for cells with 1000cc of volume. Using the two equations from the trendline fits a revised strain gage calibration equation can be generated in which the slope is itself a linear equation in T and the intercept is a quadratic equation in T. In cases where it is inconvenient to use this approach many times the apparent volume equation from Figure 2 can be used instead. It actually embodies the same effect even though it is physically incorrect. The cause of the slope in the apparent volume data in Figure 1 can now be explained with the additional fact that thermocouple measurements in the strain gage region of the cell during high rate discharge show a significant temperature rise. The higher gage temperature is reflected in a lower apparent pressure reading, which causes the slope of the P vs. t plot to be greater. From equation (8) it can be seen that a higher slope will give a smaller volume.

An example of the use of these data to predict the discharge current is shown in Figure 5 which is a plot of the derived ideal pressure, equation (4), vs time for the 10^0C test. From the slope, the current is calculated using equation (8) which gives a value of 74.93 A or within 0.09% of the actual measured value.

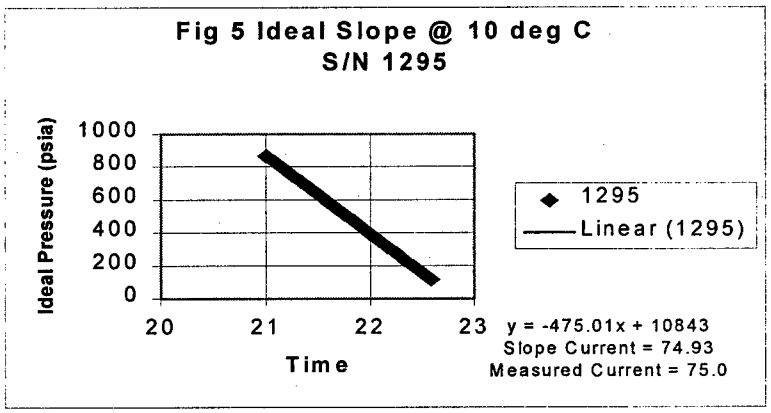

Discussion

Manipulating strain gage data is still a work in progress. Several comments can be made:

1) If no allowance is made for the effects described above (supplier calibrations are used as is) an error of 5% or more may exist especially at temperature extremes. The capacity estimate at the low temperature at the end of charge will be understated (conservative) and the capacity remaining near the end of discharge (higher temperature) will be overstated (optimistic).
2) Cursory review of application of these equations to situations involving more rapid temperature changes or to capacity retention tests has revealed large errors; for example in a ramped discharge temperature case.
3) It appears that there may be problems with local internal temperature gradients. That is during high rate discharge the cell wall temperature may be quite different from the temperature of the bulk of the hydrogen.
4) The charging process needs to be addressed.

Conclusion

The strain gage output is seen in this paper to have many peculiarities and its use to estimate capacity available in a battery needs careful attention if accuracy greater than 5% or so is required.

1999 NASA Aerospace Battery Workshop Attendance List

Jon D. Armantrout
Lockheed Martin Missiles and Space
1111 Lockheed Martin Way
B/102 O/L230
Sunnyvale, CA 94088-3504
Ph. (408) 742-1800 FAX (408) 756-0645
E-mail jon.armantrout@lmco.com

Joel K. Baker
Orbital Sciences
20301 Century Blvd.
MS E-2
Germantown, MD 20874
Ph. (301) 428-6570 FAX (301) 428-1140
E-mail baker.joel@orbital.com

Doug Bearden
Marshall Space Flight Center
ED11
Marshall Space Flight Center, AL 35812
Ph. FAX
E-mail doug.bearden@msfc.nasa.gov

Bob Bechtel
Marshall Space Flight Center
ED15
Marshall Space Flight Center, AL 35812
Ph. (256) 544-3294 FAX (256) 544-5841
E-mail bob.bechtel@msfc.nasa.gov

Michael C. Becker
The Boeing Company
POB 3707, MS AG-00
Seattle, WA 98124
Ph. (303) 307-3300 FAX (303) 307-3310
E-mail mcbecker@home.com

Yannick Borthomieu
SAFT Advanced Batteries
Rue G. Leclanche
86060 Poitiers Cedex 9
France

Ph. 33-549-55-4014 FAX 33-549-55-4780
E-mail yannick.borthomieu@saft.alcatel.fr

Bobby J. Bragg
Johnson Space Center
MS EP52
NASA Rd. 1
Houston, TX 77058
Ph. (281) 483-9060 FAX (281) 483-3096
E-mail bbragg@ems.jsc.nasa.gov

Jeffrey C. Brewer
Marshall Space Flight Center
ED11
Marshall Space Flight Center, AL 35812
Ph. (256) 544-3345 FAX (256) 544-5841
E-mail jeff.brewer@msfc.nasa.gov

Jack N. Brill
Eagle-Picher Technologies, LLC
1216 West C Street
Joplin, MO 64801
Ph. (417) 623-8000 X346 FAX (417) 623-6661
E-mail jbrill@epi-tech.com

Richard Broderick
Goddard Space Flight Center
Code 442
Greenbelt, MD 20781
Ph. (301) 286-4225 FAX (301) 286-1645
E-mail rbroderi@pop700.gsfc.nasa.gov

1999 NASA Aerospace Battery Workshop Attendance List

Bob Brown
Eagle-Picher Technologies, LLC
1216 West C Street
Joplin, MO 64801
Ph. (417) 623-8000 FAX
E-mail bbrown@epi-tech.com

Harry Brown
Naval Surface Warfare Center - Crane Div.
Code 6096 B2949
300 Highway 361
Crane, IN 47522
Ph. (812) 854-6149 FAX (812) 854-3589
E-mail brown_harry@crane.navy.mil

Ratnakumar Bugga
Jet Propulsion Laboratory
MS 277-207
4800 Oak Grove Dr.
Pasadena, CA 91109
Ph. (818) 354-0110 FAX (818) 383-6951
E-mail ratnakumar.v.bugga@jpl.nasa.gov

Jack Bullman
Marshall Space Flight Center
ED10
Marshall Space Flight Center, AL 35812
Ph. (256) 544-9009 FAX
E-mail jack.bullman@msfc.nasa.gov

John Bush
Marshall Space Flight Center
ED11
Marshall Space Flight Center, AL 35812
Ph. (256) 544-3305 FAX (256) 544-5841
E-mail john.bush@msfc.nasa.gov

William Cabrall
The Boeing Company
MS AG-00
POB 3999
Seattle, WA 98124
Ph. (303) 677-3950 FAX (303) 365-2560
E-mail bcabral9@idt.net

John E. Casey
Lockheed Martin Space Operations
2400 NASA Rd. 1, EP5
Houston, TX 77058-3799
Ph. (281) 483-0446 FAX (281) 483-3096
E-mail john.e.casey1@jsc.nasa.gov

William L. Crabtree
Marshall Space Flight Center
ED11
Marshall Space Flight Center, AL 35812
Ph. (256) 544-5305 FAX (256) 544-5841
E-mail larry.crabtree@msfc.nasa.gov

Karen Cunningham
Marshall Space Flight Center
ED11
Marshall Space Flight Center, AL 35812
Ph. (256) 544-5618 FAX
E-mail karen.cunningham@msfc.nasa.gov

Dr. Marsha Daman
Lockheed Martin Missiles and Space
1111 Lockheed Martin Way
B/102, O/L230
Sunnyvale, CA 94089
Ph. (408) 756-0749 FAX (408) 756-0645
E-mail marsha.daman@lmco.com

1999 NASA Aerospace Battery Workshop Attendance List

Eric C. Darcy
Johnson Space Center
MS EP5
Houston, TX 77058
Ph. (281) 483-9055 FAX (281) 483-3096
E-mail edarcy@ems.jsc.nasa.gov

Jerry W. David
Naval Surface Warfare Center - Crane
Code 6095, Bldg 2949
300 Highway 361
Crane, IN 47522-5001
Ph. (812) 854-4193 FAX (812) 854-3589
E-mail david_j@crane.navy.mil

Jim Degruson
Eagle-Picher Technologies, LLC
3220 Industrial Road
Joplin, MO 64801
Ph. (417) 659-9635 FAX (417) 626-2078
E-mail jdegruson@epi-tech.com

Jeff C. Dermott
Eagle-Picher Technologies, LLC
3220 Industrial Road
Joplin, MO 64804
Ph. (417) 623-8333 x21 FAX (417) 623-0233
E-mail jdermott@epi-tech.com

Andrew F. Dunnet
Fraser-Dunnet Consulting
5112 Bradford Drive
Annandale, VA 22003
Ph. (703) 256-4092 FAX (703) 256-4094
E-mail adunnet@aol.com

Ted Edge
Marshall Space Flight Center
ED11
Marshall Space Flight Center, AL 35812
Ph. (256) 544-3381 FAX (256) 544-5841
E-mail ted.edge@msfc.nasa.gov

Michel Fabre
ALCATEL
100, Bd du Midi
06150 Cannes La Bocca
France

Ph. (33) 4 92927391 FAX (33) 4 92923070
E-mail michel.fabre@space.alcatel.fr

Henry B. Flauaus
The Boeing Company
POB 516
M/C 5106-7250
St. Louis, MO 63166
Ph. (314) 233-2477 FAX
E-mail henry.b.flauaus@boeing.com

Christopher L. Fox
Eagle-Picher Technologies, LLC
C & Porter Streets
Joplin, MO 64801
Ph. (417) 623-8000 X367 FAX (417) 781-1910
E-mail cfox@epi-tech.com

Chris Garner
Naval Research Laboratory
Code 8134
4555 Overlook Ave. SW
Washington, DC 20375
Ph. (202) 767-9075 FAX (202) 767-4633
E-mail garner@ssdd.nrl.navy.mil

1999 NASA Aerospace Battery Workshop Attendance List

Pete George
Marshall Space Flight Center
ED11
Marshall Space Flight Center, AL 35812
Ph. (256) 544-3331 FAX (256) 544-5841
E-mail pete.george@msfc.nasa.gov

Donald Georgi, P.E.
Batteries Digest Newsletter
1261 Townline Road
Maple Plain, MN 55359
Ph. (612) 479-6190 FAX (612) 479-3657
E-mail donald@batteriesdigest.com

Jeffrey J. Gierloff
Lockheed Martin
4800 Bradford Dr. NW
Huntsville, AL 35807
Ph. (256) 722-4280 FAX (256) 722-4054
E-mail jeff.gierloff@lmco.com

Paul A. Gohmann
Lockheed Martin
8348 Bay Crest Ct.
Chesapeake Beach, VA 20732
Ph. (703) 293-5000 FAX (410) 257-3357
E-mail pt.gohmann@gateway.net

Guillermo A. Gonzalez
Langley Research Center
MS 257
6 East Taylor St.
Hampton, VA 23681-0001
Ph. (757) 864-7107 FAX (757) 864-8674
E-mail g.a.gonzalez@larc.nasa.gov

David Hall
Marshall Space Flight Center
ED11
Marshall Space Flight Center, AL 35812
Ph. (256) 544-4215 FAX (256) 544-5841
E-mail d.k.hall@msfc.nasa.gov

Steve Hall
Naval Surface Warfare Center - Crane Div.
Code 6095 Bldg 2949
300 Highway 361
Crane, IN 47522
Ph. (812) 854-4172 FAX (812) 854-3589
E-mail hall_s@crane.navy.mil

William R. Hart
Lockheed Martin
MS 264B
100 Campus Drive
Newtown, PA 18940
Ph. (215) 497-1649 FAX (215) 497-1564
E-mail william.r.hart@lmco.com

Jeff Hayden
Eagle-Picher Technologies, LLC
3820 South Hancock Expressway
Colorado Springs, CO 80911
Ph. (719) 392-4266 FAX (719) 392-5103
E-mail jhayden@epi-tech.com

Albert Himy
Navy / JJMA
4300 King Street
Suite 400
Alexandria, VA 22302-1503
Ph. (703) 418-4257 FAX (703) 416-1792
E-mail ahimy@jjma.com

1999 NASA Aerospace Battery Workshop Attendance List

Roger Hollandsworth
Lockheed Martin Missiles and Space
3251 Hanover St.
O/L9-21 B/204
Palo Alto, CA 94504
Ph. (650) 424-2556 FAX
E-mail roger.hollandworth@lmco.com

Nathan Isaacs
Mine Safety Appliances Company
38 Loveton Circle
Sparks, MD 21152
Ph. (410) 472-7710 FAX (410) 472-7800
E-mail nedizakmsa@aol.com

Lorna Jackson
Marshall Space Flight Center
ED11
Marshall Space Flight Center, AL 35812
Ph. (256) 544-3318 FAX (256) 544-5841
E-mail lorna.jackson@msfc.nasa.gov

Robert R. Jackson
The ENSER Corporation
PO Drawer 48548
St. Petersburg, FL 33743-8548
Ph. (727) 544-7787 x222 FAX (727) 544-7473
E-mail rjackson@ensercorp.com

Dr. Judith A. Jeevarajan
Lockheed Martin Space Operations
2101, NASA Rd 1
Mail Stop EP5
Houston, TX 77058
Ph. (281) 483-4528 FAX (281) 483-3096
E-mail jjeevara@ems.jsc.nasa.gov

Dr. P. J. Johnson
TRW Space, Defense, and Information Systems
One Space Park
Redondo Beach, CA 90278
Ph. (310) 812-7429 FAX (310) 812-4978
E-mail philip.johnson@physics.org

Bob Kapustka
Marshall Space Flight Center
ED11
Marshall Space Flight Center, AL 35812
Ph. (256) 544-3302 FAX
E-mail bob.kapustka@msfc.nasa.gov

Rick Kettner
Spectrum Astro
1440 N. Fiesta Blvd.
Gilbert, AZ 85233
Ph. (480) 892-8200 FAX (480) 892-2949
E-mail rick.kettner@specastro.com

Leonine S. Lee
Goddard Space Flight Center
Code 563, Rm 25
Greenbelt, MD 20771
Ph. (301) 286-4912 FAX (301) 286-1751
E-mail leo.lee@gsfc.nasa.gov

Dr. Harlan L. Lewis
Naval Surface Warfare Center - Crane Div.
300 Highway 361
Crane, IN 47522-5001
Ph. (812) 854-4104 FAX (812) 854-4104
E-mail lewis_h@crane.navy.mil

1999 NASA Aerospace Battery Workshop Attendance List

Eric Lowery
Marshall Space Flight Center
ED11
Marshall Space Flight Center, AL 35812
Ph. (256) 544-0080 FAX (256) 544-5841
E-mail eric.lowery@msfc.nasa.gov

Steve Luna
Marshall Space Flight Center
ED11
Marshall Space Flight Center, AL 35812
Ph. (256) 544-3402 FAX (256) 544-5841
E-mail steve.luna@msfc.nasa.gov

Charles Lurie
TRW
MS R4/1082
One Space Park
Redondo Beach, CA 90278
Ph. (310) 813-4888 FAX (310) 812-4978
E-mail chuck.lurie@trw.com

Dr. Tyler X. Mahy
U.S. Government
c/o OTS, NHB
Washington, DC 20505
Ph. (703) 874-0739 FAX (703) 641-9830
E-mail

Michelle Manzo
Glenn Research Center
MS 309-1
21000 Brookpark Rd.
Cleveland, OH 44135
Ph. (216) 433-5261 FAX (216) 433-6160
E-mail michelle.manzo@grc.nasa.gov

Jeff Martin
Marshall Space Flight Center
ED11
Marshall Space Flight Center, AL 35812
Ph. FAX
E-mail jeff.martin@msfc.nasa.gov

Dean W. Maurer
Loral Skynet
POB 7018
Bedminster, NJ 07921
Ph. (908) 470-2310 FAX (908) 470-2457
E-mail dwm@loralskynet.com

Kurt McCall
Marshall Space Flight Center
ED11
Marshall Space Flight Center, AL 35812
Ph. (256) 961-4501 FAX (256) 544-5841
E-mail kurt.mccall@msfc.nasa.gov

George Methlie
2120 Natahoa Ct.
Falls Church, VA 22043
Ph. (202) 965-3420 FAX (703) 641-9830
E-mail

John L. Michalek
Spectrum Astro
1440 N. Fiesta Blvd.
Gilbert, AZ 85233
Ph. (480) 892-8200 FAX (480) 892-2949
E-mail john.michalek@specastro.com

1999 NASA Aerospace Battery Workshop Attendance List

Martin Milden
2212 So. Beverwil Dr.
Los Angeles, CA 90034-1034
Ph. (310) 836-7794 FAX (310) 836-4494
E-mail mmilden@mediaone.net

Thomas R. Newbauer
SMC / AXEN
SMC / AXE
160 Skynet St.
Los Angeles, CA 90245-4683
Ph. (310) 363-5176 FAX (310) 363-2532
E-mail tom.newbauer@losangeles.af.mil

David O'Dell
Marshall Space Flight Center
ED11
Marshall Space Flight Center, AL 35812
Ph. (256) 544-3416 FAX
E-mail david.odell@msfc.nasa.gov

Beth Parmley
Eagle-Picher Technologies, LLC
3220 Industrial Drive
Joplin, MO 64801
Ph. (417) 659-9635 FAX
E-mail bparmley@epi-tech.com

David F. Pickett
Eagle-Picher Technologies, LLC
Power Systems Department
3820 S. Hancock Expressway
Colorado Springs, CO 80911
Ph. (719) 392-4266 FAX (719) 392-5103
E-mail dpickett@epi-tech.com

Darren Pivarnik
Loral Skynet
RR#1, Box 672
Hawley, PA 18428
Ph. (570) 226-1293 FAX (570) 226-3604
E-mail dpivarnik@loralorion.com

Gopal Rao
Goddard Space Flight Center
Code 563
Greenbelt, MD 20771
Ph. (301) 286-6654 FAX (301) 286-1751
E-mail grao@pop700.gsfc.nasa.gov

Paul L. Reinstein
The Aerospace Corporation
2350 E. El Segundo Blvd.
El Segundo, CA 99024
Ph. (310) 336-1909 FAX
E-mail paul.l.reinstein@aero.org

Ronald S. Repplinger
Eagle-Picher Technologies, LLC
1216 West C Street
Joplin, MO 64801
Ph. (417) 623-8000 FAX (417) 623-6661
E-mail rrepplinger@epi-tech.com

David P. Roller
Alliant Power Sources Company
104 Rock Road
Horsham, PA 19044
Ph. (215) 773-5405 FAX (215) 773-5499
E-mail david_roller@atk.com

1999 NASA Aerospace Battery Workshop Attendance List

Dean Roukis
INTELSAT
3400 International Dr. NW
Washington, DC 20008
Ph. (202) 944-8194 FAX (202) 944-7333
E-mail dean.roukis@intelsat.int

Kurt Salloux
Hughes Space and Communications Company
3100 W. Lomita
Building 231 Rm 2019G
Torrance, CA 90509
Ph. (310) 517-5138 FAX
E-mail kurt.salloux@hsc.com

Lee Saylors
Vaughn Associates, Inc.
8801 Willow Hills Dr.
Huntsville, AL 35801
Ph. (256) 881-1494 FAX (256) 880-6041
E-mail

Frank Scalici
INTELSAT
3400 International Dr. NW
Washington, DC 20008
Ph. (202) 944-7353 FAX (202) 944-7333
E-mail frank.scalici@intelsat.int

Darren L. Scoles
Lockheed Martin Missiles & Space
GPS IIR Flight Operations
440 Discoverer St.
Suite 79 / Rm 201
Schriever AFB, CO 80912
Ph. (719) 567-3217 FAX (719) 567-3927
E-mail darren.l.scoles@lmco.com

Annie L. Sennet
SAFT
107 Beaver Court
Cockeysville, MD 21030
Ph. (410) 771-3200 x 170 FAX (410) 771-0234
E-mail annie.sennet@saftamerica.com

Nicholas Shuster
The ENSER Corporation
PO Drawer 48548
St. Petersburg, FL 33743-8548
Ph. (727) 544-7787 x249 FAX (727) 544-7473
E-mail nshuster@ensercorp.com

E. C. Smith
Marshall Space Flight Center
ED01
Marshall Space Flight Center, AL 35812
Ph. (256) 544-3279 FAX
E-mail e.c.smith@msfc.nasa.gov

K. C. Snyder
Eagle-Picher Technologies, LLC
1216 West C Street
Joplin, MO 64801
Ph. (417) 623-8000 FAX
E-mail ksnyder@epi-tech.com

Yoshitsugu Sone
National Space Development Agency of Japan
Tsukuba Space Center
2-1-1 Sengen, Tsukuba-city
Ibaraki-pref. 305-8505 Japan

Ph. 81-(0)298-52-2285 FAX 81-(0)298-52-2299
E-mail sone.yoshitsugu@nasda.go.jp

David M. Spillman
Wilson Greatbatch Ltd.
10000 Wehrle Drive
Clarence, NY 14031
Ph. (716) 759-5378 FAX (716) 759-8579
E-mail dspillman@greatbatch.com

Joe Stockel
National Reconnesance Office
14675 Lee Rd.
Chantilly, VA 20151
Ph. (703) 808-4088 FAX
E-mail joeskl@ucia.gov

John E. Surina
Lockheed Martin
1019 Isabella Dr.
Stafford, VA 22554
Ph. (703) 619-8144 FAX (540) 720-6545
E-mail trepang@erols.com

Paul Timmerman
Jet Propulsion Laboratory
MS 277-212
4800 Oak Grove Drive
Pasadena, CA 91109
Ph. (818) 354-5388 FAX (818) 393-6951
E-mail paul.j.timmerman@jpl.nasa.gov

Mark R. Toft
Motorola
44330 Woodridge Parkway
Leesburg, VA 20176
Ph. (703) 724-8188 FAX (703) 724-8201
E-mail mark_toft-P27760@email.mot.com

Cynthia Tolliver
Marshall Space Flight Center
ED11
Marshall Space Flight Center, AL 35812
Ph. (256) 544-8590 FAX
E-mail cynthia.tolliver@msfc.nasa.gov

Dr. Hari Vaidyanathan
COMSAT Laboratories
22300 Comsat Dr.
Clarksburg, MD 20871
Ph. (301) 428-4507 FAX (301) 540-8208
E-mail hari.vaidyanathan@comsat.com

Russell Vaughn
Vaughn Associates, Inc.
3313 Memorial Pkwy., Suite 125
Huntsville, AL 35801
Ph. (256) 881-1494 FAX
E-mail

Harry Wajsgras
Goddard Space Flight Center
Code 563
Greenbelt, MD 20771
Ph. (301) 286-6158 FAX
E-mail harry.wajsgras@gsfc.nasa.gov

Harry E. Wannemacher
QSS Group
3502 Moylan Dr.
Bowie, MD 20715
Ph. (301) 286-4889 FAX (301) 286-1743
E-mail harrywannemacher@erols.com

1999 NASA Aerospace Battery Workshop Attendance List

Tom Whitt
Marshall Space Flight Center
ED11
Marshall Space Flight Center, AL 35812
Ph. (256) 544-3313 FAX (256) 544-5841
E-mail tom.whitt@msfc.nasa.gov

Doug Willowby
Marshall Space Flight Center
ED11
Marshall Space Flight Center, AL 35812
Ph. (256) 544-3334 FAX (256) 544-5841
E-mail doug.willowby@msfc.nasa.gov

Donald A. Willsher
Lockheed Martin
14608 Danville Rd.
Dale City, VA 22193
Ph. (703) 580-9723 FAX
E-mail willsher_da@mciworld.com

Dr. Michael Wixom
T/J Technologies, Inc.
VP Research & Development
POB 2150
Ann Arbor, MI 48106
Ph. (734) 213-1637 FAX (734) 213-3758
E-mail ultracap@aol.com

Wenlin Zhang
Schlumberger
14910 Airline Road
Rosharon, TX 77583
Ph. (281) 285-5564 FAX (281) 285-5575
E-mail zhang@rosharon.wireline.slb.com

Albert H. Zimmerman
The Aerospace Corporation
MS M2/275
POB 92957
Los Angeles, CA 90009-2957
Ph. (310) 336-7415 FAX (310) 336-6801
E-mail albert.h.zimmerman@aero.org

Stephane M. Zimmermann
Alcatel Space
IAC 26, avenue J-F
Champollion BP 1187
31037 Toulouse Cedex 1 France

Ph. 33.5.34.35.66.60 FAX 33.5.34.35.61.69
E-mail stephane.zimmermann@space.alcatel.fr

REPORT DOCUMENTATION PAGE

Form Approved
OMB No. 0704-0188

Public reporting burden for this collection of information is estimated to average 1 hour per response, including the time for reviewing instructions, searching existing data sources, gathering and maintaining the data needed, and completing and reviewing the collection of information. Send comments regarding this burden estimate or any other aspect of this collection of information, including suggestions for reducing this burden, to Washington Headquarters Services, Directorate for Information Operation and Reports, 1215 Jefferson Davis Highway, Suite 1204, Arlington, VA 22202-4302, and to the Office of Management and Budget, Paperwork Reduction Project (0704-0188), Washington, DC 20503

1. AGENCY USE ONLY *(Leave Blank)*

2. REPORT DATE
May 2000

3. REPORT TYPE AND DATES COVERED
Conference Publication

4. TITLE AND SUBTITLE
The 1999 NASA Aerospace Battery Workshop

5. FUNDING NUMBERS

6. AUTHORS
J.C. Brewer, Compiler

7. PERFORMING ORGANIZATION NAMES(S) AND ADDRESS(ES)
George C. Marshall Space Flight Center
Marshall Space Flight Center, AL 35812

8. PERFORMING ORGANIZATION REPORT NUMBER
M–963

9. SPONSORING/MONITORING AGENCY NAME(S) AND ADDRESS(ES)
National Aeronautics and Space Administration
Washington, DC 20546–0001

10. SPONSORING/MONITORING AGENCY REPORT NUMBER
NASA/CP—2000–209959

11. SUPPLEMENTARY NOTES
Proceedings of a workshop sponsored by the NASA Aerospace Flight Battery Systems Program, hosted by the Marshall Space Flight Center, and held at the Huntsville Hilton on November 16–18, 1999

12a. DISTRIBUTION/AVAILABILITY STATEMENT
Unclassified-Unlimited
Subject Category 44
Standard Distribution

12b. DISTRIBUTION CODE

13. ABSTRACT *(Maximum 200 words)*

This document contains the proceedings of the 32nd annual NASA Aerospace Battery Workshop, hosted by the Marshall Space Flight Center on November 16–18, 1999. The workshop was attended by scientists and engineers from various agencies of the U.S. Government, aerospace contractors, and battery manufacturers, as well as international participation in like kind from a number of countries around the world.

The subjects covered included nickel-hydrogen, nickel-cadmium, lithium-ion, and silver-zinc technologies.

14. SUBJECT TERMS
battery, cell, nickel-hydrogen, nickel-cadmium, lithium, lithium-ion, silver-zinc, separator, modeling, super capacitor

15. NUMBER OF PAGES
611

16. PRICE CODE
A99

17. SECURITY CLASSIFICATION OF REPORT
Unclassified

18. SECURITY CLASSIFICATION OF THIS PAGE
Unclassified

19. SECURITY CLASSIFICATION OF ABSTRACT
Unclassified

20. LIMITATION OF ABSTRACT
Unlimited

National Aeronautics and
Space Administration
AD33
George C. Marshall Space Flight Center
Marshall Space Flight Center, Alabama
35812